



Faculteit Landbouwkundige en
Toegepaste Biologische
Wetenschappen



Academiejaar 1999 – 2000

Buffer capacity based multipurpose hard- and software sensor for environmental applications

Een op buffercapaciteit gebaseerde multifunctionele hard- en softwaresensor voor milieutoepassingen

door
ir. LIEVEN VAN VOOREN

Thesis submitted in fulfillment of the requirements for the degree
of Doctor (Ph.D.) in Applied Biological Sciences

Proefschrift voorgedragen tot het bekomen van de graad van
Doctor in de Toegepaste Biologische Wetenschappen

op gezag van
Rector: **Prof. Dr. ir. J. WILLEMS**

Promotor:
Prof. Dr. ir. P. VANROLLEGHEM

Decaan:
Prof. Dr. ir. O. VAN CLEEMPUT

Copromotor:
Prof. Dr. ir. W. VERSTRAETE

The author and the promotors give the authorization to consult and to copy parts of this work for personal use only. Any other use is limited by the Laws of Copyright. Permission to reproduce any material contained in this work should be obtained from the author.

De auteur en de promotoren geven de toelating dit werk voor consultatie beschikbaar te stellen en delen ervan te kopiëren voor persoonlijk gebruik. Elk ander gebruik valt onder de beperkingen van het auteursrecht, in het bijzonder met betrekking tot de verplichting uitdrukkelijk de bron te vermelden bij het aanhalen van resultaten uit dit werk.

Gent, april 2000

De promotor:

De copromotor:

De auteur:

Prof. Dr. ir. P. Vanrolleghem Prof. Dr. ir. W. Verstraete ir. Lieven Van Vooren

Woord vooraf

Het woord vooraf voor de lezer is het woord achteraf van de auteur, en de ideale gelegenheid om eens achterom te kijken, en het geleverde werk te overzien in functie van iedereen die bijgedragen heeft tot de realisatie ervan.

De eerste stappen van het onderzoek werden gezet onder de hoede van Prof. Verstraete en Prof. Vansteenkiste. Vrij snel werd de tandem “Paul en Lieven” gevormd, en zijn we voor de rest van die periode onder deze noemer blijven functioneren. De tandem had als aangename eigenschap dat hij van twee walletjes kon eten, vooral als er taart geserveerd werd in de koffiepauzes . . . Willy zijn enthousiasme heeft ons toen danig geïnspireerd en menig experimenteel watertje laten doorzwemmen. De kritische opvolging door Lode, Peter en Jan werden daarin zeer gewaardeerd. Dirk gaf ons de noodzakelijke voeling met de markt en bleef steeds geloven in de uiteindelijke toepasbaarheid van het onderzoek. Ook de studenten Maarten, Ariel en Wim droegen hun steentje bij in deze periode.

Later kwam ik onder de vleugels van Prof. Ottoy en Prof. Vanrolleghem terecht, wat zeer leerrijk was. De studenten Carlo, Marijke en Tolessa leverden toen nuttige bijdragen aan dit proefschrift. Prof. Lessard in Quebec ben ik dankbaar omdat ik daar een aantal maanden intensief en in een aangename sfeer aan mijn proefschrift kon doorwerken. De familie Bertrand betekende meer dan louter een ‘gastgezin’ . . . Het FASTNAP project was de kroon op het onderzoekswerk, omdat we met een groep enthousiaste mensen tot een mooi en afgewerkt eindresultaat gekomen zijn. Hierbij wil ik vooral Marijke bedanken, haar gedrevenheid en inzet waren fantastisch. Ook Nikolaj, Peter, Anton, Piet en Dick (IMAG), Dirk (Hemmis), Hans en Fons (Eijkelkamp) en Toon (VLM) hebben een belangrijke bijdrage geleverd. Mijn promotor, Peter, wil ik toch heel speciaal bedanken. “Geef ze een pluim, en ze krijgen vleugels” weet hij als geen ander op zijn mensen toe te passen. Ook alle medewerkers van LME en BIOMATH zijn bedankt voor hun bijdrage in de aangename periode die ik daar beleefd heb.

De leden van de examen- en leescommissie wil ik bedanken voor het kritisch nalezen van dit proefschrift. Ik wil ook de financiële steun van het IWT en de firma’s Hemmis en Eijkelkamp in deze dankbetuiging betrekken. Zonder hun bijdrage was dit werk niet tot stand gekomen.

Mijn familie en vrienden wil ik bedanken voor hun steun en hun betoonde interesse voor dit werk. En tenslotte, last but not least, mijn vrouw Ria en onze kinderen Sander en Daan, die allicht blij zullen zijn voor mij dat het werk af is . . .

Gent, 5 april 2000

Lieven

Contents

List of symbols and abbreviations	v
1 Introduction	1
2 Chemical aspects of pH buffer capacity	5
2.1 The pH measurement	5
2.1.1 pH fundamentals	5
2.1.2 pH measurement cells	8
2.1.3 Practical pH measurements	10
2.2 Acid-base chemistry	14
2.2.1 The dynamic nature of chemical equilibrium	15
2.2.2 Activity corrections	15
2.2.3 Nature and strength of acids and bases	18
2.2.4 Equilibrium calculations	19
2.2.5 pH titration curve	21
2.2.6 pH buffer capacity curve	22
2.3 Dissolved organic carbon	25
2.3.1 The carbonate species and their acid-base equilibria	25
2.3.2 Alkalinity and acidity	27
2.4 Metal ions in aqueous solution	29
2.4.1 Complex formation and dissociation constants	30
2.4.2 Complexes with inorganic ligands	33
2.4.3 Complexes with organic ligands	33
2.5 Precipitation and dissolution reactions	35
2.6 Modelling tools	37
3 Mathematical pH buffer capacity modelling	39
3.1 Introduction	39
3.2 Modelling titration curves	40
3.2.1 Variable pH approach	40
3.2.2 Fixed pH approach	42
3.2.3 Generalized titration curve model	43
3.3 Linear buffer capacity model	44
3.3.1 Buffer capacity model for monoprotic acids	46

3.3.2	Buffer capacity model for diprotic acids	47
3.3.3	Buffer capacity model for triprotic acids	48
3.3.4	General linear buffer capacity model	49
3.3.5	Monoprotic approach of the general linear buffer capacity model	50
3.3.6	Ionic interaction effects	51
3.4	Non-linear symbolic buffer capacity model	52
3.5	Non-linear tableau-method based buffer capacity model	55
3.5.1	The tableau method for solving chemical equilibria problems	55
3.5.2	Precipitation and dissolution in equilibrium models	60
3.5.3	Non-linear tableau-based buffer capacity model	61
3.5.4	Ionic interaction effects	63
3.5.5	Precipitation and dissolution in the tableau-based approach	64
3.6	Comparison of the 3 buffer capacity model approaches	67
4	Field technologies for aquatic monitoring	69
4.1	On-line measurement techniques	70
4.2	Nutrient sensors: State of the art	72
4.2.1	Sample filtration	72
4.2.2	Ammonium analyzers	74
4.2.3	Nitrate analyzers	76
4.2.4	Phosphate analyzers	80
4.3	Developments in effluent and river water monitoring	81
4.4	Titrimetric sensors and applications	84
4.4.1	Data interpretation of a few specific points of a titration profile	85
4.4.2	Data interpretation of the complete titration profile	89
4.4.3	Titrimetric biosensors	93
5	Software developments	97
5.1	pH titration algorithms	97
5.1.1	The Dynamic Equivalence-point Titration (DET) algorithm	98
5.1.2	Data-based titration algorithm	103
5.1.3	Model-based titration algorithm	105
5.1.4	Combined data- and model-based titration algorithm	108
5.1.5	Validation of the combined titration algorithm	112
5.2	Tableau-method based simulation software	113
5.2.1	Software objectives	113
5.2.2	Software implementation	115
5.2.3	Functionalities description	116
5.3	Buffer capacity optimal model builder	117
5.3.1	Software objectives	117
5.3.2	Buffer capacity calculation	118
5.3.3	Non-linear function minimization	120
5.3.4	Automatic buffer capacity model building	125
5.3.5	Optimal buffer capacity model selection	131
5.3.6	Software implementation	135

5.3.7	Functionalities description	135
6	On-line effluent and river water monitoring	139
6.1	The AQMON project	139
6.1.1	Project identification	139
6.1.2	Background of the project	139
6.2	Sensor methodologies	141
6.2.1	Ammonium and ortho-phosphate measurement	143
6.2.2	Short-term BOD measurement	143
6.2.3	Nitrate measurement	146
6.3	Automatic buffer capacity based sensor	147
6.3.1	Principle of the device	148
6.3.2	Titration reproducibility and accuracy	148
6.3.3	Effluent and surface water monitoring	151
6.4	Conclusions	162
7	Tertiary algal wastewater treatment monitoring	165
7.1	Introduction	165
7.1.1	Algal wastewater treatment	165
7.1.2	Alkalinity related to algal processes	166
7.1.3	Objectives	167
7.2	Materials and Methods	168
7.2.1	The algal pilot plant	168
7.2.2	Sampling and laboratory measurements	168
7.2.3	Titration curves	168
7.2.4	Data processing software	169
7.2.5	Mathematical models	169
7.3	Results and Discussion	171
7.3.1	Alkalinity and IC buffer capacity	171
7.3.2	Ammonium and ortho-phosphate evaluation in grab samples	175
7.3.3	Dynamic nutrient evolution in a 48 hour batch experiment	175
7.4	Conclusions	181
8	Automatic titrimetric sensor for manure nutrients	183
8.1	The FASTNAP project	183
8.1.1	Project identification	183
8.1.2	Background of the project	184
8.1.3	Sensor perspectives	186
8.1.4	Measurement principles	186
8.2	Destruction of manure samples	187
8.2.1	On-line microwave destruction of manure samples	187
8.2.2	On-line UV destruction of manure samples	188
8.3	Automatic nitrogen and phosphorus measurements	190
8.4	Development of the titrimetric part of the sensor	190
8.4.1	Introduction to animal manure destruction	191

8.4.2	Titration of destructed manure samples	192
8.4.3	Modification of the destruction procedure	194
8.4.4	Mathematical model analysis	195
8.4.5	The influence of the dilution factor	207
8.4.6	Experimental method validation	208
8.4.7	Development of an adequate buffer capacity model	210
8.5	Laboratory validation and statistical data analysis	216
8.5.1	Validation experiment	216
8.5.2	Influences of alkaline stock solutions	220
8.5.3	Statistical data analysis	232
8.6	Conclusions	236
9	Automatic pH buffer capacity model building	239
9.1	Introduction	239
9.2	Buffer capacity modelling of well-known samples	240
9.2.1	Materials and methods	240
9.2.2	Evaluation of two modelling approaches with a testcase	241
9.2.3	Evaluation of six model selection criteria	247
9.2.4	Model building strategy	252
9.3	Surface water and effluent applications	254
9.3.1	Materials and methods	254
9.3.2	Automatic model building results	255
9.3.3	Conclusions	265
9.4	Algal wastewater treatment applications	266
9.4.1	Materials and methods	266
9.4.2	Automatic model building results	267
9.4.3	Conclusions	269
9.5	Destructed manure applications	270
9.5.1	Materials and methods	270
9.5.2	Automatic model building results	271
9.5.3	Conclusions	275
9.6	Summarizing conclusions	275
10	General discussion and conclusions	279
10.1	Various buffer capacity simulation approaches	280
10.2	Buffer capacity based hard- and software sensor	282
10.3	Nutrient measurements from buffer capacities	284
10.4	Buffer capacity based alarm generation	288
10.5	Automatic pH buffer capacity model building	288
10.6	Summarized conclusions	289
	Bibliography	291
	Summary – Samenvatting	317
	Curriculum Vitae	321

List of symbols and abbreviations

α :	critical significance level
β :	1. buffer capacity ($eq\ l^{-1}\ pH^{-1}$) 2. equilibrium constant for an overall formation reaction
ε :	residual value
γ :	activity coefficient
ζ :	correction factor
η :	convergence parameter
θ :	parameter vector
λ :	first order constant
σ :	standard deviation
a_i :	activity of analyte ion i
AIC :	Akaike's information criterion
AIC _C :	corrected Akaike's information criterion
AP :	algal pilot plant
AQMON :	aquatic monitor
BOD :	biological oxygen demand
BOD _{st} :	short-term biological oxygen demand
C :	concentration (M or $mmol\ l^{-1}$ or $mg\ l^{-1}$)
C :	carbonate alkalinity ($meq\ l^{-1}$ or $mg\ CaCO_3\ l^{-1}$)
C_A :	concentration of strong acid (used in titrations) (M)
C_B :	concentration of strong base (used in titrations) (M)
CFA :	continuous flow analysis
COD :	chemical oxygen demand
DET :	dynamic equivalence-point titration
DOC :	dissolved organic carbon
DON :	dissolved organic nitrogen
DW :	dry weight
EAP :	effluent algal pilot plant
EVC :	effluent of the Valcartier plant
F :	Faraday constant ($96484.56\ C\ mol^{-1}$)
FASTNAP :	fast titrimetric N and P determination in animal manure
FIA :	flow injection analysis
FPE :	final prediction error
G :	Gibbs free energy ($kJ\ mol^{-1}$)
G^0 :	standard free energy ($kJ\ mol^{-1}$)
GD :	gas diffusion
GLM :	general linear model
H :	enthalpy (heat content) ($kJ\ mol^{-1}$)
$H_2CO_3^*$:	hypothetical species representing $CO_{2(aq)}$ plus H_2CO_3
I :	ionic strength (M)
IAP :	ion activity product
IC :	inorganic carbon ($mg\ CO_2\ l^{-1}$ or $mmol\ l^{-1}$)
ICP-MS :	inductively coupled plasma - mass spectrometry

ISFET :	ion selective field effect transistor
K :	equilibrium constant
$*K$:	equilibrium constant used for hydrolysis reactions
cK :	equilibrium constant expressed in terms of concentrations instead of activities
K_a :	acidity constant expressed in terms of activities
cK_a :	acidity constant expressed in terms of concentrations
K'_a :	mixed acidity constant
K_H :	Henry's constant ($M atm^{-1}$)
K_{s0} :	solubility constant
K_w :	ion product of H_2O , $K_w = \{OH^-\}\{H^+\}$
K_w^* :	equilibrium constant for the water buffer, $K_w^* = K_w/\{H_2O\}$
M :	molar concentration ($mol l^{-1}$)
MET :	monotonic equivalence-point titration
MINAS :	mineral accounting system used in the Netherlands
N :	1. normality ($eq l^{-1}$) 2. number of data points
NaN :	not-a-number
NEN :	Dutch normalization institute
p :	1. significance level of the test statistic in a statistical test 2. $-log$ operator (used in e.g. pK_a , pK_w , ...)) 3. number of parameters 4. partial pressure (e.g. p_{CO_2}) (atm^{-1})
PRL :	proton reference level
PCA :	principal component analysis
R :	gas constant ($8.31441 J K^{-1} mol^{-1}$)
R^2 :	determination coefficient
r.s.d. :	relative standard deviation
S :	entropy ($kJ mol^{-1} K^{-1}$)
s :	sample standard deviation
SIC :	Schwartz information criterion
SSE :	sum of squared errors (or residuals)
T :	absolute temperature in K ($273.15 K +$ temperature in $^{\circ}C$)
T :	total alkalinity ($meq l^{-1}$ or $mg CaCO_3 l^{-1}$)
TOC :	total organic carbon
TP :	total phosphorus
U :	potential measured between the measuring and the reference electrode (V)
U_N :	Nernst slope (V)
V :	volume
v :	reaction rate
VFA :	volatile fatty acids
VMM :	Flemish environmental agency
VOC :	volatile organic carbon
\bar{X} :	mean value of X
z_i :	charge of analyte ion i (including sign)

Chapter 1

Introduction

In the field of environmental measurements, in the last decades, one increasingly tries to implement on-line (field) measurements to replace off-line (laboratory) measurements. In an ideal situation, the measured data should be produced in-situ, on-line, continuously in real time and cover a wide dynamic range. The largest benefit of on-line measurements compared to off-line measurements is undoubtedly the possibility to use such data for control purposes. For example in wastewater treatment, on-line sensors have been demonstrated to allow considerable savings in energy and chemical consumption [166]. On-line measurements also allow up-to-date simulation and calibration of mathematical models of treatment systems. Consequently, the benefits from computer simulation are e.g. savings in energy and chemical consumption [347], a decrease of nutrient levels in the effluent [292], and an increase of capacity of the plant [55, 56, 290]. Because the mathematical models in the field of integrated urban water system modelling (i.e. the combined modelling of sewers, rivers and wastewater treatment plants) become more advanced, on-line measurements become increasingly important for a better understanding of fast phenomena and to support the model building and simulation [321]. Continuous and on-line monitoring of aquatic streams (rivers, effluents, process waters, . . .) can also fulfil the function of alarm generation. In case of abrupt changes in the water quality, the necessary actions (e.g. activate a bypass, take an extra sample for laboratory analysis, . . .) can be taken. For some application areas, on-line automated measurements are not developed or implemented yet, but would be beneficial compared to the actually performed off-line laboratory analyses. An example of this is the monitoring of the nutrients nitrogen and phosphorus in animal manure, which is one of the applications described in this work.

Despite all advantageous aspects concerning the benefits of on-line sensors, still many difficulties and erroneous measurements are noticed during practical use of on-line sensors. Difficulties related to on-line measurements are often underestimated, and the installed on-line equipment does not always produce the results and profits expected [246]. The successful use of on-line sensors does not only depend on the sensor itself, but also, and often most importantly, on the process conditions, the sample preparation, the maintenance, calibration, . . . The sampling system is a crucial part of the measurement system. Most nutrient analyzers require a sample stream free of suspended solids, which necessitates the use of a membrane filter sampling system [250, 288]. When filtration systems are not adapted to the particular application,

they suffer from limited lifetime or clogging problems [289]. Up to half of the investment costs for the installation of an on-line analyzer can be due to the installation of a sampling and filtration system [250]. Another key factor is maintenance and surveillance [291, 334]. On the one hand, on-line analyzer companies often suggest maintenance intervals of 1 week, or even 1 month, but practical field studies show on the other hand that for complicated on-line sensors (e.g. N and P analyzers), a daily inspection should be carried out with all on-line analyzers [250]. Therefore, on-line sensor development is a challenging field for researchers because of its many aspects that need to be considered.

The developed sensor in this work is based on pH measurements. The pH measurement technology did not undergo major technical improvements in the last decades. The glass electrode, which already has a lifetime of more than 50 years, is still the standard in pH measurement [84]. A correctly implemented pH sensor is robust and suitable for field applications. However, there are a number of pitfalls and particularities related to this measurement, and there is currently no substitute for the experienced eye of a trained technician [238]. For example, the pH analyzer accuracy in the laboratory is typically around 0.02, however, once the device is brought to the plant floor, this kind of accuracy is often no longer realized [238].

The hardware part of the sensor developed in this work consists of a titrator unit, capable to perform acid-base titrations of aquatic samples. A titration curve is obtained by adding small amounts of e.g. NaOH to the sample, and measuring the pH after each addition. A titration curve has a typical S-shape, and can be transformed into a buffer capacity profile with an appropriate mathematical algorithm. The results of this work are based on advanced data processing of buffer capacity profiles. Therefore, the term 'software sensor' originally introduced in [25], is applicable to this work.

Methods and applications based on pH titrations are used in a wide variety of fields (aerobic, anaerobic and physico-chemical wastewater treatment, food and feed applications, soil science, microbiology, aquatic chemistry, ...). However, these applications mostly rely on the off-line interpretation of titration curves, and can thus not be considered 'sensors'. Sensors making use of pH titration curves are often referred to as titrimetric sensors. Traditionally, titrimetry is used for the volumetric determination of a particular substance in solution by adding a standard solution of known volume and strength until the reaction is completed, usually as indicated by a change in colour due to an indicator or by electrochemical measurements (mostly pH). However, looking into the literature, 'titrimetry' also includes all methods in which consecutive acid or base additions, followed by pH measurements, are performed.

Generally, three types of titrimetric sensors can be considered. The first category includes sensors that are automated versions of traditional laboratory methods and that can automatically perform end-point titrations. Second, titrimetric sensors can be used to record the amount of acid and/or base required to maintain a certain pH. If these sensors are applied in bioreactors with living cells, in which cell metabolism causes acidity changes that allow on-line determination of e.g. growth kinetics, they are named 'titrimetric biosensors'. The third category includes titrator based sensors that record a partial or complete titration curve. These sensors mostly work with only a few titration points and a simplified and robust data interpretation method. One of the main application fields in this area is the control of anaerobic digestion where bicarbonate and/or volatile fatty acids (VFA's) can be monitored on-line with a titrimetric sensor. The buffer capacity based sensor developed in this work belongs to the last category, but differentiates itself from the other sensors by the fact that the whole and detailed titration

profile is used for model-based interpretation (software sensing). The developed software sensor part of this work can be seen as the complete data interpretation of the recorded titration curves, to obtain useful information related to the buffers present in the sample.

An innovative aspect related to the developed hard- and software sensor in this work is the combined measurement of several buffering components in the sample with only one and relatively simple hardware set-up. Due to the simplicity of the hardware, the sensor is robust for field-use, without the necessity of a complicated sampling system (e.g. filtration unit). It is a multipurpose sensor because on the one hand it is useful for the quantification of buffering components (e.g. ammonium and ortho-phosphate in an effluent), and, on the other hand, it can be used as an alarm generator (e.g. the detection of pollutant discharges in a river). The following statement illustrates the particularities of the approach followed in this thesis: "Titration is the preferred method to discontinuously determine with a high precision relatively high concentrations of a well-known species in a pure solution. However, in this thesis, the titration technique is used for continuous or on-line measurement of multiple relatively low concentrated species with adequate precision in impure solutions" (P. Willems, Ghent University).

An important part of the research described in this thesis was performed in the framework of research projects in which industrial partners were involved (the AQMON project in chapter 6 and the FASTNAP project in chapter 8). As a consequence, the project developments strived for the practical implementation and the perspectives for later commercialisation. Therefore, the research described in this thesis is interdisciplinary and practically oriented.

The outline of this thesis consists of four parts. The first part (chapters 2, 3 and 4) describes the fundamentals and background of the research work. Chapter 2 can be seen as a summarizing introduction in aquatic chemistry topics related to pH buffer capacity. In later chapters, the described topics are of practical use for defining appropriate mathematical models, and explaining the chemical phenomena taking place in the titration vessel of the developed sensor. Chapter 3 gives a consistent overview of three different approaches of pH buffer capacity modelling. This overview is partially based on literature research, however, major parts needed to be adapted or further developed to fit the requirements of this work. An interesting aspect of this chapter is that not only buffer capacity models are developed for the simplest type of chemical reactions (acid-base equilibria), but that also more complicated buffer systems (i.e. where complexation and/or precipitation reactions occur) are considered in the same framework. Chapter 4 presents a literature review on field technologies for on-line measurement in wastewater treatment systems, rivers and other aquatic streams. To limit the scope of this very broad range of existing technologies, this review only highlights a number of techniques and sensors for which the applicability is similar compared to the developed buffer capacity based sensor. More particularly, nutrient sensors, effluent and river water monitoring equipment, titrimetric sensors and titrimetric biosensors are reviewed.

The second part of this thesis (chapter 5) summarizes the main software developments. Three software projects are worked out for the purpose of this work. The first project is the development of a robust titration algorithm for constant ΔpH titration. This type of titration algorithm is not available yet in the commonly used titrators. The developed titration algorithm is compared with a traditional end-point titration algorithm implemented in a commercial titrator. The second project is the development of general purpose buffer capacity simulation software. The innovative aspect is that buffer capacity profiles resulting from acid-base titrations in which complexation and precipitation reactions are involved can be simulated. And the last

but most important software project is the data processing software of experimental titration curves. From a particular titration curve, this software extracts information about individual buffer systems and estimates their concentrations. Further, the same software is capable to automatically and stepwise build buffer capacity models for titrated samples. In chapter 9, the latter feature is evaluated for use in alarm generation or problem detection (e.g. when unexpected buffers are found in the experimental buffer capacity profile). One can say that this software is the brain of the developed buffer capacity based sensor.

The third part of this work (chapters 6, 7 and 8) is application oriented. Chapter 6 handles the application field of wastewater treatment effluent and river water monitoring using the buffer capacity based sensor. The first part of this chapter describes the results of preliminary experiments with combined conductivity and pH titrations and the determination of nitrate and BOD_{st} , while the second part of chapter 6 focusses on ammonium and ortho-phosphate measurements in effluents and river waters. The application potential on this type of aquatic streams has to be seen in a context of alarm generation. The second application (chapter 7) describes buffer capacity based monitoring of tertiary algal wastewater treatment. Besides the nutrient measurements N and P, the inorganic carbon (IC) buffer is an important buffer system that is considered in detail. Because this buffer is the only carbon source used by the algae, its quantification is a helpful process control input. The third application (chapter 8) considers the on-line measurement of the nutrients N and P in destructed and diluted manure samples. The most important difference compared with the applications described in the two previous chapters is that the titrated sample is now free of organic interferences because of the destruction step with H_2SO_4 and H_2O_2 prior to titration. The anorganic interferences (resulting from complexation and precipitation reactions with e.g. Ca^{2+} or Fe^{3+}) are handled in software. The driving force behind this application is the official requirement in the Netherlands to determine N and P in each individual manure transport between 2 farms. In Flanders, this requirement is not adopted yet. However, a taxation system on the production and surplus of nitrogen and phosphorus has been approved (Mestdecreet, May 11th, 1999). In this framework, increasing demands for analyses of N and P in animal manure and other organic streams are to be expected in the coming years. Further, the knowledge of the nutrient concentrations in each individual manure transport can be used for a more adequate application of manure in view of environmental hygiene and fertilisation. The purpose of this application is that nutrient measurements are performed automatically and in the field, preferentially prior to application of the manure on the soil. The developed automatic buffer capacity based sensor is evaluated for its potential as an alternative for the traditional laboratory analyses, of which the results are now only available after five to ten working days.

The fourth part of this work (chapter 9) describes the automation of buffer capacity model building. The applications of part three of this work are reevaluated with this automated modelling approach. The purpose of the automation of buffer capacity model building is to efficiently find an useful and adequate buffer capacity model, tailor-made for each individual sample. The application of such approach in a buffer capacity based sensor in the field allows to automatically detect and characterize unexpected buffer systems in e.g. an effluent or a river water sample. This can be useful for alarm generating purposes. Finally, chapter 10 discusses and summarizes the results presented in this thesis.

Chapter 2

Chemical aspects of pH buffer capacity

The topics that are treated in this chapter are based on a number of reference works [198, 263, 273] on aquatic chemistry. The aim of this chapter is to define and summarize the concepts that will be needed in later chapters for the development of the buffer capacity sensor.

2.1 The pH measurement

2.1.1 pH fundamentals

Definition of pH

The hydrogen ion concentration in dilute aqueous solution generally lies between 10^{-14} and 10^0 mol l^{-1} , i.e. varies over a range of several powers of ten. It is, therefore, appropriate to express hydrogen ion concentrations on a logarithmic scale. Sørensen suggested taking the negative logarithm of the hydrogen ion concentration values. He named this the 'hydrogen exponent' and introduced the term pH (*pondus Hydrogenii; puissance d'Hydrogène*). According to present-day notation, the Sørensen scale, defined around 1909, would be expressed as

$$p\text{cH} = -\log c_{\text{H}^+} \text{ or } c_{\text{H}^+} = 10^{-p\text{cH}^+} \quad (2.1)$$

Later, Sørensen realized that it was not so much the concentration of the hydrogen ions that was significant, but rather their activity. Only the activity can be determined by normal methods, and this, therefore, forms the basis of the more recent definition of pH [84]:

$$\text{pH} \equiv p\text{aH} = -\log a_{\text{H}^+} \quad (2.2)$$

The ratio of the activity a_{H^+} over the concentration c_{H^+} is called the activity coefficient γ_{H^+} . Since it is only possible to take logarithms of dimensionless numbers, this definition

should be written correctly:

$$\text{pH} \equiv \text{paH} = -\log \frac{a_{\text{H}^+}}{a_{\text{H}^+}^0} = -\log \frac{c_{\text{H}^+} \gamma_{\text{H}^+}}{a_{\text{H}^+}^0} \quad (2.3)$$

Here $a_{\text{H}^+}^0$ is the hydrogen ion activity 1 mol l^{-1} . The definition of pH retains the concentration unit mol l^{-1} instead of converting to mol m^{-3} as is usual in analytical chemistry. The definition of the practical pH scale was only made possible by the Debye-Hückel theory of interionic interaction, developed in 1923. Some more details about this theory can be found in section 2.2.2. Many have attempted to replace pH by other units. In 1975 it was suggested, within the framework of the new international units, that hydrogen ion activities should be expressed as nmol l^{-1} instead of in logarithmic terms. None of these suggestions has received even limited acceptance [84]. One of the consequences of the logarithmic nature of the pH scale is that arithmetic mean pH and many other statistical calculations lead to substantial errors of the true H^+ ion concentration [133].

The principle of the potentiometric measurement

Potentiometry is an extremely versatile analytical method that allows rapid and simple analysis [293]. The pH measurement is a potentiometric measurement.¹ The experimental set-up for potentiometric measurements comprises a measuring and a reference electrode. An electrode is in essence a rod of metal dipping into a solution of one of its salts. Due to the metal becoming charged relatively to the solution, an electric pressure (known as an electric potential and measured in volts) is set up between the metal and the solution [336]. The measuring electrode provides a potential that depends on the composition of the analysis solution. The task of the reference electrode is to supply a potential which is as independent as possible of the analysis solution. A measuring device with as high an input resistance as possible connects the two conductors (electrodes) and allows the chain potential U to be measured. Due to the high resistance, this quasi-nonelectrical measuring method does not alter the chemical composition of the measuring solution. A charge exchange takes place at the interphases of the electrode of a galvanic chain, leading to galvanic potentials. These cannot be determined separately, since at least two interphases are present [6]. The measurable chain potential U is composed of several components:

$$\begin{array}{ccccccc} \text{Metal A} & | & \text{Electrolyte 1} & || & \text{Electrolyte 2} & | & \text{Metal B} \\ & U' & & U'' & & U''' & \\ \hline U = & U' & + & U'' & + & U''' & \end{array}$$

- U : potential measured between the measuring and the reference electrode
 U' : potential of the measuring electrode
 U'' : diffusion potential
 U''' : potential of the reference electrode

¹Non-potentiometric pH measurements (such as conductometric or colorimetric methods) also exist [84, 336], but are outside the scope of this work.

In an ideal measurement system, the potential measured between the two electrodes depends only on the activity of the analyte ion a_i . This relationship is described by the Nernst equation:

$$U = U_0 + \frac{2.303RT}{z_i F} \log a_i = U_0 + U_N \log a_i \quad (2.4)$$

- U : potential measured between the measuring and the reference electrode
 U_0 : standard potential of the electrode assembly, construction dependent
 R : gas constant ($8.31441 \text{ J K}^{-1} \text{ mol}^{-1}$)
 T : absolute temperature in K ($273.15 \text{ K} + \text{temperature in } ^\circ\text{C}$)
 z_i : charge of analyte ion i (including sign)
 F : Faraday constant ($96484.56 \text{ C mol}^{-1}$)
 a_i : activity of analyte ion i
 U_N : Nernst slope (V)
 2.303 : conversion factor \ln to \log

The Nernst slope U_N specifies the theoretical electrode slope. U_N corresponds to the potential change caused by the change in a_i to the power of ten. It depends on the condition of the electrode assembly, the temperature and the charge z of the analyte ion. It is 59.16 mV at 25°C for univalent, positively charged ions ($z = +1$).

In order to be able to compare the galvanic potentials of different electrodes, the standard hydrogen electrode (SHE) was introduced as an universal reference electrode. The potential of the SHE is by definition zero at all temperatures. The SHE consists of a platinized platinum sheet, which is immersed in a solution of $a_{\text{H}^+} = 1.0$ and surrounded by hydrogen gas at 1 bar [84].

The electrodes used throughout this work are all of the type ‘combined pH glass electrode’ with a built-in Ag/AgCl reference electrode. This type of electrode is commonly used in environmental pH measurements. The measurable chain potential U consists of several sources of potential, which are shown in Figure 2.1.

- U_1 : potential on the outside of the membrane, dependent on the pH value of the measuring solution
 U_2 : asymmetry potential, it is the potential on the glass membrane when the same solution and conducting system exist on either side of the membrane. U_2 is influenced by the thickness and production method of the glass membrane
 U_3 : potential on the inside of the membrane, dependent on the pH value of the inner buffer
 U_4 : potential of the inner Ag/AgCl lead-off electrode, dependent on the Cl^- activity of the inner buffer
 U_5 : potential of the reference electrode, dependent on the Cl^- activity of the reference electrolyte
 U_6 : junction or diffusion potential

In order to measure U_1 , and assign a definite pH value to it, all other single potentials $U_2 - U_6$ have to be constant, but not necessarily known. The diffusion potential remains the greatest cause of uncertainty in the practical measurement of pH [84].

Since pH standards are used for comparative determinations with other solutions, the measured result always contains two diffusion potentials, which compensate each other to some

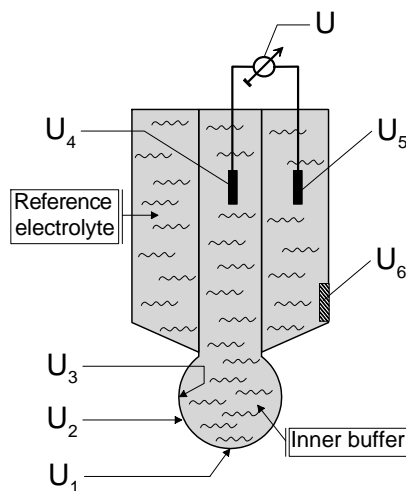


Figure 2.1: Different sources of potential in a combination electrode [6]

extent. The residual diffusion potential can be minimized by using calibration and sample solutions of similar composition. In the case of acids and bases, in particular, calibration and sample solutions should be of similar pH [84].

2.1.2 pH measurement cells

Reference electrodes with liquid junction

The standard hydrogen electrode has a fundamental importance as reference standard, but ready-to-use reference electrodes are preferred for practical determinations. The standard potentials of these electrodes are accurately known, so it is easy to recalculate the results in terms of the standard hydrogen electrode. Originally the zinc amalgam electrode in saturated zinc sulfate was used as reference electrode. In 1893 it was replaced by the mercury/calomel electrode. Nowadays the silver/silver chloride reference system is by far the most frequently employed because it is simple to prepare and very reproducible [84]. Even today the mercury/calomel electrode still remains one of the most important of all reference electrodes. Its standard potential is more reproducible and more accurately known than that of all other reference electrodes. An advantage of the Ag/AgCl electrode however, is its relatively small temperature coefficient. Compared to the calomel electrode the Ag/AgCl electrode is largely hysteresis-free and can be used even at high temperatures [6].

The junction is the critical part of the measuring chain because of the diffusion potential. The junction between the reference electrolyte and the sample solution should always have a resistance as low as possible, but at the same time prevent mixing of the two solutions. These two contradictory requirements have led to the design of many pieces of apparatus in which more or less satisfactory compromises have been made. According to different applications, the following types of junctions are used in practice: open liquid junction, ceramic plugs,

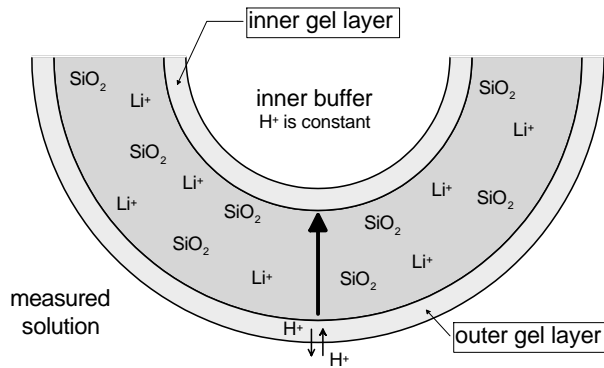


Figure 2.2: Cross-section through a glass membrane [6]

sleeve junctions, metallic junctions, ... When a reference electrode is transferred from one sample to another then, initially, the sample solution that has already diffused into the junction still remains within it. It takes several minutes for sufficient electrolyte to flow out to displace all of the old sample solution. This changing diffusion potential is known as a 'memory effect'. Reference electrodes containing thickened (gel) electrolytes are sometimes employed in order to avoid the problem of having to supply the electrode with electrolyte solution. After some time, however, classical gels suffer from syneresis (i.e. they demix with the exudation of water and contraction of the gel).

None of the typical problems of classical reference electrodes, namely liquid junction contamination, propagation resistance, stirring errors, memory effect, electrolyte bridges, and pressure compensation, would occur if a solid-state reference electrode without a liquid junction could be used. Yet, even today there is no theory for the construction of an ideal reference electrode without a liquid junction.

Glass electrodes

To explain the phenomenon of the development of a potential at the glass membrane of a pH electrode, a knowledge of the structure of the gel layer is of crucial importance. The phenomenon can be explained through the model depicted in Figure 2.2 and the different sources of potentials shown in Figure 2.1

A thermodynamic equilibrium of the hydrogen ion arises at the phase boundary between the measuring solution and the outer gel layer. If the activity of the hydrogen ions is different in the two phases, hydrogen ion transport will occur. This leads to a charge at the phase boundary, which prevents any further H^+ transport. This resulting potential is responsible for the different hydrogen ion activities in the solution and in the gel layer:

$$U_1 = \frac{2.303RT}{F} \log \frac{(a_{H^+})_{\text{solution}}}{(a_{H^+})_{\text{outer gel layer}}} \quad (2.5)$$

The number of hydrogen ions in the gel layer is imposed by the silicic acid skeleton of the

glass membrane and can be considered constant and independent of the measuring solution.

The potential in the outer gel layer is transmitted to the inside of the glass membrane by the Li^+ ions found in the glass membrane, where another phase boundary potential arises:

$$U_3 = \frac{2.303RT}{F} \log \frac{(a_{\text{H}^+})_{\text{inner buffer}}}{(a_{\text{H}^+})_{\text{inner gel layer}}} \quad (2.6)$$

The total membrane potential U is equal to the difference of the two phase boundary potentials U_1 and U_3 :

$$U = \frac{2.303RT}{F} \log \left(\frac{(a_{\text{H}^+})_{\text{solution}}}{(a_{\text{H}^+})_{\text{outer gel layer}}} \frac{(a_{\text{H}^+})_{\text{inner gel layer}}}{(a_{\text{H}^+})_{\text{inner buffer}}} \right) \quad (2.7)$$

When the H^+ activity is identical in the two gel layers (the ideal case) and the H^+ activity of the inner electrolyte is kept constant, the following equation holds:

$$U = \text{constant} + \frac{2.303RT}{F} \log(a_{\text{H}^+})_{\text{solution}} \quad (2.8)$$

The precise composition of membrane glasses are amongst the best kept secrets of electrode manufacturers. The membrane glasses in current use are always compromises for specific applications. There is no such thing as a glass of universal application, which means that a careful selection of an appropriate electrode for each particular application is necessary.

2.1.3 Practical pH measurements

Accuracy and response time

The accuracy of the measured pH value depends on the maintenance of the electrode, the measuring solution (extreme pH values, contamination, homogeneity, stirring, . . .), the temperature, the pressure, the choice of electrode, the calibration buffer solutions, and many other controllable and uncontrollable factors [6]. In a well-equipped laboratory (25 °C, 70 % relative humidity, no vibration), a pH analyzer accuracy of 0.02 or 0.03 can probably be reached. However, once the device is brought to the plant floor, this kind of accuracy can no longer be realized [238]. Basically, the accuracy and reproducibility of the measured values depend on the frequency of calibration and maintenance of the electrode. A new electrode in a standard buffer (e.g. pH values 4, 7 or 10) has a response time of less than 5 seconds to achieve a stable reading to ± 0.01 pH units. If a stable pH value is not reached over a longer period of time, the cause may be one of a wide variety of possible problems [6].

It is possible to obtain accurate estimates of pH from continuous recording field equipment [63]. In a study on an upland stream in the English Lake District, no statistically significant difference was found between continuously recorded field data and measurements made by taking samples and analyze them in the laboratory for pH, although, exceptionally differences were as high as 0.16 pH [63]. There were no problems associated with long-term drift under field conditions, and electrodes appear to perform more reproducible after long-term immersion in a relatively constant medium. This study revealed that electrodes should be completely immersed during field measurements to avoid errors associated with differences between water

and air temperature. Exposure of part of the electrode to a fluctuating temperature appears to increase the underlying unidirectional drift in potential, resulting in wrong measurements [63]. The leakage rate of the reference electrolyte in field situations was found to be between 1 and $3 \mu\text{l h}^{-1}$ [63]. Therefore a polypropylene box in an elevated location on the stream bank containing saturated KCl as reference electrolyte, ensured a positive flow of electrolyte solution irrespective of the stream level.

Calibration

Both the zero point, i.e., the point where the pH electrode delivers 0 mV potential (generally at pH 7) and the slope of the calibration line show manufacturing dependent tolerances and will change after exposure to the measuring solutions [6]. The hydrogen ion concentration (thus the pH value) in a solution is temperature dependent. Therefore, it is of great importance that the temperature curve of the buffer is known. The stability of the zero point and the slope depends on the composition of the measuring solution as well as on the temperature. It makes little sense to make general statements regarding the calibration frequency, because calibration needs are case dependent. The following factors directly influence the accuracy of the calibration as well as the pH measurement:

- buffer solutions
- temperature measurement and temperature compensation (see next paragraph)
- condition of the junction and the reference system (contamination, etc.)
- working technique

In practical pH measurement the diffusion potential is present during both calibration and pH determination. Hence, the actual determination only considers the difference between two diffusion potentials. This residual diffusion potential is small if the buffer and sample solution have similar chemical compositions. Thermal potentials can occur if parts in the measurement circuit are different in temperature (Seebeck effect). If the necessary care for this interference is not taken, errors up to 0.1 pH units can be introduced in the measurement. This implies that a pH measurement system will need relatively long stabilization periods when moved from one temperature to another. The measurement cell and the pH meter are often at different temperatures so that it should be ensured that the metallic junctions in the reference and glass electrodes are symmetrical with respect to each other and that, as is normally the case, the leads are constructed of the same material (usually copper). A thermal diffusion potential also develops when a temperature gradient exists within an electrolyte.

At high pH values (pH > 9), H^+ ions in the gel layer are partly or completely replaced by alkali ions which lead to a measured pH value which is too high. This effect is called 'the alkaline error' and can be minimized by using a special pH membrane glass [6, 336]. pH electrode calibration deviation from linearity can eventually be corrected for by considering a linear bias of electrode response (slope) at low and high pH values [144].

It was assumed, for the purpose of deriving the phase boundary potentials, equations (2.5) and (2.6), that the inner and outer gel layers are equal. In reality, this is not always true, and this effect leads to an asymmetry potential. Asymmetry potentials are eliminated by calibration so that they do not generally enter the measurement result. However, they vary with time and have

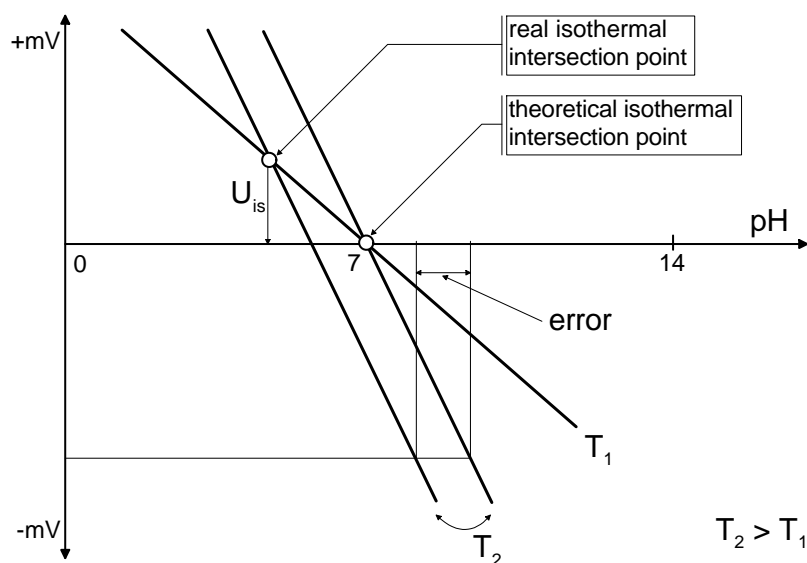


Figure 2.3: Calibration lines (isothermals) for 2 different temperatures and isothermal intersection points [6]

nonreproducible temperature coefficients so that electrodes with large asymmetry potentials are not stable [84].

Temperature compensation

The temperature influences the pH measurement through different dependent factors [6, 98]:

- temperature coefficient of the measured solution
- temperature dependence of the Nernst slope
- response time of the electrode
- position of the isothermal intersection

Every measuring solution has a characteristic temperature and pH behaviour (temperature coefficient). In general, a temperature change results in a pH change (e.g. buffer/temperature tables should be consulted when using buffer solutions for the calibration of a pH electrode). The reason for this is the temperature dependent dissociation which causes a change in $[H^+]$. This pH change is real, and not a measuring error.

An electrode would have an ideal temperature behaviour if its calibration lines (isothermals) intersect at the zero point of the electrode ($pH\ 7 = 0\ mV$) for different temperatures (see Figure 2.3). The pH value is defined as $-\log a_{H^+}$, hence, the slope of the isothermals is equal to $-U_N$ (see equation (2.4), Nernst equation). Thus an increasing temperature results in a decreasing isothermal slope, as illustrated in Figure 2.3.

Since the overall potential of the pH electrode is composed of the sum of many single potentials, which all have their respective temperature dependencies, the isothermal intersection

hardly ever coincides with the zero point of the electrode.

In the last few years, the continuous development of the electrode has concentrated on bringing the isothermal intersection and the zero point as close together as possible, since the nearer they are to pH 7 the smaller the error in the temperature compensation is. Besides, the measuring error increases with an increasing temperature difference between the calibration and the actual measurement. As a rule, the errors are in the order of 0.1 pH units. Contrary to popular belief, pH analyzers and transmitters do not compensate for the temperature effect on the actual pH of the measured solutions, they only compensate for the temperature dependence of the sensor. As already mentioned, the real pH itself is temperature dependent, so that it is useless to report pH values without mentioning the temperature [238].

New pH technologies

In industrial environments, one often finds 'intelligent' pH measuring systems, especially when the importance of a correct measured value is high (e.g. costly production processes which need an accurate pH control). This 'intelligent' system is typically based on backup pH measurements of a voting system using multiple measuring loops. Usually three measurements, taken under identical conditions with the inevitable risk of a common mode of failure, are needed (2-out-of-3) [238]. The most typical mode of failure is contamination of the electrodes, including malfunctioning of the reference electrode due to junction problems. As the electrodes are in the same medium, they will all contaminate at a similar rate, and such a fault will, hence, not be detected by the triple validation. On-line checks are by far the most important diagnostic tools for on-line pH measurement [238]. Some recent developments are based on microprocessor technology and include glass electrode breakage detection, reference electrode malfunctioning detection, ... Overall, it can be stated that pH technology did not undergo major technical improvements in the last decades.

The glass electrode already has a lifetime of more than 50 years, and is still the standard in pH measurement. However, new technologies for pH measurements are presented in literature. Ion-selective field effect transistors (ISFETs) have been developed and applied for pH measurement. The advent of ISFETs allows a considerable reduction in dimension and price of sensor electrodes. However, the expectations raised by ISFETs have as yet not been fulfilled, in spite of intensive efforts. Ideas concerning the manifold possible applications of pH ISFETs are much further advanced than is their actual state of development [84].

Because of the possibility to miniaturize ISFET based sensors and to integrate several ISFET sensors in 1 device, this technology seems promising in clinical analysis. An integrated chemical sensor with multiple ion and gas sensors, composed of four ISFETs (pH, Na⁺, K⁺ and Cl⁻) [296] was realized on a 4 × 4 mm² chip. The purpose of this sensor was to measure in real-time blood electrolytes at the bedside of seriously ill and surgical patients. All of the ISFETs show sensitivities over 50 mV per decade, and a linear range between 1 × 10⁻⁴ and 5 × 10⁻¹ mol l⁻¹. Despite the comparable selectivity and sensitivity between ISFETs and conventional ion-selective electrodes, there are still some problems with the short lifetime and the low reliability noticed with this type of ISFET based sensors [296].

The pressure and temperature sensitivity of silver chloride or calomel reference electrodes as well as their reactivity towards hydrogen sulphide –the latter causes an irreversible electrode poisoning– make sulphide bearing waters (for instance in the hypolimnion of stratified lakes,

anoxic fjords or the Black Sea) difficult to access by direct electrochemical measurements [77]. In view of these shortcomings, a novel in-situ device for the direct potentiometric detection of pH, pe and pH_2S values was developed, in which the conventional liquid-junction type reference cells for pH and pe measurements are avoided by using an alkali glass electrode as a reference [77]. The probe's main advantage lies in its high stability over large pressure, temperature and H_2S gradients.

So called AIROFs (Anodic Iridium Oxide Film) also have pH sensor properties [211]. Like ISFET they have a very fast response ($< 0.5 s$), but they are sensitive to oxygen in the solution, thus limiting their lifetime and accuracy. When the O_2 concentration is constant and the AIROF is connected to an instrumentation amplifier in such a way that the electrode remains oxidized, then the use of the AIROF as an absolute pH sensor may well be possible with an accuracy of < 0.1 pH between pH 2 and pH 11 for many hours [211]. Its small response time, large range, high sensitivity and ease of use open the possibility of using the sensor successfully as an equivalence point detector in acid-base titrations.

For on-line pH monitoring in fermenters, a fibre-optic fluorescence-based pH sensing device was developed [139]. A custom-built fluorometer, designed to provide broad-band excitation ($< 420 nm$) was used to monitor the emission of a pH-sensitive fluorophore 1,4-DHPN (1,4-dihydroxyphthalonitrile) in solution at two wavelengths. The pH-monitoring system was interfaced to the fermenter by inserting a needle connected to the optical fibre. The response time of this sensor was slower than a standard pH measurement, and the response was affected by changes in ionic strength and cell concentration [139]. Since there are no known existing protocols for immobilizing 1,4-DHPN on the distal ends of optical fibres, the fluorophore was directly dissolved in the fermentation broth. This is of course a very important drawback for implementation in other application areas, like aquatic systems.

Custom-made or modified platinum-calomel electrode systems are also used for specific purposes like the measurement of potential changes within $(Fe^{2+}/Fe^{3+}) : (Cr_2O_7^{2-}/Cr^{3+})$ solution, for measurement of COD [35], or for H_2O_2 measurement used in an enzymatic biosensor for detection of silage effluent pollution in river water [270].

Despite all technical improvements in pH measurement systems, hard- and software enhancements, etc. there is no substitute for the experienced eye of a trained technician, especially with the aid of the comprehensive data displays provided by the new age transmitters [238]. The statement "pH measurement is not only science, but also art" (N. Bogaerts, Elscolab). illustrates the particularities related to pH measurements.

2.2 Acid-base chemistry

The pH and the composition of natural waters is influenced by the interactions of acids and bases. One might say that the ocean is the result of a gigantic acid-base titration; acids that have leaked out of the interior of the earth are titrated with bases that have been set free by the weathering of primary rock. The pH of natural waters is of great significance in all chemical reactions associated with the formation, alteration, and dissolution of minerals [273]. The pH exerts such a large effect on reactions which occur in water, that it can be thought of as a *master variable*, or *control variable*, and the concentrations of most other chemical species as *response variables* [337].

Acid-base reactions in aqueous solutions generally proceed extremely rapidly. The half-life of a proton transfer reaction is below the milliseconds scale [263]. An important exception is the reaction $\text{H}_2\text{CO}_3^* \rightleftharpoons \text{H}^+ + \text{HCO}_3^-$ which will be discussed in detail in section 2.3. Equilibria characterizing hydrogen ion transfer reactions are among the simpler type of models. Metal-ion equilibria (section 2.4) and precipitation reactions (section 2.5) require more complicated types of models.

2.2.1 The dynamic nature of chemical equilibrium

Let us examine the hypothetical, elementary, reversible reaction taking place at constant temperature [263]:



The *reactants* A and B combine to form the *products* C and D . In this example, a moles of A combine with b moles of B to form c moles of C and d moles of D . If we introduce A and B into a suitable reaction vessel, the concentrations of A and B decrease until they reach values that do not change with time, while the concentrations of C and D increase from zero to time-invariant levels. If we were to add only the products of the reaction, C and D , to the reaction vessel under the same experimental conditions, we would observe a decrease in C and D , and an increase in A and B . The reaction (2.9) is only at equilibrium if the ratio of concentrations of products to reactants is the same as that attained in the previous experiment when A and B were initially present. The ratio is the so-called equilibrium constant, K .²

$$\frac{[C]^c [D]^d}{[A]^a [B]^b} = K \quad (2.10)$$

The unit of concentration as indicated by $[\cdot]$ is usually mol l^{-1} . From this we conclude that the equilibrium state can be approached from both directions.

When we investigate the rate at which the equilibrium condition is approached, we can deduce that the equilibrium condition is a dynamic one, not a static situation. Another way of stating this is that a chemical reaction is at equilibrium if its forward rate of reaction, v_f , is equal to the rate of the reverse reaction, v_r . The equilibrium constant is thus the ratio of the rate constants of the forward and the reverse reactions—a fact that underscores the dynamic nature of equilibrium. Some authors prefer a fully kinetic approach for describing chemical equilibria (e.g. acid-base equilibria) because of its advantages when coupling chemical equilibria models with other kinetic models [203].

2.2.2 Activity corrections

The theory of ideal solutions implies that there is no interaction between individual species. In real solutions, particularly solutions of ionic species in water, these conditions are not met. There are electrostatic interactions between charged ions, and the ions are generally surrounded

²Strictly speaking, the equilibrium constant is defined in terms of activity, this will be discussed in section 2.2.2.

Table 2.1: Activity coefficients (γ) of individual ions [198, 251, 273]

Approximation	Equation	Approximative applicability (Ionic Strength, M)
(1) Debye-Hückel (simplified)	$\log \gamma = -Az^2\sqrt{I}$	$< 10^{-2.3}$
(2) Debye-Hückel (extended)	$\log \gamma = -Az^2 \frac{\sqrt{I}}{1 + Ba\sqrt{I}}$	$< 10^{-1}$
(3) Güntelberg	$\log \gamma = -Az^2 \frac{\sqrt{I}}{1 + \sqrt{I}}$	$< 10^{-1}$
(4) Davies	$\log \gamma = -Az^2 \left(\frac{\sqrt{I}}{1 + \sqrt{I}} - 0.3I \right)$	< 0.5

I : ionic strength (M), $I = \frac{1}{2} \sum C_i z_i^2$
 z : charge of the ion
 a : adjustable parameter dependent on the size of the ion (\AA), see Table 2.2
 $A = 1.82 \times 10^6 (\epsilon T)^{-3/2}$ where ϵ = dielectric constant^a; $A \approx 0.5$ for water at 25 °C
 $B = 50.3 (\epsilon T)^{-1/2}$; $B \approx 0.33$ for water at 25 °C

^a The dielectric constant for water: 87.8 at 0°C; 78.3 at 25 °C; 55.6 at 100 °C [335].

by regions in which the water molecules are ordered in a structure somewhat different from that of pure water [251]. The ratio of the activity of a species to its concentration is called the activity coefficient. The activity coefficient γ_A of species A is:

$$\gamma_A = \frac{\{A\}}{[A]} \quad (2.11)$$

In general, activity coefficients of uncharged species are near unity in dilute solutions and rise above unity in concentrated solutions, largely because much of the water in concentrated solutions is involved in the hydration shells of ions and less water is available to solvate uncharged species (salting-out effect). The activity coefficients of an ion in electrolyte solution (natural waters also) is usually smaller than one.

The Debye-Hückel theory is a model that allows activity coefficients to be calculated on the basis of the effect ionic interactions should have on the free energy. Different equations have been proposed for the estimation of individual activity coefficients, see Table 2.1.

In dilute solutions ($I < 10^{-2} M$), e.g. in fresh waters, calculations are usually based on the infinite dilution activity convention and corresponding thermodynamic constants. In these dilute electrolyte mixtures, deviations from ideal behaviour are primarily caused by long-range electrostatic interactions. The Debye-Hückel equation or one of its extended forms (see Table 2.1) is assumed to give an adequate description of these interactions and to define the properties of the ions. A comparative study about different equations for activity coefficients can be found in [302]. In chapter 8, the Davies approximation is applied. However, more sophisticated

Table 2.2: Parameter a for the calculation of activity coefficients

Ion	Ion diameter a (Å) (Ångström = $10^{-10} m$)
H ⁺ , Al ³⁺ , Fe ³⁺	9
Mg ²⁺	8
Ca ²⁺ , Zn ²⁺ , Cu ²⁺ , Mn ²⁺ , Fe ²⁺	6
Pb ²⁺ , CO ₃ ²⁻	5
Na ⁺ , HCO ₃ ⁻ , H ₂ PO ₄ ⁻ , CH ₃ COO ⁻ , SO ₄ ²⁻ , HPO ₄ ²⁻ , PO ₄ ³⁻	4
K ⁺ , Ag ⁺ , NH ₄ ⁺ , OH ⁻ , Cl ⁻ , ClO ₄ ⁻ , NO ₃ ⁻	3

approaches also exist [198], but these are outside the scope of this work.

Within this framework, the earlier presented equation (2.10) for the equilibrium constant K has to be written in terms of activity instead of concentrations:

$$K = \frac{\{C\}^c \{D\}^d}{\{A\}^a \{B\}^b} = \frac{[C]^c [D]^d \gamma_C^c \gamma_D^d}{[A]^a [B]^b \gamma_A^a \gamma_B^b} = {}^c K \frac{\gamma_C^c \gamma_D^d}{\gamma_A^a \gamma_B^b} \quad (2.12)$$

We will assume that $\{H^+\}$ is the activity used in chemical equilibrium expressions for acids and bases. It can be replaced by an activity coefficient times a concentration $\gamma_{H^+} [H^+]$. When making a H^+ measurement with a combination pH electrode and calibrating with the *National Bureau of Standards* buffer solutions, the measurement is closest to an activity measurement, not a concentration. Only if one calibrates with a strong acid such as $10^{-3} M H_2SO_4$ (which has according to equation (2.1) a $pcH = 2.7$) one measures the H^+ concentration with a pH meter [251].

For water chemistry purposes, it is usually precise enough to use an approximation of ionic strength derived from a correlation with specific conductance or total dissolved solids [124, 263, 281]. Two popular expressions are:

$$I \cong 1.65 \times 10^{-5} EC \quad (2.13)$$

$$I \cong 2.5 \times 10^{-5} TDS \quad (2.14)$$

I : ionic strength (M)

EC : electrical conductivity ($\mu S cm^{-1}$)

TDS : total dissolved solids ($mg l^{-1}$)

For neutral molecules, an empirical equation for γ can be used [198, 251, 263]:

$$\log_{10} \gamma = k_s I \quad (2.15)$$

where k_s is the salting-out coefficient, to be determined experimentally, generally between 0.01 and 0.15 [263], but often set to 0.1 [198].

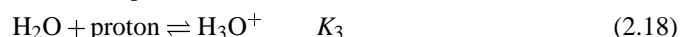
2.2.3 Nature and strength of acids and bases

It is known that a hydrogen ion, that is, a proton, cannot exist as a bare ion in water solution. Theoretical calculations show that a proton would strongly react with a water molecule to form a hydrated proton, a hydronium or a hydroxonium ion (H_3O^+). Actually, the H_3O^+ ion in an aqueous solution is itself associated through hydrogen bonds with a variable number of H_2O molecules: $(\text{H}_7\text{O}_3)^+$, $(\text{H}_9\text{O}_4)^+$, and so on. The formula H_3O^+ or H^+ is generally used, however, to denote a hydrated hydrogen ion. The hydroxide ion is also strongly hydrated in aqueous solutions. Similarly, metal ions do not occur as bare metal ions but as aqua complexes (see section 2.4).

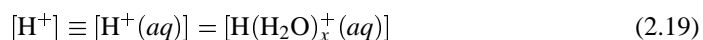
The rational measure of the strength of the acid HA relative to H_2O as proton acceptor is given by the equilibrium constant for the proton transfer reaction



which may be represented formally by two steps:



Because the equilibrium activity of the proton and of H_3O^+ are not known separately, the thermodynamic convention sets the standard free energy change ΔG^0 for reaction (2.18) equal to zero; that is, $K_3 = 1$. In dealing with dilute solutions we can, because of this convention, represent the aqua hydrogen ion by H^+ , that is,



and the free energy change ΔG involved in the proton reaction (2.16) may be expressed in terms of the equilibrium constant of equation (2.17), the acidity constant of the acid HA, K_{HA} . Ignoring activity coefficients, we have

$$K_2 = K_1 = K_2 K_3 = K_{\text{HA}} = \frac{[\text{H}^+][\text{A}^-]}{[\text{HA}]} \quad (2.20)$$

which upon rearrangement gives the equation of Henderson-Hasselbach:

$$\text{pH} = \text{p}K_{\text{HA}} + \log \frac{[\text{A}^-]}{[\text{HA}]} \quad (2.21)$$

For concentrations (activities of HA and A^-) in a molal (mol kg^{-1}) \cong molar (mol l^{-1}) scale, $\text{p}K_{\text{HA}}$ is commonly referred to as $\text{p}K_a$.

Self-ionization of water Because of its amphoteric properties, water undergoes auto-ionization, and the autoprotolysis reaction



has to be considered in all aqueous solutions. In dilute aqueous solutions ($\{\text{H}_2\text{O}\} = 1$), the

equilibrium constant for equation (2.22) usually called the ion product of water, is

$$K_w = \{\text{OH}^-\}\{\text{H}_3\text{O}^+\} \equiv \{\text{OH}^-\}\{\text{H}^+\} \quad (2.23)$$

At 25 °C, $K_w = 1.008 \times 10^{-14}$ or $pK_w = 13.997$ and the pH = 7.00 corresponds to exact neutrality in pure water ($[\text{H}^+] = [\text{OH}^-]$). The ion product of water, thus also the pH of neutrality is temperature dependent. Different equations for pK_w in function of the absolute temperature T have been developed [51, 273]:

$$pK_w = \frac{4470.99}{T} - 6.0875 + 0.01706T \quad (2.24)$$

$$pK_w = \frac{4787.3}{T} + 7.1321 \log T + 0.010365T - 22.80 \quad (2.25)$$

2.2.4 Equilibrium calculations

Because acid-base reactions in solution generally are so rapid, we can concern ourselves primarily with the determination of species concentrations at equilibrium. In the usual approach, we desire to know $[\text{H}^+]$, $[\text{OH}^-]$, and the concentration of the acid and its conjugate base that result when an acid or a base is added to the solution [263]. The mathematical modelling of acid-base equilibria (chapter 3) will use a slightly modified approach because we will desire to know the buffer capacity β in function of a *fixed* pH or $[\text{H}^+]$. Acid-base equilibrium calculations are of central importance in the chemistry of natural waters and wastewater treatment processes. The purpose of this section is to describe a general approach to the solution of acid-base equilibrium problems.

Let us consider for this purpose the equations that describe a solution which results when an acid, HA, or a salt of its conjugate base, MA (where M is a cation), is added to water [263].

Mass balances

In acid-base reactions the reacting species are conserved. When HA is added to water, the acid ionizes partially or completely.



Let us assume that the system is homogeneous and closed (i.e. no species containing A can enter from, or leave to, the atmosphere, and that precipitation or dissolution of such species cannot occur). A mass balance on all species containing A gives

$$C_a = [\text{HA}] + [\text{A}^-] \quad (2.27)$$

where C_a is equal to the analytical concentration of HA or the number of moles of HA added per litre. $[\text{HA}]$ and $[\text{A}^-]$ are the molar concentrations of the acid and conjugate base in solution at equilibrium.

When C moles of the salt MA are added per litre, it dissociates



and the base A^- , reacts with water,



If we assume that M^+ does not form complexes with A^- or other solutes, and given that MA dissociates completely, a mass balance on M and A yield respectively

$$C_m = [\text{M}^+] \quad (2.30)$$

$$C_a = [\text{HA}] + [\text{A}^-] \quad (2.31)$$

where $C_m = C_a = C$.

When MA and HA both are added to a solution, equation (2.31) holds, where C_a = sum of the moles of HA and MA added per litre of solution.

Equilibrium relationships

The second group of equations we need to consider describe equilibrium relationships. For the example of HA added to pure water the following equilibria are pertinent. In aqueous solution, we obtain for the dissociation of water:

$$K_w = \{\text{OH}^-\} \{\text{H}^+\} \quad (2.32)$$

The dissociation of HA is described by its acidity constant:

$$K_a = \frac{\{\text{H}^+\} \{\text{A}^-\}}{\{\text{HA}\}} \quad (2.33)$$

or

$${}^c K_a = \frac{[\text{H}^+][\text{A}^-]}{[\text{HA}]} = K_a \frac{\gamma_{\text{HA}}}{\gamma_{\text{H}^+} \gamma_{\text{A}^-}} \quad (2.34)$$

A so-called mixed acidity constant is frequently used [273]:

$$K'_a = \frac{\{\text{H}^+\}[\text{A}^-]}{[\text{HA}]} = K_a \frac{\gamma_{\text{HA}}}{\gamma_{\text{A}^-}} \quad (2.35)$$

This convention is most useful when pH is measured according to the IUPAC convention ($\text{pH} \approx \text{paH}$) (see section 2.1), but the conjugate acid-base pair is expressed in concentrations.

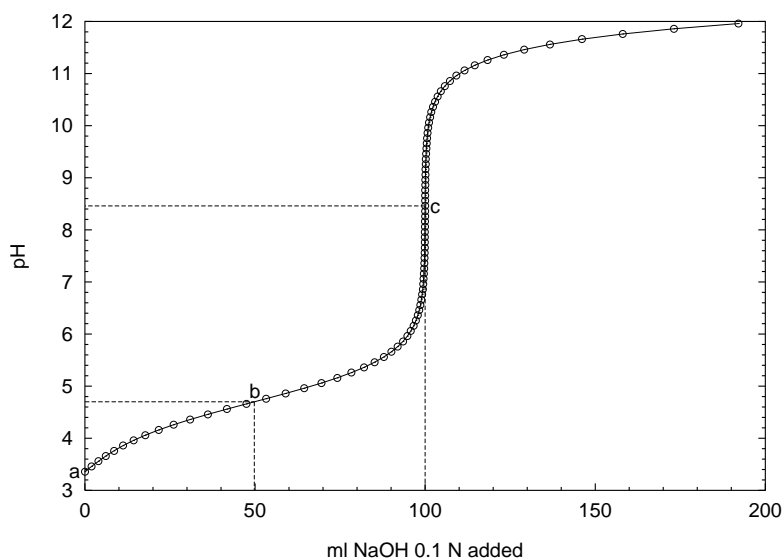


Figure 2.4: Titration curve for 1 litre of a 0.01 *M* acetic acid solution [28]

The charge balance or electro-neutrality equation

The basis of the charge balance is that all solutions must be electrically neutral. Ions of one charge cannot be added to, formed in, or removed from a solution without the addition, formation, or removal, of an equal number of ions of the opposite charge. In a solution the total number of positive charges must equal the total number of negative charges.

For the example in which the salt MA is added to water, the species present are H_3O^+ , H_2O , OH^- , M^+ , A^- and HA. The electro-neutrality equation becomes:

$$[\text{M}^+] + [\text{H}_3\text{O}^+] = [\text{OH}^-] + [\text{A}^-] \quad (2.36)$$

2.2.5 pH titration curve

A titration curve may be obtained by adding small amounts of a strong base to a weak acid solution, or by adding small amounts of a strong acid to a weak base solution, and measuring the pH after each addition. A comparative study about calculation and graphical methods to describe titration curves is given in [190]. An example of a titration curve for 1 litre of a 0.01 *M* acetic acid (HA) solution is presented in Figure 2.4. The curve has an S-shape, which suggests that the pH does not change at a constant rate with the addition of strong base. The chemical events responsible for the shape of the titration curve can be elucidated by considering the points *a*, *b* and *c* located on the plot in Figure 2.4.

Point a: This point represents the equilibrium pH established in a 0.01 *M* acetic acid solution. At this point no base has been added. Furthermore, the concentration of the ionized form is much smaller than the unionized form (4 % A^- against 96 % HA), so that the unionized acid

concentration can be considered almost equal to the initial concentration. Calculation details of this example are given in section 3.2.1 on page 40 (e.g. initial pH, which is 3.36 in this case)

Point b: This point represents the pH established when the concentration of unionized acid equals the concentration of the ionized acid; i.e.,

$$[\text{HA}] = [\text{A}^-] \quad (2.37)$$

The validity of equation (2.37) can be substantiated by considering the Henderson-Hasselbach equation (equation (2.21)) for the acetate buffer. When the measured solution pH is equal to the acid pK_a value, equation (2.21) reduces to

$$\log \frac{[\text{A}^-]}{[\text{HA}]} = 0 \quad (2.38)$$

which holds when $[\text{A}^-] = [\text{HA}]$. An examination of the titration curve in the vicinity of point *b* also shows that, around this point, the solution pH will show the smallest change per unit of strong base added. In other words, the pH buffering effect is the highest at point *b*. Because of this effect, the useful range of a buffer system is practically around 1.5 pH units on either side of its pK_a value.

Point c: This point represents the pH established when the concentration of ionized acid approaches the initial acid concentration, thus $[\text{A}^-] \cong 0.01 M$.³ In other words, the pH at this point is the equivalence-point for a 0.01 M acetate salt solution. Further addition of a strong base past point *c* will result in a continued increase in pH. The limiting pH is set by the pH of the titrant. In Figure 2.4 it is assumed that a 0.1 M NaOH (which is at pH 13) is used as the titrant. Thus, when the effects of dilution become insignificant, the pH will approach 13.

In the previous example, only 1 monoprotic⁴ buffer system in an aqueous solution was considered. A titration curve can also be obtained by adding small amounts of strong base to a solution, containing more than 1 buffer system, including polyprotic buffers. An example of such more complex titration curve is shown in Figure 2.5. The difference with the previous example is that the points *a*, *b* and *c* cannot be distinguished for the individual buffers on the graph. The mathematical aspects of this type of titration curves will be handled in chapter 3. A graphical method to determine the pK_a for simple titration curves is given in [189].

2.2.6 pH buffer capacity curve

The slope of a titration curve (pH versus C_B or C_A) is related to the tendency of the solution at any point in the titration curve to change the pH upon addition of base or acid. The buffer intensity at any point of the titration is inversely proportional to the slope of the titration curve at that point and may be defined as [273]:

$$\beta = \frac{dC_B}{dpH} = -\frac{dC_A}{dpH} \quad (2.39)$$

³Theoretically, even at high pH values, there is always a small fraction of the unionized acid [HA].

⁴A monoprotic conjugate acid-base pair, $\text{HA} - \text{A}^-$, can interchange 1 proton.

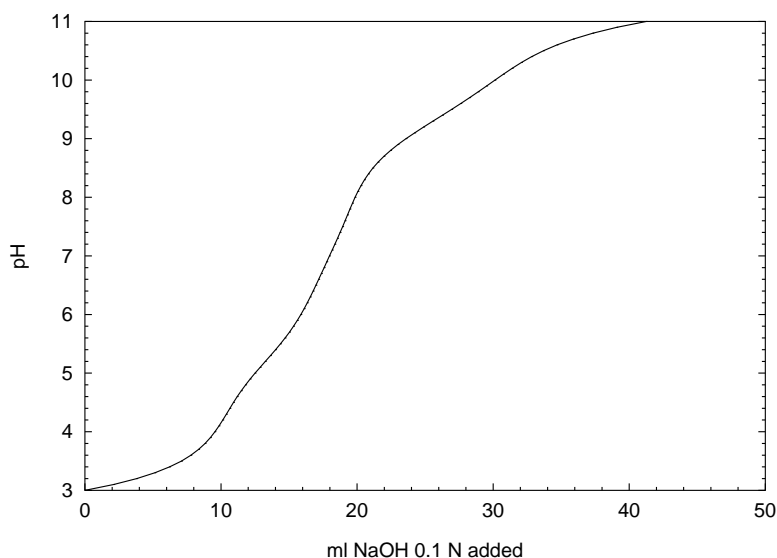


Figure 2.5: Titration curve for 1 litre of a more complex aqueous system containing $5 \text{ mg CO}_2 \text{ l}^{-1}$, $7 \text{ mg o-PO}_4\text{-P l}^{-1}$, $15 \text{ mg NH}_4^+\text{-N l}^{-1}$ and 0.6 meq l^{-1} of an unspecified soap

β : buffer intensity ($\text{eq l}^{-1} \text{ pH}^{-1}$)

dC_B, dC_A : differential quantity of strong base or acid added (eq l^{-1})

$d\text{pH}$: differential change in pH due to addition of dC

Note that β is always positive.

A graphical representation of β as a function of pH may be obtained by plotting the inverse of the slope of the titration curve versus pH. The buffer capacity curve corresponding with the titration curve in Figure 2.4 is shown in Figure 2.6. The point with the highest buffer capacity, excluding the water buffer is point *b*, the top of the buffer capacity profile. For buffer systems with pK_a values lower than 4 or higher than 10, the maximum of the bell-shaped buffer intensity profile does not necessarily correspond with the pK_a value of that buffer system, due to the presence of the buffer capacity of the water solution (see an example in the next paragraph).

The buffer capacity curve, corresponding with the titration curve in Figure 2.5 is shown in Figure 2.7. The different buffer systems that contribute to the buffer capacity curve are separately indicated on the graph. This also illustrates the additive behaviour of buffer capacities: The overall buffer capacity of the solution is the sum of buffer capacities of the different constituents to this solution. It can be noted on the graph that the maximum of the overall buffer capacity profile around pH 9 does not exactly correspond with the pK_a of ammonium, although it is the most important buffer at that pH position. A mathematical model of β will enable to simulate buffer capacities, and thus predict the buffer behaviour of solutions. This is the topic of chapter 3.

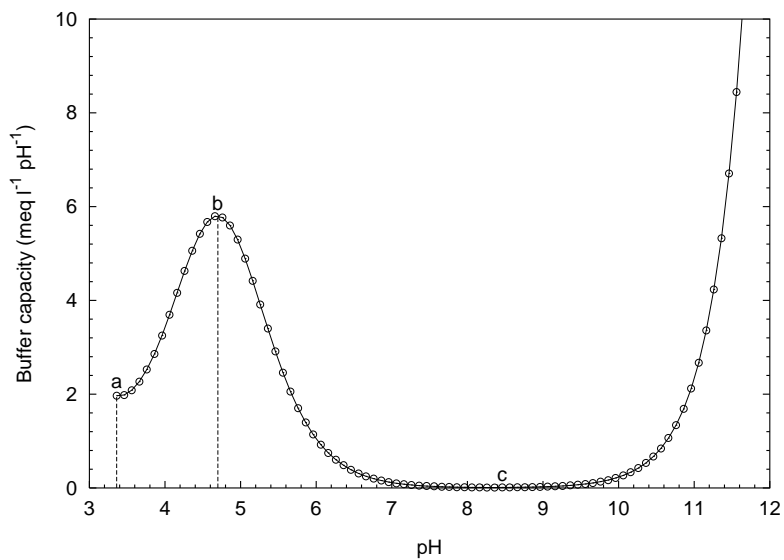


Figure 2.6: Buffer capacity curve for a 0.1 M acetic acid solution

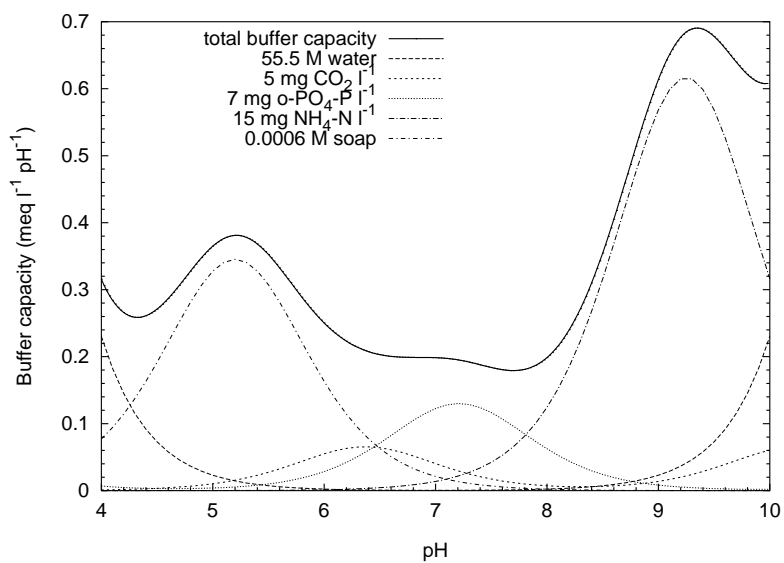


Figure 2.7: Buffer capacity curve for a more complex aqueous system containing $5 \text{ mg CO}_2 \text{ l}^{-1}$, $7 \text{ mg o-PO}_4\text{-P l}^{-1}$, $15 \text{ mg NH}_4^+\text{-N l}^{-1}$ and 0.6 meq l^{-1} of an unspecified soap

2.3 Dissolved organic carbon

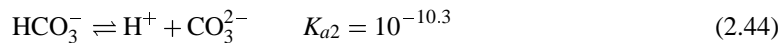
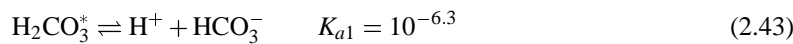
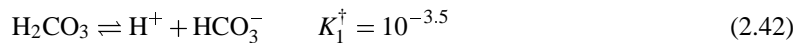
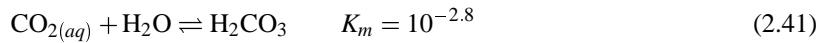
The most important acid-base system in water is often the carbonate buffer. The chemical species that make up the carbonate system are gaseous CO_2 ($\text{CO}_{2(g)}$), aqueous or dissolved CO_2 ($\text{CO}_{2(aq)}$), carbonic acid (H_2CO_3), bicarbonate (HCO_3^-), carbonate (CO_3^{2-}) and carbonate containing solids. Consequently, the carbonate system is the most important buffer in natural waters. In addition, individual species are of interest to us because they participate in important reactions other than strictly acid-base interactions [263]. Carbon dioxide is a participant in the biological processes of respiration (CO_2 produced) and biosynthesis by autotrophs such as nitrifiers or photosynthetic organisms (CO_2 consumed). The dissolution of CO_2 from the atmosphere into water or the release of CO_2 from supersaturated waters involves a heterogeneous reaction between gas and liquid phases. Similarly, the carbonate ion participates in heterogeneous reactions with solids containing carbonate, notably calcium carbonate.

2.3.1 The carbonate species and their acid-base equilibria

When we are presented with a problem involving the carbonate system, we must first make a decision concerning the nature of the system. This step is important because carbonate species can be involved in homogeneous solution equilibria as well as heterogeneous gas/liquid and liquid/solid equilibria [263]. The system can be treated as (ordered by increasing complexity):

- a closed system with no solid present,
- an open system with no solid present,
- a closed system with solid present, and
- an open system with solid present.

For the moment we will neglect the equilibria between carbonate species and metal ions (see section 2.4) and the involvement of carbonate-containing solids (see section 2.5), and treat the carbonate system as an open system with no solid present. Assuming a temperature of 25 °C, the following equilibria can be considered [263]:



K_H stands for Henry's constant. From equation (2.41) it is concluded that the concentration of hydrated carbon dioxide, $\text{CO}_{2(aq)}$, predominates over the concentration of carbonic acid, H_2CO_3 :

$$K_m = 10^{-2.8} = \frac{[\text{H}_2\text{CO}_3]}{[\text{CO}_{2(aq)}]} = 1.6 \times 10^{-3} \quad (2.45)$$

Table 2.3: Reaction rates within the carbonate system [198, 273]

Reaction	Forward rate v_f	Backward rate v_r
$\text{CO}_{2(g)} + \text{H}_2\text{O} \rightleftharpoons \text{CO}_{2(aq)}$	$6 \times 10^{-9} \text{ mol cm}^{-2} \text{ s}^{-1} a$	
$\text{CO}_{2(aq)} + \text{H}_2\text{O} \rightleftharpoons \text{H}_2\text{CO}_3$	$0.025 - 0.04 \text{ s}^{-1} (20 - 25 \text{ }^\circ\text{C})$	$10 - 20 \text{ s}^{-1} (20 - 25 \text{ }^\circ\text{C})^b$
$\text{CO}_{2(aq)} + \text{OH}^- \rightleftharpoons \text{HCO}_3^-^c$	$8.5 \times 10^3 \text{ M}^{-1} \text{ s}^{-1}$	$2 \times 10^{-4} \text{ s}^{-1} d$
$\text{H}_2\text{CO}_3 \rightleftharpoons \text{HCO}_3^- + \text{H}^+$	$1.5 \times 10^7 \text{ s}^{-1} e$	$4.7 \times 10^{10} \text{ M}^{-1} \text{ s}^{-1}$

^a Calculated for the situation of a typical lake.

^b The ratio of v_f and v_r corresponds with K_m (see equation (2.41)).

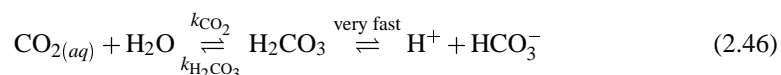
^c This reaction is kinetically insignificant at $\text{pH} < 8$.

^d The ratio of v_f and v_r corresponds with $K_{a1}K_w$ (see equation (2.43)).

^e Calculated from v_r and K_1^\dagger (see equation (2.42)).

Thus $[\text{H}_2\text{CO}_3]$ is only 0.16 % of $[\text{CO}_{2(aq)}]$. Because it is difficult to distinguish between $\text{CO}_{2(aq)}$ and H_2CO_3 by analytical procedures such as acid-base titration, a hypothetical species H_2CO_3^* is used to represent H_2CO_3 plus $\text{CO}_{2(aq)}$. The composite equilibrium constant K_{a1} of equation (2.43) is a result of the product of K_m (equation (2.41)) and K_1^\dagger (equation (2.42)). The implications of this development are important because they point out that H_2CO_3 is a fairly strong acid ($K_1^\dagger = 10^{-3.5}$), but there is very little of it in solution. This point is emphasized because K_{a1} is $10^{-6.3}$, a value that would give the impression that carbonic acid is a very weak acid. Carbonic acid has some of the properties of a strong acid, like the dissolution of minerals by CO_2 . Throughout this text we will use the hypothetical species H_2CO_3^* to represent $\text{CO}_{2(aq)}$ plus H_2CO_3 . We will treat it as a diprotic acid, but we should keep in mind its true nature.

As discussed earlier (section 2.2.1), acid-base equilibria are from a kinetical point of view extremely rapid, except for the carbonate system equilibria, and this in open as well in closed systems. The explanation of this behaviour lies in the slow (relatively to other deprotonation reactions) rate of hydration of aqueous CO_2 . The hydration of $\text{CO}_{2(aq)}$ leads to H_2CO_3 (equation (2.41)), but it may also yield H^+ and HCO_3^- [273]. The individual rate constants cannot be experimentally resolved and are reported simply as k_{CO_2} and $k_{\text{H}_2\text{CO}_3}$ corresponding to the simplified scheme:



An overview of reported rate constants for the carbonate system is given in Table 2.3. It has to be noted that the values in Table 2.3 are given as approximative values because they are dependent on many different factors. For the equilibrium where H_2CO_3^* is involved (equation (2.43)), no rate constants are given, because this equation is a ‘pooled’ equation, where a very fast proton exchange reaction, as well as a relatively slow hydration/dehydration reaction are involved. More details about these reaction rates can be found in [198, 273].

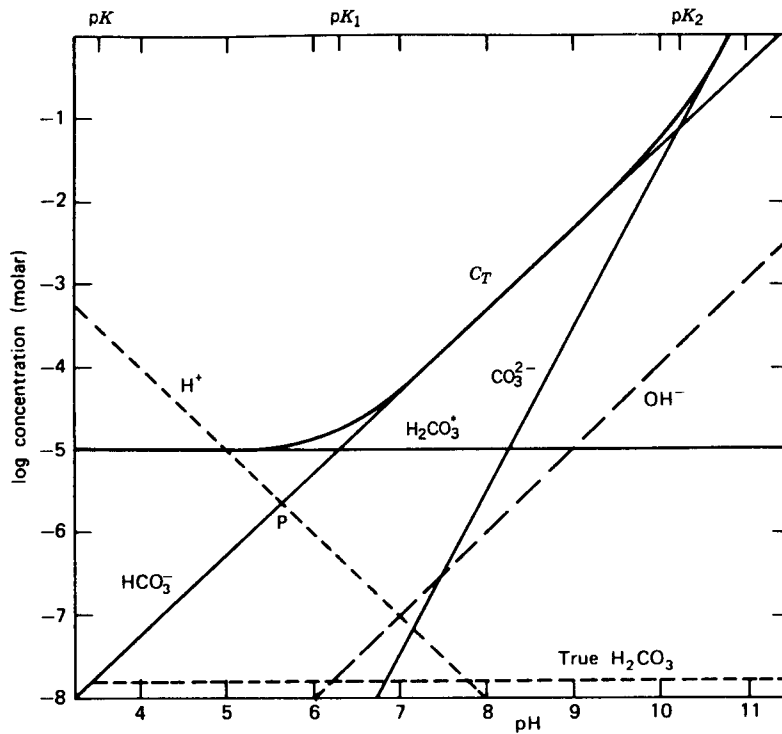


Figure 2.8: Aqueous carbonate equilibrium; atmospheric p_{CO_2} and 25 °C; pH adjusted with strong base or acid; C_T represents the sum of the solute carbonate species; point P shows equilibrium concentrations without pH adjustments [273]

A simple system illustrating some of the characteristics of the carbonate system in natural waters is provided by equilibrating pure water with a gas phase (e.g. the atmosphere) containing CO_2 at a constant partial pressure. One may then vary the pH by the addition of strong base or strong acid, thereby keeping the solution in equilibrium with p_{CO_2} . Figure 2.8 shows the distribution of the solute species in such a system. A partial pressure of CO_2 ($p_{\text{CO}_2} = 10^{-3.5} \text{ atm}$) is representative for the atmosphere. When this is in equilibrium with $\text{CO}_{2(aq)}$, we obtain from equations (2.40) and (2.45):

$$[\text{H}_2\text{CO}_3^*] \cong [\text{CO}_{2(aq)}] = K_H \times p_{\text{CO}_2} = 10^{-1.5} \times 10^{-3.5} = 10^{-5} M \quad (2.47)$$

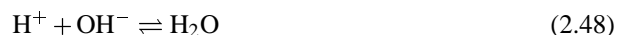
2.3.2 Alkalinity and acidity

Alkalinity is a measure of the capacity of a water to neutralize strong acid. In natural waters this capacity is attributable to bases such as HCO_3^- , CO_3^{2-} and OH^- as well as to species often

present in small concentrations such as silicates, borates, ammonia, phosphates, and organic bases [263]. *Acidity* is a measure of the capacity of a water to neutralize strong base. In natural waters this capacity is usually attributable to acids such as H_2CO_3^* and HCO_3^- and sometimes to strong acids, namely, H^+ [263].

Operational definition of alkalinity

In the determination of the total alkalinity a known volume of sample is titrated with a standard solution of a strong acid to a pH value in the approximate range of 4 to 5 and usually in the range 4.5 to 4.8. This end-point is commonly indicated by the colour change of the indicator methyl orange; therefore the total alkalinity is often referred to as the methyl orange alkalinity. Alkalinity can be expressed as meq l^{-1} or as $\text{mg CaCO}_3 \text{ l}^{-1}$. In the latter case, one takes into account that 1 *meq* of CO_3^{2-} requires 2 *meq* of H^+ , so that $1 \text{ meq l}^{-1} = 50 \text{ mg CaCO}_3 \text{ l}^{-1}$. If we consider first a closed system in which the alkalinity contributing species are only carbonate and OH^- , then the H^+ added is the stoichiometric amount required for the following reactions:



The pH at the true end-point of the total alkalinity titration should be that of a solution of H_2CO_3^* and H_2O . We refer to the pH of such a solution as pH_{CO_2} .

For the carbonate system, we can theoretically identify two more significant pH values that occur during the course of an alkalinity titration. These are $\text{pH}_{\text{HCO}_3^-}$ and $\text{pH}_{\text{CO}_3^{2-}}$. They represent, respectively, (1) the pH of a solution to which has been added the stoichiometric amount of H^+ required to complete ⁵ reaction (2.48) and the following reaction:



and (2) the pH of a solution to which has been added the stoichiometric amount of H^+ required to complete only reaction (2.48). The value of $\text{pH}_{\text{HCO}_3^-}$ is about pH 8.3 while $\text{pH}_{\text{CO}_3^{2-}}$ is generally between pH 10 and pH 11 and varies with the amount of carbonate buffer present. The experimental amount of acid required per litre of solution to lower the pH of this solution to $\text{pH}_{\text{HCO}_3^-}$ is called the carbonate alkalinity. This end-point can be determined with a pH meter or by a colour change of the indicator phenolphthalein so that it is often referred to as the phenolphthalein alkalinity. The amount of acid required to reach $\text{pH}_{\text{CO}_3^{2-}}$ (the caustic alkalinity) cannot be determined readily in the laboratory because of the poorly defined end-point, caused by the masking effect of the buffering of water (i.e. the reaction $\text{H}^+ + \text{OH}^- \rightleftharpoons \text{H}_2\text{O}$). Caustic

⁵Theoretically, equilibrium reactions are never completed, however, operationally a reaction is completed when an equivalence-point is reached. See also section 2.2.5.

Table 2.4: End-point pH values for total alkalinity measurements [104]

Test condition	End-point pH
Alkalinity 30 mg CaCO ₃ l ⁻¹	4.9
Alkalinity 150 mg CaCO ₃ l ⁻¹	4.6
Alkalinity 500 mg CaCO ₃ l ⁻¹	4.3
Silicates, phosphates known/suspected	4.5
Routine or automated analysis	4.5
Industrial waste or complex system	4.5

alkalinity can be determined by calculation if the carbonate and the total alkalinity are known [263].

The actual values that correspond to pH_{CO_2} , $\text{pH}_{\text{HCO}_3^-}$ and $\text{pH}_{\text{CO}_3^{2-}}$ are not truly fixed values, rather they vary with the total inorganic carbon buffer concentration C_{IC} in solution. If we treat the titrations as closed systems, the C_{IC} at the end-point will be the same as the C_{IC} in the initial solution. This appears to be a reasonable approach if the solution is not shaken vigorously and if the titration is conducted rapidly. Table 2.4 shows the *Standard Methods* [104] values for the total alkalinity end-points in function of the sample and its C_{IC} concentration.

Similar definitions and calculations concerning acidity measurements can be made. However, in the scope of this work, we will mainly work with the alkalinity and not with the acidity.

2.4 Metal ions in aqueous solution

Complex formation is important in the chemistry of natural waters and wastewaters from several standpoints. Complexes modify metal species in solution, generally reducing the free metal ion concentration so that effects and properties which depend on free metal ion concentration are altered. These effects include such things as the modification of solubility, the toxicity and possibly the biostimulatory properties of metals [155, 263]. Complexation equilibria will also influence the buffer capacity, which is the reason of discussing this topic here.

In aqueous solution, *free* metal ions are complexed with water. The metal ions are said to be hydrated. The interaction of these hydrated metal ions with acids and bases is a ligand exchange reaction that is commonly called hydrolysis or protolysis. These terms describe the general reaction in which a proton is transferred from an acid to water, or from water to a base. This type of reaction involving hydrated metal cations occurs readily and is of extreme importance in natural waters [263]. For example, the first step of the stepwise hydrolysis of the hydrated ferric ion, $\text{Fe}(\text{H}_2\text{O})_6^{3+}$ can be represented by the following equation:



From this equation it is easy to visualize that the hydrolysis of metal ions is a stepwise replacement of coordinated molecules of H_2O by hydroxyl ions. The hydrolysis reaction depicted in

equation (2.52) is an acid-base (proton transfer) reaction. Because of this, the pH of the solution will influence the distribution of the various species, and the presence of such reactions will influence the buffer capacity of the water. All trivalent and most divalent metal ions are complexed to some extent with OH^- at the pH of natural waters. The alkaline earth metals hydrolyse significantly only at high pH ($\text{pH} > 9$).

2.4.1 Complex formation and dissociation constants

Equilibrium constants for complexes can be written in many different ways. In literature it is not always consistent and clear what kind of constant is used and how it has to be interpreted. A minimal care has to be taken when using and interpreting values from literature. Some popular different ways of expressing complex equilibria and some examples to illustrate the confusions are presented here.

Equilibrium constants for complexes are usually stated for reactions written in the direction of complex formation, e.g.,



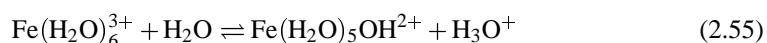
and

$$\frac{\{\text{CaPO}_4^-\}}{\{\text{Ca}^{2+}\}\{\text{PO}_4^{3-}\}} = 10^{+6.5} = \text{stability constant} \quad (2.54)$$

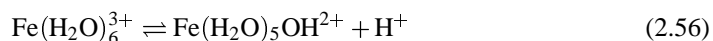
When stated for a complex formation reaction, the equilibrium constant is called a *formation* or a *stability constant*. Conversely, if the equilibrium constant is stated for the dissociation of the complex it is called a *dissociation* or an *instability constant*. Large values of stability constants indicate stable complexes.

For complexes that contain more than one ligand or central metal ion, there are two ways of writing stability constants. Stepwise formation constants are equilibrium constants for the reactions in which the central metal ion consecutively adds one ligand (symbol K). An overall formation constant is the equilibrium constant for the reaction in which the central metal ion combines with all of the ligands necessary to form a specific complex (symbol β) [263]. It is also common to omit the H_2O ligands when writing equations such as this one given here. For example $\text{Fe}(\text{H}_2\text{O})_5\text{OH}^{2+}$ is usually written as FeOH^{2+} .

Furthermore, the equation (2.52) shows hydrolysis reactions as a replacement of a water of hydration by a hydroxyl ion. Such reactions can also be written as a transfer of protons from waters of hydration to free water molecules to form a hydronium ion. The symbols for the stability and overall stability constants are often represented as *K and $^*\beta$ respectively [273]. For example, the reaction (2.52) can be written as



or as



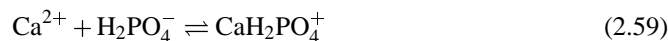
with formation constants for equations (2.52) and (2.56) respectively:

$$K_1 = \frac{\{\text{Fe}(\text{H}_2\text{O})_5\text{OH}^{2+}\}}{\{\text{Fe}(\text{H}_2\text{O})_6^{3+}\}\{\text{OH}^-\}} = 10^{+11.84} \quad (2.57)$$

$$^*K_1 = \frac{\{\text{Fe}(\text{H}_2\text{O})_5\text{OH}^{2+}\}\{\text{H}^+\}}{\{\text{Fe}(\text{H}_2\text{O})_6^{3+}\}} = 10^{-2.16} \quad (2.58)$$

Generally one can write that $^*K_1 = K_1 \times K_w$. A consistent overview of the nomenclature used for complexation constants can be found in [216].

To illustrate the confusions found in aquatic chemistry literature when looking up stability constants for complex formation, an example of complex formation between Ca^{2+} and H_2PO_4^- is presented. One of the popular tables found in modern aquatic chemistry textbooks is the one originally presented by Morel and Hering [198] and taken over in other reference works like [273] and [251]. A major issue presented by the original authors is data consistency [198]: For example, a complex formation constant reported by one author may have been calculated on the basis of a solubility constant that is not the same as that chosen in the compilation. Crosschecking the methods for estimating the constants from experimental data is advised. This can explain already some of the inconsistencies in literature, but there are also other factors that lead to wrong interpretation. For the example given here, one can find in [273] and [251] for the metal Ca^{2+} and the ligand PO_4^{3-} (notated with L) (note that H_2PO_4^- is not presented as possible ligand) that the logarithm of the overall stability constant for formation of the complex CaH_2L equals 21.0. With the information presented above, one may wish to write the following equation:



with the corresponding stability constant

$$K_1 = \beta_1 = \frac{\{\text{CaH}_2\text{PO}_4^+\}}{\{\text{Ca}^{2+}\}\{\text{H}_2\text{PO}_4^-\}} = 10^{+21.0} \quad (2.60)$$

However, this is not correct, because only when consulting the table of the original authors [198], one finds that the only correct way of writing this complexation reaction is



with the correct corresponding stability constant

$$K_1 = \beta_1 = \frac{\{\text{CaH}_2\text{PO}_4^+\}}{\{\text{Ca}^{2+}\}\{\text{H}^+\}^2\{\text{PO}_4^{3-}\}} = 10^{+21.0} \quad (2.62)$$

In an older reference [48] a reaction was found which corresponds with our example:



which logically corresponds to the following equation for K_1

$$K_1 = \beta_1 = \frac{\{\text{CaH}_2\text{PO}_4^+\}}{\{\text{Ca}^{2+}\}\{\text{H}_2\text{PO}_4^-\}} = 10^{+1.08} \quad (2.64)$$

When reaction (2.63) is summed with the 2 following reactions for the acid-base equilibria of the ortho-phosphate buffer system:



one finds the same reaction as (2.61) and a $\log K$ value equal to $1.08 + 7.2 + 12.35 = 20.62 \approx 21$, thus corresponding to K_1 in equation (2.62).

For the same example, another aquatic chemistry book [263] gives the following reaction (written as a dissociation instead of a formation reaction):



The reaction can easily be transformed into a complex formation reaction:



From this equation we can write

$$K_1 = \beta_1 = \frac{\{\text{CaH}_2\text{PO}_4^+\}}{\{\text{Ca}^{2+}\}\{\text{H}^+\}\{\text{HPO}_4^{2-}\}} = 10^{-5.6} \quad (2.69)$$

Summing reaction (2.68) with reaction (2.66) one finds

$$K_1 = \beta_1 = \frac{\{\text{CaH}_2\text{PO}_4^+\}}{\{\text{Ca}^{2+}\}\{\text{H}^+\}^2\{\text{PO}_4^{3-}\}} = 10^{-5.6+12.35} = 10^{+6.75} \quad (2.70)$$

The $\log K$ of equation (2.70) is not the same as the $\log K$ of equation (2.62), there is a difference of approximately 14 log units in the two $\log K$ values, indicating that one of the 2 equations is not correctly presented into the literature. Assuming the reference work [198] and also [48] are correct, one might eventually suggest that in [263] the author presented *K values instead of K values, but without mentioning it into the presented equation.

This illustrative example learns that there are many different ways of writing complexation reactions, and that different notations and K values eventually represent the same complexation reaction when using extra water or ligand dissociation reactions, and that extreme caution is needed when using values from tables in which it is not straightforward to assess what the tabulated values exactly mean.

Table 2.5: Percentage distribution of complex species in average river water [263]

Cation	Concentration (M)	Uncomplexed (%)	Complexed with (%)			
			OH^-	HCO_3^-	CO_3^{2-}	SO_4^{2-}
Calcium	3.8×10^{-4}	97		1	1	1
Magnesium	3.4×10^{-4}	97		1	1	1
Sodium	2.7×10^{-4}	100				
Potassium	5.9×10^{-5}	100				

2.4.2 Complexes with inorganic ligands

Natural waters contain significant concentrations of inorganic and organic ligands in addition to H_2O and OH^- . The predominant metal cations in typical fresh water are Na^+ , Ca^{2+} and Mg^{2+} ; the major ligands are HCO_3^- , Cl^- and SO_4^{2-} . At the typical natural water pH values between 6.5 and 8.5, these metals are no strong complex formers as Al^{3+} and Fe^{3+} [263].

For complicated systems such as natural waters it is necessary to use a computer program/model to determine the degree of complexation of the various cations with the ligands available. The results of a simulation study on a river water with average composition is shown in Table 2.5 [263]. This type of calculation gives us confidence in ignoring the complexes of Ca^{2+} , Mg^{2+} , Na^+ and K^+ with OH^- , HCO_3^- , CO_3^{2-} , SO_4^{2-} and Cl^- , when dealing with fresh waters of neutral pH. Increasing the pH-value or ligand concentration (like in a titration experiment), may require though that complexes of these metals be taken into consideration.

2.4.3 Complexes with organic ligands

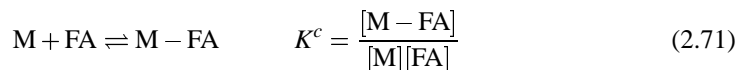
A wide variety of organic compounds in natural waters and wastewaters can act as complexing agents for metal ions. The nature and extent of metal ion complexation by natural water organics is not well defined, probably because of the poorly defined nature of these organic compounds and also because of the staggering complexity of these multimetal, multiligand systems [263]. Two categories of significant organic complexes in river waters are the 'amino acid complex' and 'inert humic complex'. For the most amino acid complexes, the values of $\log \beta_1$ range from 7 to 9; values of $\log \beta_2$ are in the approximate range of 14 to 16. However there are again some exceptions, e.g. the amino acid cysteine, which contains an $-\text{SH}$ group, forms an extremely strong complex with cuprous ion (Cu^+) with a $\log \beta_1$ value of 19.5. Humic substances are an extremely complex group of compounds. Because of this no single compound can act as a true model for this group. However, phenolic (pK_a 8.5–11) and carboxylic acid (pK_a 3–6) groups are common functional groups in humic substances [226].

Humic substances or humates are a mixture of poorly biodegradable decomposition products and by-products of natural organic matter produced by plants and animals. They are natural constituents of surface water, especially in regions with a cold climate, since low temperature is a condition for the formation of water-extractable humic substances [185]. Humic substances have been arbitrarily divided into three diverse groups of compounds on the basis

of their solubility in dilute acid and dilute base. *Fulvic acids* are soluble in both dilute acid (pH 1) and dilute base. *Humic acids* are soluble in dilute base but are precipitated by dilute acid (pH 1). *Humins* are insoluble in both dilute acid and dilute base. It is the fulvic acid fraction that appears to be the predominant group of humic substances in natural waters. Fulvic acids appear to have lower molecular weights (200 to 10000) than humic acids; they contain a higher percentage of oxygen and the oxygen appears to be located in a greater percentage of carboxyl groups. Fulvic acids, in particular, are good complexing agents for trace metals in natural waters [251]. Fulvic acid binding of trace metals is complicated. Not only is fulvic acid a distribution of a wide range of molecules, it has a variety of binding sites that are affected by pH, ionic strength, and the chemistry of ions in solution.

When chemical equilibrium models are used to assess e.g. toxicity induced by free metal ions, fulvic acid complexation should be taken into account [81], especially for metals with large $\log K$ values for metal-fulvate complexes such as Hg^{2+} , Cu^{2+} , Pb^{2+} and Cd^{2+} . Complexation of metals with fulvic acid is most significant for those ions that are appreciably complexed with CO_3^{2-} and OH^- [251]. When chemical equilibria are used for buffer capacity modelling, it are the metal ions with the highest concentrations that have to be considered first. Acid-base titrations of humic substances reflect the nature of the different pK_a values, hence the ‘smeared out’ appearance of these titration curves. While no unique equivalence-points are observed, different pK_a regions of carboxylic and phenolic groups can be discerned [273]. In a study based on titration curves of dissolved organic carbon (DOC) in wastewater, two acidity constants, 5.3 and 9.5 were found to be attributed to DOC [331]. FTIR spectra suggested the acid sites are carboxylic and amino functional groups. In the River Vouga (Portugal), the presence of sulphonic functional groups in the fulvic acids were found to originate from a pulp and paper mill effluent, that was discharged in that river [247]. These results highlight the importance of the contribution of anthropogenic sources of organic matter to the composition of humic substances from surface waters.

For describing chemical equilibria between metal ions and e.g. fulvic acid, a conditional stability constant approach can be used [251]:



where K^c is the conditional stability constant at a specified pH, ionic strength, and chemical composition. One does not always know the stoichiometry of the reaction in natural waters, e.g. whether 1:1 complexes (M-FA) or 1:2 complexes (FA-M-FA) are formed. The complexant is a macromolecule of organic carbon in which there are many different sites with varying binding energies. So, equation (2.71) simply gives a lumped-parameter conditional stability constant, but it does allow intercomparisons of the relative importance of complexation among different metal ions and dissolved organic carbon (DOC) at specified conditions. Conditional stability constants for metal-fulvic acid complexes vary in natural waters because:

- There are a range of affinities for metal ions and protons in natural organic matter resulting in a range of stability constants.
- Conformational changes and changes in binding strength of M-FA complexes in natural organic matter result from electrostatic charges (ionic strength), differential and competitive cation binding, and, most of all, pH variations in water.

The total number of metal-titratable groups is in the range of 0.1–5 *meq* per gram of carbon, and is termed the DOC complexation capacity. DOC comprises roughly 90 % of the total organic carbon in surface waters, most of which is recalcitrant [294].

Rather than using a conditional complexation constant or a distribution of discrete complexation constants, an alternative approach is to use a x -site model, with x different ligands (sites), and x different stability constants. This approach with e.g. $x = 5$ can be used to describe the complexation of dissolved fulvic acid and copper ions in natural water [251]. Many investigators have used a two site model representing fulvic acid functional groups with acidity constants $pK_{a1} \approx 3.5$ and $pK_{a2} \approx 5.0$ [251].

In a third approach for describing chemical equilibria between metal ions and humates, the humates can be described by a mixture of ligands with a continuous (Gaussian) distribution of acidity or metal-binding constants [198]. Two centres of pK_a distributions in this Gaussian approach (around pH 3 and pH 5) were found to describe the buffering capacities of humic acids fairly well [82]. In a study of the organic contribution to alkalinity in estuarine waters, it was found that humic substances have a buffer capacity around pH 4.5, pH 6.6 and pH 8.9 [49]. The authors suggest that the first two groups are carboxylic acids, and group three may be phenols or amines.

2.5 Precipitation and dissolution reactions

Precipitation and dissolution reactions are important in both natural waters [263] and water treatment processes, more particular in e.g. phosphorus removal [72, 83, 200, 346]. Dissolution of minerals is a prime factor in determining the chemical composition of natural waters. Both equilibrium considerations and the rates of reactions are important. In many instances the reaction rate controls the extent of reaction because insufficient time is available for equilibrium to be achieved. This will have important drawbacks when precipitation reactions will be considered in titration experiments. A number of caveats are in order before embarking on the study of solubility relationships in aquatic systems [198]:

1. Many precipitation-dissolution reactions are sluggish. For example, a large supersaturation of CaCO_3 is often observed in natural waters before precipitation of the solids actually occurs. Temperature, the presence of nucleating surfaces and biological activity can all dramatically alter precipitation-dissolution kinetics.
2. The solid formed is often not the most stable solid thermodynamically. The evolution of the solid to its more stable form (e.g. through recrystallization) is usually very slow.
3. The metastable solids that are initially precipitated are often 'non-stoichiometric'. Many natural solids also typically contain impurities, foreign ions incorporated in the matrix. The equilibrium constants used for such solids have operational value, but probably little true thermodynamic significance. There is a wide variation in the reported values of heterogeneous equilibrium constants.
4. The formation of pure solid phases is not the only, or perhaps even the dominant, process by which many solutes are removed from the solution. For example, surface adsorption can remove a solute from solution much below saturation conditions for pure solids.

Precipitation has generally been observed to occur in three steps:

- nucleation (homogeneous if nuclei are formed with the ions of the precipitate; or heterogeneous if foreign particles act as nuclei),
- crystal growth, and
- agglomeration and ripening of the solids.

The formation of nuclei from precipitate ions is an energy-consuming process, so solutions have to be supersaturated, or have concentrations greater than that predicted by equilibrium with the precipitate, before the precipitate will form from a homogeneous solution.

At the outset of any discussion on heterogeneous equilibria it is important to realize that heterogeneous calculations only apply when there is an *excess of the solid* of interest present. If solid is absent, the equilibrium calculations are not valid for predicting solution composition; they may only be used to test whether saturation with a particular solid exists. Although thermodynamic considerations will yield the driving force for precipitation of particular phases, their formation under a specific set of conditions may be determined much more by kinetic factors. Metastable phases may persist in supersaturated solutions [204].

The solubility product

The solubility product is the equilibrium constant that describes the reaction by which a precipitate in excess dissolves in pure water to form its constituent ions [263],



The solubility constant is defined as

$$K_{s0} = \frac{\{A^{y+}\}^z \{B^{z-}\}^y}{\{A_z B_{y(s)}\}} \quad (2.73)$$

The activity of the solid phase is taken as unity. The concentration product, or conventional solubility product [273], $\log {}^c K_{s0}$, has the same form as the equilibrium constant except that concentrations of the species in solution are used instead of their activities.

$$\log {}^c K_{s0} = [A^{y+}]^z [B^{z-}]^y \quad (2.74)$$

For the solubility of oxides and hydroxides, the symbol $\log {}^{c*} K_{s0}$ [273] can be used instead of $\log {}^c K_{s0}$, when the solubility equilibrium is expressed in terms of $[H^+]$ instead of $[OH^-]$. Similar as in section 2.4.1, caution is needed when values from the literature are used.

Available compilations of solubility products illustrate that values given by different authors for the same solubility products often differ markedly. Differences of a few orders of magnitude are not uncommon [273]. There are various reasons for these discrepancies, for example the higher complexity of solubility equilibria compared to e.g. acid-base equilibria; and the presence of solubility influencing species not accounted for in the K_{s0} .

In order to test whether a solution, or a natural water, is over- or undersaturated, the actual ion activity product (IAP), may be compared with K_{s0} [273]. E.g. for the solid $A_z B_{y(s)}$, the IAP equals $\{A^{y+}\}^z \{B^{z-}\}^y$. The state of saturation of a solution with respect to a solid is defined as:

- $IAP > K_{s0}$: oversaturated
- $IAP = K_{s0}$: equilibrium, saturated
- $IAP < K_{s0}$: undersaturated

2.6 Modelling tools

For finding solutions of a ‘large’, natural water system equilibrium model, having many reactions and many species, hand calculations are extremely slow and essentially infeasible [273]. Computers have enabled rapid computations of equilibrium composition for multicomponent, multiphase, multispecies systems [273].

Two approaches to the treatment of large systems have been developed: the Gibbs energy minimization method and the equilibrium constant approach [13, 262, 273]. Both are based on a knowledge of the chemical potentials of species under standard conditions and under actual conditions of compositions in the chemical system. In the Gibbs energy minimization approach, one guesses a solution to the equilibrium problem (the free concentrations of species) and proceeds to minimize G^{TOT} . In the equilibrium constant approach, one guesses the free component concentrations, solves the non-linear equilibrium equations for the species concentrations, and verifies the total component material expressions or mass balances. If different precipitation reactions have to be considered in one model, a thermodynamic based solution approach is preferred, rather than an equilibrium based solution approach [177]. However, if some free energies for particular components are missing, the free energy methods cannot be used [13].

Chemical modelling in hydrologic systems has become an area of active research with immediate opportunities for application to environmental problems [24]. There are many computer models available for chemical equilibrium calculations. A number of these packages are reviewed in [24]. New concepts in modelling which provide innovative advancements include model sensitivities, sampling and analytical error, computational errors, redox and metastability, thermodynamic and kinetic data advance, ... One of the more recent models, that has found wide use among environmental professionals is MINTEQA2 [10, 251]. It is freely available (public domain software) and well documented. MINTEQA2 has been supported by the U.S. Environmental Protection Agency Environmental Research Laboratory, Athens, Georgia. This package is suitable for chemical equilibrium problems in natural water (acid-base, precipitation-dissolution, complexation, surface complexation and redox reactions). Its database contains thermodynamic data for 1000 species, and can be supplemented with a user defined thermodynamic database. Partly due to the reasons mentioned in section 2.5, precipitation reactions are sometimes very difficult to model with chemical speciation programs like MINTEQA2 [176, 198]. For instance, in lead precipitation tests from aqueous solutions containing sulphate, quasi equilibrium conditions between soluble and solid phases were achieved a few hours or days after reagents blending. Significant discrepancies were found between filterable lead concentrations measured in aged precipitate suspensions and solubility predictions by MINTEQA2 [176]. Further, a flexible thermodynamic database is important to allow the user to modify e.g. K -values, because these values are case dependent [187]. Also, it is known that the precision of thermodynamic data values varies from excellent to poor, so such data is subject to constant revision [85].

Despite the wide experience with the MINTEQA2 thermodynamic database, this database still contains errors that can lead to significantly erroneous results. An example of a recently corrected significant error in reactions with organic ligands is illustrated with Cu–EDTA speciation [257]. Two typical types of errors were discovered in the thermodynamic database of MINTEQA2 [257]:

- Errors related to expressing the reaction in terms of MINTEQA2 components: All reactions in MINTEQA2 must be written as formation reactions. For solid species, the $\log K$ and ΔH^0 , needed in MINTEQA2, may be of the opposite sign to that reported in the literature (usually reported as a solubility product constant). Also both solid and dissolved reactions obtained from the literature and their associated thermodynamic constants may need to be added or subtracted from other reactions as required to reformulate the reaction in terms of MINTEQA2 components. Similar findings of confusion in the literature are also illustrated in section 2.4.1.
- Errors related to ionic strength and temperature correction of $\log K$. All log equilibrium constants in the database must be referenced to zero ionic strength and to 25 °C.

A reactive solute transport model in streams, coupled to a chemical equilibrium model based on MINTEQA2 was used for river water modelling [243, 244]. The equilibrium sub-model considers the speciation and complexation of aqueous species, precipitation, dissolution and sorption. The model provides a valuable tool for quantifying the nature and extent of pH-dependent processes within the context of hydrologic transport [244]. Alkaline precipitation and aging of Cu^{2+} in the presence of sulphate was investigated with MINTEQA2, in the framework of recovery of copper from industrial wastewaters and sludges [177]. A MINTEQA2 model with 2 ammonia species, and respectively 21 copper or 18 nickel species was used to assess the effect of these heavy metals on nitrifying bacteria [149]. Surface complexation and precipitation modelling using MINTEQA2 was successfully applied to describe the leaching of contaminants from weathered municipal solid waste incinerator bottom ash [187].

Chapter 3

Mathematical pH buffer capacity modelling

3.1 Introduction

In literature, various approaches are considered to model pH buffer capacity [198, 251, 263, 273]. Depending on the aim of the modelling, a different approach can be necessary. However, the majority of approaches focus on assessing the composition or species distribution (including pH) of a sample under a certain set of conditions. A simple example illustrates the types of questions asked: A solution contains 5 mmol of acetic acid, we add 5 ml of NaOH 0.1 N to this solution, what will be the pH at equilibrium? This we could call a single point analysis, the situation of 1 equilibrium point only is considered. This problem can be extended, considering consecutive small additions of NaOH to our acetic acid sample, resulting in a titration profile, where pH is a function of the amount of base added. Some chemical aspects of pH titration are presented in chapter 2, more particularly in section 2.2.5 on page 21 and section 2.2.6 on page 22.

Two different approaches of titration curve modelling will be discussed in section 3.2. It will be shown that buffer capacity curve modelling is preferred over titration curve modelling. For this reason, in this chapter, buffer capacity modelling will be elaborated in more detail.

Three different approaches of buffer capacity modelling will be discussed in sections 3.3, 3.4 and 3.5 respectively. To present these three methods in the same framework, in function of the objective of this work, some modifications and extensions of the methods described in literature will be presented here. The three different approaches are:

1. the linear buffer capacity model (section 3.3),
2. the non-linear symbolic buffer capacity model (section 3.4), and
3. the non-linear tableau-method based buffer capacity model (section 3.5).

These three approaches are classified towards increasing complexity and increasing possibilities. For instance the linear method can only handle simple acid-base equilibria, the

non-linear symbolic method can also handle complexation reactions, and the tableau-method based model can also handle precipitation reactions. In all of the following sections, the influence of the ionic strength on the modelling will initially not be taken into account because the incorporation of activity coefficients causes a loss of clearness in the model development. For the buffer capacity models described in sections 3.3 and 3.5, separate subsections handle the ionic strength corrections. The practical role and influence of the activity coefficients on experimental buffer capacity curves is discussed in later chapters.

3.2 Modelling titration curves

A titration curve is the result of consecutive additions of a strong acid or base to a known volume of sample, followed by a measurement of pH. Here we will assume that each pH measurement is a result of a chemical equilibrium. In other words, the kinetic aspects of the pH change as a result of strong acid-base addition will not be considered. This is a fair assumption, because the kinetics of acid-base reactions are extremely fast (see chapter 2), much faster than e.g. pH electrode kinetics. In the case we deal with non acid-base reactions, like precipitation reactions, the kinetic aspects will have to be reconsidered. The intuitive approach of titration curve modelling can be illustrated by the following question: “Given a sample with a known buffer composition, what will be the pH when x meq of strong acid or base is added?”, or in mathematical notation: $\text{pH} = f(x)$. This approach is commonly used in literature and works fine for systems with only a few buffer systems. An alternative approach can be illustrated by the following question: “Given a sample with a known buffer composition, what is the amount x of strong acid or base to be added to alter the pH to a preset pH value?”, or in mathematical notation: $x = f(\text{pH})$. The latter approach (fixed pH approach) will be shown superior from a mathematical point of view, and will be the basis for buffer capacity modelling. In the following two sections, the two approaches will be illustrated with a simple example.

3.2.1 Variable pH approach

Suppose that we have a weak acid in solution, acetic acid, CH_3COOH , 0.01 M at $25\text{ }^\circ\text{C}$ [251]. To this solution, an amount of a strong base, e.g. NaOH , is added. The concentration of base in the solution is represented by C_B (mol l^{-1} or M). Before we answer the question “What will be the pH when we add an amount of strong base?”, we can calculate the initial pH of the solution.

The relevant equilibrium equation is defined by the acidity constant K_a or often represented as pK_a , 4.7 in this case.



$$K_a = \frac{[\text{H}^+][\text{Ac}^-]}{[\text{HAc}]} = 10^{-4.7} = 2.00 \times 10^{-5} \quad (3.2)$$

Other relevant equations (details in section 2.2.4 on page 19) are the equilibrium equation for

the ionization of water

$$K_w = [\text{OH}^-][\text{H}^+] = 10^{-14} \quad (3.3)$$

the mass balance on total acetate in solution

$$C_a = 0.01 M = [\text{Ac}^-] + [\text{HAc}] \quad (3.4)$$

and the charge balance or electro-neutrality equation

$$[\text{H}^+] = [\text{Ac}^-] + [\text{OH}^-] \quad (3.5)$$

Equations(3.2)–(3.5) represent everything we know about the system. We have four unknown concentrations $[\text{H}^+]$, $[\text{OH}^-]$, $[\text{Ac}^-]$ and $[\text{HAc}]$, so we only need these 4 equations to solve for all the concentrations and the pH of the solution. Substitute (3.3) in (3.5):

$$[\text{H}^+] = [\text{Ac}^-] + \frac{K_w}{[\text{H}^+]} \quad (3.6)$$

Rearrange and substitute (3.6) in the mass balance (3.4):

$$[\text{HAc}] = 0.01 - \left([\text{H}^+] - \frac{K_w}{[\text{H}^+]} \right) \quad (3.7)$$

Lastly, substitute (3.6) for $[\text{Ac}^-]$ and equation (3.7) into the equilibrium expression, equation (3.2). We now have just one equation with one unknown, being $[\text{H}^+]$.

$$K_a = \frac{[\text{H}^+] \left([\text{H}^+] - \frac{K_w}{[\text{H}^+]} \right)}{0.01 - \left([\text{H}^+] - \frac{K_w}{[\text{H}^+]} \right)} \quad (3.8)$$

$$[\text{H}^+]^3 + K_a[\text{H}^+]^2 - (0.01K_a + K_w)[\text{H}^+] - K_aK_w = 0 \quad (3.9)$$

Equation (3.9) is a third degree polynomial. The easiest way to solve it algebraically is by trial and error. The Newton-Raphson method can solve this iteratively using a computer. In this particular example, the solution of equation (3.9) is $[\text{H}^+] = 4.37 \times 10^{-4} M$ or pH 3.36. The two other solutions of equation (3.9) are negative numbers and do not have to be considered.

If we add now the strong base to the solution of which we just calculated the equilibrium pH, we will reach a new equilibrium state. The strong base is considered to be completely dissociated into Na^+ and OH^- . It is also noted that Na^+ does not undergo any chemical reaction with the species already present in the solution, so we can write that $[\text{Na}^+] = C_B$. From the 4 equations we wrote to completely specify our system (equations(3.2)–(3.5)), only the charge balance (3.5) has to be rewritten.

$$C_B + [\text{H}^+] = [\text{Ac}^-] + [\text{OH}^-] \quad (3.10)$$

Equations (3.6), (3.7), (3.8) and (3.9) will respectively change into the following equations:

$$[\text{H}^+] = [\text{Ac}^-] + \frac{K_w}{[\text{H}^+]} - C_B \quad (3.11)$$

$$[\text{HAc}] = 0.01 - \left([\text{H}^+] - \frac{K_w}{[\text{H}^+]} + C_B \right) \quad (3.12)$$

$$K_a = \frac{[\text{H}^+] \left([\text{H}^+] - \frac{K_w}{[\text{H}^+]} + C_B \right)}{0.01 - \left([\text{H}^+] - \frac{K_w}{[\text{H}^+]} + C_B \right)} \quad (3.13)$$

$$[\text{H}^+]^3 + (K_a + C_B)[\text{H}^+]^2 - (0.01K_a + K_w + K_a C_B)[\text{H}^+] - K_a K_w = 0 \quad (3.14)$$

One notices that the order of the polynomial describing the equilibrium pH does not change when a strong base is added to the solution. A completely similar approach holds for adding a strong acid, like HCl, to a solution containing buffering systems. The resulting equations are not presented here. The preceding example was very simple. As one increases the number of solutes and the number of equations, the polynomials become very large, an n -degree polynomial. Trial-and-error solutions become impractical, and are the most important drawback of this approach.

3.2.2 Fixed pH approach

Basically, the fixed pH approach follows the same path as the variable pH approach, but it differs in the way the mathematical equations are solved. Its advantage is that it avoids the impractical trial-and-error solution technique. Let's retake the same example of 0.01 M acetic acid in aqueous solution, and rearrange equation (3.10):

$$C_B = [\text{Ac}^-] + [\text{OH}^-] - [\text{H}^+] \quad (3.15)$$

Substitute [HAc] from equation (3.4) into equation (3.2) and rearrange for [Ac⁻]:

$$[\text{Ac}^-] = \frac{K_a(0.01 - [\text{Ac}^-])}{[\text{H}^+]} \quad (3.16)$$

$$[\text{Ac}^-] = \frac{0.01K_a}{[\text{H}^+] + K_a} \quad (3.17)$$

After substitution of equation (3.17) and $[\text{OH}^-]$ from equation (3.3) into equation (3.15), one obtains an expression for C_B in function of $[\text{H}^+]$.

$$C_B = \frac{0.01K_a}{[\text{H}^+] + K_a} + \frac{10^{-14}}{[\text{H}^+]} - [\text{H}^+] \quad (3.18)$$

From computational point of view, equation (3.18) can easily be solved for C_B when $[\text{H}^+]$ or the pH is given. There is no need for trial-and-error solutions. For more complex solutions, containing several buffer systems (monoprotic, diprotic, triprotic buffer systems), equation (3.18) will be expanded with more additive terms, but will never require complicated computational techniques to solve.

A particularity of both the variable and fixed pH approach is that the amount of acid or base needed to obtain a ΔpH change, is always calculated starting from a reference point which is the equilibrium point reached before any acid or base addition. In this example, the equilibrium pH was 3.36 (the reference point where $C_B = 0$). Correspondingly, e.g. for the fixed pH approach this means that the calculation of C_B to bring the solution to a particular pH is only applicable when the system was originally at pH 3.36. The reference point can easily be changed to any other pH value by adding or subtracting a constant value to C_B in both equations (3.14) and (3.18). This particularity has important drawbacks for the practical use of mathematical models that are based on a titration curve. The necessity of a reference point means that measurement errors and pH electrode calibration errors will have a pronounced effect when evaluating the 'fit' between experimental and simulated titration profiles. The buffer capacity approach is not suffering from this problem because it is based on derivative data instead of raw pH data. This is an important reason for preferring buffer capacity models instead of titration curve models.

The effect of a small pH electrode calibration error on the experimental and corresponding theoretical titration or buffer capacity profiles is illustrated in Figure 3.1. For this purpose, the 'pseudo-experimental' data was derived from the theoretical data by introducing a 0.08 pH offset error and a 1 % slope error on the pH measurement. The unwanted deviation between the experimental and the theoretical buffer capacity curves (Figure 3.1(b)) can easily be corrected for, by allowing to vary to a small extent the pK_a values of the modelled buffer systems. For the titration curves (Figure 3.1(a)), such similar correction is not straightforward. Moreover, allowing a small variation in the pK_a values of buffer systems to be modelled is also advantageous to correct for other disturbing effects, like small temperature effects, small ionic strength effects, etc.

Comparing the 2 different approaches of titration curve modelling, one can conclude that from the experimental point of view (which is adding a fixed amount of strong acid or base to a solution and measure the pH) the variable pH method is to be preferred, but from a computational point of view the fixed pH approach is to be preferred.

3.2.3 Generalized titration curve model

For the sake of completeness, a generalized model for a titration curve of solutions containing monoprotic, diprotic and triprotic buffers, based on the fixed pH approach, can be written down. The calculation details for this model are similar as for the corresponding buffer capacity model, worked out in more detail in section 3.3. Therefore, only the titration curve model

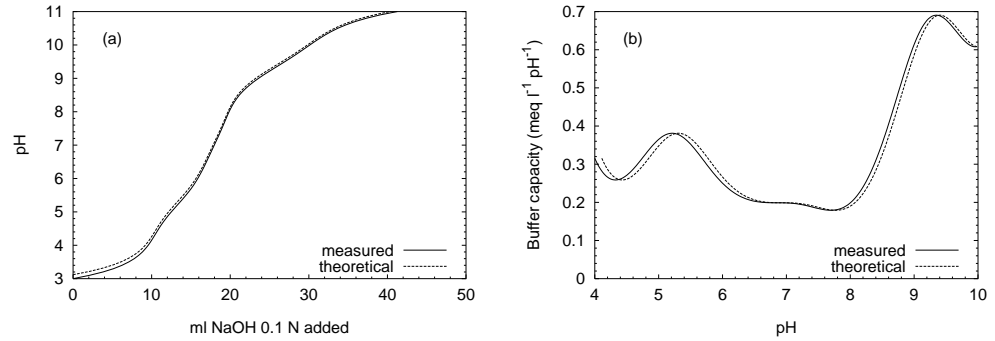


Figure 3.1: Illustration of the effect of a small pH electrode calibration error on the difference between the experimental and theoretical titration (a) or buffer capacity (b) profiles

without the equation details is presented here.

The equation (3.18) for 1 monoprotic buffer can be extended for l monoprotic (H_2O buffer not included), m diprotic and n triprotic weak acids:

$$C_B = \sum_i^l (\text{term}_1)_i + \sum_j^m (\text{term}_2)_j + \sum_k^n (\text{term}_3)_k + \frac{10^{-14}}{[\text{H}^+]} - [\text{H}^+] \quad (3.19)$$

$$\text{term}_1 = \frac{C_a K_a}{[\text{H}^+] + K_a} \quad (3.20)$$

$$\text{term}_2 = C_a K_{a1} \frac{[\text{H}^+] + 2K_{a2}}{[\text{H}^+]^2 + K_{a1}[\text{H}^+] + K_{a1}K_{a2}} \quad (3.21)$$

$$\text{term}_3 = C_a K_{a1} \frac{[\text{H}^+]^2 + 2K_{a2}[\text{H}^+] + 3K_{a2}K_{a3}}{[\text{H}^+]^3 + K_{a1}[\text{H}^+]^2 + K_{a1}K_{a2}[\text{H}^+] + K_{a1}K_{a2}K_{a3}} \quad (3.22)$$

In the next 3 sections, different approaches for buffer capacity models will be presented. The intuitive approach of a buffer capacity model can be formulated as “What is the buffer capacity for a particular measured pH during a simulated titration experiment?”. This corresponds with the ‘fixed pH approach’, which is also the preferred one for computational reasons.

3.3 Linear buffer capacity model

The term ‘linear buffer capacity model’ was chosen because in this approach the buffering properties of the system can be represented by a set of equations which are linear in the concen-

trations. In case one only considers acid-base chemical equilibria (either monoprotic, diprotic or triprotic weak acids, or a combination of these), a linear buffer capacity model can always be used. Non-linearities are the result of considering, among others, complexation or precipitation reactions, e.g. reactions between Ca^{2+} and OH^- , or between Ca^{2+} and HPO_4^{2-} . These more complicated reactions are handled in sections 3.4 and 3.5.

If we reconsider the acetic acid example of the previous section, where a concentration C_B of NaOH is added to the solution, we can write the general equation for the buffer capacity β ($\text{eq l}^{-1} \text{pH}^{-1}$) (see also section 2.2.6 on page 22):

$$\beta = \frac{dC_B}{d\text{pH}} \quad (3.23)$$

The 4 basic equations completely describing the system were discussed before, and the equations (3.2), (3.3), (3.4) and (3.15) from the variable and fixed pH approach will be used as starting point for the development of the linear buffer capacity model.

A generalization that will be introduced here is the consideration of H_2O as a regular monoprotic buffer system. This will facilitate the incorporation of the water buffer system in later software implementations. Instead of using equation (3.3), we will use the following 2 equations, respectively for the mass balance and dissociation equation of the water buffer:

$$C_w = [\text{H}_2\text{O}] + [\text{OH}^-] \approx [\text{H}_2\text{O}] = 55.5 \text{ mol l}^{-1} \quad (3.24)$$

$$K_w^* = \frac{[\text{H}^+][\text{OH}^-]}{[\text{H}_2\text{O}]} \text{ where } K_w^* = \frac{K_w}{[\text{H}_2\text{O}]} \quad (3.25)$$

Practically, for $pK_w = 14$ (at $T = 25^\circ\text{C}$), the corresponding $pK_w^* = 15.74$.

If we rewrite the charge balance of equation (3.15):

$$C_B = -[\text{H}^+] + [\text{Ac}^-] + [\text{OH}^-] \quad (3.26)$$

then we can write for an infinitesimal addition of C_B :

$$dC_B = -d[\text{H}^+] + d[\text{Ac}^-] + d[\text{OH}^-] \quad (3.27)$$

or in terms of buffer capacity β :

$$\beta = \frac{dC_B}{d\text{pH}} = -\frac{d[\text{H}^+]}{d\text{pH}} + \frac{d[\text{Ac}^-]}{d\text{pH}} + \frac{d[\text{OH}^-]}{d\text{pH}} \quad (3.28)$$

The first right-hand term of equation (3.28) can be written as (using $d(\log u) = \frac{1}{u} \log e du$):

$$-\frac{d[\text{H}^+]}{d\text{pH}} = \frac{d[\text{H}^+]}{d \log[\text{H}^+]} = \ln(10) [\text{H}^+] \quad (3.29)$$

Using equations (3.2) and (3.4), an expression for $[\text{Ac}^-]$ yields:

$$[\text{Ac}^-] = \frac{C_a K_a}{[\text{H}^+] + K_a} \quad (3.30)$$

Further, equation (3.29) can be reorganized:

$$d\text{pH} = -\frac{d[\text{H}^+]}{\ln(10)[\text{H}^+]} \quad (3.31)$$

Using equations (3.30), (3.31) and $\frac{d}{dx}\left(\frac{1}{u}\right) = -\frac{1}{u^2}\frac{d}{dx}(u)$, the second right-hand term of equation (3.28) can be written as:

$$\frac{d[\text{Ac}^-]}{d\text{pH}} = -\frac{\ln(10)[\text{H}^+]}{d[\text{H}^+]} d\left(\frac{C_a K_a}{[\text{H}^+] + K_a}\right) = \ln(10)[\text{H}^+] \left(\frac{C_a K_a}{([\text{H}^+] + K_a)^2}\right) \quad (3.32)$$

Using the mass balances (3.4) and (3.24), together with the equilibrium equations (3.2) and (3.25), followed by differentiation as illustrated in equations (3.29) and (3.32), one can rewrite (3.28):

$$\beta = 2.303 \left([\text{H}^+] + C_a K_a \frac{[\text{H}^+]}{([\text{H}^+] + K_a)^2} + C_w K_w^* \frac{[\text{H}^+]}{([\text{H}^+] + K_w^*)^2} \right) \quad (3.33)$$

Due to the generalized notations of the H_2O buffer, one can notice the similarities between the terms for H_2O and HAc in equation (3.33).

If different monoprotic weak acids are present in the sample, the equation for β can be extended with similar additional terms. For polyprotic acids the additional terms are somewhat more complex. In the remainder of this section, a generalization of equation (3.33) will be developed.

3.3.1 Buffer capacity model for monoprotic acids

A weak monoprotic acid ($C_a \text{ mol l}^{-1}$) dissolved in water will dissociate until an equilibrium between the acid (HA) and the dissociated base (A^-) form is established.



A mathematical representation of this chemical equilibrium after addition of a strong base with concentration in the solution $C_B \text{ mol l}^{-1}$, is based on 3 equations (mass balance, dissociation equation and charge balance) which were already introduced before.

$$C_a = [\text{HA}] + [\text{A}^-] \quad (3.35)$$

$$K_a = \frac{[\text{H}^+][\text{A}^-]}{[\text{HA}]} \quad pK_a = -\log K_a \quad (3.36)$$

$$C_B + [\text{H}^+] = [\text{OH}^-] + [\text{A}^-] \quad (3.37)$$

As illustrated above, this set of 3 equations, together with the dissociation equation of H_2O leads to the following equation for β :

$$\beta = 2.303[\text{H}^+] \left(1 + C_w K_w^* \frac{1}{([\text{H}^+] + K_w^*)^2} + C_a K_a \frac{1}{([\text{H}^+] + K_a)^2} \right) \quad (3.38)$$

For the development of a general β -model, the following notation for a monoprotic weak acid HA with concentration C_a is introduced (index 1 stands for monoprotic):

$$\text{term}_1 = C_a K_a \frac{1}{([\text{H}^+] + K_a)^2} \quad (3.39)$$

3.3.2 Buffer capacity model for diprotic acids

A weak diprotic acid ($C_a \text{ mol l}^{-1}$) dissolved in water will dissociate until an equilibrium between the acid (H_2A) and the dissociated base forms (HA^-) and (A^{2-}) is established.



A mathematical representation of these chemical equilibria after addition of a strong base with concentration in the solution $C_B \text{ mol l}^{-1}$, is based on 4 equations (mass balance, 2 dissociation equations and a charge balance).

$$C_a = [\text{H}_2\text{A}] + [\text{HA}^-] + [\text{A}^{2-}] \quad (3.42)$$

$$K_{a1} = \frac{[\text{H}^+][\text{HA}^-]}{[\text{H}_2\text{A}]} \quad pK_{a1} = -\log K_{a1} \quad (3.43)$$

$$K_{a2} = \frac{[\text{H}^+][\text{A}^{2-}]}{[\text{HA}^-]} \quad pK_{a2} = -\log K_{a2} \quad (3.44)$$

$$C_B + [\text{H}^+] = [\text{OH}^-] + [\text{HA}^-] + 2[\text{A}^{2-}] \quad (3.45)$$

This set of 4 equations, together with the dissociation equation of H_2O leads to the following equation for β :

$$\beta = 2.303[\text{H}^+] \left(1 + C_w K_w^* \frac{1}{([\text{H}^+] + K_w^*)^2} + C_a K_{a1} \frac{[\text{H}^+]^2 + 4K_{a2}[\text{H}^+] + K_{a1}K_{a2}}{([\text{H}^+]^2 + K_{a1}[\text{H}^+] + K_{a1}K_{a2})^2} \right) \quad (3.46)$$

Similar as for a monoprotic acid, we introduce for a diprotic acid H_2A with concentration

C_a the following notation (index 2 stands for diprotic):

$$term_2 = C_a K_{a1} \frac{[H^+]^2 + 4K_{a2}[H^+] + K_{a1}K_{a2}}{([H^+]^2 + K_{a1}[H^+] + K_{a1}K_{a2})^2} \quad (3.47)$$

3.3.3 Buffer capacity model for triprotic acids

A weak triprotic acid ($C_a \text{ mol l}^{-1}$) dissolved in water will dissociate until an equilibrium between the acid H_3A and the dissociated base forms H_2A^- , HA^{2-} and A^{3-} is established.



A mathematical representation of these chemical equilibria after addition of a strong base with concentration in the solution $C_B \text{ mol l}^{-1}$, is based on 5 equations (mass balance, 3 dissociation equations and a charge balance).

$$C_a = [H_3A] + [H_2A^-] + [HA^{2-}] + [A^{3-}] \quad (3.51)$$

$$K_{a1} = \frac{[H^+][H_2A^-]}{[H_3A]} \quad pK_{a1} = -\log K_{a1} \quad (3.52)$$

$$K_{a2} = \frac{[H^+][HA^{2-}]}{[H_2A^-]} \quad pK_{a2} = -\log K_{a2} \quad (3.53)$$

$$K_{a3} = \frac{[H^+][A^{3-}]}{[HA^{2-}]} \quad pK_{a3} = -\log K_{a3} \quad (3.54)$$

$$C_B + [H^+] = [OH^-] + [H_2A^-] + 2[HA^{2-}] + 3[A^{3-}] \quad (3.55)$$

This set of 5 equations, together with the dissociation equation of H_2O leads to the following equation for β :

$$\beta = 2.303[H^+] \left(1 + C_w K_w^* \frac{1}{([H^+] + K_w^*)^2} + C_a K_{a1} \frac{[H^+]^4 + 4K_{a2}[H^+]^3 + (K_{a1} + 9K_{a3})K_{a2}[H^+]^2 + (4[H^+] + K_{a2})K_{a1}K_{a2}K_{a3}}{([H^+]^3 + K_{a1}[H^+]^2 + K_{a1}K_{a2}[H^+] + K_{a1}K_{a2}K_{a3})^2} \right) \quad (3.56)$$

Similar as above, we introduce for a triprotic acid H_3A with concentration C_a the following

notation (index 3 stands for triprotic):

$$term_3 = C_a K_{a1} \frac{[H^+]^4 + 4K_{a2}[H^+]^3 + (K_{a1} + 9K_{a3})K_{a2}[H^+]^2 + (4[H^+] + K_{a2})K_{a1}K_{a2}K_{a3}}{([H^+]^3 + K_{a1}[H^+]^2 + K_{a1}K_{a2}[H^+] + K_{a1}K_{a2}K_{a3})^2} \quad (3.57)$$

3.3.4 General linear buffer capacity model

In a water sample containing several buffering components, one can write that the total buffer capacity β is equal to the sum (hence, the linearity) of the buffer capacity β_i of the different components in the sample. Due to our general notation for the water buffer system, the H₂O buffer is considered in the same way as any other monoprotic weak acid HA. This offers an advantage compared to most β models in the literature, where the H₂O buffer is considered separately from the other monoprotic buffers.

$$\beta = \sum_{i=1}^n \beta_i \quad (3.58)$$

Based on this additive property of β , one can write a general equation for the buffer capacity of a sample containing l monoprotic (including H₂O), m diprotic and n triprotic weak acids:

$$\beta = 2.303[H^+] \left(1 + \sum_i^l (term_1)_i + \sum_j^m (term_2)_j + \sum_k^n (term_3)_k \right) \quad (3.59)$$

Equation (3.59) is very convenient and easy to be implemented in a spreadsheet or computer program. Contrary to the titration curve models (section 3.2), the general buffer capacity model does not contain any variable referring to the amount of strong base C_B added. This means that there is no need any more for a ‘reference point’ in the simulated buffer capacity profile, a major advantage for implementation and accuracy. Further, the model presented in equation (3.59) is usable for titrations with both strong acids and strong bases.

Some authors [138, 273] present the buffer capacity model (3.59) in terms of protolysis degree (α_i), being the ratio of the concentration of the species to the total concentration. This approach does not offer computational advantages above the approach presented here. In another approach [235–237], the buffer capacity is defined as a dimensionless value. The definition of buffer capacity in section 2.2.6 is an operational definition, but it is not adequate in a mathematical treatment of e.g. ampholytes [235].¹ The dimensionless definition of buffer capacity of a weak protolyte is defined as the amount in moles of strong base (or acid) added to the solution of the protolyte, divided by the resulting increase (or decrease) in pH caused exclusively by the protolyte in question and by the amount in moles of the protolyte present.

$$\beta = - \frac{dz}{dpH} \quad (3.60)$$

¹Ampholytes are substances which have both weak acid and base functional groups, e.g. amino acids.

β : buffer capacity per mole of ampholyte; dimensionless
 z : valence or mean valence with sign according to charge

This buffer capacity, which is the molar buffer capacity is consequently useful in a theoretical treatment of individual weak protolytes. However, in practice, it is not useful since it is an in-operational definition: it cannot be measured directly [235]. What can be measured, of course, is the added buffer capacities of the protolyte, the solvent, and other solutes if present. This approach offers some computational advantages for buffer systems like ampholytes, but offers no advantage above the approach presented here for the treatment of larger buffer systems (i.e. mixtures of different mono- and polyprotic weak acids).

3.3.5 Monoprotic approach of the general linear buffer capacity model

The general linear buffer capacity model can be written in an alternative way [74, 101, 299] by stating that a m -protonic acid with concentration C_a is mathematically equivalent with m monoprotic acids with each a concentration C_a . However, if one replaces a m -protonic acid with dissociation constants $K_{a1}, K_{a2}, \dots, K_{am}$ by m monoprotic acids with dissociation constants $K_{a1}^\dagger, K_{a2}^\dagger, \dots, K_{am}^\dagger$ respectively, the dissociation constants need to be altered, as presented in the following scheme:

$$\begin{aligned} K_{a1} &= \sum_{i=1}^m K_{ai}^\dagger \\ K_{a1}K_{a2} &= \sum_{i=1}^{m-1} \sum_{j=i+1}^m K_{ai}^\dagger K_{aj}^\dagger \\ &\vdots \\ K_{a1}K_{a2} \dots K_{am} &= K_{a1}^\dagger K_{a2}^\dagger \dots K_{am}^\dagger \end{aligned} \quad (3.61)$$

This property can be used to study amphoteric substances with small ΔpK differences, e.g. to investigate stepwise and parallel dissociation schemes of ampholytes [272]. If all polyprotic acids are replaced by monoprotic acids, as defined in the set of equations (3.61), then the general mathematical model (3.59) can be rewritten as

$$\beta = 2.303[\text{H}^+] \left(1 + \sum_i^{l+2m+3n} (\text{term}_1^\dagger)_i \right) \quad (3.62)$$

in which

$$\text{term}_1^\dagger = C_a K_a^\dagger \frac{1}{([\text{H}^+] + K_a^\dagger)^2} \quad (3.63)$$

The computational advantage of equation (3.62) disappears when one realizes that for each di- or triprotic weak acid, one needs to solve a non-linear set of equations (3.61) in order to find the corresponding K_a^\dagger values. Some properties of equations (3.61) are presented in [74].

3.3.6 Ionic interaction effects

The foregoing expressions need to be examined for the effects of nonideality. We will assume that, during titration, activity coefficients are constant over the pH range where they exert significant influence in the equations. The validity of this assumption will depend, of course, on experimental conditions [101].

The most convenient way to apply ionic strength corrections is the introduction of mixed acidity constants (see section 2.2.4 on page 19) in the models. A mixed acidity constant is characterized by H^+ written as an activity $\{H^+\}$, and the other species, like A^- and HA written as concentrations $[A^-]$ and $[HA]$. Its symbol is K'_a instead of K_a . A pH meter actually provides the activity of the H^+ ions (see section 2.1 on page 5 and section 2.2.2 on page 15), so subsequently instead of $\beta = f([H^+], \dots)$, the model can more correctly be written as $\beta = f(\{H^+\}, \dots)$. Important to note is that the mass balances and charge balance have to be written in terms of concentrations and *not* activities. With the above information, the corrected general equation (3.59) becomes:

$$\beta = 2.303\{H^+\} \left(\frac{1}{\gamma_{H^+}} + \sum_i^l (term'_1)_i + \sum_j^m (term'_2)_j + \sum_k^n (term'_3)_k \right) \quad (3.64)$$

The equations for $term'_1$, $term'_2$ and $term'_3$ are derived from equations (3.39), (3.47) and (3.57) respectively.

$$term'_1 = C_a K'_a \frac{1}{(\{H^+\} + K'_a)^2} \quad (3.65)$$

$$term'_2 = C_a K'_a \frac{\{H^+\}^2 + 4K'_{a2}\{H^+\} + K'_{a1}K'_{a2}}{(\{H^+\}^2 + K'_{a1}\{H^+\} + K'_{a1}K'_{a2})^2} \quad (3.66)$$

$$term'_3 = C_a K'_a \frac{\{H^+\}^4 + 4K'_{a2}\{H^+\}^3 + (K'_{a1} + 9K'_{a3})K'_{a2}\{H^+\}^2 + (4\{H^+\} + K'_{a2})K'_{a1}K'_{a2}K'_{a3}}{(\{H^+\}^3 + K'_{a1}\{H^+\}^2 + K'_{a1}K'_{a2}\{H^+\} + K'_{a1}K'_{a2}K'_{a3})^2} \quad (3.67)$$

The mixed acidity constants K'_a are derived from the acidity constants K_a using the activity coefficients for the weak acids (e.g. HA) and their dissociated bases (e.g. A^-).

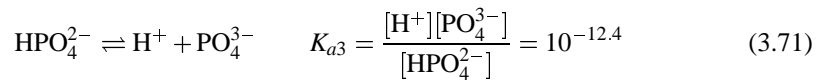
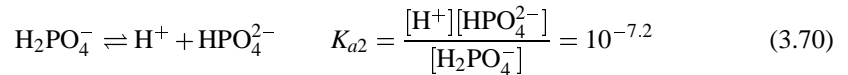
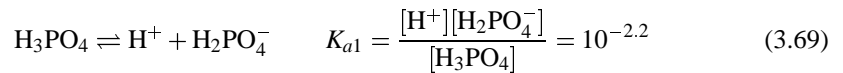
$$K'_a = K_a \frac{\gamma_{HA}}{\gamma_{A^-}} \text{ or } pK'_a = pK_a - \log \gamma_{HA} + \log \gamma_{A^-} \quad (3.68)$$

Equation (3.68) is valid for monoprotic as well for polyprotic weak acids. The activity coefficients γ_{H^+} , γ_{A^-} , ... can be calculated with e.g. the Davies approximation (see section 2.2.2 on page 15).

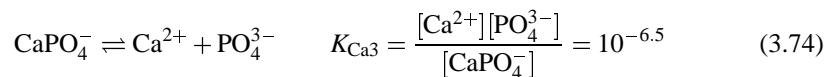
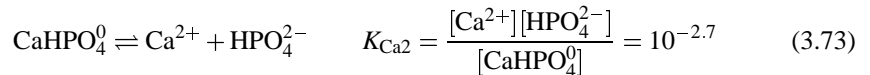
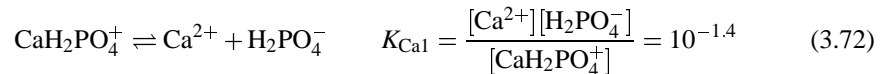
3.4 Non-linear symbolic buffer capacity model

As already introduced in section 3.3, non-linearities are involved when reactions different from acid-base equilibrium reactions have to be modelled. As it becomes very difficult and complicated to obtain an algebraic expression for the buffer capacity, a ‘symbolic solution’ approach will be introduced here. The example that we will consider is an aquatic solution, containing phosphoric acid with concentration C_a and calcium with concentration C_{Ca} . The chemical relevance of which buffers and reactions that have to be considered in aquatic samples is discussed in later chapters. The aim of this section is to develop a mathematical framework that can be used to solve non-linear chemical equilibria.

The chemical equilibria and dissociation equations for the triprotic phosphoric acid can be written in a similar way as presented in section 3.3:



Up to this point, the buffer capacity of the buffer system could be described with the linear buffer capacity equation (3.59). Now we will consider the chemical equilibria between the Ca^{2+} and the different forms of phosphate that are present in the solution. It is important at this point to consider all species in aqueous form. If precipitation reactions occur, this mathematical framework will not suffice. The reactions we consider are the following:



For this system, two mass balances have to be considered:

$$C_a = [\text{H}_3\text{PO}_4] + [\text{H}_2\text{PO}_4^-] + [\text{HPO}_4^{2-}] + [\text{PO}_4^{3-}] + [\text{CaH}_2\text{PO}_4^+] + [\text{CaHPO}_4^0] + [\text{CaPO}_4^-] \quad (3.75)$$

$$C_{Ca} = [\text{Ca}^{2+}] + [\text{CaH}_2\text{PO}_4^+] + [\text{CaHPO}_4^0] + [\text{CaPO}_4^-] \quad (3.76)$$

The dissociation equation of water (3.25) also has to be considered to completely determine the system. After addition of a strong base with concentration in the solution $C_B \text{ mol l}^{-1}$, one

can write the electro-neutrality equation or the charge balance:

$$C_B + [\text{H}^+] + 2[\text{Ca}^{2+}] + [\text{CaH}_2\text{PO}_4^+] = [\text{H}_2\text{PO}_4^-] \\ + 2[\text{HPO}_4^{2-}] + 3[\text{PO}_4^{3-}] + [\text{CaPO}_4^-] + [\text{OH}^-] \quad (3.77)$$

For a given C_a and C_{Ca} , and a particular chosen pH, the 8 equations (3.69)–(3.76) contain 8 unknown species concentrations, so they fully determine the system with respect to the concentrations of the calcium and phosphate species. Further, the dissociation equation of the water buffer (3.25) and the charge balance (3.77) can be used to calculate C_B for any given pH value. In other words, referring to section 3.2.2, we have developed a ‘fixed pH approach’ model for the titration profile. However, it is the aim to develop a buffer capacity model. For that, we will first try to find an analytical solution for C_B as a function of $[\text{H}^+]$, and then use equation (3.23) to find an analytical solution for β as a function of pH.

Summarized, the equations (3.25) and (3.69)–(3.77) have to be solved simultaneously, where $[\text{H}^+]$ is a fixed value (fixed pH approach).

$$\left\{ \begin{array}{l} [\text{H}^+][\text{OH}^-] = K_w^*[\text{H}_2\text{O}] \\ [\text{H}^+][\text{H}_2\text{PO}_4^-] = K_{a1}[\text{H}_3\text{PO}_4] \\ [\text{H}^+][\text{HPO}_4^{2-}] = K_{a2}[\text{H}_2\text{PO}_4^-] \\ [\text{H}^+][\text{PO}_4^{3-}] = K_{a3}[\text{HPO}_4^{2-}] \\ [\text{Ca}^{2+}][\text{H}_2\text{PO}_4^-] = K_{\text{Ca}1}[\text{CaH}_2\text{PO}_4^+] \quad (\star) \\ [\text{Ca}^{2+}][\text{HPO}_4^{2-}] = K_{\text{Ca}2}[\text{CaHPO}_4^0] \quad (\star) \\ [\text{Ca}^{2+}][\text{PO}_4^{3-}] = K_{\text{Ca}3}[\text{CaPO}_4^-] \quad (\star) \\ C_a = [\text{H}_3\text{PO}_4] + [\text{H}_2\text{PO}_4^-] + [\text{HPO}_4^{2-}] + [\text{PO}_4^{3-}] \\ \quad + [\text{CaH}_2\text{PO}_4^+] + [\text{CaHPO}_4^0] + [\text{CaPO}_4^-] \\ C_{\text{Ca}} = [\text{Ca}^{2+}] + [\text{CaH}_2\text{PO}_4^+] + [\text{CaHPO}_4^0] + [\text{CaPO}_4^-] \\ C_B + [\text{H}^+] + 2[\text{Ca}^{2+}] + [\text{CaH}_2\text{PO}_4^+] = [\text{H}_2\text{PO}_4^-] \\ \quad + 2[\text{HPO}_4^{2-}] + 3[\text{PO}_4^{3-}] + [\text{CaPO}_4^-] + [\text{OH}^-] \end{array} \right. \quad (3.78)$$

The equations marked with a (\star) are those introducing the non-linearities in the set of equations (3.78). Solving such a set of non-linear equations can be done with iterative techniques. However the aim is here to find an algebraic solution for each of the unknowns in the set of equations (3.78). Finding algebraic solutions for non-linear equations can be done with the technique of the ‘Groebner bases’. Symbolic software packages like REDUCE [112] and MuPAD [284] are equipped with the groebner package. To illustrate how this practically works, the processing of this example in REDUCE can be done with the following syntax:

```
f:=part(groebner(
{h*oh=h2o*kw,
h*h2po4=h3po4*kb1,
h*hpo4=h2po4*kb2,
h*po4=hpo4*kb3,
ca*h2po4=cah2po4*kca1,
ca*hpo4=cahpo4*kca2,
```

```

ca*po4=capo4*kca3,
c_a=h3po4+h2po4+hpo4+po4+cah2po4+cahpo4+capo4,
c_ca=ca+cah2po4+cahpo4+capo4,
c_b+h+2*ca+cah2po4=h2po4+2*hpo4+3*po4+capo4+oh},
{c_b,oh,h3po4,h2po4,hpo4,po4,ca,cah2po4,cahpo4,capo4}),1);

```

This command will algebraically solve the set of equations between the first pair of $\{\cdot\}$, in which the unknown variables are listed in the second pair of $\{\cdot\}$. For the development of the buffer capacity model, only the algebraic solution for C_B is required, in this case the first variable in the list of unknown variables. The isolation of the solution for C_B from the generated list of solutions for all unknowns is obtained with the ‘part(. . . , 1)’ command in the example code.

The further development of the buffer capacity model from this point on is similar with the linear buffer capacity approach of section 3.3. Equation (3.23) can be written as :

$$\beta = \frac{dC_B}{d\text{pH}} = -\frac{dC_B}{d\log[\text{H}^+]} = -\frac{dC_B}{d[\text{H}^+]}[\text{H}^+]\ln(10) \quad (3.79)$$

As we have a symbolic solution for $C_B = f([\text{H}^+])$, the same symbolic software package can be used to find a symbolic solution for the first derivative of C_B towards $[\text{H}^+]$.

```
g:=df(f,h)
```

This command generates a symbolic solution for $g = \frac{dC_B}{d[\text{H}^+]}$. Substitution of this solution in equation (3.79) results in the non-linear symbolic buffer capacity model in which β is expressed as $eq\ l^{-1}\ \text{pH}^{-1}$.

$$\beta = -g[\text{H}^+]\ln(10) \quad (3.80)$$

From a practical point of view, the solution for g will eventually need some further processing and rearrangement before it can be automatically translated into executable program code. The advantages of the symbolic manipulation method compared to an iterative numerical approach are twofold. First, the solution of the equation set (3.78) and the buffer capacity calculation (3.79) is fully algebraic, so that potential convergence problems for iterative or numerical solutions are avoided. Second, the computation speed of the symbolic buffer capacity model is probably much faster than any iterative solution technique. The disadvantage of the symbolic manipulation method is that for each other model (e.g. obtained by adding or removing chemical equilibria) the complete cycle of implementing the equations in a package like REDUCE, solving the equations with the groebner approach, transforming the solution into programmable code, compiling and linking the code into the simulation software, has to be repeated. The calculation time is considerable high, e.g. for the illustrated example, solved on a ‘Sun SPARCstation SLC’ workstation with 16 MBytes RAM, it took around 1 hour to obtain the programmable code. Further, our experience is that for more complicated examples (e.g. incorporation of calcium hydroxides), the calculation time increased to many hours, and the memory limits were quickly reached. Furthermore, there is no guarantee that a symbolic solution is found for each particular problem.

3.5 Non-linear tableau-method based buffer capacity model

Two approaches for the treatment of ‘large’ natural water systems were introduced in section 2.6 on page 37, i.e. the Gibbs minimization method, and the equilibrium constant approach. The latter approach is most commonly used in chemical software, like MINEQL or MINTEQA2 [10]. The equilibrium method, also called the ‘tableau-method’ will be presented in the following two sections [198,273]. In a further section, the tableau method will be adapted for its use in defining a buffer capacity model.

3.5.1 The tableau method for solving chemical equilibria problems

A systematic approach to organization of aquatic chemical equilibrium problems using the tableau format [198] will be adopted. The ‘canonical form’ entails:

1. A *recipe*, for example, how the system is constructed from reagents, including the molar amounts, the imposition of phases at equilibrium and the imposition of fixed activities;
2. A list of *species* at equilibrium;
3. A list of *independent* reactions among the species and their associated equilibrium constants.

Species are formed from *components*, “a set of chemical entities that permits a complete description of the stoichiometry of the system” [198]. A compact and convenient way to represent the relationship between components, species, formulae and mole balance equations is to organize the stoichiometric data in the form of a ‘tableau’. In the following paragraph, a numerical solution technique [251] for a chemical equilibrium example will be presented. Consider the example of 0.01 M acetic acid from section 3.2.1. At this point, we only consider the chemical equilibrium of acetate in water, without any strong base or acid added to the solution. The first thing one needs to determine in setting up a numerical solution is the number of *species* in solution. In this case, we have four.

- Species : HAc, Ac⁻, OH⁻ and H⁺

Second, we need to determine a minimum number of species necessary to solve the system of equilibrium equations. These are the independent variables which are called *components*. There are two equilibrium equations, the acid dissociation equation (3.2) of HAc with equilibrium constant K_a , and the ionization equation (3.3) of water with equilibrium constant K_w . These two equilibrium expressions contain the four chemical species (two equations and four unknowns), but we also have the mass balance (3.4) for total acetate and the charge balance (3.5), which can be substituted into equations (3.2) and (3.3) to leave us with two equations and two unknowns. Thus, we really only need two components (independent variables) to specify the system. In this example HAc and H⁺ are chosen as components.

- Components : HAc and H⁺

The choice of components is arbitrary as long as they are independent components. A more formal way of writing the rules for choosing a proper component set is [198]:

1. All species can be expressed stoichiometrically as a function of the components, the stoichiometry being defined by the chemical reactions.
2. Each species has a unique stoichiometric expression as a function of the components.

A necessary, but not sufficient, condition to fulfil these requirements is that the number of components be equal to the number of species minus the number of independent reactions considered to take place in the system.

Next, we need to write chemical equations for the four species in terms of the components, including the formation of the components themselves.

- Formation of HAc : $\text{HAc} \rightleftharpoons \text{HAc} \quad \log K_1 = 0$
- Formation of Ac^- : $\text{HAc} \rightleftharpoons \text{Ac}^- + \text{H}^+ \quad \log K_2 = -4.7$
- Formation of OH^- : $\text{H}_2\text{O} \rightleftharpoons \text{OH}^- + \text{H}^+ \quad \log K_3 = -14$
- Formation of H^+ : $\text{H}^+ \rightleftharpoons \text{H}^+ \quad \log K_4 = 0$

The formation equations of HAc and H^+ are chemically not really relevant, but they are needed as supporting equations in the matrix notation.

The chemical equations are, in reality, mass action expressions that form a set of algebraic equations for the activity of each species in terms of the components. We will assume that all activity coefficients are 1. For our example of 0.01 M HAc in H_2O , the activity corrections are indeed negligible.

$$[\text{HAc}] = K_1 [\text{HAc}]^1 \quad (3.81)$$

$$[\text{Ac}^-] = K_2 [\text{HAc}]^1 [\text{H}^+]^{-1} \quad (3.82)$$

$$[\text{OH}^-] = K_3 [\text{H}^+]^{-1} \quad (3.83)$$

$$[\text{H}^+] = K_4 [\text{H}^+]^1 \quad (3.84)$$

These equations define the system completely, together with the mass balance equation for acetate (3.4) and the charge balance (3.5). Taking the logarithm of both sides of equations (3.81)–(3.84), we find

$$\log[\text{HAc}] = 1 \log[\text{HAc}] + \log K_1 \quad (3.85)$$

$$\log[\text{Ac}^-] = 1 \log[\text{HAc}] - 1 \log[\text{H}^+] + \log K_2 \quad (3.86)$$

$$\log[\text{OH}^-] = -1 \log[\text{H}^+] + \log K_3 \quad (3.87)$$

$$\log[\text{H}^+] = 1 \log[\text{H}^+] + \log K_4 \quad (3.88)$$

Equations (3.85)–(3.88) define a linear set of equations that can be solved using matrix algebra. The species comprise the rows of the matrix and the components are the columns. This information is summarized in Table 3.1. For the example being considered, equations (3.85)–(3.88) can be written in matrix notation:

$$\begin{bmatrix} \log[\text{HAc}] \\ \log[\text{Ac}^-] \\ \log[\text{OH}^-] \\ \log[\text{H}^+] \end{bmatrix} = \begin{bmatrix} 1 & 0 \\ 1 & -1 \\ 0 & -1 \\ 0 & 1 \end{bmatrix} \cdot \begin{bmatrix} \log[\text{HAc}] \\ \log[\text{H}^+] \end{bmatrix} + \begin{bmatrix} 0 \\ -4.7 \\ -14.0 \\ 0 \end{bmatrix} \quad (3.89)$$

Table 3.1: Species, components and stoichiometric matrix of the HAc example

Species	Components		
	HAc	H ⁺	log <i>K</i>
HAc	1	0	0
Ac ⁻	1	-1	-4.7
OH ⁻	0	-1	-14.0
H ⁺	0	1	0
	10 ⁻²	10 ⁻⁷	

There is one final step before solving the matrix equation. We must provide an initial estimate of the [H⁺] to get the program started, and we must provide the mass balance equation. The initial estimate of [H⁺] is in lieu of the charge balance. The manner in which we provide this information in computer packages is to specify the *mode* of each component, that is, whether the concentration specified is the *total* or *free* concentration. The total concentration of acetate is 10⁻² *M* and we specify it at the bottom of the column, and the initial guess for H⁺ is 10⁻⁷ *M*.

The programs that implement the tableau method will recognize the concentrations specified to be the mass balance HAc + Ac⁻ = 0.01 *M* and pH = 7 (initial guess). We will calculate the distribution of species as a function of pH.

In matrix notation, we will use {·} to designate one-dimensional arrays (column vectors) and square brackets [·] for two-dimensional matrices. The stoichiometric coefficients, which came from the exponents of the mass action expressions, equations (3.81)–(3.84), comprise the matrix, and all the species are expressed in terms of concentration, *mol l*⁻¹, or *M*. In matrix notation, we can rewrite equations (3.85)–(3.88) in a general form.

$$\{C^*\} = [A]\{X^*\} + \{K^*\} \quad (3.90)$$

{C*} : column vector of log species concentrations, *n* dimension
 [A] : matrix of stoichiometric coefficients, *n* × *m* dimension
 {X*} : column vector of log component concentrations, *m* dimension
 {K*} : column vector of log equilibrium constants, *n* dimension
n : the number of species
m : the number of components

The material balance equations are determined in the computer program from the modes that were specified and the concentrations given at the bottom. There is exactly one material

balance equation for each component.

$$0.01 = C_a = 1 [\text{HAc}] + 1 [\text{Ac}^-] \quad (3.91)$$

$$10^{-7} = 1 [\text{H}^+] \quad (3.92)$$

In general, the material balance equations can also be written in matrix notation. It is the transpose of the $[A]$ matrix of stoichiometric coefficients times the concentration vector for the species, minus the total concentration of each component. This is not a logarithmic equation as is equation (3.90). The equation is cast in terms of a differential error term that will be calculated by the Newton-Raphson numerical solution technique until it is within an acceptable closure tolerance.

$$[A]^T \{C\} - \{C_{\text{TOT}}\} = \{Y\} \quad (3.93)$$

$[A]^T$: transposed stoichiometric coefficient matrix, $m \times n$ dimension
 $\{C\}$: column vector of species concentration, n dimension
 $\{C_{\text{TOT}}\}$: column vector of component total concentrations, m dimension
 $\{Y\}$: column vector, which is the remaining error in the material balance equations, m dimension

For the example being considered, equation (3.93) becomes

$$\begin{bmatrix} 1 & 1 & 0 & 0 \\ 0 & -1 & -1 & 1 \end{bmatrix} \cdot \begin{bmatrix} [\text{HAc}] \\ [\text{Ac}^-] \\ [\text{OH}^-] \\ [\text{H}^+] \end{bmatrix} - \begin{bmatrix} 10^{-2} \\ 10^{-7} \end{bmatrix} = \begin{bmatrix} y_1 \\ y_2 \end{bmatrix} \quad (3.94)$$

Note that the second equation in (3.94) is the charge balance of the system. The equilibrium problem is solved when $\{Y\} = 0$, or when $\{Y\} < \eta$, the acceptable closure tolerance.

In the numerical scheme, the log concentration of each species is computed from equation (3.90) based on an initial guess for the concentration of the components. Then the error, or remainder, is estimated from equation (3.93). An iterative technique is used to find improved values of $\{X\}$, the component concentrations, such that the value of $\{Y\}$ is reduced. Typically, the Newton-Raphson method is applied. Improved values for $\{X\}$, the component concentration array, are found from the matrix equation

$$[Z]\{\Delta X\} = \{Y\} \quad (3.95)$$

$[Z]$: square matrix that is the Jacobian of Y with respect to X , $\frac{\partial Y}{\partial X}$, $m \times m$ dimension
 $\{\Delta X\}$: column vector for the improvement in component concentrations, m dimension

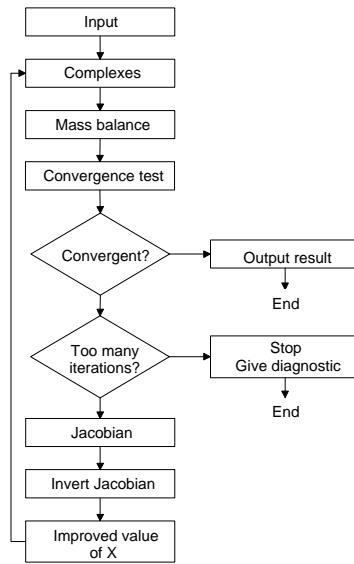


Figure 3.2: Flowchart of a typical chemical equilibrium program with the Newton-Raphson iterative solution technique (modified from [251])

The Jacobian operator can be written in terms of the stoichiometric coefficients

$$Z_{jk} = \frac{\partial Y_j}{\partial X_k} = \sum_{i=1}^n \frac{a_{ij}a_{ik}C_i}{X_k} \quad \begin{cases} \text{for all species } (i = 1, \dots, n) \\ \text{for all components } (j = 1, \dots, m) \\ \text{and } (k = 1, \dots, m) \text{ and } j \neq k \end{cases} \quad (3.96)$$

Equation (3.95) can be solved for ΔX by inversion of the Z matrix.

$$\{\Delta X\} = [Z]^{-1}\{Y\} \quad (3.97)$$

$$\therefore \{X\}_{\text{improved}} = \{X\}_{\text{original}} - [Z]^{-1}\{Y\} \quad (3.98)$$

Since $\{Y\}$ is an array of error terms that may vary widely (orders of magnitude), the convergence criterion is chosen to reflect the magnitude of Y_j , relative to the maximum of terms of which Y_j is the sum [251]. Therefore, a possible criterion for convergence is

$$\frac{|Y_j|}{\max(Y_j)} < \eta \text{ for all components } (j = 1, \dots, m) \quad (3.99)$$

η : convergence parameter

When the error term is within closure limits, the program can exit and the equilibrium problem is 'solved'. A flowchart of a typical computer program is presented in Figure 3.2. The Newton-

Raphson method is one of the oldest and still most widely used numerical technique for solving a set of nonlinear equations [262].

3.5.2 Precipitation and dissolution in equilibrium models

One of the powerful features of the tableau-based method for solving chemical problems is the possibility to include precipitation and dissolution of species. From a chemical point of view, precipitation and dissolution reactions are conditional, they only occur if certain conditions (solubility product) are fulfilled. From a mathematical point of view, this means that such reactions will introduce discontinuities in e.g. an algebraic model, or from a numerical point of view the introduction of *if... then* structures in the model. As a result of this, buffer capacity modelling approaches presented in sections 3.3 and 3.4 cannot be used when one wants to include precipitation or dissolution reactions.

Chemical equilibrium models are quite structured in the manner that one designates precipitation and dissolution of species. Several models [10, 198] use a format where each chemical species is assigned a ‘Type’ upon data entry.

- Type I species – all the aqueous chemical species designated as *components*.
- Type II species – all other aqueous species not designated in Type I.
- Type III species – all fixed species including solids designated to be present at chemical equilibrium and not subject to complete dissolution.
- Type IV species – all finite solids that are presumed to be present initially and have the potential to be completely dissolved if the solution becomes undersaturated.
- Type V species – all solids that may precipitate from solution but are presently undersaturated.
- Type VI species – all species that are excluded from mass balance calculations (e.g. gases, electrons, ...).

The number of degrees of freedom of the chemical equilibrium problem is the number of independent variables. The Gibbs’ phase rule for computer modelling purposes is

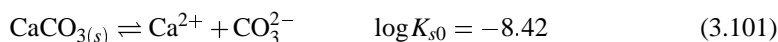
$$F = C - P \quad (3.100)$$

F : number of degrees of freedom

C : number of chemical components

P : number of Type III + Type IV species

By specifying Type III and Type IV species, we decrease the number of degrees of freedom. As long as F is positive, the computer calculations will proceed. If F is zero or less, a diagnostic will prompt the user to restructure the problem. To understand why Type III and Type IV species decrease the number of degrees of freedom, consider the case of $\text{CaCO}_{3(s)}$ dissolution as a type IV solid.



As long as $\text{CaCO}_{3(s)}$ is present, the product of calcium ions and carbonate ions is fixed; they are not both independent variables, therefore we loose 1 degree of freedom. If carbonate

anion increases, calcium ion must decrease.

$$[\text{Ca}^{2+}] = \frac{10^{-8.42}}{[\text{CO}_3^{2-}]} \quad (3.102)$$

3.5.3 Non-linear tableau-based buffer capacity model

The tableau-based method for solving chemical equilibria can be adapted and used for the simulation of buffer capacity profiles. However, there are some slight modifications necessary. The available software is mainly focused on speciation calculations, and, although, the step towards buffer capacity curve modelling is theoretically possible, it is not readily implemented in software like MINTQA2 [10]. The following steps will be taken in order to develop a tableau-based buffer capacity model:

1. According to sections 3.3 and 3.4, for mathematical and computational reasons, the approach will be a ‘fixed pH approach’. Because the concentrations of the *components* are iteratively changed in the tableau-based method until a certain convergence is reached, $[\text{H}^+]$ is no longer a component, but will be treated as constant value, similar to the K values.
2. Because $[\text{H}^+]$ is kept fixed in the equilibrium calculations, the degrees of freedom can be decreased with 1.
3. Leaving out $[\text{H}^+]$ as a component means also that the mass balance for this component (here, the charge balance) is not included in the iterative Newton-Raphson procedure.
4. If we assume titration with a strong base (e.g. NaOH), and the counter-ion (Na^+ in this case) is assumed not to enter in any specified chemical reaction, the concentration C_B is present in only 1 equation, being the charge balance (cfr. example discussed in the set of equations (3.78). For this reason, together with the previous point, it’s useless to include the $[\text{Na}^+]$ with concentration C_B in the tableau.
5. When for a particular pH, the tableau method has found a chemical equilibrium solution, and found the concentrations for all species, the excluded charge balance will be used to calculate the value of C_B , because all species in the charge balance will be known, except for $[\text{Na}^+]$ with concentration C_B .
6. Once $C_B = f(\text{pH})$ is established, the buffer capacity β can be calculated. However the approach for β will be different from the approach in sections 3.3 and 3.4 because the relationship between C_B and pH will be numerical in the tableau method, while it was algebraic or symbolic in the 2 previous approaches. In other words, the expression for β in equation (3.23) will be modified from $\frac{dC_B}{d\text{pH}}$ to $\frac{\Delta C_B}{\Delta \text{pH}}$.

To illustrate these six different steps to build a tableau-based buffer capacity model, the same example of a solution containing phosphoric acid and Ca^{2+} of section 3.4 will be repeated. The number of components for the approach of the conventional tableau-method would be 3. But because we take a ‘fixed pH approach’, the number of independent components reduces to 2. The components which are chosen preferentially are H_3PO_4 and Ca^{2+} .

Table 3.2: Species, components and stoichiometric information of the $\text{Ca}^{2+} - \text{H}_3\text{PO}_4$ example

Species	Components		H^+	$\{\log K\}$
	H_3PO_4	Ca^{2+}		
H_3PO_4	1	0	0	0
H_2PO_4^-	1	0	-1	-2.2
HPO_4^{2-}	1	0	-2	-2.2 - 7.2
PO_4^{3-}	1	0	-3	-2.2 - 7.2 - 12.4
Ca^{2+}	0	1	0	0
$\text{CaH}_2\text{PO}_4^+$	1	1	-1	-2.2 + 1.4
CaHPO_4^0	1	1	-2	-2.2 - 7.2 + 2.7
CaPO_4^-	1	1	-3	-2.2 - 7.2 - 12.4 + 6.5
OH^-	0	0	-1	-14
	C_a	C_{Ca}		

The species, components and stoichiometric matrix information for this example is presented in Table 3.2. Table 3.2 summarizes the equilibria and mass balances that were presented in equations (3.69)–(3.76) and equation (3.25). Note that in order to write the species equilibrium equations in function of the 2 components, substitutions of equations into other equations was necessary in order to find the appropriate $\{\log K\}$ values. This is a mainly manual process, and it appears difficult to automate this for general purposes. For example, the equilibrium equation for $\text{CaH}_2\text{PO}_4^+$ is found by rewriting equations (3.69) and (3.72) respectively into:

$$\log[\text{CaH}_2\text{PO}_4^+] = \log[\text{H}_2\text{PO}_4^-] + \log[\text{Ca}^{2+}] + 1.4 \quad (3.103)$$

$$\log[\text{H}_2\text{PO}_4^-] = \log[\text{H}_3\text{PO}_4] - \log[\text{H}^+] - 2.2 \quad (3.104)$$

followed by substitution of equation (3.104) into (3.103):

$$\log[\text{CaH}_2\text{PO}_4^+] = \log[\text{H}_3\text{PO}_4] + \log[\text{Ca}^{2+}] - \log[\text{H}^+] - 2.2 + 1.4 \quad (3.105)$$

The latter equation is formulated in the stoichiometric information matrix in Table 3.2. The general equation (3.90) of the tableau method needs to be extended here for buffer capacity calculations with one term due to $[\text{H}^+]$ being excluded as a component:

$$\{C^*\} = [A]\{X^*\} + \{B\}\log[\text{H}^+] + \{K^*\} \quad (3.106)$$

$\{B\}$: column vector of stoichiometric H^+ coefficients, n dimension

Equation (3.106) together with equation (3.93) can now be solved for a particular chosen pH value with the iterative Newton-Raphson numerical solution technique, as illustrated in section 3.5.1. This will result in equilibrium concentrations for all considered species. The buffer capacity β at the considered pH can be calculated with equation (3.23) if we know the concentration C_B . C_B can easily be found by rearranging equation (3.77), which was not used until this point.

$$C_B = [\text{H}_2\text{PO}_4^-] + 2[\text{HPO}_4^{2-}] + 3[\text{PO}_4^{3-}] + [\text{CaPO}_4^-] \\ + [\text{OH}^-] - [\text{H}^+] - 2[\text{Ca}^{2+}] - [\text{CaH}_2\text{PO}_4^+] \quad (3.107)$$

Unfortunately, the analytical approach of calculating β by taking the first derivative of C_B towards pH, equation(3.79), cannot be taken here because the relationship between C_B and pH is purely numerical in this tableau based approach. This forces us to use a numerical derivative procedure to find β . Because of the high numerical precision that can be reached with modern software and computers, a simple first derivative algorithm like the Euler algorithm will mostly suffice.

$$\beta = \frac{dC_B}{dpH} \approx \frac{\Delta C_B}{\Delta pH} = \frac{C_B(pH + \Delta pH) - C_B(pH - \Delta pH)}{2\Delta pH} \quad (3.108)$$

where ΔpH is a sufficiently but not too small value, in order to obtain a correct value for β in function of pH. The illustrated example did not contain any precipitation or dissolution reactions. However, a similar approach can be followed for systems with this kind of chemical reactions. An extra step at the end of each iteration loop will have to be included. This will be illustrated with an example in section 3.5.5.

3.5.4 Ionic interaction effects

A similar ionic strength correction as presented for the general linear buffer capacity model (section 3.3.6) can be applied here too. The introduction of mixed acidity constants K'_a (see section 2.2.4 on page 19) instead of acidity constants K_a , makes that all species can be written as concentrations, except for H^+ , that has to be written as an activity, $\{\text{H}^+\}$. Because a pH meter delivers the H^+ activity (see section 2.1 on page 5 and section 2.2.2 on page 15), the buffer capacity is expressed in function of $\{\text{H}^+\}$ instead of $[\text{H}^+]$. Subsequently, the stoichiometric information can be written in terms of concentrations for all species, and in terms of activity for H^+ . However, as also noted in section 3.3.6, the mass balances and charge balance should be written in terms of concentration. Therefore, the equation (3.107) has to be corrected:

$$C_B = [\text{H}_2\text{PO}_4^-] + 2[\text{HPO}_4^{2-}] + 3[\text{PO}_4^{3-}] + [\text{CaPO}_4^-] \\ + [\text{OH}^-] - \frac{\{\text{H}^+\}}{\gamma_{\text{H}^+}} - 2[\text{Ca}^{2+}] - [\text{CaH}_2\text{PO}_4^+] \quad (3.109)$$

Summarized, and in general, ionic strength effects can be introduced in the tableau method when the following steps are taken:

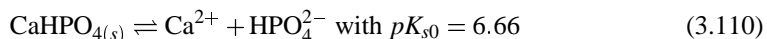
- Replace $[\text{H}^+]$ by $\{\text{H}^+\}$ in all equations.

- Use K'_a values instead of K_a values.
- Replace in the charge balance $\{H^+\}$ by $\frac{\{H^+\}}{\gamma_{H^+}}$.

3.5.5 Precipitation and dissolution in the tableau-based approach

The introduction of Type IV and Type V species (see section 3.5.2) into a chemical equilibrium model lead to mathematical discontinuities, which need a careful approach. If we consider reaction (3.101), the corresponding equilibrium equation (3.102) is only valid as long as $CaCO_{3(s)}$ is present. When the solution becomes undersaturated, the equilibrium equation (3.102) is not valid any more and has to be eliminated from the model, for as long as the solution stays undersaturated.

We will consider the example of section 3.5.3 of which the stoichiometric information is presented in Table 3.2. We will consider a titration from low pH (e.g. pH = 4) until the pH where $CaHPO_{4(s)}$ with $pK_{s0} = 6.66$ starts to precipitate. Because the calculation of the buffer capacity curve is based on simulations with increasing pH-values which are defined by the user, it is possible to verify at each simulated pH value if there is a possibility for precipitation. This can be done by comparing the ion-product of the possible precipitate with the solubility product K_{s0} . In the example, Ca^{2+} and HPO_4^{2-} ions are present, so we can consider a $CaHPO_{4(s)}$ precipitate.



There will be no precipitation as long as $[Ca^{2+}] \cdot [HPO_4^{2-}] < K_{s0}$. From the moment the ion product exceeds K_{s0} , we need to take into consideration a new species, being $CaHPO_{4(s)}$. However, from a stoichiometric and mathematical point of view, this means that the complete system has to be restructured.

As discussed in section 3.5.2, the number of degrees of freedom will decrease with 1 due to the precipitate, so the amount of components also decreases with 1. Practically we will have to set up a completely different stoichiometric matrix. The new species, components and stoichiometric matrix is presented in Table 3.3. The chemical equilibria presented in Table 3.3 are the result of restructuring the original equations and write them all down in function of H_3PO_4 and H^+ . The precipitated $CaHPO_{4(s)}$ is normally not considered as species because we cannot write down an equation expressing the concentration of precipitate. We need to consider the precipitate to be present as long as the IAP of Ca^{2+} and HPO_4^{2-} is higher than K_{s0} . Often in chemical equilibria problems, solids are chosen as components if one wants to calculate dissolution or precipitation amounts [251], but we didn't need to do that for this example. The mass balance for the H_3PO_4 component is not straightforward, because an unknown concentration of HPO_4^{2-} is precipitated with Ca^{2+} . We can express that the amount of Ca^{2+} precipitated from the pool of calcium is equal to the amount of HPO_4^{2-} precipitated from the pool of phosphorus.

$$\begin{aligned} C_{Ca} - [Ca^{2+}] - [CaH_2PO_4^+] - [CaHPO_4^0] - [CaPO_4^-] &= C_a - [H_3PO_4] \\ -[H_2PO_4^-] - [HPO_4^{2-}] - [PO_4^{3-}] - [CaH_2PO_4^+] - [CaHPO_4^0] - [CaPO_4^-] & \quad (3.111) \end{aligned}$$

Table 3.3: Species, components and stoichiometric information of the $\text{Ca}^{2+} - \text{H}_3\text{PO}_4$ example, in the presence of a $\text{CaHPO}_{4(s)}$ precipitate

Species	Component		
	H_3PO_4	H^+	$\{\log K\}$
H_3PO_4	1	0	0
H_2PO_4^-	1	-1	-2.2
HPO_4^{2-}	1	-2	-2.2 - 7.2
PO_4^{3-}	1	-3	-2.2 - 7.2 - 12.4
Ca^{2+}	-1	2	-6.66 + 2.2 + 7.2
$\text{CaH}_2\text{PO}_4^+$	0	1	-6.66 + 1.4 + 7.2
CaHPO_4^0	0	0	-6.66 + 2.7
CaPO_4^-	0	-1	-6.66 - 12.4 + 6.5
OH^-	0	-1	-14
$C_a - C_{\text{Ca}}$			

or after rearranging

$$[\text{H}_3\text{PO}_4] + [\text{H}_2\text{PO}_4^-] + [\text{HPO}_4^{2-}] + [\text{PO}_4^{3-}] - [\text{Ca}^{2+}] = C_a - C_{\text{Ca}} \quad (3.112)$$

Equation (3.112) makes it possible to write a mass balance for the phosphorus component, as included in Table 3.3.

A simulated buffer capacity profile of the $\text{Ca}^{2+} - \text{H}_3\text{PO}_4$ example, including a precipitation reaction of $\text{CaHPO}_{4(s)}$ is shown in Figure 3.3. The component concentrations used in the simulation are for Ca^{2+} : $C_{\text{Ca}} = 1.25 \text{ mmol l}^{-1}$ and for H_3PO_4 : $C_a = 2 \text{ mmol l}^{-1}$. First, a simulation without considering the precipitation reaction was performed (using the stoichiometric information of Table 3.2). From that simulation, by comparing the IAP of Ca^{2+} and HPO_4^- with K_{s0} , it was found that a precipitation of $\text{CaHPO}_{4(s)}$ might occur between pH 6.35 and pH 9.45. Second, a model including the $\text{CaHPO}_{4(s)}$ precipitate was simulated between pH 6 and pH 10 (using the stoichiometric information of Table 3.3). Third, a combined buffer capacity model was obtained by considering the simulation result of the first model outside the pH range 6.35–9.45, and the simulation result of the second model inside the pH range 6.35–9.45. The species concentrations found with both models at the ‘model switching’ points (pH 6.35 and pH 9.45) were exactly the same. The latter finding was a confirmation of the correctness of both models and their simulations. However, the derivatives of the species concentrations towards the pH at the ‘model switching’ points are very different in both models, thus explaining the 2 discontinuities in the combined buffer capacity model. The practical question is if these discontinuities will also appear in experimental buffer capacity measurements of such solutions. A practical case-study where precipitation reactions are involved is presented in section 8.4.4 on page 195.

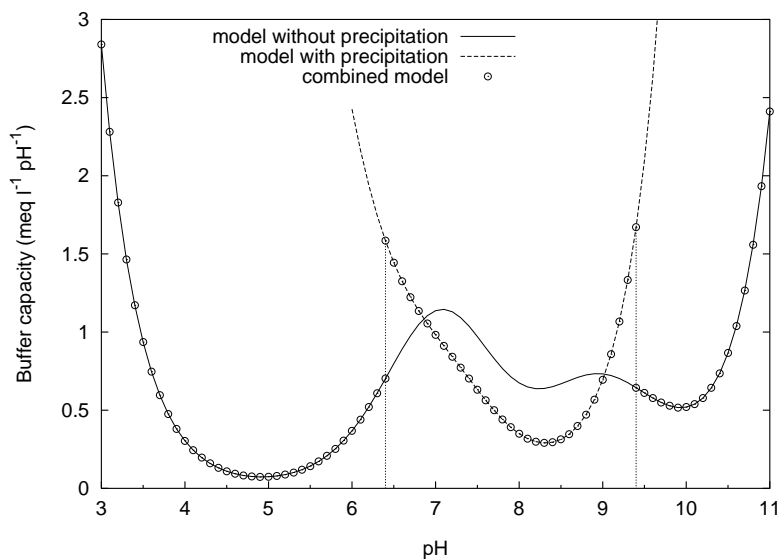


Figure 3.3: Simulated buffer capacity profile of the $\text{Ca}^{2+} - \text{H}_3\text{PO}_4$ example, including a precipitation reaction of $\text{CaHPO}_4(s)$

To summarize the approach for non-linear modelling of buffer capacity in function of pH for models including precipitation reactions, the following steps are taken:

- One starts with a model taking into account all species that are assumed to be present at the considered initial pH.
- One simulates the model and finds species concentrations and the buffer capacity for increasing pH values.
- At the end of every equilibrium calculation, one checks the ion-product (IAP) of 1 or more possible precipitates.
- If the IAP exceeds the solubility product, one switches to another model including the precipitate and continues the calculations for increasing pH values.
- If the IAP for a precipitate that is present in the model becomes smaller than the solubility product, then again a model switch to a model without that precipitate is necessary.

It is not always possible to guess correctly whether a given solid phase should or should not be present at a given pH. When there are few such solids, a trial and error procedure yields the correct answer [198]. In complex situations where there are many possible solids involving common components, this procedure can become quite difficult and short of trying all possibilities (which can number in the thousands), there is in fact no easy way to obtain the correct set of solids [198].

Table 3.4: Comparison of three types of buffer capacity models

	linear buffer capacity model	non-linear symbolic buffer capacity model	non-linear tableau-based buffer capacity model
acid-base equilibria	yes	yes	yes
complexation	no	yes	yes
precipitation and dissolution	no	no	yes
calculation speed	very fast	fast	slow
implementation	very easy, e.g. spreadsheet	difficult, specialized software like REDUCE needed	moderate iterative solution technique needed
adaptation to new models	easy, supply extra additive term	difficult, repeat the symbolic manipulation and code compilation	moderate, change of stoichiometric matrix
robustness	very robust	symbolic solution not always found; however, the compiled code is very robust	robust, but possible convergence problems in matrix calculations may occur

3.6 Comparison of the 3 buffer capacity model approaches

Which of the three presented buffer capacity models (sections 3.3, 3.4 and 3.5) is to be preferred for a certain case is dependent on the reactions and the equilibria that are included in the model. Table 3.4 gives an overview of the possibilities and some specifications for buffer capacity modelling.

If only simple acid-base equilibria have to be modelled, the linear buffer capacity model is by far to be preferred. If complexation and/or precipitation reactions have to be considered, the tableau-based method is a good choice, because of its flexibility and widest range of possibilities. However, if only acid-base and complexation equilibria have to be considered, and speed and numerical robustness are important (e.g. in on-line field applications), the non-linear symbolic model is the preferred model.

Among implementations found in literature, two spreadsheet approaches [210, 295] and one matrix approach [20] are mentioned here. The first spreadsheet approach was developed because in the early stage of developing a candidate compound as a new drug, its solubility and stability in aqueous solutions have to be investigated in function of pH [210]. A number

of methods and/or computer programs for calculation of solution pH and buffer capacity were reviewed by the authors, but these were found to be inconvenient for use in designing a buffer solution, since they ignore effects of ionic strength, do not involve effects of temperature, treat acids, bases and/or ampholytes separately, and eventually do not run on Windows[®] which is now widely used at workplaces. The developed program in Excel[®] is useful for identifying appropriate buffer solutions at various temperatures and/or ionic strengths [210]. The program is useful for prototyping, but not for simulations. One of the drawbacks for simulation applications was found to be the limited possibility of Excel[®] to deal with computational 'loops'. The second spreadsheet application was developed for water conditioning purposes [295]. The author points out that the main advantages of the use of spreadsheets for solving problems of equilibrium chemistry are: its cheap implementation, the easy reuse, and the higher accessibility for users. The disadvantage is that spreadsheets are limited to relatively simple problems. The developed spreadsheet could handle a number of topics related to the CO₂ – H₂O system, like carbonate equilibria, construction of a lime titration curve, finding pH of a blend of two water sources, calcium carbonate precipitation, and buffer capacity curves of inorganic carbon species [295].

For more complex problems in chemical equilibria, a set of FORTRAN routines (MAGIK) have been developed, which perform all of the necessary arithmetic for the solution of many types of complex equilibria [20]. Its calculation engine is based on the Newton-Raphson method of steepest descents (see also section 3.5), which is similar to packages presented before like MINTEQA2 [10]. The main feature of the program is that it can handle titrations, contrary to many other programs, that can only handle single point equilibrium problems. More particular, MAGIK calculates species concentrations in function of a stepwise added titrant. The dynamic equilibria also include precipitation and dissolution. However, with a chemical event such as precipitation, the concentration of one or more species will usually suffer an abrupt change, which is ultimately reflected as a mathematical discontinuity. The mathematical discontinuity is a situation in which not only specific variables will change drastically, but entire equations will no longer be valid. To overcome this problem, a possibility to swap between 2 sets of equations was implemented in the software. A model swap is necessary when a precipitation reaction starts, or when the precipitate redissolves. These model swaps must occur at the precise instant that both models overlap and where one supersedes the other in order to get a smooth continuity of results [20]. The models and the model swapping condition have to be entered by the user in a subroutine, so that in case there are several possible precipitates/dissolutions, this approach will also be infeasible or impossible to implement. Eventually, off-line studies with several sets of models can help to determine which precipitation/dissolution reactions will occur first, and once the sequence of reactions is found, this sequence can be implemented in e.g. MAGIK [20] to obtain a full titration profile of the system. For each chemical equilibrium problem, a user-defined FORTRAN subroutine needs to be compiled and linked with the main program MAGIK. This is a serious drawback for field applications, or in an automatic model building approach (see chapter 9).

Chapter 4

Field technologies for aquatic monitoring

In this chapter, a literature review on technologies, practical experiences, relevance, problems, equipment, etc. related to the on-line measurements in activated sludge systems, rivers and other aquatic streams is presented. Because of the very broad range of existing technologies and applications in this area, this literature study will only highlight these techniques and sensors for which the developed buffer capacity sensor in this work can be considered as a possible alternative. Taking this into account, the techniques that will be considered are chosen by the following criteria:

1. On-line or potential on-line application;
2. Application in wastewater effluent, river water, process water and other aquatic streams;
3. Measurement of chemical substances that directly or indirectly (after transformation into another chemical) induce a pH buffer capacity in the measurable range between pH 3 and pH 11. More particular, ammonium, nitrate, phosphate, alkalinity and VFA's are among measurements that will be treated in this chapter;
4. Application measurement range in the order of magnitude of 0.1 mmol l^{-1} for each chemical substance. This is one of the main reasons that drinking water applications are not discussed here, because in this area, the minimal measurable concentrations that are necessary cannot be achieved with a buffer capacity based sensor.

Furthermore, the benefits of on-line measurements compared to off-line measurements is highlighted in section 4.1. Existing sensors which are based on pH titration or buffer capacity profiles will be discussed separately in section 4.4 because they can be of direct importance to compare with the results obtained in this work. The goal of this chapter is to present a framework of existing sensors/methods, in order to make a positioning of the developed buffer capacity sensor into existing technologies.

4.1 On-line measurement techniques

In the field of environmental measurements, in the last decades, one increasingly tries to implement on-line measurements to replace off-line measurements. However, the results obtained with on-line measurements are sometimes unsuccessful. In cases where the expectations from on-line measurements are high, and the difficulties related to these measurements are underestimated, installed on-line equipment will probably not produce the results as they were expected. This already highlights the difficulties and particularities related to on-line measurements.

The highest benefit of on-line measurements compared to off-line measurements is undoubtedly the possibility to use this data for control purposes. In the field of biotechnological process control, better processing will come with the improvement of the biological knowledge and the application of automatic control [265]. In an ideal situation, the measured data should be produced in-situ, on-line, continuously in real time and cover a wide dynamic range in order to exploit them for process control. Aspects related to a successful implementation of on-line sensors are discussed widely in literature [22, 127, 159, 161, 163, 265, 271, 332]. These aspects are related to the data reduction, database management [159, 265], data interpretation [160, 161, 163], the human interface [265], maintenance and calibration related topics [161, 332].

One of these application fields for on-line sensors that will be discussed in somewhat more details is the activated sludge wastewater treatment. The main objective of sewage treatment was previously to remove organic carbon compounds from the wastewater. However, the range of demands has greatly increased nowadays. Efforts now extend to complete elimination of nitrogen and phosphorus [179]. At present, the most economical method for nitrogen removal seems to be biological nitrification-denitrification [26]. Until now chemical precipitation using aluminium and iron salts and lime has been adopted in phosphate removal. However, this has major disadvantages (large amount of chemicals, expensive, additional sludge, ...) and, consequently, biological phosphorus removal appears to be economically very attractive [26, 150]. Alternating anaerobic/aerobic conditions of the biomass is one of the key factors triggering off phosphorus removal in excess of the normal assimilation (luxury uptake). The release of $o\text{-PO}_4$ in the anaerobic phase depends on several factors which can act separately or simultaneously: e.g. the concentration of organic substrates and nitrates [109]. The alternating mode of operation involves that the concentrations of ammonium, nitrate and phosphate increase and decrease periodically in the mixed liquor. By monitoring these dynamics with on-line measurements, the rates of nitrification, denitrification and phosphate uptake or release can be determined. This in turn provides valuable information for the understanding, modelling and on-line control of this process [18, 19, 128]. Besides on-line nutrient sensors for nitrate and ammonium, ortho-phosphate and TOC, on-line alkalinity and turbidity measurements [256] are shown to be useful for process control purposes.

A major difficulty faced by plant operators in controlling the activated sludge process is the inability to adequately monitor the process [271]. However, nowadays on-line sensors for dissolved oxygen, suspended solids, pH, temperature and flow are found accurate enough for control purposes, under the conditions of correct use, frequent maintenance and calibration etc. Today almost all plants are equipped with some of these sensors. A more interesting range of instruments related to this work are the on-line nutrient sensors (e.g. ammonium, nitrate, phosphate). These sensors get a lot of attention nowadays and a lot of research and

commercialisation efforts are focused on this category of sensors. These sensors are expensive equipment, but the benefits of these sensors can be very high, as will be illustrated with some examples below.

On-line analyzers to monitor the effluent levels of ammonia and phosphate have been used for operational control of 4 nutrient removal activated sludge plants in Johannesburg [166]. Savings of 1 million US dollar per year in the purchase of phosphate precipitation chemicals have been achieved. Other authors point out two major obstacles to be considered with on-line nutrient sensors: First, that on-line measurements of ammonium, nitrate and phosphate are too unstable to be used for on-line control; Second, that no efficient control strategies are documented in the literature [291]. However, studies at several plants in Denmark have shown that obstacle 1 is now overcome as these measurements are now used for direct control [291]. The same study also showed that a responsible maintenance and surveillance is the key factor. Closed loop control strategies have been found efficient and robust for practical implementation, and are economically favourable at most large plants with biological nutrient removal [291]. Another key factor is sample preparation. In order to obtain nutrient measurements in the mixed liquor, most on-line apparatus need an extra membrane filtration step, because the measurements would be disturbed by clogging in the small tubes of the nitrogen and phosphorus monitors [292].

Data of on-line analyzers allow also up-to-date simulation using mathematical models of the treatment system [57, 213]. It is shown that computer simulation is a very powerful tool for the optimization of the operation of wastewater treatment plants. Considering the benefits of computer simulation for plant operation, it is worth its price for medium to very large wastewater treatment plants [213]. The benefits from computer simulation are e.g. savings in energy and chemical consumption [347], a decrease of nutrient levels in the effluent [292], and an increase of capacity of the plant [55, 56, 290]. An important point when designing and implementing a control system for wastewater treatment purposes is to make the control system as simple as possible [347]. This includes the usage of simple control laws and few sensors, which reduces the implementation and maintenance cost of the control system. The most recent studies give promising results of upgrading treatment plants to N and/or P removal using on-line sensors and appropriate control strategies [55, 266]. A Danish study on 14 treatment plants has shown that the introduction of control systems based on on-line sensors for ammonia, nitrate and phosphate has resulted in a more stable effluent quality and an increased capacity [266]. This study also concludes that it may be better to incorporate a considerable flexibility into the design, allowing the processes to be adjusted to the time-varying operational conditions. In another study, a simulation supported scenario analysis for the upgrading of a municipal wastewater treatment plant was used [55]. A comparison was made between extending the plant with new reactors, or re-design the existing reactors for increased performance. It was found that the most cost-effective solution was to create optimal aerobic and anoxic conditions within existing reactor volumes [55].

Despite all advantageous aspects concerning the benefits of on-line sensors, still many difficulties and wrong measurements are noticed in practical use of on-line sensors. Instrument faults are to blame for many control problems and plant upsets, but the actual culprits often are hard to identify or are completely overlooked [246]. Unfortunately, most sensor errors may go unrecognised, particularly if those signals are used in feedback control loops. Some typical causes of errors are: wrong sensor application, transmitter not properly calibrated, signal drift,

electrical problems of wiring, shielding, grounding, ... [246]. Another particularity related to on-line measurements for control purposes is the limitation of the measurement range of the sensors. E.g. typical values for nitrate used as set-point in the control strategy are around 1 mg N l^{-1} . The problem with this form of control is the inaccuracy of nitrate measurements in the lower measuring range, i.e. the range used for the controlling variable. Frequent recalibration and high maintenance efforts are required in such cases [164].

As the instrumentation systems become more complex, it becomes less satisfactory to deal separately with designers, instrument manufacturers, information transfer specialists and operators [334]. As a consequence of this there is e.g. a lack of process knowledge with instrument developers which can result in measurement systems which are very expensive but quickly become non-functional and mistrusted by operators [334]. Maintenance has always been one of the most important functions of wastewater treatment operation. The increasing complexity of treatment, required standards and necessary control systems with the resultant possible heavy costs make proper maintenance increasingly important [334]. On the one hand, on-line analyzer companies often suggest maintenance intervals of 1 week, or even 1 month, but on the other hand practical field studies show that for complicated on-line sensors (e.g. N and P analyzers), a daily inspection should be carried out with all on-line analyzers [250]. This inspection can vary from a visual inspection to a full cleaning and calibration. In general, 20 minutes per instrument and per day, including sample pre-treatment, are to be expected [250].

On-line measurements undoubtedly offer high benefits compared to off-line measurements, however, on-line measurements may not be considered as straightforward measurements. The successful use of on-line sensors does not only depend on the sensor itself, but also, and often most importantly, on the process conditions, the sample preparation, the maintenance, calibration, ... On-line sensor development is a challenging field for researchers because of these many aspects related to on-line measurements. The next section will present a number of sensors that are related to the results of this work, being the nutrient sensors.

4.2 Nutrient sensors: State of the art

The aim of this section is to present the current situation of existing nutrient sensors for on-line environmental applications. More particular, sensors for ammonium, nitrite/nitrate and ortho-phosphate will be presented. Besides the measurement principle, attention will focus on accuracy, precision, stability, maintenance requirements and common problems. Basically, the on-line analyzers make use of known laboratory measuring principles [307]. However, it is important to note that the measuring principles have often been modified (=simplified) compared to the standard laboratory method when applied to on-line analyzers [87].

4.2.1 Sample filtration

Most NH_4^+ , NO_3^- and PO_4^{3-} -analyzers require a sample stream free of suspended solids, which necessitates the use of a membrane filter sampling system [87, 250, 288, 289, 317]. Up to 46 % of the investment costs for the installation of an on-line analyzer can be due to the installation of a sampling and filtration system [250].

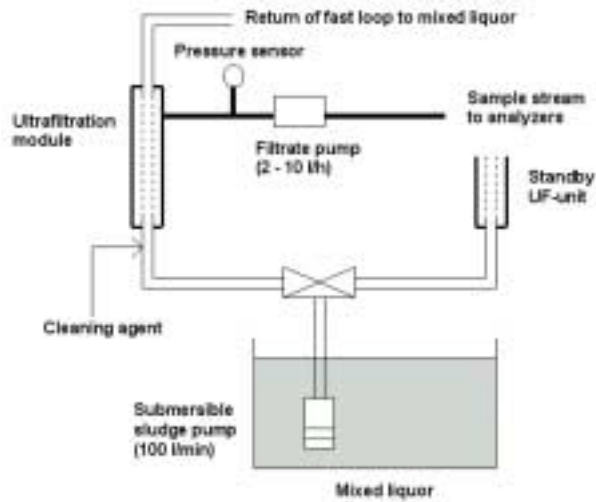


Figure 4.1: Diagram of a typical ultrafiltration (UF) module [89]

The sampling system is a crucial part of the measurement system. An ultrafiltration cross-filter system fed with a submerged shredding pump has been evaluated as being the most appropriate filter in activated sludge (influent, reactor, effluent) applications [220, 250, 288, 289, 317]. The membrane filtration is carried out by means of a cross-flow filter in which a large main flow (several $m^3 h^{-1}$) is pumped vertically through the filter thus allowing a small sub-flow (approximately $3 l h^{-1}$) to pass horizontally through the filter membrane. The unfiltered wastewater is returned to the plant/river. The filtered sample is distributed to the on-line meters [288, 289]. The high flow and the resulting shear forces prevent the deposit of small particles on the membrane surface [289].

In the past, other filter systems, like dialysis [220], a gauze filter equipped with a compressor for cleaning purposes [261], or smaller filter systems [289] have been tested but they often suffer from limited lifetime or clogging problems. Possible problems are case dependent (e.g. influent versus effluent). A schematic presentation of a typical sampling system is given in Figure 4.1. In practice, a set-up with two parallel ultrafiltration (UF) units (Figure 4.1) offers the possibility to maintain a continuous sample flow to the analyzers [87, 317]. Built-in filtrate flow meters or pressure drop meters can automatically switch off the active unit and activate the spare one. Another filter control system consists of an electronic permeate weighing system, for early clogging detection [105].

The self cleaning power of the filtration unit is mostly not sufficient for continuous operation. Therefore, cleaning with chemicals may be necessary at periodic intervals [250]. Automatic cleaning can be obtained by an air blow or a hypochlorite chemical treatment [317]. The manual maintenance frequency for an UF unit (e.g. manual cleaning) can vary from 1 day for wastewater influent to 2 – 6 weeks for an effluent type of water [250]. The lifetime of a

cross filter is typically 1 year [289]. The additional response time introduced by an UF unit can vary between 3 and 20 minutes [288,289]. Typical technical problems that occur when on-line filtration is implemented, are discussed in [96]. The authors have based their results on a case study of a newly developed on-line river water measurement station, and conclude that considerable time is needed for the testing, calibrating, site-adaptation, . . . before reliable measurements can be obtained. Similar experiences were also obtained in [41,96].

To overcome the difficulties related to sample filtration, recently on-line colorimetric sensors without need for a separate sampling and filtration unit have been developed [171]. Such devices are constructed as completely closed small containers, that are directly placed in e.g. the activated sludge aeration tank. The innovative part of this type of sensor is the particular membrane that contacts the sludge. The membrane functions as an ion sieve with, in practice, no mass transportation of water. The thickness of the membrane is 50 μm and the molecular weight cut-off of the membrane is approximately 100 Daltons. The lifetime of the membrane is tested to be well over one month, and no fouling of the membrane was observed [171]. The prototype sensors are believed to have a big potential for further refinement, and the authors suggest that the use of the sensors can be extended into other areas such as monitoring of receiving waters, sewer and drinking water systems [171]. However, no practical results in these areas are available yet. Also, the announced commercialisation within wastewater treatment operation has not been established, which make us believe the initial reports were too optimistic.

4.2.2 Ammonium analyzers

On-line ammonium analysis is mostly performed with a potentiometric (gas electrode) or a colorimetric method.

In the potentiometric or electrochemical method, the pH in the sample is raised above 11, thus converting all NH_4^+ to NH_3 . The NH_3 is then measured by means of an NH_3 gas sensitive electrode [289]. The gas electrode based ammonium analyzers are shown to have the widest measuring range (0.1–1000 mg N l^{-1}) [250], and the shortest response time (less than 8 minutes) [175,250,289]. Tests in nutrient removal activated sludge plants have shown that the electrochemical method is the more accurate and reliable [289], has the lowest reagent expenses [289] and is free of interfering ions [175,289,326]. A disadvantage is that some commercial electrode monitors lack temperature compensation capabilities [289,326]. Some other reported problems include air building up under the electrode tip and electrode drifting [11]. Electrochemical methods perform better in effluents than in influents, because of the lower demand of chemicals and lower maintenance needs in effluents [165]. A recent development is the measurement of ammonia with a fibre optical analogue of the conventional electrochemical ammonia electrode [103]. Despite that no field experiences are available yet, the authors anticipate that many positive developments in this field are to be expected in the years to come.

Colorimetric flow injection analysis (FIA) is most frequently applied for the analysis of ammonia in a diverse range of liquid samples, including those using the Berthelot reaction, in which ammonia reacts with phenol and hypochlorite to produce indophenol blue, and those using Nessler's reagent to form a yellow azo dye [14]. The higher chemical reagent consumption [289], the slower response time (5 to 20 minutes) [250], the sensitivity to temperature variation

[326] and possible interferences from NO_2^- , S^{2-} , Fe^{3+} and ethanolamine [326] are some of the drawbacks noticed in these systems.

The carryover effect, this is the situation where the current measurement is affected in some way by the previous measurement is a known problem in many FIA systems [126]. Carryover is caused by a variety of factors, not all of which are completely understood.

A further spectrophotometric method utilises gas diffusion, in which the sample is mixed with an alkaline stream to convert all dissolved ammonium ions to gaseous ammonia. The latter diffuses across a hydrophobic microporous membrane into an acid-base indicator stream, and the resulting colour is detected [126, 127, 220, 221]. This method is particularly well suited to complex sample matrices since the membrane provides a physical barrier, excluding potential interferences from the measured stream [14]. Also a relatively high measurement rate and a lower reagent consumption are reported with this method [127]. Unsatisfactory long-term stability and unreliability of this type of analyzer were found [220], but technical improvements of the system lead to more satisfactory results, especially a longer lifetime (> 6 months) of the gas diffusion membrane [127, 221]. Alkylamines are reported as interferences for ammonia determination with gas diffusion methods [14]. For very low NH_3 levels (e.g. $1 \mu\text{M}$), atmospheric CO_2 has to be removed from the acid-base indicator solution for accurate determinations [14]. Despite all improvements and efforts, such type of sensors cannot be left unattended for more than 1 week [14, 221].

A few measurement systems that do not require sample filtration are reported. First, an optical-chemical sensor based on a flow-through cell with a microporous PTFE membrane with immobilized pH indicator was optimized to analyze wastewater without pre-treatment of the sample [255]. The long term stability of this type of sensor is better than 6 months, and the response time depends on the ammonium concentration and ranges between 1 and 60 minutes. Second, a FIA based auto-calibrating colorimetric NH_4^+ analyzer is reported, with a response time of less than 5 minutes [171]. The response time could be limited, on the one hand because the analyzer could immediately be placed in the mixed liquor, on the other hand because colour reactions did not have to complete for a reliable concentration estimation. Although the analyzer is operated continuously, reagent consumption is limited to less than 3 litres per month through use of semi-micro continuous flow analysis (μCFA). For comparison reasons, a conventional FIA system as presented before consumes around 20 litres of reagents per month [127]. The most innovative part of this system is the choice of the membrane, as tests show very little, if any, fouling problems due to the membrane materials used. Third, an ammonium meter based on gas diffusion, and coupled to a hydroxide electrode was developed for on-line monitoring of a pilot-scale trickling filter [339]. The ammonium meter consists of a beaker, a stirrer, a hydroxide sensor, a temperature sensor and a slope pump. The slope pump continuously pumps the sample, together with a strong NaOH solution, into the beaker. Because of the sodium hydroxide, the ammonium entering the beaker turns into ammonia, which, due to differences in partial pressure, diffuses through a membrane into an electrolyte surrounding the hydroxide sensor. Because the electrolyte has a high and approximately constant concentration of ammonium chloride, the hydroxide sensor gives a measurement of the ammonia concentration in the electrolyte through an equilibrium relation, and hence, the ammonium concentration in the beaker [339]. The step response time is rather slow (around 50 minutes before the meter reaches 90 % of the end-value), and the author indicates that some information about the effluent transients is hidden by the dynamics of the ammonium meter. Results on long-term field

Table 4.1: Comparison of different on-line ammonium analyzers

Principle	Ref.	Detection limit	Range	Accuracy	R.s.d.	Maintenance interval	Response time
		$(mg\ NH_4^+-N\ l^{-1})$		(%)	(%)	(weeks)	(min.)
NH ₃ sensitive electrode	[289]		0.5–10	+4	8	1	10–15
	[11]		> 1	–28 to +178	40–120	1	10–15
	[288]		0–12	–4 to –20	12–33	1	
	[165]		0–100			< 1	
FIA	[326]	0.05–0.2	0–20000		1–14	1	6–12
	[288]		0–10	–7 to +3	2–32	1	
	[165]		0–80			1–4	
FIA + GD unit	[326]	0.17–0.9	0–100		0.7–18	1–4	2–21
	[126]		0.5–50			1	
optical/chemical (no filtration)	[14]	0.6	1–100	±15	1–5	1	30
	[255]	0.01	0–14		9		1–60
μ CFA	[171]	0.1	0–25	±5	3	4	< 5

experience of this type of sensor are not reported yet.

Alternative methods for ammonium measurement, but at this moment only used in laboratory off-line analysis include a multi-component determination in which chloride and ammonia are determined in the same sample with a single FIA system [306]; a centrifugal ammonia analyzer [186]; laboratory FIA systems based on the Berthelot reaction [232]; salicylate and enzymatic methods [143]. Typically these methods have low detection limits in the order of magnitude $1 - 50\ \mu g\ N\ l^{-1}$, but are not (yet) suited for on-line applications.

Comparison results of field studies with different types of ammonium sensors are presented in Table 4.1. It can be seen that the reported values for detection limit, range, accuracy and repeatability vary very much depending on measurement principle and the particular case study.

A detailed field test with 9 commercial ammonium sensors on the same location reported differences of more than 200 % between measurements performed by the different sensors under test [326]. This is illustrated in Figure 4.2. An important offset difference between different sensors was noticed. The main concern was that some monitors often failed and needed extra intervention and cleaning, multiple trials of calibration, changing of plastic pipes or other parts, ... This field test has shown that every detail is important when installing and running a monitor. Particularly the filtration unit and piping are among the high maintenance parts.

4.2.3 Nitrate analyzers

Numerous methods have been proposed for the determination of nitrate. Commercial on-line nitrate sensors are mainly based on ion-selective electrodes, colorimetric reactions or UV absorption. Due to many interferences of other chemical species, alternative systems have been

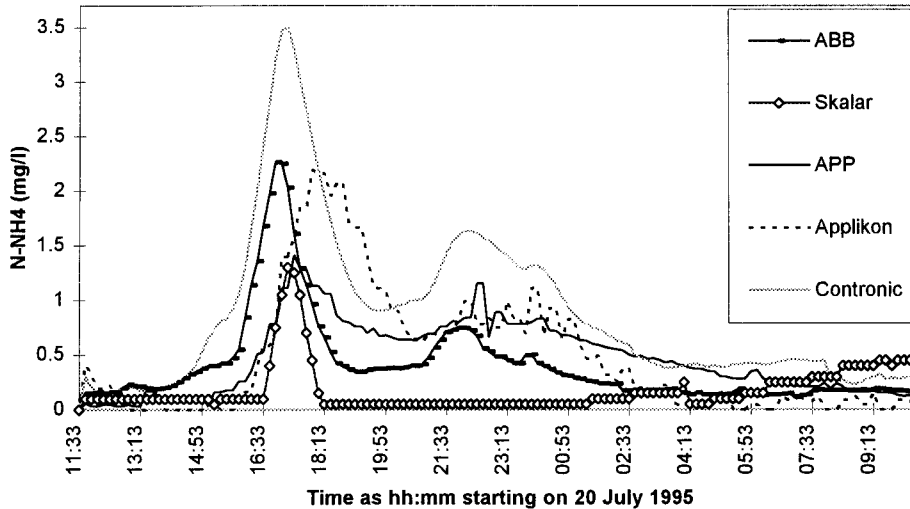


Figure 4.2: Field test of NH_4^+ monitors [326]

developed for specific purposes. However the latter are often not commercialised as on-line sensor. Some of these ‘alternatives’ will be discussed here too.

The analyzers based on UV absorption are considered to be the best choice for field-use [87, 261, 289]. The advantages of this type of sensor are: A short response time (10 seconds), low maintenance needs and no need for chemicals [261, 289]. Due to interference of particles with the UV absorption measurement, an ultra filter is needed for reliable operation [261]. Nitrate and nitrite are measured together, as they both absorb UV at 210 nm [269]. A calibration frequency of only once in 6 months can be sufficient [261], but in some applications UV absorption NO_3^- analyzers were reported to have a moving baseline, which could be solved by a frequent automatic zero calibration [11]. In some applications, interferences of UV-absorbing organic matter (e.g. aromatic compounds) may influence the measurements [11, 165, 269, 288, 289]. A possible solution is the dual wavelength approach, where the strong absorbance of nitrate in the 210 nm region is measured relative to the absorbance in a region where nitrate does not absorb. The wavelength 275 nm can be used to compensate for mainly organic interferences [104, 269].

The electrochemical meters based on an ion-selective NO_3^- -electrode are good because of their low pre-treatment demand resulting in a short response time (less than 10 minutes), and their low chemical consumption [250, 289]. However the nitrate electrode is sensitive to electrode drift [221], disturbing ions (e.g. HCO_3^-) and fouling of the electrode [261]. Chloride and bicarbonate ions interfere when their weight ratios to NO_3^- -N are > 10 or > 5 , respectively [104]. Erratic responses have been noted when the pH and ionic strength are not held constant

in all samples and standards [104]. Another drawback of this system is the limited lifetime (2–3 months) of the expensive electrodes [261]. Sample pre-treatment, frequent automatic calibration (including pH and ionic strength corrections) and availability of a spare electrode can partly alleviate such problems [87].

Colorimetric NO_3^- analyzers are considered to be the most accurate [165], but also have the highest maintenance needs, making them less favourable for field-use. Some studies illustrate that these sensors are sometimes too unreliable for use as process equipment in situations where several days unsupervised operation is necessary [220, 289]. Colorimetric sensors first convert NO_3^- to NO_2^- . This reduction step can either be done with a Cd column [126, 220, 288, 289] or with hydrazine [104, 171, 288]. In the following step, a yellow or red azo-dye which can be measured optically is formed with NO_2^- . In such a way NO_2^- eventually present in the sample is measured together with NO_3^- . The installation of two injection valves, one before and one after the Cd column, results in a double peak, which can be associated with nitrate and the sum of nitrate and nitrite [165, 221]. In order to minimize the analyzer complexity, it is not worthwhile to include this extra step in cases where NO_2^- is normally quite low [126]. Some of the problems of the unreliability in the field can be related to the Cd column. Suspended matter can restrict the sample flow, oil and grease will coat the Cd column, reducing its efficiency [104]. A reliable sensor, without filtration needs was realised by placing the analyzer directly in the measurement stream (e.g. mixed liquor) and using a membrane device that functions as an ion sieve [171] (see also section 4.2.1).

Another type of NO_3^- analyzer is a flow-injection analysis system with an amperometric detection system [269]. Nitrate is determined as nitrite after reduction in a Cd column. The working electrode is glassy carbon modified with a crosslinked redox polymer. Its main advantages are twofold; first of all no sample pre-treatment is needed and fast sample throughput is possible. Secondly, with this measurement technique the effect of interferences is reduced considerably since only species with an appropriate redox potential are detected with these polymer modified electrodes. Only nitrite and iron could possibly interfere in the reduction process [269]. At this stage the sensor has been designed for the laboratory environment only.

Other continuous flow methods, but so far only used off-line, use titanium(III)chloride as reducing agent for NO_3^- [9, 15]. Nitrate can be reduced to nitrite with TiCl_3 , and determined spectrophotometrically as usual [9], or it can be reduced to ammonia in alkaline medium by TiCl_3 [15]. In the latter method, the interference of nitrite initially present in the sample can be masked with sulfonic acid. A NH_3 determination before and after the reduction step makes a simultaneous determination of nitrate and ammonium possible. The detection limits of these methods are between 3 and $20 \mu\text{g NO}_3^- \cdot \text{N l}^{-1}$. Despite the fact that from a technical point of view, these methods are not more complicated than e.g. the Cd reduction method, no examples were found where this principle is implemented as on-line sensor.

The usual reducing agents for NO_3^- are not sufficiently specific and it is normally difficult to obtain a quantitative reduction of nitrate to nitrite [34]. Methods based on enzymatic or bacterial reduction of nitrate are assumed to be more specific [34] and free from interferences [136]. However, a possible drawback and reason why these methods are not found in commercial sensors, is the necessity to have specialised personnel for the preparation/handling and use of enzymatic or bacterial suspensions. Consequently, such methods are typically found in laboratory environments instead of in the field. Although in special cases (e.g. carbonization wastewater), where commercial available on-line nitrate sensors were not suitable due

to interferences, an on-line FIA system including a biological nitrate to nitrite reduction using immobilized *E. coli* cells combined with selective nitrite determination was implemented [196].

Basically there are two different approaches to the biological conversion of nitrate. First, there are the enzymatic methods, where the enzyme is used in purified or unpurified form (including other cell material); the enzyme can be immobilised in pellets or kept in suspension. Second, living cell methods exist where the biological nitrate conversion is mostly obtained with a specific bacterial strain. The latter method offers some advantages like: an increased electrode lifetime, regeneration of electrode response, and the elimination of tedious, time-consuming enzyme isolation and purification steps [140]. The use of bacteria would be particularly superior for systems in which more than one enzymatic step along with cofactors are required to produce the measured product [140]. A disadvantage of living cell sensors is their higher sensitivity for toxic substances in the measurement solution.

Enzymatic methods which reduce nitrate into nitrite using nitrate reductase were reported by [34, 137, 167, 196, 342]. The nitrite formed can be measured by a standard diazoting colorimetric method [34, 167, 196] or by fluorometric detection in which NADH is used as electron donor [137]. In these methods special care has to be taken that NO_2^- is not further reduced to N_2O etc. [167]. The detection limit of these methods is around $10\text{--}50\ \mu\text{g NO}_3^- \text{-N l}^{-1}$ in laboratory conditions [137, 167]. An on-line sensor using this method [196], in which bacterial *E. coli* cells were immobilized in spherical alginate beads with diameter $4\text{--}5\ \text{mm}$ obtained a lower sensitivity compared to other commercial available instruments. The detection limit was around $1\ \text{mg NO}_3^- \text{-N l}^{-1}$, which is still sufficient for most monitoring purposes. The sensor used a built-in continuous data correction to compensate for activity loss of the biologically catalysed reduction process [196].

An enzymatic sensor in which nitrate was reduced to nitrite (using nitrate reductase), followed by a second reduction step to ammonia (using nitrite reductase) overcame the problem that the colorimetric NO_2^- measurement method is rather complicated [136]. The ammonia produced is monitored, using an air-gap ion-selective electrode. A measurement range between 0.7 and $140\ \text{mg NO}_3^- \text{-N l}^{-1}$ was obtained [136].

A novel approach to the development of bioselective sensors has been the use of intact bacterial cells in place of isolated enzymes at the surface of a membrane electrode [140]. A potentiometric sensor has been devised for nitrate by coupling the bacterium *Azotobacter vinelandii* with an ammonia gas sensing electrode [140]. The response of this sensor was found to be linear over the concentration range 0.1 to $10\ \text{mg NO}_3^- \text{-N l}^{-1}$. The electrode was useful for a period up to two weeks. The bacterial electrode must be stored in growth medium when not in use. Another type of microbial NO_3^- -electrode consists of immobilised *Pseudomonas aeruginosa* and a carbon dioxide gas-sensing probe [114]. In this system nitrate was determined by measuring carbon dioxide with a gas sensing probe under anaerobic conditions accompanying an excess carbon source, ethanol in this case [114]. As carbonate interfered with the determination, pre-treatment was made to remove CO_2 by adjusting the pH of the sample at 4.0 and bubbling with nitrogen gas for 1 minute. The electrode was tested on samples from a wastewater treatment plant. The cycle time for 1 measurement was 30 minutes and the response was linear between 5 and $50\ \text{mg NO}_3^- \text{-N l}^{-1}$.

On-line analyzers for total nitrogen also become available [73, 141, 250]. The measurement principle of these sensors can be based on the hot catalytic conversion of bonded nitrogen to

Table 4.2: Comparison of different on-line and semi on-line[‡] nitrate analyzers

Principle	Ref.	Detection limit	Range	Accuracy	R.s.d.	Maintenance interval	Response time
		($mg\ NO_3^- \cdot N\ l^{-1}$)		(%)	(%)	(weeks)	(min.)
UV absorption	[250]		0.1–100				< 5
	[288]		0–5	–3 to +260	5–20	1	
	[165]		0–50				
	[289]		1–7	< 0.5	4	4	3–9
	[11]			+47	32	1	
NO_3^- selective electrode	[269] [‡]	0.4	0.4–30	2–4	1.7		
	[288]		0–10	–1	15	1	
Colorimetric with Cd	[288]		0.5–7	–10	20–24	1	
	[165]		0–50			1	20
	[126]		0.5–20			1	
	[218]	0.1	0–4	±3	< 1		
Colorimetric with hydrazine	[156]	1	0–25				
	[22, 171]	0.07	0–10	±10	5	4	5
Enzymatic $NO_3^- \rightarrow NO_2^-$	[196]	1					

nitrogen monoxide [250] or on in-line UV catalysed oxidation of organic nitrogen to nitrate, which is measured colorimetrically [73]. The latter method found recoveries of different nitrogen forms between 90 and 100 %. However comprehensive practical experience is not yet available [250].

A comparative literature review on different nitrate analyzers is presented in Table 4.2.

4.2.4 Phosphate analyzers

The majority of on-line phosphate sensors are colorimetric methods, thus requiring a filtration unit prior to the analyzer unit. As a consequence of the fact that no phosphate selective electrode is available, often FIA methods are chosen for this measurement [221]. Phosphate can either be determined as ortho-phosphate or as total phosphate. Total phosphate analysis requires more manipulations because phosphorus compounds must be decomposed into ortho-phosphate.

Two colorimetric ortho-phosphate analysis methods are employed: the molybdenum blue method and the vanado-molybdate method [250]. The molybdenum blue complex is formed by the reduction of the reaction product between ortho-phosphate and ammonium molybdate. The reducing agents that can be used include ascorbic acid [288] and stannous chloride (Tin(II)chloride) [32]. Some reducing agents are reported to have a limited lifetime so that the reagent autonomy is reduced to maximum 1 week [220]. Tin(II)chloride as reductant makes that the wavelength maxima of the blue complex are at 690–700 nm compared with 882 nm for ascorbic acid. This offers the advantage of greater sensitivity when a solid state detector

which uses a red light-emitting diode light source ($\lambda_{max} \approx 635 \text{ nm}$) is used [32]. Similar to the molybdenum blue method, the vanado-molybdate method also starts with a reaction between ortho-phosphate and ammonium molybdate to form molybdophosphoric acid. In the presence of vanadium, yellow vanado-molybdophosphoric acid is formed [104]. This compound is measured photometrically at a wavelength of usually 470 nm .

Field studies have shown that automatic ortho-phosphate analyzers are more stable and reliable than ammonium or nitrate analyzers, mainly because no membranes and columns are needed [220]. The chemical expenses for ortho-phosphate determinations are very high which is, however, to some degree balanced by a low purchase price [289]. More recent studies [288] show that phosphate analyzers have been optimized in the last 5 years, so that its operating cost is nowadays comparable with the operating costs of ammonium and nitrate analyzers.

Despite all technical improvements and longer autonomy of the analyzers noticed in the last years, the weakest part of the measurement chain remains the filter system [33]. Further, the molybdenum blue colour complex can give precipitation problems on the inner walls of the transport tubes and on the detector's flow cell windows [126]. In such situations more frequent manual cleaning (e.g. 0.5 M HCl) is advised. The use of ascorbic acid as reductant for the molybdenum blue complex was found to be unaffected by the presence of organic phosphates, pyrophosphates and polyphosphates [39].

Besides colorimetric measurement systems, other methods are available too, like the combined enzymatic and amperometric FIA biosensor system [174]. This sensor contains two immobilised enzymes (nucleoside phosphorylase and xanthine oxidase). In a laboratory set-up, response times were less than 6 minutes. However, no on-line results with this sensor are available [174].

In water and wastewater systems, total phosphorus (TP) concentration is commonly used as an indicator of water quality and as control parameter in wastewater treatment processes. On-line techniques for TP are available [30, 73, 141]. They are based on a colorimetric measurement of ortho-phosphate after a destruction of TP into ortho-P. The methods differ in the way the on-line destruction step is performed. Polyphosphates can be hydrolysed with acid and heat, while organophosphates can be digested with UV-catalysed persulfate oxidation [73]. Others use nitric-sulphuric acid, perchloric acid or potassium peroxodisulphate as oxidising agent [31, 141], eventually at high temperature and pressure. Other on-line digestion systems include a flow-through reactor in a modified microwave oven [30] or a combined UV/thermal induced digestion [31, 73]. The latter method can be used without sample pre-treatment prior to analysis. For separate determinations of ortho- and polyphosphates, no on-line method is reported, but rapid laboratory methods like anion exchange chromatography are available [132].

A comparative study of different phosphate analyzers is presented in Table 4.3. The accuracy and repeatability of phosphate analyzers is better than for ammonium and nitrate analyzers. This can possibly be due to less interferences in the phosphate colorimetric reactions.

4.3 Developments in effluent and river water monitoring

The detection of accidental discharges of pollutants in effluents and river waters is important to get more insight in the sources of pollution and take the necessary control actions. In this

Table 4.3: Comparison of different on-line phosphate analyzers

Principle	Ref.	Detection limit	Range	Accuracy	R.s.d.	Maintenance interval	Response time
		($mg\ P\ l^{-1}$)		(%)	(%)	(weeks)	(min.)
Colorimetric molybdenum blue	[22, 171]	0.2	0–10	± 5	3	4	5
	[126, 220]		0.5–50			1	
	[250]		0.01–5				< 12
	[288]		0.2–4	–1 to +23	5	1	
	[165]		variable			1	20
Colorimetric vanado-molybdate	[32, 33]	0.05	0–25	–2.5	0.4	> 1	
	[289]		0.05–1	–1	4	1	8–13
	[11]			3	9	1	
	[250]		0.1–20				< 12
	[288]		0–4	–4 to +40	8–13	1	
TP (including digestion step)	[165]		0–15			> 1	
	[156]	0.3	0–25				
	[30]	0.09	0–18	$\pm(1-30)$	2		
	[31]	0.15	0–18	$\pm(1-20)$	1		

section, a number of methods and sensors are presented that can be used for alarm generating purposes. Most of the presented sensors are on-line systems, measuring non-specific substances. Special attention is given to UV based sensors, because their application area is most similar to the developed buffer capacity based sensor in this work.

A number of specific techniques for evaluating the biological quality of river waters have been developed in the past 15 years. Two categories of methods can be distinguished: First, off-line methods based, among others, on quality indices. For example, in Belgium, the BBI (Belgian Biotic Index) [193, 313] is used, while in the United Kingdom, the microcomputer-based system RIVPACS (River InVertebrate Prediction And Classification System) [343, 344] is used to evaluate the biological quality of rivers. Indices are useful for long-term evaluations (e.g. over a period of years), but are not suitable for on-line problem detection. The second category is more interesting in the framework of this work and considers on-line biosensor methods for environmental biomonitoring and especially for the detection of water pollutants. These systems are developed in view of continuous and real-time analysis. A review and state of the art of biosensors for environmental monitoring is given in [212]. Three categories can be defined: biosensors using aquatic vertebrates and invertebrates (fish, microcrustacea, bivalves), cellular sensors (bacteria, yeast, microalgae [297], ...) and biosensors measuring an 'affinity' response and a specific binding between enzyme/substrate or antibody/antigen [212]. These biosensors can be very sensitive to specific or non-specific toxicants in low concentrations ($\mu g\ l^{-1}$). Some interesting examples in the framework of this work are the following [212]:

- Ammonium sensitivity ($110\ \mu g\ N\ l^{-1}$) of the fish *Oncorhynchus mykiss*, detected by ventilation after 17 minutes of exposure.
- Phosphate sensitivity ($16\ \mu g\ P\ l^{-1}$) of the fish *Gnathonemus petersii*, detected by emission of electrical signals after 15 minutes of exposure.

- Nitrate sensitivity (2 mg N l^{-1}) of immobilized bacteria *Pseudomonas aeruginosa*, detected by CO_2 respiration after 15 minutes of exposure.

It should be mentioned that the first two examples are non-specific, because these fish are sensitive to a range of toxicants. Taking into account the sensitivity of the mentioned biosensors, they are only applicable in low-polluted rivers. Practical experiences with an automatic biosensor measurement station on a river in Flanders used for drinking water intake are described in [172].

On-line physico-chemical river water quality can be assessed with automated measurement stations. Dissolved oxygen, ammonia, pH, electrical conductivity, turbidity, temperature and flow were among the first determinants to be included in automatic measurements relating to the quality of the water [274]. Although a high degree of automation can nowadays be implemented at the levels of measurement, maintenance, data communication and data management, the resulting data series easily inherit errors and uncertainties [41, 96].

Sensors based on UV absorption were already discussed in section 4.2.3 for the purpose of nitrate measurement. However, this type of sensors is also used for the monitoring of organic material in wastewaters and river waters. Useful correlations have been established between the COD in various types of waters and the UV absorbance at 254 nm [201]. Absorbance measurement in the UV spectrum range is very rapid and a sufficiently precise method permitting a simple automatic indication of the organic pollution extent in some types of surface waters [201]. However, some compounds (especially saturated hydrocarbons and carbohydrates), and also urea, either do not absorb or only absorb below 200 nm , and thus cannot be considered with UV spectrophotometry [287]. The UV absorption spectrum is dependent both on the chemical nature and concentration of their absorbing dissolved components and on the physical characteristics and concentration of particulate material that induces light scattering. Thus, the UV spectrum is related to the total suspended solids and a part of the dissolved components (organic and mineral) [287]. The negative influence of particulate material on the correlation between e.g. the absorbance at 254 nm and the COD or TOC can be reduced with the help of measurements at a second wavelength (e.g. 380 nm) [182]. A deterministic deconvolution method has been applied on UV spectra [287]. In short, an UV spectrum can be considered as a linear combination of defined spectra (reference spectra) of compounds in the water. The acquisition of the reference spectra must be carefully carried out for a given type of water. The deconvolution method consists in finding a linear combination of reference spectra that reconstitute the real spectrum. The presence of an unknown pollutant in a sample can easily be detected through a poor restitution, corresponding to an unusual spectrum for a wastewater or a surface water sample. The application of the latter described technique has to be seen in the survey of discharges in rivers and the control of wastewater treatment plants. However, note that the spectrophotometric developments are waiting for the design of a simple field portable device [287].

Fluorometry-based sensors have found useful applications in the monitoring of activated sludge processes [125, 282]. The principle of the measurement is based on the exposure of a sample to light at a certain wavelength and subsequently the registration of resulting fluorescent light at another wavelength. The application in [125] is based on the property that intracellular reduced NAD(P)H (nicotinamide adenine dinucleotide (phosphate)) fluoresces at 460 nm when the cells are irradiated by 366 nm light. In a case study with an alternating ac-

tivated sludge process, an abrupt rise in the fluorescence signal was found to occur upon the transition from anoxic to anaerobic conditions [125]. In the same activated sludge application area, a multiple excitation–multiple emission fluorometry technique was tested [282]. A correlation was developed between COD-removal rate and the fluorescence signals. Stepwise multiple regression and principal component analysis were employed for the data analysis. In another study, BOD measurements in river and effluent samples were compared with absorbance and fluorescence determinations on the same samples [58]. Absorbance at 650 nm showed a moderately high, positive correlation with BOD ($R^2 = 0.48$) for sewage effluent samples. The use of absorbance measurements in the development of a relatively inexpensive on-line monitor would provide an early warning system of deteriorating quality in a sewage effluent discharge [58]. No clear association was found between the BOD of industrial effluents or river waters with absorbance values at 4 wavelengths (250, 350, 400 and 650 nm). Similarly, no clear association between fluorescence and BOD was observed for all samples. The only benefit of the use of fluorescence is that measurements are less influenced by sample turbidity than are absorbance data [58]. In a recent study, effluents from sewage wastewater treatment plants showed characteristic fluorescence signatures when excited by UV light in the 240–300 nm wavelength band [7]. A nice correlation between the BOD and the normalized fluorescence intensity at 340 nm (excitation wavelength 248 nm) was obtained ($R^2 = 0.94$). However, the results were obtained on only 1 selected domestic wastewater treatment plant, and the measurement conditions were optimized for that plant, which prohibits comparisons with e.g. the results described in [58]. The authors conclude that the fluorescence technique has potential for use in noninvasive continuous water quality monitoring. However, the necessary equipment is still very expensive and bulky, and further research is still necessary before commercial applications are to be expected.

4.4 Titrimetric sensors and applications

Nowadays, the term ‘titrimetry’ is used in a much broader sense than it was initially defined for analytical chemistry purposes. Originally titrimetry was used for ‘end-point’ titration methods only, but in the current literature one can notice that the criterion for a titrimetric sensor includes all kinds of systems where consecutive acid or base additions to a sample, followed by a pH measurement, are performed. In the following paragraphs the presented sensors are selected on this broad criterion.

A titrimetric sensor basically consists of two different parts. First, there is a ‘wet’ part, including sample preparation, pH adjustment and titration. A major advantage of these systems is that filtration of the sample is mostly not necessary. Despite the fact that this technology is well suited for field applications, most of the titrimetric systems found in literature are based on laboratory set-ups. Second, there is a ‘data processing’ part, the most important and diverse part. In the literature that was found on this topic, often the ‘wet part’ is limited to a few lines describing which titrator and which conditions were used.

It is straightforward that the data analysis of a titration experiment is the real heart of a titrimetric sensor. Some publications only discuss chemical and mathematical aspects of titration data, without pointing to a specific application field. The application fields for titrimetric sensors are twofold. First, there are the on-line applications, used for process control purposes.

These titrimeters often work with only a few titration points and a simplified and robust data interpretation. One of the major application fields in this area is the control of anaerobic digestion where bicarbonate and/or volatile fatty acids (VFA's) can be monitored on-line with a titrimetric sensor. Second, there are the off-line applications, where the data processing often is more complicated. Some of the applications like analysis of wine, cheese whey, milk, tomatoes, ... are uniquely lab applications. However, many of these data processing techniques discussed as off-line systems can possibly be adopted to field-use in other application areas.

4.4.1 Data interpretation of a few specific points of a titration profile

The determination of bicarbonate and total volatile acid concentration in anaerobic digesters is a popular application area for this type of titration sensors. These methods are based on the physico-chemical equilibria in anaerobic digesters, which are summarized and mathematically modelled in [239]. The pH in a normally functioning digester is close to neutral and controlled by a buffering system that consists of bicarbonate and volatile fatty acids (VFA). Because fluctuations of organic loading rate or other operational conditions may often cause variation of VFA concentration, VFA is a useful parameter for digester control [12]. Organic or toxic overload in anaerobic digesters can lead to a higher acid production or to a reduced production of methane from acetic acid. Both situations lead to an increase of VFA concentration in the reactor. Consequently, a decrease of bicarbonate alkalinity and of pH and an increase of CO₂ partial pressure in the gas [241]. Depending on the buffer capacity in the digester, the drift in pH values could be negligible until the operating conditions of the digester are appreciably out of balance, while the variation of bicarbonate concentration becomes readily apparent at any buffer concentration. Therefore, the potential of bicarbonate concentration both as stability indicator and control variable was found to be as good or better than the pH [241].

To maintain a quasi-constant pH, sufficient buffering capacity should be provided. Traditionally, the alkalinity measurement (determined by titrating a sample to a pH of 4.3) is used to estimate the buffering capacity in an anaerobic digester. However, the total alkalinity includes all the bicarbonate and approximately 80 % of the volatile fatty acids [12]. Because only bicarbonate is usable for neutralising VFA's, total alkalinity does not represent the available buffering capacity in a digester. A simple, alkalimetric method is described that can be used to determine bicarbonate and total volatile fatty acid concentrations in anaerobic digesters by a two-stage titration [12]. The sample is titrated through two stages (first to pH 5.1, then from pH 5.1 to pH 3.5), and the VFA and bicarbonate are calculated by means of equations (4.1) and (4.2) that were derived from the acid-base equilibrium equations and mass balances [12].

$$A1 = \frac{[\text{HCO}_3^-]([\text{H}^+]_2 - [\text{H}^+]_1)}{[\text{H}^+]_2 + K_1} + \frac{[\text{VFA}]([\text{H}^+]_2 - [\text{H}^+]_1)}{[\text{H}^+]_2 + K_2} \quad (4.1)$$

$$A2 = \frac{[\text{HCO}_3^-]([\text{H}^+]_3 - [\text{H}^+]_1)}{[\text{H}^+]_3 + K_1} + \frac{[\text{VFA}]([\text{H}^+]_3 - [\text{H}^+]_1)}{[\text{H}^+]_3 + K_2} \quad (4.2)$$

A1 and A2 : molar equivalents of acid consumed to the first and second end-points (*M*)

[HCO₃⁻] : bicarbonate concentration (*M*)

- [VFA] : volatile fatty acid concentration (M)
 $[H^+]_{1,2,3}$: hydrogen ion concentrations of the original sample and at the first and the second end-points (M)
 K_1 : first dissociation constant of carbonic acid ($6.6 \cdot 10^{-7}$)
 K_2 : combined dissociation constant of the volatile fatty acids ($2.4 \cdot 10^{-5}$)

It was found that the experimental pK_a 's for bicarbonate and VFA (considered as acetic acid) were 0.14 pH units lower than the corresponding thermodynamic dissociation constants. The ionic strength in anaerobic digestors that have a total alkalinity of 1000 to 1500 $mg\ CaCO_3\ l^{-1}$, is typically around 25 $mmol\ l^{-1}$. The authors indicate that this ionic strength largely explains the difference between the experimental and thermodynamic dissociation constants. This method was evaluated in standard solutions of mixtures of bicarbonate and volatile fatty acids. The average recovery in all of the measurements is more than 96 % [12].

A further refinement of this method uses 5 pH points instead of 3 [197]. The titrimetric method incorporates a computer program to calculate the necessary results from a 5 pH point acid titration experiment. The 5 pH points include the initial pH, a pH pair (pH_1 , pH_2) located symmetrically around the first dissociation constant of the inorganic carbon buffer, and a pH pair (pH_3 , pH_4) located symmetrically around the dissociation constant of the acetate buffer. An extra benefit of this method is that errors in pH due to the residual liquid junction effects or poor calibration can be determined and corrected. This was achieved by including an asymmetrical pH pair as set-points around the theoretical pK_a (e.g. pH pair (pH_1 , pH_3) located around the first dissociation constant of the inorganic carbon buffer). An average standard deviation on the estimates of 5–8 % around the expected values were found [197]. The authors point out that in anaerobic systems, weak acids/bases other than bicarbonate and VFA may be present, e.g. phosphate, ammonium, sulfide, etc. which influence the estimates derived from the 5 pH point titration described above. However, if their total species concentrations are measured by wet chemical methods, their presence can be taken into account readily, and their effect can be eliminated. This method was tested for measurement of HCO_3^- and VFA's in primary sludge, settled sewage and anaerobic digester sludge (under process failure conditions) [65]. Comparisons were made between this titrimetric method, a colorimetric method and an HPLC method for VFA determination [65]. The titrimetric method was found to over-predict the VFA content of failed anaerobic digester samples by approximately 15 %, relative to the colorimetric method. No immediate explanation was found. Good recovery of VFA from spiked samples of settled sewage in the range of 40 to 80 $mg\ l^{-1}$ as acetic acid was obtained. Using pure solutions of carbonate and acetate, the detection limits for the titrimetric method were found to be 10 $mg\ l^{-1}$ as $CaCO_3$ and 5 $mg\ l^{-1}$ as acetic acid [65]. Scrupulous attention to pH probe maintenance and calibration was found to be very important, particularly at low concentrations when the systematic pH error estimate by the computer program cannot be relied upon.

A recent study compares the 5 pH point method described above with a new 4 pH method [46]. It is shown that both methods have similar accuracy for VFA determination. The 5 pH point method does make an estimation of the carbonate alkalinity, whereas the 4 pH point method doesn't. From a practical point of view the 5 pH point method does not require reaching target pH points exactly, but allows a tolerance of ± 0.1 pH units. A disadvantage of the latter method is its necessity to handle both a strong base and a strong acid. The initial pH of the samples is frequently below pH 6.7 (= first target pH point in the 5 pH point procedure); thus the procedure requires a pH increase to begin with. The first target point of the 4 pH point

method is at pH 5, which is so low that a base is actually never in demand [46]. In this respect the 4 pH point method is regarded as superior, but whenever there is interest in the specification of the carbonate alkalinity, the 5 pH point procedure is recommended.

In the same application area of anaerobic digestion, an automatic on-line titration unit for routine or event-initiated monitoring of alkalinity, buffer capacity and VFA levels is presented [228]. The acid and base additions to the titration vessel are performed with a pump but for accuracy reasons the amount of titrant added to the vessel is recorded by the change in weight of the titration vessel. A sequence of pH adjustment to pH > 11, acid titration, sparging and an alkali backtitration are performed during which the pH and weight are recorded continuously and a titration curve constructed. From the acid titration curve, 4 characteristic points are used in the calculation model for the total carbonate concentration (2 points) and the total bicarbonate concentration (2 points). From the alkali titration curve, well chosen titration points are used for the VFA determination. The titrations are performed fast, because the dosing of acid or base is done continuously and no equilibrium time is allowed for the pH measurement. A typical titration cycle takes about 15 minutes, of which 9 minutes is spent sparging. The application of this sensor has to be seen as an early warning system of digester perturbations, indicating possible reactor failure. If the alkalinity is subsequently found to be below a critical value, or VFA's above a critical value, more sophisticated monitoring equipment, like hydrogen level monitoring, is suggested to automatically switched in [228].

If only bicarbonate has to be monitored, a number of alternatives for the described titration methods are available. They are based on the application of physico-chemical equilibria in gas-liquid systems. A review of the methods which can be used to determine bicarbonate alkalinity in solutions where weak acid-base couples other than the inorganic carbon buffer are present is given in [219]. The methods which seem to be promising for automation are discussed in [240]. Bicarbonate from the sample is decomposed to carbon dioxide by strong acid addition and measured as CO₂. The CO₂ can be measured as a flow rate with a sensitive gas meter [108, 110, 111] or as a pressure build-up [71].

A further simplification of determination of VFA's was realized by 1 single pH measurement [298].¹ For this purpose, a fundamental relationship between pH, VFA concentration and alkalinity in prefermenters was used. The relationship can be used to monitor prefermenter performance (with respect to VFA production rates) from pH measurements alone, without the need to measure VFA concentrations. The model used was based on a number of rather dangerous assumptions (e.g. the governing acid-base equilibrium of the system is determined by the CO₂/HCO₃⁻ buffer only, total alkalinity in the system remains constant, . . .). In 4 prefermenters studied, 70 % of the variability of VFA (as HAc) could be explained by the pH [298].

Some applications make use of Gran functions or modified Gran functions for the interpretation of titrimetric data [162, 197, 273]. The Gran functions represent one of the first attempts to linearize titration curves, thereby making it possible to calculate the equivalence volumes by using several points on the titration curve instead of only the inflection point [222]. The Gran functions for titrations of weak acids with strong base are given in equations (4.3) and (4.4). Equation (4.3) is used on the acid side of the equivalence-point, whereas equation (4.4) is used on the alkaline side of the equivalence-point [222].

¹The application of a VFA-pH model is not considered as a titrimetric method, because no addition of acid/base is involved.

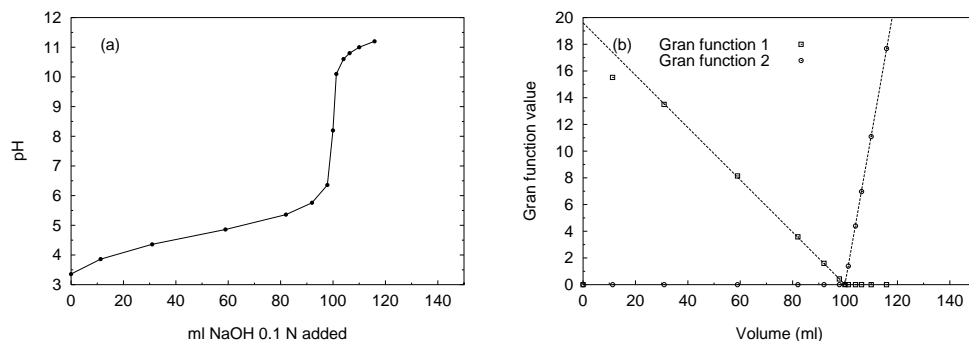


Figure 4.3: Titration curve for 1 litre of a 0.01 M acetic acid solution (a) and corresponding Gran functions with graphical determination of the equivalence-point V_e (b)

$$V10^{(k-\text{pH})} = f(V) \quad (4.3)$$

$$(V_0 + V)10^{(\text{pH}-k')} = f(V) \quad (4.4)$$

V : volume of titrant added

V_0 : volume of the sample solution before the titration is started

k and k' : arbitrarily chosen constants

Similar functions exist for the titration of strong acids with strong bases [222]. The use of Gran functions is illustrated in Figure 4.3 with a simple example that was introduced before (Figure 2.4 on page 21). Figure 4.3(a) shows a simulated titration curve, but with a low measurement point density. Figure 4.3(b) shows the calculated points with the two Gran functions of equations (4.3) and (4.4). To make the scale of the two Gran functions in the same order of magnitude, the arbitrarily chosen constants k and k' are set to 4 and 13 respectively. Further, a straight line through the linear part of the Gran function values is constructed to find the intersection with the V -axis at $V = V_e$, with V_e the equivalence volume. The Gran functions given in equations (4.3) and (4.4) will not give a straight line for any acid. However, for moderately weak acids, having pK_a values in the range 5.0–8.5, more than 50 % of the function will lie on a straight line intersecting the V -axis at V_e (assuming concentrations of the order of 0.01 M). There is a range of acids between strong and moderately weak acids within which neither of these simple Gran functions will yield satisfactory results and this has not been generally recognized [222].

The great advantage of the Gran functions is that it is not necessary to determine absolute $[\text{H}^+]$ values; it suffices to determine values proportional to $[\text{H}^+]$ which means that it is not necessary to calibrate the electrode system [222]. In a publication about the use of Gran functions on titration profiles of mixtures of two acids [223], it was found that the two acids

can be separated provided the stability constants (K_a 's) of the acids differ enough. As a rule of thumb, a difference of 4 logarithmic units is considered satisfactory for instrumental detection of the end-point. In case the K_a values of both acids are known precisely, a difference in K_a of 2 logarithmic units is considered minimal for separation of the 2 acids [223]. Later, by using more sophisticated data interpretation techniques (see section 4.4.2), a separation of 2 acids with differences in K_a much smaller than 2 logarithmic units can be obtained correctly.

Gran (1950) proposed a method for the determination of alkalinity/acidity, in which he formulated a function based on equilibrium and stoichiometric considerations, which allows accurate determination of the proton accepting capacity of a solution without the need of titrating to an end-point [162]. This method was successfully applied for low COD determinations, where titrimetric colour end-point detection was totally inadequate [162]. The method hinges on the utilisation of a modified Gran function coupled with a potentiometric titration of digested test solutions with ferrous ammonium sulphate (FAS) titrant. The detection limit was found to be 3 mg COD l^{-1} . A possible drawback of applying this method to more complex situations is that the stoichiometry of the buffer systems must be known and that the method is not reliable when several buffer systems are present. Further, the Gran plot method has limited accuracy when the dissociation constants are low or high [36, 222]. It is possible to correct for this problem using trial and error or an iterative technique, but this becomes computationally unwieldy [36]. Further, when the Gran function analysis is applied to titration data from typical acidified surface waters, the strong acid acidity is almost always overestimated and the weak acid acidity is underestimated. When CO_2 contamination of the titrant is present, total acidity will be overestimated [23].

4.4.2 Data interpretation of the complete titration profile

The interpretation of the complete titration or buffer capacity profile is performed in a wide variety of systems, especially environmental systems. Applications are found in sanitary landfill leachate [94, 248], micro-organisms growth media [305], cheese wheys [115] and cheese homogenates [169], canned vegetables [66], cattle slurry [124], anaerobic digester liquid [36, 38], ... However, most of these applications are limited to a qualitative approach, to find or to illustrate the most important buffer systems in the titrated sample. Mathematical modelling of the titration or buffer capacity curve in order to find the concentrations of the buffer systems present is rather limited compared to the qualitative approach, e.g. [36, 38]. The most advanced data interpretation of buffer capacity profiles found in literature is a stepwise model building approach to construct a suitable mathematical model for an unknown solution [101, 102]. The last mentioned category is important in the framework of this work. The following paragraphs will go into some more details on the above mentioned applications.

Sanitary landfill leachate is an important source of pollution to both surface and ground waters [94]. More particularly, the pH of leachate determines the solubility, predominant ionic species, complex formation and toxicity in the aqueous solution. A simplified buffer capacity model was used to predict pH changes in the leachate. The model took into account: organic acids (lumped together as acetic acid because the dissociation constants for the organic acids present are grouped within a ΔpK of 0.1), ammonia, hydrogen sulfide and carbonic acids. Because leachate samples cannot be considered as dilute solutions, the dissociation constants were corrected for ionic strength using the Davies equation. Off-line concentration

measurements of the buffering components were introduced in the mathematical model and the simulated buffer capacity curves were compared with the experimental curves. The model was found to be an adequate predictor of the buffer capacity in the pH range 3–10. The lack of agreement between the model and the actual buffer capacity at pH > 10 can possibly be explained by e.g. the presence of phosphate species, precipitation of metal hydroxides, the presence of other organic compounds like phenol, ... The maximum buffer capacity pH was predicted with the model within a $\Delta\text{pH} = 0.35$, and the magnitude of the buffer capacity at this pH value was underestimated with 16 %. These results were found to be acceptable for this application. In a similar study on titration of landfill leachate, a multicomponent chemical equilibrium program SURFEQL was used to predict buffer capacity curves [248]. It was found that ferrous hydroxide buffering caused a sharp peak in the simulated and experimental buffer capacity profile. However, the quantitative agreement was inadequate and two observed buffering systems were not predicted. Although these findings have increased the fundamental understanding of leachate chemistry, the buffering capacity analysis needs to be refined in order to improve these results [248].

Another application of the use of the complete titration profile is the buffer capacity of cheese and cheese wheys [115, 169]. For the cheese wheys, an equation was developed to define whey pH as a function of the pH at dipping (i.e. the pH at which curd is separated from whey), and the concentration and level of HCl or NaOH added [115]. The buffer capacity of whey is mainly determined by the contents of lactate and phosphate. Titration curves of 24 experimental units were defined by 14–16 volumes of titrant for a total of 400 observations. A regression model was used for the whey pH in function of pH at dipping, % solids and titrant added. A multiple linear regression model failed for this purpose, but a cubic regression model gave satisfying results. At alkaline pH, the equilibration time after base addition ranged up to 1 hour, pointing to precipitation phenomena. The buffering capacity curves were not modelled with an acid-base equilibrium model, which probably would reveal more information than a simple regression model. In the same application area, titrations were performed on Emmental cheese homogenate, to investigate the changes in acid-base buffering properties during ripening [169]. The buffer capacity curves were interpreted in a qualitative way but were not modelled. The maximum buffering occurred at pH 5 which was probably due to solubilisation of colloidal calcium phosphate. Again the same remark holds that a more mathematical oriented approach, e.g. with software like MINTEQA2 to incorporate precipitation phenomena, would, eventually combined with advanced data interpretation like PCA, reveal more information than a visual interpretation of the data only.

The role of the buffer system in the ammonia loss from cattle slurry by the use of acidifying additives was investigated by interpretation of titration and buffer capacity curves [124]. The major buffer components were found to be ammonium, bicarbonate and a solid phase of carbonates. A deterministic model that simulated the slurry as an ammonium bicarbonate solution plus a solid phase of calcium carbonate was used to fit the experimental data. Although cattle slurry is a complex mixture of various dissolved and solid compounds, the buffer capacity model described the experimental data fairly well. The model, combined with experimental data, was used to investigate the pH stability of the slurry in response to addition of increasing levels of additives like HCl, superphosphate, FeCl_3 , $\text{Ca}(\text{NO}_3)_2$ and CaCl_2 [124].

A numerical method for the determination of VFA's using all available titration data could resolve acetic and propionic acid components in anaerobic digester samples [36]. A titration

curve linear model that includes acetate ($pK_a = 4.75$), propionate ($pK_a = 4.87$) and bicarbonate ($pK_{a1} = 6.35$; $pK_{a2} = 10.25$) was used. The set of 4 equations were simultaneously solved using a Gauss-Jordan matrix elimination procedure. This method was chosen because it is relatively efficient and not susceptible to ill-conditioned matrices. The authors point to the problem that ill-conditioned matrices are often encountered when logarithmic data (e.g. pH) are used. Another numerical problem that must be dealt with to ensure robustness of the procedure is negative equivalent volumes. A further computational problem arises due to the closeness of the dissociation constants for acetic and propionic acids. In cases where the concentration of one or the other of these acids is relatively small, the procedure distributes the smaller acid concentration into the larger acid concentration. For these cases, the distribution of the VFA components is incorrect, but total VFA concentration is accurate. In a recent paper [38] the authors have modified their procedure to make it more accurate by introducing the effect of ionic strength and combining the acetic and propionic acid component into a composite buffer. The latter modification simplified the total calculation procedure and resulted in a more robust method with less computational problems. The influence of ionic strength was found to be significant and should be considered to yield accurate results [38]. Complications introduced by not knowing the ionic strength I of an unknown sample, were dealt with by *swamping* the sample with an indifferent electrolyte at a high enough concentration to make the original sample's ionic strength and the contribution to ionic strength from the added titrant negligible. KCl in a concentration of 0.1–0.2 M was used for this purpose. Accurate results were obtained for all of the swamped samples, but without swamping, poor results were obtained for a number of samples. VFA concentrations determined with this method yielded estimates that had a mean absolute error of 6–10 % compared to the more accurate chromatographic procedure [38]. These errors were still within the acceptable range for anaerobic digester analysis. Despite the positive results obtained with this method, a possible shortcoming of this procedure is that the authors do not include a model validation step (e.g. based on residual analysis on the differences between simulated and experimental data) to verify if no extra buffering components need to be considered when an unknown sample is analyzed with this method.

An advanced mathematical modelling approach for titration data can be found in two publications [101, 102]. The major difference with previously mentioned methods is that without a priori information about the buffering components present in a sample, a titration or buffer capacity model is constructed for an unknown solution. The method is based on a monoprotic approach, in which titration of a polyprotic acid can be rigorously represented as a mixture of monoprotic acids, by replacing the thermodynamic constants with fictitious titration constants (see also section 3.3.5 on page 50). In the proposed method, titration points are fitted to a one component model, a two component model, and so on; and this is carried to the point where further resolution becomes meaningless. The curve fitting is performed with linear least-squares analysis, and the linear equations are solved with the Gauss-Newton method. A major advantage of Gauss-Newton is that it readily yields statistical measures of confidence in the estimates (standard deviations and covariances). The curve fitting is performed on the first derivative data (buffer capacity curve) rather than on the titration data (titration curve). The criterion to stop the model building process is based on an indicator that detects when the fitted curve falls within the scatter range of the data. Two indicators were used: First a 'randomness' index, that is related to the randomness in sign of the deviations of the first derivative data points from the fitted curve. The second index, called 'relative σ ', is the standard deviation of

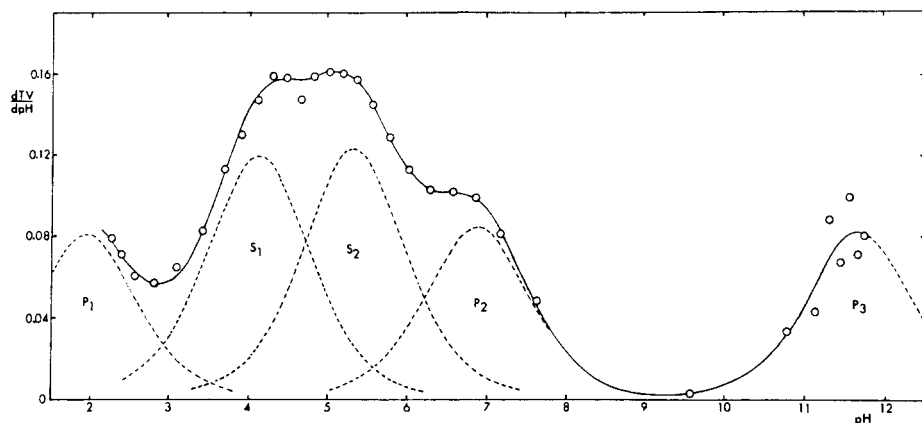


Figure 4.4: Curve-fitting analysis of buffer capacity data for a five-component system. Data points are from titration of a mixture of phosphoric and succinic acids with KOH. The solid line is the fitted curve obtained by superposition of the dashed curves for the individual components. Peaks P_1 , P_2 and P_3 are due to phosphoric acid; S_1 and S_2 , to succinic acid [101]

the derivative data points, expressed as a relative percentage. The main reasons for using the derivative function as a basis for the search analysis are (1) a simple rule can be used to estimate pK starting values, and (2) the two indices, randomness index and relative σ , when used in conjunction, provide the basis for a reliable termination criterion. The main reason these indices provide more reliable criteria for termination than standard deviation of pH (from the primary data analysis) is that differentiation virtually eliminates the effect of systematic errors.

An example of curve-fitting analysis of buffer capacity data for a five-component system is shown in Figure 4.4. A consequence of the monoprotic approach is that the protonicity type of an unknown acid cannot be determined by a curve-fitting analysis, except by inference from finding that two or more concentrations are not significantly different.

A limit obviously exists in the ability to resolve components in a solution by least-squares analysis. This will be imposed, on the one hand, by imprecision in the measurements, and, on the other, by characteristics of the solution [101]. The failure to resolve two components present in a solution by curve-fitting of the composite buffer capacity curve, may be due to a small pK separation, to a small concentration of one component relative to the other, or, in general, to a combination of both factors to some degree. It was shown that data imprecision, relative concentration and pK separation are interrelated. They were used to define a criterion for the limit of resolution, given by:

$$X_2 \Delta pK^2 \approx 4\sigma_{pH} \quad (4.5)$$

X_2 : the fraction of the minor component

ΔpK : the pK separation

σ_{pH} : the standard deviation of pH for the primary data points (titration curve)

Using this formula and practical examples, the authors concluded that a pK separation of 0.1–0.2 is borderline for most applications. On the other hand, a pK separation of 0.5 or more should permit resolution of a component below the 10 % level of the total buffer capacity, even when experimental precision is just average [101]. In a later publication [102] the author applies the proposed stepwise modelling system to titration curves of different types of wine. Titrations of undiluted wine showed sluggish response and evidence that the electrode was being fouled. Therefore the samples were diluted with a ‘buffered diluent’, i.e. a diluent solution of 0.002 M with respect to phosphoric, acetic, and boric acids. The reason for the use of ‘buffered diluent’ was related to the adjustment period for a glass electrode which should be kept as constant as possible during the stepwise titration. Further optimizations of the titration conditions were ionic strength adjustment to 0.1 M by addition of KCl and headspace flushing with water saturated nitrogen in a thermostatic titration cell. Further, the titration data were corrected for the presence of 2.7 % carbonate in the titrant by using hypothetical data subtracted from the measured data. The buffers present in the wine samples were carboxylic acids (between pH 3 and pH 6) and tannins (or phenolics) in the region between pH 9 and pH 11. The contribution of the buffers from the diluent were deleted from the experimental data by subtracting these buffer capacities from the experimental data. Models ranging from 1 to 8 buffering components were fitted to the data. At each step, the level of the residuals decreased, as illustrated in Figure 4.5.

Introducing an eight-component model (not shown in Figure 4.5) resulted in only an insignificant further reduction in the residuals. Thus, both the seven- and eight-component models fit the data about equally well, and the fit is much better for these two models than for those with fewer than seven components. From these data, suggested species were proposed (amino acids, fumaric acid, lactic acid, malic acid, succinic acid, tartaric acid and phenolics). Moreover, the values of the different buffers appeared to correlate with the ‘quality of wine’, but further work would be needed to support a firm conclusion to this effect. Unfortunately, the methods described in [101, 102] were developed 15 years ago, and no recent literature based on this approach was found.

4.4.3 Titrimetric biosensors

Titrimetric biosensors include sensors in which the amount of titrant required to maintain a certain pH is recorded. In these systems, cell metabolism causes acidity changes that allow on-line determination of growth kinetics [129], nitrification rate [88, 92, 180, 231], denitrification rate [40], VFA [242], ammonium [88, 180] and nitrate [40]. A biological reactor, in which the pH is kept constant, and the titrant used is acid, base or growth medium, is called a ‘pH-auxostat’. In spite of its simplicity and general applicability, the information obtainable from titrant measurements does not seem to be widely used to obtain information about growth kinetics in batch culture [129]. However several recent sensor developments in wastewater treatment nitrogen control [91, 181] illustrate that a ‘pH auxostat’ is a useful system to obtain very ‘rich’ process information. These instruments open new perspectives for efficient on-line monitoring of wastewater treatment plants.

During the last two decades, more stringent effluent standards for nutrients (N and P) imposed by legislation have in many countries led to the development of more complicated activated sludge process configurations specifically designed to achieve biological nutrient re-

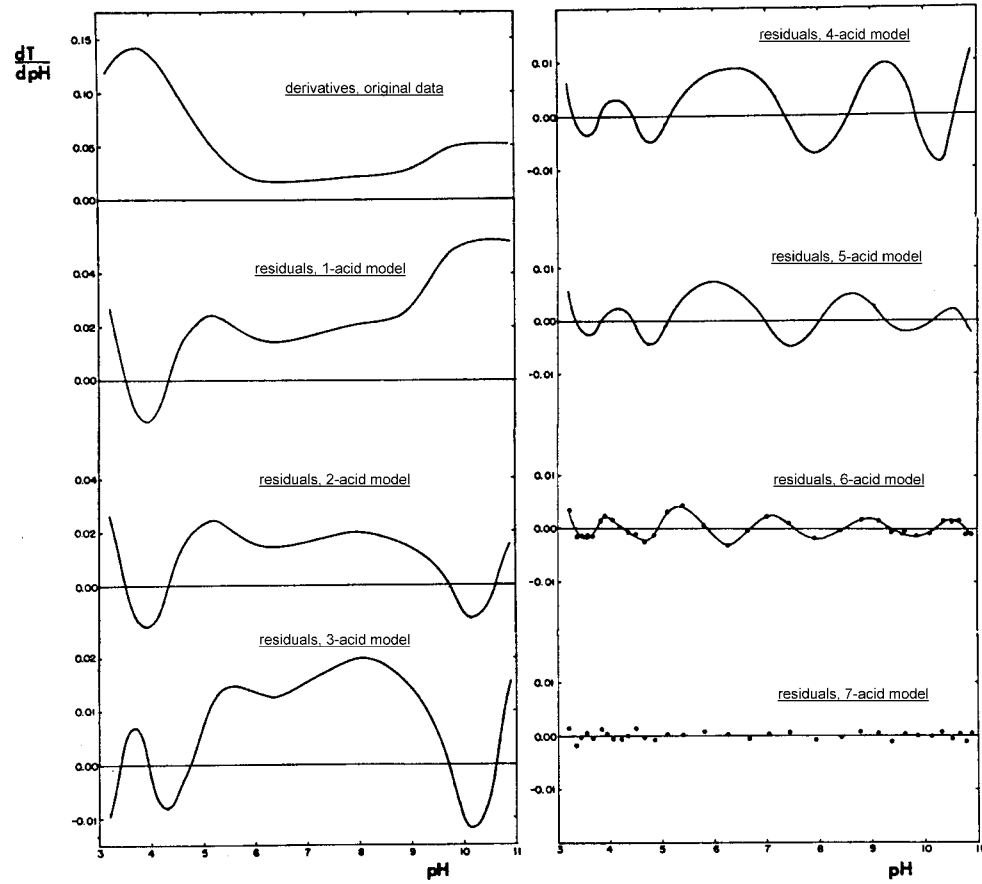


Figure 4.5: Buffer capacity data for a French wine (top) and residuals generated in the search analysis. Points have been omitted from all except the last 2 figures [102]. (note changes in scale)

removal [91]. Biological nitrogen removal includes hydrolysis and degradation of N-containing organic compounds, nitrification (biological oxidation of NH_4^+ to NO_3^-) and denitrification (NO_3^- reduction to N_2). Monitoring the reaction rates of these processes is possible with regular sampling and laboratory analyses. These measurements are expensive, time consuming and often not usable for on-line control. In activated sludge systems with highly varying process conditions, such as for instance in sequencing batch reactors or alternating activated sludge plants, on-line estimation of in-situ nitrification and denitrification rates is possible based on the data provided by on-line NH_4^+ and NO_3^- analyzers [171] (see also section 4.2). For continuous flow activated sludge systems, however, batch experiments are needed to obtain similar information on the sludge characteristics because continuous input of influent results in data with very little dynamics so that no clear interpretation can be made [316]. Therefore, the concept of adaptive in-sensor-experiments was developed [315, 316]. An in-sensor-experiment is typically performed in a down-scaled bioreactor in which the full-scale process is simulated in hardware, and to which specific manipulations such as substrate additions are performed to observe the dynamic response of the biological process. The experimental conditions for which an in-sensor-experiment provides the most interesting data may vary as the conditions in the full-scale process change. It is therefore an essential feature of measuring systems operating according to the in-sensor-experiment principle to be capable to automatically adjust the experimental conditions in the sensor. This automated adaptation leads to the concept of the adaptive sensor [316]. Some applications based on the principle of (adaptive) in-sensor-experiments are presented in the next paragraphs.

In similar sensors (BRAM: Biological Residual Ammonium Measuring system; ANITA: Ammonium NITrification Analyzer) the stoichiometric conversion of NH_4^+ into NO_3^- producing H^+ is used to measure the residual ammonium concentration and the activity of the nitrifiers in an activated sludge sample [88, 92, 180]. The biosensor is made of a reactor vessel and a pH titration unit. Activated sludge, taken from a WWTP, is transferred to the vessel. Acid or base is added to adjust the pH to a chosen set-point. After this phase, cumulative alkali addition is recorded to maintain the set-point pH. The slope of the linear part of the alkali addition profile is closely related to the actual NH_4^+ -N removal velocity, unless aerobic acidifying microbial populations other than nitrifiers are present [181]. The total amount of base needed is related to the NH_4^+ present. Recovery experiments in which a range of concentrations from 0.5 to 4 mg NH_4^+ -N l^{-1} was added to mixed liquors free of ammonium resulted in errors from 1 to 8 % [181]. Further refinement of the sensor consisted in a pulse dosing of approximately 1.3 mg NH_4^+ -N l^{-1} at the beginning of each measurement cycle. This enabled to measure the nitrification rate of an activated sludge sample even when almost no NH_4^+ -N was initially present in the sludge sample [88]. Theoretically, the calculation of the results could be simplified by choosing the pH set-point exactly the same as the equilibrium pH. Eventually the equilibrium pH could be changed by adjusting the % CO_2 in the gas phase of the aeration air, but this would make the titration system more complicated and more expensive to operate [88]. The influence of changes in operational factors such as pH, temperature and bicarbonate alkalinity on the NH_4^+ measurements has been examined [180]. An increase in the amount of bicarbonate buffer in the mixed liquor had a considerable effect on the accuracy of the results, even for a variation of 1 meq l^{-1} , because the increase in the amount of bicarbonate buffer decreased the sensitivity of the pH sensor and therefore the accuracy of the titration. A decrease in total ammonium with increasing bicarbonate concentration was observed [180]. This error can be overcome by

independent determinations of the alkalinity, allowing variable quantities of strong acid in the reaction vessel to be added. In this way, the titration system is operated at constant alkalinity [180]. With the same sensor, it was possible to estimate the volumetric nitrification capacity of the mixed liquor and the Monod half-saturation coefficient for the *Nitrosomonas* bacteria in the sludge. These kinetic parameters are determined with an existing parameter estimation procedure on the basis of information provided by a titration in-sensor-experiment using a nitrifying activated sludge sample [92]. The same method was also used to quantify the effect of low concentrations of a toxic compound on the kinetic parameters of ammonium oxidizing bacteria [90]. The experimental results showed that two sludge samples reacted completely different in the presence of a certain concentration of the same toxic compound.

DECADOS (DENitrification CARbon source DOSage System) is a biosensor for denitrification control in activated sludge WWTP [40, 91, 181, 312]. It is based on two simple and robust probes (pH and ORP). The sensor provides relevant information concerning the kinetics and stoichiometry of the denitrification process and, under some conditions of the in-sensor-experiment, the concentration of nitrate [91]. The sensor is equipped with 3 pumps: acid, base and carbon source dosage pumps. A sample of activated sludge mixed liquor is pumped into a 1 litre vessel and the titration with the carbon source is started. The titration end-point is detected by monitoring the Oxidation Reduction Potential (ORP) of the mixed liquor, based on a particular pattern when all nitrate is consumed (nitrate knee) [181]. The proton consumption is measured via the acid/base addition rate of a pH controller that keeps the pH at a set-point. A pH controller is used, rather than a mere pH measurement, because this excludes the influence of buffering components and simplifies the theoretical background of the sensor [40]. From the volume of carbon source solution added, the nitrate concentration and denitrification rate can be calculated. In case a readily biodegradable substrate is used as titrant, the volume of that carbon source of unknown composition that is needed per volume unit mixed liquor to completely remove the nitrate present can also be measured with the DECADOS.

Another denitrification based sensor is the DENICON (DENitrification CONtroller). It is based on a titration unit similar to the one described for the BRAM system [181]. DECADOS is a closed system, while DENICON is an open system with N_2 and CO_2 sparging. The information provided by the DENICON is similar to that of DECADOS [181]. In the DENICON, anoxic conditions are created with a mixture of N_2 and CO_2 bubbled through the measuring vessel. Nitrate and sodium acetate are added to the mixed liquor in excess to the assumed maximum required nitrate concentration in the ratio of 1 : 5 ($N : CH_3COO^-$). A modified version of the DENICON was used to measure VFA concentration in digested anaerobic liquors as readily biodegradable COD. A sample of the digested effluent is mixed to denitrifying microorganisms in the presence of excess nitrate. The concentration of readily biodegradable COD is then derived from the consumption of nitrates, as measured by titration [242]. This sensor might allow for a better process control of the majority of the anaerobic reactors, which are fed on variable feed both as flow and concentration [242].

Chapter 5

Software developments

5.1 pH titration algorithms

Commercial automatic titrators have built-in algorithms for the control of a titration experiment. A complete titrator set-up consists of a dosing unit for the titrant, a pH meter and titration algorithms. These titration algorithms perform tasks like

- pH measurement and pH stabilization detection,
- calculation of the amount of titrant to be dosed during the titration course, and
- end-point detection.

The details of titration algorithms are kept secret by the titrator developers, because of their commercial value. Two similar titrator set-ups, with and without built-in titration algorithms have a purchase price difference of minimum € 3000. In the framework of this research, only a limited number of functionalities out of the wide range of possibilities that commercial titration algorithms offer, are needed. Therefore the objective of this section is to develop a titration algorithm, capable of performing just the titration task as is needed for this work.¹

The commercial titrator used throughout this work is the Metrohm Titrino 716 [168], however other commercial titrators (Orion 960 Titrator Plus System and Mettler DL70 Titrator) were also evaluated and found similar concerning the capabilities of the titration algorithms.

In the following sections, first the built-in algorithms of the Titrino 716 will be presented and discussed; then three sections follow describing alternative titration algorithms developed in the framework of this research. These alternatives will be classified into a data-based approach, a model-based approach and a combined data- and model-based approach.

¹It should be mentioned that the research results described in this thesis are based on titrations performed with a commercial titrator with built-in titration algorithms. The alternative titration algorithm developed in this chapter has been implemented in a prototype sensor, however, only at the end of this Ph.D. study.

5.1.1 The Dynamic Equivalence-point Titration (DET) algorithm

The Metrohm Titrino 716 is an advanced titrator system for laboratory use. The titration mode determines the manner in which the titration is performed. The following titration modes can be selected on the Titrino 716 [168]:

DET : Dynamic Equivalence-point Titration. With this type of titration, the titrant is added in differently sized volume increments: In the flat part of the curve, the increments are large, whereas in the steep part small increments are added. This mode is suitable for most titrations. However, the algorithm for reagent dispensing functions perfectly only if the curve does not deviate too much from an S-shaped profile.

MET : Monotonic Equivalence-point Titration. With this type of titration, the titrant is added in volume increments whose size does not change throughout the entire titration. This mode is suitable for slow titration reactions (e.g. diazotisations, coupling reactions) or for titrations with asymmetrical curves.

SET : Set Endpoint Titration. This mode is suitable for very fast routine determinations, and dispenses continuously until the stop criterion is reached.

Throughout this work, titration curves were taken with the DET algorithm. The choice for this algorithm was straightforward, because of the following reasons:

- The DET algorithm tends to ensure a constant measurement point density and ensures a constant weight of all pH regions for further data processing.
- The SET algorithm does not take into account electrode kinetics and equilibration times; therefore it is not useful in the framework of this research.
- The MET algorithm with a medium volume step works too slow in the pH regions where the buffer capacity is high (e.g. pH < 4 or pH > 10) and works too fast in the low buffer capacity regions (e.g. pH 7), with as consequence a lack of data points in the low buffer capacity regions.

The technical details of the DET algorithm are not available for the end-user, except that the algorithm is sensitive to deviations from the S-shape ... However, the available titration parameters that can be tuned by the user illustrate the basic functioning of the algorithm. The most important titration parameters of the DET algorithm are:

- Measurement point density (0 – 9): 0 is the highest density. For a value of 4 (default), experimental results show a point density that typically varies between 2 and 20 measurement points per pH unit. An example of a titration, with the lowest and highest possible measurement point density in the DET algorithm, is shown in Figure 5.1.
- Minimum increment: Minimum volume to be dispensed between 2 successive titration points. The DET algorithm always dispenses 3 times this volume at the beginning of the titration.
- Titration rate: Dosing rate for increments (default = maximum).
- Signal drift: Drift criterion for measured value acquisition (default 1 mV min^{-1}).
- Equilibration time: Waiting time for measured pH value acquisition. It is used in combination with the signal drift. The algorithm proceeds to the next point when the signal drift criterion or the equilibration time criterion is reached (default = 60 s).
- Stop pH: End pH value. The algorithm stops when the stop pH or the stop volume is reached.

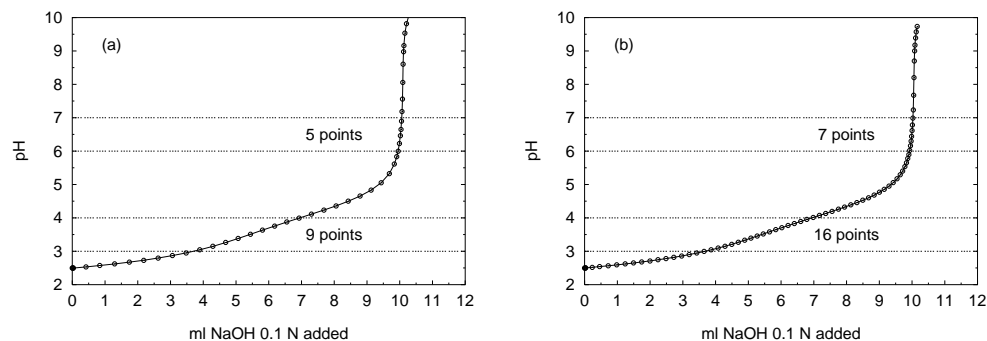


Figure 5.1: Lowest (a) and highest (b) measurement point density with the DET [168] algorithm for a titration of 10 ml oxalic acid 0.1 N in 150 ml water with NaOH 0.1 N as titrant

- Stop volume: Maximum allowed titrant volume for a complete titration.

Besides the titration parameters, there are also parameters related to equivalence-point evaluation. In the framework of this research, equivalence-point determination was only used for titrations of e.g. oxalic acid, for the calculation of the exact normality of the NaOH titrant.

Despite the fact that the DET algorithm gave satisfactory results throughout this work, a number of remarks about this algorithm are given below. First, the measurement point density controls only partially what we want to realize, i.e. a constant ΔpH step, or in other words a constant number of measurement points per pH unit. This equidistant measurement point density is advantageous for the further data processing, more particularly for the calculation of the buffer capacity from the titration profile, because this calculation is based on a moving window parabolic regression on the raw titration data. The DET algorithm gives a high or low measurement point density in regions with respectively high or low buffer capacities. This often results in too low measurement point densities in these parts of the titration curve that are very important for the later data processing part, e.g. the region around pH 7. This is clearly illustrated in Figure 5.1. Plot (a) with the lowest measurement point density realizes a density of 9 points between pH 3 and 4 (a high buffer capacity region), and only 5 points between pH 6 and 7 (a low buffer capacity region). Plot (b) with the highest measurement point density, realizes for the same pH regions 16 and 7 points respectively. The minimum realized volume increment between pH 6 and pH 7 was $60\ \mu\text{l}$, which is still above the minimum increment volume, that was set to $10\ \mu\text{l}$ in this example. Based on this, one can conclude that the measurement point density parameter mainly controls the number of points in the high buffer capacity region (often the less interesting part of the curve), but does not highly influence the number of points in the low buffer capacity region. Further it is not possible with the DET algorithm to obtain a titration curve with a constant, and user-adjustable ΔpH step.

Second, the successively realized ΔpH steps during the course of a titration show slow and fast changes which cannot be controlled by the user. This is illustrated in Figure 5.2. Plot (a) shows a titration curve of oxalic acid, titrated with a measurement point density of 4, the

default value. Plot (b) are the calculated successive ΔpH values from plot (a). The titration curve was taken with a well maintained pH electrode and under the best possible laboratory conditions. The first 3 steps are steps of $10\ \mu\text{l}$, the minimum dispensable volume, which is one of the DET titration parameters presented before. Based on these 3 steps, a first relevant ΔpH of 0.03 is realized. Then the titration algorithm slowly increases the ΔpH to 0.1, and keeps this pH step for a number of points. After this, the titration algorithm slowly increases its pH step size to about 0.2 units, until the point where the equivalence-point is almost reached. Around the equivalence-point, the ΔpH is not stable and varies between 0.2 and 0.45. In that region, the titrator controller also reaches two times its saturation value for the minimal increment volume ($10\ \mu\text{l}$, indicated with an arrow). From this ΔpH analysis, it can be concluded that the titration algorithm uses other rules for the titration advancement than a constant ΔpH . The primary function of the DET algorithm is to detect and quantify end-points, and related K_a values (inflection points) of simple buffer systems.

From Figure 5.2(b) it can be suggested that the DET titration algorithm initially proceeds with a constant, and positive second derivative, followed by a region with second derivative equal to 0 (in particular the region that starts after the inflection point of the oxalic acid buffer, indicated with a filled symbol on the plot). The ΔpH 's in the final part of the titration curve are more irregular, and more difficult to interpret in function of the titration algorithm. Further the 'Instructions guide' [168] mentions also something about the second derivative approach, but without any details: "The evaluation of EP's is based on the zero crossing of the second derivative with a Metrohm correction for the distortion of the curve from superimposed jumps". Both the end-point and pK_a value are inflection points on the titration curve, which points to the necessity of a second derivative analysis of the titration data. From this, one can conclude that the DET algorithm is based on a second derivative analysis, in function of inflection point determination, but that for the purpose of this work, a first derivative approach (constant ΔpH) would be sufficient. Further, a second derivative analysis is very sensitive to data taken under unideal circumstances (e.g. noisy data). This will be illustrated in the next point.

Third, some remarks can be made when the DET titration algorithm is used in situations where the recorded titration curve differs from an ideal smooth, S-shaped titration curve. Situations where the titration curve deviates from the ideal case are manifold:

- pH electrode related: fouled diaphragm, electrolyte level too low, electrode too slow, ...
- pH amplifier related: electrical interferences, noisy amplification, ground loops, ...
- Titrant related: contamination with e.g. CO_2 in NaOH titrant.
- Dosing unit related: air bubbles in the tubings, ...
- Sample related: Slow chemical reactions, exchanges with atmosphere, ...

Two such examples are given in Figure 5.3. In this particular case, some problems existed with the pH electrode, where the electrolyte level was no longer high enough to ensure the necessary positive outflow of electrolyte to the solution. At first sight the electrode seemed to work correctly, so the problem related to the low electrolyte level was not noticed immediately. The plots (a)+(c) and corresponding plots for ΔpH (b)+(d) illustrate 2 noisy titration curves of oxalic acid. The DET algorithm was set to find 1 equivalence-point, and then stop the titration (as only oxalic acid was present, it was considered that the algorithm would find only 1 equivalence-point, similar as in Figure 5.2). However in both cases the algorithm stopped too early, far before the real equivalence-point. Plots (c) and (d) shows a situation where the ΔpH

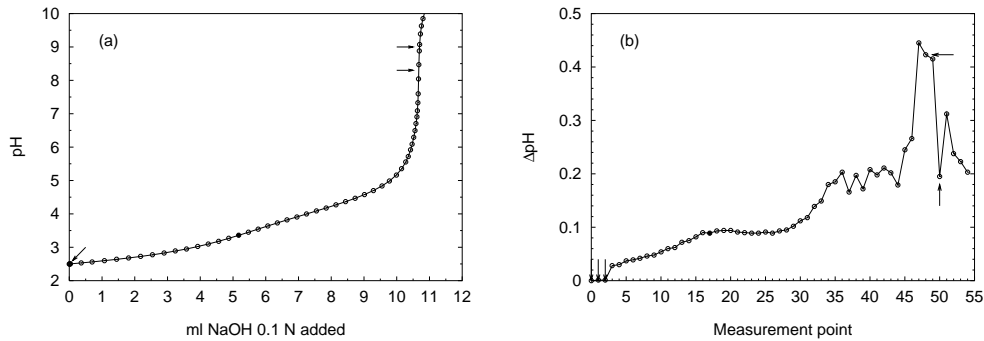


Figure 5.2: Titration curve (a) and corresponding steps in pH for successive titration points (b) for a titration of 10 ml oxalic acid 0.1 N in 150 ml water with NaOH 0.1 N as titrant (the arrows indicate that the minimum allowable volume was dosed; the filled symbol on the titration curve corresponds with the pK_a value of oxalic acid as determined by the DET algorithm)

is even negative. From a theoretical point of view this is not possible, because consecutive alkali additions should result in a pH increase. This phenomenon is e.g. also noticed when an air bubble from the titrant tubing is brought into the titration vessel, or when the pH electrode is not stable yet when the pH measurement is already performed. In such cases, the DET algorithm typically will give a too high titrant step volume for the next point in the titration curve. Data as shown in Figure 5.3 also create difficulties in further data processing, e.g. for the calculation of the buffer capacity, which is based on the first derivative of the titration data. A typical problem in the calculation of derivatives is the amplification of noise present in the original raw data. From these findings one can conclude that the DET algorithm is not a very robust algorithm for our purpose, and it can possibly fail in situations deviating from the ideal situation. This is justified by the fact that the algorithm was developed for a titrator that is used in a laboratory environment, under perfect measurement conditions, and for equivalence-point detection only.

It was mentioned before that the majority of the titration curves in this research were taken in the lab with the Titrino 716 titrator and with the DET algorithm, because this titration system was readily available in the lab and generally gave good results. Titrations where the DET algorithm failed were repeated again until an acceptable titration curve was obtained. How the DET algorithm performs on more complex samples is illustrated in Figure 5.4, which is a titration curve of a destructed and diluted manure sample, containing at least carbonate, orthophosphate and ammonium (see chapter 8). The DET algorithm realizes ΔpH steps that vary between 0.02 and 0.4 pH units.

The aim of this work includes the development of a field applicable on-line measuring system, and therefore alternative, tailor-made algorithms are worked out in the next three sections. Three different approaches are taken: First, an approach is proposed where the titration algorithm only relies on the titration points (data) which are already collected (this corresponds

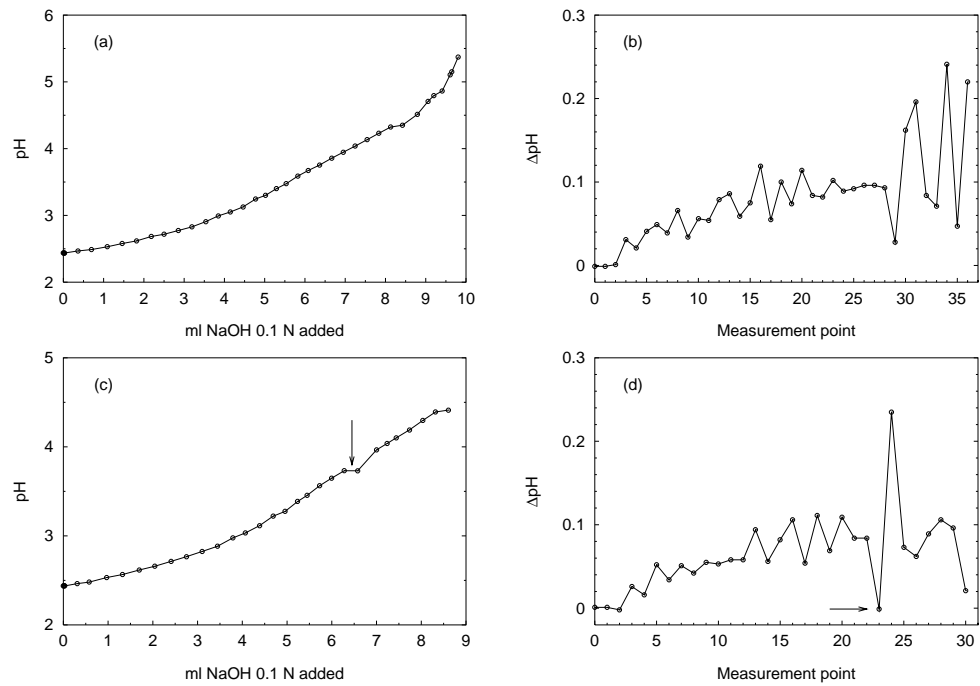


Figure 5.3: Titration curves (a)+(c) and corresponding steps in pH for successive titration points (b)+(d) for a titration of 10 ml oxalic acid 0.1 N in 150 ml water with NaOH 0.1 N as titrant (an arrow indicates that even negative ΔpH 's can be found in real curves)

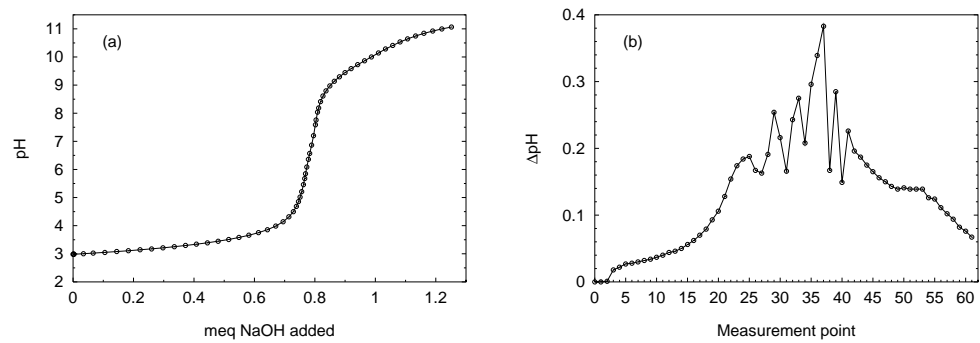


Figure 5.4: Titration curve (a) and corresponding steps in pH for successive titration points (b) for a titration of a destructed and diluted animal manure with NaOH as titrant

with the DET algorithm, so no a priori knowledge about the sample is used). This is the data-based approach. In the second approach, a priori knowledge about the buffer systems that are to be expected is introduced in the titration algorithm. This approach is the model-based approach. The third approach is a combined data- and model-based approach. The two most important criteria that were used for the algorithm development are:

- a user-defined set-point for ΔpH , and
- a robust algorithm that will not give irregular jumps in ΔpH when the titration is not performed under ideal conditions.

5.1.2 Data-based titration algorithm

In its simplest form the data-based approach is an algorithm that can predict the consecutive titrant volume steps to be dispensed, in order to change the pH with the set-point ΔpH . It is based on an extrapolation of the titration curve based on the titration points realized thus far. Two approaches are presented in this section: First, a moving window regression approach, and second, a proportional-integral (PI) controller approach.

In the first approach, practically, a moving window containing the x last titration points is used to predict the next point. An initial titration sequence to initiate such extrapolation algorithm is a necessity (e.g. in a similar approach the DET algorithm uses the first 3 titration points that are a result of dispensing 3 times the minimal incremental volume). Two further questions need to be answered in this framework:

- What is the number of titration points that will be used in the moving window?
- Which mathematical algorithm will be used for the prediction of the next point?

Experimental analysis of typical titration curves has shown that in a situation in which each titration step is around 0.2 – 0.5 pH units, the ideal number of points in the moving window is more than 2, but less than 5. Thus 3 or 4 points make a good compromise between robustness or smoothness of the prediction (more points = more robust) and the actual dynamical response of the pH signal (less points = better pH dynamics). In the following examples 3 points will be used for the window width.

If 3 points are used for the window width, the possible choices for the mathematical model that can be used for the prediction of the next point are rather limited. A linear or parabolic regression model are reasonable choices that will be further discussed. Two examples with both a linear and parabolic regression model are given in Figure 5.5. Under ideal measurement conditions, i.e. a smooth S-shaped titration curve, the parabolic regression is superior to the linear regression, especially in the low and high pH regions. This is illustrated in Figure 5.5(a), and can be interpreted as follows: Assume that one has titrated until point 3, and we want to predict the next titrant volume step ΔV for a chosen set-point $\Delta\text{pH} = 0.2$. The predicted volume steps with respectively the linear and the parabolic regression are ΔV_1 and ΔV_2 . It can be seen that the linear regression line predicts a too high volume step ΔV_1 for the desired set-point ΔpH , whereas the parabolic regression line predicts an almost perfect volume step ΔV_2 . In the high pH range (not shown on the figure), the linear regression predicts too small volume steps, whereas the parabolic regression predicts correct volume steps. In the pH range 5 – 8, both regression types give similar results. Thus, in an ideal case, the parabolic regression is

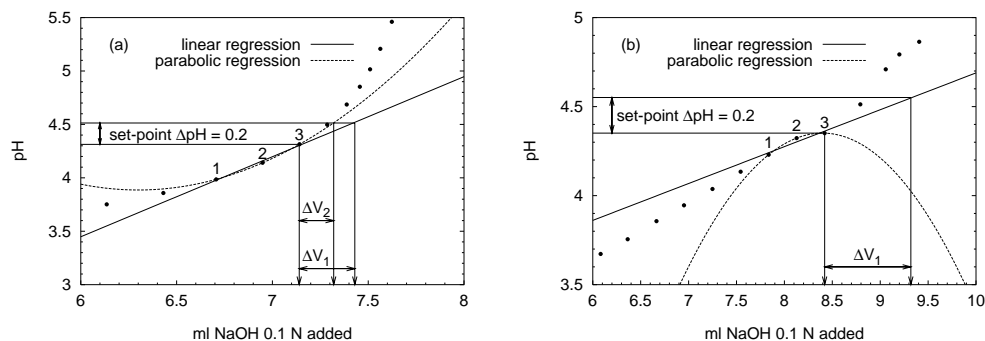


Figure 5.5: Illustration of linear and parabolic regression used for the data-based titration algorithm. Plot (a): titration curve taken under ideal circumstances. Plot (b): non-ideal situation. Points 1, 2 and 3 are used in the regressions

the best choice. The situation is, however, completely different when titrations are performed under non-ideal circumstances (see also section 5.1.1). Such example is given in Figure 5.5(b). Assume again that one has titrated until point 3, and we want to predict the next titrant volume step ΔV for a chosen set-point $\Delta \text{pH} = 0.2$. For the illustrated example, the titrant volume step needed to increase the pH with the set-point ΔpH cannot be predicted with the parabolic curve. This is explained by the noisy data in that part of the titration curve, and consequently a calculated parabolic regression curve that completely fails to represent the shape of the titration profile. On the other hand, the linear regression over-predicts with a factor 2 the volume step to be dispensed. Therefore, algorithms based on extrapolation of titration points fail in case the titration curve differs from ideality. In other words these algorithms are not very robust, a disadvantage for e.g. field-use of such algorithm. This finding corresponds with what was illustrated in section 5.1.1, because the DET algorithm is also a data-based algorithm.

In the second approach, a PI-controller is evaluated for the purpose of constant ΔpH titration. The PI-model in discrete notation is shown in equation (5.1).

$$\Delta V(k+1) = \Delta V(k) + K_C \varepsilon(k) + \frac{K_C}{\tau_I} \sum_{i=1}^k \varepsilon(i) \quad (5.1)$$

- k : titration point number
- $\Delta V(k)$: volume pulse to be dispensed at titration point k
- K_C : proportional control constant
- τ_I : integral control constant
- ε : $\Delta \text{pH}_{\text{realized}} - \Delta \text{pH}_{\text{set-point}}$

The performance of this PI-controller was evaluated with simulation examples, and optimum values for K_C and τ_I were searched. However, no optimum values were found, and no decent control was realized. The non-linear behaviour of the pH in function of the volume steps of

titrant added is pointed to be the reason why this type of control was not working. Thus it was concluded that PI-control is not suited for the purpose of constant ΔpH titration. This is in correspondence with literature findings, that pH control by conventional means is very difficult because of the highly non-linear response of the pH value to the addition of acid or base [188]. A more advanced and adaptive pH controller was successfully implemented for a pH wastewater neutralisation process [135]. The controller is based on a neural network, and both the network structure and the related parameters (weights) are updated on-line. Another successful pH controller, based on fuzzy logic was found useful for pH control of laboratory reactors, waste streams, ... [188]. The pH controller is based on fuzzy logic because it permits the inclusion of subjective knowledge, often based on experience and not on a theoretical model. The knowledge supplied to the control system includes e.g. prior experimental results. However, for the purpose of titration algorithm development, there is theoretical knowledge about the system available. Therefore it should be worthwhile to include this a priori knowledge in the algorithm. Such type of titration algorithm is the topic of the next section.

5.1.3 Model-based titration algorithm

Up to this point, no a priori knowledge about the sample was used in the titration algorithm. However, in most cases, quite a lot of information about the sample to be titrated is available. Useful information can be a list of buffer systems that are to be expected, as well as a first, rough, estimation of their concentrations. As all titrations in this work are in aqueous solution, we know that the water buffer system will be the most significant buffer when the $\text{pH} < 4$ or $\text{pH} > 10$.

Therefore, in this approach, the prediction of the volume step that has to be dispensed in order to have a change in pH equal to the desired ΔpH , will be based on a mathematical model (called titration model) of a hypothetical titration curve calculated with the a priori knowledge that is available about the sample (expected concentrations and pK_a values of buffers). A major concern of this approach is the effect incomplete a priori information has on the titration curve that is being recorded. For instance one may lack information concerning the buffers that are present, or the expected concentrations may be deviating too much from the real concentrations.

A specific computer program (*dyntit*) was developed to simulate a model-based titration based on 2 input files, containing a 'real' titration curve and a 'titration model' curve respectively. The first input file contains the data of a titration experiment conducted with the laboratory titrator and the DET algorithm. The second input file contains simulated titration data, based on the assumed composition of the sample to be titrated. With this software, it was possible to investigate the effect of the 'titration model' on a recorded titration curve, but without having to conduct the model-based titration experimentally. The principle implemented in *dyntit* is illustrated in Figure 5.6. A two-step sequence is needed for the calculation of each titration point with *dyntit*. Assume that one has titrated until pH 4, and we want to simulate the next titrant volume step for a chosen set-point $\Delta\text{pH} = 0.8$.² First, the actual pH and the set-point pH (which is 4.8) are needed to calculate with the titration model curve the volume ΔV to be dispensed (points (1) and (2) on Figure 5.6(a)). Second, this volume step is used to

²A more realistic set-point would be $\Delta\text{pH} = 0.1 - 0.2$, however, for illustration purposes a higher set-point is taken.

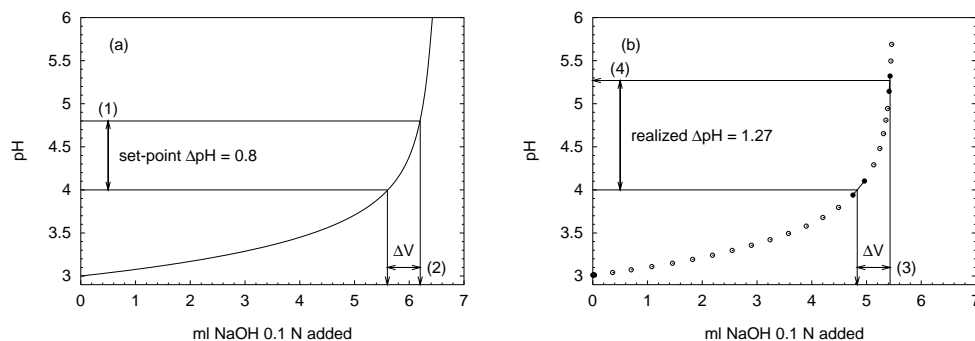


Figure 5.6: Illustration of model-based titration as implemented in the software *dyntit*. Plot (a): ‘titration model’ curve. Plot (b): ‘real’ titration curve. The numbers (1)–(4) indicate the consecutive steps in the algorithm

calculate with the real titration curve the realized ΔpH (points (3) and (4) on Figure 5.6(b)). As illustrated, linear interpolation between the real experimental data points is used for this purpose. In this example the realized $\Delta\text{pH} = 1.27$, thus the model-based titration algorithm has overpredicted the required titrant volume step at pH 4. The new actual pH value is now 5.27, and the two-step sequence can be repeated to calculate the next point of the hypothetical recorded titration curve. Summarized, *dyntit* generates a hypothetical model-based recorded titration curve, based on a titration model and a real experimental titration curve. Two examples below will illustrate the model-based titration approach using *dyntit*.

A first example is a study based on a simulated titration curve that was introduced in section 2.2.5 on page 21. This titration curve (here the ‘reality model’ because it represents the ‘real’ titration curve in *dyntit*) represents an aquatic sample containing some carbonate, orthophosphate, ammonium and an organic acid buffer. A simulation study was set up to investigate the effect of a wrongly defined ‘titration model’ in terms of the model versus the real buffer concentrations. For the simulation study, two titration models were tested: Model 1 incorporates all buffers that are present in the ‘reality model’, but with concentrations equal to 50 % of the real concentrations (except the water buffer concentration, which is always 55.5 M). Model 2 is a similar model, but with concentrations equal to 200 % of the real concentrations. With these 2 titration models, and the ‘reality model’, the model-based titration algorithm was tested. The pH interval was chosen between pH 3 and pH 11, and the set-point ΔpH was chosen at 0.1 pH units. Thus, for each simulated titration step, model 1 or model 2 were used to predict the volume needed to increase the pH with 0.1 units, and the ‘reality model’ was used to find the realized ΔpH . The obtained simulation results are shown in Figure 5.7. At the beginning and at the end of the titration experiment, the model-based titration algorithm is able to maintain the set-point ΔpH of 0.1 units. This is due to the water buffer which is the main buffer in the pH regions outside the pH interval 4 – 10, and which is correctly defined in the titration model (55.5 M). Inside the pH interval 4 – 10, it can be seen that if the titration

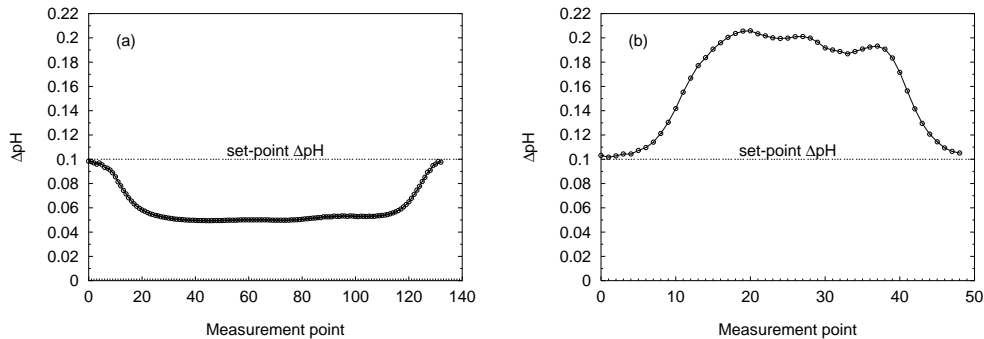


Figure 5.7: Realized ΔpH values in a simulated titration experiment using a model-based titration algorithm. Plot (a): Titration model 1, concentrations 50 % of real concentrations. Plot (b): Titration model 2, concentrations 200 % of real concentrations

model underestimates (model 1) or overestimates (model 2) the real buffer concentrations, the realized ΔpH steps are smaller or bigger than the set-point ΔpH respectively. Further, the ratio between realized and set-point ΔpH equals the ratio between the titration model concentrations and the real concentrations. For example for model 1, the realized ΔpH is 0.05, compared to the set-point 0.1; and the model 1 buffer concentrations are 50 % of the real concentrations. However, it would be dangerous to generalize the latter remark for all practical cases, because the ‘real’ titration curve in this example is in fact also the result of a simulation. Therefore a second example, using experimental titration curves will be presented below.

The second example is a more realistic approach, based on experimental titration data of destructed animal manure samples (see chapter 8) obtained with the Metrohm 716 automatic titrator. This example will illustrate the usefulness of model-based titration using a ‘titration model’ obtained with the mean composition of destructed animal manure samples. 19 different manure samples were used for this study, originating from cattle or pig farms. The destructed and 6.6 times diluted manure samples were titrated with 0.1 N NaOH from pH 3 to pH 11. The titrated sample volume was 165 ml. The mean concentrations of NH_4^+ and $o\text{-PO}_4$ calculated on the 19 samples were used to define the ‘titration model’. This titration model was then used as an input for the program *dyntit*, and 19 ‘new’ hypothetical titration curves were generated using the model-based titration algorithm. The concentrations of 3 selected samples, together with the mean concentrations of ammonium and ortho-phosphate, are presented in Table 5.1. Figure 5.8 shows the pH steps obtained with the model-based titration algorithm, with a set-point ΔpH equal to 0.1. Plot (a) shows the result of Sample 1, which is a sample with one of the highest concentrations for both ammonium and phosphate. Because the concentrations of the ‘real’ curve are significantly higher than the ‘titration model’ concentrations, the realized ΔpH values are up to a factor 3 lower than the set-point 0.1. Plot (b) shows the results of Sample 2, which is the lowest loaded sample in the study. Consequently, the realized ΔpH values are continuously higher than the set-point, up to a factor 5. In all cases, the realized ΔpH values

Table 5.1: Concentrations of ammonium and ortho-phosphate of three selected manure samples and the concentrations used in the titration model used for the evaluation of the model-based titration algorithm

	Concentrations in destructed and diluted manure samples		Model-based titration results
	$mg\ NH_4^+-N\ l^{-1}$	$mg\ o-PO_4-P\ l^{-1}$	
Sample 1	36.0	9.7	Figure 5.8(a)
Sample 2	7.6	0.5	Figure 5.8(b)
Sample 3	21.4	9.4	Figure 5.9(d)
Titration Model	18.7	5.9	

varied between 0.03 and 0.5, which are still acceptable in the framework of buffer capacity modelling. When these results are compared with the results that were obtained with the DET algorithm (see e.g. Figure 5.4), one notices that the model-based ΔpH results are less noisy than the DET results.

5.1.4 Combined data- and model-based titration algorithm

A data- and a model-based titration algorithm were presented in sections 5.1.2 and 5.1.3 respectively. It was already suggested that the data-based algorithm is sensitive to fail when noise or irregular jumps are encountered in the titration data. The model-based algorithm is suggested to be much more robust on this point, because the titration data that are already obtained are *not* used for the prediction of the volume to be dispensed for a next titration point. On the other hand, the data-based algorithm is expected to keep the realized ΔpH close to the set-point ΔpH in different types of samples (low and high loaded samples), compared to the model-based approach where the realized ΔpH is only close to the set-point ΔpH when the titration model does not deviate too much from the ‘real’ titration curve. The question is now if it is worthwhile to combine the 2 approaches and thus use a combined data- and model-based titration algorithm.

An example introduced in section 5.1.3 (Table 5.1, Sample 3) was evaluated for this purpose, and the results are shown in Figure 5.9. Plots (a) and (b) show the experimental titration curve and the corresponding pH steps as obtained with the automatic titrator in the lab, using the DET algorithm. Plot (c) is the application of a linear and parabolic regression method for the data-driven prediction of the next point of the titration curve with a ΔpH set-point of 0.1 (see also section 5.1.2). A moving window width of 3 points gave the best results, and is shown on the graph. The parabolic regression method keeps the ΔpH very close to the set-point, except for 2 peaks in the beginning and in the middle of the curve. The linear regression line overpredicts the volume to be dispensed in the beginning of the titration, and underpredicts the volume to be dispensed in the last part of the titration. Similar to Figure 5.8, plot (d) represents the ΔpH values realized when the model-based titration algorithm is used. Because the real

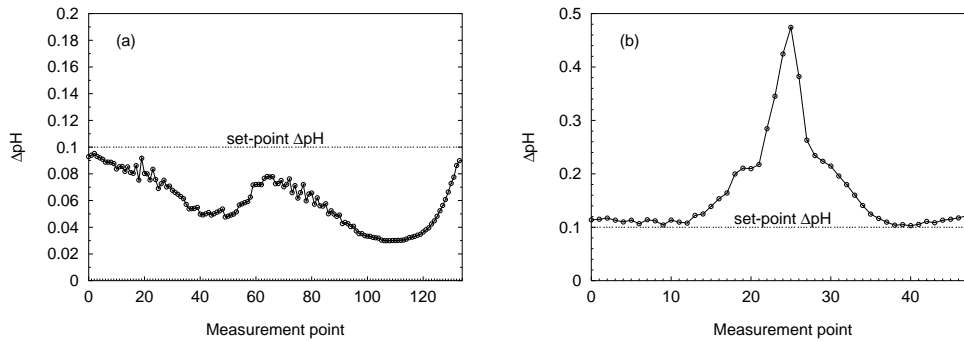


Figure 5.8: Realized ΔpH values in a simulated titration experiment using a model-based titration algorithm. Plot (a): Based on an experimental titration curve of Sample 1 (high concentrations). Plot (b): Based on an experimental titration curve of Sample 2 (low concentrations).

buffer concentrations of manure sample 3 are higher than the mean concentrations used in the titration model, the ΔpH values in plot (d) are somewhat lower than the set-point 0.1.

Based on this example, and the results from the previous sections, it can be concluded that:

- Both the data-based and the model-based algorithm give satisfying results.
- The parabolic algorithm is superior to the linear one for maintaining the desired ΔpH .
- The model-based algorithm is less sensitive to irregular jumps in the realized ΔpH .

Therefore a combined data- and model-based algorithm is suggested for a robust and accurate titration algorithm with constant ΔpH steps and with a user-defined set-point for ΔpH . The idea is to have a dual algorithm that predicts the volume to be dispensed with both approaches, and a built-in selector that can select from point to point which of the two calculated volumes will be dispensed. A flowchart of such dual algorithm is presented at the left side of Figure 5.10. The algorithm is proposed for field-use, thus it starts with some diagnostics test to verify if the titration system is 'ready for use'. These diagnostics can include a liquid level check in the titration vessel, an electrode check, etc. The selector algorithm needs to be chosen in function of the particular application. The selector can either strictly select to dispense the volume calculated with the model-based or with the data-based approach; or it can select a weighted average of the calculated volumes obtained with both approaches. A high weight for the model-based approach can be chosen if robustness or fail-safety are important, or a high weight for the data-based approach can be chosen if it is uncertain that the titration model is representative for the titrated sample. A more complicated selector would, for instance, include a detection of a possible irregular jump for a data-based volume step, thus resulting in a lower weight factor for the data-based approach.

A possible alternative for the selector algorithm is a sequential algorithm, with a model-based volume step, supplemented with a data-driven factor to correct the model-based volume for previously realized ΔpH 's. Such correction factor approach is illustrated at the right side of Figure 5.10. An example is worked out in the next paragraph.

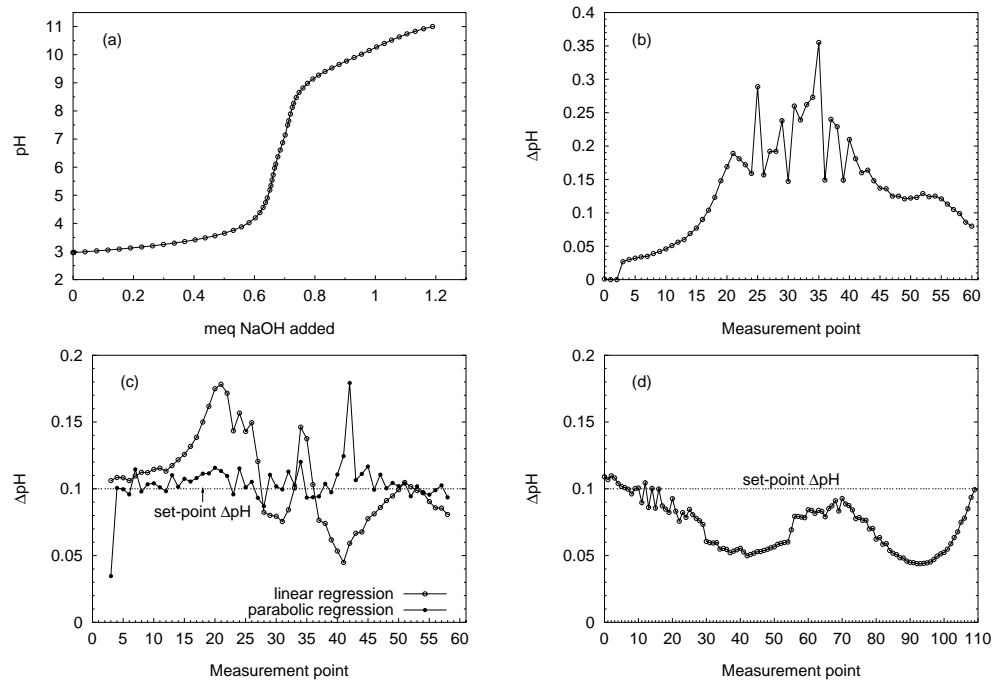


Figure 5.9: Experimental titration curve (a) and corresponding steps in pH for successive titration points (b) obtained with an automatic titrator using the DET algorithm. Realized ΔpH values in a simulated titration experiment using a data-based (c) and model-based (d) titration algorithm based on the experimental titration curve

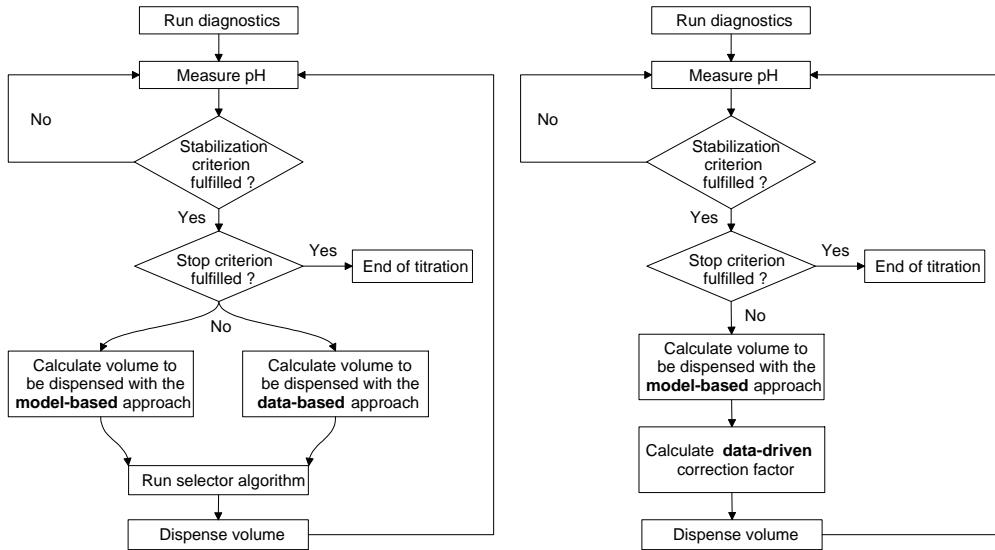


Figure 5.10: Flowcharts of a combined (left side) and sequential (right side) model- and data-based titration algorithm for constant ΔpH titration

A discrete first-order correction factor ζ was applied to the model-based calculated volumes in order to keep the realized ΔpH 's closer to the set-point ΔpH .

$$\zeta(k+1) = \zeta(k) - \lambda \varepsilon(k) \text{ and } \zeta(0) = 1 \quad (5.2)$$

$$\Delta V(k) = \Delta V(k)_{\text{model}} \times \zeta(k) \quad (5.3)$$

k : titration point number
 ζ : correction factor
 λ : first order constant
 ε : $\Delta\text{pH}_{\text{realized}} - \Delta\text{pH}_{\text{set-point}}$

$\Delta V(k)$: volume pulse to be dispensed at titration point k

$\Delta V(k)_{\text{model}}$: volume to be dispensed as calculated with the titration model

In equation (5.3), it can be seen that the volume pulse to be dispensed depends on a model-driven term $\Delta V(k)_{\text{model}}$ and a data-driven term $\zeta(k)$. Equations (5.2) and (5.3) were implemented in the program *dynTit* (introduced in section 5.1.3) to simulate a model-based titration. The example that is presented in section 5.1.3 (Table 5.1, Sample 3) was evaluated again, and some results are shown in Figure 5.11. The effect of the algorithm tuning parameter λ was evaluated and for this particular example a value of λ between 2 and 15 gave significantly better results compared to the results obtained without the correction factor, presented in Fig-

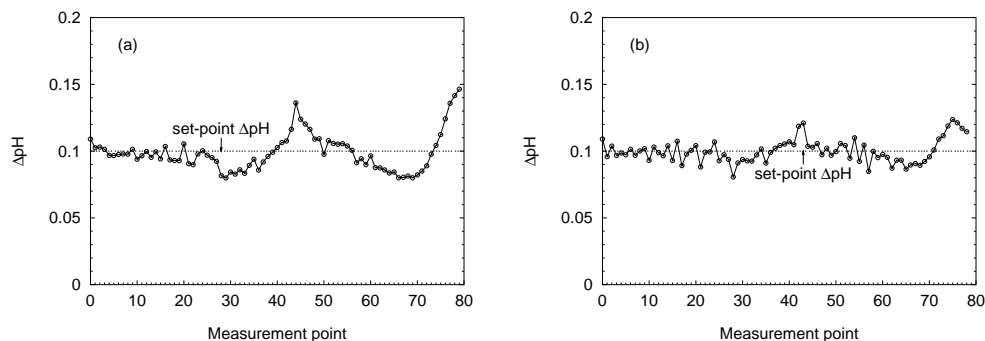


Figure 5.11: Realized ΔpH values in a simulated titration experiment using a model-based titration algorithm with a first-order correction factor ζ . Plot (a) $\lambda = 4$. Plot (b) $\lambda = 10$

ure 5.9(d). For higher λ values the algorithm became unstable due to an overcompensating effect of the data-driven correction factor ζ , resulting in a heavily oscillating ΔpH around its set-point.

The 19 different manure samples that were used to define the titration model (section 5.1.3), were evaluated for the effect of λ and it was found that $\lambda = 4$ is a safe value, in terms of stability of the algorithm, giving satisfying ΔpH steps around the set-point ΔpH . The results for $\lambda = 4$ for 2 selected samples are shown in Figure 5.12. This figure can be compared with Figure 5.8, that presents the same examples, but without the correction factor ζ .

The combined data- and model-based algorithm includes at least the following user-defined titration parameters:

- Set-point ΔpH : The desired increment in pH between 2 successive titration points.
- Minimum increment, signal drift, equilibration time, stop volume and stop pH. These parameters are explained in section 5.1.1.
- For the model-based approach: A list of buffers, their pK_a 's and concentration(s).
- For the data-based approach: Moving window width for the regressions.
- For the selector: depending on the user-defined selector algorithm.
- For the data-driven correction: First order constant λ .

5.1.5 Validation of the combined titration algorithm

The sequential model- and data-based titration algorithm developed in section 5.1.4 was evaluated for its usefulness under more realistic conditions. A preliminary set-up for field-use was realized with a titration vessel, a computer controlled NaOH dosing unit, a high impedance pH amplifier and an industrial PC with the titration algorithm. Thirty destructed and diluted manure samples (10 pig, 10 cattle, 10 poultry) were used for the validation experiment. The mathematical titration curve model used in the titration algorithm was based on the mean composition of respectively pig, cattle and poultry manure (see also chapter 8).

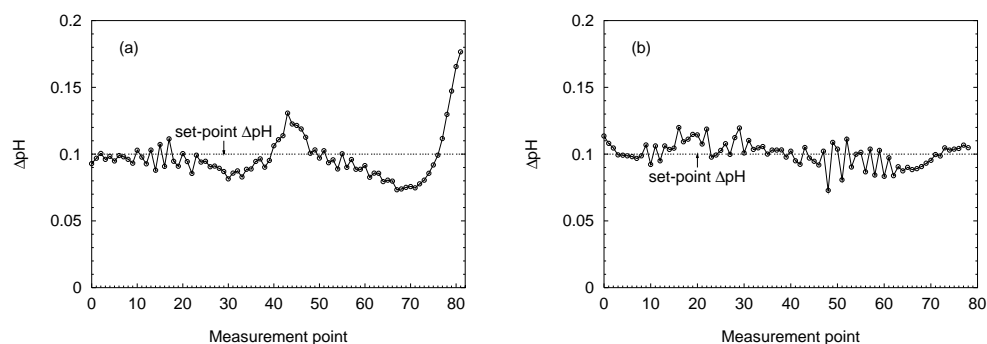


Figure 5.12: Realized ΔpH values in a simulated titration experiment using a model-based titration algorithm with a first-order correction factor ζ . Plot (a): Sample 1 (high concentrations). Plot (b): Sample 2 (low concentrations).

The titration curve and the corresponding ΔpH steps for 1 selected sample are shown in Figure 5.13. The results for the other samples are comparable. Despite the fact that the pH measurement was not very stable yet (signal noise of 3 mV or 0.05 pH units), the titration algorithm succeeded within acceptable deviations to maintain the set-point ΔpH of 0.2 during the complete titration, and for the 30 different tested samples. Based on these results, it is concluded that the developed titration algorithm is sufficiently robust for field-use.

5.2 Tableau-method based simulation software

5.2.1 Software objectives

The program *bctab* is an acronym for “Buffer Capacity simulation using the chemical equilibrium Tableau method”. A compact and convenient way to represent stoichiometric data of a chemical equilibrium problem is in the form of a ‘tableau’ [198]. This tableau representation is treated in section 3.5 on page 55. The tableau method is used to solve chemical equilibrium problems, including complexation and precipitation reactions. In section 3.5.3 on page 61, it is illustrated that, with some slight modifications of the original tableau concept (e.g. excluding H^+ as a component), it is possible to adapt this method for buffer capacity simulation. Extensions to also include ionic activity corrections and precipitation reactions in the buffer capacity simulation are presented respectively in sections 3.5.4 on page 63 and 3.5.5 on page 64.

From literature, it was found that several software programs exist for chemical equilibrium problems. Two of them were evaluated in more detail for the purpose of buffer capacity modelling. The first program is MINTEQA2 [10], which has found wide use in environmental application areas (see section 2.6 on page 37). The second program is MAGIK [20], which is a set of mathematical routines to solve complex chemical equilibria problems. This software uses similar matrix concepts as in the tableau method (see section 3.6 on page 67).

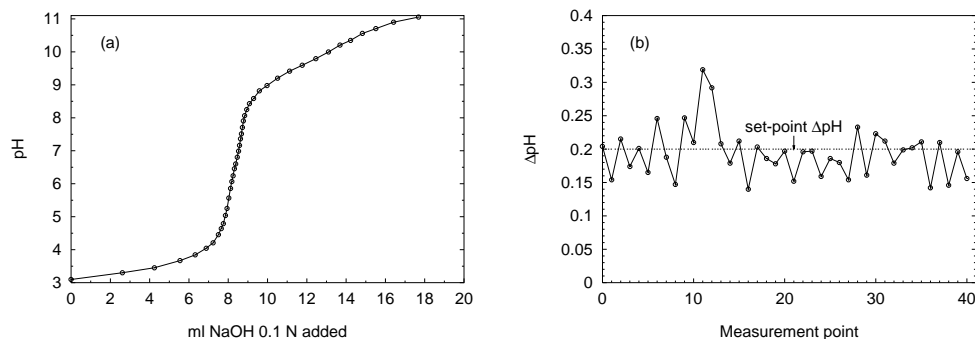


Figure 5.13: Experimental titration curve (a) and corresponding steps in pH for successive titration points (b) obtained with the combined model- and data-based titration algorithm and with a preliminary titration set-up for field-use

The program MINTEQA2 [10] is a speciation program. For a particular set of chemical components specified by the user, MINTEQA2 will equilibrate the chemical solution to a specified pH and/or Eh , to the partial pressure of a gas phase and/or to a specified solid phase composition. The molality and activity of the free ions and aqueous complexes are calculated. In addition, the percent distribution of each component among the aqueous species is determined. Metal adsorption submodels and the calculation of saturation indices of solid phases are also included in the package. The program consists of a number of FORTRAN routines, of which the source code is freely available for the user. The interaction with the user is via in- and output files. The problem should be entered in a specific format file, and this file is then processed by the main program. The results enter in an output file. For a beginning user, it was experienced that it is difficult to understand and use the program when one is not very familiar with the chemical background of the included processes. Even for a small chemical problem, one should consider all possible phenomena, even if one is not interested in those phenomena. The simulation of a titration experiment and the related calculation of buffer capacities is not readily implemented. However, it should be possible to add this functionalities with some modifications in the source code by an experienced user. It was concluded that MINTEQA2 is a very powerful program, with many features, but not well suited for the purpose of simulation of buffer capacity curves in the framework of this work.

The program MAGIK [20] is less extensive in possibilities compared to MINTEQA2. However, it can simulate titration curves for complex chemical equilibrium systems. The program is written in FORTRAN, and the source code is also available. The chemical equilibrium problem should be entered by the user in the form of a FORTRAN subroutine. This user-defined subroutine contains the chemical equilibrium equations and the mass balances. In case of possible precipitation reactions, a set of *if ... then* statements should be entered by the user. The organization of the chemical problem in a set of FORTRAN commands is not well-structured, compared to the tableau method. As a consequence, it is difficult to overview,

modify, extend or correct a chemical problem that is entered as a FORTRAN subroutine. The main program is an implementation of what is described in section 3.5.1 on page 55, i.e. the Newton-Raphson method of steepest descents and partial derivative calculations to construct a Jacobian matrix. Buffer capacity calculations are not readily implemented in the software. A major disadvantage of this program is that for each equilibrium problem, the user-defined source code needs to be modified, and recompiled with a FORTRAN compiler.

Based on the experiences mentioned above, it was concluded that in the framework of this research, the best option was to develop a new program, *bctab*, to simulate acid-base titrations and calculate buffer capacity curves. The objectives for this software are:

- A representation of the chemical problem in a tableau, which can easily be modified.
- A direct output of buffer capacities in function of a user-defined pH range.
- The availability of a facility to recognize pH intervals where precipitation can occur, based on a user-defined list with possible precipitates and their solubility products.
- User interaction with in- and output files only, to keep the program simple, easy-to-use and hardware platform independent.
- A possibility to integrate this software in the software *bomb*, presented in section 5.3.

Similar to the programs discussed above, *bctab* is based on equilibrium models. Therefore, it is assumed that the chemical system is at equilibrium at each point of the titration. This equilibrium assumption is important to remember because natural systems can be kinetically constrained.

5.2.2 Software implementation

The program *bctab* is developed in C++, and can be compiled on different computer platforms. For this research, a C++ compiler (GNU project C++ compiler, v2.7) on a unix workstation (SGI Origin 200) was used for the development of *bctab*. The algorithm for matrix inversion was adopted from the library 'Numerical Recipes in C' [229]. A PC version of *bctab* (compiled with DJGPP, DJ's GNU Programming Platform, free C++ compiler) and a set of illustrative examples is also made available for other users.

The methodology of *bctab* is based on an implementation of the tableau method, described in section 3.5.3 on page 61. The criterion for convergence was slightly modified compared to the criterion found in [251], and earlier presented in equation (3.99):

$$\frac{|Y_j|}{C_j} < \eta \text{ for all components } (j = 1, \dots, m) \quad (5.4)$$

Y_j : remaining error in the material balance for component j

C_j : total concentration for component j

η : convergence parameter

The buffer capacity β is calculated from the species concentrations found with the tableau method, as illustrated in equation (3.108). It was first investigated and then concluded that the relatively simple Euler approach for the calculation of the first derivative was sufficiently accurate. The step value ΔpH in the Euler algorithm is a user-defined value. Ionic interaction

effects were implemented as described in section 3.5.4 on page 63. Therefore, an extra user-defined activity coefficient γ_{H^+} is included in the software.

5.2.3 Functionalities description

The program *bctab* has an elementary user interface and is command-line driven. The necessary input data is supplied to the program by a specific format input file, with a fixed name 'intab'. An illustrative example of a valid 'intab' file is given below.

```
# bctab input file version 3.0
2      # number of components (H+ is NOT a component)
9      # number of species
1      # number of solubility products to be tested
1      # 0 or 1 for log-file function off or on
1      # activity coefficient for H+
1e-07 # convergence criterion for Newton-Raphson algorithm
3      # simulation start pH
11     # simulation stop pH
.1     # simulation step pH
0.05  # internal delta pH for Euler algorithm
      H3PO4   Ca(2+)   H+   log_K   e-   CaHPO4(s)
      0.0019  0.0012
H3PO4   1      0      0    0      0    0
Ca(2+)  0      1      0    0      2    1
H2PO4-  1      0     -1   -2.2   -1    0
HPO4(2-) 1      0     -2   -9.4   -2    1
PO4(3-)  1      0     -3  -21.8  -3    0
CaH2PO4+ 1      1     -1   -0.8   1     0
CaHPO4(aq) 1      1     -2   -6.7   0     0
CaPO4-  1      1     -3  -15.3  -1    0
OH-     0      0     -1  -14    -1    0
      0.002   0.00125
      -6.66
```

The 10 user-defined parameters are explained in the 'intab' file, to make editing convenient for the user. Lines or parts of lines starting with # are considered as comment. The tableau information is entered in the 'intab' file in a format as illustrated above. Fields can be separated by spaces or tabs. The first column contains the labels of the species. The next columns contain the information of the components. More particularly, in each component column, the following information is supplied: a component label, an initial value for the component concentration (mol l^{-1}) used in the Newton-Raphson algorithm, the stoichiometric coefficients and the total concentration (mol l^{-1}). If m components are defined, then the first m species should be in the same order as the components. The tableau information finishes with a column for the stoichiometric coefficients in H^+ , and the $\log K$ values for each species. A following column with the label e^- , contains the charge of each species. This information is needed in equation (3.109), for the calculation of the buffer capacity. The next columns are optional columns, that contain the precipitation conditions to be tested at each pH value. In the example,

the last column should read as: Precipitation of $\text{CaHPO}_4(s)$ will occur if

$$1 \log[\text{Ca}^{2+}] + 1 \log[\text{HPO}_4^{2-}] > -6.66 \quad (5.5)$$

The command

```
bctab myfile
```

will read the 'intab' file, and will generate 2 or 3 new files, with the following names:

myfile.sim : A two-column file with the simulation results. The first column contains the pH values, and the second column contains the corresponding buffer capacities β ($\text{meq l}^{-1} \text{pH}^{-1}$).

myfile.spc : A multi-column file with the species concentrations and precipitation information. The first column contains the pH values, and for each species, a column with the concentration (mol l^{-1}) is added. And last, for each precipitate to be tested, a column is foreseen for the message 'precip', if precipitation is expected at the corresponding pH.

myfile.log : This file is only generated when the corresponding parameter in the 'intab' file is set to 1. This file contains detailed iteration information of the Newton-Raphson algorithm and can be consulted in cases where convergence or numerical problems are noticed.

Throughout this work, several illustrative stoichiometric tableaus have been developed, as input for the program *bctab*. They are given in Tables 3.1, 3.2, 3.3, 8.11 and 8.13.

5.3 Buffer capacity optimal model builder

5.3.1 Software objectives

The program *bomb* is an acronym for "Buffer capacity optimal model builder". The three main objectives for this software are:

- Calculate buffer capacity curves from titration curves.
- Fit mathematical models to experimental buffer capacity curves with a non-linear least squares optimization routine. The optimized parameters are concentrations and/or pK_a values of selected buffer systems included in the mathematical buffer capacity model.
- Stepwisely and automatically construct the optimal buffer capacity model for samples with a lack of a priori knowledge about the buffers that are expected in the sample.

A literature research on advanced buffer capacity modelling software yielded rather poor results. Some software implementations and their related applications are described in more detail in chapters 3 and 4. The majority of available software programs were developed for one specific application, e.g. the determination of VFA and HCO_3^- in anaerobic digesters (more examples in section 4.4.2 on page 89). Such programs are not portable to other application areas for other types of buffer systems. One important exception is the software described in [101, 102], which is also discussed in section 4.4.2 on page 89. This computer program (TI-TAN) analyzes titration data for an unknown solution, and is developed for 'general purpose'

use. However, no references more recent than 1982 about this program, its applications, or similar programs were found.

In two research projects related to this work (AQMON and FASTNAP, described in respectively chapters 6 and 8), the final goal is to develop an on-line, robust and field-usable buffer capacity based sensor. The central part of this sensor is the data processing, which is the software *bomb*. Both projects are driven by commercial final goals, and need specific requirements or criteria for the developed software, such as stability, fail-safety, reusability, robustness, ... Therefore it was chosen throughout the software development to use only techniques and methods that have proven to be stable and robust.

5.3.2 Buffer capacity calculation

The buffer capacity β as a function of pH may be obtained by plotting the inverse of the slope of the titration curve versus pH (see section 2.2.6 on page 22). Several numerical algorithms for derivative calculations were tested on their accuracy and robustness. These algorithms are based on a moving window, that progresses over the experimental data points (ml , pH), and then calculates the first derivative in the middle or midpoint of the window. A compromise had to be found between the smoothness and the dynamical response of the first derivative. Titration curves can be considered as relatively smooth signals, thus derivative calculations are expected to be easily done. First, a geometrical algorithm for differentiation of an experimental function at a point [148] was evaluated for the purpose of this work. The approach is based on the existence of an arc of circle through any three experimental points. It was found that a window width of 3 points is not enough to obtain smooth derivative results. Two other approaches, based on least squares regression of experimental data points in the moving window, were evaluated. These approaches are a linear and parabolic regression through n experimental points, with n a user-defined window width. Both methods are implemented in *bomb*. The parabolic regression with a window width of 5 points was found to give the best results. The S-shaped titration curve is very well suited for fitting parabolic functions through a moving window containing n points of the experimental titration curve. This is illustrated in Figure 5.14, where some examples of parabolic functions fitted to the raw titration data are shown.

For a set of data points (x_i, y_i) , $i = 1, 2, \dots, n$, a parabola of the form

$$y = a + bx + cx^2 \quad (5.6)$$

is fitted by the least squares method. The regression coefficients a , b , and c are calculated by solving the following system of linear algebraic equations:

$$\begin{bmatrix} n & \sum x_i & \sum x_i^2 \\ \sum x_i & \sum x_i^2 & \sum x_i^3 \\ \sum x_i^2 & \sum x_i^3 & \sum x_i^4 \end{bmatrix} \cdot \begin{bmatrix} a \\ b \\ c \end{bmatrix} = \begin{bmatrix} \sum y_i \\ \sum x_i y_i \\ \sum x_i^2 y_i \end{bmatrix} \quad (5.7)$$

The first implemented solution for equation (5.7) was an analytical approach (the so-called method of Cramer). A symbolic solution for equation (5.7) can easily be written down and implemented. However, accumulated roundoff errors in the solution process swamped the true solution. This problem typically arises when a set of linear algebraic equations is almost singular, or when the number of equations is too large [229]. However, in this application, the major

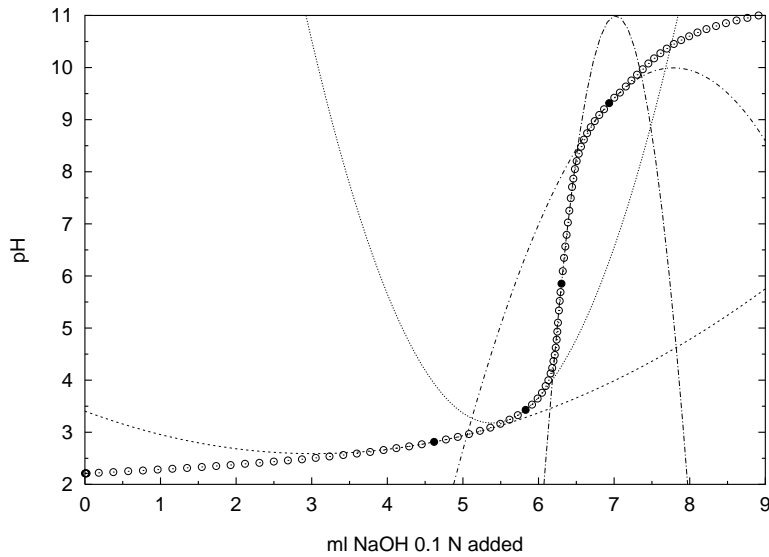


Figure 5.14: Four selected parabolic regression functions fitted to experimental titration points in a moving window with $n = 5$, with the purpose of buffer capacity calculation. The filled symbols are the midpoints of each window

cause for numerical failures was none of the two above mentioned reasons. Rather, the differences in the order of magnitude of the equation coefficients (e.g. n versus $\sum x_i^4$) was the culprit. The numerical procedure does not fail algorithmically, however, it returns a wrong solution, as can be discovered by direct substitution back into the original equations. Therefore, another solution technique, which is more robust for roundoff errors, was implemented. A routine for Gauss-Jordan elimination with full pivoting was adopted from the library 'Numerical Recipes in C' [229]. The full pivoting is important, because Gauss-Jordan elimination without pivoting is numerically unstable in the presence of roundoff errors [229].

In the program *bomb*, the buffer capacities are calculated as function of equidistant pH values. Consequently, an equally distributed weight for the buffer capacities as function of the pH is realized in the further non-linear parameter optimization. Often, in experimental titration curves, the less interesting pH ranges (mostly at low and high pH) contain most titration points as function of pH (see two examples in Figure 5.1). If no special care is taken, the parameter optimization procedure will put more weight on the less interesting pH ranges, because those pH ranges contain more titration points.

Practically, the buffer capacity at a particular pH is calculated by searching the nearest n neighbouring points in the titration profile, followed by the calculation of the regression coefficients a , b and c with equation (5.7). Taking into account the definition of the buffer capacity (see section 2.2.6 on page 22) and the first derivative $\frac{dy}{dx}$ of equation (5.6), the calculation

formula for β becomes

$$\beta = \frac{N}{V} \left| \frac{1}{b + 2cx} \right| \quad (5.8)$$

- β : buffer capacity at a particular pH ($meq\ l^{-1}\ pH^{-1}$)
 b, c : parabolic regression coefficients
 x : titrant volume, calculated as function of pH with equation (5.6) (ml)
 N : normality of the titrant ($eq\ l^{-1}$)
 V : sample volume in the titration vessel (l)

Note that the absolute sign in equation (5.8) ensures a correct β for both acid and base titrations. A number of diagnostics are calculated for each buffer capacity point, including the coefficient of determination of the parabolic regression and a singular matrix detection in the Gauss-Jordan elimination method. If numerical problems are detected, an automatic and temporary switch from the parabolic regression algorithm to the more robust, but less accurate linear regression algorithm is included in the software *bomb*.

5.3.3 Non-linear function minimization

Finding the minimum of a multivariate function f is a common problem in many research fields. For example, fitting a model to a set of data points involves minimizing the deviation of the model's predictions from the data points [86]. In this particular case, a mathematical buffer capacity model is fitted to a set of calculated buffer capacity data points. The sum of squared errors define the cost function value, which is mathematically written as follows:

$$f(\theta) = \sum_{i=1}^N (\beta_i - \hat{\beta}_i(\theta))^2 \quad (5.9)$$

- $f(\theta)$: error function or cost function to be minimized
 θ : parameters in the buffer capacity model that are allowed to vary (concentrations and/or pK_a values of selected buffers)
 N : number of buffer capacity points
 β_i : experimental buffer capacity at point i
 $\hat{\beta}_i(\theta)$: simulated buffer capacity at point i

The purpose is to find as efficiently as possible estimations of θ that make $f(\theta)$ minimal. However, the minimum can either be *global* (truly the lowest function value) or *local* (the lowest function value in a finite neighbourhood and not on the boundary of that neighbourhood) [229]. Unfortunately, there is no perfect non-linear optimization algorithm, and consequently, finding the global minimum for non-linear problems cannot be guaranteed [229]. A helpful visualization of a non-linear cost function is a landscape with hills and valleys [318]. The minimization algorithm should search now the lowest point in this landscape, but can eventually end up in a local minimum instead of the global minimum. Related to this, a property of non-linear function minimization is that the minimum found by the algorithm (global or local) can be influenced by the choice of the starting values for the parameters θ [318].

For linear problems (e.g. linear regression using least squares), the parameter estimates are easily found by differentiating the error function with respect to each of the parameters, set these derivatives to 0, and solve the resulting system of equations for the unknown parameters. This standard recipe, however, fails in many cases when the model function is more complicated. In those cases we have to resort to numerical methods that search the parameter space in a systematic way [86].

The most intuitive minimization technique is the method of steepest descent. The main idea is to change the current parameter estimates in the direction of the largest decrease in f with respect to the parameters. However, this method has some serious drawbacks, making it slow and inefficient [86, 229]. The only search directions used in this procedure are the ones orthogonal to the gradient at the starting point. In the case where the minimum is not located in one of those directions from the current point, the procedure typically meanders in small steps along a valley, instead of making large steps in the direction of the minimum. To improve convergence, one can make use of the fact that most functions are fairly well approximated by a quadratic function near their minima. Algorithms with this property are called *quadratically convergent*. These algorithms can be classified by the kind of information they use to find the minimum. The first class of methods are the derivative methods. They use information on the partial derivatives of the function. Typically, during one iteration, the matrix of second partial derivatives is built up and used to solve for the minimum of the quadratic function. The second class of methods are the ‘direction-set’ methods. They minimize f along a set of directions chosen to make the algorithm quadratically convergent. This approach is taken in Brent’s method [44], and implemented as PRAXIS [86], as will be described further in this section. Derivative methods are generally more efficient than the direction-set methods. On the other hand, the direction-set methods are more general and work even when derivatives are not available. The roundoff errors involved in the calculation of derivatives are significant, and diminish the efficiency advantage. Furthermore, methods using derivatives do have problems in certain cases, which makes the derivative-free methods appear more stable and robust [86].

As mentioned previously, PRAXIS is an algorithm for minimization of multi-dimensional functions. It is based on a ‘direction set’ method by Powell (1964) with some modifications by Brent [44]. Direction-set methods consist of prescriptions for updating the set of directions as the method proceeds, attempting to come up with a set which either (i) includes some very good directions that will take us far along narrow valleys, or else (ii) includes some number of ‘non-interfering’ directions with the special property that minimization along one is not ‘spoiled’ by subsequent minimization along another, so that interminable cycling through the set of directions can be avoided [229].

This concept of ‘non-interfering’ directions, more conventionally called *conjugate directions*, is worth making mathematically explicit [229]. Take some particular point \mathbf{P} in the p -dimensional space, as the origin of the coordinate system with coordinates \mathbf{x} . Then, any function f can be approximated by a quadratic form using Taylor series

$$\begin{aligned} f(\mathbf{x}) &= f(\mathbf{P}) + \sum_i \left. \frac{\partial f}{\partial x_i} \right|_{\mathbf{P}} x_i + \frac{1}{2} \sum_{i,j} \left. \frac{\partial^2 f}{\partial x_i \partial x_j} \right|_{\mathbf{P}} x_i x_j + \dots \\ &\approx c - \mathbf{b} \cdot \mathbf{x} + \frac{1}{2} \mathbf{x} \cdot \mathbf{A} \cdot \mathbf{x} \end{aligned} \quad (5.10)$$

where

$$c \equiv f(\mathbf{P}) \quad \mathbf{b} \equiv -\nabla f|_{\mathbf{P}} \quad [\mathbf{A}]_{ij} \equiv \left. \frac{\partial^2 f}{\partial x_i \partial x_j} \right|_{\mathbf{P}} \quad (5.11)$$

The matrix \mathbf{A} whose components are the second partial derivative matrix of the function is called the *Hessian matrix* of the function at \mathbf{P} . In the approximation of equation (5.10), the gradient of f is easily calculated as:

$$\nabla f = \mathbf{A} \cdot \mathbf{x} - \mathbf{b} \quad (5.12)$$

This implies that the gradient will vanish—the function will be at an extremum—at a value of \mathbf{x} obtained by solving $\mathbf{A} \cdot \mathbf{x} = \mathbf{b}$.

Moving along some direction \mathbf{u} , the gradient ∇f will change according to $\delta(\nabla f) = \mathbf{A} \cdot (\delta \mathbf{x})$. Suppose that we have moved along some direction \mathbf{u} to a minimum and now propose to move along some new direction \mathbf{v} . The condition that motion along \mathbf{v} does not spoil our minimization along \mathbf{u} is just that the change in the gradient stays perpendicular to \mathbf{u} :

$$0 = \mathbf{u} \cdot \delta(\nabla f) = \mathbf{u} \cdot \mathbf{A} \cdot \mathbf{v} \quad (5.13)$$

When equation (5.13) holds for two vectors \mathbf{u} and \mathbf{v} , they are said to be *conjugate*. Minimization along p linearly independent, mutually conjugate directions will exactly provide the minimum of the quadratic form (5.10). For functions f which are not exactly quadratic forms, this will not exactly be the minimum of f ; but repeated cycles of p line minimizations will, in due course, *quadratically* converge to the minimum of f [229]. A detailed discussion of the praxis algorithm used in this work is given in [44, 86]. Interesting to mention is that Brent also incorporated some random steps into the procedure to avoid ‘local minima’ problems.

It should be noted that PRAXIS does not allow one to specify constraints on the problem. For example, it could be useful to restrict the range of values for a parameter to be optimized (e.g. all buffer concentrations should be positive, or a pK_a value should be between a minimum and maximum value). This is not a big problem, however, since constrained problems can usually be converted into unconstrained ones by parameter transformations or simple penalty functions [86]. An example of a useful parameter transformation is the scaled tan function (corrected from [233]): The parameter p_i within the interval between $p_{\min,i}$ and $p_{\max,i}$ is mapped to the whole real axis by the transformation:

$$p'_i = \tan \left(\frac{\pi}{2} \frac{2p_i - p_{\max,i} - p_{\min,i}}{p_{\max,i} - p_{\min,i}} \right) \quad (5.14)$$

The minimization with the unconstrained algorithm as described before is performed in the coordinates p'_i and the solution in the original coordinates is obtained by the inverse transformation:

$$p_i = \frac{1}{2}(p_{\max,i} + p_{\min,i}) + (p_{\max,i} - p_{\min,i}) \frac{\arctan(p'_i)}{\pi} \quad (5.15)$$

which maps the real axis to the interval between $p_{\min,i}$ and $p_{\max,i}$. The other approach, the penalty or barrier function method [205], considers inequality constraints by returning an extremely high cost function value for parameter values not fulfilling the constraints. Practical experiences showed, however, that this algorithm had problems to proceed a descending direction along a constraint [233]. To overcome this problem, it is suggested to linearly increase the ‘high cost function value’ in function of the distance that a constrained parameter drifts away outside its boundaries. In other words, the high cost function plateau suggested in [205] is replaced by a high cost function steep hill with a positive slope. The latter method is implemented in *bomb* and was found to perform without any problems.

The PRAXIS algorithm does not yield estimates of the standard deviations and the correlations of the optimized parameters, although this information is very useful for the interpretation of the optimized results. Confidence information of parameter estimates from measured data is an important aspect of practical identifiability of highly non-linear models [50, 158, 322, 338]. In a first approach, it was attempted to use the internal matrix of search directions, which is built up by PRAXIS, and calculate from this Hessian matrix the variance-covariance matrix of the parameter estimates.³ However, the implementation of this method was not successful, sometimes yielding unrealistic results. The reason for this can possibly be found in the way the Hessian matrix is built up in PRAXIS. Direction-set methods, like PRAXIS, do not compute the Hessian but rather compute a matrix that begins as an identity matrix and is updated on each iteration. This matrix *eventually* converges to the inverse of the Hessian [76]. Especially for constrained problems, it is expected that this approach yields problems for the calculation of the confidence information.

In a second approach, the variance-covariance matrix was calculated separately from the parameter optimization routine PRAXIS. A method proposed by [268], and extended by Nelder and Mead [205] was adopted to calculate the variance-covariance matrix around the minimum. The technique is again based on the construction of a quadratic surface around the minimum of the cost function f . If $(p+1)$ points in p dimensions are given by P_0, P_1, \dots, P_p , then ‘half-way points’ $P_{ij} = (P_i + P_j)/2$, $i \neq j$ are calculated, and a quadratic surface to the combined set of $(p+1)(p+2)/2$ points is fitted. The points P_i may be taken as:

$$\begin{aligned}
 P_0 &= (\hat{\theta}_1, \hat{\theta}_2, \dots, \hat{\theta}_p) \\
 P_1 &= (\hat{\theta}_1 + \delta_1, \hat{\theta}_2, \dots, \hat{\theta}_p) \\
 P_2 &= (\hat{\theta}_1, \hat{\theta}_2 + \delta_2, \dots, \hat{\theta}_p) \\
 &\vdots \\
 P_p &= (\hat{\theta}_1, \hat{\theta}_2, \dots, \hat{\theta}_p + \delta_p)
 \end{aligned} \tag{5.16}$$

$\hat{\theta}_i$: the estimated optimum parameter value

δ_i : stepsize, a user-defined small step or a step automatically chosen as function of the machine precision. In order not to exceed the parameter boundaries (constrained optimization), the step may be chosen positive or negative.

³The relationship between the Hessian matrix and the variance-covariance matrix is illustrated in the second approach starting in the next paragraph.

A matrix with the step sizes δ_i is called the direction matrix \mathbf{Q} .

$$\mathbf{Q} = \begin{bmatrix} \delta_1 & 0 & \cdots & 0 \\ 0 & \delta_2 & \cdots & 0 \\ \vdots & \vdots & \ddots & \vdots \\ 0 & 0 & \cdots & \delta_p \end{bmatrix} \quad (5.17)$$

The quadratic approximation to the function in the neighbourhood of the minimum is used again, see equation (5.10). The coefficients of the Hessian matrix \mathbf{A} are estimated as:

$$a_{ii} = 2(y_i + y_0 - 2y_{0i}) \quad i = 1, \dots, p \quad (5.18)$$

$$a_{ij} = 2(y_{ij} + y_0 - y_{0i} - y_{0j}) \quad i \neq j \quad (5.19)$$

where y_i is the function value at P_i and y_{ij} that at P_{ij} . The Hessian or information matrix in the original coordinate system is given by⁴

$$2(\mathbf{Q}^{-1})' \cdot \mathbf{A} \cdot \mathbf{Q}^{-1} \quad (5.20)$$

so that the variance-covariance matrix is given by

$$\frac{1}{2} \mathbf{Q} \cdot \mathbf{A}^{-1} \cdot \mathbf{Q}' \quad (5.21)$$

In our case, the sum of squares of residuals is minimized, and normal equal-variance independent errors are assumed, thus this matrix must be multiplied by $2 \sigma^2$ [205]. As usual σ^2 is estimated by $SSE/(N - p)$, N being the total number of observations, and p the number of parameters fitted.

The latter method was implemented in *bomb*. The effect of the step sizes δ_i was investigated, and it was found that the final results were not much influenced for different choices of the δ_i 's. This points to the robustness of the algorithm. In the program *bomb*, a stepsize $\delta_i = 10^{-5} \hat{\theta}_i$ was implemented. The choice of the stepsize should also depend on the rounding errors, and it is advised in [205] that the stepsize would be at least 10^3 times that rounding error. Further, for a number of buffer capacity models, a comparison was made between our implementation and the non-linear regression algorithm of SPSS[®] (Statistical Product and Service Solutions, version 7.5). The results (i.e. the optimized parameter values and the variance-covariance matrix) were, except for some small rounding errors, exactly the same. One of the drawbacks of the implemented method from [205] is that it requires a considerable number of additional function evaluations [233]. However, in our particular case, the extra calculation time necessary to run this extra algorithm is negligible compared to the overall data processing time.

Besides PRAXIS, other optimization packages were evaluated too. Among them, the commercial OPTIM module within the M++ Class Library [76] was tested within the *bomb* environment. This library contains 8 well-known algorithms for parameter optimization (e.g. Newton-Raphson, conjugate gradient, steepest descent, Brent's, ...). The M++ Class Library

⁴Note that in the original paper [205], the factor 2 was erroneously omitted [206].

needs to be linked with self-written software in C++. An attractive feature of this package is that it allows algorithm switching during optimization. E.g. the steepest descent algorithm is insensitive to poor start values but can be slow to converge, whereas the Newton-Raphson method may converge quickly but often requires good start values. This suggests that a useful optimization strategy might be to start with the steepest descent method, and at some point in the optimization switch to the Newton-Raphson method. This software was performing satisfactory, and was found very flexible due to the many included features. However, M++ was rejected for possible use in the field, because it was not robust enough. In approximately 1 % of the optimization trials, the program completely crashed within the optimization module, from which it was impossible to recover and proceed with the main program. In those cases, it was mostly sufficient to slightly change the initial conditions or some other parameter settings, to obtain a correct optimization. For field-use, however, this cannot be tolerated. User-support was not available to solve the problem, despite numerous attempts.

A comparative study of linear, non-linear and combined parameter optimization techniques for the purpose of buffer capacity optimization problems is described in [340]. A neural net based optimization technique was found to be very performing, however, is strictly limited to linear problems. For the linear buffer capacity model presented in equation (3.59) on page 49, this neural net based technique was successfully used for problems in which only buffer concentrations had to be estimated. However, in practical situations, it is also necessary to have the option to estimate K_a values, and those are highly non-linear parameters in the model. The Levenberg-Marquardt algorithm [214] has the property that it separately estimates the linear and non-linear parameters. The linear parameters are estimated by linear regression, and the non-linear parameters are estimated with a second derivative technique. In an example where 4 concentrations and 1 K_a value had to be estimated, the Levenberg-Marquardt algorithm was very performing, as only 1 parameter needed to be estimated with an iterative technique. The other 4 parameters were estimated afterwards with linear regression. However, there are a number of drawbacks for this algorithm. First, the choice of the initial values is quite important not to end up in a local minimum. Thus, the algorithm is not so robust. Second, the method is not suited for constrained optimization. And third, the separation of the linear and non-linear parameters requires extra model manipulations, and is only possible for simple buffer capacity models (see section 3.3 on page 44). It is not applicable for the more complicated approaches in section 3.4 on page 52 and section 3.5 on page 55. Therefore, for the above mentioned reasons, the PRAXIS algorithm was found to be the best choice for our purposes.

5.3.4 Automatic buffer capacity model building

If there is a lack of a priori knowledge about the buffer systems that are to be expected in a titrated sample, it is not straightforward to construct and end up with a 'satisfying' buffer capacity model. In the initial phase of this work, the model building process was performed manually. The fit between the experimental and the simulated buffer capacity curves was evaluated visually, and buffer systems were added, shifted, ... until a satisfying model was found. In a later phase, an automatic model building algorithm has been developed [299] and evaluated. Buffer capacity models of a large amount of experimental titration files were automatically built, and a number of shortcomings in the algorithm were found. Based on these results, the model building algorithm was modified and further developed. The final algorithm

is implemented in *bomb* and used as such in this work (see results in chapter 9). There are major differences between our algorithm and the algorithm described by Gordon in [101, 102] (see also section 4.4.2 on page 89). First, the Gordon algorithm does not allow variation on the pK_a values, except for the lastly introduced pK_a value and its closest neighbouring pK_a value. Second, the Gordon algorithm uses a priori information about the buffers to be expected in the sample only to a minor extent. Third, the Gordon algorithm is only considering monoprotic buffer systems. And fourth, the Gordon algorithm does not use advanced model selection criteria.

To describe efficiently the automatic buffer capacity model building algorithm, it is necessary to introduce a specific terminology:

Automatic model building: Procedure in which an initial model or zero model is stepwisely modified. This is generally a sequence of model extensions and/or model tunings.

B-buffer: A candidate buffer for model extension. Each B-buffer has a ranking number indicating its priority for incorporation in the buffer capacity model. It can be a known or a blind buffer.

Blank buffer: A known buffer, but without a particular attributed name.

Blind buffer: A monoprotic unknown buffer used for model extension, of which the acidity constant K_a is automatically determined in the automatic model building procedure.

Final model: Automatically selected best model using a model selection criterion.

Known buffer: A buffer of which the acidity constant(s) are exactly known or known within a minimum-maximum interval. It can be a named or a blank buffer.

Model extension: Model building subprocess in which the first ranked B-buffer is incorporated in the buffer capacity model.

Model tuning: Model building subprocess in which the minimum and/or maximum boundaries of the acidity constant of a blind buffer are modified.

Named buffer: A known buffer, with an attributed name, e.g. phosphate, ammonium, ...

Optimization: Non-linear parameter estimation with the PRAXIS algorithm to fit the buffer capacity model to the experimental buffer capacity curve. Which concentrations and/or acidity constants of known and/or blind buffers that are to be estimated is user-defined.

Residual: Difference between the experimental and the simulated buffer capacity for a particular pH value (symbol ϵ).

Run: A sequence of consecutive positive or negative residuals in function of the pH.

Zero model: The user-defined buffer capacity model containing the a priori information of the buffer systems to be expected in the titrated sample. More particularly, this a priori information includes the concentration range(s) and the acidity constant(s) range(s) of one or more buffer systems.

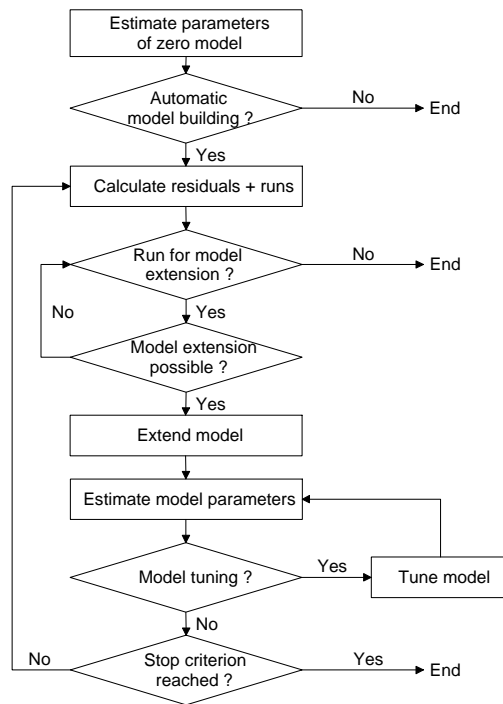


Figure 5.15: Flowchart of the automatic model building algorithm

Model building algorithm

The model building algorithm is designed for an automatic, stepwise and robust buffer capacity model development. The objective of the algorithm is to combine a priori information of the sample buffer composition with lack of fit information to build buffer capacity models, fit those models to the experimental data and obtain concentrations of known and unknown buffers. An overview of the different steps in the algorithm is given in Figure 5.15.

The algorithm starts with the optimization of the zero model. If automatic model building is requested by the user, the residuals and runs obtained with the zero model are calculated. This information is then used to define the candidate pH ranges for model extension. A number of criteria to define the best position for model extension in the buffer capacity profile are described and investigated in [299]. Among them are the number of points per run, the mean, median, mode, minimum, maximum, sum and standard deviation of the residuals within each run. The selection of the pH for model extension based on the highest mean or median of the residuals within each run gave acceptable results. However, it was experienced that a high number of points within each run is also important for an appropriate position for model extension. The criterion ‘sum of residuals’ within each run combines the above mentioned criteria. Therefore, the best candidate pH (and corresponding pK_a) for model extension was obtained when the run with the highest positive sum of residuals was selected, and within that run the pH with the maximum residual value [299]. This is illustrated in Figure 5.16.

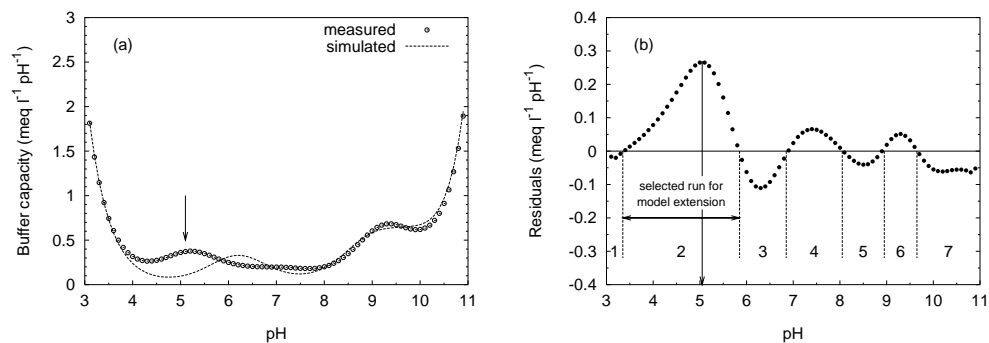


Figure 5.16: Experimental and simulated buffer capacity curves (a) and calculated residuals (b), with indication of the runs, the best candidate run for model extension, and the best candidate pH within that run

The runs are classified towards their priority as candidate positions for model extension. Then, the algorithm will evaluate for the best ranked run if model extension is possible at that pH position (e.g. check if that position and its neighbourhood is not occupied by other buffers). If model extension is not possible at the first ranked pH position, the algorithm proceeds to the second ranked run for model extension, etc. A number of rules for model extension are described below. When an extended model is optimized, the algorithm proceeds, if necessary, with one or several model tuning cycles. Model tuning is the process in which the boundaries (minimum and maximum) for acidity constants of blind buffers that have been estimated, are moved if the estimated value is too close to one of its boundaries. The rules for model tuning are described and illustrated below. After each model tuning cycle, the tuned model is optimized again, and the tuning cycle is eventually repeated several times. Finally, after each tuning session, the model building stop criteria are calculated and evaluated. Such criterion can simply be to enter a maximum defined number of buffers in the model, or a more advanced model selection criterion based on e.g. a statistical test. These criteria are presented in section 5.3.5.

Model extension

The basic idea of model extension is that the ranges (defined by their minimum and maximum boundaries) of all acidity constants to be estimated may never overlap with each other. Initially, this 'limitation' was not set [299]. However, it was found that the optimization routine ran sometimes into difficulties (e.g. local minima), and the final results could not always be interpreted. A number of possible scenarios for model extension are illustrated in Figure 5.17. In short, the rules for model extension that are implemented in *bomb* are the following:

- The blind buffers have a user-defined maximum and minimum width for their acidity constant range. This is illustrated in scenarios 1–3 in Figure 5.17.

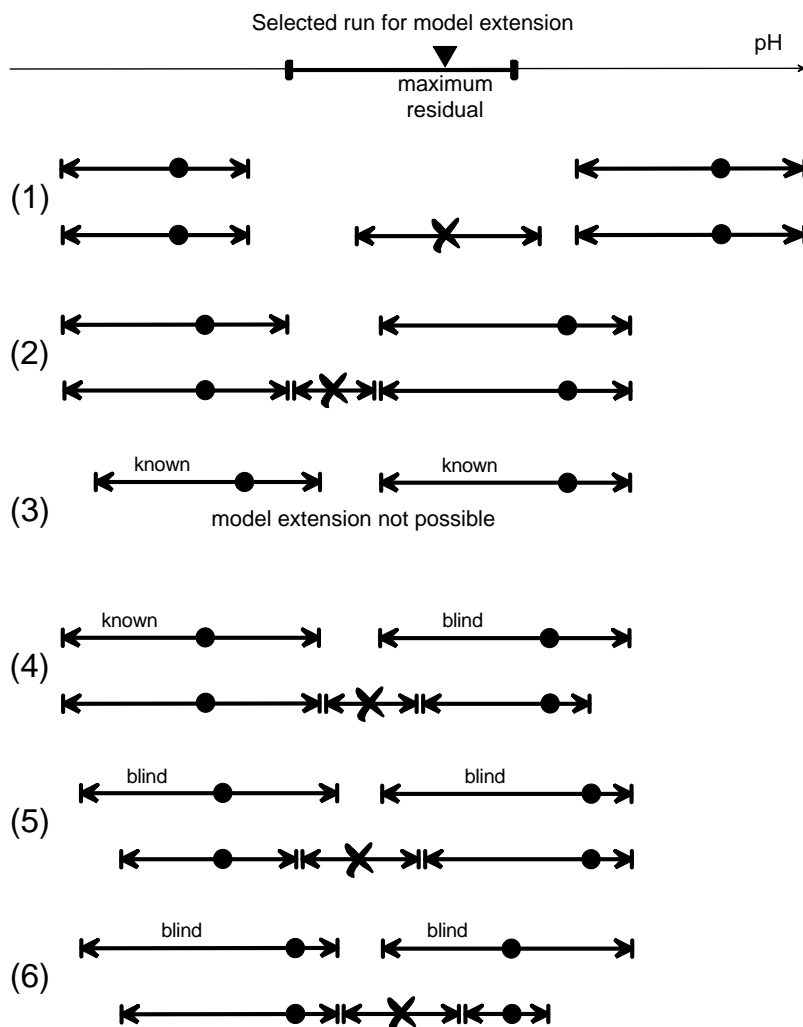


Figure 5.17: Six different scenarios for buffer capacity model extension in the neighbourhood of the candidate pH value. Each scenario shows the situation before and after model extension. The double arrow intervals indicate the optimization boundaries, the filled circles indicate the position of an estimated pK_a value and the cross marks with their interval indicate the position of the new blind buffer

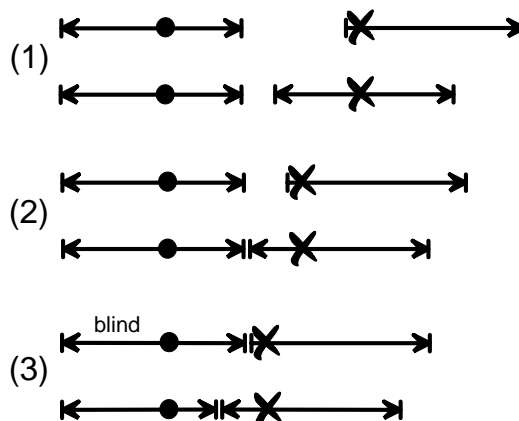


Figure 5.18: Three different scenarios for buffer capacity model tuning. Each scenario shows the situation before and after model tuning. The double arrow intervals indicate the optimization boundaries, the filled circles indicate the position of an estimated pK_a value and the cross marks with their interval indicate the boundary problem and its solution

- A known buffer in the buffer capacity model always has a user-defined range which is never changed during the automatic model building process. For example, when the user defines an ammonium buffer with acidity constant between 9.0 and 9.4, no blind buffer with an acidity constant in that range will enter in the model.
- If model extension with a blind buffer is suggested at a position where another blind buffer is already present in the model, the acidity constant range of the latter blind buffer is symmetrically narrowed with a user-defined factor. However, the estimated pK_a value of the latter blind buffer should always stay included in the narrowed interval. Therefore, the algorithm will eventually narrow the interval asymmetrically or not narrow the interval at all. This is illustrated in scenarios 4–6 in Figure 5.17.
- The initial value for the concentration of a blind buffer is calculated as the mean of the minimum and maximum concentration defined by the user.
- If model extension with a blind buffer is not possible at the position of the first ranked candidate run, then the algorithm proceeds with the other candidate runs. The algorithm stops if the model building stop criterion is reached, or if no more runs are available for model extension.

Model tuning

A buffer capacity model has to be tuned when the estimated acidity constant of a blind buffer is too close to one of its boundaries. The minimal needed boundary distance is user-defined, as a fraction of the actual range of the blind buffer. As mentioned before, the boundaries of known buffers are never changed by the automatic model building algorithm. A number of possible scenarios for model tuning are illustrated in Figure 5.18. In short, the rules for model tuning that are implemented in *bomb* are the following:

- If the estimated acidity constant of a blind buffer ‘touches’ one of its boundaries, the range is shifted (tuned) until the estimated value is centralized (if possible) within the allowed range. As mentioned earlier, it is not allowed that ranges of acidity constants overlap with each other. This is illustrated in scenarios 1 and 2 in Figure 5.18.
- If the range of a blind buffer cannot be shifted because it is restricted by another blind buffer, then a new boundary value is calculated for both blind buffers. More particularly, the mean of the two estimated acidity constants is used as respectively the maximum and the minimum boundary for the two blind buffers. This is illustrated in scenario 3 in Figure 5.18.
- Several blind buffers can be tuned together in one tuning cycle. Each tuning cycle is followed by a parameter estimation of the tuned model. Several tuning cycles can be performed before the algorithm proceeds to the next stage.

A specific model coding system is used to make the distinction between model extension and model tuning within a model building process. The zero model is coded as model 0.0, and the first model extension results in model 1.0. If model tuning cycles are performed, this will result in model 1.1, 1.2, etc. The next model extension will result in model 2.0 etc.

5.3.5 Optimal buffer capacity model selection

When the automatic model building algorithm described in section 5.3.4 is applied, one ends up with a set of mathematical models that have all been fitted to the experimental buffer capacity data. The next logical step is a selection of the most appropriate model for the purpose the model will be used for. Model structure selection techniques, also called model structure characterization, are widely available from literature [107, 157, 264, 319].

Choosing the best possible model for a particular problem, always induces an error that has two components [319]: The first component, the *bias error*, is due to the error between the true model structure and the model structure chosen from the set of candidate models with restricted complexity. The second component, the *variance error*, is caused by the particular realization of the noise in the limited number of data used in the modelling process. The variance error also includes the effect of overparametrization: the more parameters included in the model, the more uncertain their values will be. If N is the number of data points and p the number of parameters in the model, the variance error typically decreases like $\frac{1}{N}$, but increases like p . The bias error, on the other hand, will decrease as p increases, but is independent from N [99, 319]. The goal of model structure characterization will be to find the compromise between bias error and variance error. An important principle in this framework is the *parsimony principle*, that says that out of two or more competing models which all explain the data well, the model with the smallest number of independent parameters should be chosen [264].

The techniques and considerations that can be used for structure characterization can be split into different categories [157]:

- A priori considerations: Certain aspects are independent of the data set and can be evaluated a priori, before the data have been measured. For example, the need for a carbonate buffer in any buffer capacity model can be justified by the fact that there is always some CO_2 in the titrant or headspace entering the sample during titration.

- Techniques based on preliminary data analysis: These techniques are also termed a *a priori structure characterization*, and can be classified into two groups of methods. One type of methods is generally applicable (e.g. pattern recognition using neural networks [217]), while the other type of methods take advantage of specific features of the model structures present in the set of candidate models [322, 323, 325]. A major difficulty of feature-based methods is finding appropriate features, therefore only limited successful applications are found.
- Comparing different model structures: These techniques are also termed a *posteriori structure characterization*. If the computational demand for parameter estimation is high, it is clearly advantageous to apply a priori methods, since they only require estimation of the parameters of the selected model. However, if a posteriori methods show good selection results (as is most often the case), a combined strategy can be devised in which a priori methods are used to make up a first ranking of the different structures, after which a posteriori methods are used to make the final selection among the model structures with highest ranking [315].

In the framework of this research, the promising idea to use a priori structure characterization for the selection of the best buffer capacity model was investigated in more detail in [217]. A pattern recognition algorithm, successfully used for e.g. the recognition of hand written characters, was adapted for the recognition of the number of buffers present in a titrated sample. A set of titration curves resulting from prepared samples with exact known composition were used to test the feature-based pattern recognition algorithm, however, without satisfying results. Two major conclusions could be drawn: First, it is very difficult to find appropriate features to distinguish titration or buffer capacity curves containing 1, 2 or more buffers with varying concentrations. Second, for the majority of the ‘field’ samples used throughout this work, the a priori available information about the samples (e.g. presence of carbon, ortho-phosphate, ammonium, etc.) was mostly so ‘rich’ that the tested a priori structure characterization technique could not bring extra information. For the above mentioned reasons, it was chosen to implement in *bomb* only a posteriori structure characterization techniques. As mentioned earlier, a posteriori techniques require more calculation time, however, for the purpose of this work, this aspect is not so important because the calculation requirements are much lower than e.g. for the non-linear differential equation models described in [315].

A number of a posteriori structure characterization techniques found in literature were evaluated for buffer capacity model selection in [299]. Seven useful model selection criteria are implemented in *bomb* and are presented below. The first two criteria are statistical tests, the four next criteria include information about the model ‘complexity’ and the last criterion is a robust criterion taking into account the limitations of the parameter estimation routine.

The Run-test or testing changes of sign

Let R be the number of changes of sign in the residual sequence $\varepsilon(1), \varepsilon(2), \dots, \varepsilon(N)$, with N the number of data points. E.g. for the illustrated example in Figure 5.16, R is equal to 6. Under the assumption of the null hypothesis $H_0: \varepsilon(t)$ is a zero mean white noise, a test statistic

can be constructed [264]:

$$u = \frac{R - N/2}{\sqrt{N/2}} \rightarrow N(0, 1) \quad (5.22)$$

If the residual sequence is a zero mean white noise, the test statistic is distributed as a standard normal distribution. Hence a 95 % confidence interval for u is given by $|u| \leq 1.96$ for $\alpha = 0.05$. If several models have to be compared with each other, the model with the lowest number of parameters for which $|u|$ is lower than u_α is selected. A particular remark about the use of the number of runs for model selection, is that this method can be applied only if the process description is nearly perfect [320].

The F-test for comparison of model structures

Let M_1 and M_2 be two model structures, such that $M_1 \subset M_2$ (for example M_1 corresponds to a lower-order model than M_2). In such a case they are called hierarchical model structures [264]. Further, let SSE_i denote the sum of squared errors (or residuals) in the structure M_i ($i = 1, 2$) and let M_i have p_i parameters. Although the concept is applicable for different loss functions, the presented F-test is based on the least squares approach. The test statistic

$$F_w = \frac{(SSE_1 - SSE_2)/(p_2 - p_1)}{SSE_2/(N - p_2)} \quad (5.23)$$

is used to compare the model structures M_1 and M_2 . If F_w is 'large', one concludes that the decrease in loss function from SSE_1 to SSE_2 is significant and, hence, that the model structure M_2 is significantly better than M_1 . On the other hand, when F_w is 'small', the conclusion is that M_1 and M_2 are almost equivalent and according to the parsimony principle the smaller model structure M_1 should be chosen as the more appropriate one. The selection criterion becomes:

$$\begin{aligned} F_w > F_{\alpha; p_2 - p_1; N - p_2} &\rightarrow M_2 \text{ is selected} \\ F_w < F_{\alpha; p_2 - p_1; N - p_2} &\rightarrow M_1 \text{ is selected} \end{aligned} \quad (5.24)$$

Akaike's information criterion (AIC)

Another approach to model structure selection consists of using a criterion that in some way penalizes the decrease of the loss function with increasing model complexity. A widely used criterion is Akaike's information criterion [264, 319]:

$$\text{AIC} = N \log \left(\frac{\text{SSE}}{N} \right) + 2p \quad (5.25)$$

with SSE the sum of squared errors, and N and p as defined before. The first term in equation (5.25) decreases with increasing p (increasing complexity) while the second term penalizes too complex (overparametrized) models. The model structure with the smallest criterion value is selected. This selection criterion was designed for models fitted by least squares. However, Akaike-type criteria applicable to a wide variety of loss functions are also available [47].

Final Prediction Error (FPE)

The FPE criterion is similar to the AIC criterion, but with a different penalizing term [264, 319]:

$$\text{FPE} = \frac{\text{SSE}}{N} \left(1 + \frac{2p}{N-p} \right) \quad (5.26)$$

The FPE criterion only holds for selection among model structures which are flexible enough to include the true system. In a model structure selection application one will also have to consider underparametrized model structures. For such structures, equation (5.26) loses its interpretation as an estimate of the ‘final prediction error’. Nevertheless, equation (5.26) can still be used to assess the difference between the prediction ability of various underparametrized model structures [264]. FPE and AIC have been proven not to be consistent (i.e., do not guarantee that the probability of selecting the wrong model tends to zero as the number of data points tends to infinity) [264]. For example, if in particular $p_2 - p_1 = 1$, the risk of choosing the larger structure M_2 when M_1 is more appropriate, will asymptotically be 15.7 % [264].

Schwarz or Bayesian Information Criterion (SIC or BIC)

An example of a consistent criterion is the Schwarz Information Criterion [123, 319]:

$$\text{SIC} = N \log \left(\frac{\text{SSE}}{N} \right) + p \log(N) \quad (5.27)$$

If $p \geq 8$, it can easily be seen that SIC will tend to favour models of lower complexity than those chosen by AIC. Discussions between the original authors of both criteria [8, 253] learn that it is not possible as such to point to one criterion being superior to the other one. Both criteria are based on different assumptions, making comparisons difficult.

Corrected Akaike’s information criterion (AIC_C)

The AIC criterion is a biased criterion, leading to overfitting or the selection of overdimensioned models. Therefore, a bias corrected form of the AIC criterion was introduced [121, 122]:

$$\text{AIC}_C = N \log \left(\frac{\text{SSE}}{N} \right) + N \frac{1 + p/N}{1 - (p+2)/N} \quad (5.28)$$

The bias correction is of particular use when the sample size is small, or when the number of parameters p is a moderate to large fraction of the sample size N [122].

Smallest SSE criterion

This very simple criterion favours the model with the lowest SSE as such. Theoretically spoken, this is not an equilibrated structure characterization criterion, because it does not include any penalization term for the model complexity. However, practical experiences have learned

that for models with increasing complexity, the parameter estimation routine can run into difficulties to find the real minimum of the cost function. Therefore, it can happen that a simple model structure M_1 , which is a subset of a more complex model M_2 ($M_1 \subset M_2$), does fit better (lower SSE) than the more complex model. If such a problem remains unnoticed, it is a dangerous situation to proceed with the automatic model building, because new blind buffers could be added at wrongly chosen pH values. Thus, when the smallest SSE criterion is selected, the automatic model building process will continue until the parameter estimation routine returns a higher SSE for a more complex model compared to a previous and simpler model. Even if another model selection criterion is chosen in *bomb*, the user will always be warned if the SSE of a more complex model is higher than the previous model, but the model building cycle will eventually proceed until the selected criterion is fulfilled.

5.3.6 Software implementation

The program *bomb* is developed in C++, and can be compiled on different computer platforms. For this research, a C++ compiler (GNU project C++ Compiler, v2.7) on a unix workstation (SGI Origin 200) was used for the development of *bomb*. The algorithm for Gauss-Jordan elimination was adopted from the library 'Numerical Recipes in C' [229] and the PRAXIS algorithm in C is available from the author at no cost [86]. A PC version of *bomb* (compiled with DJGPP, DJ's GNU Programming Platform, free C++ compiler) is also available.

5.3.7 Functionalities description

The program *bomb* has an elementary user interface and is command-line driven. The parameter settings and the mathematical model descriptions are supplied to the program through a specific format input file, with a fixed name 'in'. The titration data (*ml*, pH) should be stored in a file with extension '.dat'. An illustrative example of a valid 'in' file is given below.

```
##### BOMB version 8.0 parameter and model input file #####
# * The settings are in a predefined order: do not change the order !!      #
# * A line of comment should start with a '#' (FIRST character on the line) #
#   Comments can also be added at the end of each line, starting with '#'   #
# * Values can be separated by tabs or spaces                               #
#=====
# Software related settings
#
#       # software version number
#=====
# Installation related settings
#
0.15  # volume titration vessel (l)
#=====
# Experimental data related settings
#
0.1015 # calculation factor ml -> meq for the raw titration data
1      # algorithm for buffer capacity calculation (0: linear, 1: parabolic)
5      # window width for the calculation of the buffer capacity (ODD !)
1      # Ionic strength correction: Activity coefficient for H+
#=====
# General settings for simulation and optimization
#
1      # 0: simulate, 1: optimize, 2: only buffer capacity calculation
```

```

0      # optimization routine (0: PRAXIS, 1: not available)
3      # minimum of the pH simulation interval
11     # maximum of the pH simulation interval
.1     # pH simulation step
1      # model to be used (0: not available, 1: linear model)
0      # info from optimizer (0: to screen, 1: to file)
10     # minimum correctly ended trials for optimizer
20     # maximum allowed trials for optimizer (if NaN values are returned!)
=====
# Optimization control settings
#
0      # controls the quantity of iteration info (0: none, 1, 2, 3: most)
1.0e-8 # tolerance for precision solution
4      # number of times tolerance criterion should be fulfilled to stop
0.01   # steplength
1      # PRAXIS internal scaling parameter (1: no scaling)
1      # is the optimization problem illconditioned? (0: no, 1: yes)
10000  # max number of function calls for optimization
1      # confidence information calculation (0: no, 1: yes)
=====
# Automatic model building settings
#
1      # Automatic model building (0: off, 1: on)
1      # How to stop model building (0: add all B-buffers, 1: model selection)
7      # Selection criterion: 1..7: AIC, AICc, SIC, FPE, Run-test, F-test, SSE
0.05   # Alpha for Run-test and F-test
0.005  # Boundary touch condition: touch if distance from boundary < x * range
2      # Symmetrical narrowing factor for blind buffers ; should be > 1
4      # Maximum number of optimization cycles within 1 model building cycle
0.25   # Minimum width for pKa-interval of BLIND-buffers
2      # Initial and maximum width for pKa-interval of BLIND-buffers
#
#####
# Model descriptions for simulation, optimization and model extension
# A line contains 7 items for each model component:
# * Name (MAX 15 chars), it is advised not to edit the names
# * Initial value for optimization or fixed value for simulation
# * Minimum: minimum boundary condition for optimization
# * Maximum: maximum boundary condition for optimization
# * Molecular weight: only for concentrations!
# If = 0 : the concentration values are expressed as mol/l
# If < > 0 : the concentration values are expressed as mg/l
# * Ranking number for B-buffers that will be used for model extension
# * Optimization settings for the zero model (0: fixed, 1: optimize)
#
# NAME----->  INITIAL    MIN      MAX     MOLW  B-  OPT # comments
PKA_WATER      15.744   15.62   15.82   0     0   0 # water
PKA1_CARBON    6.3      6.2     6.5     0     0   1 # carbonate
PKA2_CARBON    10.3     9.5     10.5    0     0   0 # carbonate
PKA1_PHOS      2.15     2.1     2.2     0     0   0 # phosphate
PKA2_PHOS      6.7      6.3     6.9     0     0   1 # phosphate
PKA3_PHOS     12.35    11.5    12.5    0     0   0 # phosphate
PKA_AMMON      9.25     9.15    9.35    0     0   1 # ammonium
PKA_SOAP       3.8      3.0     4.0     0     0   1 # soap
PKA_SULPHATE   1.99     1.98    2.0     0     0   0 # sulphate
PKA_BLANK1     8         7        8       0     0   0 # monoprotic
PKA_BLANK2     5         5         6       0     0   0 # monoprotic
PKA_BLANK3     7         0         0       0     0   0 # monoprotic
PKA1_BLANK4    0         0         0       0     0   0 # diprotic
PKA2_BLANK4    0         0         0       0     0   0 # diprotic
PKA1_BLANK5    0         0         0       0     0   0 # diprotic

```

```

PKA2_BLANK5      0      0      0      0      0      0 # diprotic
PKA1_BLANK6      0      0      0      0      0      0 # triprotic
PKA2_BLANK6      0      0      0      0      0      0 # triprotic
PKA3_BLANK6      0      0      0      0      0      0 # triprotic
PKA_BLIND1       6      2      11     0      1      0 # blind 1
PKA_BLIND2       8      2      11     0      2      0 # blind 2
PKA_BLIND3       7      2      12     0      3      0 # blind 3
PKA_BLIND4       7      2      12     0      4      0 # blind 4
PKA_BLIND5       7      2      12     0      5      0 # blind 5
PKA_BLIND6       7      2      12     0      6      0 # blind 6
PKA_BLIND7       7      2      12     0      0      0 # blind 7
PKA_BLIND8       7      2      12     0      0      0 # blind 8
CONC_WATER       55.5     0      0      0      0      0 # water! in mol/l
CONC_CARBOON     1.0      0.75   5.5    44     0      1 # carbonate
CONC_PHOS        10      0      25     31     0      1 # phosphate
CONC_AMMON       20      0      45     14     0      1 # ammonium
CONC_SOAP        0.0001   0      0.005  0      0      1 # soap
CONC_SULPHATE    0.0      0      0      0      0      0 # sulphate
CONC_BLANK1      0.0      0      0      0      0      0 # monoprotic
CONC_BLANK2      0.0      0      0.001  0      0      0 # monoprotic
CONC_BLANK3      0.0      0      0.001  0      0      0 # monoprotic
CONC_BLANK4      0.0      0      0      0      0      0 # diprotic
CONC_BLANK5      0.0      0      0      0      0      0 # diprotic
CONC_BLANK6      0.0      0      0      0      0      0 # triprotic
CONC_BLIND1      0.0      0      0.001  0      1      0 # monoprotic
CONC_BLIND2      0.0      0      0.001  0      2      0 # monoprotic
CONC_BLIND3      0.0      0      0.001  0      3      0 # monoprotic
CONC_BLIND4      0.0      0      0.001  0      4      0 # monoprotic
CONC_BLIND5      0.0      0      0.001  0      5      0 # monoprotic
CONC_BLIND6      0.0      0      0.001  0      6      0 # monoprotic
CONC_BLIND7      0.0      0      0.001  0      0      0 # monoprotic
CONC_BLIND8      0.0      0      0.001  0      0      0 # monoprotic
#####

```

The user-defined settings in the 'in' file are explained in the file itself, to make editing convenient for the user. The command

```
bomb myfile.dat
```

will read the file 'myfile.dat' with the experimental titration data, and 'in' with the user-defined settings. The program *bomb* will generate a number of new files, with the following names:

- myfile.bc : A two-column file with the calculated buffer capacities from the experimental titration data. The first column contains the pH values, and the second column contains the corresponding buffer capacities β ($meq\ l^{-1}\ pH^{-1}$).
- myfile.sim : A similar two-column file with simulated buffer capacities. If optimization is requested, then this file contains the simulated buffer capacities obtained with the optimized model. If automatic model building is requested, then this file contains the simulated buffer capacities of the final or selected model.
- myfile.sim?? : These files are only generated when automatic model building is requested. ?? equals 00, 01, 02, ... These files contain the simulated buffer capacities of the different models that are created and optimized during the model building process.
- myfile.log : This file contains detailed information about the simulation, optimization and model building processes. More particularly, it contains information about the

titration data quality, simulation model summary and results, confidence information, optimizer information, model building summary, model selection criteria, error messages, detailed warnings and final results.

myfile.lg : Short result file. For each optimization, 1 line with the optimized concentrations and/or pK_a values is added to this file. If automatic model building is requested, this file will contain the optimization results of the different models that have been fitted to the data. If model selection is requested, the last line entered in the .lg file are the optimization results of the final or selected model.

Throughout this work, the software *bomb* was modified, adapted, extended and made robust for field-use. It was tested intensively, and used for all buffer capacity calculations, simulations and optimization exercises in this work.⁵ In chapters 6, 7 and 8, *bomb* is used to optimize user-defined models. In chapter 9, *bomb* is used and evaluated for automatic model building and model selection.

⁵The program *bomb* has been used to solve around 10^6 parameter estimation problems, or an equivalent of around 100 days processor occupation.

Chapter 6

On-line effluent and river water monitoring

Some of the results described in this chapter were also published in [89, 310, 311].

6.1 The AQMON project

6.1.1 Project identification

The AQMON acronym stands for “Aquatic monitor”. This project was a cooperation between three partners:

- Hemmis N.V., Kortrijk
- Ghent University, BIOMATH department, Gent
- Ghent University, Department for biochemical and microbial technology, Gent

The aim of the project was to develop an automated on-line sensor for use in water quality monitoring. The end-result should be applicable for the control and monitoring of effluents of wastewater treatment plants, surface waters and internally recycled process waters within e.g. textile or food production plants. Due to the principles that are used, the methodology is not applicable for heavily loaded waters (influent), neither for very low loaded waters like drinking waters. The developed methodology is designed for alarm generating purposes, rather than for precision analytical purposes.

6.1.2 Background of the project

The Flemish physico-chemical surface water quality does not meet the required surface water quality criteria on around 90 % of around 1000 sampling points in Flanders [193]. The chemical oxygen demand (COD), nitrogen (mainly nitrate in winter times) and phosphorus are the most alarming parameters, as they exceed the desired criteria in 50 to 90 % of the cases. The main sources of river water pollution are summarized in Table 6.1. It is concluded that

Table 6.1: Percentage distribution of the main river water pollutants among three types of activities in 1998 [192]

	industry	agriculture	households
COD	31	-	69
nitrogen	14	46	40
phosphorus	18	26	56

households are the major source of river water pollution, however, industrial activities and agriculture are important as well. Particularly threatening for river water quality are accidental discharges from industrial and agricultural activities, malfunctioning of wastewater treatment plants and discharges of untreated wastewaters [191]. Continuous monitoring of surface waters and potentially polluting river inputs (e.g. effluents) is a promising supporting tool for a better supervision and control of surface water quality.

Wastewater treatment plants do not always reach the effluent discharge requirements [193]. This is, among others, due to the lack of reliable on-line measurements and related adequate automatic control. Some particularities and difficulties related to on-line measurements are presented in section 4.1 on page 70. In the last decade, increased research towards reliable, robust, on-line measurement systems was performed, of which an overview is presented in chapter 4.

Since 1991, the quality of surface waters and effluents is expressed in ‘polluting units’. The mathematical expression for the calculation of the ‘polluting units’ considers three categories of pollutants: First, the oxygen binding substances (COD and BOD) and suspended solids; second, the nutrients nitrogen and phosphorus; and third, the heavy metals. Within this framework, the goal of the AQMON project is twofold. First, the development of an on-line sensor that can be used to assess several components of the ‘polluting units’. And second, the development of an automatic sensor that can be integrated in an automatic measurement network, e.g. to monitor a river network.

The central idea is to develop a new instrument based on simple, reliable and robust measurements, with minimal maintenance requirements, with a high measurement frequency and usable in the field. The followed approach is holistic, e.g. the production of new polluting substances (waste) during the measurements should be avoided.

A new idea originating from the AQMON project is ‘quality proportional sampling’. This is proposed as an alternative for time or flow proportional sampling, and allows to economize on the amount of samples that should be analyzed in the laboratory. For instance, suppose that an on-line automatic sensor is continuously monitoring an aquatic stream (river, effluent, process water), and yields a more or less general ‘fingerprint’ of the water quality at every measurement cycle. Further, suppose that an automatic sampler, that takes samples for laboratory analyses, is coupled to the sensor, and can receive an activation signal from the sensor. Then a sampling strategy can be implemented, that no samples are collected if the water quality ‘fingerprint’ is not significantly changing. Only if the sensor detects a change in the water quality ‘fingerprint’, a sample is taken for laboratory analysis. In those cases where the water

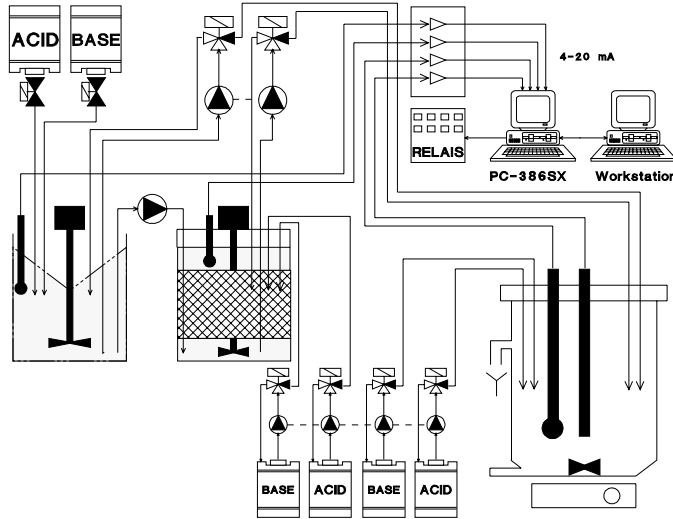


Figure 6.1: Scheme of the research set-up used in the initial phase of the AQMON project. From left to right: pretreatment reactor, bioreactor and titration vessel

quality changes are slow or not frequent, the quality proportional sampling strategy is expected to be economically advantageous compared to time or flow proportional sampling, leading to a significantly lower number of laboratory analyses to be performed.

6.2 Sensor methodologies

In the initial phase of the AQMON project, a research set-up was realized, with the aim of developing a sensor for ammonium, ortho-phosphate and short-term biological oxygen demand (BOD_{st}). The basic idea is a combined and advanced interpretation of relatively simple and robust measurements (e.g. pH and conductivity) to obtain more 'upgraded' information compared to the interpretation of the single measurements alone. A scheme of this set-up is shown in Figure 6.1. This set-up provided the following functionalities:

- A pretreatment reactor for pH adjustments and CO_2 stripping of the raw water sample;
- A bioreactor with poly-urethane foam as carrier material, with the possibility for pH adjustments and automatic pH control;
- A titration vessel for pH and conductometric acid and base titrations.

The basic measurements used in the AQMON research set-up are pH and conductivity. The information that can be extracted from acid-base titrations is more or less complementary for pH and conductivity titrations. For example, sulphate can theoretically be estimated from the conductivity profile, but not from the pH buffer capacity profile. On the other hand, some ions like ortho-phosphate can theoretically be estimated from both types of profiles which will enhance the reliability of the final result. For example, conductometric acid-base titration based

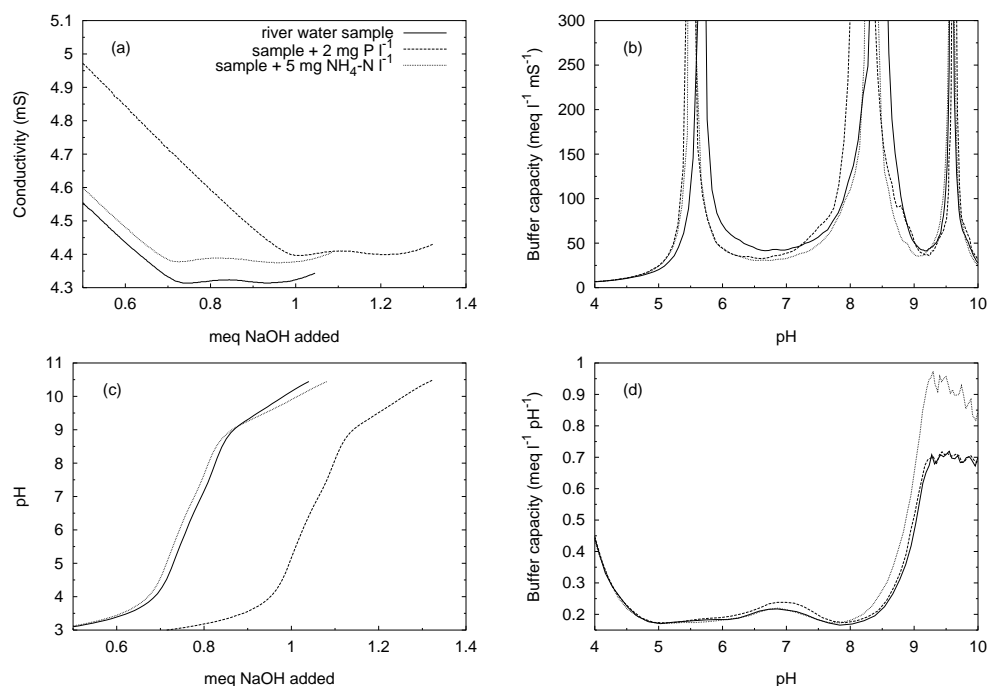


Figure 6.2: Simultaneous conductivity and pH titration curves of a river water sample, and the sample supplemented with ortho-phosphate or ammonium: plots (a) and (c). Corresponding buffer capacities shown in function of the pH: plots (b) and (d). The legend in (b), (c) and (d) is the same as in (a)

sensors are available for the determination of alkalinity and acidity [254], or the indirect assessment of microbial populations by the absorption of metabolic CO₂ in an alkaline absorbant solution whose conductance is monitored [215], or to monitor a well-known waste stream [60]. However, none of the mentioned sensor applications apply mathematical modelling for the interpretation of the conductometric titration curves.

It was found to be very difficult to find a realistic mathematical model for the conductometric titration profiles obtained from aquatic samples like river waters. An example of a combined pH and conductivity titration is shown in Figure 6.2. A heavily loaded river water was made CO₂ free at low pH and titrated to high pH. The raw signals of pH and conductivity, and the calculated pH and conductivity buffer capacities (respectively $\text{meq l}^{-1} \text{pH}^{-1}$ and $\text{meq l}^{-1} \text{mS}^{-1}$) in function of the pH are given in Figure 6.2. The pH buffer capacity profiles clearly illustrate an increased buffer capacity around pH 7 and pH 9.5 for respectively ortho-phosphate and ammonium standard additions to the river water sample. This buffer capacity effect could not clearly be deduced from the conductivity signal and corresponding conductivity buffer capacity profile. Because the pH buffer capacity profiles were more 'rich' for our

purposes, and very suitable for mathematical modelling, it was decided to focus on the pH titration profiles alone.

The initial research performed in the AQMON project was exploratory, and rather ambitious. An overview of the research subjects and the most relevant results are given below. In further stages of the project, the attention was focussed towards those topics that had the best potential value for field application and possible commercialisation, and of which the necessary research aspects could be finished within the scope of the project. These results are presented in more detail from section 6.3 onwards.

6.2.1 Ammonium and ortho-phosphate measurement

Experiments with the research set-up given in Figure 6.1 showed good perspectives for ammonium and ortho-phosphate assessment from the buffer capacity profile. The acid and base dosing system consisted of a peristaltic pump that was continuously dispensing acid or base into the titration vessel. While the titration was running, the dosing speed could not be changed. A difficult compromise between dosing speed and satisfactory accuracy in the low buffer capacity regions of the titration profile had to be found. The dosing accuracy of the peristaltic pump was also found to be less than what should be expected from the specifications of the pump manufacturer. Despite the fact that 1 titration from pH 3 to pH 11 took around 30 minutes, the dynamics of the pH electrode response in the low buffer capacity regions could not be neglected, and the corresponding buffer capacity curves were not closely following the theoretical buffer capacity model. An exception can be made for the heaviest loaded waters, that had the best reproducibility, and were also easier to model. Illustrative buffer capacity curves of three different Flemish surface waters (sampled in October, 1992) with various loads of ammonium and ortho-phosphate are given in Figure 6.3. The illustrated titration curves were collected with the research set-up discussed above, and were thus not very useful for modelling purposes. Ortho-phosphate buffers around pH 7, while the ammonium buffer can be found around pH 9.25.

Based on the difficulties described above, it was decided that for ortho-phosphate and ammonium assessment from the buffer capacity profile, a more accurate and reproducible titration system would be necessary. Therefore it was chosen to proceed the research with a commercial titrator (Metrohm Titrino 716 [168]). As a consequence, automatic and on-line validations with this new titrator set-up were no longer possible and all field samples to be analyzed were thus brought to the laboratory.

6.2.2 Short-term BOD measurement

Overviews of available techniques for the measurement of BOD in aquatic streams are given in [61, 79]. The most important drawback of the classical laboratory method for BOD_5^{20} is that 5 measurement days are necessary before the result is available. On-line BOD methods have been developed, but they are mostly limited to the monitoring of rather heavily loaded waste streams, like influents. It was noticed in [61, 79] that there is a lack of on-line biosensor methods for quick determination of the BOD_{st} in low loaded waters like effluents or river waters. Thus, this particular niche was explored with the AQMON sensor set-up illustrated in Figure 6.1 [61, 79].

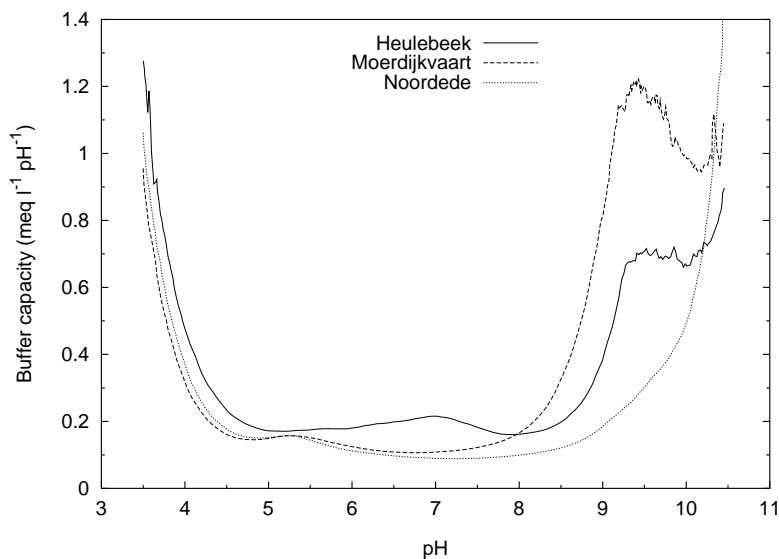


Figure 6.3: Buffer capacity curves from 3 different surface waters: Heulebeek ($10.6 \text{ mg } o\text{-PO}_4\text{-P l}^{-1}$; $3.5 \text{ mg NH}_4^+\text{-N l}^{-1}$), Moerdijkvaart ($1.0 \text{ mg } o\text{-PO}_4\text{-P l}^{-1}$; $9.6 \text{ mg NH}_4^+\text{-N l}^{-1}$) and Noordede ($0.5 \text{ mg } o\text{-PO}_4\text{-P l}^{-1}$; $1.0 \text{ mg NH}_4^+\text{-N l}^{-1}$)

The principle developed for the BOD_{st} measurement starts with the removal of the inorganic carbon (IC) buffer, by strong agitation of the sample at low pH. Next, the sample is adjusted to a pH suitable for bioreactions (e.g. pH 8) and transferred into a bioreactor filled with poly-urethane foam colonized with a bacterial biofilm. Two complementary principles for BOD_{st} determination were investigated in detail. The first principle is to record the acid and/or base consumption by a pH controller while the pH is kept as constant as possible as the bioreactions proceed [61]. This work was the initiation of further research that has resulted in a number of successful sensor implementations for the monitoring of nitrification and denitrification processes, such as BRAM and DECADOS [40, 87, 88, 91, 92, 180, 181, 312]. These sensors are described in more detail in section 4.4.3 on page 93. The second principle is to record a titration curve of the sample before and after the bioreaction. This titration curve is then transformed into a buffer capacity curve and interpreted. The disappearance of buffers, and the formation of new buffers (e.g. IC buffer) is then correlated with the BOD_{st} present in the sample [79]. The latter principle is illustrated in Figure 6.4.¹ A complete measurement cycle typically needs 1 hour. A mathematical model that describes the CO_2 evolution in bioreactors, related to acid-base additions is given in [208].

The most important conclusions from this study on BOD_{st} measurement can be summarized as follows:

¹Note that the buffer capacity curves in Figure 6.4 are obtained from titration curves recorded with the new laboratory titrator set-up, mentioned in section 6.2.1.

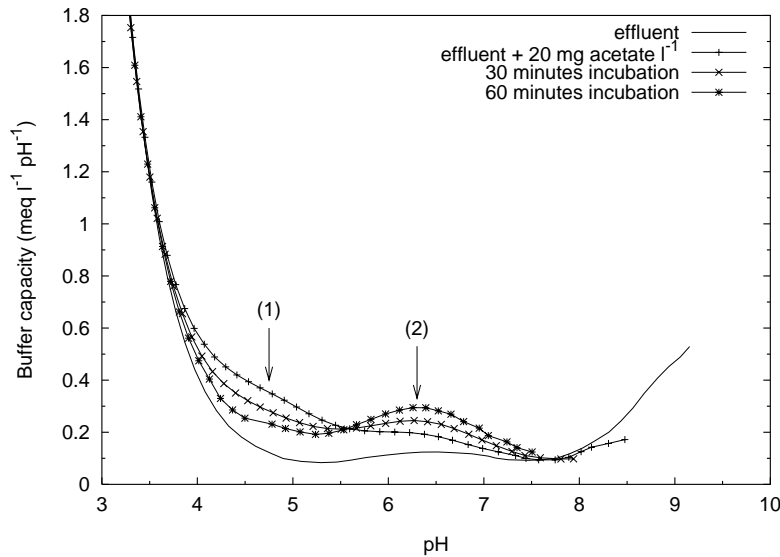


Figure 6.4: Buffer capacity curves of an effluent supplemented with 20 mg l^{-1} acetate buffer, before and after bioreaction. Arrow (1) indicates the decrease of acetate; arrow (2) indicates the increase in IC buffer capacity

- If a readily biodegradable substrate like acetate or sugar is added to the bioreactor, the calculated amount of CO_2 that is theoretically formed corresponds quantitatively with the IC buffer found in the buffer capacity profile. This is also illustrated in Figure 6.4.
- Effluent BOD is only partially degraded in the bioreactor due to the slow biodegradation kinetics. Thus, for practical purposes, calibrations are necessary.
- The biomass in the bioreactor requires an adaptation period of 1 to 2 weeks to a particular water. Despite the fast, accurate and reproducible laboratory results with e.g. acetate additions, the biomass response to an effluent feed pulse under field conditions is not very reproducible. If the biomass is exposed to a high pulse load (e.g. accidental discharge), it takes several measurement cycles (or, equivalently, several hours) before the biomass is at its background response level in absence of substrate, and sometimes the background response level is not reached at all.
- Technical problems with the research set-up (electrical, mechanical, hydraulical, . . .) made that a considerable part of the project time was used to deal with hardware problems. Especially for the measurements in the field, the research set-up often failed.

In a later phase of the project, the experimental set-up was extended with an unit for UV irradiation of aquatic samples [79, 202]. The central idea of those experiments was that increases and decreases of buffer systems due to the photocatalytic UV destruction of the organic material in aquatic samples would correlate with the COD or BOD. The conclusions that were obtained from a number of experiments described in [79, 202] can be summarized as follows:

- The photocatalyst TiO_2 favours the destruction of organic material with UV light, and is

- not an interfering compound in the buffer capacity profile.
- UV irradiation of organic components with buffer capacity (e.g. malonic acid, acetic acid, ...) generates new buffering components, including IC.
 - Stoichiometrically, it was not possible to find a useful relationship between the original COD of a sample and the IC measured from the buffer capacity profile of the UV irradiated sample. It should be noted that the reactor set-up was not completely closed, thus CO₂ exchanges with the atmosphere could not be avoided.
 - The two different low-pressure mercury vapour lamps that were used (monochromatic peaks at respectively 254 and 370 nm) were not sufficiently destructive to transform e.g. effluent COD into CO₂.
 - Optimized conditions for UV destruction were 1 g TiO₂ l⁻¹, pH 1.5–2, 60 minutes irradiation time and the 254 nm lamp.
 - Measurements of COD in effluent samples before and after UV irradiation (in optimized conditions) found only 10–20 % COD removal due to the UV treatment.

Combined treatments with UV and biotransformations were also investigated, albeit not in detail [79]. Despite the poor results obtained in [79, 202], the idea of using UV treatment combined with buffer capacity measurements in various types of aquatic samples is still suggested to be promising, provided a high-pressure mercury vapour lamp in a completely closed reactor would be used.

Measuring the BOD_{st} in low loaded waters, with the technology presented above, seems possible. However, more research is required before this technology is ready for field-use.

6.2.3 Nitrate measurement

As described in section 6.1.2, also nitrate is an important component that contributes in the 'polluting units' formula. However, nitrate as such does not have an observable effect on the pH buffer capacity profile. A number of possible strategies for nitrate measurement based on pH buffer capacity profiles were worked out [61, 70]. The central idea is to include an extra sample pretreatment step in the current sensor approach. This pretreatment step should transform the nitrate quantitatively into a component with measurable buffer capacity. This extra facility should make it possible to measure ammonium, ortho-phosphate and nitrate together from a single buffer capacity profile.

Two reduction strategies were tested and evaluated in detail. The first strategy was based on the reduction of NO₃⁻ into NH₄⁺. This was performed with TiCl₃ in alkaline medium (based on [15]) and with Fe⁰ at low pH (based on [120, 304]). The second strategy was based on a reduction of NO₃⁻ into NO₂⁻. This was investigated with a microbiological method described in [196]. Among the methods and procedures tested [61, 70], the best results were obtained when nitrate was reduced to nitrite, followed by direct determination of nitrite ($pK_a = 3.4$) from the buffer capacity profile, or indirect determination of nitrite with a selective nitrite reacting chemical with a measurable buffer capacity. Good results for the nitrate reduction were obtained with a microbiological method [61] adopted from [196]. The organism *E. Coli K12 DSM 498* has a high nitrate to nitrite reducing activity, but possesses no nitrite reducing activity (see also section 4.2.3 on page 76 for more details about this method). Aniline was found to have an accurately measurable buffer capacity ($pK_a = 4.5$), and having the property to

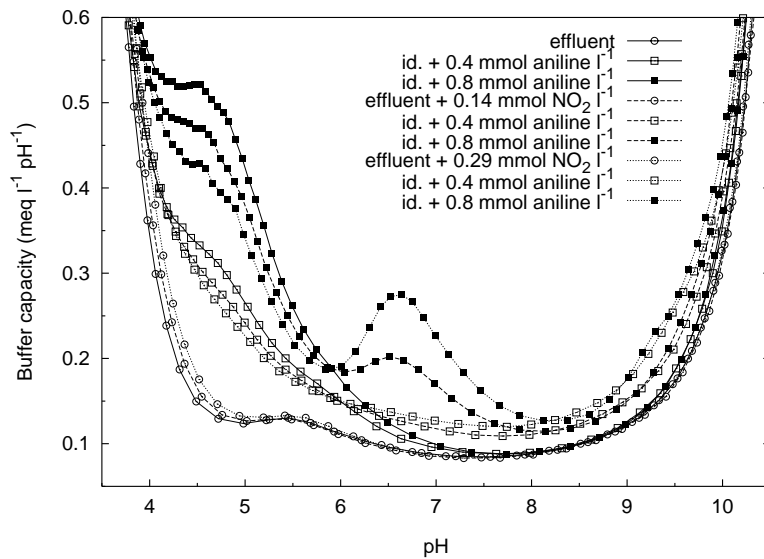


Figure 6.5: Buffer capacity curves of an effluent supplemented with nitrite (0.14 and 0.28 mmol l^{-1}) and/or aniline (0.4 and 0.8 mmol l^{-1}) with the purpose to illustrate a buffer capacity related measurement technique for nitrite

bind nitrite more or less selectively, with the formation of benzenediazohydroxide ($pK_a = 6 - 7$) or phenol ($pK_a = 9.9$). Figure 6.5 shows buffer capacity curves of an effluent supplemented with nitrite and/or aniline. Around pH 4, it can be seen that nitrite itself has a measurable buffer capacity, and that aniline reacts with nitrite with a new buffer formation. Further and more detailed investigations are described in [70].

The nitrate measurement principle, with the technology presented above, gave acceptable results on a number of samples. For example, nitrite standard addition experiments in effluent samples and its measurement through aniline buffer capacity decrease yielded nitrite recoveries between 70 and 110 % [70]. However, the method suffers from interferences which are not fully understood at this moment. Certainly more research is necessary before this technique is ready for field implementation. Further, the extra investments (bioreactor for *E. Coli* cells, aniline dosing system, ...) and the use of hazardous chemicals (aniline), make this rather complicated method less attractive.

6.3 Automatic buffer capacity based sensor

Based on the research results presented in section 6.2, it was decided in the framework of the AQMON project, to narrow the scope of the research towards the detailed interpretation of pH buffer capacity curves only. The ammonium and ortho-phosphate assessment from the buffer capacity profile showed good potentials for field-use, and it was expected that the buffer capacity curve itself could serve as a sort of 'fingerprint' of the water quality. The AQMON

sensor is thus proposed as an automatic buffer capacity based hard- and software sensor. The AQMON measurement principle and the research results with river waters and effluents are presented in the following sections.

6.3.1 Principle of the device

The elementary measurement used in this sensor is a pH measurement. Successive measurements of pH in function of stepwise acid or base addition (with known concentration) to the sample is called a titration curve. In this application, only stepwise base addition is used. From this measured titration curve (typically around 30 to 50 points), the buffer capacity in each point is calculated as the derivative of the amount of base needed (in $meq\ l^{-1}$) for a pH increase of one pH unit. The function obtained as the buffer capacity ($meq\ l^{-1}\ pH^{-1}$) in function of the pH is called the buffer capacity profile. The pH('s) at which a certain component gives its maximum buffer capacity is (are) called the pK_a ('s) of that component. For samples containing several pH buffering components, the buffer capacity curve consists of the sum of the buffer capacities of each individual component. From the buffer capacity curve, estimates of the different buffering components can be computed using a mathematical model. The principle of the decomposition of a complex buffer capacity curve into its components is illustrated in section 2.2.6 on page 22.

The principle of the sensor is illustrated in Figure 6.6. In the wet part, the first step is the sampling (typically 100 – 200 ml) and a pH adjustment to pH 3, followed by a short aeration of 5 minutes to strip the dissolved CO_2 . In the second step a dynamic titration is effected from pH 3 to pH 11. The data processing part is performed in a computer connected to the titration apparatus. First, the titration data are filtered (smoothed, outliers removed) if necessary. Second, the buffer capacity in each point of the titration curve is calculated as the derivative of the amount of base needed for a pH increase of one pH unit. The next step is the mathematical model selection followed by parameter estimation. The candidate models differ in the number of buffering components they include. After the parameter estimation, the concentrations and eventually corresponding pK_a values for the buffering components defined in the model, are obtained. Eventually, a different model can be selected if the fit is not satisfying. The mathematical models used describe the chemical equilibria taking place in the reaction vessel during titration. Models were built using different chemical reaction equilibria described in chapter 2 and mathematically worked out in chapter 3.

In the final output of the sensor, a list of concentrations of buffering components is given. If certain preset values are exceeded an alarm is given and/or an automatic sampler is activated to take a sample for further laboratory analysis. The time for 1 complete run is approximately 30 minutes.

6.3.2 Titrator reproducibility and accuracy

The reproducibility of the ammonium and ortho-phosphate measurement with the research set-up shown in Figure 6.1 was unsatisfactory (see also section 6.2.1). Therefore, the new titration system (based on the laboratory titrator Metrohm Titrino 716 [168]) was evaluated for its reproducibility and accuracy for the assessment of ammonium and ortho-phosphate from buffer capacity curves.

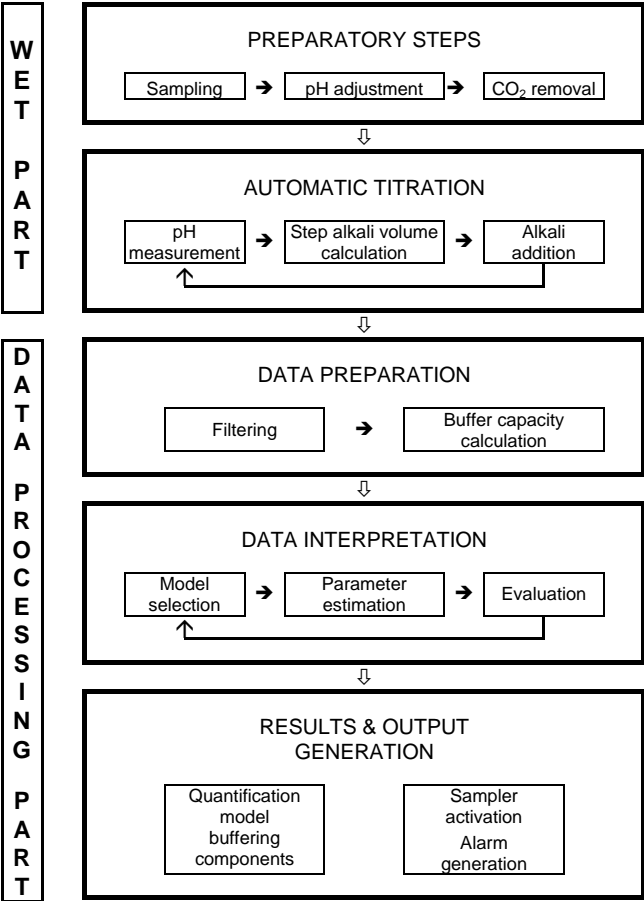


Figure 6.6: Principle of the buffer capacity based AQMON sensor

Table 6.2: Standard addition experiment with the means and standard deviations of the concentrations ammonium and ortho-phosphate estimated from the buffer capacity profiles

Ammonium ($mg\ N\ l^{-1}$)			Ortho-phosphate ($mg\ P\ l^{-1}$)		
Addition	Mean	Std. dev.	Addition	Mean	Std. dev.
0	0.03	0.06	0	0.05	0.10
50	50.2	0.37	12.5	11.8	0.79
75	76.3	1.83	18.75	18.1	0.93
100	101	2.19	25	24.6	0.92

A two-factorial standard addition experiment was designed in which known amounts of ammonium and/or ortho-phosphate were added in 150 ml demineralized water. Samples were adjusted to pH 3 with HCl 1 N, agitated open to the air for 20 minutes to strip off CO₂ and titrated from pH 3 to pH 11. Four different concentrations of ammonium (NH₄Cl) and ortho-phosphate (KH₂PO₄) were used, thus resulting in 16 treatments. Each treatment was replicated in threefold. Summarized results are given in Table 6.2. The different sources of variability in this experiment included: Prepared stock solution variability, manual pipetting and volume adjustment, titrator variability and data processing variability.

Concluded from Table 6.2, the recovery for ammonium is around 101 %, or in other words, 1 % overestimation compared to the amount of ammonium added. For ortho-phosphate, a recovery around 95 % was obtained. The reproducibility or precision can be expressed as a relative standard deviation (r.s.d.), and is found around 2 and 5 % for ammonium and ortho-phosphate respectively. This standard addition experiment was performed with rather high concentrations of ammonium and ortho-phosphate. Other, less extensive experiments, with lower concentrations of N and P were also performed, with similar results for accuracy and reproducibility (results not shown). Ortho-phosphate estimations are generally found to be less accurate and less reproducible compared to ammonium estimations. This is possibly due to higher amounts of interferences present in the buffer capacity region where ortho-phosphate is buffering. Also, ortho-phosphate is more sensitive to complexation reactions with other components, masking its buffer capacity effect. However, this should not be the case in standard addition experiments in demineralized water.

Additions of ammonium and ortho-phosphate were also performed in river waters and effluents. It was experimentally found that the minimum amount of ammonium and ortho-phosphate that can be successfully recovered with the titration method is respectively around 0.5 $mg\ N\ l^{-1}$ and 0.5 $mg\ P\ l^{-1}$. These values are only indicative, because they are case dependent. Further, if a number of interferences related to the NaOH titrant (see section 8.5.2 on page 220) would have been better controlled in these experiments, the accuracy, reproducibility and detection limits can be expected to be better than reported in this section.

6.3.3 Effluent and surface water monitoring

Materials and methods

The experiments to evaluate the performance of the buffer capacity sensor were first performed on the effluents of 26 different domestic wastewater treatment plants. Two to eleven different samples were analyzed per plant. The samples were collected in October 1993 and June 1994. Second, the effluent of an industrial activated sludge wastewater treatment plant of a food company was monitored for 3 months (February to May 1994), with a sampling frequency of 3 to 5 samples per week. This plant was in a start-up phase, so that the effluent concentrations, especially of ammonium, showed a large variation (200 to $500 \text{ mg NH}_4^+ \cdot \text{N l}^{-1}$ in the beginning and between 10 and $20 \text{ mg NH}_4^+ \cdot \text{N l}^{-1}$ at the end of the measurement period). Third, 118 different surface waters in Flanders were sampled in September 1993. From each sample, two or more titration curves were recorded.

All titration curves were obtained with a laboratory construction of the titration sensor. This experimental set-up consisted of a pH adjustment unit to lower the pH of the sample to pH 2–3; an aeration unit, to strip off the carbonate buffer; and an automatic titration unit (Metrohm Titrino 716 [168]). The titration algorithm used was DET (dynamic equivalence-point titration), but in order to obtain the complete titration curve, no end-points were defined in the algorithm. Details about the titrator and its titration algorithms are given in section 5.1 on page 97. A PC-XT was coupled to the titrator via RS-232 for data acquisition.

The off-line laboratory analyses of ammonium, ortho-phosphate and COD were performed by two independent, certified laboratories, respectively referred to as laboratory A and B.

The data processing of the collected titration data was performed off-line, using a unix workstation (HP Apollo 425e or SGI Origin 200). The software *bomb*, described in section 5.3 on page 117, was used for the titration data processing.

A mathematical buffer capacity model containing the following components was used for the validation: water, IC, ortho-phosphate, ammonium and an undefined component (called soap, expressed as mol l^{-1}) with a pK_a between 4.0 and 6.0. The latter component stands for a range of substances (e.g. organic acids) that all have a buffer capacity in the range around pH 5. The detailed model specifications of the buffer capacity model are given in Table 6.3.

The aim of the performed experiments was twofold. First, it is investigated how accurate and reliable the ammonium and ortho-phosphate concentrations in effluents and surface waters can be estimated with the titrimetric sensor. Second, it is evaluated whether the buffer capacity profiles contain particular buffers that can be used to assess e.g. the organic load of the sample, or that can be used as a functional water quality fingerprint.

Domestic wastewater effluent results and discussion

The average ammonium concentration in the domestic wastewater effluents was $11.8 \pm 9.1 \text{ mg N l}^{-1}$ for laboratory A; $11.2 \pm 7.8 \text{ mg N l}^{-1}$ for laboratory B and $26.7 \pm 10.9 \text{ mg N l}^{-1}$ with the titration based sensor. The average concentration for ortho-phosphate in the domestic wastewater effluents was $2.2 \pm 1.6 \text{ mg P l}^{-1}$ for laboratory A; $2.4 \pm 1.6 \text{ mg P l}^{-1}$ for laboratory B and $5.6 \pm 3.8 \text{ mg P l}^{-1}$ with the titration based sensor. Hence, for both ammonium and ortho-phosphate, the titration based sensor overestimates the mean concentrations with a factor 2 to 3 in comparison with the laboratory results. This can be explained by the fact that other

Table 6.3: Model specifications for a simulation interval between pH 4 and pH 10

Buffer	Variable	Initial guess or value	Estimated?	Lower limit	Upper limit
Water	pka_water	15.74	No		
	conc_water	55.5 mol l ⁻¹	No		
IC	pka1_carbon	6.37	No		
	pka2_carbon	10.25	No		
o-PO ₄	conc_carbon	2 mg CO ₂ l ⁻¹	Yes	0	5
	pka1_phos	2.15	No		
	pka2_phos	7.21	Yes	6.5	7.4
	pka3_phos	12.35	No		
NH ₄ ⁺	conc_phos	5 mg P l ⁻¹	Yes	0	200
	pka_ammon	9.25	Yes	9	9.75
	conc_ammon	20 mg N l ⁻¹	Yes	0	600
Soap	pka_soap	5	Yes	4	6
	conc_soap	5 · 10 ⁻⁴ mol l ⁻¹	Yes	0	0.02

buffering components than ammonium and phosphate are present in the effluents, and they are modelled as ammonium or phosphate in the buffer capacity model. Figure 6.7 presents scatterplots with the concentrations of ammonium and ortho-phosphate obtained with the laboratories A and B analyses and with the titrimetric sensor. Comparisons are made between the two laboratories and between the titrimetric sensor and laboratory A or B respectively. The differences between the two laboratories are remarkable (see Figure 6.7 plots (a) and (d)). Typical differences between 2 and 10 mg N l⁻¹ are noticed for ammonium, and between 0.5 and 2 mg P l⁻¹ for ortho-phosphate. This is not surprising when taking into account other studies in which different laboratories are compared with each other [69]. Even under ideal controlled circumstances, differences of ± 10 % between laboratories for measurements in environmental samples of e.g. ortho-phosphate are still very acceptable. Recent so-called Aquacheck tests [62, 301] have found that the relative standard deviation (r.s.d.) of measurements of 1 sample in several laboratories is 6 % and 5 % for ammonium and ortho-phosphate respectively.

The least squares linear regression equations (see Figure 6.7 plots (b), (c), (e) and (f)) are given by equations (6.1)–(6.4):

$$N_{\text{AQMON}} = 10.7 + 1.16 N_{\text{lab A}} \quad (6.1)$$

$$N_{\text{AQMON}} = 11.5 + 1.30 N_{\text{lab B}} \quad (6.2)$$

$$P_{\text{AQMON}} = 1.20 + 0.78 P_{\text{lab A}} \quad (6.3)$$

$$P_{\text{AQMON}} = 1.22 + 0.92 P_{\text{lab B}} \quad (6.4)$$

Each regression equation has a very significant ($\alpha = 0.01$) intercept and slope. The positive intercept is interpreted as a consequence of interfering unknown buffering components present in the effluent samples, and estimated as respectively ammonium or ortho-phosphate. However,

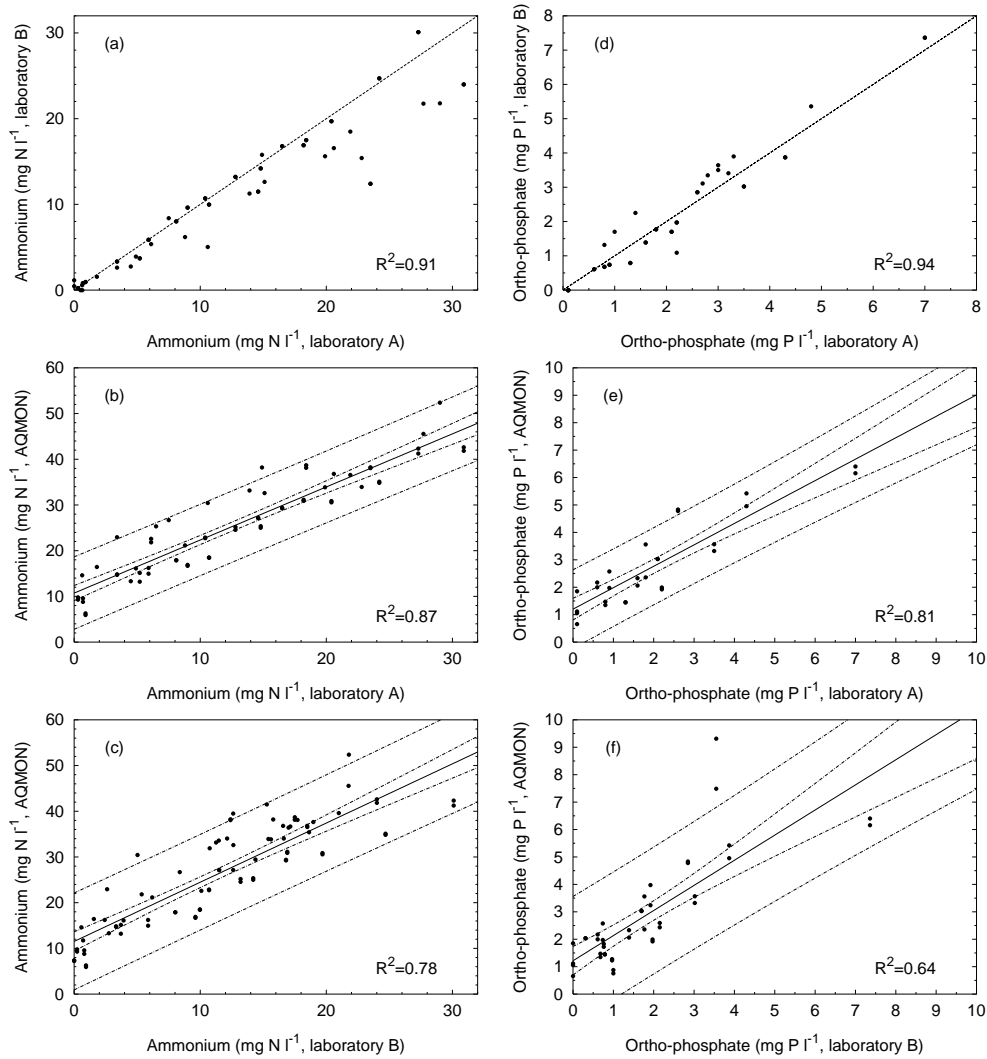


Figure 6.7: Concentrations of ammonium (plots (a), (b) and (c)) and ortho-phosphate (plots (d), (e) and (f)) in 26 domestic wastewater effluents determined with standard methods in laboratories A and B, and estimated with the titrimetric sensor. Bisection lines are plotted on top of scatterplots (a) and (d). Linear regression lines with their 95 % model confidence and prediction intervals are plotted on top of scatterplots (b), (c), (e) and (f)

there is a different interpretation of the regression slopes for ammonium and ortho-phosphate: For ammonium, the slope is significantly ($\alpha = 0.05$) higher than 1 in both regressions (laboratory A and B). This points to increasing concentrations of interfering buffering components with increasing ammonium concentrations. On the other hand, the slope for ortho-phosphate is not significantly different from 1 in the regression equation of laboratory B, but significantly lower than 1 in the regression equation of laboratory A ($\alpha = 0.05$). Two possible explanations for this phenomenon can be formulated: First, interfering buffering components around the pK_{a2} value of ortho-phosphate are not changing or even decrease in concentration with increasing ortho-phosphate concentrations. Second, in samples with higher ortho-phosphate concentrations, it is plausible that a considerable quantity of ortho-phosphate is complexed with other substances, thus masking the ortho-phosphate buffer capacity effect around pH 7. The latter explanation or a combination of the two explanations are considered most realistic.

Nevertheless, an useful correlation between the laboratory results and the titration sensor was obtained, as illustrated in Figure 6.7. Taking into account the residual standard deviations of the linear regressions (4 to 5 $mg\ N\ l^{-1}$ and 0.7 to 1.2 $mg\ P\ l^{-1}$), compared to the standard deviation of the paired differences between the laboratories A and B (2.8 $mg\ N\ l^{-1}$ and 0.25 $mg\ P\ l^{-1}$), one can conclude that the variability between the two laboratories is comparable to the variability between the titrimetric sensor and each of the laboratories. The obtained results show that the buffer capacity sensor is a useful measurement system for on-line monitoring of ammonium and ortho-phosphate in domestic wastewater effluents. Because the titrimetric measurement methodology is undoubtedly sensitive to interferences, the sensor application has in the first place to be seen in the context of an alarm generator. Field research with an automatic and on-line titration system would be very useful to validate and work out the latter statement.

The relationship between the 'soap' buffer (see Table 6.3) and the COD in the domestic wastewater effluents is illustrated in Figure 6.8. An useful determination coefficient $R^2 = 0.75$ was found between the COD and the 'soap' buffer concentration. In the domestic wastewater effluents, the COD varied between 30 and 300 $mg\ l^{-1}$, and the 'soap' buffer concentration is interpreted as a potentially useful alarm generating criterion in case of e.g. accidental discharges in a river. It is also expected that for one particular wastewater treatment plant, the correlation between the 'soap' buffer (or eventually more extra buffers) and the COD can be more significant than this global approach including 26 treatment plants. The latter statement was evaluated with the industrial effluent that was monitored for a consecutive period of 3 months. These results are presented in the next section.

Industrial wastewater effluent results and discussion

The average ammonium concentration in the effluent of the industrial wastewater treatment plant was $115 \pm 92\ mg\ N\ l^{-1}$ for laboratory A; $108 \pm 117\ mg\ N\ l^{-1}$ for laboratory B and $141 \pm 110\ mg\ N\ l^{-1}$ with the titration sensor. The average concentration for ortho-phosphate in the industrial effluent was $3.9 \pm 1.8\ mg\ P\ l^{-1}$ for laboratory A; $5.8 \pm 2.0\ mg\ P\ l^{-1}$ for laboratory B and $10.8 \pm 4.9\ mg\ P\ l^{-1}$ with the titration based sensor. A comparison of the three independent ammonium analyses during the measurement period is shown in Figure 6.9. In the beginning of the measurement period the ammonium concentrations were very high because of the start-up phase of the plant. At the end of the measurement period, the ammonium concentration

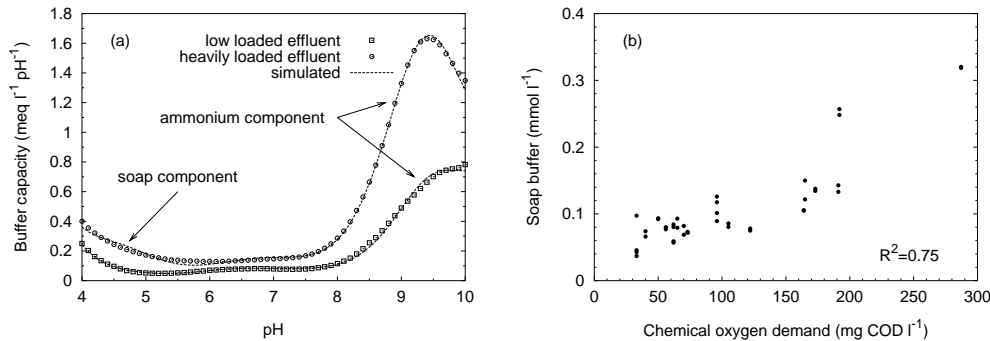


Figure 6.8: Experimental and simulated buffer capacity curves of respectively a low ($1.8 \text{ mg } o\text{-PO}_4\text{-P } l^{-1}$; $5.9 \text{ mg NH}_4^+\text{-N } l^{-1}$; $33 \text{ mg COD } l^{-1}$) and a heavily ($2.7 \text{ mg } o\text{-PO}_4\text{-P } l^{-1}$; $23 \text{ mg NH}_4^+\text{-N } l^{-1}$; $287 \text{ mg COD } l^{-1}$) loaded domestic wastewater effluent (a); Scatterplot of the COD of 26 domestic effluents versus the concentration of the ‘soap’ buffer obtained with the buffer capacity sensor

decreased below $10 \text{ mg NH}_4^+\text{-N } l^{-1}$. Over the whole period the titration sensor was able to estimate the ammonium concentration in the effluent. The determination coefficient between the titration sensor and the laboratory measurements was $R^2 = 0.92$, almost the same value as the determination coefficient of the ammonium concentration measured in the two independent laboratories ($R^2 = 0.94$).

The ortho-phosphate concentrations in the industrial effluent samples were rather low compared to the ammonium and COD concentrations (around $4 \text{ mg P } l^{-1}$). Further, the ortho-phosphate concentrations measured in laboratories A and B showed a bad agreement (results not shown, $R^2 = 0.65$). The titrimetric estimations of ortho-phosphate did not show an useful correlation with the laboratory measurements. This can possibly be explained by the high COD load in the effluent (between 150 and $1500 \text{ mg } l^{-1}$), causing too many interferences with the ortho-phosphate buffer capacity effect.

The determination coefficient between the concentration of the undefined buffering component between pH 4 and 5 (assumed to be the ‘soap’ component) and the COD in the effluent was $R^2 = 0.69$. This buffering component was consequently evaluated as an indicator of sudden organic loads in the effluent, as illustrated in Figure 6.10. Figure 6.10(a) shows the buffer capacity curves of the effluent during normal operation ($200 \text{ mg COD } l^{-1}$), and two unexpected peak loadings (800 and $1500 \text{ mg COD } l^{-1}$ respectively). The buffering components between pH 4 and 5 were not identified conclusively. Figure 6.10(b) illustrates the correlation between the effluent COD and the ‘soap’ buffer concentration ($R^2 = 0.69$). The two unexpected COD peak loadings in the effluent were perfectly recognized by the increasing ‘soap’ buffer concentration. This illustrates that for this particular industrial effluent, the AQMON sensor is suited for alarm generating purposes in case of unexpected effluent COD discharge peaks.

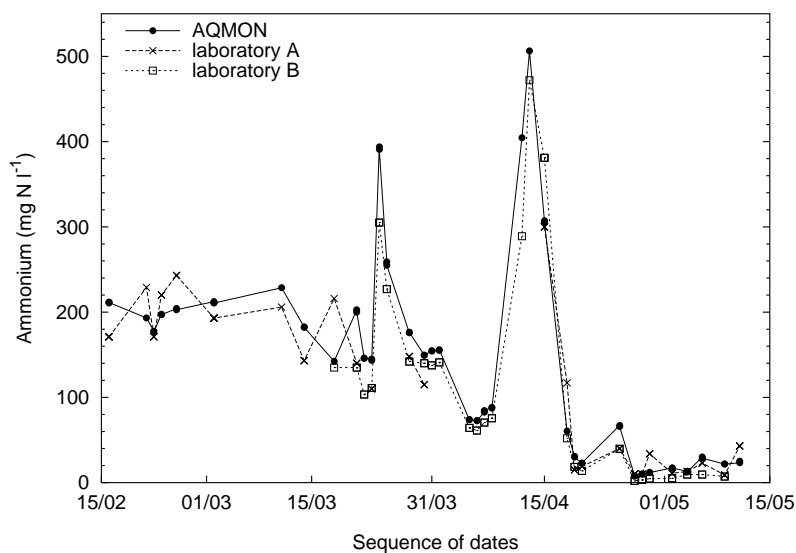


Figure 6.9: The ammonium concentration measured by two independent laboratories A and B and the titrimetric sensor in the effluent of an industrial wastewater treatment plant

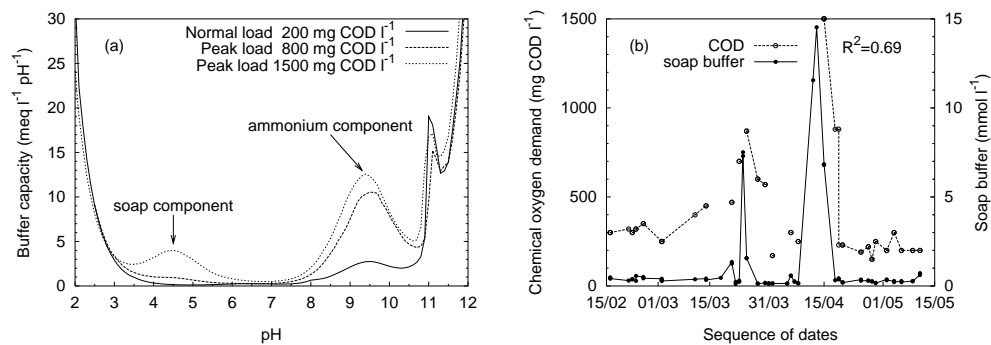


Figure 6.10: Experimental industrial effluent buffer capacity curves of three selected days with various COD loadings (a); Corresponding COD and 'soap' buffer concentrations in function of time (b)

Surface water results and discussion

The average ammonium concentration in the sampled surface waters was $6.7 \pm 8.2 \text{ mg N l}^{-1}$ for laboratory A; $6.6 \pm 8.6 \text{ mg N l}^{-1}$ for laboratory B and $14.3 \pm 10.7 \text{ mg N l}^{-1}$ with the titration based sensor. The average concentration for ortho-phosphate in the surface waters was $2.5 \pm 3.8 \text{ mg P l}^{-1}$ for laboratory A; $3.0 \pm 4.4 \text{ mg P l}^{-1}$ for laboratory B and $3.4 \pm 4.0 \text{ mg P l}^{-1}$ with the titration based sensor. Hence, for both ortho-phosphate and ammonium, the titration based sensor overestimates the mean concentrations with respectively 20 – 30 % and 100 % in comparison with the laboratory results. This overestimation is clearly lower than the 200 – 300 % overestimation in the effluent samples. This points to possibly less interferences of unmodelled buffer components in surface waters compared to effluents. Figure 6.11 presents scatterplots of the concentrations of ammonium and ortho-phosphate obtained with the laboratories A and B analyses and with the titrimetric sensor. Comparisons are made between the two laboratories and between the titrimetric sensor and laboratory A or B respectively. The analyses differences between the two laboratories are similar as observed for the effluents.

The least squares linear regression equations (see Figure 6.11 plots (b), (c), (e) and (f)) are given by equations (6.5)–(6.8):

$$N_{\text{AQMON}} = 5.95 + 1.24 N_{\text{lab A}} \quad (6.5)$$

$$N_{\text{AQMON}} = 6.64 + 1.16 N_{\text{lab B}} \quad (6.6)$$

$$P_{\text{AQMON}} = 0.87 + 0.99 P_{\text{lab A}} \quad (6.7)$$

$$P_{\text{AQMON}} = 0.86 + 0.84 P_{\text{lab B}} \quad (6.8)$$

Each regression equation has a very significant ($\alpha = 0.01$) intercept and slope. Similarly to the effluents, the positive intercept is interpreted as a consequence of interfering unknown buffering components present in the surface water samples, and estimated as respectively ammonium or ortho-phosphate. However, these interferences are clearly lower than in the effluent samples. For ammonium, the slope is significantly ($\alpha = 0.05$) higher than 1 in both regressions (laboratory A and B). The slope for ortho-phosphate is not significantly different from 1 in the regression equation of laboratory A, but significantly lower than 1 in the regression equation of laboratory B ($\alpha = 0.05$). These findings lead to the same conclusions as formulated for the domestic wastewater effluents.

Again, an useful correlation between the laboratory results and the titration sensor was obtained, as illustrated in Figure 6.11. Taking into account the residual standard deviations of the linear regressions (3 to 4 mg N l^{-1} and 1.5 to 1.7 mg P l^{-1}), compared to the standard deviation of the paired differences between the laboratories A and B (1.8 mg N l^{-1} and 0.95 mg P l^{-1}), one can conclude that the variability between the two laboratories is comparable to the variability between the titrimetric sensor and each of the laboratories. The results obtained show that the buffer capacity sensor is a potentially useful measurement system for on-line monitoring of ammonium and ortho-phosphate in surface waters. It is expected that in case an AQMON buffer capacity sensor would be installed on-line at a particular sampling point in a river, even better results can be obtained if local model adjustments or extra local calibrations would be implemented. However, up to now the latter statement was not validated in the field.

Figure 6.12 illustrates the correlations between the concentration of the ‘soap’ component found with the titration sensor and the COD and the BOD respectively. Both correlations are

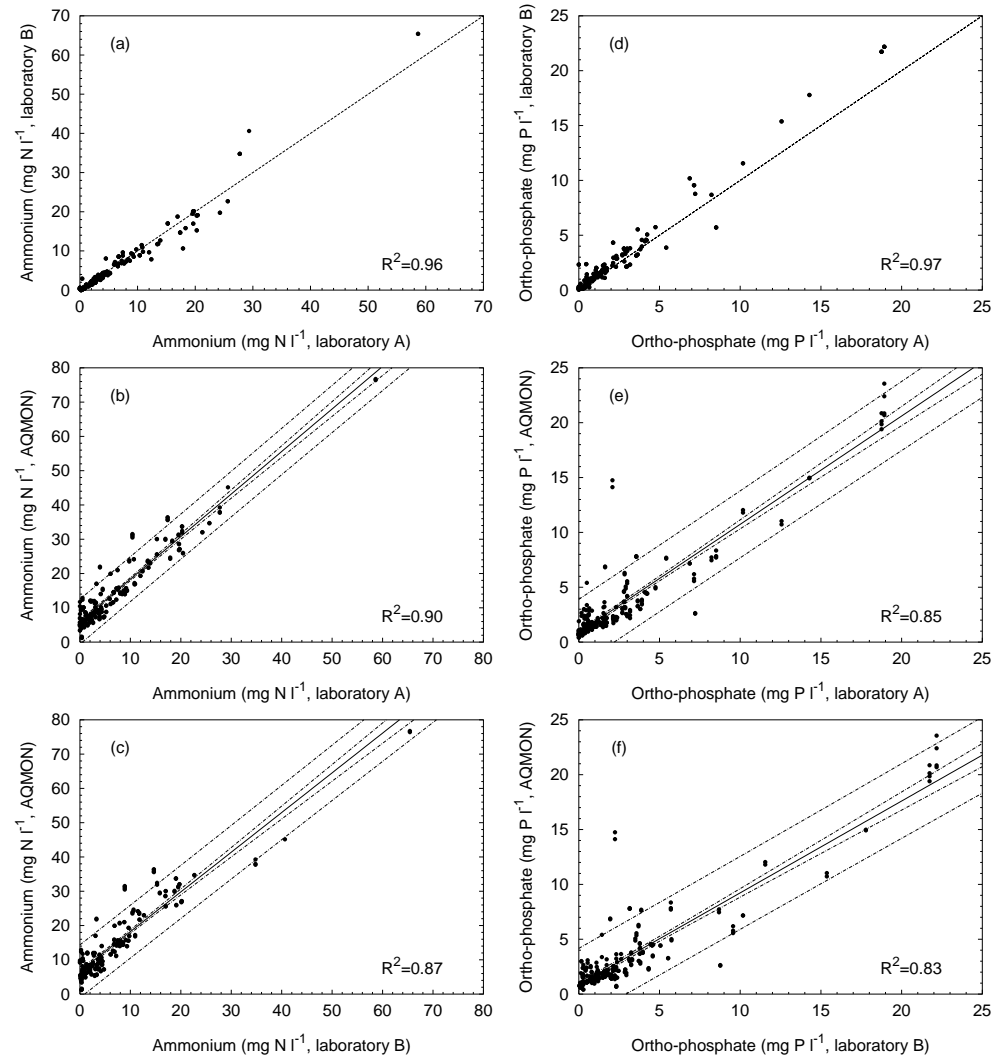


Figure 6.11: Concentrations of ammonium (plots (a), (b) and (c)) and ortho-phosphate (plots (d), (e) and (f)) in 118 Flemish surface waters determined with standard methods in laboratories A and B, and estimated with the titrimetric sensor. Bisection lines are plotted on top of scatterplots (a) and (d). Linear regression lines with their 95 % model confidence and prediction intervals are plotted on top of scatterplots (b), (c), (e) and (f)

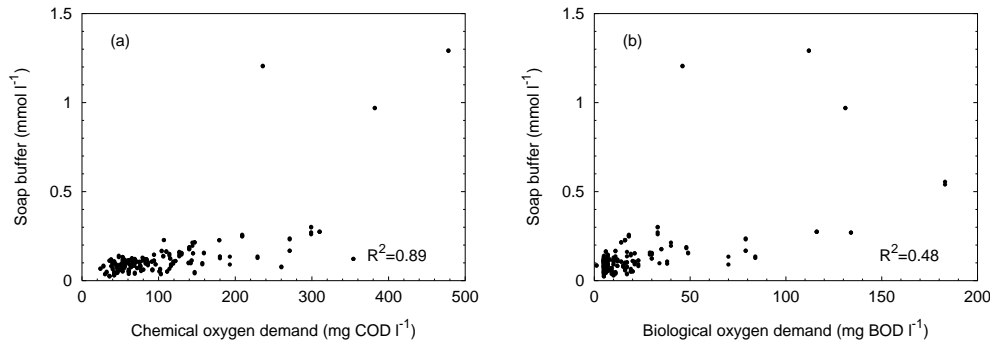


Figure 6.12: Scatterplot of the COD (a) and BOD (b) of 118 Flemish surface waters versus the concentration of the ‘soap’ component obtained with the buffer capacity sensor

statistically significant ($\alpha = 0.01$), and the amount of ‘soap’ buffer correlates better with the COD than with the BOD of surface water samples. It should be mentioned that the variability of BOD measurements between and within laboratories is much higher compared to COD measurements [69]. On theoretical basis, there should not be a strict relationship between buffer capacities and COD (e.g. sugars have no buffer capacity, but a high COD). Nevertheless, a useful correlation between the ‘soap’ signal and the organic load of a river is established. As discussed above, it is again expected that for one particular sampling point, better correlations can be obtained when the buffer capacity model is ‘tuned’ for that location.

Buffer capacity model evaluation

A detailed study of the buffer capacity curves of the effluents and surface waters in relationship with their ammonium and ortho-phosphate concentrations was performed, and some observed phenomena were related to the selected buffer capacity model and the model fit. The buffer capacity model of which the model specifications are given in Table 6.3 was fitted to all experimental buffer capacity curves. The experimental and the best-fit simulated buffer capacity curves of 6 selected surface water samples are given in Figure 6.13. The ammonium and ortho-phosphate concentrations found in laboratories A and B, and with the AQMON set-up respectively are given in Table 6.4.

Example (a) in Figure 6.13 illustrates a typical example of an almost perfect model fit, with a good estimation of ortho-phosphate, but around 80 % overestimation of ammonium. The most probable explanation is the presence of one or more extra buffer systems around pH 9–10, that are modelled as ammonium.

Example (b) shows a heavily loaded river water, with a good model fit, and reliable estimations of ammonium and ortho-phosphate. Some other heavily loaded waters (results not shown) showed a bad model fit, sometimes coupled to wrong estimations mostly of ortho-phosphate (e.g. one dark brown river water with a COD of 2500 mg l^{-1} , had a seven times overestimation of ortho-phosphate compared to the laboratory measurements; this particularly

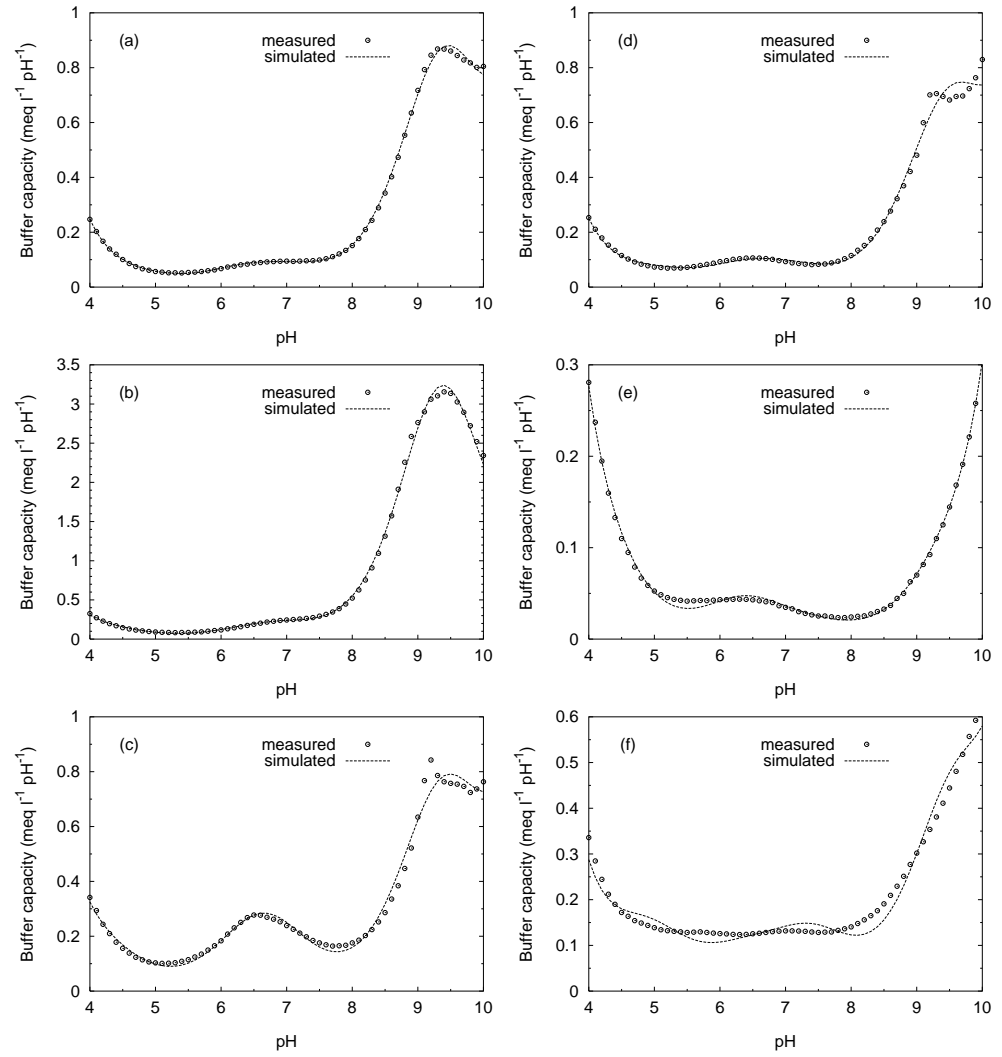


Figure 6.13: Experimental and simulated buffer capacity curves of 6 selected Flemish surface waters: Bassin Smedenstraat, Roeselare (a); Vuile beek, Ieper (b); Uyttenhovebeek, Roeselare (c); Zwinnevaart, Knokke-Heist (d); Scherpenbergbeek, Poperinge (e); Zarrenbeek, Staden (f). Note the remarkable differences in buffer capacity scale.

Table 6.4: Ammonium and ortho-phosphate concentrations of 6 selected Flemish surface waters determined in laboratories A and B, and with the titrimetric sensor

Figure 6.13		Ammonium ($mg\ N\ l^{-1}$)			Ortho-phosphate ($mg\ P\ l^{-1}$)		
Subplot	Code ^a	lab. A	lab. B	AQMON	lab. A	lab. B	AQMON
(a)	6260	12.0	9.7	19.3	3.0	2.2	2.4
(b)	9740	58.6	65.4	76.7	8.2	8.7	7.7
(c)	6230	3.3	3.1	16.9	10.2	11.6	11.8
(d)	260	4.5	8.1	15.2	7.2	8.8	2.6
(e)	9750	0.4	0.3	1.2	0.2	0.2	0.6
(f)	9270	3.0	2.6	9.0	2.8	3.7	6.2

^a Identification number of the sampling point, attributed by the VMM.

extreme case corresponds with the two high outlier points in Figure 6.11(e) and (f).

Example (c) illustrates a surface water with difficulties for the ammonium estimation. The buffer capacity around the ammonium buffer had a typical unstable behaviour and the estimated ammonium concentration is 5 times too high compared to the laboratory results. Remarkable for this surface water is the high concentration of chlorides ($> 500\ mg\ Cl\ l^{-1}$). Similar phenomena were observed in some other samples with high chloride concentrations.

The surface water in example (d) is located near the Northsea and has a very high amount of chlorides ($2005\ mg\ Cl\ l^{-1}$). The concentration of ortho-phosphate estimated from the buffer capacity profile is rather exceptional because it is three times lower than the laboratory results; this particular case can easily be located as an outlier point in Figure 6.11(e) and (f). Moreover, this sample contained $260\ mg\ COD\ l^{-1}$, which was one of the highest values in the study. Possibly, some ortho-phosphate remained complexed with other components during titration, and was thus not available as a buffer around pH 7. One could suggest to introduce ionic strength corrections in the buffer capacity model. However, from the graph it can be concluded that it is unlikely that this would have a significant improving effect on the estimated buffer concentrations, due to the presence of interfering buffers in the neighbourhood of ortho-phosphate.

Example (e) is obtained from a clean river water. The laboratory results indicate that both ammonium and ortho-phosphate are below $1\ mg\ l^{-1}$. The model fit is satisfying, except that there is probably an extra buffer present at pH 5.5 which is not accounted for in the buffer capacity model. A typical phenomenon observed in low loaded waters is a relatively large overestimation of ammonium and ortho-phosphate (a factor 3 in this particular case). This could be explained by the higher relative amount of interferences, that are modelled as ammonium or ortho-phosphate.

Example (f) is the most extreme example where the model fit is not satisfying. The experimental buffer capacity profile indicates that more buffer systems are distributed in the considered pH interval, compared to the theoretical buffers included in the buffer capacity model specified in Table 6.3. As a consequence, the estimated concentrations of ortho-phosphate and ammonium cannot be trusted.

From detailed visual explorations of the experimental and corresponding simulated buffer capacity profiles of effluents and river waters in relationship with their laboratory analyses, a number of conclusions can be drawn:

- There is no strict relationship between the goodness of fit and the agreement between the ammonium and ortho-phosphate laboratory analyses and the titrimetric results.
- Examples with a perfect model fit have often good estimations for ammonium and ortho-phosphate, but sometimes suffer from interferences present at the same pK_a value of the modelled buffer systems.
- Estimated concentrations of samples with a bad model fit should be interpreted very carefully. They are mostly suffering from extra interferences compared to well fitting examples. It could be suggested to use a modified or extended mathematical buffer capacity model in those cases.

Among different evaluated mathematical models (i.e. fixed or variable pK_a values, fixed or variable amount of IC buffer, wide or small simulation interval), the model specified in Table 6.3 was found to be the best 'general purpose' model. This is an important aspect for field implementations, because it is not always possible or realistic to set up preliminary experiments to define the best site-specific buffer capacity model. In this framework, it was also investigated whether it is advantageous with respect to ammonium and ortho-phosphate assessment, to implement an automatic buffer capacity model builder (available in the software *bomb* described in section 5.3 on page 117). These results are presented in chapter 9.

6.4 Conclusions

The proposed titration sensor can be used for effluent and surface water monitoring of pH buffering substances. Experiences with different types of samples have shown that the accuracy and precision are affected by the composition of the sample. The sensor is capable of giving an indication of the ammonium and ortho-phosphate level in the tested effluents and surface waters. The results in Figures 6.7 and 6.11 illustrate that the variability between the laboratory analyses and the titrimetric estimations is comparable to the variability between the two independent laboratory results.

The buffer capacity at certain pK_a 's is suggested to give an indication of the organic load. More particularly, the buffer capacity around pH 5 (named the 'soap' buffer) was found to have an useful correlation with the COD of the sample, both for surface waters and effluents.

Due to possible interferences of buffering components and the presence of unmodelled buffering components in the effluent, this titration sensor cannot be proposed for use as an analytical instrument. Rather it should be used as an effluent or surface water quality indicator and detector of possible changes in the sample composition. The titration sensor is suitable for integration in a robust and reliable automated instrument. An important advantage of the sensor is that no filtration is required. The model database can be easily extended and fully adjusted to particular requirements. The proposed buffer capacity model has been shown to be useful for general purposes. However, it is suggested that a site-specific tuning of the mathematical model could offer some perspectives for better and more specific predictions.

The sensor can be used for alarm triggering when the buffer capacity profile changes. However, this should be further investigated and validated with field experiments. This sensor coupled to an automatic sampler can be used for quality dependent sampling. In this case the buffer capacity profile is used as a fingerprint for the water composition, and when the fingerprint is changing, a sample is taken for further laboratory analysis. The quality dependent sampling is superior to the time- or flow proportional sampling if such sampling strategy would lead to a significantly lower number of laboratory analyses to be performed.

Chapter 7

Tertiary algal wastewater treatment monitoring

The results of this chapter were also published in [308].

7.1 Introduction

7.1.1 Algal wastewater treatment

Traditionally, the aims of wastewater treatment have been to reduce the concentration of organic matter and the number of pathogens. However, in many treatment plants typical primary and secondary treatments cannot meet the increasingly stringent requirements of water pollution control. Although secondary effluents may contain low levels of BOD and COD, they still contain high levels of inorganic nutrients (NH_4^+ , NO_3^- , PO_4^{3-}). These nutrients are primarily responsible for eutrophication of the receiving waters [147, 230].

Nowadays more and more plants adapt and/or extend their secondary treatment facilities towards 'nutrient removal capacity' [18, 128, 220], but even effluents with low concentrations of these pollutants can have a negative impact on the environment if they are discharged in high volume, especially if the receiving water is a rather small river. Tertiary treatment is becoming a necessity to minimize the harmful impact of effluents on the environment.

Besides biological nitrogen and phosphorus removal, numerous physico-chemical treatments such as chemical coagulation, breakpoint chlorination, NH_3 -stripping, reverse osmosis and filtration have been proposed for removing nitrogen and phosphorus. However, due to costs and operational practices, these technologies are not implementable for municipal wastewater treatment of small communities [151].

As an alternative, tertiary treatment involving micro-algae or cyanobacteria is shown to be effective in nitrogen and phosphorus removal [147, 151]. The process is quite attractive because of its capacity to transform wastes into useful biomass using sunlight as an energy source. However these algal treatment systems also have some drawbacks: The generation time of the organisms involved is long compared to bacteria; there is a necessity for sunlight;

the active part of the biomass is small and harvesting of biomass is difficult [67, 230].

In recent years, research has been conducted to overcome the problems related to algal tertiary wastewater treatment, and to optimize the treatment process [68, 146, 151, 275, 280]. The harvesting problem of the algal biomass has been solved by using organisms like the cyanobacterium *Phormidium bohneri*, which has the ability to form flocks that settle, thus facilitating harvest [258].

Algal wastewater treatment processes often are discontinuous, of SBR (sequencing batch reactor) type, where one treatment cycle consists of a filling phase, an aeration phase, a settling phase and an effluent discharge phase. Such processes need continuous monitoring of the most important process variables, in order to obtain an optimal nutrient removal capacity at minimal costs. Especially when one realizes that nutrient removal processes are often related to phases of luxury uptake (e.g. phosphates) and phases of nutrient release, the usefulness of on-line measurements is obvious.

7.1.2 Alkalinity related to algal processes

The alkalinity of a water sample is defined as the amount of acid necessary to decrease the pH to a predefined end value. Two end values are considered [104]:

- End value 8.3 (only relevant if the sample pH is higher than 8.3): this is called the phenolphthalein or carbonate alkalinity (symbol C), and is a measure of the amount of strong bases, carbonates and alkali present in the sample.
- End value 4.5 (only relevant if the sample pH is higher than 4.5): this is called the total alkalinity (symbol T), and is a measure of the amount of strong and weak bases (like bicarbonates).

The alkalinity can be measured in the laboratory using a recipient of known volume of sample and a burette containing a strong acid (e.g. HCl 0.02 N). It can be expressed in $meq\ l^{-1}$ or in $mg\ CaCO_3\ l^{-1}$.

Alkalinity is a popular measurement used in the process control of diverse water treatment processes, e.g. in activated sludge treatment [249, 256, 283] or in anaerobic wastewater treatment [46, 71]. In practice alkalinity is often used as a practical measure of the amount of carbonates and bicarbonates in the water. There are some particular remarks concerning the use of alkalinity as '(bi)carbonate' estimator:

- In cases the sample is loaded with weak acid buffering systems other than the CO₂ subsystem (like ammonium, phosphates and VFA's), these components will be included in the alkalinity and will suggest that more (bi)carbonates are present than in reality [65].
- For the pH meter method, it is advised to choose the end value in function of the alkalinity (end-value ranging from pH 4.3 to pH 4.9 for high to low alkalinity respectively) [281]. For colour indicator methods, like the bromcresol method, the pH value 4.5 corresponds with the inflection point on the titration curve where the colour indicator will switch to its other state. In case the inflection point is not so sharp, or the solution contains strong colouring substances, the colour switch will be difficult to observe. For this reasons, the pH meter method is mostly preferred above the older colour indicator methods.

In the application area of wastewater treatment, modified or extended methods of the alkalinity measurement have been developed. Examples of extended methods where more than 1 end value in the titration profile are considered are a three-point method [12] and a five-point method [197] for the determination of bicarbonate and VFA. Methods using more than 5 points for bicarbonate and VFA estimation have also been developed [36, 228]. To eliminate the effect of interfering pH buffers when one is only interested in bicarbonate content, a method was developed where the CO_2 is stripped from the sample by addition of strong acid. The stripped CO_2 can be directly measured by the volumetric [108, 111] or pressure [71] build-up of CO_2 . The described methods have been used in the application area of anaerobic treatment, where high concentrations of both bicarbonate and VFA's are present [46, 65]. An overview of measurement methods for CO_2 and bicarbonate is given in [75, 219].

Alkalinity related techniques for bicarbonate estimation are well developed in applications where CO_2 is continuously generated by micro-organisms degrading organics. In these areas possible interferences with other pH buffering components are negligible. In the area of algal treatment, on the other hand, CO_2 is consumed by the algae, resulting in relatively low or even limiting concentrations of bicarbonate in the water samples. Inorganic carbon (IC) is of major importance, because it is the only carbon source used by algae. Among the different forms of IC ($\text{CO}_{2(aq)}$, HCO_3^- and CO_3^{2-}), only the two first ones are taken up by the algal biomass, and thus useful as a carbon substrate [80, 97, 278]. The preference for $\text{CO}_{2(aq)}$ or HCO_3^- uptake is pH dependent [286] and an adaptation period to switch between the $\text{CO}_{2(aq)}$ and HCO_3^- transport system may be required [80]. The importance of the IC buffer system in relation to photosynthetic algal growth is widely described in literature [199, 259, 277, 279]. Therefore, the usefulness of quantifying the IC buffer for algal wastewater treatment is twofold. First, a precise knowledge of the inorganic carbon content can indicate whether the IC becomes limiting [199], and whether IC supply is needed [259, 279]. Second, because IC is the only carbon source used by the algae, the rate of IC consumption under light conditions can be used as a process and control variable, e.g. indicating a possible reactor failure if the IC consumption is too low.

7.1.3 Objectives

The objective of this chapter is to develop a pH buffer capacity based sensor, capable of extracting concentrations of pH buffering components from on-line measured titration curves coming from the influent, effluent and reactor content of an algal pilot plant. The information that can be extracted from the buffer capacity profiles using mathematical modelling is evaluated towards its usefulness related to tertiary algal treatment processes. The relationship between the alkalinity and the IC buffer capacity will be discussed, as well as the ammonium and orthophosphate assessment from the buffer capacity profile. In the latter case, IC, NH_4^+ and $o\text{-PO}_4$ will be incorporated in equation (3.59) on page 49 as diprotic, monoprotic and triprotic weak acids respectively. The results obtained with the buffer capacity sensor seem promising as input to develop a control strategy, although this is not the objective of this chapter.

7.2 Materials and Methods

7.2.1 The algal pilot plant

A pilot reactor with algal biomass, installed at the outlet of the activated sludge plant Valcartier near Quebec city (Canada), was used for the sample collection between July 22 and August 12, 1997. The activated sludge plant was treating domestic wastewater of the military base Valcartier, and received an influent flow of around $2500 \text{ m}^3 \text{ d}^{-1}$. The plant was operating in partially nitrifying mode and the secondary effluent nitrogen was present in two forms, NH_4^+ and NO_3^- .

The algal bioreactor with a triangular cross-section had a volume of 6 m^3 and combined aeration and mixing was obtained by means of a perforated flexible tube at the bottom of the reactor. This pilot reactor was in use for 2 years and its function was to further decrease the nutrient concentrations of the secondary effluent. The reactor was used in batch mode, in cycles of 1 or 2 days. A cycle consisted of a filling phase (in the morning), an aeration phase of 12 or 36 hours, a sedimentation phase (at night) to allow the algae to settle down, and a decantation phase (in the morning) to remove an upper liquid layer of around 75 % of the total reactor volume. The biomass concentration in the reactor was kept between 100 and 600 mg DW l^{-1} .

7.2.2 Sampling and laboratory measurements

Light, pH, DO and temperature were monitored continuously in the algal pilot plant. Three different kinds of samples were taken for further analysis in the laboratory:

- The Effluent of the ValCartier plant (sample code EVC), being the influent of the algal pilot reactor;
- The content of the Algal Pilot (sample code AP), 3 hours after the reactor was filled and completely mixed by the aeration;
- The Effluent of the Algal Pilot plant (sample code EAP).

The EVC and EAP samples were taken with a peristaltic pump in the inlet and outlet of the pilot plant during filling and decantation phases respectively. The AP samples were taken as manual grab samples. All samples were stored immediately in the fridge (4°C) and processed in the laboratory within 1 day.

Prior to the laboratory analyses (NH_4^+ , NO_3^- , $o\text{-PO}_4$), all samples were filtered on a Whatman 934 AH filter, with a pore size of $1.5 \mu\text{m}$. The analyses were conducted according to Standard Methods [104]. For the total alkalinity measurements in the laboratory, the pH meter method was used [104].

7.2.3 Titration curves

Titrations were performed with a laboratory titrator (Metrohm Titrino 716 [168]). Data acquisition was performed with a 386 PC connected to the titrator. The titrated sample volume was 100 ml , and titration took place in a completely closed magnetically stirred titration vessel containing a CO_2 scrubber (bowed glass tube with soda lime pellets) to prevent entrance of CO_2 from the air. The headspace of the titration vessel was 150 ml . Prior to titration, the

refrigerated samples were equilibrated to 25 °C with a warm water bath, and they were immediately titrated at room temperature, which varied between 20 and 25 °C. Two different types of titration profiles were collected:

Down titration profile: The sample as such was titrated with 0.1 N HCl from the actual pH to pH 2.5 using a monotonic end-point titration (MET) method [168], with fixed steps of 0.05 ml. This type of titration was used for the determination of the IC buffer.

Up titration profile: The down titrated sample was strongly agitated with a magnetic stirrer for 15 minutes to remove all CO₂, while the titration vessel was open to the air. Next, the vessel was closed and the sample was titrated with 0.1 N NaOH to pH 11 using a dynamic end-point titration (DET) method [168]. The difference with the MET method is that the DET method does not take fixed volume steps, but variable volume steps (small versus big steps when the buffer capacity is low or high respectively). This type of titration was used for the determination of ammonium and ortho-phosphate.

7.2.4 Data processing software

The software *bomb*, described in section 5.3 on page 117, was used for the calculation of the buffer capacity profiles. Such a profile is the inverse of the first derivative of the titration profile. The calculation of the derivative was performed using a parabolic regression in a moving window of 5 experimental data points of the titration curve. No further smoothing algorithms were necessary to obtain a smooth buffer capacity profile. The same software was used to fit several mathematical models to the calculated buffer capacity curve. The mathematical model specifications were defined in a special input file, read by the program. The software was running on an INDIGO workstation (Silicon Graphics, U.S.) and the data processing of 1 experimental data file needed approximately 1 minute.

7.2.5 Mathematical models

The mathematical models used were all based on the general buffer capacity equation (3.59) on page 49. For each model used, the following considerations were taken into account:

- The pH interval used for data processing.
- Which pH buffering components to be included in the model.
- The initial guesses for the concentrations and pK_a values.
- Which concentrations and pK_a values had to be adjusted in order to fit the simulation model to the experimental data. The parameters that are to be estimated are specified with a lower and upper limit (constrained optimization). The reason for optimizing pK_a values instead of keeping them fixed at the pK_a^0 or another value is to take into account the residual effects of temperature, ionic strength and possible electrode errors on the position of the pK_a values in the experimental buffer capacity curve.

For the down titrations a simulation interval between pH 4 and pH 7.3 was taken. Even if the initial pH of the sample was much higher than 7.3, it was not worthwhile to extend the simulation interval and incorporate ortho-phosphate or ammonium in the model, because the magnitude of the IC buffer would interfere with the other smaller buffer systems. For

Table 7.1: Down titration model specifications for a simulation between pH 7.3 and pH 4

Buffer	Variable	Initial guess or value	Estimated?	Lower limit	Upper limit
Water	pka_water	15.74	No		
	conc_water	55.5 mol l ⁻¹	No		
IC	pka1_carbon	6.37	Yes	6	7
	pka2_carbon	10.25	No		
	conc_carbon	1 meq IC l ⁻¹	Yes	0	2.5
Soap	pka_soap	4.8	Yes	4	5.5
	conc_soap	5 · 10 ⁻⁵ mol l ⁻¹	Yes	0	1 · 10 ⁻³

the up titrations, a simulation interval between pH 4 and pH 10 was chosen. In the software, concentrations can be specified in mol l⁻¹ or mg l⁻¹. More detailed model specifications for the down and up titrations are shown in Table 7.1 and Table 7.2 respectively. The ‘soap’ term in the models stands for a range of components that all have a buffer capacity in the range between pH 4 and pH 5.5, e.g. numerous organic acids. The ‘blank1’ term represents an unknown buffering component around pH 10, found to be present in almost all samples analyzed. The reason for incorporating the ‘carbon’ component in the up titration model, despite the fact that the sample is made CO₂ free, is that during up titration the CO₂ initially present in the headspace above the vessel, or small amounts of CO₂ present in the titrant, can enter the sample and typically account for 0.07 meq IC l⁻¹.

Furthermore, once the total concentration C_{IC} (which is [CO₃²⁻] + [HCO₃⁻] + [CO_{2(aq)}]) is determined using the simulation model, the partitioning of these 3 forms can be calculated as function of the actual pH [281]. Using the mass balance and the 3 equilibrium equations for IC, the concentrations [CO_{2(aq)}], [HCO₃⁻] and [CO₃²⁻] are given by equations (7.1), (7.2) and (7.3) respectively. Details on obtaining these equations can be found in [273, 281].

$$[\text{CO}_{2(aq)}] = \frac{10^{-2\text{pH}}}{10^{-2\text{pH}} + 10^{-(\text{pH} + \text{p}K_{a1})} + 10^{-(\text{p}K_{a1} + \text{p}K_{a2})}} C_{\text{IC}} \quad (7.1)$$

$$[\text{HCO}_3^-] = \left(1 - \frac{10^{-2\text{pH}} + 10^{-(\text{p}K_{a1} + \text{p}K_{a2})}}{10^{-2\text{pH}} + 10^{-(\text{pH} + \text{p}K_{a1})} + 10^{-(\text{p}K_{a1} + \text{p}K_{a2})}} \right) C_{\text{IC}} \quad (7.2)$$

$$[\text{CO}_3^{2-}] = \left(1 - \frac{10^{-2\text{pH}} + 10^{-(\text{pH} + \text{p}K_{a1})}}{10^{-2\text{pH}} + 10^{-(\text{pH} + \text{p}K_{a1})} + 10^{-(\text{p}K_{a1} + \text{p}K_{a2})}} \right) C_{\text{IC}} \quad (7.3)$$

It is important to remark that the latter 3 equations are valid only in a completely closed and equilibrated system. As the algal reactor is an open system, the concentration of CO_{2(aq)} is also driven by Henry’s law [260]:

Table 7.2: Up titration model specifications for a simulation between pH 4 and pH 10

Buffer	Variable	Initial guess or value	Estimated?	Lower limit	Upper limit
Water	pka_water	15.74	No		
	conc_water	55.5 mol l^{-1}	No		
IC	pka1_carbon	6.37	No		
	pka2_carbon	10.25	No		
o-PO ₄	conc_carbon	0.07 meq l^{-1}	Yes	0	0.25
	pka1_phos	2.15	No		
	pka2_phos	7.21	Yes	7	7.8
	pka3_phos	12.35	No		
NH ₄ ⁺	conc_phos	3 mg P l^{-1}	Yes	0	30
	pka_ammon	9.25	Yes	9	9.5
Soap	conc_ammon	2 mg N l^{-1}	Yes	0	30
	pka_soap	4.8	Yes	4	5.5
Blank1	conc_soap	$5 \cdot 10^{-5} \text{ mol l}^{-1}$	Yes	0	$1 \cdot 10^{-3}$
	pka_blank1	9.6	Yes	9.4	11.5
	conc_blank1	$5 \cdot 10^{-5} \text{ mol l}^{-1}$	Yes	0	$1 \cdot 10^{-3}$

$$[\text{CO}_{2(aq)}] = K_H \times p_{\text{CO}_{2(\text{air})}} \quad (7.4)$$

With $K_H = 3.4 \cdot 10^{-2} \text{ M atm}^{-1}$ (at $T = 25^\circ\text{C}$) and $p_{\text{CO}_{2(\text{air})}} = 3 \cdot 10^{-4} \text{ atm}$, equation (7.4) leads to an air/liquid equilibrium concentration of $[\text{CO}_{2(aq)}] = 10^{-5} \text{ M}$ or 0.01 meq l^{-1} , which is a very low value. Furthermore, one has to take into account that a biological active system like and algal system is quite seldom in equilibrium with the atmosphere [37], so careful use of equation (7.4) is advised.

7.3 Results and Discussion

7.3.1 Alkalinity and IC buffer capacity

A random sample from the algal pilot reactor AP, taken in the morning of a sunny day was analyzed with the titrator and in the laboratory. A filtered and an unfiltered sample were titrated from the actual pH to pH 2.5 (Figure 7.1). Both samples were also analyzed on the total alkalinity with two standard methods. From the titration curves, the corresponding buffer capacity curves (Figure 7.2) were calculated and the simulation model (equation (3.59) on page 49 and Table 7.1) was used to quantify the concentration of the IC buffer. The best fit simulation result for the unfiltered and filtered sample is given in Figure 7.2.

For the total alkalinity determination, the end-point pH value for the pH meter method was

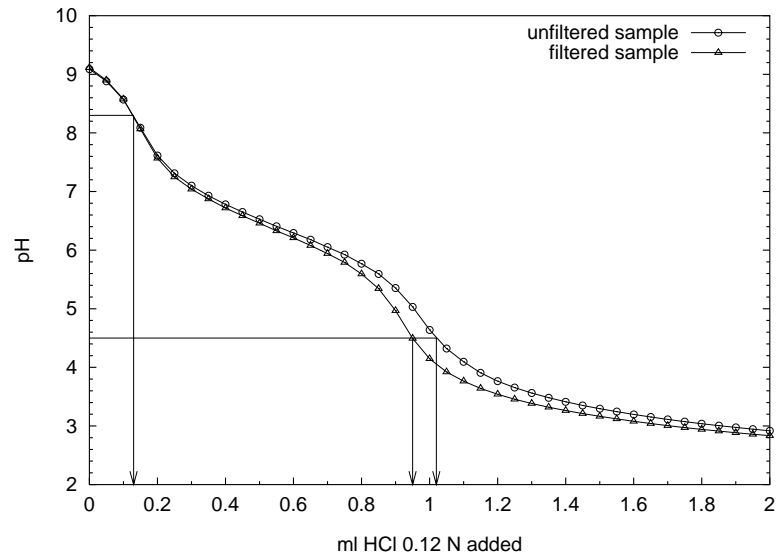


Figure 7.1: Titration curves of an unfiltered and filtered AP sample

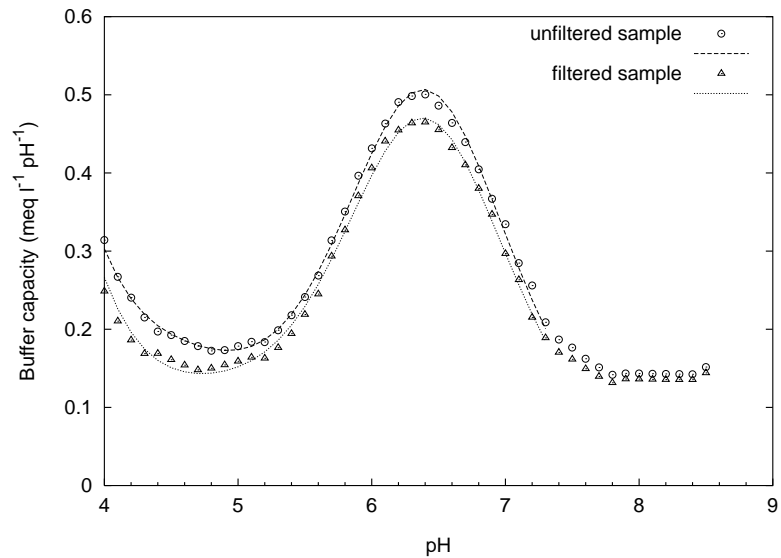


Figure 7.2: Measured (points) and simulated (lines) buffer capacity curves of an unfiltered and filtered AP sample

Table 7.3: Alkalinity measurements and IC simulation results

	Filtered sample $meq l^{-1}$	Unfiltered sample $meq l^{-1}$
Total alkalinity (pH meter method [104])	1.09	1.17
Total alkalinity from titration curve (T)	1.11	1.20
Carbonate alkalinity from titration curve (C)	0.15	0.15
(T–C) alkalinity from titration curve	0.96	1.05
(T–2C) alkalinity from titration curve	0.81	0.90
Simulated C_{IC} from titration curve	0.80	0.85
Simulated $[HCO_3^-]$ using equation (7.2)	0.75	0.80

set at pH 4.5, according to the standard method [104]. This method was also applied to the titration curves of Figure 7.1, where an interpolation between 2 successive data points was used to make a reading of the amount of acid necessary to bring the pH to 8.3 and 4.5 respectively. For comparison reasons, the simulation results to quantify the IC buffer were also expressed as $meq l^{-1}$.

The results of the alkalinity measurements and the simulation results for IC are presented in Table 7.3. The precision of the total alkalinity measurements (both the pH meter method and from the titration curve), expressed as relative standard deviation (r.s.d.), was between 1 and 2 %. The r.s.d. of the simulated IC concentration based on down titration profiles was 2 %. One can notice that the results for the filtered sample are only about 7 % lower than the unfiltered sample. This means that the alkalinity or IC buffer capacity is mainly related to the soluble phase and not to the algal biomass phase. The total alkalinity with the standard pH meter method was not significantly different from the total alkalinity calculated from the titration curves in Figure 7.1 (t-test; $\alpha = 0.05$). An interesting feature of this experiment is found when comparing the IC content found with the modelled buffer capacity curves and the alkalinity calculated from the same experimental titration curve. From Table 7.3, it can be seen that the total alkalinity is about 40 % higher than the corresponding simulated IC concentration and that the (T–C) alkalinity is still more than 20 % higher than the simulated IC concentration. This is the case in both the filtered and unfiltered sample. This indicates that the alkalinity of the sample is mainly, but not completely determined by the amount of IC.

To make a further interpretation of the different results in Table 7.3, a summarizing table with the buffers that are included in these results is presented in Table 7.4. None of the measurements in Table 7.4 exactly represents the amount of $CO_{2(aq)}$ or HCO_3^- in the water, which are the only two IC species that are available to the algae. The IC obtained with the simulation model will be the closest to the real amount of IC because interferences in the pH range 7 or higher (ammonium, ortho-phosphate) and in the pH range of 5.5 and lower (organic acids, detergents) are excluded in the simulation method. For the sample studied, the initial pH was 9.1, and the partitioning between the 3 different carbon species was 0.2 % $CO_{2(aq)}$,

Table 7.4: Different buffers that are included in the alkalinity measurements and IC simulation results (assuming actual pH of sample > 8.3)

Measurement	Buffers that are included in the measurement
Total alkalinity (T)	$2\text{CO}_3^{2-} + \text{HCO}_3^- + \text{other buffers between actual pH and pH 4.5}$
Carbonate alkalinity (C)	$\text{CO}_3^{2-} + \text{other buffers between actual pH and pH 8.3}$
(T–C) alkalinity	$\text{CO}_3^{2-} + \text{HCO}_3^- + \text{other buffers between pH 8.3 and pH 4.5}$
(T–2C) alkalinity	$\text{HCO}_3^- + \text{other buffers between pH 8.3 and pH 4.5}$ – other buffers between actual pH and pH 8.3
Simulated C_{IC}	$\text{CO}_3^{2-} + \text{HCO}_3^- + \text{CO}_{2(aq)} + \text{buffers with } pK_a \approx pK_{a1} \text{ of IC}$
Simulated $[\text{HCO}_3^-]$	$\text{HCO}_3^- + \text{other buffers with } pK_a \approx pK_{a1} \text{ of IC}$

93.9 % HCO_3^- and 5.9 % CO_3^{2-} , calculated with equations (7.1), (7.2) and (7.3) respectively. From this, it is concluded that the algal available carbon was mainly in the bicarbonate form. From Table 7.4, it can be concluded, that in case the only buffer in the sample is the IC buffer, then both (T–2C) and the simulated $[\text{HCO}_3^-]$ represent exactly the bicarbonate content. If also other buffer systems (ammonium, ortho-phosphate, organic acids, ...) are present in the sample, the situation is different. On the one hand, the simulated $[\text{HCO}_3^-]$ will overestimate the real bicarbonate content when extra buffers with the same pK_a as the pK_{a1} of IC are present. On the other hand, the bicarbonate assessment from the (T–2C) measurement will be influenced by a much wider range of buffers. All extra buffers between pH 8.3 and pH 4.5 (e.g. ortho-phosphate, organic acids) will lead to an overestimation of the bicarbonate content, and all extra buffers between the actual pH and pH 8.3 (e.g. ammonium) will lead to an underestimation of the bicarbonate content. Practically, in this example, when comparing the (T–2C) to the simulated $[\text{HCO}_3^-]$ for bicarbonate estimation, an overestimation of the real amount of bicarbonate by (T–2C) is minimal 8 and 12 % for the filtered and unfiltered samples respectively (concluded from Tables 7.3 and 7.4 together). From 36 unfiltered samples (pH between 7.1 and 9.1) taken at various times in the algal reactor, it was found that the (T–2C) measurement always gave 4 to 22 % overestimation of the bicarbonate content compared to the $[\text{HCO}_3^-]$ from the simulation method. In case the IC would become more limiting in the algal reactor, or the interfering buffers would become more pronounced, the simulation method is to be preferred by far for the determination of available bicarbonate for the algae. Besides, the result of the simulation method does not depend on the choice of the end-point (pH 4.3 to 4.9, depending on the method and alkalinity range).

For this particular case-study, an automated alkalinity measurement possibly would reveal similar process information as the IC determination with the buffer capacity sensor. However, because the hardware and the hardware related practical difficulties (maintenance, calibration, ...) of an automated alkalinity measurement are very similar to this buffer capacity sensor, the main advantage of the buffer capacity sensor is that more parameters are obtained with a single measurement device.

7.3.2 Ammonium and ortho-phosphate evaluation in grab samples

During a period of 14 days, samples were taken in the influent of the algal pilot reactor (EVC), in the reactor itself (AP) and in the effluent of the algal pilot plant (EAP). These samples were analyzed in the laboratory for NH_4^+ and $o\text{-PO}_4$. Subsamples of 100 ml were used to perform up titrations to obtain the buffer capacity profiles. For the AP samples, containing algal biomass, 2 different titration experiments were performed:

- Titration of the raw sample as such (including 100 to 600 mg DW l^{-1} of the algae);
- Titration of the supernatant after the algae were settled.

After the titration data were collected, the data processing was performed. The reproducibility for repeated sampling, titrating and optimization, expressed as relative standard deviation (r.s.d.), was less than 2 % for the ammonium concentration and less than 5 % for the ortho-phosphate concentration. The results of the AP samples with or without biomass were comparable for the ammonium prediction but different for the ortho-phosphate prediction. For the $o\text{-PO}_4$, the samples with biomass gave 50 to 100 % higher values than the samples without the biomass. This might indicate that a considerable amount of phosphate is related to the biomass fraction, or that this biomass fraction contains other weak acid buffering systems that interfere with the titrimetric ortho-phosphate determination. The validity range of the measurements using this approach is case dependent (e.g. presence or absence of interfering buffers) and depends on the titration conditions (e.g. sample volume, titrant normality, measurement point density). Based on the experience for this particular case, the minimum validity values are considered around 1 mg N l^{-1} and 1 mg P l^{-1} .

Using the mathematical model (equation (3.59) on page 49) and Table 7.2), a perfect fit between the experimental and simulated buffer capacity curves was obtained for all experimental data. An illustration of the experimental data and the model fitting for 3 selected EAP samples taken at different days is illustrated in Figure 7.3. On the graph, one can easily distinguish the profiles of samples that are high or low in ammonium and/or phosphate concentration. For the samples shown in Figure 7.3, together with the other grab samples, the laboratory measurements of NH_4^+ and $o\text{-PO}_4$ and the concentrations estimated with the model (titrator) are presented in Table 7.5. For the AP samples, only the results of the titration experiments without the algal biomass are shown, because they correspond most closely to the laboratory procedure where all samples were filtered prior to analysis. Overall, the linear relationship between laboratory and titrator results is shown in Figures 7.4 and 7.5. The constructed linear regression lines with their 95 % confidence intervals are comparable to the results obtained in chapter 6 on secondary effluents with a similar buffer capacity sensor.

7.3.3 Dynamic nutrient evolution in a 48 hour batch experiment

A 48 hour batch experiment was set up to monitor the nutrient removal in the algal pilot plant. The experiment started with a filling phase with EVC water at 08:00 in the morning. In the first 36 hours of the experiment, the aeration was activated, ensuring a completely mixed reactor. During the last 12 hours, the aeration was stopped. An automatic time-proportional sampler was used to obtain combined samples every 3 hours. During this experiment, 19 samples were titrated, among which the first 11 were samples from a completely mixed system (when aeration was activated). The last 8 samples were taken during the second night of the experiment,

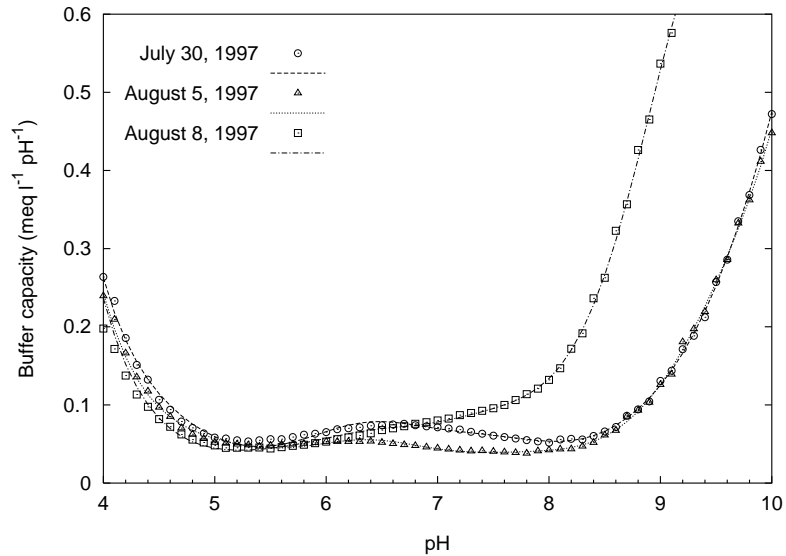


Figure 7.3: Measured (points) and simulated (lines) buffer capacity curves for 3 selected EAP samples

Table 7.5: Laboratory measurements and simulation results for all grab samples

Sample	Date	NH_4^+ (mg N l^{-1})		$o\text{-PO}_4$ (mg P l^{-1})	
		laboratory	titrator	laboratory	titrator
EVC	July 30, 1997	4.6	9.0	3.4	3.2
	August 5, 1997	21	23	3.7	3.1
	August 6, 1997	19.6	21	3.9	3.4
	August 8, 1997	15.2	18.6	4.3	3.5
EAP	July 30, 1997	0.6	0.8	3.8	2.1
	August 5, 1997	0.8	1.0	1.2	1.2
	August 6, 1997	9.4	10.8	4.2	3.4
	August 8, 1997	12	13.4	3.9	2.9
AP	August 4, 1997	2.8	2.7	3.3	2.7
	August 5, 1997	13.2	14.6	4.6	3.9
	August 6, 1997	16.9	19.5	4.3	3.6
	August 8, 1997	14.3	16.9	4.1	3.6
	August 12, 1997	13	9.3	3.2	3.0

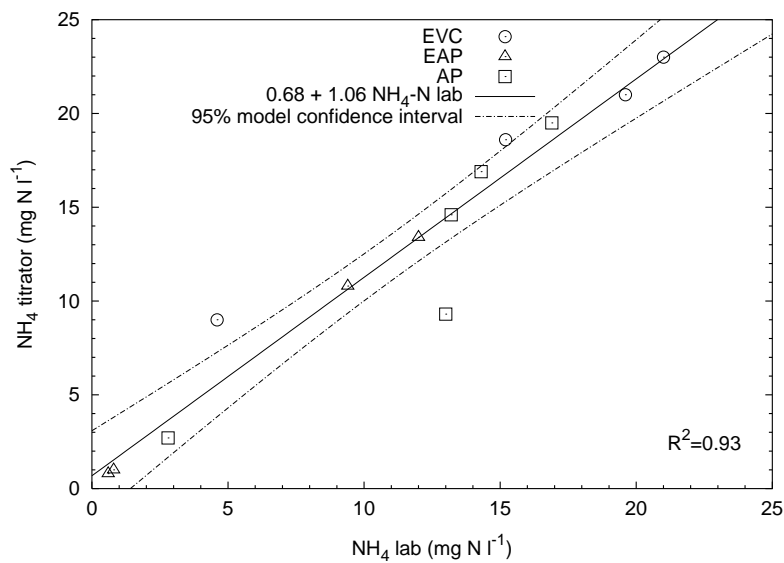


Figure 7.4: Scatterplot of laboratory and titrator ammonium results for all grab samples

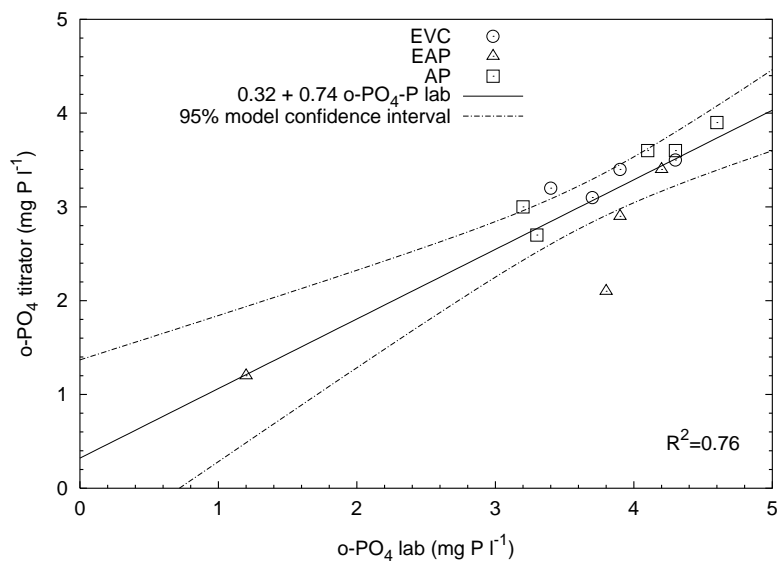


Figure 7.5: Scatterplot of laboratory and titrator ortho-phosphate results for all grab samples

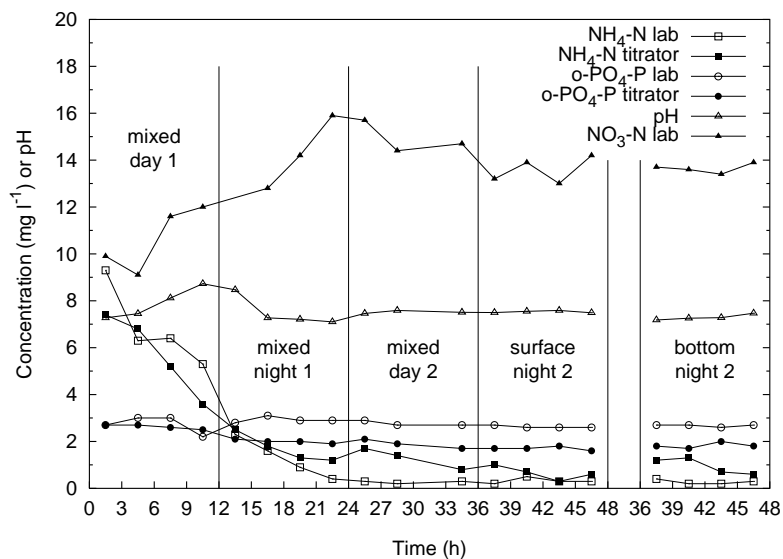


Figure 7.6: Laboratory and titrator concentrations for ammonium and ortho-phosphate; laboratory measurements of pH and nitrate

when the aeration was stopped and the algae had settled to the bottom of the reactor (4 samples close to the surface and 4 samples at the bottom). Based on the results of the grab samples mentioned above, it was decided to take titration curves of samples without algae only (titration of the supernatant after the algae were settled to the bottom of the sampling vessel).

For each sample, a down titration was performed to estimate the IC buffer capacity, followed by a 15 minutes stirring at pH 2.5 to remove the IC. Subsequently an up titration to pH 11 was performed to estimate the ortho-phosphate and ammonium. The specifications of the buffer capacity model in equation (3.59) on page 49 for the down and up titrations are given in Tables 7.1 and 7.2 respectively. In Figure 7.6 the results are given for the laboratory and titrator analyses of NH_4^+ and o-PO_4 , and for the laboratory measurements of pH and NO_3^- .

Ammonium was mainly removed in the first day, dropping from around 9 mg N l^{-1} during the first 24 hours. The fit between the experimental and simulated buffer capacity was very good for all samples, indicating that an adequate model was used. The ammonium concentrations determined in the laboratory showed good correspondence with the titrator results in the first 18 hours, but from 18 hours onward, the concentrations resulting from the titrator showed an overestimation with 0 to 1.5 mg N l^{-1} . This might be explained by the fact that a rather strong buffer is present between pH 9.8 and pH 10.3 in all samples, possibly giving some interference with the ammonium buffer only. This extra unknown buffer was modelled and its concentration was estimated at 0.3 mmol l^{-1} . If this buffer was ignored in the model, the fit between experimental and simulated buffer capacity profiles was poor, and the estimation of the ammonium concentration was 2 mg N l^{-1} higher than the laboratory result. The nature of the interfering compound remains, however, unknown.

The ortho-phosphate concentration did not change very much during this 48 hour batch

experiment, and both the laboratory results and the titrator results varied between 2 and 3 $mg\ P\ l^{-1}$. Again, a small systematic deviation between the results of the 2 measurement methods was observed. This time, the titration results were lower than the laboratory results. A possible explanation can be found in the complex equilibria that exist between the different forms of phosphorus [285]. These different forms of phosphorus play the role of 'PO₄ reservoir' through chemical exchanges. It is reported [285] that standard methods, like the molybdenum blue method used here, can give a significant overestimation of *o*-PO₄ under such conditions. The standard molybdenum blue method can potentially hydrolyze organic P compounds or displace P from colloids, and thus the level of ortho-phosphate ions present may be severely overestimated [21].

The results show that *o*-PO₄ is not removed from the secondary effluent by this pilot reactor. On the other hand NH₄⁺ is almost completely removed after 1 day of treatment. From the viewpoint of nutrient removal process control, the batch cycle time could have been shortened to 1 day. An exact comparison of the laboratory results and the titrator results is difficult, because the titrator used the samples as such (or in case algae were present, only the upper part without the algal biomass), while the laboratory analyses were preceded by a filtration.

In Figure 7.7 the results are shown for the titrator based determinations of the IC present in the AP samples. As discussed above the estimated IC concentration with the titration system corresponds most closely to the amount of carbon available to the algal biomass. The IC concentration at the beginning of the experiment was around 1.6 $meq\ l^{-1}$. During day 1, this concentration decreased to 0.9 $meq\ l^{-1}$. During night 1 the concentration of IC increased a bit, pointing to algal respiration. During day 2, the IC further decreased to around 0.7 $meq\ l^{-1}$. During night 2, in the upper part of the reactor, where no algae were present, no further decrease in concentration could be observed. At the bottom of the reactor, where the algae were settled, one notices a higher IC concentration in the first 3 hours, decreasing to the same level as the upper part of the reactor. An explanation for this can be found when looking at the oxygen concentration at the bottom of the reactor during night 2. In the first 3 hours after the aeration was stopped, the concentrated algal biomass consumed all oxygen for their respiration, resulting in a high IC concentration. In the remaining part of night 2, under anoxic conditions, an equilibrium in IC concentration between the upper and lower part of the reactor was established.

In order to make an interpretation of the changes in NH₄⁺, *o*-PO₄ and IC, at least 2 different biological processes may be considered to be responsible for the observed phenomena. First, there is algal photosynthesis and respiration, with a consumption and release of inorganic carbon respectively. During photosynthesis nitrogen (NH₄⁺ or NO₃⁻) and phosphorus are taken up together with inorganic carbon (CO₂ or HCO₃⁻) in the proportion C : N : P ≈ 106 : 16 : 1 [273]. Second, there is the bacterial autotrophic nitrification, with a transformation of NH₄⁺ into NO₃⁻ with a small consumption of IC, in the proportion NH₄⁺-N : NO₃⁻-N : C ≈ 1 : 1 : 0.08 [91]. The IC consumed for the formation of new nitrifying biomass is too low to be used to quantify the nitrification rate accurately. This nitrification process is in accordance with the NO₃⁻ evolution measured with off-line laboratory analysis, where an increase in NO₃⁻ from 10 to 16 $mg\ N\ l^{-1}$ was observed in the first 24 hours of the experiment. The next 48 hours, almost no further changes in NO₃⁻ occurred because NH₄⁺ became limiting. Besides the biological consumption of the inorganic carbon for assimilation into new biomass, the decrease of the IC buffer can also be partially explained by the H⁺ production by both biological processes, resulting in an

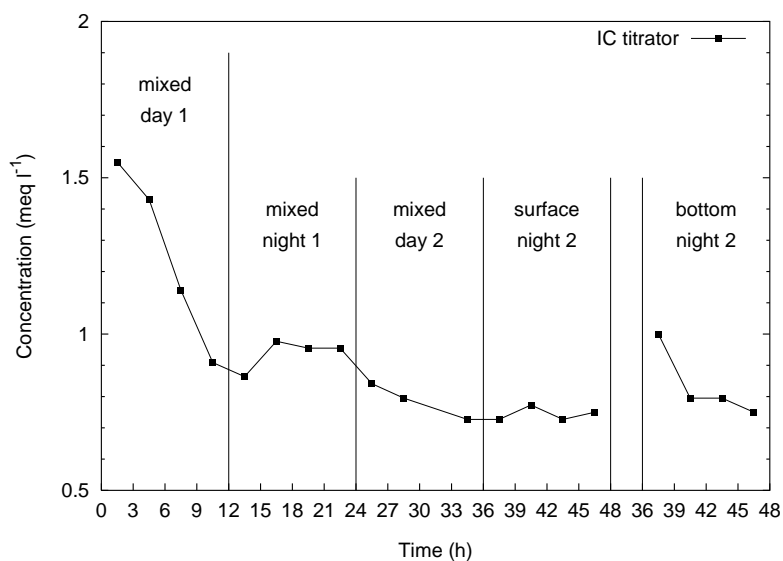


Figure 7.7: Titrator concentrations for inorganic carbon

alkalinity decrease [273]. On the other hand, the algal uptake of dissolved CO_2 during day-time, resulted in a net pH increase from pH 7.3 to pH 8.7, as observed during the first 12 hours. The pH of all samples was between pH 7.1 and pH 8.7, meaning that the bio-available carbon was always higher than 95 % of the quantified IC buffer system (equations (7.1) and (7.2)). In this case study, the IC never dropped below 0.7 meq l^{-1} , which is a rather safe value compared to the 0.5 meq l^{-1} reported to be needed [199] for normal operation. From an industrial point of view, this algal wastewater treatment appears to be a viable alternative for small communities [151]. However, the pilot-plant experiments in this study have shown that especially for the phosphate removal, the % P removed (by precipitation and/or biologically) is lower than previous, smaller-scale studies [146, 230]. In the viewpoint of possible eutrophication of the receiving waters, further insights in the phosphorus removal mechanisms and further process optimization are necessary. The role of phosphorus in the eutrophication of receiving waters is complex because phosphorus is a very dynamic, biologically active element [54, 59].

As the results of the titration method can be influenced by interfering buffering components, this measurement method cannot be considered to be an analytical device, replacing the standard laboratory methods. As illustrated above, the application of this titration method has to be seen in the context of process monitoring and alarm generation. An innovative aspect of the presented buffer capacity sensor, is that it gives a multivariate response (IC, NH_4^+ , $o\text{-PO}_4$) supplemented with extra information, e.g. the appearance or disappearance of extra buffer systems, that are useful for process monitoring.

Further research will focus on the implementation of a fully automatic sensor, including automatic buffer model selection to accommodate for (dis)appearing buffer systems. Further, an appropriate control strategy will be developed in which this device is providing the necessary data in due time. The time needed to perform a full measurement cycle was approximately

1 hour (down titration, up titration and data interpretation). Further optimization of the titration parameters can reduce this cycle time with 10 – 20 minutes. The cycle time can be further decreased to 20 – 25 minutes if the down and up titrations are performed in parallel titration vessels. Electrode problems were never observed during the performed experiments. The maintenance of the titration vessel and electrode is comparable to the maintenance of a pH meter.

7.4 Conclusions

The proposed methodology of a pH buffer capacity based measurement system was evaluated for its usefulness for multivariate monitoring of tertiary wastewater treatment with algae. In waters which are low or even limiting in IC buffer capacity (like in algal treatment plants), standard alkalinity measurements can give an overestimation of the IC buffer system, because the alkalinity is a general composite measurement, including all pH buffering components in the considered pH interval. For the samples analyzed, the (T–C) alkalinity was around 20 % higher than the IC concentration obtained with the buffer capacity sensor, explaining that other buffering components than IC are included in the (T–C) alkalinity (*o*-PO₄, NH₄⁺, organic acids, ...). It is concluded that the HCO₃⁻ concentration assessed with the simulation method is preferred, rather than the (T–2C) alkalinity, when one wants to quantify the available bicarbonate.

The NH₄⁺ and *o*-PO₄ assessment from the up titration profiles were comparable with the laboratory measurements. An exact comparison of the laboratory results and titration results was difficult, because of the filtration step preceding laboratory analyses, and possible interferences by buffer systems not accounted for in the model.

During a 48 hours batch experiment, the measured IC concentration reflected the day/night difference in activity of the algal biomass fairly well. The data of the titrimetric sensor showed that there was no carbon limitation and that the treatment cycle could have been halved to 24 hours, still allowing complete NH₄⁺-removal. The IC reduction rate during daytime was an indicator of the biological activity.

The application of the sensor developed here has to be seen in the context of process monitoring and alarm generation. The developed methodology can be realistically implemented in an on-line automatic measurement system. The sensor does not need any sample filtration, a major advantage for field-use. The chemicals used are environment friendly and inexpensive.

Chapter 8

Automatic titrimetric sensor for manure nutrients

Some of the results of this chapter were registered in a patent [78].

8.1 The FASTNAP project

8.1.1 Project identification

The FASTNAP acronym stands for “FAST titrimetric Nitrogen And Phosphorus determination in animal manure and other organic slurries”. The project was a cooperation between 3 Flemish and 2 Dutch partners:

- Hemmis N.V., Kortrijk
- Flemish Land Agency (V.L.M.), manure bank department, Brussel
- Ghent University, BIOMATH department, Gent
- Eijkelkamp Agrisearch Equipment b.v., Giesbeek, The Netherlands
- DLO Institute of Agricultural and Environmental Engineering (IMAG-DLO), manure technology department, Wageningen, the Netherlands

The aim of the project was the development of an automated on-line sensor, that can be used to quantify the total amounts of nitrogen and phosphorus in animal manure and other organic slurries. The innovative aspect of this project is that, eventually, these measurements should be conducted on a driving transport vehicle for animal manure, and the results should be available within 1 hour after loading the transport vehicle.

This project could only be realized with an interdisciplinary approach. Physico-chemical analytical and destruction techniques are combined with mathematical simulation techniques and resulted in a combined hard- and software sensor, capable of extracting upgraded information from a pH titration profile. The use of such intelligent sensor in the application area of animal manure measurements is a new research topic.

8.1.2 Background of the project

Due to an increase of the livestock population in Flanders and the Netherlands during the last decades, the production of animal manure has increased. Especially the number of pigs increased drastically in the past 40 years (in the Netherlands from 3 million pigs in 1960 to 14.4 million pigs in 1996) [330]. The application of large quantities of animal manure to agricultural soils created environmental problems such as leaching of nitrate to the groundwater and eutrophication of surface waters due to surface runoff of phosphate [330].

On the first of January 1998, a mineral accounting system (MINAS) was introduced in the Netherlands to reduce excess mineral losses to the environment. MINAS obliges farmers to balance the in- and output of nitrogen and phosphorus in manure. The introduction of MINAS created a need for rapid and accurate determination of the nitrogen and phosphorus content in animal manure on site [330]. In Flanders, a similar legislation exists, but it is less intensive as the Dutch MINAS system. Some important differences between the Flemish and Dutch situation are:

- In the Netherlands, all organic and inorganic mass flows containing nitrogen and/or phosphorus should be included accurately in the mineral bookkeeping. Mass flows containing nitrogen and/or phosphorus are amongst others animals, roughage, feed stuff, crops, animal products and manure. In Flanders (Mestdecreet, December 20th, 1995), the farmers have to make a bookkeeping of the volumina of manure that is transported and they should announce beforehand to the Flemish authorities (Mestbank) each quantity of manure that is going to be transported from and to the farm.
- In the Netherlands, for each manure transport between 2 farms, the concentrations of nitrogen and phosphorus need to be determined in the laboratory with official methods. In Flanders, the farmer has the choice between two declaration systems: a system where no laboratory analyses are needed (fixed mean values for nitrogen and phosphorus content of animal manure are used); or a system where exact concentrations, measured in the laboratory, are used for the declaration.
- The Dutch authorities make up the accounts at the end of each year. For each surplus of a kilogram phosphorus (as P_2O_5) and nitrogen, farmers have to pay €5.00 and €0.75 respectively. In Flanders, a taxation system on the production and the surplus of nitrogen and phosphorus has been adopted (Mestdecreet, May 11th, 1999). All nitrogen and phosphorus, originating from production of animal manure, other organic sources (compost, sludge) and chemical fertilizers is levied with €0.022 for 1 kg of N or P_2O_5 . Further, a supertax is imposed for each kilogram of N and P_2O_5 that is produced above a production quota allotted to each individual farmer (dependent on the manure production of the farm in the past). The supertax is set to €0.25 for 1999 and 2000, increasing to €0.5 in 2001 and 2002, and further increasing to €1.0 after 2002.

Depending on the farming system, manure is an important input/output flow of nitrogen and phosphorus. Livestock producers, for example, produce manure (output) and arable farmers use manure as fertiliser (input). To create a balanced situation, livestock producers with mineral surpluses on their own farm, have to transport animal manure to arable land of other farms.

Accurate determination of the quantity of transported nitrogen and phosphorus requires

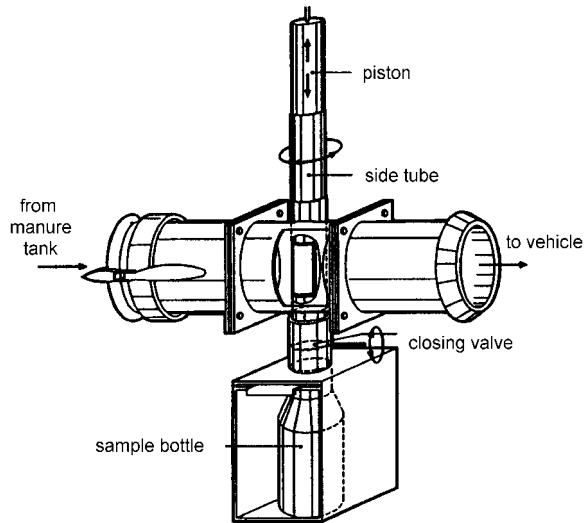


Figure 8.1: Representative sampling with the side tube technique [330]

weighing and sampling of each individual load [330]. Representative samples can be taken with the side tube technique [119]. The principle of this sampling system is illustrated in Figure 8.1. During loading or unloading of the manure-transporting vehicles, five samples of about 150 ml each are taken and collected in a sample bottle. A completely automated version of this technique is on sale. The operator cannot influence the time of sampling nor the composition of the sample. This increases the tamperproofness of the technique. After sampling, the samples are sent to the laboratory for analyses. After five to ten working days, the analytical results are available [330]. In case of direct transport and use of manure (e.g. fertilisation), farmers cannot take the results of the analyses into account for e.g. adjusting the quantity of manure applied per unit of soil surface. This complicates an adequate use of manure in view of environmental hygiene and fertilisation. Practice shows that farmers with arable land are not eager to use manure from livestock producers when the mineral composition is unknown. The reason for this is that fertilisation of arable land with a shortage of nitrogen and phosphorus can result in poor crop yields, whereas an overuse is punished by levies because of the imbalance in the mineral accounting system [330].

Summarized, in the framework described above, there is a necessity for a robust and automatic sensor, that can measure the most important manure nutrients N and P. The sensor should have the ability to be placed or mounted near the place where the manure is loaded (eventually mounted on the driving vehicle itself). Preferentially, the analyses results should be available for the receiving farmer prior to the application of the transported manure on his arable land. The measurement principle should be accurate, reliable and susceptible to official acceptance and certification.

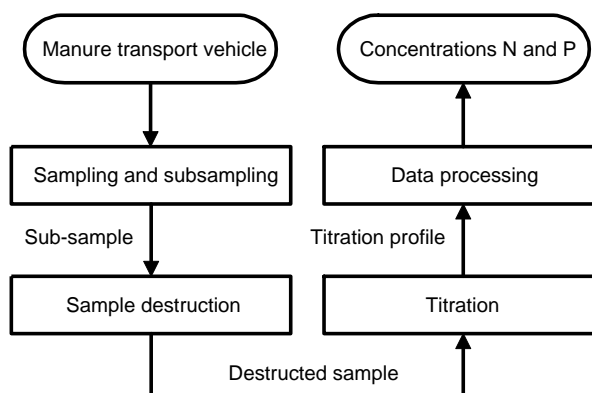


Figure 8.2: Methodology of the FASTNAP sensor

8.1.3 Sensor perspectives

A market study revealed that the needed capacity for Flanders is around 70–100 automatic measuring units. In Flanders, there are about 50 big manure transportation companies, who transport each more than 10.000 tons per year. These 50 (from a total of 500) transporters together realize 62.000 transports or 1.900.000 tons per year. The needed capacity for the Netherlands is about 150 automatic measuring units for 75 transporting companies with a total of 350 vehicles for ‘long distance’ manure transport. In the Netherlands, a total of 800.000 transports of manure are registered per year.

The end-user-price for such automatic sensor is estimated to be around €25.000. The price for a laboratory analysis (N and P) is around €50, so that approximately 500 analyses per instrument are needed to pay back the investment cost.

8.1.4 Measurement principles

The sensor methodology is presented in Figure 8.2. The aim of the project is the on-line measurement of nitrogen and phosphorus in manure samples and this can be realized in four consecutive steps. Steps one and two (left side of Figure 8.2) are developed by the Dutch partners in the project, and steps three and four (right side of Figure 8.2) are developed by the Flemish partners. In the sequel, an overview of the presented topics in this chapter is given.

The sampling of manure, with the side tube technique, is existing technology. The subsampling consists of a homogenization of the sample in the sample bottle (750 ml), followed by a subsampling for further analyses. Several techniques for subsampling were investigated, including pipetting arms, dispensers and pumps [328]. The sample destruction is discussed in section 8.2, where a number of techniques are summarized and compared. It was chosen to use microwave digestion with H_2SO_4 and H_2O_2 [329]. Possible techniques for on-line measurement of nitrogen and phosphorus in manure are presented in section 8.3. A similar titrimetric method, as presented in chapters 6 and 7, was adopted for the measurement of nitrogen and phosphorus in destructed manure samples. Ammonium and ortho-phosphate both have

a measurable pH buffer capacity, and they can be quantified from the buffer capacity profile. However, because different buffer systems are present in the sample, a conventional end-point titration cannot be used, so advanced data processing is necessary to find the concentrations of nitrogen and phosphorus. The development of the titrimetric part of the sensor is worked out in section 8.4. In the final part of this chapter, a validation and statistical data analysis of the developed methods are presented in section 8.5.

8.2 Destruction of manure samples

Prior to analytical determination of the nutrients N and P in animal manure, it is necessary to digest the manure sample, thus bringing nitrogen and phosphorus in solution. For this purpose, two possible methods that can be automated, were investigated: microwave and UV destruction. The first method was studied experimentally, while the latter was mainly evaluated on the basis of a literature review.

8.2.1 On-line microwave destruction of manure samples

For the microwave destruction, 2 different systems were tested and evaluated in the framework of the FASTNAP project [329]: an open microwave system (Microdigest 3™, Prolabo) and a closed microwave system (Mega 1200, Milestone). The chemicals added to the manure sample prior to the destruction step are based on a reference laboratory destruction method for animal manure and related products (NEN 7433) [1]. They are H_2SO_4 , H_2O_2 and $\text{CuSO}_4 \cdot 5\text{H}_2\text{O}$. The reference method demands a certain temperature profile of which the highest needed temperature is 330°C .

Destruction of animal manure samples in an open microwave system gave results (within $\pm 5\%$) that are comparable with destruction in the lab using a conventional destruction block. Also in other application fields, microwave digestion methods for total nitrogen and phosphorus in natural waters [131] and COD in wastewater effluents [130] gave promising results as compared with the conventional laboratory methods. A destruction time of 30–50 minutes with the open microwave results in a nitrogen recovery of 95–99%. However, the results with the closed microwave showed a nitrogen recovery of maximum 90%. This can probably be explained by the fact that the closed microwave could only heat until 220°C (due to teflon components), which is below the boiling point of the sulphuric acid. In both microwave systems, the phosphorus recovery is around 100%. It was also found that the catalyst $\text{CuSO}_4 \cdot 5\text{H}_2\text{O}$ could be omitted for the same destruction result. The open microwave has facilities for automatic reagent addition and a reflux system for vapour, which are advantageous aspects for automation. The lower nitrogen recovery and the difficulties to automate the closed microwave system are the two most important reasons why the open microwave was chosen for further optimization in the framework of the project [329].

An automated destruction of animal manure is possible with an open microwave system within 1 hour and with a combination of sulphuric acid and hydrogen peroxide. However, some disadvantages of this method for field application are: very high apparatus cost (€ 15.000); extreme working conditions (330°C and $\text{pH} < 1$) and high, expensive consumption of dangerous chemicals, with associated safety problems for application in the field. Because of these limi-

tations, an alternative destruction method based on UV-light was investigated for the purpose of manure destruction.

8.2.2 On-line UV destruction of manure samples

Literature overview of UV photodegradation applications UV destruction of organic material is applied for many different purposes: disinfection of water or wastewater [3, 154, 303], destruction of recalcitrant chemical substances (often aromatic structures) [52, 134, 245], measurement of nitrogen, phosphorus, ... in water or soil solutions by photochemical decomposition [16, 113], etc. Photo-oxidation can enhance the biodegradability of wastewaters due to removal of toxic pollutants [106, 153, 224], however a possible consequence of ultraviolet photo-oxidation can also be the induction of biotoxicity (e.g. algicidal effect) in treated waters [95, 252].

UV lamps can be classified by their radiation spectrum. This spectrum can be very narrow, e.g. a monochromatic radiation at 254 nm, realized with a low-pressure mercury vapour lamp [29], or the spectrum can be very broad, e.g. a strong emission over the entire region between 190 and 400 nm, realized with a high-pressure mercury vapour lamp [227]. Oxidation of chemicals by the UV process using low and medium pressure mercury vapour lamps hinges on the generation of hydroxyl radicals [227]. Hydrogen peroxide (H₂O₂) is often used in combination with low or medium pressure lamps, because the quantum yield of hydroxyl radicals from hydrogen peroxide is almost 1 when the wavelength of UV light approaches 254 nm. Applications based on this type of process are manifold: UV/H₂O₂ treatment of industrial wastewater [117, 134, 194] or groundwater [152]. Sometimes the UV/H₂O₂ process is accelerated by adding Fe²⁺ [245, 345] or ferrioxalate [245]. It is also possible to use H₂O₂ in combination with a catalyst (iron, graphite, activated carbon) without UV for the degradation of e.g. phenolic compounds [170]. For groundwater contaminated with volatile organic compounds (VOC's), the *Ultrax* process (UV/H₂O₂/ozon) achieved VOC removals greater than 90 % [152]. The oxidation of organic material with a combined persulphate/UV treatment is a common technique used in TOC analyzers [42, 45]. A high-pressure mercury vapour lamp is effective not only at generating hydroxyl radicals from H₂O₂ but also causing electronic transitions in many organic molecules. Thus, this type of lamp is potentially capable of degrading organics without the presence of a hydroxyl radical source [178, 227].

Titanium dioxide powder in aqueous solution is a well-known photocatalyst for the degradation of organics with solar or near-UV irradiation [27, 106, 142, 153, 195, 225]. A typical concentration for chemicals that can be mineralized with such treatment is around 1 mmol l⁻¹, in a time period of 1 – 3 hours [184]. Full mineralization is not always possible, e.g. photocatalytic degradation of atrazine [224]. The possible use of solar-illuminated TiO₂ for the disinfection of water is suggested [183]. By photocatalytic degradation with TiO₂, dissolved organic nitrogens (DON's) in natural waters are converted to inorganic nitrogens such as ammonium, nitrate and nitrite [276]. Other photocatalysts include magnetite and aluminium oxide [52], dyes like riboflavin [5, 333] and methylene blue [4, 5, 53], or naturally occurring substances like proteins [116]. Experiments with magnetite and a high-pressure mercury lamp [52] have shown that it is possible to reduce the COD of a shale dry distillation wastewater from 2500 ppm COD to 1500 ppm COD in 1 hour illumination time.

Photochemical decomposition of organic and inorganic phosphorus compounds into ortho-

phosphate has been developed for the determination of total phosphorus in natural and sewage water [100, 209, 324, 348]. These methods rely on a combined strong acid (e.g. sulphuric acid) and strong UV treatment (e.g. 1000 W high pressure mercury lamp). This method is typically used in a range from 1–5000 $\mu\text{g P l}^{-1}$. The determination of total nitrogen in water using on-line UV digestion is a possible alternative for the Kjeldahl method, especially for wastewater samples with high nitrate content [145]. In this method, the organic and inorganic nitrogen is converted into nitrate by potassium peroxodisulphate. In some cases (e.g. in the presence of H_2O_2), nitrate acts like a filter and reduces the UV light intensity in the photoreactor [267]. Without the addition of photocatalysts, it was found that organic nitrogen compounds are first oxidized almost completely to nitrate which is then slowly reduced to nitrite on further irradiation [17].

Potential use of UV for manure destruction Based on the literature review presented above and some preliminary experiments, a comparative evaluation between UV and microwave destruction of animal manure samples was made. The advantages of UV compared to microwave digestion are:

- UV treatment can be done with cheaper equipment (€ 3.000 for an UV reactor compared to € 15.000 for a microwave oven).
- The technical construction of an UV photoreactor is more suited for automation compared to a microwave oven.

The disadvantages of UV compared to microwave digestion are:

- Organic nitrogen compounds are transformed into nitrate/nitrite with photo-oxidation. An oxidizing reagent (e.g. hydrogen peroxide or persulphate) is needed to transform all nitrogen containing organics (e.g. ureum) into nitrate/nitrite. It is uncertain if ammonium is also transformed into nitrate/nitrite.
- Organic phosphorus compounds are transformed into ortho-phosphate. However, extra addition of oxidizing reagent is necessary to transform all phosphorus (including polyphosphates) into ortho-phosphate. Further, preliminary experiments showed that even without UV treatment, almost 100 % recovery of phosphorus compounds from animal manure was realized when only sulphuric acid was added to the sample (personal communication, N. Walraven).
- Particulate materials are decreasing the efficiency of UV destruction due to light scattering. Therefore, perfect homogenization of the manure sample prior to destruction is necessary. Also, the nutrient concentrations in animal manure are very high compared to wastewaters and natural waters, so that a high dilution factor is required for the UV treatment. However, this will consequently result in a lower accuracy of the N and P measurements, due to the high heterogeneity of (even homogenized) animal manure.

Based on these points, it can be concluded that UV destruction is not a very strong alternative for microwave digestion in the framework of this project. Especially if titrimetry is used in a further stage as measurement technique for nitrogen and phosphorus (see section 8.4), nitrogen should be in the ammonium form for accurate quantification from a buffer capacity profile. Further, some preliminary experiments with a low pressure UV system were not very promising, because of a low nitrogen recovery (personal communication, N. Walraven). Experiments

with a high pressure UV system could not be performed until now. In the framework of the FASTNAP project, further developments and optimizations were only based on the microwave digestion.

8.3 Automatic nitrogen and phosphorus measurements

Before deciding on titration as the most adequate measurement technique for the automatic manure sensor in the FASTNAP project, an exploratory study has been done to determine potential techniques for automatic nitrogen and phosphorus determinations in manure [330, 341]. In this study, the following techniques were evaluated:

- inductively coupled plasma - atomic emission spectroscopy (ICP-AES),
- X-ray fluorescence (XRF),
- near infrared spectroscopy (NIR), and
- titrimetry.

All techniques show both advantages and disadvantages. Test measurements with an ICP-AES indicated that the phosphorus content in manure could be determined accurately [341]. However, an ICP-AES is not capable of quantifying nitrogen [341]. In addition, it is a massive device and it is labour-intensive to operate. Further, samples must be digested before analysis. With XRF it is also impossible to quantify nitrogen. However, it should be able to measure phosphorus without sample pretreatment. NIR and titrimetry are non-proven technologies with respect to the determination of nitrogen and phosphorus in manure. NIR has the advantage that it is non-destructive and does not require digestion. There are examples in which nitrogen and phosphorus content in forage, food and beverage is determined with NIR [330]. Titrimetry was successfully used for the determination of phosphate and ammonia in effluents, river waters and algal treatment systems (see chapters 6 and 7). However, a disadvantage of titrimetry is that manure samples must be digested. The measuring time with NIR is much shorter than with titrimetry (minutes compared to 1 hour). This puts NIR in favour of titrimetry with respect to speed.

Based on:

- the possibility to analyze both nitrogen and phosphorus in a short amount of time, and
- the successful analytical results in related research fields,

it is concluded that NIR and titrimetry are promising techniques for automatic measurement of nitrogen and phosphorus in manure samples [327, 330]. Because of the positive experiences with the pH buffer capacity based measurement method (see chapters 6 and 7), the latter technique was chosen for the further developments, which are presented in the next sections.

8.4 Development of the titrimetric part of the sensor

In this section, the different stages in the development of the titrimetric method for manure samples are presented. First, the destruction method and its relation with the titration procedure is highlighted in sections 8.4.1, 8.4.2 and 8.4.3. A detailed simulation study with comparisons

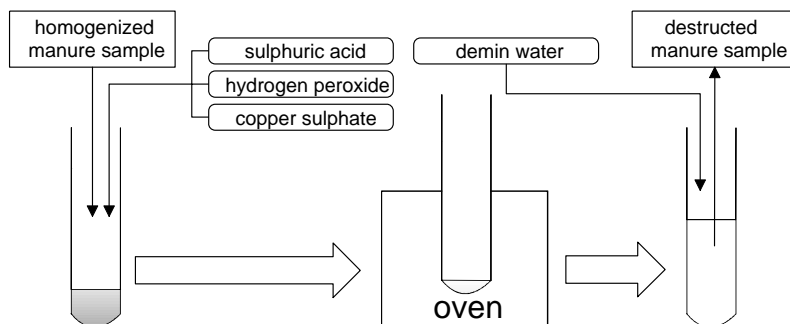


Figure 8.3: Scheme of the different steps in the animal manure destruction method

of different mathematical buffer capacity models is performed in section 8.4.4. The influence of the dilution factor and the first experimental validation experiments are described in respectively sections 8.4.5 and 8.4.6. Finally, an adequate buffer capacity model is developed, and evaluated with a measurement campaign in section 8.4.7.

8.4.1 Introduction to animal manure destruction

In 1998, official NEN (Nederlands normalisatie-instituut, Dutch normalization institute) methods for diverse measurements in manure were adopted [1]. These methods include NEN 7430 for the sample pre-treatment and homogenization, and NEN 7433 for the sample destruction with sulphuric acid, hydrogen peroxide and copper sulphate. The determination of nitrogen (NEN 7434) is a distillation/titration method, and the phosphate determination (NEN 7435) is based on the colorimetric molybdenum blue method. The official procedures adopted in Flanders [93] are also the Dutch NEN methods, however, for some methods (e.g. total nitrogen) minor modifications are introduced. Other methods like ISO 7150 for the determination of ammonium, or an alternative method for total phosphorus based on a complete destruction into ash with an oven at 550°C are also accepted methods in Flanders [93]. For the development of the titrimetric part in the FASTNAP project, animal manure samples were destroyed with the NEN 7433 method, then diluted and titrated.

Without going into the technical details of the destruction method, it is necessary to know the different steps of the destruction procedure. These steps are illustrated with a scheme in Figure 8.3. First, approximately 5 g of homogenized wet sample is transferred into a destruction tube. Second, 20 ml 18 M H_2SO_4 , 15 ml 9.8 M H_2O_2 and 1 ml 0.4 M $\text{CuSO}_4 \cdot 5\text{H}_2\text{O}$ are added (stepwisely or not). Third, a destruction at 330°C is performed, until the sample is colourless or light-blue. In the automatic version, where the visual inspection of the destruction tube is no longer possible, a sufficiently long enough destruction time should be chosen. Finally, after cooling down the destroyed sample, the sample volume is adjusted with water to a total volume of 250 ml. The organic and inorganic nitrogen compounds from the original manure sample are now transformed into ammonium and the phosphorus compounds are transformed into ortho-phosphate. Untreated animal manure does normally not contain nitrate.

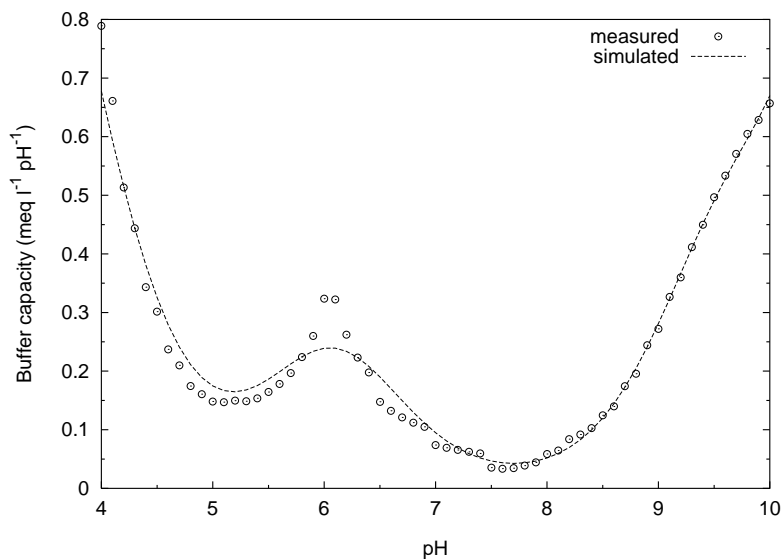


Figure 8.4: Calculated buffer capacity points and corresponding simulation curve of a destructed and 10 times diluted manure sample

However, if nitrate is present due to extra additions or treatments (e.g. aeration), a modified destruction method should be adopted [1, 173]. The concentrations of the added chemicals (except for H_2O_2 which is completely disintegrated) in the final destructed sample can be calculated and are 1.5 M sulphuric acid and 0.0016 M copper sulphate.

8.4.2 Titration of destructed manure samples

Experimental versus simulated buffer capacities In a first preliminary experiment, titration curves of a destructed and 10 times diluted sample were recorded and interpreted. A mathematical model was used to simulate the buffer capacity curves. Prior to titration, the diluted sample was adjusted to a pH 3 with NaOH 10 N. Figure 8.4 shows the calculated buffer capacity points from a recorded titration profile and the corresponding simulated buffer capacity profile. The simulation model contained: a water buffer, an IC buffer (to take into account the IC present in the titrant, or the headspace CO_2 that eventually enters the sample during titration), an ortho-phosphate buffer, an ammonium buffer and a buffer around pH 3.7. A first comparison between laboratory and simulated concentrations is shown in Table 8.1. Figure 8.4 illustrates that the simulated buffer capacity does not follow the experimental points around pH 6. When additional buffers were added to the model, a better fit could not be obtained (results not shown). This points to a possible phenomenon (e.g. precipitation) that is not included in the simulation model. Further, from Table 8.1 it can be concluded that the phosphate in the titrated sample was not found back as ortho-phosphate with the simulation model. Also, the simulated concentration for IC is four times more than expected from calculations and previous experiments. The extra buffer at pH 3.7 could not be explained at this stage.

Table 8.1: Laboratory and simulated concentrations of a destructed and 10 times diluted sample

Component	Unit	Laboratory	Simulated
NH_4^+	mg N l^{-1}	9.1	7.3
<i>o</i> - PO_4	mg P l^{-1}	3.2	0.003
IC	meq l^{-1}		0.41
extra buffer pH 3.7	meq l^{-1}		0.9

The influence of the copper catalyst In a second preliminary experiment, the influence of phosphate in the titration profile was investigated. To this end, the same destructed sample was used, but with a dilution factor 2 instead of 10. Based on the laboratory analysis, 16 $\text{mg } o\text{-PO}_4\text{-P l}^{-1}$ was to be expected as titration result. A standard addition experiment with KH_2PO_4 was performed, and the results of extra additions of 4 and 10 mg P l^{-1} are shown in Figure 8.5. The phosphate that was added to the sample was found back in the titration profile as buffer capacity around pH 6, but could not be modelled with a simple buffer capacity model (same findings as illustrated in Figure 8.4). Further, a precipitation formation was observed during the titration at $\text{pH} > 6$. It was investigated which precipitate was formed and what its influence was on the titration profile. A destructed and undiluted sample was brought to pH 6–7 and kept at that pH during 30 minutes. Then, the blue-white precipitate was removed by filtration on a Schleicher & Schuell folded filter nr. 595. The resulting filtrate was diluted 2 times, put at pH 3 with HCl and then titrated as before. The same was repeated for a destructed and undiluted sample that was brought to pH 12 instead of 6–7. The precipitate was yellow-brown instead of blue-white. The resulting titration curves are also shown in Figure 8.5. It can be concluded that the precipitate plays a very important role in the pH ranges 5–7 and 9–11.

Laboratory analysis with ICP-MS (Inductively coupled plasma - mass spectrometry) indicated the following cations in the precipitates, in order of importance: Cu (15–34 %), Ca (1–14 %), P (2–10 %), Na (3–5 %), Mg (3 %) and Fe (1 %). The Cu mainly originated from the added $\text{CuSO}_4 \cdot 5\text{H}_2\text{O}$ as catalyst in the destruction step. More specific, 102 $\text{mg Cu}^{2+} \text{ l}^{-1}$ destructed sample was added, which is at least 30 times higher than Cu^{2+} concentrations originating from the manure itself. Details on concentrations are given in section 8.4.4, Tables 8.2–8.5.

From the results of the second preliminary experiment, it is concluded that Cu^{2+} is an important interfering component for the determination of N and P from the titration profile. Therefore, 2 possible actions to avoid interference of Cu^{2+} were considered:

- The influence of the Cu^{2+} -precipitates should be accounted for in the simulation model. This is not straightforward, as discussed earlier in chapters 2 and 3 and illustrated further in section 8.4.4.
- The Cu^{2+} from the catalyst should not be present in the destructed samples to be titrated. This is discussed in the next section.

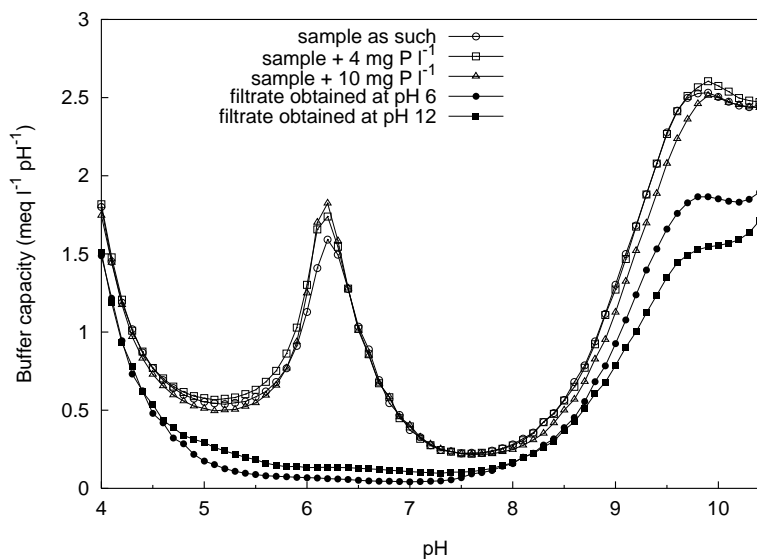


Figure 8.5: Experimental buffer capacity curves of a destructed and 2 times diluted manure sample. Titration of the sample as such, the sample with standard additions of o - PO_4 , and filtrates obtained at pH 6 and pH 12

8.4.3 Modification of the destruction procedure

A separate study by the Dutch partners in the FASTNAP project showed that the catalyst $\text{CuSO}_4 \cdot 5\text{H}_2\text{O}$ (NEN 7433) is not really necessary to obtain complete destruction. There were no significant differences between laboratory measurements of nitrogen and phosphorus in destructed samples obtained with or without the catalyst. Therefore, it was decided to simplify the destruction procedure and perform all further destructions in the framework of the FASTNAP project without the copper catalyst (modified NEN 7433).

The consequences for the titrimetric measurement of the destructed manure samples without Cu^{2+} addition were twofold. First, precipitation during titration was not observed any more (results not shown), and second, the sharp peak in the buffer capacity around pH 6 was no longer present. When experimental buffer capacity curves were modelled with the same model as presented in section 8.4.2, a good fit between the experimental and simulated buffer capacity curves was obtained, but still differences between laboratory and titrimetric results in the order of magnitude 20 % for ammonium and 100 % for phosphate were found (results not shown). Therefore, a more detailed study of the factors influencing the titrimetric nitrogen and phosphorus determination was performed, and is presented in the following sections.

Table 8.2: The composition of pig manure, based on 379 samples [118]

Component	Unit	Mean	Minimum	Maximum
Nitrogen	$mg\ N\ l^{-1}$	130	50	212
Phosphorus	$mg\ P\ l^{-1}$	17	1	52
Potassium	$mg\ K\ l^{-1}$	56	20	90
Calcium	$mg\ Ca\ l^{-1}$	50	7	217
Magnesium	$mg\ Mg\ l^{-1}$	18	2	36
Chlorine	$mg\ Cl\ l^{-1}$	34	12	88
Sodium	$mg\ Na\ l^{-1}$	7	ND ^a	24
Sulfur	$mg\ S\ l^{-1}$	13	ND ^a	25
Boron	$mg\ B\ l^{-1}$	0.088	ND ^a	0.17
Cadmium	$mg\ Cd\ l^{-1}$	0.0006	ND ^a	0.0036
Copper	$mg\ Cu\ l^{-1}$	1.0	ND ^a	2.4
Zinc	$mg\ Zn\ l^{-1}$	1.0	ND ^a	3.5

^a ND: not detectable

8.4.4 Mathematical model analysis

Composition of destructed manure samples

To study which chemical phenomena influence the recorded titration curves, an insight in the complete composition of the destructed manure samples is necessary. With this information, and using mathematical models, a simulation study can be used to assess which reactions have to be considered when modelling buffer capacity profiles. It should be mentioned that the main purpose of the buffer capacity modelling is to estimate the ammonium and ortho-phosphate concentrations in the destructed manure samples.

A Dutch study [118] about animal manure composition was used to tabulate the mean, minimum and maximum concentrations of measured components in animal manure. The original results are expressed as $mg\ kg^{-1}$ manure, but for the purpose of this work, all values are expressed as $mg\ l^{-1}$ destructed and undiluted manure. Tables 8.2, 8.3 and 8.4 show the results for respectively pigs, poultry and cattle.¹ Note that the concentration of sulfur originating from the H_2SO_4 added prior to the destruction step, is not included in the tables. This concentration in the destructed samples is $1.5\ M\ H_2SO_4$.

A second study considered 19 different manure samples, originating from 2 mixed (pigs and cattle) farms in Flanders, taken in May 1998. The samples were analyzed for the same elements as in the first study [118] (except for chlorine and sulfur), but supplemented with 50 extra, mainly minor elements, all measured, except for nitrogen, with ICP-MS. Only the components with a mean concentration higher than $0.1\ mg\ l^{-1}$ and Cd are listed in Table 8.5.

¹To convert values from l^{-1} destructed sample to kg^{-1} manure, the tabulated values should be multiplied with 50.

Table 8.3: The composition of poultry manure, based on 436 samples [118]

Component	Unit	Mean	Minimum	Maximum
Nitrogen	$mg\ N\ l^{-1}$	212	112	412
Phosphorus	$mg\ P\ l^{-1}$	34	6	88
Potassium	$mg\ K\ l^{-1}$	51	27	115
Calcium	$mg\ Ca\ l^{-1}$	244	47	617
Magnesium	$mg\ Mg\ l^{-1}$	24	4	54
Chlorine	$mg\ Cl\ l^{-1}$	32	16	68
Sodium	$mg\ Na\ l^{-1}$	8	4	18
Sulfur	$mg\ S\ l^{-1}$	18	6	42
Boron	$mg\ B\ l^{-1}$	0.11	0.046	0.22
Cadmium	$mg\ Cd\ l^{-1}$	0.001	0.0002	0.0046
Copper	$mg\ Cu\ l^{-1}$	0.28	0.09	1.3
Zinc	$mg\ Zn\ l^{-1}$	1.5	0.48	3.5

Table 8.4: The composition of cattle manure, based on 429 samples [118]

Component	Unit	Mean	Minimum	Maximum
Nitrogen	$mg\ N\ l^{-1}$	98	48	156
Phosphorus	$mg\ P\ l^{-1}$	9	3	34
Potassium	$mg\ K\ l^{-1}$	51	10	76
Calcium	$mg\ Ca\ l^{-1}$	44	7	507
Magnesium	$mg\ Mg\ l^{-1}$	17	7	33
Chlorine	$mg\ Cl\ l^{-1}$	34	6	64
Sodium	$mg\ Na\ l^{-1}$	7	1	16
Sulfur	$mg\ S\ l^{-1}$	14	5	23
Boron	$mg\ B\ l^{-1}$	0.06	0.02	0.14
Cadmium	$mg\ Cd\ l^{-1}$	0.0006	ND ^a	0.0016
Copper	$mg\ Cu\ l^{-1}$	0.14	0.032	1.7
Zinc	$mg\ Zn\ l^{-1}$	0.5	0.12	3.4

^a ND: not detectable

Table 8.5: The composition of 19 manure samples from Flemish pigs and cattle

Component	Unit	Mean	Minimum	Maximum
Nitrogen	$mg\ N\ l^{-1}$	128	53	241
Phosphorus	$mg\ P\ l^{-1}$	40	4	102
Potassium	$mg\ K\ l^{-1}$	94	42	137
Calcium	$mg\ Ca\ l^{-1}$	52	7	152
Magnesium	$mg\ Mg\ l^{-1}$	29	1	63
Sodium	$mg\ Na\ l^{-1}$	16	3	32
Boron	$mg\ B\ l^{-1}$	0.13	0.06	0.26
Cadmium	$mg\ Cd\ l^{-1}$	0.001	0.0003	0.002
Copper	$mg\ Cu\ l^{-1}$	0.75	0.06	4.3
Zinc	$mg\ Zn\ l^{-1}$	5	0.21	38
Aluminum	$mg\ Al\ l^{-1}$	3	0.07	10
Titanium	$mg\ Ti\ l^{-1}$	0.11	0.004	0.3
Manganese	$mg\ Mn\ l^{-1}$	0.8	0.03	1.7
Iron	$mg\ Fe\ l^{-1}$	7	0.7	22
Strontium	$mg\ Sr\ l^{-1}$	0.14	0.02	0.4
Barium	$mg\ Ba\ l^{-1}$	0.13	ND ^a	0.8

^a ND: not detectable

Table 8.6: Ionic strength calculations in destructed manure samples for different dilution factors and the corresponding corrections for pK_a and γ_{H^+} to be included in buffer capacity models

	Dilution factor			
	undiluted	2 times	6.6 times	10 times
SO_4^{2-} (M)	1.5	0.75	0.227	0.15
Na^+ (M)	3	1.5	0.454	0.3
I (M)	4.5	2.25	0.68	0.45
ΔpK_a $H_3PO_4/H_2PO_4^-$			-0.12	-0.13
ΔpK_a $H_2PO_4^-/HPO_4^{2-}$			-0.37	-0.4
ΔpK_a HPO_4^{2-}/PO_4^{3-}			-0.62	-0.67
ΔpK_a $H_2CO_3^*/HCO_3^-$			-0.12	-0.13
ΔpK_a HCO_3^-/CO_3^{2-}			-0.37	-0.4
ΔpK_a NH_4^+/NH_3			+0.12	+0.13
ΔpK_a H_2O/OH^-			-0.12	-0.13
ΔpK_a HSO_4^-/SO_4^{2-}			-0.37	-0.4
γ_{H^+}			0.75	0.74

Ionic strength influence

The ionic strength of the destructed manure mainly originates from the quantity of H_2SO_4 added to the manure prior to the destruction step, and the quantity of strong $NaOH$ added to the destructed sample to bring it to pH 3, prior to the titration. All other ionic substances (e.g. NH_4^+ , HPO_4^{2-} , Ca^{2+}) are mostly far below 15 mmol l^{-1} , before as well as during the titration. These quantities are negligible compared to the quantities of SO_4^{2-} and Na^+ which are respectively 1.5 and 3 M in the destructed and undiluted manure sample.

Table 8.6 reports the ionic strength in function of different dilution factors. The ionic strength is calculated with the formula for I given in Table 2.1 on page 16. Next, the activity coefficients γ were calculated for a number of ions that need to be considered in the mathematical models for buffer capacity. However, only the Davies approximation (see Table 2.1 on page 16) is useful, because its applicability reaches an ionic strength upper level of 0.5 M . Next, the necessary calculations were done to correct the mathematical models for the influence of ionic strength (see section 3.3.6 on page 51 and section 3.5.4 on page 63). The symbol ΔpK_a is used for the difference between the pK_a' (taking into account the effect of ionic strength) and the pK_a (assuming no influence of ionic strength). A ΔpK_a value can be positive or negative, depending on the considered buffer system. The ΔpK_a values for some important buffer systems in the destructed samples, and the activity coefficient of H^+ are also given in Table 8.6. Note that the latter calculations are only performed for the two highest dilution factors, because for the lower dilution factors, the ionic strength is too high for reliable calculations, even with the Davies approximation. The dilution factor 6.6 is included because this factor was experimentally found as the optimal dilution factor (see section 8.4.5). Therefore, the further

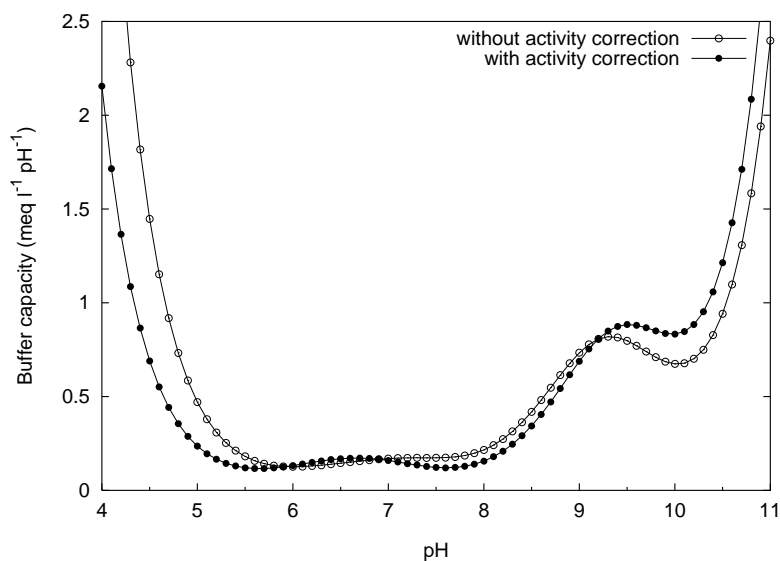


Figure 8.6: Simulated buffer capacity curves of a destructed and 6.6 times diluted manure sample, with and without ionic strength correction in the model

simulation examples in this section are performed with this particular dilution factor.

The effect of the ionic strength correction is illustrated in Figure 8.6. The buffer capacity curve of a destructed and 6.6 times diluted manure sample with mean concentrations for ammonium and ortho-phosphate, was simulated. A small amount of inorganic carbon (IC) (0.11 mmol l^{-1}) was also included in the model. The simulation was performed with and without the ionic strength correction. No complexation or precipitation reactions were included in this model. It can be concluded that the ionic strength correction has a significant effect on the buffer capacity profile, and should be considered in the mathematical models.

Complexation and precipitation

Based on the complete analysis of 19 manure samples (see Table 8.5), it was investigated which complexation and precipitation reactions might have an influence on the buffer capacity profile in the pH range between pH 3 and pH 11. This is a difficult task, in the first place because of the caveats related to precipitation and dissolution reactions, formulated in section 2.5 on page 35. Experimental findings have shown that buffer capacity curves are not very reproducible when precipitation reactions are involved. Further, in section 3.5.5 on page 64, it was discussed that in systems where different possible solids involving common components exist, it is not straightforward to obtain the correct set of solids to be included in the mathematical model. These aspects make the modelling of precipitation phenomena difficult and unwieldy. Complexation reactions (see section 2.4 on page 29) are equilibrium reactions that from a kinetic point of view are in most cases fast or very fast. They are easy to incorporate in mathematical models for buffer capacity (e.g. with the tableau-method discussed in section

Table 8.7: Concentrations of different components included in the buffer capacity model with the purpose to evaluate precipitation and complexation reactions

Component	Concentration
SO_4^{2-}	0.227 mol l^{-1}
NH_4^+	2.6 mmol l^{-1}
<i>o</i> - PO_4	0.5 mmol l^{-1}
Ca^{2+}	0.58 mmol l^{-1}
Fe^{3+}	0.06 mmol l^{-1}

3.5 on page 55). However, the difficulty is that there are possibly hundreds of complexation reactions that can be considered in destructed manure. Based on the composition of destructed manure (see Table 8.5), the metal cations known as complex formers are Ca^{2+} , Mg^{2+} , Fe^{3+} , Al^{3+} , Zn^{2+} and Cu^{2+} . Rare complex formers, but present in high concentrations are K^+ and Na^+ . Possible ligands in destructed manure are H_2O , OH^- , SO_4^{2-} , NH_3 , PO_4^{3-} , HPO_4^{2-} , H_2PO_4^- . During titration, some CO_2 can enter in the titration vessel, thus at high pH, also CO_3^{2-} can be considered as a possible ligand.

With preliminary simulation tests, using the software *bctab* (see section 5.2 on page 113), a number of complexation and precipitation reactions were investigated for their effect on the buffer capacity profile. With the above mentioned cations and ligands, hundreds of possible complexation or precipitation reactions must be considered. Therefore, more detailed simulation studies were restricted to a choice of 2 cations, Ca^{2+} and Fe^{3+} , that are present in rather high concentrations, and that are considered to have an important influence on the buffer capacity profile between pH 4 and pH 11. It was also chosen not to include carbonate equilibria at this stage. The concentrations of the different components included in the buffer capacity model, for the purpose of complexation and precipitation modelling, are tabulated in Table 8.7. The concentrations are chosen as the maximum values from Table 8.5, and take into account a 6.6 times dilution.

First, a number of simple chemical equilibrium reactions were considered in the mathematical model, given in Table 8.8. The $\log K$ values are given at 25°C [273], and the $\log K'$ values (mixed acidity constants, see section 2.2.4 on page 19) were calculated to account for ionic activities in the model. Contrary to preliminary simulation experiments (see section 8.4.2), the sulphuric acid buffer was now included in the model. Despite the fact that H_2SO_4 is a strong acid, its influence on the buffer capacity is considered significant due to its high concentration in the destructed manure. Second, also complexation reactions were included in the model. Table 8.9 summarizes the complex formation reactions and corresponding $\log \beta$ values ($\log \beta$ values were taken from [273] at 25°C). Because some reactions involve the binding of more than 1 ligand anion, overall formation constants (symbols β and β') and not stepwise formation constants (symbol K) were used (see also section 2.4.1 on page 30). Third, a number of precipitation reactions were investigated with the *bctab* software. They are summarized in Table 8.10 ($\log K_{s0}$ were taken from [263, 273] at 25°C). The concentration product $\log {}^c K_{s0}$

Table 8.8: Simple chemical equilibrium reactions included in the mathematical model

Chemical reaction	$\log K$	$\log K'$
$\text{H}^+ + \text{H}_2\text{PO}_4^- \rightleftharpoons \text{H}_3\text{PO}_4$	2.15	2.03
$\text{H}^+ + \text{HPO}_4^{2-} \rightleftharpoons \text{H}_2\text{PO}_4^-$	7.2	6.83
$\text{H}^+ + \text{PO}_4^{3-} \rightleftharpoons \text{HPO}_4^{2-}$	12.35	11.73
$\text{H}^+ + \text{NH}_3 \rightleftharpoons \text{NH}_4^+$	9.24	9.36
$\text{H}^+ + \text{SO}_4^{2-} \rightleftharpoons \text{HSO}_4^-$	1.99	1.62
$\text{H}^+ + \text{OH}^- \rightleftharpoons \text{H}_2\text{O}$	14	13.88

Table 8.9: Complex chemical equilibrium reactions included in the mathematical model

Chemical reaction	$\log \beta$	$\log \beta'$
$\text{Ca}^{2+} + \text{H}_2\text{PO}_4^- \rightleftharpoons \text{CaH}_2\text{PO}_4^+$	1.45	0.96
$\text{Ca}^{2+} + \text{HPO}_4^{2-} \rightleftharpoons \text{CaHPO}_4^0$	2.75	1.76
$\text{Ca}^{2+} + \text{PO}_4^{3-} \rightleftharpoons \text{CaPO}_4^-$	6.5	5.01
$\text{Ca}^{2+} + \text{OH}^- \rightleftharpoons \text{CaOH}^+$	1.15	0.66
$\text{Ca}^{2+} + \text{SO}_4^{2-} \rightleftharpoons \text{CaSO}_4^0$	2.31	1.32
$\text{Fe}^{3+} + \text{H}_2\text{PO}_4^- \rightleftharpoons \text{FeH}_2\text{PO}_4^{2+}$	4.35	3.61
$\text{Fe}^{3+} + \text{HPO}_4^{2-} \rightleftharpoons \text{FeHPO}_4^+$	10.15	8.66
$\text{Fe}^{3+} + \text{OH}^- \rightleftharpoons \text{FeOH}^{2+}$	11.8	11.1
$\text{Fe}^{3+} + 2\text{OH}^- \rightleftharpoons \text{Fe}(\text{OH})_2^+$	22.3	21.07
$\text{Fe}^{3+} + 4\text{OH}^- \rightleftharpoons \text{Fe}(\text{OH})_4^-$	34.4	32.9
$\text{Fe}^{3+} + \text{SO}_4^{2-} \rightleftharpoons \text{FeSO}_4^+$	4.0	2.51
$\text{Fe}^{3+} + 2\text{SO}_4^{2-} \rightleftharpoons \text{Fe}(\text{SO}_4)_2^-$	5.4	3.42

(introduced in equation (2.74) on page 36) is used for the ionic activity corrected $\log K_{s0}$ value, where concentrations instead of activities can be used.

Note that hydroxy-apatite ($\text{Ca}_5(\text{PO}_4)_3\text{OH}_{(s)}$) is a precipitate that is typically found in animal manure. However, this reaction proceeds very slowly to an equilibrium, i.e. the solution can highly, and for a long time, be supersaturated before any precipitation starts (unless there are already crystal seeds present in the solution) [263].

In a first stage, the simulation study only considered the simple and the complex chemical equilibria. In a later phase, the precipitation reactions were evaluated. The chemical reactions in Tables 8.8 and 8.9 need to be organized into a stoichiometric matrix and a corresponding input file for the program *bctab*. This process is described and illustrated with an example in section 3.5.3 on page 61. The species, components and stoichiometric information, representing the reactions presented in Tables 8.8 and 8.9, is organized in a tableau in Table 8.11.

Table 8.10: Precipitation and dissolution reactions included in the mathematical model

Chemical reaction	$\log K_{s0}$	$\log {}^c K_{s0}$
$\text{Ca}^{2+} + \text{HPO}_4^{2-} \rightleftharpoons \text{CaHPO}_4(s)$	-6.65	-5.66
$\text{Ca}^{2+} + 2\text{H}_2\text{PO}_4^- \rightleftharpoons \text{Ca}(\text{H}_2\text{PO}_4)_2(s)$	-1.14	-0.40
$\text{Ca}^{2+} + 2\text{OH}^- \rightleftharpoons \text{Ca}(\text{OH})_2(s)$	-5.19	-4.45
$\text{Ca}^{2+} + \text{SO}_4^{2-} \rightleftharpoons \text{CaSO}_4(s)$	-4.62	-3.63
$\text{Fe}^{3+} + \text{PO}_4^{3-} \rightleftharpoons \text{FePO}_4(s)$	-(21.9 - 26.4)	-(19.7 - 24.2)
$\text{Fe}^{3+} + 3\text{OH}^- \rightleftharpoons \text{Fe}(\text{OH})_3(s)$	-(38.8 - 42.7)	-(37.3 - 41.2)
$5\text{Ca}^{2+} + 3\text{PO}_4^{3-} + \text{OH}^- \rightleftharpoons \text{Ca}_5(\text{PO}_4)_3\text{OH}(s)$	-55.9	-50.0

The simulation results of 2 models, with and without the complex formation reactions, are shown in Figure 8.7. There are 3 regions in the buffer capacity profile that are influenced by the complex formation reactions from Table 8.9. They are indicated with arrows on the graph. Extra simulations, where complex formation reactions were evaluated separately or in smaller groups, revealed the responsible reactions for the buffer capacity increases. Region (1), around pH 5.5, is related to iron and phosphate; region (2), around pH 8, is related to iron hydroxides; and region (3), around pH 10, is originating from calcium and phosphate. It should be noted that, in the simulation study, the maximum concentrations of Ca^{2+} and Fe^{3+} found in a set of manure samples (see Table 8.5) were used. Thus, in real situations, the influences of the complex formation reactions are probably lower than illustrated in Figure 8.7.

The final purpose of the buffer capacity modelling in this application is to make an estimation of the ortho-phosphate and ammonium concentrations in the destructed and diluted manure samples. Therefore, an interesting conclusion from this simulation study is that the buffer capacities around pH 6.7 and pH 9–9.5 are influenced only to a minor extent by the complex formation reactions. As a consequence, a reliable estimation of ortho-phosphate and ammonium is still possible, even if the exact concentrations of calcium and iron are unknown.

In a second stage, the simulation study evaluated the precipitation reactions in Table 8.10 on their occurrence between pH 2 and pH 11 during the simulation of the model shown in Table 8.11. The program *bctab* has a built-in facility to calculate the ionic concentration product of 2 or more species that can form a possible precipitate at each pH value. This concentration product is then compared with the $\log {}^c K_{s0}$ value, to find the state of saturation of the solution with respect to that solid. If the solution is oversaturated, a message for that solid is logged in a file. The precipitates that are theoretically formed and their corresponding pH ranges, are tabulated in Table 8.12. Three possible precipitates were found under the modelled conditions. As mentioned before, the precipitation of hydroxy-apatite is most uncertain, and will not be further considered. An interesting point is that there are no calcium precipitates formed, but only two iron precipitates. The precipitate that is theoretically formed at first during a pH increase is iron hydroxide. The consequences for the simulated buffer capacity profile when $\text{Fe}(\text{OH})_3(s)$ precipitation is considered, are presented in the following paragraphs.

Table 8.11: Species, components and stoichiometric information for simple and complex chemical equilibrium reactions in destructed and diluted manure

Species	Components					H ⁺	{log K}
	H ₃ PO ₄	NH ₄ ⁺	HSO ₄ ⁻	Ca ²⁺	Fe ³⁺		
H ₃ PO ₄	1	0	0	0	0	0	0
NH ₄ ⁺	0	1	0	0	0	0	0
HSO ₄ ⁻	0	0	1	0	0	0	0
Ca ²⁺	0	0	0	1	0	0	0
Fe ³⁺	0	0	0	0	1	0	0
H ₂ PO ₄ ⁻	1	0	0	0	0	-1	-2.03
HPO ₄ ²⁻	1	0	0	0	0	-2	-8.86
PO ₄ ³⁻	1	0	0	0	0	-3	-20.6
NH ₃	0	1	0	0	0	-1	-9.36
SO ₄ ²⁻	0	0	1	0	0	-1	-1.62
CaH ₂ PO ₄ ⁺	1	0	0	1	0	-1	-1.08
CaHPO ₄ ⁰	1	0	0	1	0	-2	-7.1
CaPO ₄ ⁻	1	0	0	1	0	-3	-15.6
CaOH ⁻	0	0	0	1	0	-1	-13.23
CaSO ₄ ⁰	0	0	1	1	0	-1	-0.3
FeH ₂ PO ₄ ²⁺	1	0	0	0	1	-1	1.58
FeHPO ₄ ⁺	1	0	0	0	1	-2	-0.2
FeOH ²⁺	0	0	0	0	1	-1	-2.82
Fe(OH) ₂ ⁺	0	0	0	0	1	-2	-6.69
Fe(OH) ₄ ⁻	0	0	0	0	1	-4	-22.6
FeSO ₄ ⁺	0	0	1	0	1	-1	0.89
Fe(SO ₄) ₂ ⁻	0	0	2	0	1	-2	0.18
OH ⁻	0	0	0	0	0	-1	-13.88
<i>C (mol l⁻¹)</i>	0.0005	0.0026	0.227	0.00058	6 10 ⁻⁵		

Table 8.12: Theoretical precipitations found with the simulation model for destructed and diluted manure between pH 2 and pH 11

Precipitate	Precipitation in pH interval
FePO _{4(s)}	3.35–8.45
Fe(OH) _{3(s)}	2.75–11
Ca ₅ (PO ₄) ₃ OH _(s)	7.35–11

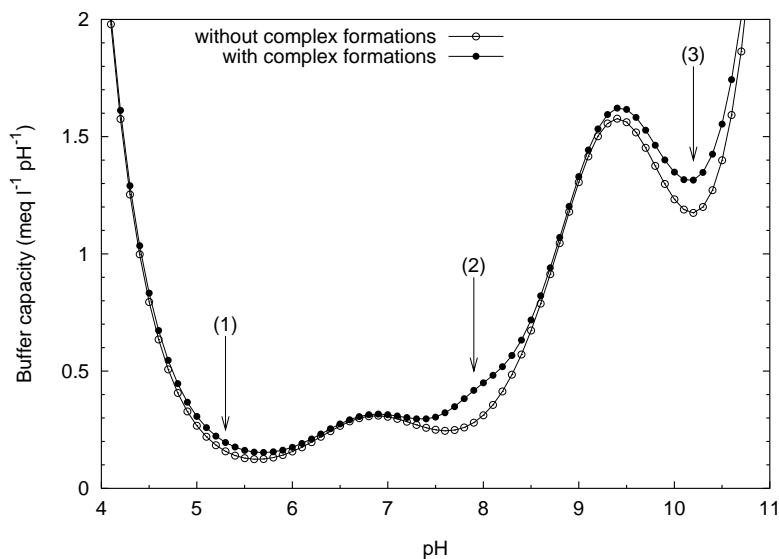


Figure 8.7: Simulated buffer capacity curves of a destructed and diluted manure sample, with and without complex formation reactions in the model. Three arrows indicate a buffer capacity increase due to the complex formation reactions

When considering precipitation reactions, the stoichiometric information has to be rewritten in function of the precipitates that are considered. An example that illustrates how a precipitation reaction has to be included in the stoichiometric information is given in section 3.5.5 on page 64. It is mentioned there, that if more than one precipitation reaction needs to be considered, a trial and error procedure may be necessary to find the correct stoichiometric matrix. And further, for each simulation pH step, the stoichiometric matrix should be reconsidered for its validity, because the set of precipitates can change along increasing pH values. This is unwieldy for practical purposes, and therefore, it is advised to consider only a minimal number of precipitates (1 or 2 precipitates) for buffer capacity simulation purposes. Also, as described in section 2.5 on page 35, precipitation reactions are sluggish, slow, non-stoichiometric, ... Thus, mathematical modelling results of such reactions during a relatively 'fast' titration process (from pH 3 to pH 11 in around 30 minutes), should be interpreted with carefulness.

The $\text{Fe}(\text{OH})_{3(s)}$ is considered as a type IV solid (see section 3.5.2 on page 60) in this example. Its presence decreases the number of degrees of freedom for solving this equilibrium problem. More particularly, the concentration of free iron $[\text{Fe}^{3+}]$ is directly linked to the pH by the following reaction:

$$[\text{Fe}^{3+}][\text{OH}^-]^3 = 10^{-40} \text{ or } \log[\text{Fe}^{3+}] = 1.64 + 3 \log[\text{H}^+] \quad (8.1)$$

Thus, the stoichiometric information in Table 8.11 needs to be adjusted when $\text{Fe}(\text{OH})_{3(s)}$ is involved. Fe^{3+} is not considered any more as a component, and species including Fe^{3+} need to be rewritten using equation (8.1). The new stoichiometric matrix is presented in Table 8.13.

The simulation with the model from Table 8.13 learns that in the presence of $\text{Fe}(\text{OH})_{3(s)}$, the complex formation reactions involving iron are not influencing the buffer capacity profile any more. In other words, the iron is practically unavailable for other reactions due to the solid phase of iron. This can also be logically deduced when interpreting equation (8.1): The free iron concentration decreases with 3 log units for each increase of 1 pH unit. The resulting buffer capacity profile (figure not shown) is similar as in Figure 8.7, except that the increased buffer capacities in regions (1) and (2) disappear when precipitation is included in the model. However, as mentioned above, it should also be noticed that the occurrence and completeness of this precipitation reaction is uncertain, thus strong conclusions cannot be made from this simulation result.

Conclusions

Simulation experiments have learned that ionic strength corrections should be taken into account for the simulation of buffer capacity curves of destructed and diluted manure samples. Further, it is illustrated that the ortho-phosphate and ammonium buffers can be modelled with a simple chemical equilibrium model, because the buffer capacities around pH 7 and pH 9 are only slightly influenced by the considered complex formations. Only complex formation reactions with Ca^{2+} and Fe^{3+} are investigated, because these cations are present in the highest concentrations, and considered to have a noticeable influence on the buffer capacity between pH 4 and pH 11. Other cations, like Mg^{2+} and Al^{3+} , however, can eventually also have minor influences on the buffer capacity profile. Some precipitation reactions with Ca^{2+} and Fe^{3+} were investigated, and it was found that iron hydroxide is a possible candidate for ‘mathematical’ precipitation. Its influence on the buffer capacity profile is positive rather than negative, because the iron precipitate immobilises the iron for complex formation reactions. It is uncertain if in real situations, the competition between complex formation and precipitation will occur. It should be noted that the simulation experiments are based on maximum concentrations found in real samples. Thus, the practical influence of complex formation and precipitation is to be expected lower than what is illustrated.

With the final aim of field application, it is chosen for the practical model development (see section 8.4.7) to start the modelling exercise with a simple model without complex formation and precipitation reactions. The reason for this is threefold. First, in field situations, the concentrations of complexing cations are not known, and they should be estimated (e.g. by using the mean values in Tables 8.2–8.5). Second, if the influence of the complex formation and precipitation reactions is not significant on the end result (the estimation of ortho-phosphate and ammonium), there is no need to consider those reactions. Third, from a mathematical point of view, the complex formation reactions can approximately be modelled as extra monoprotic buffers. This simplifies the modelling because the underlying complexation reactions do not have to be known in detail for incorporating their influence in the model. If it is found that these extra buffers are needed in the model to obtain reliable end results, then the underlying complexation reactions can eventually be taken into account in a later modelling phase as real complexation reactions.

Table 8.13: Species, components and stoichiometric information for simple and complex chemical equilibrium reactions in destructed and diluted manure, in the presence of iron hydroxide precipitate. The bold items mark the differences with Table 8.11

Species	Components				H ⁺	{log K}
	H ₃ PO ₄	NH ₄ ⁺	HSO ₄ ⁻	Ca ²⁺		
H ₃ PO ₄	1	0	0	0	0	0
NH ₄ ⁺	0	1	0	0	0	0
HSO ₄ ⁻	0	0	1	0	0	0
Ca ²⁺	0	0	0	1	0	0
Fe ³⁺	0	0	0	0	3	1.64
H ₂ PO ₄ ⁻	1	0	0	0	-1	-2.03
HPO ₄ ²⁻	1	0	0	0	-2	-8.86
PO ₄ ³⁻	1	0	0	0	-3	-20.6
NH ₃	0	1	0	0	-1	-9.36
SO ₄ ²⁻	0	0	1	0	-1	-1.62
CaH ₂ PO ₄ ⁺	1	0	0	1	-1	-1.08
CaHPO ₄ ⁰	1	0	0	1	-2	-7.1
CaPO ₄ ⁻	1	0	0	1	-3	-15.6
CaOH ⁻	0	0	0	1	-1	-13.23
CaSO ₄ ⁰	0	0	1	1	-1	-0.3
FeH ₂ PO ₄ ²⁺	1	0	0	0	2	3.22
FeHPO ₄ ⁺	1	0	0	0	1	1.44
FeOH ²⁺	0	0	0	0	2	-1.18
Fe(OH) ₂ ⁺	0	0	0	0	1	-5.05
Fe(OH) ₄ ⁻	0	0	0	0	-1	-20.96
FeSO ₄ ⁺	0	0	1	0	2	2.53
Fe(SO ₄) ₂ ⁻	0	0	2	0	1	1.82
OH ⁻	0	0	0	0	-1	-13.88
<i>C (mol l⁻¹)</i>	0.0005	0.0026	0.227	0.00058		

Table 8.14: Titrimetric nitrogen and phosphorus determination in destructed manure for different dilution factors. The concentrations are expressed as $mg\ l^{-1}$ in the undiluted destructed sample

Dilution factor	NH_4^+ ($mg\ N\ l^{-1}$)		<i>o</i> - PO_4 ($mg\ P\ l^{-1}$)	
	Mean	Std. dev.	Mean	Std. dev.
Undiluted	208	4.6	77	4.9
2 ×	202	3.6	71	2.7
3 ×	197	5.6	74	4.4
6 ×	191	6.3	74	4.4
15 ×	182	14.2	77	13.2
Laboratory	171		76	

8.4.5 The influence of the dilution factor

Destructed manure samples contain 1.5 M H_2SO_4 , and have an extremely low pH value. Prior to titration, the pH needs to be adjusted with a strong alkaline solution (e.g. NaOH 1.5 N) to bring the pH around 3. Next, a titration with NaOH 0.1 N is performed until pH 11 is reached. If destructed manure samples are titrated without dilution, a number of problems can arise. First, the alkaline consumption, NaOH 1.5 and 0.1 N in this case, would be very high. Second, the ionic strength would be very high and its effect on the activities of ions cannot be predicted any more by approximate formulas (see Table 8.6). Third, unwanted chemical reactions, like precipitation, can interfere with the buffer capacity measurement. On the other hand, when destructed samples are diluted too much, the concentrations of phosphate and ammonium in the solution become too low, and the effect of measurement noise and interferences of e.g. inorganic carbon become too large. Consequently, the variability and accuracy of the final result would be negatively influenced. An experiment was set up to test different dilution factors and evaluate their effects on the estimates of ortho-phosphate and ammonium concentrations.

A destructed manure sample was used to prepare 5 different dilutions, ranging from undiluted to 15 times diluted. Each diluted series was titrated in fourfold. The laboratory analyses of the nitrogen and phosphorus concentrations of that sample were $171\ mg\ N\ l^{-1}$ and $76\ mg\ P\ l^{-1}$. The ammonium and the ortho-phosphate concentrations were also estimated from the experimental buffer capacity curves, and the results are tabulated in Table 8.14. Two examples of experimental and corresponding simulated buffer capacity curves for respectively undiluted and 15 times diluted sample are shown in Figure 8.8.

For the undiluted samples, the experimental buffer capacity curves became irregular for pH values higher than 9, as illustrated in Figure 8.8(a). This can possibly be explained by slow reactions like precipitation reactions. This was also observed in the 2 times diluted sample, but no longer for the higher dilutions. Despite the irregular buffer capacity curves for the undiluted and two times diluted sample, the estimates for N and P are still reproducible, as can be seen in the rather low standard deviations on the N and P estimates in Table 8.14. The simulated buffer

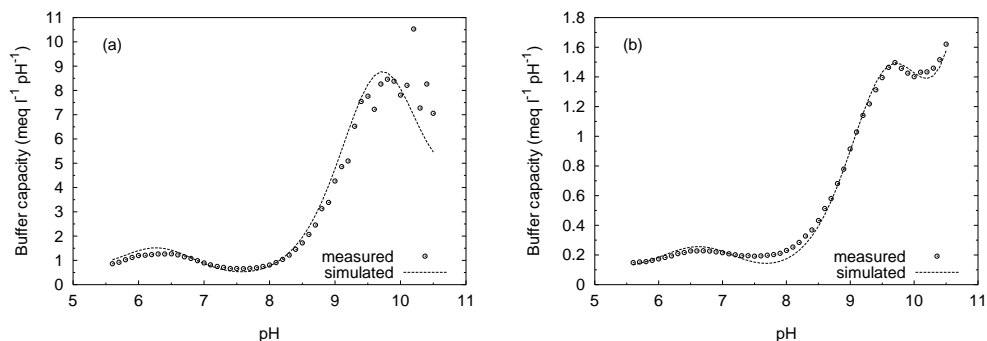


Figure 8.8: Experimental and simulated buffer capacity curves of destructed manure. Plot (a) undiluted sample. Plot (b) $15 \times$ diluted sample. Note the difference in scale

capacity curves for the highest dilution factor (see Figure 8.8(b)) fit much better in the high pH range, compared to the fit of the undiluted samples. However, the standard deviations obtained through the 4 replicate concentration values, become too high for the highest dilution factor compared to the lower dilution factors (see Table 8.14). The dilution factors 3 and 6 gave the best results, because unwanted precipitations or other reactions were avoided, and still reproducible results were obtained. Because of the corresponding lowest chemical demands, factor 6 was chosen as the ideal dilution factor for further experiments.

8.4.6 Experimental method validation

A number of experiments were set up to experimentally study some anticipated phenomena that were already investigated with simulations in section 8.4.4. In a first stage, the influence of sulphuric acid, ionic strength and Ca^{2+} were investigated. In a second stage, a standard addition experiment with $o\text{-PO}_4$ was performed to validate the followed approach.

Without going into the details of the the first stage experiments (full results in [300]), there are some important conclusions to be made from these experiments. Despite the fact that sulphuric acid is a strong acid, its influence on the buffer capacity in destructed and diluted manure samples (e.g. 0.23 M in 6.6 times diluted sample) is clearly felt up to pH 6.5. Therefore, the $\text{HSO}_4^- \rightleftharpoons \text{H}^+ + \text{SO}_4^{2-}$ reaction needs to be incorporated in the buffer capacity model. Addition experiments with NaCl (up to 0.3 M) to change the ionic strength of titrated samples have illustrated that the ΔpK_a 's predicted by the Davies approximation fairly well correspond with the observations in the buffer capacity profiles (see also Table 8.6). Addition experiments with CaCl_2 (up to $150\text{ mg Ca}^{2+}\text{ l}^{-1}$) have shown that the Ca^{2+} did not have a significant effect on the buffer capacity profile of destructed and diluted manure. This confirms that a simple mathematical model (without complexation and precipitation) may be sufficient for the modelling of the buffer capacity curves of destructed manure samples.

In the second stage, a standard addition experiment with KH_2PO_4 on a destructed manure sample was performed. The concentrations in the sample were 117 mg N l^{-1} and 25 mg P l^{-1} .

Table 8.15: Titrimetric nitrogen and phosphorus determination in destructed manure for different standard additions of ortho-phosphate. The concentrations are expressed as $mg\ l^{-1}$ in destructed and undiluted sample

Standard addition ($mg\ P\ l^{-1}$)	NH_4^+ ($mg\ N\ l^{-1}$)		<i>o</i> - PO_4 ($mg\ P\ l^{-1}$)		<i>o</i> - PO_4 recovery	
	Mean	Std. dev.	Mean	Std. dev.	($mg\ P\ l^{-1}$)	(%)
0	118.9	0.57	23.2	0.61		
4.76	119.2	0.22	27.6	0.50	4.37	92
9.52	119.0	0.26	31.6	0.21	8.35	88
19.0	119.4	0.25	40.3	0.55	17.1	90
28.6	119.4	0.55	49.2	0.31	26.0	91
38.1	120.0	0.13	57.9	0.57	34.7	91
47.6	120.5	0.63	67.1	0.58	43.9	92

The stock solution of KH_2PO_4 was tested on its concentration with a colorimetric method (Cuvette test LCK049, Dr. Lange®). Subsamples were prepared as follows: 25 ml from the destructed manure sample was diluted with 100 ml water. Around 70 ml of NaOH 1 N was added manually to bring the pH of the sample to pH 3. Thus, the total sample volume was around 195 ml and therefore, the dilution factor was 7.8. The titrations were performed with a laboratory titrator (Metrohm Titrino 716) with the DET titration mode (details of the DET titration algorithm can be found in section 5.1.1 on page 98). The normality of the titrant was 0.1 N and the end pH value was 11. Around 10 ml of titrant was added during the titration. The temperature of the samples was the same as the room temperature during the experiment (24 to 25 °C). Seven series of samples (blank and standard additions between 5 and 50 $mg\ P\ l^{-1}$ destructed and undiluted sample, see Table 8.15) were titrated in fivefold. Contrary to the previous and following experiments reported in this section, the NaOH stock solutions 1 N and 0.1 N were not prepared in the laboratory with NaOH pellets and demineralized water, but were bought as 10 litre, completely closed, plastic bags (Titripack®, Merck). The reason for this is described in detail in section 8.5.2.

The mathematical modelling of the experimental buffer capacity curves was performed in two steps. First, the ‘blank’ curves (without extra ortho-phosphate addition) were modelled and it was found that besides the ortho-phosphate and ammonium buffers, two additional small buffers around pH 5.1 and pH 8.4 were present. These 2 buffers were quantified as respectively 0.060 and 0.095 $mmol\ l^{-1}$ in the diluted samples. Second, another model was used, in which the 2 extra buffers were included as fixed buffer capacities. The second model was applied to other experimental buffer capacity curves and the amount of ortho-phosphate and ammonium was estimated.

The results of this standard addition experiment are given in Table 8.15. The ammonium and ortho-phosphate concentrations estimated from the buffer capacity profiles showed a good reproducibility, with a standard deviation around 0.5 $mg\ l^{-1}$ for both N and P. The ammonium concentrations estimated from the buffer capacity profiles increased with increasing additions

of ortho-phosphate. This increase was small ($< 2 \text{ mg N l}^{-1}$), however, statistically significant ($p < 0.001$). The recovery of ortho-phosphate for the different standard additions was in all cases around 90 %. With a paired t-test, it was concluded that the recovered concentrations of ortho-phosphate were significantly different ($p < 0.001$) from the added concentrations. This could point to possible other chemical reactions with ortho-phosphate, which are not included in the model, e.g. complexation reactions. The small increases in the estimated ammonium concentration with increasing ortho-phosphate standard additions points to possible formation of ortho-phosphate complexes that are buffering around pH 9, and being modelled as ammonium instead of ortho-phosphate (see also arrow (3) in Figure 8.7).

8.4.7 Development of an adequate buffer capacity model

A measurement campaign was organized to evaluate different mathematical buffer capacity models. The estimated ammonium and ortho-phosphate concentrations from the buffer capacity profile were compared with the laboratory analyses. A most adequate model is formulated, that will be proposed for further validations and later field-use.

The manure samples were collected in May 1998 on two mixed farms (pigs and cattle) in Flanders. At very different places on both farms, 19 samples were taken. All samples were destructured with the modified NEN 7433 method (see section 8.4.3) and analyzed in the lab for N and P. The destructured samples were titrated as follows: 25 ml of destructured sample was diluted with 100 ml water. Around 40 ml of NaOH 1.5 N was added manually to bring the pH of the sample to pH 3. Thus, the total sample volume was around 165 ml, corresponding with a dilution factor 6.6. This dilution factor was chosen in correspondence with the results of section 8.4.5. Between the manual pH adjustment and the titration, the samples were stirred for 20 minutes at pH 3 with a magnetic stirrer at high speed, to remove inorganic carbon (CO_2) originating from the NaOH 1.5 N stock solution. The titrations were performed with a laboratory titrator (Metrohm Titrino 716) with the DET titration mode (details of the DET titration algorithm can be found in section 5.1.1 on page 98). The normality of the titrant was 0.1 N and the end pH value was 11. Around 10 ml of titrant was added during the titration. The temperature of the samples was the same as the room temperature (around 20 °C), but no extra temperature control was used during the titrations. All samples were diluted and titrated in threefold.

Two criteria were used to interpret the results obtained with different buffer capacity models. First, the fit between the experimental and the simulated buffer capacity data was visualized and interpreted. Second, tables and scatterplots with the laboratory measurements of nitrogen and phosphorus against the estimated concentrations from the titrimetric measurements were interpreted. Different mathematical models were fitted to the experimental data. The software *bomb* (see section 5.3 on page 117) was used for the buffer capacity calculation and modelling. An overview of the model specifications of 4 selected models is given in Table 8.16. The results of 1 selected manure sample for the different models are tabulated in Table 8.17 and the corresponding experimental and simulated buffer capacity curves are shown Figure 8.9.

Model 1 is the initial model, containing the main buffer components to be expected in the destructured and diluted manure samples. Ionic activity corrections as calculated theoretically in section 8.4.4 were applied to the zero ionic strength pK_a values at 25 °C. All pK_a values were

Table 8.16: Model specifications of 4 selected models used during the development of the most adequate model for destructed and 6.6 times diluted manure samples. The concentrations are expressed per volume of destructed and diluted sample. The bold items mark the differences with the previous model

	Unit	Model 1	Model 2	Model 3	Model 4
$pK_a \text{H}_2\text{O}$		15.62	15.62–15.82	15.62–15.82	15.62–15.82
$pK_{a1} \text{IC}$		6.25	6.1	6.1	6.1
$pK_{a2} \text{IC}$		9.88	9.85	9.85	9.85
$pK_{a1} o\text{-PO}_4$		2.0	1.9	1.9	1.9
$pK_{a2} o\text{-PO}_4$		6.84	6.7	6.7	6.7
$pK_{a3} o\text{-PO}_4$		12.05	11.9	11.9	11.9
$pK_a \text{SO}_4^{2-}$		1.52	1.1	1.1	1.1
$pK_a \text{NH}_4^+$		9.2–9.5	9.25–9.75	9.25–9.75	9.25–9.75
$pK_a \text{blank1}$				4.5–5.5	
$pK_a \text{blank2}$					7.5–8.4
C_{IC}	$\text{mg CO}_2 \text{ l}^{-1}$	0.75–2.2	0.75–2.2	0.75–2.2	0.75–2.2
$C_{o\text{-PO}_4}$	mg P l^{-1}	0–25	0–25	0–25	0–25
$C_{\text{SO}_4^{2-}}$	mol l^{-1}	0.227	0.227	0.227	0.227
$C_{\text{NH}_4^+}$	mg N l^{-1}	0–45	0–45	0–45	0–45
C_{blank1}	mmol l^{-1}			0–1	
C_{blank2}	mmol l^{-1}				0–1
γ_{H^+}		0.75	0.75	0.75	0.75
pH interval		5.6–10.5	5.6–10.5	4–10.5	5.6–10.5

Table 8.17: Simulation results of 1 selected sample for the 4 different models. The concentrations are expressed as mg l^{-1} or mmol l^{-1} in destructed and diluted sample

	Unit	Laboratory	Model 1	Model 2	Model 3	Model 4
$pK_a \text{H}_2\text{O}$				15.72	15.72	15.72
$pK_a \text{NH}_4^+$			9.5	9.74	9.74	9.75
$pK_a \text{blank1}$					5.18	
$pK_a \text{blank2}$						7.88
C_{IC}	$\text{mg CO}_2 \text{ l}^{-1}$		1.08	2.2	0.75	2.15
$C_{o\text{-PO}_4}$	mg P l^{-1}	9.82	8.56	9.32	9.18	8.14
$C_{\text{NH}_4^+}$	mg N l^{-1}	36.5	35.9	38.3	38.8	38.3
C_{blank1}	mmol l^{-1}				0.12	
C_{blank2}	mmol l^{-1}					0.063

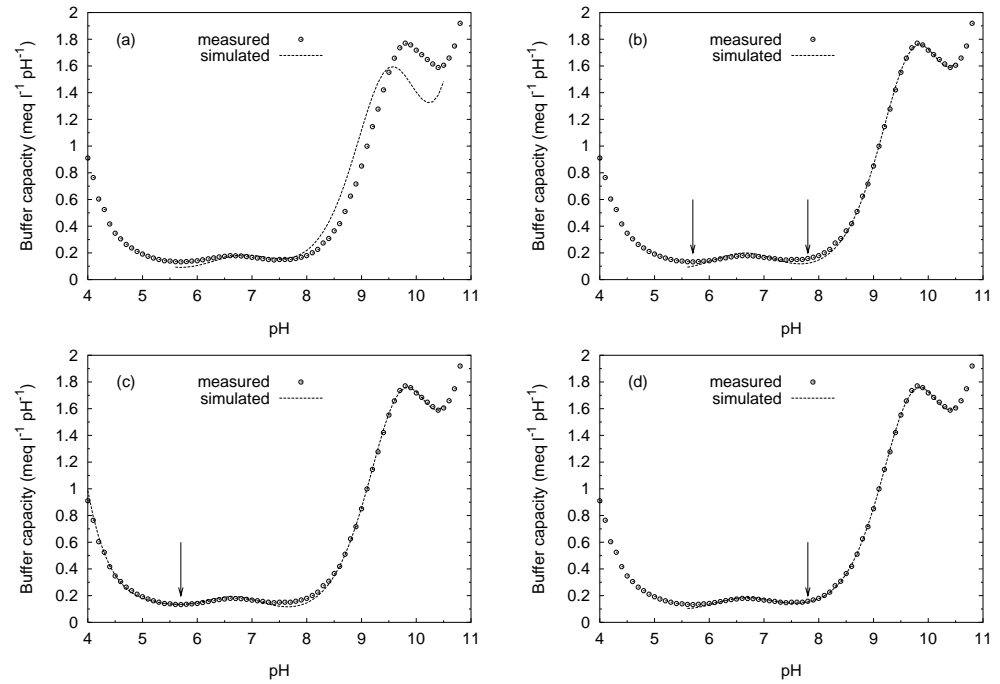


Figure 8.9: Experimental and simulated buffer capacity curves of 1 selected sample. Plots (a), (b), (c) and (d) for models 1, 2, 3 and 4 respectively. The arrows in plot (b) indicate the 2 pH ranges where extra buffer capacity was observed. The arrows in plots (c) and (d) indicate the positions where this extra buffer was incorporated in the model

kept fixed, except for the pK_a of the ammonium buffer, which was allowed to vary between a value 9.2 and 9.5. A fixed or variable pK_a value for ammonium did not make much difference in the estimates of the concentrations, but a variable pK_a for ammonium gave a better fit between the experimental and simulated buffer capacity profiles. When the pK_{a2} value for ortho-phosphate allowed to vary, the estimations of phosphate became worse. Therefore, it was chosen to set the pK_a of ammonium as a parameter to be optimized and to keep the other pK_a 's fixed. It was experienced in chapters 6 and 7 that a small amount of inorganic carbon (IC) is found back in the buffer capacity profile. Initially, a variable amount of IC between 0 and $5 \text{ mg CO}_2 \text{ l}^{-1}$ was included in the buffer capacity model. Later, it was found, generally, that a more narrow range gives somewhat more realistic results, especially in the samples with a low phosphate concentration ($< 10 \text{ mg P l}^{-1}$). This can be explained by the fact that the IC buffer is located near the ortho-phosphate buffer in the buffer capacity profile, thus those two buffers are more or less exchangeable with each other. Therefore, the amount of IC was allowed to vary between 0.75 and $2.2 \text{ mg CO}_2 \text{ l}^{-1}$ only. On the experimental buffer capacity curves, it was noticed that some buffer capacity around pH 5 was present, which could not originate from the buffer components included in model 1. Because at this stage, this buffer capacity was not of interest, it was chosen to limit the pH range for the simulation from pH 5.6 to pH 10.5. Generally spoken, the estimated concentrations of N and P obtained with model 1 were acceptable. However, the experimental and simulated buffer capacity curves did not fit very well. This is illustrated in Figure 8.9(a).

Model 2 is the result of manual adjustments of the 'fixed' pK_a values in the model, in order to obtain a better fit and a more accurate prediction of the concentrations. The adjustments that were made can be read from Table 8.16 when comparing model 1 with model 2. It can be noticed that for all buffers (except for H_2O), the adjustments of the fixed pK_a values are in the same direction as if the samples would have a higher ionic strength than the values used for a 6.6 times diluted sample in Table 8.6. More particular, all pK_a values were decreased a little bit, except for the NH_4^+ and the H_2O buffer, where the pK_a 's were increased. It was found that the pK_a of the H_2O buffer influenced the quality of the NH_4^+ prediction and the fit around pH 10. The best value for the pK_a of H_2O was 15.69. However, because this pK_a value was so determining for the estimated ammonium concentration, it was investigated if the result was still acceptable if the pK_a of water was allowed to vary instead of being a fixed value. The conclusion was that a variable pK_a for water gives similar results as a fixed pK_a . The advantage of a variable pK_a is that biased pH measurements (e.g. due to calibration errors) and deviations of the real pK_a compared to the theoretical pK_a (e.g. ionic interaction effects) can slightly be 'corrected' in the model by allowing some extra flexibility on the considered pK_a in the model. Therefore, for robustness reasons, a variable pK_a was preferred. There are several explanations possible why the theoretical pK_a values did not correspond with the practical observations. There could be a calibration error or an alkaline error in the pH measurement (see section 2.1.3 on page 10). Also, there can be an effect of the temperature, which was not kept at 25°C . The pH meter did not have automatic temperature compensation, and internally kept the Nernst slope always as if the temperature of the solution was 25°C . The theoretical pK_a values that were used, were those tabulated at 25°C . Finally, due to the high ionic strength in the samples (even at 6.6 times diluted), the formulas for the activity corrections (Davies approximation in this case) are at their limit of applicability. Therefore, the real ΔpK_a 's can differ from the values calculated in Table 8.6.

Considering the results of the selected manure sample (see Table 8.17) and the other 18 manure samples in the study (results not shown), model 2 was found to be better than model 1. The estimated concentrations C_{IC} for the different samples varied between the minimum and maximum boundary values (respectively 0.75 and 2.2 mg CO₂ l⁻¹). However, in around 50 % of the samples, the estimated IC concentration equalled the maximum boundary value (see also the example in Table 8.17). Increasing the boundary value resulted in a worse estimation of ortho-phosphate. This points to the important interfering property of IC for the quantification of ortho-phosphate. In Figure 8.9(b), one notices that in the experimental data, some buffer capacity exists around pH 5 and pH 8 (indicated with arrows) which can not be modelled with model 2, because no buffer systems around these pH ranges are included in the model. This phenomenon was noticed in most samples. Therefore, the two next models respectively incorporated an extra buffer in those two pH ranges.

Model 3 is an extension of model 2, with the incorporation of an extra monoprotic buffer in the model, whose pK_a may vary between pH 4.5 and pH 5.5. The pK_a and the concentration of that buffer are estimated by fitting the model to the experimental data. The simulation pH interval was extended, and set from pH 4 to pH 10.5. The typical result is a better fit in the pH range 4 to 7, as illustrated with the selected example in Figure 8.9(c). The estimations of NH₄⁺ did not change in model 3 compared to model 2. However, the estimations of *o*-PO₄ were slightly worse in model 3 compared to model 2. The extra buffer in model 3 was at most 0.17 mmol l⁻¹. There is a remarkable difference in the concentration of IC found with model 2 compared to model 3 (see Table 8.17). In model 2, the estimated IC is at its upper limit (2.2 mg CO₂ l⁻¹), whereas in model 3, the estimated IC is at its lower limit (0.75 mg CO₂ l⁻¹). This suggests that the extra monoprotic buffer in model 3 is interfering to some extent with the IC buffer. Also, in Figure 8.9(c), it can be noticed that around pH 8, there is some extra experimental buffer capacity, not accounted for in the simulated buffer capacity profile.

Model 4 is an alternative extension of model 2, with an extra monoprotic buffer whose pK_a may vary between pH 7.5 and pH 8.4. Again, the fit between the experimental and the simulated data was better than in model 2, illustrated for the selected sample in Figure 8.9(d). The extra buffer in model 4 was at most 0.16 mmol l⁻¹. The estimations of *o*-PO₄ were systematically underestimated and with a higher variability (not shown in Table 8.17) in model 4 compared to model 2. Unfortunately, this extra buffering component is thus interfering with the ortho-phosphate buffer estimations at pH 6.7.

To get more insight in the origin of the two extra buffers around pH 5 and pH 8, a correlation analysis was performed between the data obtained with ICP-MS on those samples (see section 8.4.4 and Table 8.5) and the concentrations of 'blank1' and 'blank2' obtained with models 3 and 4 respectively. The Pearson correlation coefficients with their significance level are tabulated in Table 8.18. From these correlations, it can be concluded that Ca²⁺, Mg²⁺, N and P correlate best with 'blank1' at pH 5, and that Cu²⁺ and Zn²⁺ correlate best with 'blank2' at pH 8. Fe³⁺ and Al³⁺ correlate very significant with both blank buffers. This is fairly well in correspondence with the findings of the simulation study in section 8.4.4, more particularly with what is illustrated in Figure 8.7. The 'blank1' and 'blank2' buffers exactly correspond with the 2 regions in the buffer capacity profile influenced by complex formation reactions with Ca²⁺ and Fe³⁺. In the simulation study, it was found that the buffer capacity in 'blank1' was originating from iron and phosphate. In this correlation study, iron and phosphate are both correlating very significant with 'blank1'. Further, the simulation study also revealed that the

Table 8.18: Pearson correlation coefficients between the concentrations of the 'blank1' and 'blank2' buffers and the most important components in destructed manure

	Blank1 pH 5	Blank2 pH 8
Blank1	1.000	0.59**
Blank2	0.59**	1.000
Nitrogen	0.30*	0.08
Phosphorus	0.37**	0.16
Potassium	0.26	0.19
Calcium	0.33*	0.11
Magnesium	0.43**	0.20
Sodium	0.05	0.03
Copper	0.18	0.53**
Zinc	0.18	0.61**
Aluminum	0.75**	0.78**
Iron	0.40**	0.45**

* : Significant at $\alpha = 0.05$
** : Significant at $\alpha = 0.01$

buffer capacity around pH 8 was originating from iron hydroxides, which is also confirmed by the very significant correlation between iron and 'blank2'. In a following step, it was investigated if the incorporation of this knowledge in the mathematical model would result in better estimations of ortho-phosphate and ammonium. This is discussed in the next paragraph.

Due to the clear interpretation of the 2 extra buffers around pH 5 and pH 8, it was decided to validate a number of extra models incorporating this supplementary knowledge. The experimental results with model 3 and model 4 suggested already that the incorporation of just an extra blank buffer around pH 5 or pH 8 does not ameliorate the final results. Also the simultaneous incorporation of the same 2 extra buffers (results not shown) did not have the desired effect. The knowledge of the exact concentration of Fe^{3+} for each individual sample would be helpful, because both buffers were earlier suggested to depend on the concentration of iron. However, in field situations, this concentration is unknown. Therefore, a first attempt was made to include 2 extra monoprotic buffers at pH 5.3 and pH 8.0, with a fixed concentration 0.08 mmol l^{-1} . This concentration represents the 'mean interference', obtained from the simulation results with models 3 and 4. The obtained fit was good, however, the estimated ortho-phosphate concentrations were not better than the results with model 2. It can also be remarked that the real Fe^{3+} concentration in animal manure is quite variable (see Table 8.5), thus being a disadvantage for this approach. In a second attempt, the knowledge that the concentrations of the 2 extra buffers are coupled (high correlation between 'Blank1' and 'Blank2', see Table 8.18) and the finding that those buffers have variable concentrations among samples,

were implemented in a new model. The model contained again the 2 extra buffers at pH 5.3 and pH 8.0, but with concentrations that were allowed to vary, however, with the restriction that both concentrations must be equal within 1 sample. The minimum boundary for the simulation interval was also slightly modified from pH 5.6 to pH 5.3. The fit of this model was excellent, but the estimated ortho-phosphate concentrations were again systematically underestimated. From all the studied models considering the extra buffers around pH 5 and/or pH 8, this model was found to perform the best when comparing the estimated concentrations with the laboratory concentrations.

Besides the buffer capacity models described above, some more mathematical models were evaluated. The other models that were studied contained the same buffer systems as described in models 1 to 4. However, they contained different boundary values on the pK_a values and concentrations (e.g. C_{IC}) that were allowed to vary. It was also investigated if the pK_a 's of sulphate, IC and ortho-phosphate are best kept fixed or allowed to vary. Finally, model 2 was found to be the most adequate model for further validations and possible field-use. A scatterplot of the laboratory analyses against the titrimetric estimations with model 2 for respectively ammonium and ortho-phosphate are presented in Figure 8.10(a) and (b). Further, a relative error (%) was calculated to express the difference between the titrimetric and the laboratory concentrations.

$$\text{relative error (\%)} = \frac{C_{\text{titrimetric}} - C_{\text{laboratory}}}{C_{\text{laboratory}}} \times 100 \quad (8.2)$$

The corresponding graphs with the relative errors for ammonium and ortho-phosphate are presented in Figure 8.10(c) and (d).

Figure 8.10(a) and (b) illustrates that the linearity between the 2 measurement techniques is very good. However, the ammonium concentrations estimated from the buffer capacity profile were in most cases overestimated compared to the corresponding laboratory measurements. For ortho-phosphate, only one, very low loaded sample (3.5 mg P l^{-1} , measured in the laboratory) was overestimated with more than 25 %. All other samples were within relative differences between -2% and $+18\%$ for ammonium and between -15% and $+30\%$ for ortho-phosphate, as illustrated in Figure 8.10. Based on these results, a new experiment was set up, to validate the 'most adequate model' with completely new manure samples. This validation experiment is described in the following section.

8.5 Laboratory validation and statistical data analysis

8.5.1 Validation experiment

A second measurement campaign was organized to validate the results and the most adequate model described in section 8.4.7. Fifty-three samples were collected in April 1999, at farms randomly selected in the Netherlands and Flanders. More particularly, several manure transportation companies have cooperated to collect samples at the most diverse places. Each sample was homogenized, and two subsamples (duplo A and B) were taken. Each subsample was destructured and analyzed in the laboratory for N and P. All destructured samples were 6.6 times diluted and titrated in threefold, with the same procedures as described in section 8.4.7. In

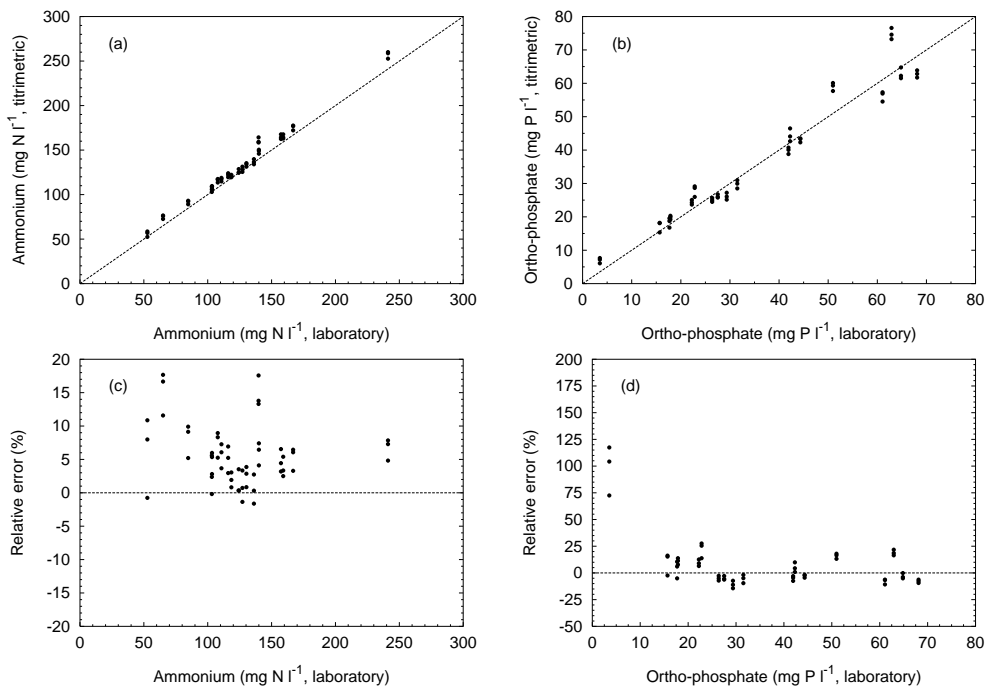


Figure 8.10: Laboratory and titrimetric analyses of ammonium (a) and ortho-phosphate (b) with the corresponding relative error of the titrimetric analyses of ammonium (c) and ortho-phosphate (d) for 19 different manure samples and using the most adequate buffer capacity model. The concentrations are expressed as $mg\ l^{-1}$ destructed and undiluted sample

total, 318 titration curves (53 samples, 2 subsamples and 3 replicates) were recorded, in a period of 14 days. The sequence of those 318 titrations was split in 12 blocks, of which 1 block contained 27 different manure samples of 1 subsample (duplo A or B) and 1 replicate. Each block corresponded with one measurement day. With such experimental design, eventual uncontrollable effects (e.g. of temperature, electrode, titrant, ...) could be determined with an analysis of variance, including a block effect. The temperature in the laboratory was around 22 °C, and fairly well constant due to the isolated location of the laboratory. No extra measures were taken to keep the temperature as constant as possible, and the minimum and maximum temperature recorded in the lab during the complete experiment was respectively 20 and 24 °C.

During this experiment, the stock solutions of NaOH 0.1 N and 1.5 N had to be prepared several times (6 times 1 litre for the stock of NaOH 0.1 N and at least 10 times 1 litre for the stock of NaOH 1.5 N). These stocks were prepared with pro analyse NaOH pellets, and the exact titre was determined with oxalic acid dihydrate ((COOH)₂ · 2H₂O) titrations. The pro analyse pellets were taken from two different pots (an almost empty one and a new one) that were in use in the lab at that moment. The stock solutions were stored in dark brown glass bottles, equipped with a bowed CO₂ absorption tube. Contrary to the first measurement campaign (see section 8.4.7), the majority of destructed samples were brought to pH 3 with the automatic titrator. Only a few samples were manually brought to pH 3, for which an older NaOH 1.5 N stock that was standing in the lab, was used. The above rather detailed description of stock solution origin, storage, etc. is necessary to introduce a prior unnoticed problem of interferences in the buffer capacity profiles. It was found that for almost 50 % of the samples, the reproducibility of the 3 replicates (recorded at different days, with different stock solutions) was worse than in previous experiments. The problems were related to the stock solutions, and are described and investigated in section 8.5.2. For this reason, a number of titration curves were eliminated for further data analysis. A total of 253 titration curves were considered as acceptable and were further processed with the software *bomb*.

A number of mathematical models were fitted to the experimental buffer capacity curves of this data set, and comparisons between laboratory and titrimetric measurements were made. The same methodology as applied in section 8.4.7 was used here, i.e. first trying with a simple, basic model, then extending the model with extra buffers, while at the same time also evaluating the pK_a values, i.e. whether they are best kept fixed or allowed to vary, etc. It was concluded that the most adequate model found in section 8.4.7 also applied as such for the new data set. This points to the robustness of this model in different situations. A scatterplot of the laboratory analyses against the titrimetric estimations with the most adequate model for respectively ammonium and ortho-phosphate are presented in Figure 8.11(a) and (b). The corresponding graphs with the relative errors for ammonium and ortho-phosphate are presented in Figure 8.11(c) and (d).

The titrimetric ammonium estimations are all lying between -7 % and +8 % relative error compared to the laboratory measurements. This result is even better than what was found in the first measurement campaign, used for the model development. The results of the titrimetric ortho-phosphate estimation are similar as in the previous experiment. For the samples with a laboratory ortho-phosphate concentration higher than 10 mg Pl⁻¹, a relative error between -15 % and +45 % was found. However, the relative errors of the samples with a low laboratory ortho-phosphate concentration are unexpectedly high. More particularly, the titrimetric concentrations are systematically higher than the laboratory concentrations. The origin

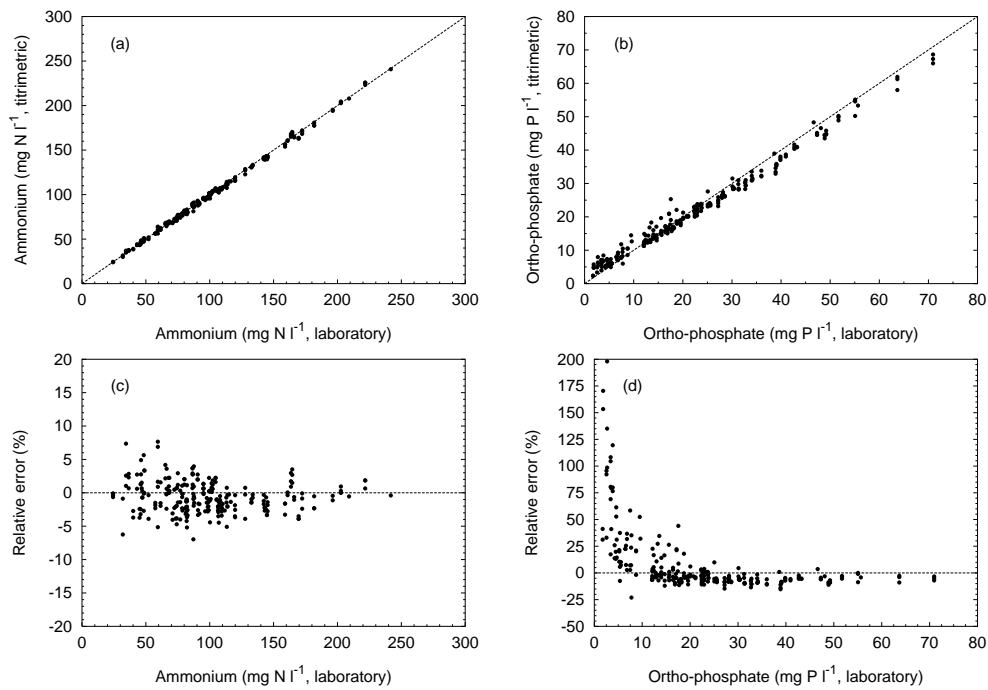


Figure 8.11: Laboratory and titrimetric analyses of ammonium (a) and ortho-phosphate (b) with the corresponding relative error of the titrimetric analyses of ammonium (c) and ortho-phosphate (d) using the buffer capacity model developed in section 8.4.7 (53 different manure samples). The concentrations are expressed as $mg\ l^{-1}$ destructed and undiluted sample

of these rather bad results was pointed out to be interferences originating from the NaOH stock solutions. These are described and further investigated in section 8.5.2.

From the samples with a laboratory ortho-phosphate concentration lower than 10 mg P l^{-1} (12 samples from the 53), duplo A and B were titrated again. New NaOH stock solutions 0.1 and 1.5 *N* with pellets from an almost new pot NaOH ‘pro analyse’, were prepared at the same day of the titrations. The other experimental conditions were the same as before. The same mathematical model was used, with one small modification. In the original model, the minimum and maximum boundaries for the amount of inorganic carbon were respectively set to 0.75 and $2.2 \text{ mg CO}_2 \text{ l}^{-1}$. For the newly recorded titration curves, the amount of inorganic carbon was found to be more constant than before, around $1.6 \text{ mg CO}_2 \text{ l}^{-1}$. Therefore, the range for the concentration of CO_2 in the model, was set between 1.3 and $1.8 \text{ mg CO}_2 \text{ l}^{-1}$. A similar scatterplot with the laboratory analyses against the titrimetric estimations for respectively ammonium and ortho-phosphate are presented in Figure 8.12(a) and (b). The corresponding graphs with the relative errors for ammonium and ortho-phosphate are presented in Figure 8.12(c) and (d).

On the one hand, the differences between the titrimetric and laboratory ammonium concentrations are in a similar range as noticed in the first data set of the validation experiment (compare Figure 8.12(a) and (c) with respectively Figure 8.11(a) and (c)). However, there is a tendency that in the samples containing less phosphorus, the estimations of ammonium are systematically around 5 % lower than the corresponding laboratory values. On the other hand, a very significant increase in accuracy was reached for the titrimetric ortho-phosphate estimation (compare Figure 8.12(b) and (d) with respectively Figure 8.11(b) and (d) in the range between 0 and 10 mg P l^{-1}). The relative errors on P of the 12 repeated low-loaded samples are now in the same order as the relative errors of the high-loaded samples.

A first conclusion that can be drawn from this validation experiment is that the estimated concentrations for N and P with the titrimetric method are in a practical useful and acceptable range compared to the official laboratory methods. However, a more detailed statistical analysis of the variability and measurement errors is necessary to formulate a more statistically supported conclusion. This statistical analysis is described in section 8.5.3. A second conclusion resulting from this validation experiment is that important interferences are originating from the NaOH stock solutions. Especially in the low loaded samples, the ‘quality’ of the stock solutions is of major importance for the accuracy of the P estimations. The interferences originating from the NaOH are presented and discussed in section 8.5.2.

8.5.2 Influences of alkaline stock solutions

During the validation experiment described in section 8.5.1, it was found that the reproducibility of the buffer capacity profiles of several destructed and diluted manure samples, titrated with different NaOH stock solutions, was poor. When putting all the measurement results together, it was quickly recognized that the poor reproducibility was originating from the NaOH stock solutions, and not from temperature effects, calibration errors, etc. A detailed description on how the alkaline stock solutions were prepared and stored was already given in section 8.5.1.

A series of new experiments were set up, to investigate and define the origin of the poor reproducibility. A pool of 6 different destructed manure samples was made, to be able to

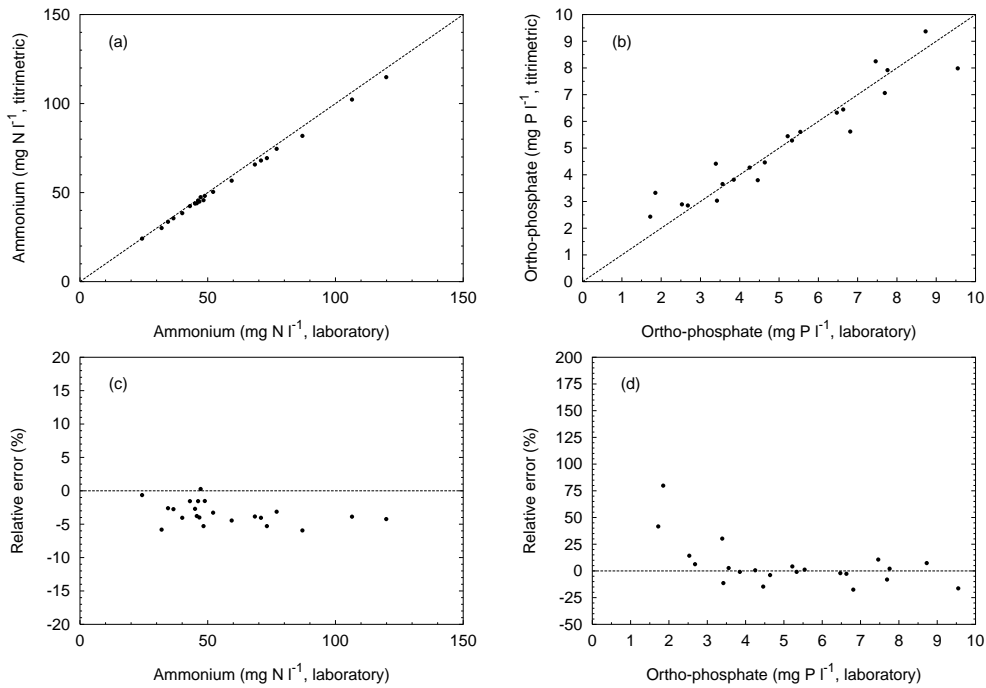


Figure 8.12: Laboratory and titrimetric analyses of ammonium (a) and ortho-phosphate (b) with the corresponding relative error of the titrimetric analyses of ammonium (c) and ortho-phosphate (d) using the buffer capacity model developed in section 8.4.7 (12 repeated manure samples). The concentrations are expressed as $mg\ l^{-1}$ destructed and undiluted sample

titrate the same sample under varying conditions. The sample preparations and titrations were performed as described in section 8.4.7. In short, a destructed and diluted manure sample was first set to pH 3 with around 40 ml of a 1.5 N NaOH stock solution. Next, the sample was stirred for 20 minutes to remove CO₂ originating from the alkaline stock solution. Last, the sample was titrated to pH 11 with around 10 ml of a 0.1 N NaOH stock solution.

The following 4 stock solutions of NaOH were used in a first series of experiments:

Stock 1.5(a) : Stock solution of 1.5 N, prepared in the laboratory at the day of the measurements, with pellets from a new pot 'NaOH pro analyse'. The solution was kept in a dark brown glass bottle, equipped with a CO₂ scrubber (bowed glass tube with soda lime pellets).

Stock 1.5(b) : Two months old stock solution of 1.5 N, kept in a closed dark brown glass bottle, but without a CO₂ scrubber. This solution was earlier used for manual pH adjustments of destructed manure samples. When not in use, the bottle was kept closed. It is noteworthy that during this period of 2 months, a brown precipitate was formed at the bottom of the bottle.

Stock 0.1(a) : Stock solution of 0.1 N, prepared in the laboratory at the day of the measurements, with pellets from a new pot 'NaOH pro analyse'. The solution was kept in a dark brown glass bottle, equipped with a CO₂ scrubber.

Stock 0.1(b) : Nine days old stock solution of 0.1 N, prepared with pellets from an older, almost empty pot 'NaOH pro analyse'. The solution was kept in a dark brown glass bottle, equipped with a CO₂ scrubber.

In the following paragraphs, first, problems related to the 1.5 N stock solution will be presented. Second, the interferences originating from the 0.1 N stock solutions will be illustrated. Third, an extra validation experiment with a new pool of destructed samples, and a possible alternative stock solution will be discussed. And last, a number of conclusions and precautions will be formulated.

Interferences from the 1.5 N NaOH stock solution

A comparison was made between the stock solutions 1.5(a) and 1.5(b). Three samples from the pool were prepared and titrated identically, except that for one sample, the old stock solution 1.5(b) was used, and for the other two samples, the new stock solution 1.5(a) was used. The sample pretreatment included the CO₂ scrubbing prior to titration, except for one of the two latter samples, which was not made CO₂ free. The titration itself was performed with the new stock solution 0.1(a). The three corresponding buffer capacity curves are shown in Figure 8.13.

Very important differences between the buffer capacity profiles can be noticed in Figure 8.13. The buffer capacity profile of the sample prepared with the old stock solution 1.5(b) is much higher than the corresponding curve with the new stock solution. It is concluded that the extra buffer capacity is originating from the old stock solution 1.5(b). This extra buffer capacity was modelled, and buffer concentrations of 0.16 mmol l⁻¹ around pH 4.8, 0.11 mmol l⁻¹ around pH 8.4 and 1.1 mmol l⁻¹ around pH 10 were found. The latter buffer concentration is so important that under these conditions, a reliable estimation of the NH₄⁺ buffer is impossible.

It was investigated in more detail where these extra buffer capacities could originate from.

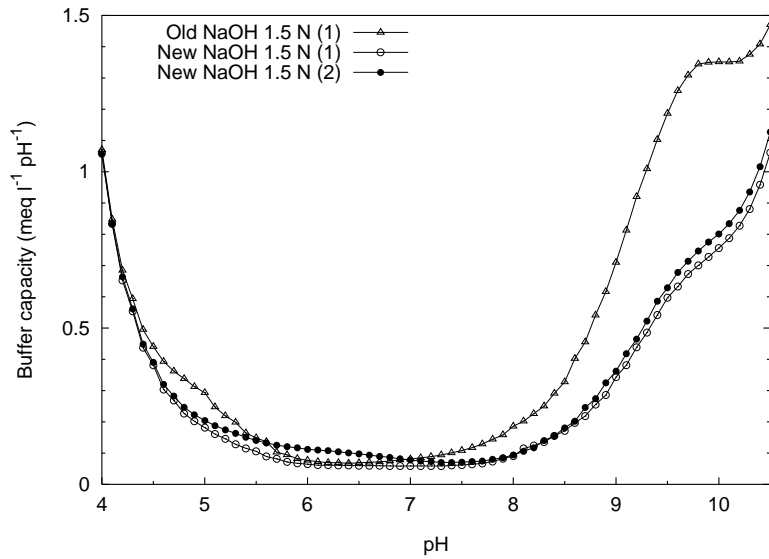


Figure 8.13: Experimental buffer capacity curves of 1 sample, prepared with an old and new NaOH 1.5 N stock solution, with (1) and without (2) CO₂ scrubbing prior to titration

The small amount of brown precipitate at the bottom of the stock solution was a first indicator that the glass of the bottle could be the source of extra buffer capacity. The dissolution rate of quartz (SiO₂) is reported to be $10^{-9} \text{ mol m}^{-2} \text{ h}^{-1}$ at pH 6, and $10^{-7} \text{ mol m}^{-2} \text{ h}^{-1}$ at pH 11 [273]. At high pH, where Si – OH surface sites are deprotonated and therefore carry negative charge, detachment of silicon appears to control overall silicate dissolution rates [43]. There is a direct proportionality between the dissolution rate of quartz and the concentration of negatively charged surface sites at high pH. However, above pH 12, the quartz dissolution rate decreases, reflecting the saturation of all Si – O⁻ sites [43]. The 1.5 N stock solution has a theoretical pH of more than 14, but no exact values for the dissolution rate of quartz were found for this pH. If SiO₂ from the glass is entering in the stock solution, it influences the buffer capacity through the two following silicate weak acid/base proton exchange reactions [198]:



It is a fair assumption that the first dissociation step of silicic acid (equation (8.3)) is responsible for the high buffer capacity observed around pH 10. Taking into account the volume of the titration vessel, and the amount of stock solution 1.5(b) needed for one titration, it is calculated that the stock solution 1.5(b) would contain around 3 mmol Si l^{-1} . Taking into account the dimensions of the bottle (0.04 m^2 liquid-glass contact surface and 0.8 l titrant) and the standing period (60 days), it is calculated, under the hypothesis that only Si⁴⁺ is responsible for the extra buffer capacity around pH 10, that the dissolution rate of SiO₂ would be $4 \cdot 10^{-5} \text{ mol m}^{-2} \text{ h}^{-1}$.

This value is a factor 100 higher than the value at pH 11, reported above. The two other smaller extra buffers, around pH 4.8 and pH 8.4, could eventually originate from iron, aluminum or other components used in the production of the glass, and also set free during the dissolution of SiO_2 . Iron complexes with phosphate and hydroxide (see also Figure 8.7) are introducing extra buffer capacities at those pH values. However, more experimental analyses are needed to confirm the latter hypothesis. With simulation experiments using *bctab*, it was investigated whether complex formations with SiO_3^{2-} and e.g. Ca^{2+} or Fe^{3+} should be considered. It was found that Si-complexes do not have a significant effect on the buffer capacity between pH 4 and pH 11.

Further, another important difference was noticed between the buffer capacity curves of the two samples prepared with the new stock solution 1.5(a), but with and without CO_2 scrubbing prior to titration (see Figure 8.13). The extra buffer capacity was modelled, and found to originate solely from the inorganic carbon (IC) buffer, representing $4 \text{ mg CO}_2 \text{ l}^{-1}$. Despite the fact that the stock solution 1.5(a) was freshly prepared in the laboratory, with a new pot of NaOH pellets, an important interfering amount of IC was entering in the sample to be titrated. Such amount of IC in the titration vessel makes the estimation of phosphorus unreliable, especially in destructed manure samples with phosphate concentrations lower than 10 mg P l^{-1} . This inorganic carbon cannot originate from the destructed sample itself (very low pH), neither can it enter during sample preparation because the pH is lower than 3. Thus, it is concluded that this IC is originating from the stock solution 1.5(a). Taking into account the volume of the titration vessel, and the amount of stock solution 1.5(a) needed for one titration, it can be calculated that the stock solution 1.5(a) contains at least $15 \text{ mg CO}_2 \text{ l}^{-1}$. The latter experiment illustrates that CO_2 scrubbing of the sample after addition of 1.5 N NaOH , and prior to titration, is necessary to obtain reliable results.

In another similar experiment, part of the 1.5(a) stock solution was strongly agitated for 30 minutes with a magnetic stirrer in an open beaker. The aim was to absorb as much CO_2 as possible from the air into the stock solution. As usual, the sample at pH 3 was stirred for 20 minutes prior to titration. There was no change in the buffer capacity profile of destructed manure samples that were set to pH 3 with this IC-rich 1.5 N stock solution compared to samples that were set to pH 3 with the 'untreated' $1.5(a)$ stock solution. This illustrates that 20 minutes CO_2 scrubbing of the sample at pH 3, prior to titration, is sufficient to remove the IC originating from the 1.5 N NaOH stock solution.

Interferences from the 0.1 N NaOH stock solution

Six samples were prepared from the pool and titrated identically. The samples were set to pH 3 with the new stock solution 1.5(a). Three samples were titrated with the new stock 0.1(a) and three samples were titrated with the old stock 0.1(b). The resulting buffer capacity curves are presented in Figure 8.14. The reproducibility of the buffer capacity curves, illustrated by plotting 3 replicates of each treatment on the graph, is very good. The buffer capacity curves were modelled and the increased buffer capacities with the stock solution 0.1(b) versus the stock solution 0.1(a) are given in Table 8.19. The differences in buffer capacity between the stock solutions 0.1(b) and 0.1(a) are found to be very significant. Increases in buffer capacities were noticed at the same pH values as found before in stock solution 1.5(b). It was realized that the modelling of IC entering the titration vessel via the titrant is a simplification of the reality,

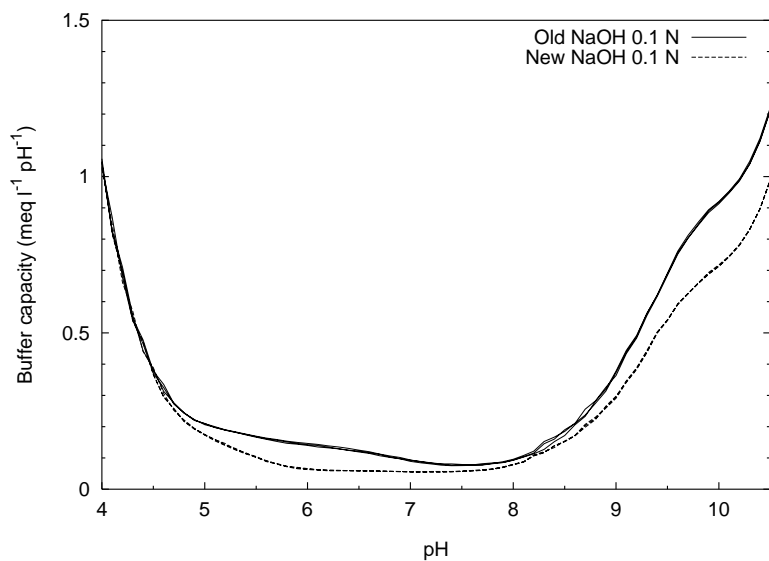


Figure 8.14: Experimental buffer capacity curves of 1 sample, titrated with an old and a new NaOH 0.1 N stock solution (a). Three replicates with each stock solution are plotted on top of each other

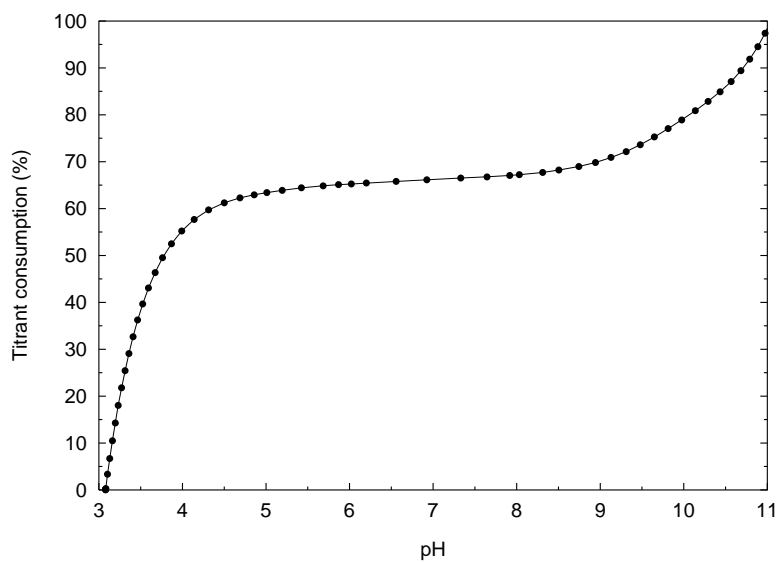


Figure 8.15: Typical titrant consumption profile in function of the pH for a titration with NaOH from pH 3 to pH 11

Table 8.19: Means, standard deviations and statistical significance of the differences in buffer capacity in a destructed and diluted sample, titrated with the old 0.1(b) and the new 0.1(a) NaOH stock solution

Buffer component	Difference 0.1(b)–0.1(a)		
	Mean ($mmol\ l^{-1}$)	Std. dev. ($mmol\ l^{-1}$)	Significance (p -value)
IC	0.13	0.003	<0.001
pH 4.8	0.019	0.002	<0.001
pH 8.3	0.017	0.004	0.008
pH 10.3	0.28	0.003	<0.001

i.e. the amount of IC buffer capacity entering the titration vessel increases along the titration, while in the mathematical model, the IC is considered constant during the complete titration. An example of the titrant consumption and the related interfering amount of IC entering in the titration vessel in function of the pH is illustrated in Figure 8.15. Around 60 % of the titrant is dispensed in the pH range $pH < 6$, and it is considered that only in the mentioned pH range, the CO_2 can be stripped from the solution during titration. Thus, it may be assumed that the real amount of IC present around pH 10.3 is maximally 40 % more than the modelled amount of IC under the above mentioned simulation conditions. Consequently, using the values given in Table 8.19, around $0.05\ mmol\ l^{-1}$ of the $0.28\ mmol\ l^{-1}$ extra buffer concentration found around pH 10.3 can possibly be explained by IC. If similar calculations as before are performed, it is found that if the non IC buffer capacity around pH 10.3 ($0.23\ mmol\ l^{-1}$) is originating from silicates in the stock solution 0.1(b), the concentration in the stock solution would be at least $4.2\ mmol\ Si\ l^{-1}$. This is a similar value as found in the experiment with the 1.5 N stock solution. This is rather surprising, because the normality is lower (0.1 N instead of 1.5 N) and the standing time in the laboratory is also lower (9 days instead of 60 days). An explanation could be that the dissolution rate of SiO_2 at pH 13 (0.1 N NaOH) is possibly higher than at pH 14.2 (1.5 N NaOH) [43]. However, it should also be mentioned that both stock solutions were kept in different types of brown glass bottles, thus making comparisons difficult. Further, the bottle of stock 0.1(b) was already a long time in use with NaOH 0.1 N, without cleaning the bottle prior to filling with fresh NaOH solution when the bottle was almost empty. This may eventually have lead to a concentrating effect of silicates.

A particular problem related to the 0.1 N stock solutions is the interference of inorganic carbon. As described before, IC present in the 1.5 N stock solutions does not really introduce interferences in the buffer capacity profile, due to the CO_2 scrubbing prior to titration. However, the situation is different for the 0.1 N stock solution. All IC present in the 0.1 N stock solution enters the titration vessel during the titration, and causes a direct interference. More particularly, as illustrated in section 8.5.1, the accuracy of the phosphate estimation is negatively influenced by the presence of a bicarbonate buffer system. The amount of IC present in the buffer capacity profile of the samples titrated with the freshly prepared stock solution

0.1(a) was modelled to be around $1.5 - 2 \text{ mg CO}_2 \text{ l}^{-1}$. In a following experiment, it is verified if this modelled IC buffer capacity is indeed originating from CO_2 .

Six new titration curves were recorded with the 0.1(a) stock solution. As in the previous experiment, all samples were prepared with the 1.5(a) stock solution, and stirred for 20 minutes prior to titration. Three different treatments, each with 2 replicates, were compared with each other. First, a titration was performed as usual, with a closed titration vessel. Second, a titration curve was obtained with the titration vessel open to the air (a circular opening with a diameter of 1 cm). Third, a titration profile was recorded while N_2 was continuously bubbled through the sample. There was no significant difference between the mean concentrations of IC obtained with the first two treatments. This indicates that it is not strictly necessary to keep the titration vessel airtight. The amount of IC with treatment 1 and 2 was estimated to be $1.8 \text{ mg CO}_2 \text{ l}^{-1}$. A very significant difference ($p = 0.01$) in IC was found between treatment 3 and the first two treatments. The estimated amount of IC in treatment 3 was $1.0 \text{ mg CO}_2 \text{ l}^{-1}$. Thus, $0.8 \text{ mg CO}_2 \text{ l}^{-1}$ from the $1.8 \text{ mg CO}_2 \text{ l}^{-1}$ is removed by the N_2 bubbling, and is considered as IC. It is uncertain if the remaining amount of buffer capacity ($1 \text{ mg CO}_2 \text{ l}^{-1}$) is originating from IC, or resulting from other buffer systems in the same pH range of IC.

The discussed interferences (IC and non-IC) are directly related to the accuracy and precision of the ammonium and ortho-phosphate estimations from the buffer capacity profile. Therefore, they should be kept as low as possible. To get more insight in these interferences and to find possible solutions or alternatives, further experiments are presented in the next paragraph.

Validation and alternatives

A new experiment was designed to confirm and extend the findings of the experiments previously described in this section. More particularly, the objectives of this experiment are to:

- Validate whether silicate dissolution from the glass bottle containing the 0.1 N NaOH titrant is responsible for the interfering buffer capacity found around pH 10.
- Determine whether the IC found in the buffer capacity profiles (estimated $0.8 \text{ mg CO}_2 \text{ l}^{-1}$ in the previous experiment) is originating from the NaOH 0.1 N stock solution, or rather originating from the CO_2 in the headspace of the titration vessel.
- Evaluate the performance of commercially prepared NaOH solutions, stored in completely closed, headspace free plastic bags (Titripack[®], Merck).

A new pool of destructed manure samples was made, to be able to titrate the same sample under varying conditions. Sample preparations and titrations were performed as before. To bring the sample to pH 3, NaOH 1 N (Titripack[®]) was used. Three different stock solutions NaOH 0.1 N were used for the titrations from pH 3 to pH 11:

Stock 0.1(c) : One litre of NaOH solution was prepared with NaOH pellets from an almost empty pot 'NaOH pro analyse' (the same pot as used in the previous experiment for solution 0.1(b)). Half of this freshly prepared solution was kept in a completely closed glass bottle for 9 days at room temperature. After this 'incubation period', the bottle was connected as usual to the titrator (with CO_2 scrubber) and used for the titrations.

Stock 0.1(d) : The other half litre of the freshly prepared NaOH was kept in a completely closed plastic bottle for 9 days prior to titration.

Stock 0.1(e) : A commercial NaOH 0.1 *N* 10 litre stock solution (Titripack[®], Merck).

With each of these stock solutions, three different treatments, each in threefold, were applied for titrations of destructed and diluted manure samples from the pool:

- titration as usual, in a closed titration vessel,
- titration while bubbling N₂ through the liquid, and
- titration while flowing N₂ through the headspace of the vessel.

The exact titres of the stock solutions were determined with oxalic acid titrations. Despite the fact that solution 0.1(c) and 0.1(d) should theoretically have the same titre, the normality of solution 0.1(c) after nine days incubation in the glass bottle was 0.7 % lower than the normality of the same solution kept in the plastic bottle. This difference is small, but was found to be statistically significant ($p < 0.001$). Further, the buffer capacity curves obtained with the 3 different titrant solutions were compared to confirm the hypothesis that silicates or other substances enter the stock solution kept in the glass bottle. Rather surprisingly, the extra buffer capacity expected around pH 10 or elsewhere was not found in the titration curves obtained with solution 0.1(c). When using the most adequate mathematical model (see section 8.4.7) on the titration curves obtained with N₂ bubbling in the liquid, no significant differences were found in the estimated N and P concentrations resulting from titrations with the 3 different NaOH stock solutions (on the $\alpha = 0.01$ level). This means that the earlier formulated hypothesis of the silicate interference is not valid here. A possible explanation could be that in the previous experiment, stock solution 0.1(b) was the result of a longer than 9 days 'aging period' due to the bottle refilling method used in many previous experiments. When the glass bottle of the titrant solution 0.1 *N* was almost empty (e.g. 10 % of the volume left), the bottle was refilled (without emptying and cleaning) with freshly prepared NaOH solution. Thus, stock solution 0.1(b) was kept in a glass bottle that was continuously exposed to NaOH for at least 3 weeks. It was also noticed in the past that titration curves obtained with titrant of an almost empty titrant bottle are often 'noisy' and not very reproducible. This points to possible concentrating interferences at the bottom of bottle. Extra results, from longer 'incubation' times, are presented further in this section.

To evaluate the origin of IC in the buffer capacity profiles, the effect of the 3 different treatments on the IC was investigated with an analysis of variance (GLM). First, the buffer capacity curves of the samples with N₂ bubbling in the liquid were modelled with the most adequate mathematical model (see section 8.4.7). As mentioned above, no significant differences were found in N and P estimations obtained with the 3 different NaOH titrant solutions. Second, the estimated concentrations of N and P were kept fixed in a new model, that was fitted to the 27 buffer capacity curves (3 titrant solutions, 3 treatments, 3 replicates), with the purpose of a more correct estimation of the IC. The mean IC concentrations found with this model are tabulated in Table 8.20. The residual standard deviation on the IC concentrations, obtained from the GLM analysis, was 0.15 mg CO₂ l⁻¹. From pairwise comparisons in the GLM analysis, it was concluded that there is no significant difference in IC between titrant 0.1(c) and 0.1(d). The IC found with titrant 0.1(e) was found to be significantly different from the 2 other NaOH solutions. There was no significant interaction between the effect of the titrant solution and the effect of the treatments. Further, among the 3 treatments, all were found to be significantly

Table 8.20: Mean concentrations of IC ($mg\ CO_2\ l^{-1}$) obtained in the validation experiment with 3 titrant solutions and 3 treatments. The estimated standard deviation is $0.15\ mg\ CO_2\ l^{-1}$

	normal titration	N ₂ bubbling in the liquid	N ₂ flowing in the headspace
Titrant 0.1(c)	1.33	0.26	0.94
Titrant 0.1(d)	1.33	0.45	0.94
Titrant 0.1(e)	0.85	0.11	0.71

different from each other. Their effects are interpreted in more detail in the next paragraphs.

For the titration curves obtained without N₂ bubbling or flowing, the IC found with the titrant solutions 0.1(c) and 0.1(d) are similar as in previous experiments, $1.33\ mg\ CO_2\ l^{-1}$ in this case. As described earlier in this section, this amount of CO₂ is an interfering substance for the ortho-phosphate determination from the buffer capacity profile, and should be kept as low as possible. The IC found with solution 0.1(e) is significantly lower than the IC found with the two other solutions. Further, scrubbing of CO₂ in the headspace of the titration vessel results in a $0.1\text{--}0.4\ mg\ CO_2\ l^{-1}$ reduction of IC in the buffer capacity profile, compared to the normal titration. This value was compared with a theoretical calculated value, based on the ideal gas law:

$$pV = nRT \quad (8.5)$$

p : gas partial pressure (*atm*)

V : volume (*l*)

n : moles of gas (*mol*)

R : gas constant ($0.082\ l\ atm\ K^{-1}\ mol^{-1}$)

T : absolute temperature in *K* ($273.15\ K +$ temperature in *°C*)

With $p_{CO_2} = 3 \cdot 10^{-4}\ atm$ and $0.1\ l$ headspace volume, the amount of CO₂ in the headspace at room temperature is $1.2 \cdot 10^{-6}\ M$, or $0.05\ mg\ CO_2$. If this quantity of CO₂ enters the titration vessel during titration, its concentration in the vessel is $0.3\ mg\ CO_2\ l^{-1}$. This corresponds with the experimental values that were found, and it can be concluded that the headspace CO₂ can be completely absorbed into the sample during titration of that solution. Note also that the sample is strongly stirred during titration, thus enhancing gas-liquid exchange processes.

A following point to be discussed is the quantity of IC that originates from the NaOH stock solution itself, and enters the titration vessel during titration of the sample. This amount of CO₂ can be deducted from Table 8.20 when subtracting the IC found when N₂ is injected in the headspace with the IC found when N₂ was bubbled in the solution. This amount is for the 3 titrant solutions $0.5\text{--}0.6\ mg\ CO_2\ l^{-1}$. The latter calculation is made with the assumption that the headspace flushing with N₂ does only strip the CO₂ from the headspace and does not induce extra stripping of IC from the liquid. If the latter assumption is not true, and taking into account the $0.1\text{--}0.4\ mg\ CO_2\ l^{-1}$ reduction of IC when flushing the headspace only, the amount

of IC originating from the titrant is estimated to be between 0.6 and 1 $\text{mg CO}_2 \text{l}^{-1}$.

Another finding of this experiment is that the modelled amount of IC with titrant solutions 0.1(c) and 0.1(d) is always higher than the concentration found with solution 0.1(e). Especially from the treatment with N_2 bubbling in the liquid, it can be concluded that higher amounts of buffering interferences, not stripped off by N_2 bubbling, are originating from the NaOH solutions 0.1(c) and 0.1(d) compared to solution 0.1(e).

From the results described above, it can be concluded that the NaOH solution 0.1(e), i.e. the commercial Titripack[®]NaOH solution gives more reliable and more accurate titration results compared to NaOH 0.1 *N* solutions prepared in the lab. Because the Titripack[®] plastic bags are completely closed and headspace free, it is also expected that interferences are smaller and more constant in function of time, making it easier to incorporate them in the mathematical buffer capacity models. There are two more advantages of this Titripack[®] solutions that were not mentioned before. First, these solutions have an exact titre (deviation from 0.1 *N* is maximum 0.02 %), which eliminates the necessity to determine the normality with e.g. oxalic acid titrations. Second, these solutions are degassed, and consequently, no air bubbles are formed on the moving piston of the titrator burette. Such air bubbles appear quickly when self prepared NaOH solutions are used (NaOH pellets and demineralized water). When such an air bubble releases the piston, it induces a titrant dosing error. There is, however, a major price difference between Titripack[®] solutions (€ 8.5 per litre NaOH 0.1 *N*) and self prepared NaOH 0.1 *N* solution (€ 0.05 for NaOH pro analyse pellets and € 0.5 for demineralized water per litre of NaOH 0.1 *N*). Taking into account the extra products and working hours necessary to prepare stock solutions and determine the exact titre with e.g. oxalic acid titrations, the price difference is not an obstruction any more. For example, to prepare 1 litre of NaOH 0.1 *N* and determine the exact titre with an oxalic acid end-point titration in 4 replicates, it costs 15 minutes labour (€ 6) and 2 hours occupation of an automatic laboratory titrator with sample carousel (roughly estimated at € 4).

Because it was considered important to validate the hypothesis of the silicate dissolution in the NaOH titrant, the validation experiment was extended, and a longer incubation period (20 days) was tested with solution 0.1(c). Also, the SiO_2 dissolution rate is highly temperature dependent [43], thus part of the 0.1(d) stock solution, previously not in contact with glass, was kept at 45 °C in a closed glass bottle for 4 days. Summarizing, extra titration curves were obtained with

- Stock 0.1(c), kept for 20 days in a closed brown glass bottle at room temperature.
- Stock 0.1(d), kept for 16 days in a closed plastic bottle at room temperature, and then transferred into a completely closed brown glass bottle at 45 °C for 4 days.

With these stock solutions, destructured and diluted samples from the pool were titrated once normally and in threefold while bubbling N_2 in the liquid. Buffer capacity curves obtained with titrant solutions 0.1(e) and 0.1(d) are given in Figure 8.16. The curves obtained with solution 0.1(c) are very similar to the curves obtained with solution 0.1(d) and are therefore not shown in Figure 8.16.

The results were compared with the previous titration experiments, and similar buffer capacity increases around pH 10 were found with both stock solutions 0.1(c) and 0.1(d). Thus, it was concluded that an aging period of 20 days, or an aging period of 4 days at elevated temperature, introduces significant amounts of extra buffers into the stock solution. These increases

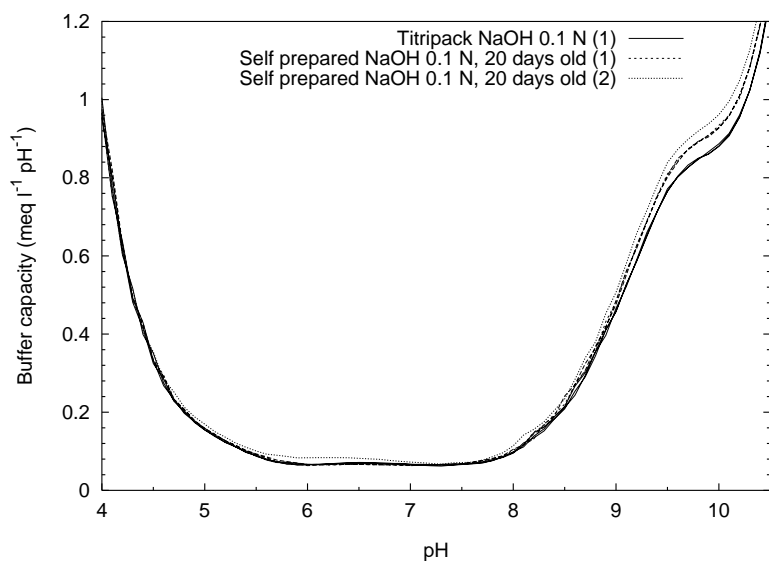


Figure 8.16: Experimental buffer capacity curves of 1 sample, titrated with a Titripack[®] and self prepared NaOH 0.1 *N* stock solution, with (1) and without (2) CO₂ scrubbing during titration. For the treatments (1), three replicates with each stock solution are plotted on top of each other

were quantified to be around $9 \cdot 10^{-5} M$. As discussed before, part of this extra buffer capacity can originate from IC entering continuously in the titration vessel, and not completely accounted for in the mathematical model. If this extra buffer capacity is originating from SiO₂ dissolution, the concentration in the stock solution would be maximally $1.9 \text{ mmol Si l}^{-1}$ or 54 mg Si l^{-1} . Taking into account the dimensions of the bottle (0.02 m^2 liquid-glass contact surface and 0.2 l titrant) and the standing period (20 days), it is calculated that the dissolution rate of SiO₂ would be $3.8 \cdot 10^{-5} \text{ mol m}^{-2} \text{ h}^{-1}$. This is again the same value as found before. Finally, laboratory analyses of the amount of silicates in both stock solutions at the end of all experiments were performed (molybdenum blue colorimetric method). These found respectively 52 and 67 mg Si l^{-1} in stock solutions 0.1(c) and 0.1(d). As an extra verification, the quantity of Si in stock solution 0.1(e) (Titripack[®]) was also determined, and found to be less than 0.5 mg Si l^{-1} . The high quantity of Si in stock solutions 0.1(c) and 0.1(d) clearly confirms the hypothesis of the silicate dissolution and its interference in the buffer capacity profiles.

Conclusions

A number of conclusions and precautions with respect to the stock solutions 1.5 and 0.1 *N* NaOH can be summarized as follows:

- Inorganic carbon present in the NaOH stock solution 1.5 *N* does not interfere with the N and P estimations from the buffer capacity profile, as long as the sample is made CO₂ free at pH 3 by stirring, prior to titration with NaOH 0.1 *N*.

- Very important interferences were found in ‘aged’ stock solutions 1.5 *N* (2 months old) and 0.1 *N* (9 days old, however in a bottle that was a couple of weeks in use with NaOH, without completely emptying and cleaning). The main interfering buffer was found around pH 10 and was quantified as 1.5–5 *mmol l*⁻¹ of an extra monoprotic buffer. It is hypothesized that this extra buffer is a silicate buffer originating from SiO₂ dissolution of the glass bottle. An extra validation experiment under similar conditions, as well as laboratory analyses of Si in ‘aged’ stock solutions clearly confirmed this hypothesis.
- Inorganic carbon buffer capacity interferes with the ortho-phosphate determination, and should be kept as low as possible. Under normal titration conditions, the amount of IC that can enter the solution via a 100 *ml* headspace is 0.3 *mg CO*₂ *l*⁻¹. The amount of IC that enters the titration vessel via the titrant solution is around 0.5–0.6 *mg CO*₂ *l*⁻¹.
- If the interfering amount of IC would be constant, its influence can easily be corrected by accounting this amount of IC in the mathematical buffer capacity model. Otherwise, the ortho-phosphate overestimation error from the buffer capacity profile could be around 0.4 *mg P l*⁻¹ diluted sample or 3 *mg P l*⁻¹ undiluted destructed sample.
- The titration vessel does not have to be completely closed to obtain reliable results. No significant differences were found between buffer capacity profiles obtained in a closed vessel, and in an open to the air vessel (opening of 1 *cm*²).
- The commercial NaOH 0.1 *N* solution (Titripack[®], Merck) was evaluated and found more reliable (less sensitive to possible contaminations), more accurate and containing less interferences than self prepared NaOH stock solutions. A price comparison was made, and it was concluded that Titripack[®] solutions are not necessarily more expensive than self prepared stock solutions.

8.5.3 Statistical data analysis

The results of the validation experiment described in section 8.5.1 were statistically evaluated, and the different sources of variability were quantified and interpreted. The investigated sources of variability are the method variability (laboratory versus titrimetric result), the duplo variability (2 subsamples from each raw manure sample are analyzed) and the residual variability (uncontrolled variability due to sample preparation, titration, data analysis, ...).

The available data for this study originates from 53 different manure samples. From each manure sample, 2 subsamples (or duplos) of approximately 5 *g* were taken. The exact weight of each subsample was recorded, because this weight factor is needed to transform the analytical results from *mg l*⁻¹ destructed sample to *mg kg*⁻¹ manure, in which the final results should be expressed. The subsample weight typically varies between 4 and 6 *g*, and the duplo variability can only be investigated when this weight factor is included in the statistical analyses. Therefore, the statistics are performed on data expressed as *mg kg*⁻¹. Each subsample was analyzed once in the laboratory for N and P with the official NEN methods. Further, each destructed subsample was diluted and titrated in threefold, thus resulting in 3 independently estimated N and P concentrations for each subsample. Later, 20 subsamples (originating from 12 samples with P < 10 *mg l*⁻¹ in destructed, undiluted sample) were repeated because of the interferences discussed in section 8.5.2. There was not enough sample left to include replicate titrations, thus each of the 20 repeated subsamples was titrated only once.

An introductory remark that should be made prior to statistical interpretations, is that the

Table 8.21: Duplo and residual variability analysis obtained with two GLM's for respectively the laboratory and the titrimetric data

Variable	Source of variation	Method	Significance (<i>p</i> -value)	Mean \bar{X} ($mg\ kg^{-1}$)	Std. dev. s_X ($mg\ kg^{-1}$)	r.s.d. (%)
N ₅₃	duplo	laboratory	0.007	4941	14	0.3
N ₅₃	duplo	titrimetric	0.01	4898	21	0.4
P ₄₁	duplo	laboratory	0.09	1361	3.7	0.3
P ₄₁	duplo	titrimetric	0.001	1318	30	2.3
P ₁₂	duplo	laboratory	0.008	246	2.4	1.0
P ₁₂	duplo	titrimetric	0.13	247	15	6.1
N ₅₃	residual	titrimetric		4898	64	1.3
P ₄₁	residual	titrimetric		1318	54	4.1
P ₁₂	residual	titrimetric		247	37	15

data set is highly unbalanced, because no replicate analyses were available for the laboratory measurements compared to the threefold titrimetric measurements. Therefore, it was chosen in a first stage to assess the duplo variability on the laboratory data, and the duplo plus residual variability on the titrimetric measurements, with two separate GLM studies. The variables that were investigated are

N₅₃ : Ammonium on all of the 53 samples

P₄₁ : Ortho-phosphate on 41 samples with $P > 10\ mg\ l^{-1}$

P₁₂ : Ortho-phosphate on 12 repeated samples with $P < 10\ mg\ l^{-1}$

The duplo effect and the sample effect were included as two random factors in the GLM. For the titrimetric data, an interaction effect $sample \times duplo$ was also included in the GLM. Summarized results are given in Table 8.21. The duplo variability, expressed as a standard deviation, can be interpreted as follows: If many subsamples originating from 1 sample are analyzed either in the laboratory or with the titrimeter, 95 % of the results are expected in the interval $\bar{X} \pm 2s_{duplo}$.² Similarly, for the residual variability of the titrimetric measurement: If one subsample is titrated many times, 95 % of the results are expected in the interval $\bar{X} \pm 2s_{resid}$. Theoretically, the duplo variability is expected to be the same with both measurement methods. This is fairly well the case, except for P₄₁ and P₁₂, where the duplo standard deviations are found to be higher in the titrimetric method. The duplo variability, expressed as r.s.d., is between 0.3 and 1 % for the laboratory measurements, which confirms that the subsampling is a reproducible process. The titrimetric reproducibility was evaluated, and it was found that the titrimetric variability is homogeneous along the range from low loaded to high loaded samples (homoscedasticity). This is also reflected when comparing the residual standard deviation of P₄₁ and P₁₂. As a logical consequence, the relative error in the low loaded P samples is higher (15 %) compared to the high loaded P samples (4.1 %). The re-

²The latter statement is somewhat simplified, because the effect of the residual variability should also be considered.

Table 8.22: Method variability analysis obtained with paired t-tests for laboratory versus titrimetric analyses results

Variable	Nbr. of pairs	Sign.	Paired differences (lab. – titrimetric) ($mg\ kg^{-1}$)		
			Mean \bar{d}	Std. dev. s_d	95 % conf. interval of \bar{d}
N ₅₃	106	<0.001	43	95	25 – 61
P ₄₁	82	0.001	43	115	18 – 68
P ₁₂	20	0.91	-0.97	37	-18 – 16

producibility of the ammonium estimation with the titrimer is very good, 1.3 %. Such low residual error indicates that further optimization of the titrimetric reproducibility is not needed for the ammonium measurement. However, the situation is different for the ortho-phosphate reproducibility. This is in correspondence with earlier experimental findings, that the buffer capacity of ortho-phosphate is much more influenced by external uncontrolled factors, in the first place the inorganic carbon. A quick calculation learns that a residual ortho-phosphate standard deviation of $37\ mg\ kg^{-1}$ manure corresponds with an ortho-phosphate concentration in the titration vessel of $0.11\ mg\ P\ l^{-1}$, or $0.004\ mmol\ l^{-1}$. A typical amount of IC entering the titration vessel via the headspace and the titrant is $1\ mg\ CO_2\ l^{-1}$, or $0.02\ mmol\ l^{-1}$. Hence, the molar amount of interfering IC is 5 times higher than the amount of phosphate representing the residual standard deviation. Thus, further optimization of the titrimetric procedure, to keep the IC as low and as constant as possible, is the strategy to be followed to decrease the variability of the titrimetric P measurement.

In a second stage, the method variability (laboratory versus titrimetric) was investigated. Therefore, in the second stage, it was chosen to aggregate the replicate titrimetric measurements and calculate their means as values for a new data set. The aggregated and thus balanced data set contains 53 samples, each with 2 subsamples (duplos), and each subsample has one laboratory and one titrimetric N and P measurement. A GLM with 1 fixed factor (method) and 2 random factors (sample and duplo) was constructed. Three main effects and three two-way interactions were included in the model and could be interpreted. Only for P₁₂, the interpretation is simple and straightforward: None of the interactions are significant, and there are no significant effects of duplo and method. In other words, the P₁₂ results of the laboratory are not statistically different from the titrimetric results. For N₅₃ and P₄₁, the interpretation is more complicated. The interactions method × sample and method × duplo are very significant, thus masking possible interpretation of the main effect 'method'. The method effect should be interpreted as significant through its interactions with the two random factors. In other words, it is concluded that this GLM study cannot be used to give a simple and clear answer to the question whether the laboratory and titrimetric results are significantly different from each other for N₅₃ and P₄₁.

In a third stage, another approach was followed to specifically interpret the method effect. Based on the results of the previous stage, a paired t-test was chosen as the best option to evaluate the method effect. The summarized results of these tests are given in Table 8.22. From

Table 8.23: Official accreditation requirements for the measurement of nitrogen and phosphorus in animal manure [1] compared with the obtained results

	Required	Obtained
Minimum measurable concentration N	150 mg kg ⁻¹	190 mg kg ⁻¹
Minimum measurable concentration P	40 mg kg ⁻¹	110 mg kg ⁻¹
Reproducibility N (0 – 2500 mg N kg ⁻¹)	150 mg kg ⁻¹	67 mg kg ⁻¹
Reproducibility N (> 2500 mg N kg ⁻¹)	6 % relative	1.4 % relative
Reproducibility P (0 – 500 mg P kg ⁻¹)	40 mg kg ⁻¹	40 mg kg ⁻¹
Reproducibility P (> 500 mg P kg ⁻¹)	8 % relative	3.6 % relative

these results, it is concluded that there is a significant difference between the laboratory and titrimetric measurements for N₅₃ and P₄₁. In both cases, the mean laboratory values are higher than the titrimetric results. For the repeated samples, P₁₂ is not significantly different for both methods. This can partially be explained because in the low loaded samples, the mean concentration for P is much lower compared to the high loaded samples, thus for the same residual variability, it is statistically more difficult to find significant differences in the lower range. The confidence intervals in Table 8.22 are best suitable to interpret the difference in results between the laboratory and the titrimetric measurement. E.g. if many samples are analyzed in the laboratory and with the titrimer, the mean difference in ammonium concentration (laboratory – titrimetric) will be with 95 % confidence between 25 and 61 mg kg⁻¹.

Finally, the obtained statistical results were compared with the requirements for an official accreditation in the Netherlands [1] for nitrogen and phosphorus measurement in animal manure. These requirements include the minimum measurable concentration (expressed as three times the residual standard deviation s_X) and the reproducibility (including the subsampling or duplo effect and the analysis effect). The obtained results are calculated from Table 8.21. The accreditation requirements and the obtained results are summarized in Table 8.23.

The obtained minimum measurable concentrations N and P, calculated from the residual standard deviations of the titrimetric measurements are still higher than the required values. Especially for P, the results are not fully acceptable yet. However, it should be taken into account that the titrimetric data used in this validation study (see section 8.5.1) were obtained without appropriate control and minimizations of the interferences discovered afterwards (silicates and IC). Therefore, taken into account the results obtained in section 8.5.2, it is expected that by taking care of the described interferences, the minimum measurable concentrations for N and P will be within the requirements for accreditation. The obtained reproducibility (including the effects of subsampling and analysis) is already within the requirements.

A recent but unofficial comparative study among 8 different Dutch laboratories for N and P measurement in one pig manure sample has been organized by a pig farmers association [2]. This small scale study showed differences between the minimum and maximum reported analysis results of 24 % and 87 % for respectively N and P. A similar comparative test in Flanders (called ‘ringtest’) [64] in which 30 laboratories were involved, found differences between the

minimum and maximum reported analysis results of 54 % and 39 % for respectively N and P. This official test was also used in an accreditation procedure to select the laboratories that are officially allowed to perform these measurements. From these two recent studies, one can conclude that nutrient measurements in manure are sensitive to many sources of error which are in some of the tested laboratories not completely under control yet.

8.6 Conclusions

The final goal of the FASTNAP project is to build a functional model of the device. This hardware model should be able to demonstrate the functionality of an automatic and on-line N and P measurement in manure samples. In the current stage of the project, the functional model will be constructed on a non-driving vehicle. However, in a further post-project stage, the aim is to have measurements conducted on a driving vehicle. Within this framework, the techniques used in the project were chosen in function of this ultimate goal. The followed methodology can be summarized in four consecutive steps. First, a representative manure sample is taken from a transporting vehicle during loading or unloading of the vehicle. This is existing technology, and available on the market. This sample is homogenized and a sub-sample is taken (5 ml out of 750 ml manure). Second, the sample is destructed with the aid of chemicals and heat (microwave oven). Third, a titration curve is recorded from pH 3 to pH 11. And last, an advanced data-processing step, based on buffer capacity modelling, is performed. The development of the latter two steps was the main topic of this chapter.

The official NEN 7433 manure destruction procedure includes the addition of $\text{CuSO}_4 \cdot 5\text{H}_2\text{O}$ as a catalyst. However, this high amount of Cu^{2+} caused an interfering precipitation reaction with $o\text{-PO}_4$ during titration, such that it was investigated if this catalyst is really necessary to obtain a complete destruction of the animal manure. It was found that this catalyst could be omitted, and therefore, all further destructions in the framework of this project were performed without the Cu catalyst.

Destructed manure samples contain in order of importance: sulphuric acid, ammonium, ortho-phosphate, calcium, potassium, iron, and a whole range of minor elements. The effect of ionic strength on the buffer capacity is important, and ionic activity corrections should be included in the mathematical models. The effect of dilution of the destructed manure sample prior to titration was investigated. Undiluted or too much diluted destructed manure samples give unreliable titration results, and a dilution factor between 3 and 6 was experimentally found to give the best results. The effect of simple chemical equilibrium reactions can easily be modelled, and it is also straightforward to include complexation reactions in a mathematical model for buffer capacity of destructed manure. Complexation reactions with Ca^{2+} and Fe^{3+} were investigated in more detail, and it was found that iron and calcium complexes could be responsible for buffer capacities around pH 5, pH 8 and pH 10. It was also found that the buffer capacities of $o\text{-PO}_4$ and NH_4^+ (the buffers of main interest) are only influenced by the complex formation reactions to a limited extent. Possible precipitation reactions during titration were also investigated with simulation studies, and a number of potential precipitates were found. However, literature research learned that precipitation reactions are sluggish, slow, non-stoichiometric, incomplete, ... Simulation studies with precipitation reactions included learned that their effect is negligible for ammonium and ortho-phosphate estimation. It was

chosen for the further model developments to exclude precipitation reactions from the models.

A first measurement campaign was organized for the development of an adequate buffer capacity model. Titrimetric N and P estimations were compared with laboratory results using standard NEN methods. Four selected mathematical models were compared with each other, and it was found that the best N and P estimations are obtained with a rather simple model, only including buffer capacities originating from H_2O , H_2SO_4 , IC, $o\text{-PO}_4$ and NH_4^+ . With this model, a lack of fit was observed due to extra experimental buffer capacity found around pH 5.5 and pH 8. Referring to the simulation study, these extra buffer capacities could be attributed to the complex formation reactions. With another model, that took those 2 extra buffers into account, the estimations of $o\text{-PO}_4$ were, however, slightly worse compared to the most adequate model. A correlation study between the concentrations of these extra two buffers and the concentrations of the most important components in destructed manure confirmed the hypothesis of the complexation reactions at these two pH ranges.

A second measurement campaign (53 samples, 2 subsamples, 3 replicates) was organized to validate the most adequate buffer capacity model. Also for the new data set the developed model was optimal. This points to the robustness of this model in different situations. The ammonium concentrations found with the titrimetric analyses are all between -7 and $+8$ % relative error compared to the laboratory measurements. The relative errors for the titrimetric ortho-phosphate concentrations are between -25 and $+200$ % compared to the laboratory measurements. The highest deviations were noticed for the 20 % lowest loaded P samples (or $\text{P} < 10 \text{ mg l}^{-1}$). A number of interferences originating from the NaOH stock solutions were found to be the reason of the high relative errors particularly for P. The low loaded P samples were titrated again, using freshly prepared NaOH stock solutions, and the relative errors became in an acceptable range between -15 and $+25$ % compared to the laboratory results.

The influences of the alkaline stock solutions were investigated in more detail with separate experiments to characterize and quantify the interfering buffers in the NaOH stock solutions. There are two different interfering substances that should be kept as low and constant as possible. The first one is IC, found to originate from the stock solution 0.1 N and the headspace of the titration vessel. Its quantity is typically around $1 \text{ mg CO}_2 \text{ l}^{-1}$, and causes an important interference for the ortho-phosphate determination in case it is not known or not constant. The second interfering substance is found to originate from SiO_2 dissolution from the glass bottle where the alkaline stock solution was kept. Its quantity is around 1.5 mmol l^{-1} in 20 days old stock solutions of NaOH 0.1 N. This interfering amount of silicates interferes with the ammonium estimation. It is concluded that commercially prepared NaOH stock solutions (Titripack[®], Merck) are a strong and reliable alternative to avoid interferences, both from IC and silicates. These solutions are stored in completely closed, headspace free plastic bags of 10 l, and are not necessarily more expensive than self prepared stock solutions.

A detailed statistical analysis of the data obtained with the second measurement campaign was performed to quantify and interpret the different sources of variability. It was found that the duplo or subsampling variability is low, pointing to reproducible subsampling. The relative residual standard deviation obtained with the titrimetric measurements is 1.3 % for ammonium, and between 4 and 15 % for ortho-phosphate. This indicates that further optimization of the titrimetric reproducibility for ortho-phosphate should be considered. Especially when the interferences discussed in the previous paragraph are avoided, it is expected that the reproducibility

and accuracy will still become better.

The goal of the project was to develop an automatic technique for N and P measurements in animal manure in the field. Taking into account some further optimizations discussed above, the analysis results with this titrimetric sensor are expected to be as reliable as the laboratory results. A first comparison between the obtained results and the requirements for accreditation was performed, and it was concluded that the developed methodology is promising for official acceptance. Thus, it can even be suggested to implement the titrimetric measurement technique in the laboratory, with a laboratory titrator, coupled to a computer, as a reliable alternative for the classical laboratory methods. The strongest points of the titrimetric method are: simultaneous N and P measurement with 1 method, minor sample manipulations, N and P results within 30 minutes, low and inexpensive chemical consumption, consumption of only one and non-hazardous reagent (NaOH) and the possibility to measure continuously in the lab with a sample carousel coupled to the titrating unit.

Chapter 9

Automatic pH buffer capacity model building

Some of the results of this chapter are submitted for the conference “Watermatex 2000” [309].

9.1 Introduction

In the previous chapters, user-defined buffer capacity models were fitted to various experimental buffer capacity data, with the aim to quantify the concentration of known buffer systems defined in the mathematical buffer capacity model. At that stage, the interpretation of the goodness of fit of the model still was a manual process. If necessary, the mathematical model was extended or modified and refitted to the data. In each chapter, an adequate field-usable model was developed. More particularly, models were formulated for river and effluent samples (chapter 6), samples from algal wastewater treatment systems (chapter 7) and destructured and diluted animal manure samples (chapter 8).

The aim of this chapter is to automate the process of buffer capacity model building, and find an useful and adequate buffer capacity model, tailor-made for each individual sample. Such approach is expected to yield useful information in the framework of alarm generation, because for example, the appearance of unexpected buffers (e.g. pollutants) in the buffer capacity profile would be automatically detected and their characteristics quantified. In situations with a lack of a priori knowledge about the buffers present in a titrated sample, an automatic buffer capacity model building environment can be useful to find an appropriate model for that sample.

The tools needed for the automatic buffer capacity model development are implemented in the software *bomb*, which is described in detail in section 5.3 on page 117. In this context, the automatic model building algorithm (see section 5.3.4 on page 125) and the implemented buffer capacity model selection criteria (see section 5.3.5 on page 131) are of prior importance.

In section 9.2, a number of titration curves of samples with well-known composition will be used to evaluate the model building algorithm and the model selection criteria. Based on these results, a model building strategy will be formulated. In sections 9.3, 9.4 and 9.5, the

Table 9.1: Chemicals for the preparation of samples of which titration curves were collected

Chemical	Code	Protogenicity	pK_{a1}	pK_{a2}	pK_{a3}
Oxalic acid	oxa	2	1.23	4.19	
Sodium acetate	ace	1	4.75		
Ammoniumchloride	amm	1	9.20		
Malonic acid	mal	2	2.83	5.69	
Sodium tripolyphosphate	pho	3	2.12 ^a	7.21 ^a	12.67 ^a
Citric acid	cit	3	3.14	4.77	6.39

^a Values of ortho-phosphate. The real values have to be determined experimentally.

automatic model building environment will be evaluated with titration curves presented earlier in chapters 6, 7 and 8 respectively. An important aspect that will be investigated and discussed in this chapter is the benefit of automatic model building compared to the use of fixed buffer capacity models.

9.2 Buffer capacity modelling of well-known samples

9.2.1 Materials and methods

A number of titration curves with known composition were collected in the framework of adequate buffer capacity model development. The titration data collection is described in [202]. Initially, a manual model building algorithm was evaluated in [202]. The goodness of fit was interpreted visually and the 'best' model was compared with the 'theoretical' model. Later, this model building algorithm was modified and automated in [299]. Also, automatic model selection criteria were introduced in [299]. Finally, based on the experiences in [202, 299], some further modifications to the algorithm were proposed and finally implemented in the software *bomb*, presented in section 5.3 on page 117.

The database contains 146 titration curves, originating from 66 different samples, each titrated in two- or threefold. The chemicals that were used to prepare the samples are presented in Table 9.1. Four different concentrations of each chemical were used for the preparation of the samples: 0.5, 1, 2 and 5 $meq\ l^{-1}$. First, samples were prepared with only 1 component, and with each of the concentrations mentioned above (in total 24 samples). Second, combinations of 2 components were made: being oxa-amm, amm-ace, oxa-ace, pho-amm, pho-ace, oxa-mal, cit-ace, pho-mal and cit-mal. Each combination was prepared in the concentrations 1-1, 0.5-1 and 1-0.5 $meq\ l^{-1}$ (in total 27 samples). Third, combinations of 3 components were formed: being oxa-amm-ace and pho-amm-cit in the concentrations 0.5-1-0.5, 0.5-0.5-1, 1-0.5-0.5 and 1-1-1 $meq\ l^{-1}$ (in total 8 samples). Fourth, the combination oxa-pho-amm-ace was prepared in the concentrations 1-0.5-0.5-0.5, 0.5-1-0.5-0.5, 0.5-0.5-1-0.5, 0.5-0.5-0.5-1 and 1-1-1-1 $meq\ l^{-1}$ (in total 5 samples). Fifth, the combination oxa-pho-amm-ace-cit was prepared in the concentration 0.5

meq l^{-1} for each component. Sixth, the combination oxa–pho–amm–ace–cit–mal was prepared in the concentration 0.5 meq l^{-1} for each component.

Prior to titration, the samples were adjusted to pH 2–3 with HCl 1 N, and made CO_2 free by strong agitation with a magnetic stirrer during 10 minutes. The titrated sample volume was 100 ml, and the samples were titrated with NaOH 0.1 N from pH 2–3 to pH 11. The titration curves were obtained with a laboratory titrator (Metrohm Titrino 716 [168]). The details about the titration algorithm are described in section 5.1.1 on page 98. The titration data was later processed with the software *bomb*, described in section 5.3 on page 117.

9.2.2 Evaluation of two modelling approaches with a testcase

One of the samples cit–ace with concentrations 1–0.5 meq l^{-1} was selected as testcase to compare two modelling approaches. The first approach is based on the availability of a priori knowledge about the buffers present in the sample, while in the second approach, it is assumed that no information about the composition of the sample is available. These two approaches are presented and compared in the following paragraphs.

A priori knowledge based buffer capacity model

The buffer capacity model that was fitted to the experimental data included the water buffer, an inorganic carbon buffer, a citric acid buffer and an acetate buffer. In the previous chapters, it was found that it can be useful to allow some flexibility on the pK_a values of the considered buffer systems. Such flexibility corrects for small deviations of the real pK_a compared to the experimental pK_a , due to measurement errors, ionic strength effects, temperature effects, ... Therefore, the buffer capacity model was fitted twice to the experimental data, without and with extra flexibility on the theoretical pK_a values. The model specifications are summarized in Table 9.2.

The experimental and simulated buffer capacity curves of the selected sample, respectively without and with the extra flexibility on the pK_a values are shown in Figure 9.1. The corresponding results for the estimations of the pK_a values and the concentrations together with their standard deviations (calculated with the method of Nelder and Mead (1964), see section 5.3.3 on page 120) are given in Table 9.3.

The applied buffer capacity models (a) and (b) have respectively 4 and 8 parameters to be estimated. Both models succeeded in a satisfying estimation of the concentrations of respectively the citric and the acetic acid buffer. As can be expected, the fit of the simulated to the experimental buffer capacities, however, is worse for model (a) compared to model (b) (see Figure 9.1). With model (b) the pK_{a1} value of the blank6 buffer and the pK_a value of the blank1 buffer are estimated respectively at their maximum and minimum allowed boundary value. Allowing a wider flexibility range for these pK_a values resulted in slightly worse estimated concentrations of these two buffers (results not shown). An advantage of the flexible pK_a approach compared to the fixed pK_a approach is that the flexible pK_a approach allows to detect more easily extra unexpected buffers (e.g. interferences) in the buffer capacity profile. E.g. for this particular example in the situation (b), it can be seen that the fitted mathematical model describes the experimental data fairly well, except that between pH 8 and pH 9, there is probably a buffer present, not accounted for in the model. On the other hand in the situation

Table 9.2: Model specifications for a simulation interval between pH 3.5 and pH 10.5

Buffer	Variable	Initial guess or value	Estimated?	Lower limit	Upper limit
Water	pka_water	15.74	Yes	15.70	15.82
	conc_water	55.5 mol l ⁻¹	No		
IC	pka1_carbon	6.37	No		
	pka2_carbon	10.25	No		
	conc_carbon	0.5 mg CO ₂ l ⁻¹	Yes	0	5.5
Citric acid	pka1_blank6	3.14	No/Yes ^a	3.01	3.27
	pka2_blank6	4.77	No/Yes ^a	4.6	4.9
	pka3_blank6	6.39	No/Yes ^a	6.2	6.52
	conc_blank6	0.1 mmol l ⁻¹	Yes	0	1
Acetic acid	pka_blank1	4.75	No/Yes ^a	4.6	4.9
	conc_blank1	0.1 mmol l ⁻¹	Yes	0	1

^a 'Yes' for the incorporation of extra flexibility on the considered pK_a .

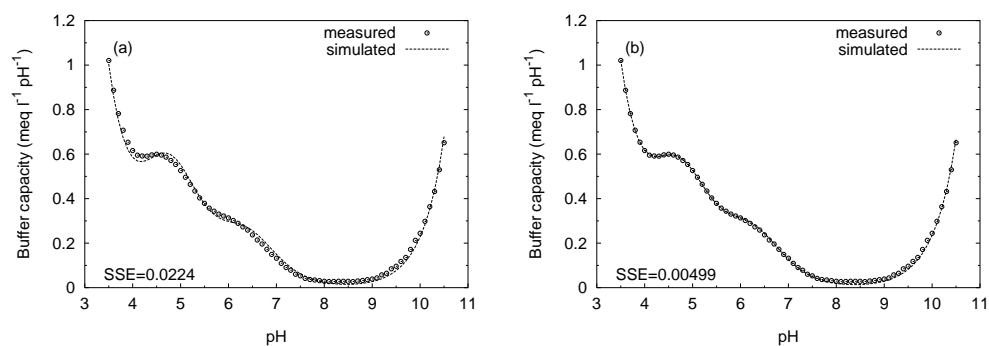


Figure 9.1: Experimental and simulated buffer capacity curves of a sample with well-known composition. Results are shown for the buffer capacity model without (a) and with (b) extra flexibility on the pK_a values of the citric and acetic acid buffer

Table 9.3: Simulation results of the selected and well-known sample for the buffer capacity model without (a) and with (b) extra flexibility on the pK_a values of the citric and the acetic acid buffer

	Unit	Model (a)		Model (b)		Expected
		Estimate	Std. dev.	Estimate	Std. dev.	
pK_a H ₂ O		15.79	0.012	15.81	0.0078	
pK_{a1} blank6				3.27	0.11	3.14
pK_{a2} blank6				4.88	0.09	4.77
pK_{a3} blank6				6.25	0.03	6.39
pK_a blank1				4.60	0.07	4.75
C_{IC}	mg CO ₂ l ⁻¹	1.69	0.72	3.03	0.49	
C_{blank6}	mmol l ⁻¹	0.35	0.016	0.33	0.014	0.33
C_{blank1}	mmol l ⁻¹	0.56	0.023	0.55	0.039	0.5

(a), it is not clear whether extra buffers are necessary and at what pH they should be included in order to fit the experimental buffer capacity profile more closely. Therefore, the extra buffer between pH 8 and pH 9 in situation (a) remains unnoticed due to the overall lack of fit. There is a notable difference in the estimated IC concentration (see Table 9.3). However, considering the standard deviations on these estimates, the difference is statistically not significant. Despite the fact that model (b) has more degrees of freedom compared to model (a), there is not more uncertainty in the estimates of the concentrations with model (b) (the standard deviations on the concentrations are similar for model (a) compared to model (b)). This aspect will further be investigated with other examples and more complicated models.

The above presented approach is based on the a priori knowledge that the selected sample contains at least a monoprotic and a triprotic acid (respectively acetic and citric acid). In the next approach, it is considered that this a priori information is not available.

Automatic model building in absence of a priori knowledge

The second modelling approach is based on the automatic model building algorithm included in the software *bomb*. The selected and well-known sample is considered again, and the stepwise model building process is initiated, starting from a zero model that only contains the water buffer. As described in chapter 5, the stepwise model building algorithm will systematically add new buffers at pH values near the run with the highest sum of residuals. When the model building process is finished, a list of blind buffers with their pK_a values and concentrations has to be interpreted by the user.¹ At this stage, an appropriate model selection criterion (e.g. AIC, Run-test, ...) is not considered yet. The model building process will continue until all available blind buffers are incorporated in the model (*bomb* can include at most 8 blind

¹For the specific automatic model building terminology, the reader is referred to section 5.3.4 on page 125.

Table 9.4: Simulation results of a well-known sample for the automatically built buffer capacity models illustrated in Figure 9.2, plots (b) until (f). The concentrations are expressed as mmol l^{-1} and the table entries are estimate \pm standard deviation

	Model 1.0 Plot (b)	Model 2.0 Plot (c)	Model 3.0 Plot (d)	Model 4.0 Plot (e)	Model 5.0 Plot (f)
pK_a blind1	4.78 ± 0.06	4.51 ± 0.03	4.50 ± 0.02	4.74 ± 0.01	4.74 ± 0.007
pK_a blind2		6.08 ± 0.06	6.08 ± 0.05	6.24 ± 0.01	6.22 ± 0.008
pK_a blind3			9.88 ± 0.21	9.90 ± 0.04	9.99 ± 0.03
pK_a blind4				3.50 ± 0.05	3.50 ± 0.03
pK_a blind5					8.21 ± 0.13
C_{blind1}	1.00 ± 0.05	0.93 ± 0.02	0.93 ± 0.02	0.83 ± 0.008	0.83 ± 0.006
C_{blind2}		0.47 ± 0.02	0.47 ± 0.02	0.40 ± 0.004	0.40 ± 0.003
C_{blind3}			0.08 ± 0.02	0.08 ± 0.003	0.08 ± 0.002
C_{blind4}				0.32 ± 0.007	0.32 ± 0.005
C_{blind5}					0.02 ± 0.002

buffers) or until the situation that the algorithm cannot further extend the model (e.g. due to the restriction in the model building algorithm that pK_a ranges may never overlap with each other, it is possible that no runs are available any more for model extension).

The stepwise model building process with the testcase is illustrated in Figure 9.2. The pH simulation interval was set between pH 3.5 and pH 10.5 and the pK_a of the water buffer was set to 15.81, based on previous models where the pK_a of water was allowed to vary. At the last modelling step (i.e. a sixth model extension at pH 7.1 of the fitted model shown in Figure 9.2(f)), the parameter estimation routine PRAXIS ran into a local minimum problem because it did not find a cost function value that was lower than the previous model (which is theoretically not possible in case of correct optimization, because the less complicated model is always a subset of the more complicated model). Apparently, the optimization problem became overparametrized, and thus it was not useful to proceed the model building process. The simulation results with the models illustrated in Figure 9.2(b)–(f) are summarized in Table 9.4.

The interpretation of the results of this example is straightforward. In the first modelling step, a buffer with $pK_a = 4.78$ is introduced in the model. Its final concentration is 0.83 mmol l^{-1} (with only a small modification of the pK_a to 4.74), and represents the dissociation of acetic acid. Of course, but this cannot be determined by the algorithm, it falls together with the second dissociation step of citric acid (the theoretical concentration can be calculated as $0.5 + 0.33 = 0.83 \text{ mmol l}^{-1}$). In the second step, a buffer with $pK_a = 6.08$ is introduced, with an estimated concentration of 0.40 mmol l^{-1} . This buffer represents the third dissociation step of citric acid (0.33 mmol l^{-1}) together with some extra buffer (0.07 mmol l^{-1} , probably IC). The third buffer that is entered in the model has an estimated $pK_a = 9.99$ and a concentration of 0.08 mmol l^{-1} . This is an unexpected buffer, however, with the experiences described in section 8.5.2 on page 220, it is a fair assumption that this buffer originates from interfering sil-

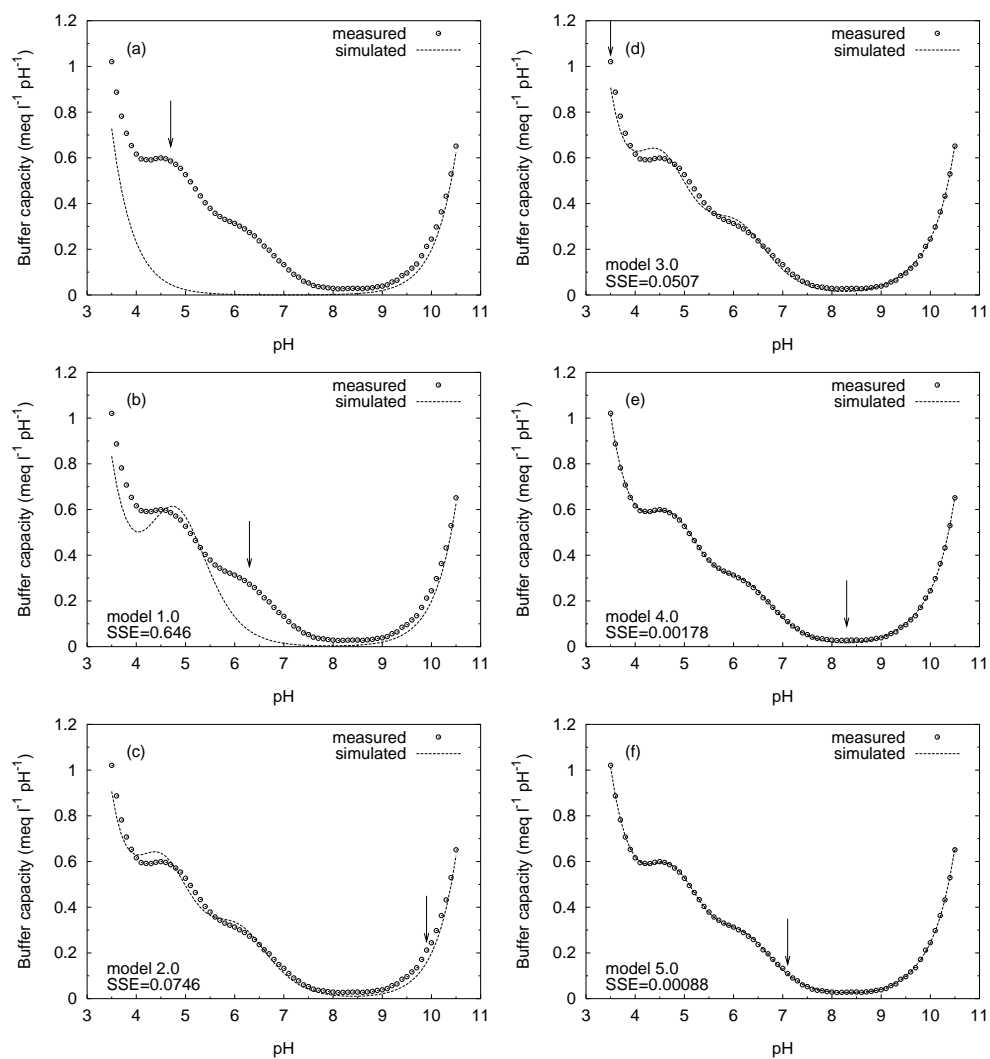


Figure 9.2: Experimental and simulated buffer capacity curves of a well-known sample. The stepwise model building process starts with plot (a) (the zero model) and ends with plot (f) (the final model). The arrows indicate the automatically proposed pK_a positions for model extension

Table 9.5: Model selection criteria calculated for the consecutive models in the automatic model building process of the well-known testcase. The bold items mark the selected models based on each considered criterion. For the last two criteria, the significance level $\alpha = 0.0001$ was chosen

	Model 1.0	Model 2.0	Model 3.0	Model 4.0	Model 5.0	Model 6.0
AIC	-330	-479	-502	-736	-782	-729
AIC _C	-256	-405	-428	-660	-705	-649
FPE	0.0096	0.0012	0.00085	0.000031	0.000016	0.000035
SIC	-325	-470	-489	-718	-760	-701
Run-test (p)	$< 10^{-6}$	$< 10^{-6}$	0.000001	0.00013	0.00047	0.00047
F-test (p)	$< 10^{-6}$	$< 10^{-6}$	0.000003	$< 10^{-6}$	$< 10^{-6}$	1.00000 ^a

^a An insignificant p -value for model 6.0 means that model 5.0 is selected.

icates entering the titration vessel through the NaOH titrant. The fourth buffer has an estimated $pK_a = 3.5$ and a concentration of 0.32 mmol l^{-1} . This pK_a value equals the minimum pH value of the considered pH interval, and the model building algorithm does not allow to introduce buffers with pK_a values outside the simulation interval. Therefore, the real pK_a value of that buffer could be lower than 3.5. Its concentration indicates that this buffer is most probably the first dissociation step of citric acid (theoretically $pK_a = 3.1$ and 0.33 mmol l^{-1}). The last buffer entered in the model is located at pH 8.21, with a very low concentration 0.02 mmol l^{-1} . Probably, it is again a small interfering buffer, but with unknown origin. The latter buffer is not considered very important. However, taking into account the standard deviation on the estimate, the concentration is still significantly different from 0 (t-test, $\alpha = 0.01$). As mentioned before, the model building process has finally tried to introduce a next buffer with $pK_a = 7.1$ (model 6.0, results not shown), but then the optimization problem became overparametrized, and the optimization algorithm failed to find an acceptable solution. Such optimization failure mostly ends up with an SSE of the current model that is higher than the SSE of the previous model (which is theoretically not possible in case of correct optimization, because the less complicated model is always a subset of the more complicated model). An appropriate message is foreseen in the software when this happens. Further, if the optimization algorithm doesn't find a correct solution, often the calculation of the variance-covariance matrix afterwards also ends up in numerical problems (e.g. Not-a-Number or NaN values). Such problems are also logged to the user.

Although the evaluation of model selection criteria is the topic of section 9.2.3, it is useful at this stage to summarize and interpret the different model selection criteria calculated at each model building step for the selected testcase. More particularly, it is interesting to know whether the model selection criteria would stop the model building process earlier than model 6.0 (which is the model that resulted in an optimization failure). The 6 model selection criteria, applied to the testcase, are summarized in Table 9.5.

If the automatic model selection was activated, all criteria would select model 5.0 as the

final model, except for the Run-test, that would favour model 4.0. Of course, the latter finding completely depends on the choice of the critical significance level α . Also, model 6.0 ended up in a wrong optimization result, thus forcing all criteria (including the F-test) to select the simpler model 5.0. The first four criteria (AIC, AIC_C, FPE and SIC) show their highest decrease in value from model 1.0 to 2.0 and from model 3.0 to 4.0. This points to very important increases in model adequacy at those two stages. This is also nicely reflected in Figure 9.2. A more detailed evaluation of the 6 model selection criteria on each of the 146 titration curves of the samples with well-known composition is described in section 9.2.3.

Conclusions

At this stage, a number of conclusions related to the automatic buffer capacity model building algorithm can be formulated. First, the algorithm succeeds in a stepwise construction of a buffer capacity model in which the buffer systems are incorporated in order of importance. It was straightforward to relate the final result to the available a priori knowledge. Second, the results of the automatic model building revealed extra information on top of the available a priori knowledge. More particularly, prior unknown interfering buffers at pH 8 and pH 10 were detected and quantified.

Third, the standard deviations on the pK_a and concentration estimates are very important for the interpretation. On the one hand, they are useful to statistically test if certain small concentrations of e.g. interfering buffers are significant; or to calculate confidence intervals on the estimates. On the other hand, if the standard deviation becomes too high, it indicates that the optimization problem is overparametrized. In the testcase, the standard deviations became systematically lower for increasing model complexity. This strongly points to the validity of the more complex models. The latter conclusion was also reflected in the model selection criteria, that pointed to the model with 5 blind buffers as the most appropriate one. In the next section, the three formulated conclusions will be further evaluated with the other samples with well-known composition.

9.2.3 Evaluation of six model selection criteria

The titration curves of the samples with well-known composition were classified in 4 groups, that are discussed separately in this section:

Group 1 : 27 titration curves with 1 monoprotic buffer (oxalic acid is also considered in this group, because of its very low pK_{a1} value)

Group 2 : 27 titration curves with 1 di- or triprotic buffer

Group 3 : 60 titration curves with 2 buffers (mono-, di- or triprotic)

Group 4 : 32 titration curves with more than 2 buffers

All titration curves were used as input data to the automatic model building environment in the software *bomb*. It was assumed that no a priori knowledge about the buffers to be expected in the samples was available. Consequently, the zero model only contained the water buffer. The model building process was repeated for each of the 6 model selection criteria. The significance level for the Run-test and the F-test was set to $\alpha = 0.0001$.

Summarizing frequency tables for each of the 4 groups of titration curves, with the counts of titration curves corresponding with the final (or selected) model degree ² are given in Table 9.6 for each of the 6 model selection criteria. In general, the first four criteria (AIC, AIC_C, PFE and SIC) select the same model as final model. However, large differences in the selected final model are noticed for the Run-test and the F-test. A more detailed analysis of the selected final model as function of the selected criterion, and for each of the 4 considered groups of titration curves is given in the next paragraphs.

In group 1, the automatic model building algorithm perfectly detects the single monoprotic buffer in the experimental buffer capacity profile, and in all cases incorporates this buffer as the first blind buffer in the model. The estimated concentrations were not significantly different from the theoretically expected concentrations. However, the model building process does not stop at this stage in most cases, but continues with the incorporation of new blind buffers. In order of importance, first a buffer around pH 10 with a typical concentration of 0.1 mmol l⁻¹, and second a buffer around pH 6.5 with a typical concentration between 0.05 and 0.1 mmol l⁻¹ are added to the model. As discussed before, these two buffers are assumed to be silicate and inorganic carbon respectively. Their concentrations are mostly found significantly different from 0. The Run-test and F-test generally stop at this stage. However, the AIC and related criteria mostly extend the model with 1 or even 2 extra buffers of unknown origin (around pH 7 and pH 4). The concentrations of these extra buffers are very low, and sometimes not significantly different from 0. Practically, it is concluded that the AIC and related criteria go rather far in the model building process. In 7 out of the 27 cases, the F-test selected the model with only 1 buffer as the final model, thus not recognizing the silicate and/or the IC buffer. This behaviour could be attributed to an optimization problem. It was noticed that for some 'uncomplete' models (thus models still deviating a lot from the final model), the parameter estimation routine ended in a local minimum (5 cases out of the 27) at the second modelling step, i.e. the model with 2 blind buffers, with an SSE of the more complex model higher than the SSE of the simpler model. Consequently, the simpler model was selected by the F-test. The AIC and related criteria too suffered from this flaw, and as a result selected in 4 (AIC, AIC_C and FPE) or 5 (SIC) cases the model with 1 buffer as the final model. Only the Run-test was not influenced by local minima problems, because this test examines only the randomness of the residuals. As a first preliminary conclusion, the Run-test was found to perform most 'realistically' for this group of titration curves.

For the titration curves of group 2, similar findings as for group 1 can be formulated. The final models mostly contain, as expected, 1 or 2 supplementary buffers compared to the final models of group 1. For example, in 17 out of 27 cases, the Run-test selects the model with 4 blind buffers. These 4 buffers include 2 or 3 buffers from the added di- or triprotic component, and 1 or 2 interfering buffers, like silicates or IC. The AIC and related criteria often select a model with 5 or 6 blind buffers. This is again a higher model degree than what should be considered practically. Further, these high degree models illustrate certain weaknesses in the model building algorithm. More particularly, sometimes buffers are added in the model (interfering buffers, in small but significant concentrations), that in a later modelling stage become insignificant, because a neighbouring buffer takes over the buffer capacity of the previously introduced buffer. The model building algorithm does not allow to remove a buffer

²The degree of a model is here defined as the number of blind buffers incorporated in the model.

Table 9.6: Frequency tables per group of titration curves, classified towards the final model degree and the applied model selection criterion

Group	Final model degree	Criterion for model selection					
		AIC	AIC _C	FPE	SIC	Run-test	F-test
1	1	4	4	4	5	1	7
1	2	2	2	2	4	7	5
1	3	2	2	2	4	19	9
1	4	14	14	14	11	0	6
1	5	5	5	5	3	0	0
2	1	1	1	1	1	0	4
2	2	0	0	0	2	0	10
2	3	1	1	1	2	5	2
2	4	7	7	7	7	17	2
2	5	11	11	11	9	5	6
2	6	7	7	7	6	0	3
3	1	0	0	0	0	0	3
3	2	0	0	0	1	1	5
3	3	2	2	2	2	14	1
3	4	13	13	13	16	19	23
3	5	36	36	36	34	17	26
3	6	9	9	9	7	3	2
3	7	0	0	0	0	0	0
3	8	0	0	0	0	6	0
4	3	0	0	0	0	1	0
4	4	3	3	3	3	7	6
4	5	9	9	9	10	16	10
4	6	16	16	16	15	8	16
4	7	4	4	4	4	0	0

from the model in case the concentration of this buffer is not significantly different from 0. It could be suggested to include this feature in the model building algorithm of the software *bomb* (e.g. based on a similar F-test based method that is also implemented in stepwise linear regression algorithms). This is further discussed in section 9.2.4. Local minima problems with ‘uncomplete models’, as described earlier, did occur less frequently (only 1 out of the 27 cases). In groups 3 and 4, this particular problem was no longer noticed. Thus it is concluded that only the simplest type of titration curves sometimes lead to a too low final model degree due to an optimization problem. Again, the Run-test was found to select the most realistic final model.

The titration curves of group 3 have an increased complexity, and should theoretically contain at least between 2 (e.g. amm–ace) and 5 (e.g. cit–mal) pK_a values. For the simplest type of combinations (e.g. the combination of a monoprotic and a diprotic buffer), the final model could be interpreted perfectly: The quantified buffers corresponded with the buffers present, both for the pK_a positions, and the respective concentrations. Again, supplementary buffers were sometimes found around pH 10 (silicates) or elsewhere. A typical example of one of these titration curves was described earlier in section 9.2.2. At this stage, another particularity related to the model building algorithm was discovered. In the example cit–mal, the $pK_{a2} = 5.69$ of malonic acid is only 0.7 different from the $pK_{a3} = 6.39$ of citric acid. In most examples of this type, a blind buffer was incorporated in the model somewhere between these 2 theoretical pK_a values, and was accounting for both buffer systems. This points to a certain ‘limit of resolution’ which is further discussed in the next paragraph. For the simplest type of curves in group 3, the Run-test was slightly favoured for practical purposes. However, for the more complicated titration curves, the performance of the Run-test was not found most appropriate in a number of situations. More particularly, for 6 out of 60 titration curves, the Run-test selected a final model with 8 blind buffers, whereas all other criteria considered only 6 blind buffers as the maximum number of buffers needed in the final model. There is a clear explanation for this behaviour. The maximum number of buffers that are available in the automatic model building algorithm is 8. Therefore, in those cases where the Run-test selected 8 blind buffers, the necessary Run-test criterion was never reached. This phenomenon occurred only in examples with polyphosphate as one of the buffers. It can be pointed that the uncertain position of the pK_{a2} value of polyphosphate could be the reason why an acceptable fit was not found with the Run-test criterion. By lowering the significance level α , this problem would partially be solved. However, this is an important limitation for field applications. An illustrative titration example of pho–mal is given in Figure 9.3. The fitted buffer capacity model contains 4 blind buffers (with respectively the pK_a values in order of importance 5.7, 9.3, 3.5 and 6.8). A further model extension proposed at pH 8.1 results in an insignificant F-test result ($p = 0.26$), whereas the Run-test result is still very significant ($u = -4.5$ or $p = 0.000007$). Further model extensions do not make the fit better than what is illustrated in Figure 9.3. When 6 or more blind buffers are included in the model, the optimization problem becomes overparametrized, and the parameter estimation algorithm ends up in local minima. Thus, when the Run-test criterion is selected for this particular example (with $\alpha = 0.0001$), the model building algorithm will proceed until all available blind buffers are incorporated in the model, and will finally not find any model that fulfils the requested criterion.

The final model results of the easiest type of titration curves in group 4 (e.g. the combination of 2 monoprotic buffers and a diprotic buffer) could easily be related with the buffers to be

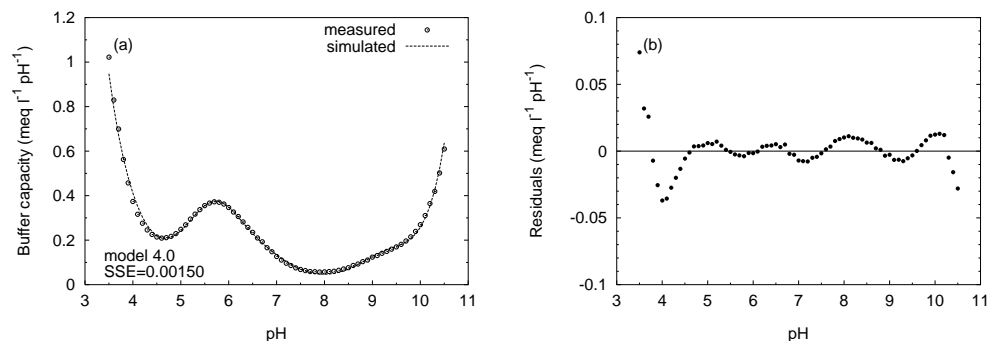


Figure 9.3: Experimental and simulated buffer capacity curves (a) and calculated residuals (b) of a sample pho-mal

expected. The F-test criterion mostly selected the same model as the AIC and related criteria. The Run-test criterion often selected models of lower complexity. The results obtained with the F-test criterion were found to correspond most closely to the reality. The interfering buffer at pH 10 (silicates) was still detected and quantified in most cases. The ‘limit of resolution’ mentioned in the previous paragraph, was further investigated. Again, it was found that 2 buffers with neighbouring pK_a values are pooled together in the model building algorithm. It was found that the practical limit of resolution for the considered examples is between 0.5 and 1 pH units. This can be related with two parameter settings of the model building algorithm (see chapter 5): The initial range³ of a blind pK_a value is chosen 1.5, and the minimal range of a blind pK_a value is set to 0.2. The intervals of the pK_a values are not allowed to overlap, thus this automatically limits the number of buffers that can enter in the model around the same pK_a . However, detailed analysis of the pK_a ranges that were automatically narrowed during the model building process showed that only in a few cases, the minimal range was used by the algorithm. This indicates that the model building algorithm did not request to enter new blind buffers with a pK_a separation of 0.5 or less compared to pK_a values of previously incorporated buffers in the model. A comparison with the Gordon algorithm described in [101, 102] was made, and the defined criterion for the limit of resolution (see equation (4.5) on page 92) was compared with the obtained results. The authors found that a minimal pK_a separation of 0.1–0.2 is borderline for most applications, whereas 0.5 is a common value. However, it should be noted that the Gordon algorithm only allows variation on the pK_a value that is lastly entered in the model, together with the neighbouring pK_a value, whereas in the *bomb* algorithm, variation may be allowed on any pK_a . As mentioned and illustrated in section 4.4.2 on page 89, such approach is only useful under well controlled laboratory conditions. It can be concluded that the limit of resolution obtained here is somewhat lower than what is described

³The range is defined as the difference between the maximum and minimum boundary value set as an interval in which the considered pK_a value is allowed to vary.

in [101, 102], but still in an acceptable range. It is also expected that our approach is more robust, because of the higher flexibility on the pK_a values, the built-in model 'tuning' in case an estimated pK_a value touches one of its boundary values, and the use of model selection criteria.

Based on the results presented and discussed here, some generalizations and a proposed model building strategy are presented in the next section.

9.2.4 Model building strategy

In the previous section, no a priori knowledge was used for the buffer capacity model development of a number of samples with well-known composition. The approach followed has illustrated that it is possible to extract and interpret correctly at least 3 or 4 different buffer systems in a concentration around 1 mmol l^{-1} and 1, 2 or 3 mostly smaller and interfering buffers (IC, silicates, ...) from an experimental buffer capacity profile. One of the limitations of the approach was found to be that two experimental buffers with a pK_a separation less than 0.5 are pooled together in the model as one buffer.

The application of this modelling approach is suggested for samples in which an unbiased⁴ characterization of different buffer systems is required. An example could be the evaluation of the correctness of end-point titrations used in many analytical laboratory methods. Automatic titrators search for an equivalence-point, and the corresponding equivalence titrant volume is attributed to the expected buffer. However, such algorithms are not able to detect small interferences like IC, silicates, ... Therefore, automatic buffer capacity modelling can be used to find out if there is indeed one buffer system present, or if other (interfering) buffers are present as well.

For the majority of environmental samples (river waters, effluents, ...) a priori knowledge is available about (some of) the buffer systems to be expected in an experimental buffer capacity profile. The expected buffers that need to be quantified, are best incorporated as known buffers in the zero model (in the first place to avoid 'pooling' of the expected buffers to be quantified and the neighbouring buffers). The range in which the theoretical pK_a of such known buffer is allowed to vary should be considered carefully. If the pK_a position is known rather precisely, then a small range can be used (e.g. 0.2), so that neighbouring blind buffers are allowed to approach the known buffer quite closely. If the exact pK_a position is unknown or if it is preferred that blind buffers do not approach the known buffer too closely (e.g. to avoid that the buffer capacity of the known buffer is partially modelled as the neighbouring blind buffer), it is suggested to choose a wider range for the known buffer (e.g. 1).

At the previous stages, no 'best' model selection criterion was found. The AIC, AIC_C, FPE and SIC criteria mostly selected the same model. The Run-test criterion performed best for the simplest type of buffer capacity curves, whereas the F-test was better for the more complicated type of curves. The AIC and related criteria tend to select highly parametrized (almost overparametrized) models. In another field, the same model selection criteria were compared for the selection of oxygen uptake rate (OUR) models fitted to respirometric data [315]. It was found that traditional information criteria (AIC, AIC_C, FPE and SIC) result in

⁴The term 'unbiased' is used here in a non-statistical sense to indicate that the user does not impose his knowledge about the sample into the buffer capacity model.

overfitting of the model compared to the ‘human expert advice’. In particular, some small oscillations in the data were accounted for to a significant extent by flexible, more complex models. To the human expert, however, these phenomena seemed not essential [315]. The latter statement also applies to the results obtained in this work. In the next sections, only three model selection criteria will further be considered and evaluated, being AIC, Run-test and F-test.

If the F-test criterion is selected, an useful comparison can be made with multiple linear regression search procedures for the selection of independent variables in a multiple linear regression model. There is, however, a fundamental difference in approach between the automatic buffer capacity model building procedure and multiple linear regression. In linear regression problems, the independent or exploratory variables X_i are known in advance, and a subset from the pool of a priori known X_i variables is included in the final or ‘best’ regression model. With the buffer capacity model building algorithm, the buffers that are entered in the model (cfr. the X_i) are not a priori known, but determined as function of the residual pattern of the previous model. The different procedures for multiple linear regression [207] are shortly reviewed and discussed in relation with stepwise buffer capacity modelling.

- *All-possible-regressions*: This procedure calls for considering all possible subsets of the pool of potential X_i variables and identifies for detailed examination a few ‘good’ subsets according to some criterion. For example with 4 exploratory variables, there are altogether 16 subset regression models that can be formed. First, there is the regression model with no X_i variables, then with one X_i variable, with two X_i variables, etc. Due to the fundamental difference mentioned above, such approach would not be feasible for automatic buffer capacity modelling.
- *Forward stepwise regression*: Essentially, this search method develops a sequence of regression models, at each step adding or deleting an X_i variable. It is probably the most widely used method and it was developed to economize on computational efforts, as compared with the all-possible-regressions procedure. The criterion for adding or deleting an X_i variable is mostly an F-test. Further, two critical significance levels need to be chosen: a minimum significance level to enter, and a maximum significance level to remove. Note that the stepwise regression algorithm allows an X_i variable, brought in the model at an earlier stage, to be dropped subsequently if it is no longer helpful in conjunction with variables added at later stages. The current algorithm in *bomb* does not allow to remove buffers from the buffer capacity model once they are incorporated. However, as described in section 9.2.3, it happens that the concentration of a buffer introduced at an earlier stage becomes insignificant at later stages. Consequently, an useful extension of the current algorithm would be to allow the removal of insignificant buffers from the model. On the other hand, this would make the algorithm more complicated, and certainly would require extra research to make it robust enough for field-use.
- *Forward selection*: This search method is a simplified version of forward stepwise regression, omitting the test whether a variable once entered into the model should be dropped. This corresponds best with the current algorithm in the program *bomb*.
- *Backward elimination*: The backward elimination search procedure is the opposite of forward selection. It begins with the model containing all potential X_i variables and identifies the one with the smallest F-test value. If the significance of this value exceeds

a maximum significance level to remove, that X_i variable is dropped. Such procedure is not foreseen in the current version of *bomb*, however, it should be possible in further research to extend the algorithm with a backward elimination method. Because the elimination method is simpler than the stepwise method mentioned above, it is expected that the robustness of the new algorithm would be similar as the current algorithm. Some statisticians argue for backward methods over forward methods because it is useful as a first step to look at each X_i in the regression function adjusted for all the other X_i variables in the pool [207]. For buffer capacity modelling purposes, a backward algorithm would not suffer from a particular problem described in section 9.2.3, being the selection of a too low degree model caused by local minima problems in still very ‘uncomplete’ models.

9.3 Surface water and effluent applications

9.3.1 Materials and methods

The titration curves that were used for the evaluation of the automatic buffer capacity modelling are described earlier in chapter 6, more particularly in section 6.3.3 on page 151. Summarized, 421 titration curves were analyzed, originating from

- domestic wastewater effluents (26 different plants),
- an industrial effluent sampled during three months, and
- 118 Flemish surface waters.

The a priori knowledge that holds for all titration curves is that an ortho-phosphate buffer, an ammonium buffer and an IC buffer are to be expected. As discussed in section 9.2.4, it is considered important to use such a priori knowledge in the automatic buffer capacity model development. Therefore, the zero model or starting model is chosen in correspondence with the model specifications given in Table 6.3 on page 152, except for the following two modifications:

- The ‘soap’ buffer is not included any more. The automatic modelling algorithm has now the flexibility to include no, one, two or more buffer systems that account for the previously used ‘soap’ buffer between pH 4 and pH 6.
- The simulation interval (between pH 4 and pH 10 in the work presented in chapter 6) is now extended to an interval between pH 3.5 and pH 10.5. This offers the possibility to take into account more potentially present buffer systems. A further extension of the simulation interval is not advised, for two reasons. First, outside the above mentioned interval, the water buffer capacity is masking all other buffers, and thus it is not worthwhile to search for extra buffers with such low or high pK_a values. Second, it was found that the optimization algorithm easily ends up in local minima when the simulation interval is set very wide, e.g. between pH 3 and pH 11. The most probable reason is that the buffer capacities at pH 3 and pH 11 are approximately ten times higher than the buffer capacities at pH 5 – 7. Therefore, the optimization algorithm will focus too much on the goodness of fit at the lowest and highest pH values, and neglect the goodness of fit in the central part of the buffer capacity profile, which is undoubtedly the most important part

of the profile. For future versions of the program *bomb*, it is suggested to implement a relative weighing option in the cost function to overcome this problem. More particularly, it is proposed to use a high cost function weight in the low buffer capacity regions, and vice versa.

Based on the above described zero model, the automatic model building algorithm may stepwise enter blind buffers in the model, but not with pK_a 's in the 2 pH ranges 6.5 – 7.4 and 9 – 9.75, which are the lower and upper limits for the variable pK_a values of respectively ortho-phosphate and ammonium. Other important settings for the automatic model building algorithm in *bomb* are: $\alpha = 0.0001$ as the critical significance level for the Run-test and F-test, and 0.2 as the minimal range for a pK_a of a blind buffer. In section 9.2.3, it was found that the AIC, AIC_C, FPE and SIC model selection criteria performed very similar. Therefore, in this section, only AIC, Run-test and F-test will be evaluated and compared with each other.

In the next section, the following points will be investigated:

- What are the differences in the final model results when considering the different model selection criteria?
- Is the automatic model building algorithm able to detect and quantify other buffers than ammonium and ortho-phosphate, and does this reveal extra information about the titrated sample?
- Is the automatic model building advantageous for ammonium and ortho-phosphate assessment, compared to the fixed model approach that was used in chapter 6?

9.3.2 Automatic model building results

Evaluation of three model selection criteria

Summarizing frequency tables for the surface waters (259 titration curves) and effluents (162 titration curves), with the counts of titration curves corresponding with the final model degree for each of the three model selection criteria are given in Table 9.7.

For most surface waters and effluent samples, the three model selection gave satisfying results. A strict comparison between the 'selected' model degree and the 'real' model degree is not possible, because the 'real' model degree is unknown, and differs from sample to sample. Therefore, an 'expert judgement' was needed for each titrated sample. The AIC criterion again tends to select higher degree models. Two typical problems were noticed. First, the Run-test criterion is not reached in 33 % of the cases, resulting in a final model in which the maximum allowable (6) blind buffers are entered in the model, whereas the other criteria have selected a final model of lower degree. In most of these cases, the optimization algorithm ends up in local minima and the variance-covariance calculation is not correctly finished due to numerical problems. This is a serious limitation for field-use, and thus the Run-test criterion as such is found not very robust. Second, in 20 % of the cases the F-test criterion concludes that model 1.x (zero model plus 1 blind buffer) is not significantly different from model 0.0 (zero model), and therefore selects the zero model as the final model. Visual inspection of the experimental versus the simulated buffer capacity curve shows in most of these cases that there is still unmodelled experimental buffer capacity, and thus the F-test has selected a final model with a too low degree. Moreover, when the further model building steps (e.g. model 2.x or

Table 9.7: Frequency tables of surface water and effluent samples, classified towards the final model degree and the applied model selection criterion

Final model degree	259 surface water samples			162 effluent samples		
	AIC	Run-test	F-test	AIC	Run-test	F-test
0	14	0	41	2	3	44
1	28	4	93	15	8	53
2	49	10	71	36	15	34
3	116	61	38	64	38	22
4	47	55	15	40	22	9
5	5	40	1	5	25	0
6	0	89	0	0	51	0

3.x) are performed anyway, it can happen that the F-test criterion again becomes significant for these higher degree models. The origin of this problem can be found in the way the automatic model building algorithm proceeds, i.e. the algorithm can only introduce one blind buffer at a time. If the model fit of the zero model is bad at several positions of the buffer capacity profile, then the algorithm can increase the fit at only one position of the profile. Consequently, it is possible that such a ‘small’ increase in fit by adding one blind buffer is not significant due to lack of fit of the other positions in the buffer capacity profile, despite that a blind buffer is always introduced at the pK_a position that suits best for a model extension.⁵ This particular problem automatically disappears for more complicated models with several blind buffers. Note that the backward elimination suggestion formulated in section 9.2.4 would automatically solve this problem.

From this analysis, it can be concluded that the three model selection criteria have a clearly different behaviour. At this moment, none of the three criteria can be proposed as the ‘best’ criterion, which was also concluded in section 9.2.4. In the next paragraphs, a number of case studies will be presented in detail for further evaluation and interpretation of the model selection criteria and their corresponding final models.

Surface waters

Four selected Flemish surface waters samples, that were introduced and discussed earlier (see Table 6.4 on page 161 and Figure 6.13 on page 160), are reconsidered for detailed analysis of the automatic model building results. Summarized results are presented in Table 9.8, and the corresponding graphs are shown in Figures 9.4, 9.5, 9.6 and 9.7. Note that the standard deviations of the concentration estimates are calculated with the Nelder and Mead method (see section 5.3.3 on page 120), and not from replicate samples.

The first case, shown in Figure 9.4, illustrates the two above mentioned problems with

⁵How this pK_a position for model extension is determined is illustrated in Figure 5.16 on page 128.

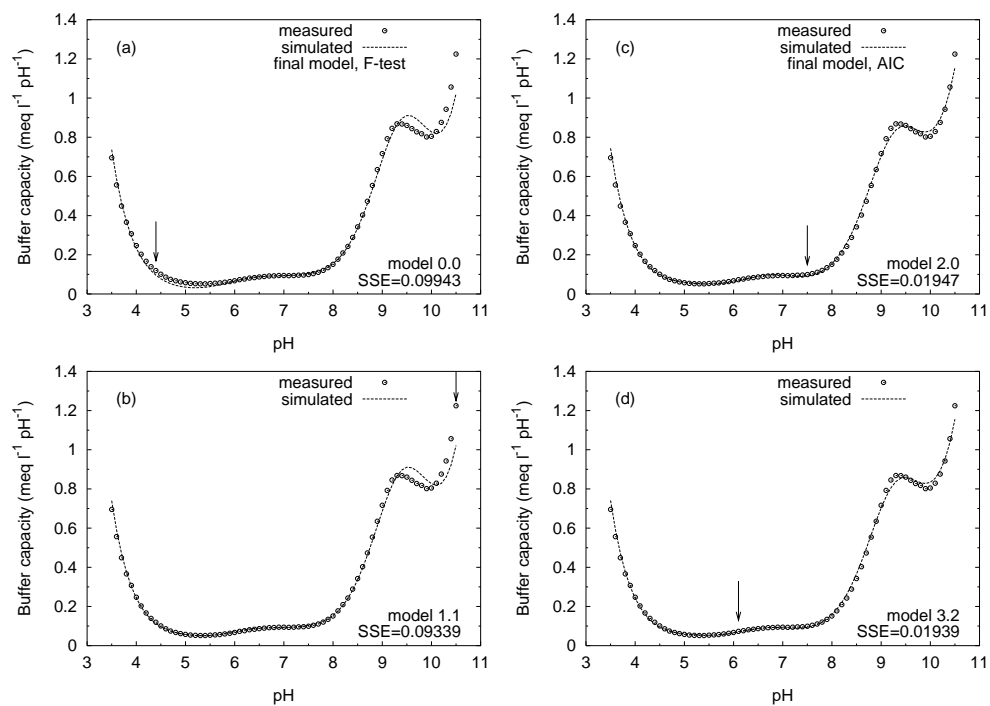


Figure 9.4: Experimental and simulated buffer capacity curves of the surface water Bassin Smedenstraat, Roeselare. The stepwise model building process starts with plot (a) (the zero model) and ends with plot (d). The final model for each model selection criterion is indicated on the graph. The arrows indicate the automatically proposed pK_a positions for model extension

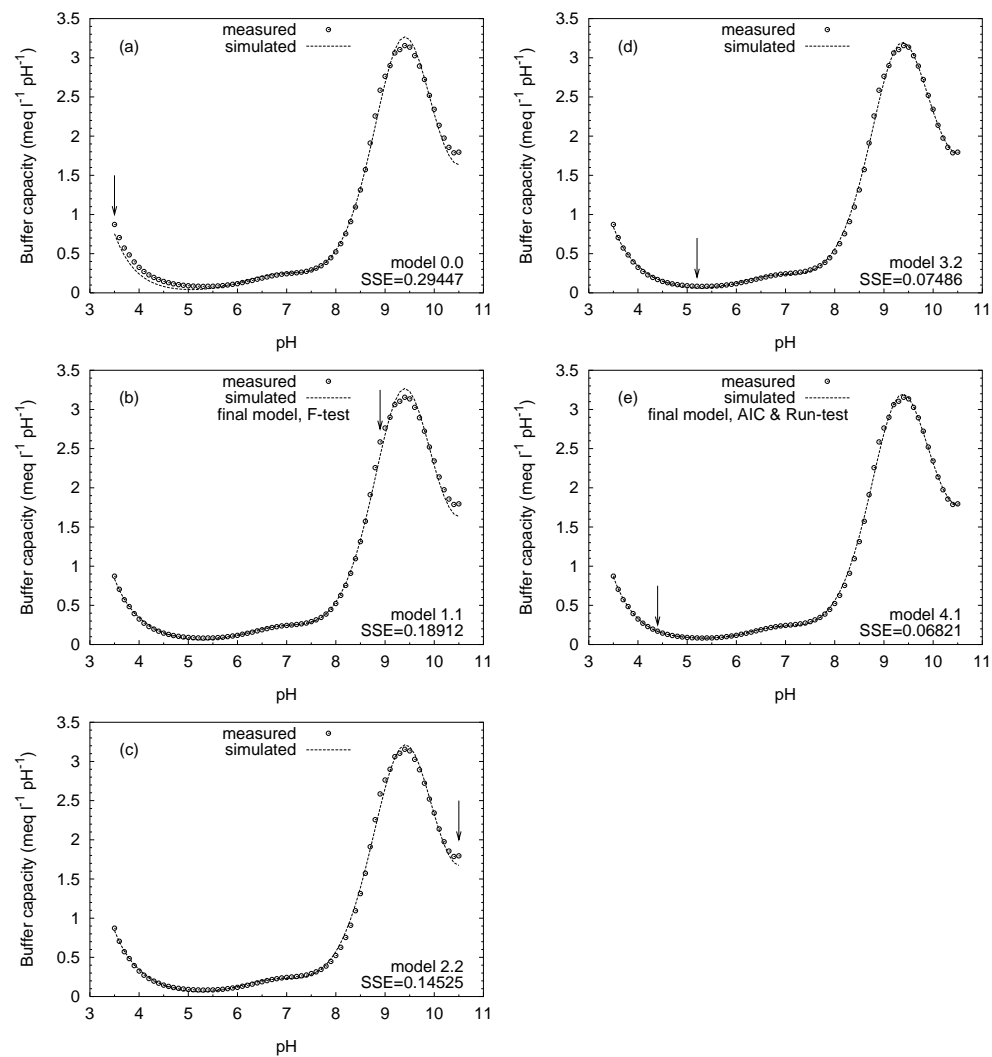


Figure 9.5: Experimental and simulated buffer capacity curves of the surface water Vuile beek, Ieper. The stepwise model building process starts with plot (a) (the zero model) and ends with plot (e). The final model for each model selection criterion is indicated on the graph. The arrows indicate the automatically proposed pK_a positions for model extension

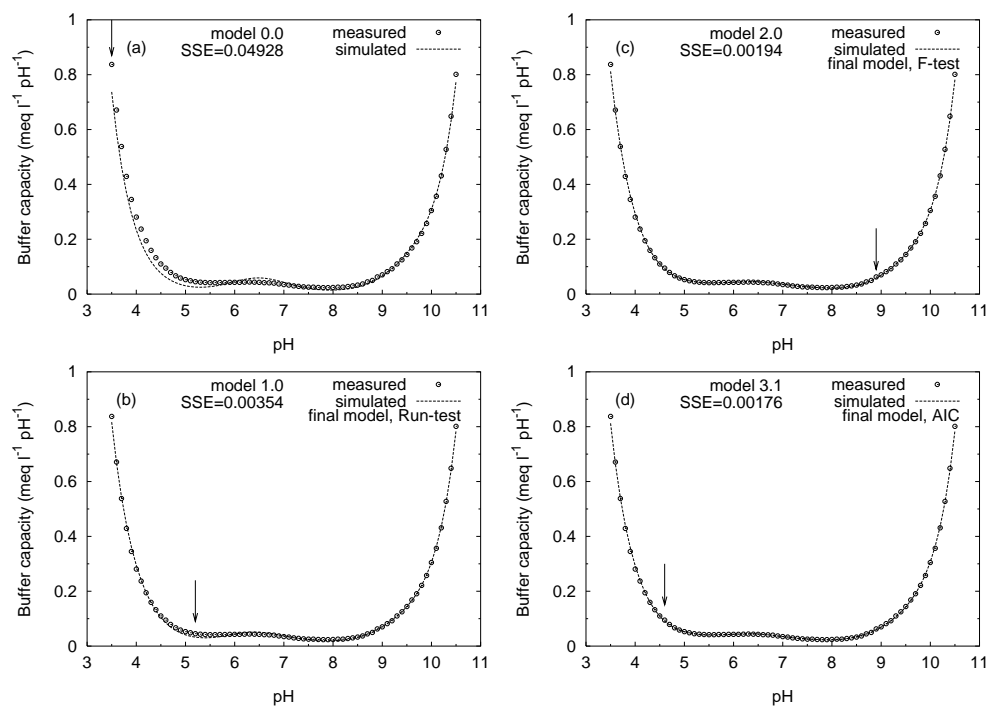


Figure 9.6: Experimental and simulated buffer capacity curves of the surface water Scherpenbergbeek, Poperinge. The stepwise model building process starts with plot (a) (the zero model) and ends with plot (d). The final model for each model selection criterion is indicated on the graph. The arrows indicate the automatically proposed pK_a positions for model extension

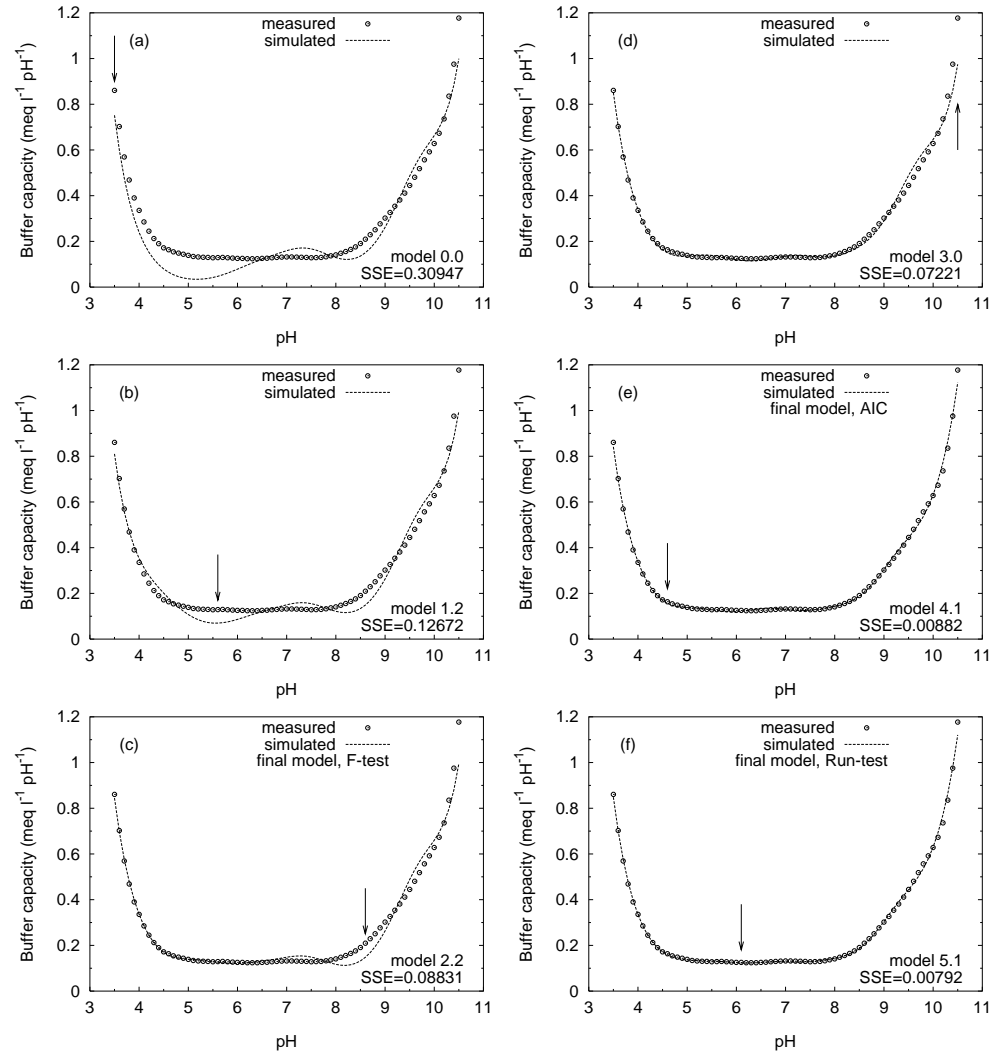


Figure 9.7: Experimental and simulated buffer capacity curves of the surface water Zarrenbeek, Staden. The stepwise model building process starts with plot (a) (the zero model) and ends with plot (f). The final model for each model selection criterion is indicated on the graph. The arrows indicate the automatically proposed pK_a positions for model extension

Table 9.8: Ammonium and ortho-phosphate model building results for 4 selected Flemish surface waters, compared with results previously described in chapter 6. The concentrations are expressed as $mg\ N\ l^{-1}$ or $mg\ P\ l^{-1}$ and the table entries are estimate \pm standard deviation

Buffer	Automatic model building results				Results of chapter 6		
	Figure	AIC	Run-test	F-test	laboratory ^a	AQMON	Figure
NH_4^+	9.4	17.8 ± 0.61	—	19.7 ± 0.48	10.9 ± 1.63	19.3 ± 0.12	6.13(a)
NH_4^+	9.5	72.7 ± 1.54	72.7 ± 1.54	77.3 ± 0.77	62.0 ± 4.81	76.7 ± 0.68	6.13(b)
NH_4^+	9.6	1.08 ± 1.20	1.15 ± 0.07	1.32 ± 0.08	0.33 ± 0.06	1.22 ± 0.04	6.13(e)
NH_4^+	9.7	6.29 ± 0.44	6.34 ± 0.37	9.82 ± 0.79	2.80 ± 0.28	8.98 ± 0.40	6.13(f)
<i>o</i> - PO_4	9.4	4.03 ± 3.67	—	2.68 ± 0.91	2.60 ± 0.57	2.36 ± 0.30	6.13(a)
<i>o</i> - PO_4	9.5	8.65 ± 2.89	8.65 ± 2.89	8.17 ± 2.10	8.45 ± 0.35	7.73 ± 2.13	6.13(b)
<i>o</i> - PO_4	9.6	0.70 ± 0.35	0.48 ± 0.18	0.79 ± 0.13	0.19 ± 0.04	0.62 ± 0.08	6.13(e)
<i>o</i> - PO_4	9.7	4.84 ± 1.06	4.19 ± 0.93	6.52 ± 0.96	3.25 ± 0.64	6.17 ± 0.60	6.13(f)

^a Mean and standard deviation of the laboratory A and B results in Table 6.4 on page 161.

respectively the F-test and the Run-test. The F-test selects the zero-model as the final model, although there is a clear extra buffer present at pH 4.5 (estimated in further models as a significant concentration of $0.05\ mmol\ l^{-1}$). The second problem is the Run-test criterion, which was never fulfilled in this case. For models 1.x, 2.x and 3.x the test statistic for the Run-test is still very significant ($u = -4.5$ or $p = 0.000007$), and becomes even more significant for the higher degree models (theoretically this is not possible, however as described earlier, optimization problems are the origin of this behaviour). The AIC criterion selects model 2.0, which is probably the best choice. A comparison of the titrimetric ammonium and ortho-phosphate estimations with the laboratory analysis (see Table 9.8) does not clearly indicate which model selection criterion gave the best estimations of N and P. The incorporation of an extra buffer at pH 10.5 has a positive influence on the estimated concentration of ammonium. However, the ortho-phosphate concentration estimated with model 2.0 is less reliable (very high standard deviation) and less accurate than the estimate with model 0.0. Even in the model with the highest degree, i.e. model 3.2 in Figure 9.4(d), still a visible lack of fit between pH 9 and pH 10 is noticed. This is caused by the ammonium buffer in the model, which is not perfectly fitted, together with the restriction that the model building algorithm may not introduce blind buffers at the pK_a positions reserved for known buffers, like ammonium.

In the second example, illustrated in Figure 9.5, the F-test selects model 1.1. This is an acceptable result, because the model fit for model 2.2 is only slightly better than model 1.1. The AIC and Run-test criterion select the model with 4 blind buffers as the final model. The two blind buffers at pH 8.9 and 10.2 make that the ammonium estimation is around $5\ mg\ N\ l^{-1}$ lower than in e.g. model 1.1. In this particular case, this has as a result that the ammonium estimation is closer to the laboratory value for model 4.1 compared to the result for model 1.1. The estimated ortho-phosphate concentrations differ only slightly when comparing the consecutive fitted models.

The third selected sample, shown in Figure 9.6, is an example of a clean surface water, with laboratory concentrations of N and P far below 1 mg l^{-1} . The F-test and AIC criterion select model 2.0 and model 3.1 respectively, which can be considered realistic models. However, the Run-test criterion selects model 1.0, which, from a practical point of view, is a model of too low degree. Earlier interpretations (see e.g. Figure 6.13(e)) have illustrated that at least two buffers are present in the pH range lower than 6. With the AIC and F-test criteria, two buffers in that range are detected, with pK_a 's respectively equal to 3.5 and 5.3. The behaviour of the Run-test criterion in this example is rather exceptional, because the Run-test more often selects models of too high degree (or the criterion is never reached). The final estimated concentrations of N and P are slightly influenced by the automatically built models compared to the previously obtained AQMON results.

The last selected sample, illustrated in Figure 9.7, was earlier described as the most extreme example for which the previously obtained model fit was unacceptable (see Figure 6.13(f)). Therefore, the earlier estimated concentrations of N and P could not be trusted. The automatically built models need at least 4 blind buffers for a reasonable model fit. This time, the F-test criterion fails because it selects a model of too low degree. The AIC and Run-test criteria select respectively model 4.1 and model 5.1, which are both considered realistic models. The N and P concentrations estimated with the latter two mentioned models are more closely to the laboratory data compared to the previously obtained AQMON results. This clearly illustrates the advantage of the automatic model building in this particular case.

At the current stage, for samples of the type 'surface water', it might be concluded that the AIC criterion is superior to the Run-test and F-test criterion. Although the AIC criterion sometimes tends to select high degree models, it does not suffer from the two major disadvantages of respectively the Run-test (i.e. that the criterion sometimes never fulfils) and the F-test (i.e. the selection of a too low degree model).

The ammonium and ortho-phosphate estimations resulting from automatically built buffer capacity models based on the AIC selection criterion were compared with the laboratory determined concentrations. This was performed for the 118 Flemish surface waters, similarly to what is illustrated in Figure 6.11 on page 158. The only but important difference is that the results of chapter 6 were obtained with a fixed buffer capacity model, whereas in this chapter, the results are derived from automatically built models, custom-made for each individual sample. Despite the significantly better results for a number of individual samples (see also some of the selected samples above) with the automatic modelling approach, the overall comparison between laboratory and titrimetric results via scatterplots was only slightly different from the results described in chapter 6 (results not shown). In about 5 % of the samples, it was found that the automatically built final model did not fit sufficiently to the experimental data, due to the selection of a model with a too low degree. This problem was already described in section 9.2.3 and originates from a local minimum problem of the parameter estimation algorithm. Fortunately, the problem is well-defined, and a suggestion for an alternative algorithm (backward elimination) that doesn't suffer from this shortcoming was formulated in section 9.2.4. Also the Run-test is a reasonable alternative for these problematic cases.

Table 9.9: Ammonium and ortho-phosphate model building results for 3 selected effluent samples, compared with prior obtained results in chapter 6. The concentrations are expressed as $mg\ N\ l^{-1}$ or $mg\ P\ l^{-1}$ and the table entries are estimate \pm standard deviation

Buffer	Automatic model building results		Previously obtained results	
	Figure	AIC	laboratory ^a	AQMON
NH_4^+	9.8(a1)–(a2)	10.8 ± 0.42	5.89 ± 0.02	14.9 ± 0.19
NH_4^+	9.8(b1)–(b2)	17.0 ± 0.82	16.4 ± 3.68	23.1 ± 0.60
NH_4^+	9.8(c1)–(c2)	4.87 ± 0.94	2.03^b	8.03 ± 0.33
<i>o</i> - PO_4	9.8(a1)–(a2)	2.89 ± 2.38	1.79 ± 0.02	2.36 ± 0.30
<i>o</i> - PO_4	9.8(b1)–(b2)	5.95 ± 7.07	5.75 ± 2.62	9.43 ± 1.41
<i>o</i> - PO_4	9.8(c1)–(c2)	6.43 ± 4.79	6.55 ± 1.06	14.7 ± 0.87

^a Mean and standard deviation of the laboratory A and B results.

^b There is only 1 laboratory result.

Effluents

The automatic buffer capacity model building of effluent samples gives results similar to the surface waters. However, some new interesting phenomena were observed for the industrial effluent samples. One domestic wastewater effluent (Hofstade, sampled at October 19, 1993) and two industrial effluent samples (sampled respectively at April 20 and 27, 1994) are selected for more detailed analysis and discussion. The summarized results of the selected samples are given in Table 9.9, and the corresponding graphs are shown in Figure 9.8.

The first example, illustrated in Figure 9.8(a) is a typical case of buffers interfering with the ammonium estimation. Without automatic model building, the estimated ammonium concentration was about three times higher than the measured laboratory concentration. With automatic model building, two interfering buffers at pH 9 and 10.5 of respectively 0.1 and 0.6 $mmol\ l^{-1}$ are recognized. As a consequence, the ammonium estimation becomes lower than before, but the estimation is still almost two times higher than the laboratory concentration. This indicates that other interferences could be present at the same pK_a as ammonium. No interfering buffers around the ortho-phosphate pK_{a2} are found, and, thus the estimated ortho-phosphate concentration is not significantly different compared to the previously obtained results. The standard deviations on the estimates of ortho-phosphate are rather high, indicating a high uncertainty of the estimated values. The presence of the IC buffer and blind buffers in the neighbourhood of the ortho-phosphate buffer is pointed to as a reason for this.

The second and third example represent industrial effluent samples that were both taken in the third month of the measurement period. As mentioned in section 6.3.3 on page 151, the wastewater treatment plant was in a start-up phase, with very high ammonium concentrations ($> 200\ mg\ N\ l^{-1}$) in the first two months and lower concentrations ($< 20\ mg\ N\ l^{-1}$) in the last month of the measurement period. For the samples taken in the first two months, the fixed model approach (chapter 6) resulted already in an acceptable agreement between the exper-

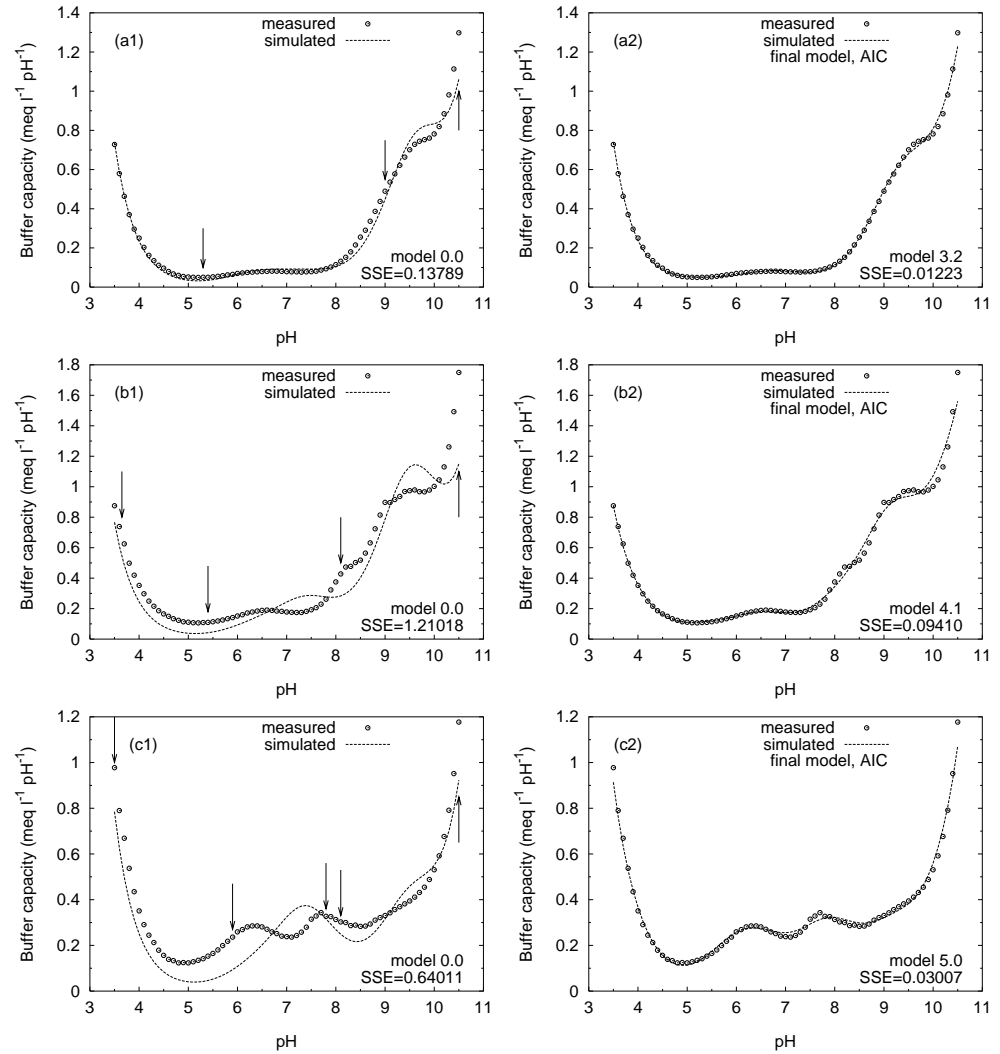


Figure 9.8: Experimental and simulated buffer capacity curves of a domestic wastewater effluent (a) and an industrial effluent (b) and (c). Two plots per sample show respectively the zero model (1) and the AIC selected final model (2). The arrows indicate the automatically proposed pK_a positions for model extension

imental and simulated data, and the automatic modelling approach produced similar results (results not shown). However, in the third month, extra buffer systems on top of the expected buffers appeared in the buffer capacity profiles, resulting in the bad fixed model fit reported in chapter 6. It is in the latter period that the automatically built models are found superior compared to the previously used fixed model with only water, ammonium, ortho-phosphate, IC and a 'soap' buffer. The extra added blind buffers were not always found at the same pK_a positions for the different samples, as illustrated in Figure 9.8(b1) and (c1). Consequently, it was found that the ortho-phosphate and ammonium concentrations estimated with the automatically built models are much closer to the laboratory data compared to the previously obtained results (see Table 9.9).

9.3.3 Conclusions

It has been illustrated that the application of automatically built buffer capacity models mostly results in similar or better estimations of ammonium and ortho-phosphate compared to fixed buffer capacity models. For a number of selected samples (e.g. the industrial effluent samples in the last weeks of the measurement period), the estimations with automatically built models are highly superior to the fixed model approach.

In general, for all samples, the agreement or correlation between the estimated ammonium and ortho-phosphate concentrations and the laboratory concentrations was found similar for the fixed model approach compared to the automatic modelling approach. This can be explained by the following reasons. First, buffers with pK_a values that differ less than 0.5 from the pK_a value of ammonium or the pK_{a2} value of ortho-phosphate are modelled as respectively ammonium or ortho-phosphate. Both the fixed and the automatic modelling approach are influenced by such interfering buffer systems. Second, the uncertainty on the laboratory measurements is reflected by the residual variance that was noticed between the two laboratories (see e.g. differences between laboratories A and B on Figure 6.11 on page 158). Consequently, it is not expected that for any buffer capacity modelling approach, the obtained results would be much better than what was previously illustrated.

The benefits of the automatic buffer capacity model building compared to the fixed buffer capacity modelling can be summarized as follows:

- With the automatic modelling approach, it is possible to use a wider simulation pH range (e.g. between pH 3 and pH 11), whereas with the fixed model approach, one attempts to choose an as small as possible interval, to avoid problems of interfering buffers outside the strict pH range of interest. A larger simulation interval allows to detect more interfering buffers, without a negative influence on the ammonium and ortho-phosphate estimations.
- An automatic modelling approach allows to adapt the model quickly and efficiently to changing sample compositions. In the case of the industrial effluent, it has been shown that the most adequate buffer capacity model at the end of the measurement period was different from the best model at the beginning of the measurement period.
- If detailed a priori knowledge about the sample composition is available, one can define this buffer information in a 'rich' zero model. If the automatic model building environment does select this zero model as the final model, it ensures that the zero model is

still valid as an adequate model. If the final model is different from the zero model, it points to changing buffer compositions in the sample. Further, the concentrations of ammonium and ortho-phosphate estimated with the zero and final model can be compared. If there are notable differences, it points to possible interferences in the neighbourhood of the buffers of interest. Consequently, the estimated ammonium and ortho-phosphate concentrations should be considered uncertain.

- Automatic buffer capacity modelling is useful for alarm generating purposes in case there are extra buffers detected and quantified on top of the expected buffers defined in the zero model. The model building algorithm will add blind buffers in order of importance, and therefore the interpretation of the sequentially added buffers ‘blind1’, ‘blind2’, ... is automatically performed in order of importance. The corresponding standard deviations on the estimates can be used to statistically test whether the reported concentrations are significantly different from 0.

9.4 Algal wastewater treatment applications

9.4.1 Materials and methods

The titration curves described in chapter 7 are reconsidered for automatic buffer capacity modelling. The up titration profiles (from pH 2.5 to pH 11) of the algal reactor influent (sample code EVC), the content of the algal bioreactor (sample code AP) and the effluent of the algal pilot plant (EAP) were used to validate and extend the findings of the previous section. The details about the sampling, the data collection and the applied mathematical models are given in section 7.2 on page 168.

The applied methodology is very similar to the methodology described in section 9.3.1. The zero model or starting model is chosen in correspondence with the model specifications given in Table 7.2 on page 171, except for the following modifications:

- The ‘soap’ buffer and the ‘blank1’ buffer are not included in the zero model.
- The simulation interval (between pH 4 and pH 10 in chapter 7) is now extended to an interval between pH 3.5 and pH 10.5.

Based on the above description, the automatic model building algorithm may stepwise enter blind buffers in the model, but not with pK_a 's in the pH ranges 7 – 7.8 and 9 – 9.5, which are the lower and upper limits for the variable pK_a values of respectively ortho-phosphate and ammonium. All other settings for the automatic model building algorithm in *bomb* are the same as used in section 9.3.

There is an important particularity about the previously introduced fixed buffer capacity model (specifications in Table 7.2 on page 171). This model contains a ‘blank1’ buffer with pK_a between 9.4 and 11.5. In the first stage of the model development, this buffer was not included in the model, and the ammonium estimations were systematically too high (the estimated NH_4^+ concentration was 2 mg N l^{-1} higher than the laboratory result). After careful manual interpretation of the goodness of fit on different samples, it was recognized that there was probably an unknown buffer present with a higher pK_a than the pK_a of ammonium. In a later stage, the ‘blank1’ buffer was added in the model, and the minimum and maximum

Table 9.10: Frequency table of 37 algal pilot plant samples, classified towards the final model degree and the applied model selection criterion

Final model degree	AIC	Run-test	F-test
0	13	0	22
1	12	13	8
2	7	18	7
3	5	2	0
4	0	2	0
5	0	1	0
6	0	1	0

allowable value for its pK_a were chosen on the basis of the obtained results with a number of samples. Finally, the extended model was tested with all available titration curves, and the estimated ammonium concentrations were found to correspond significantly better with the laboratory determined concentrations. Later, the interfering buffer around pH 10 was suggested to originate from silicates, however, this was not analytically validated. Summarized, it can be concluded that quite some ‘expert’ time and knowledge were necessary to define an useful fixed buffer capacity model for the algal pilot plant application. Consequently, an interesting point that will be investigated in the next section is whether the automatic buffer capacity modelling algorithm will be able to automatically detect and quantify the interfering buffer around pH 10, without influencing the correctness of the ammonium estimation.

9.4.2 Automatic model building results

The three model selection criteria, being AIC, Run-test and F-test, were evaluated on all available titration curves. Summarizing frequency tables with the counts of titration curves corresponding with final model degree for each of the three model selection criteria are given in Table 9.10. The interpretation of these results is similar as in section 9.3.2. In many cases, the F-test criterion selects a too low degree model, whereas in the majority of the samples the Run-test criterion yields the most realistic final model.

The simulation results previously obtained with the fixed buffer capacity model, and the automatic model building results of one selected AP sample (August 4, 1997) are illustrated in Figure 9.9. The summarized results for the ortho-phosphate and ammonium estimations with the different models are presented in Table 9.11. The automatic model building process proceeds as expected, i.e. it detects and quantifies a number of buffers which were not included in the zero model. The first blind buffer is located at pH 5.1 and quantified as 0.1 mmol l^{-1} . The second blind buffer is located at pH 10.5 (which is the upper limit for pK_a values of blind buffers, thus the real pK_a of this buffer could be higher) and is quantified as 0.3 mmol l^{-1} . The third blind buffer at pH 7.8 has a concentration of 0.09 mmol l^{-1} , which is not significantly different from 0. Thus, the model with 3 blind buffers can be considered ‘overparametrized’ for this particular case.

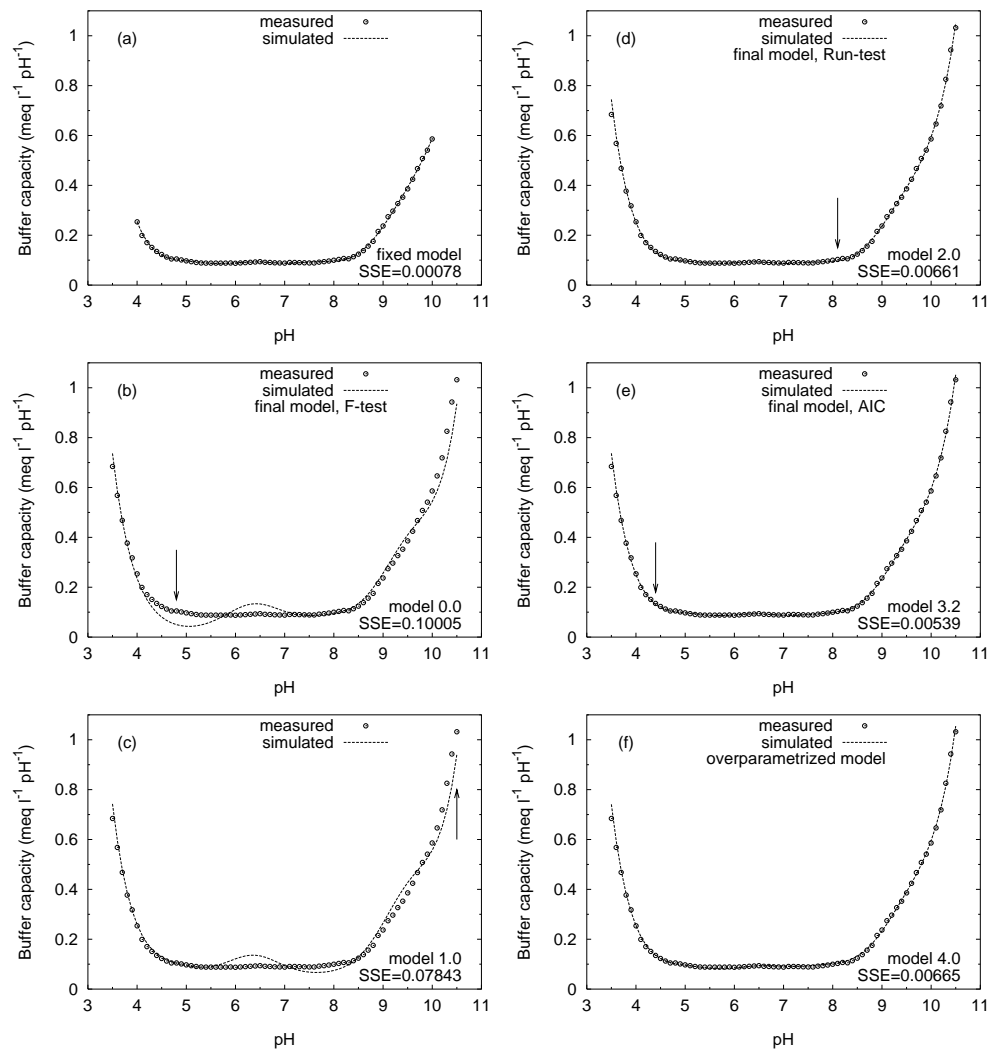


Figure 9.9: Experimental and simulated buffer capacity curves of an AP sample. Plot (a) shows the previously obtained results (chapter 7) and plots (b)–(f) show the results obtained with the stepwise model building process. The arrows indicate the automatically proposed pK_a positions for model extension

Table 9.11: Ammonium and ortho-phosphate model building results for the selected AP sample, compared with results previously obtained in chapter 7. The concentrations are expressed as $mg\ N\ l^{-1}$ or $mg\ P\ l^{-1}$ and the table entries are estimate \pm standard deviation

Buffer	Automatic model building results			Previously obtained results	
	AIC	Run-test	F-test	laboratory	AQMON
NH_4^+	5.07 ± 0.45	4.80 ± 0.47	6.53 ± 0.43	2.8	3.74 ± 0.66
$o\text{-}PO_4$	0.79 ± 1.87	3.38 ± 0.22	2.57 ± 0.83	3.3	3.45 ± 0.66

When comparing the final model degree for the different model selection criteria, one can conclude that the F-test selects a too low model degree (see also the previously described problem typically related to the F-test), whereas the AIC criterion selects a too high model degree. In this example, the Run-test practically selects the most appropriate model. Figure 9.9(f) illustrates a parameter estimation problem when 4 blind buffers are entered in the model. The fitted model has a higher SSE compared to the model with only 3 blind buffers. This is theoretically not possible because the simpler model is a subset of the more complex model. In the software *bomb*, the user is warned for such problem.

The effect of the selected model on the ammonium and ortho-phosphate estimation is illustrated in Table 9.11. The ammonium estimates of the automatically built models are all higher than the laboratory and previously obtained results. For model 0.0 (final model, F-test), the highly overestimated ammonium concentration can easily be explained because this model does not include the interfering buffer around pH 10. For both other final models, the estimated ammonium is also higher than the previously obtained results, however, this could be due to the wider simulation interval (the upper limit for simulation is pH 10.5 and not pH 10 as before). The AIC selected final model completely fails to properly estimate the ortho-phosphate concentration, because the neighbouring and insignificant blind3 buffer at pH 7.8 is interfering with ortho-phosphate. A wider interval for the variable pK_{a2} of ortho-phosphate, in which no blind buffers are allowed to enter would partially solve this problem. The Run-test selected model and the original fixed model produce the best estimates of ortho-phosphate.

9.4.3 Conclusions

Generally, the ammonium and ortho-phosphate concentrations estimated with the automatically built buffer capacity models were not very different from the results previously obtained with the fixed buffer capacity model. This points to the correctness and usefulness of the fixed buffer capacity model. On top of the a priori expected buffers IC, ortho-phosphate and ammonium, the automatic modelling algorithm introduces two significant extra buffers around pH 5 and pH 10.5. This corresponds with the two blank buffers that were already foreseen in the fixed buffer capacity model. The Run-test criterion selected in most cases the model with these 2 blind buffers, which agreed best with the practical observations.

The most important benefit of the automatic modelling approach is that the algorithm de-

tests and quantifies a priori unexpected buffers, without direct negative influence on the accuracy of the estimated concentrations of the a priori known buffers. More particularly, the specifications of the fixed buffer capacity model (chapter 7) are the result of manual interpretations of experimental buffer capacity profiles, followed by trial and error simulation experiments with various ranges for the simulation interval and the pK_a values that are allowed to vary. The optimal settings for the fixed buffer capacity model were obtained by comparison of the estimated concentrations of ammonium and ortho-phosphate with their respective laboratory concentrations. This is a manual and labour intensive process, that can only be performed by an expert user. Therefore, the automatic modelling approach can take over some of the efforts needed in the fixed model development phase. Consequently, the automatic modelling can adapt quickly to new situations or new types of samples. The task of the expert user in the model development phase is then limited to the interpretation of the final models and eventually modify a number of settings like the simulation interval, the buffers to be included in the zero model and the selection of an appropriate model selection criterion.

9.5 Destructed manure applications

9.5.1 Materials and methods

The collection and modelling of buffer capacity curves originating from destructed and diluted manure samples is described in chapter 8. In the framework of automatic buffer capacity model building the model development results described in section 8.4.7 on page 210 are important to consider. A number of specific particularities about the modelling of destructed manure samples can be summarized as follows:

- The a priori knowledge about the destructed manure samples is much higher compared to e.g. effluent or surface water samples. The main buffers that are expected in the experimental buffer capacity profiles are ortho-phosphate and ammonium. Inorganic carbon and silicates are two known interfering buffers, and a number of complexation reactions with e.g. Fe^{3+} are responsible for extra buffer capacities around pH 5 and pH 8. This a priori knowledge was intensively used in the development phase of an adequate fixed buffer capacity model in chapter 8.
- The fixed buffer capacity models that incorporated the extra buffers around pH 5 and/or pH 8 resulted in a better model fit compared to the models without these extra buffers. However, the estimated N and P were best in the simpler type of buffer capacity models (see e.g. Table 8.17 on page 211 and Figure 8.9 on page 212). This illustrates that the goodness of fit for this application is not the best criterion for accurately estimated concentrations of ammonium and ortho-phosphate.

With the information presented above, it is doubtful whether automatically built models will be the preferred models for practical use in the framework of accurate N and P estimations. Therefore, the benefit of automatic model building has to be seen in the context of finding 'extra' knowledge and information on top of the estimated N and P concentrations. Therefore, the following topics will be investigated in more detail in the next section:

Table 9.12: Frequency table of 253 destructed manure samples, classified towards the final model degree and the applied model selection criterion

Final model degree	AIC	Run-test	F-test
0	2	29	3
1	59	162	113
2	42	53	91
3	52	8	38
4	98	1	8

- Can the automatic model development detect and quantify at least the two known interfering buffers at pH 5 and 8?
- Are the automatically built models useful to obtain confidence information on the estimates of N and P (e.g. interfering buffers close to ammonium or ortho-phosphate can induce a higher standard deviation on the N and P estimates)?
- Can the automatically built final model be used for the detection of problems related to the experimental titration conditions (e.g. the appearance of unexpected buffer systems)?

The applied model building methodology is similar as described in the previous sections. The zero model is based on the model specifications of model 2 in Table 8.16 on page 211, except for the following modifications:

- The fixed pK_{a2} of ortho-phosphate (which was 6.7) is now allowed to vary between 6.3 and 7.1. This ensures that no blind buffers are entering in that pH range.
- The simulation interval (between pH 5.6 and pH 10.5 in chapter 8) is now between pH 4 and pH 10.5.

The settings of the automatic model building algorithm are the same as used in section 9.3, except that the maximum number of blind buffers that may stepwise enter in the model is 4 instead of 6. The experimental data (53 manure samples, 253 titration curves) used for the evaluation of three model selection criteria is described in section 8.5 on page 216.

9.5.2 Automatic model building results

The model selection criteria AIC, Run-test and F-test were tested with the 253 titration curves. Summarizing frequency tables with the counts of titration curves corresponding with the final model degree for each of the three model selection criteria are given in Table 9.12. These results are different compared to the interpretations described in previous sections. The F-test criterion does not wrongly select the zero model as final model any more, and the Run-test no longer suffers from the problem that this criterion never becomes fulfilled. However, especially the Run-test and also the F-test tend to select a too low final model degree. This problem and its possible solution are discussed later in this section. In the cases where 4 blind buffers are

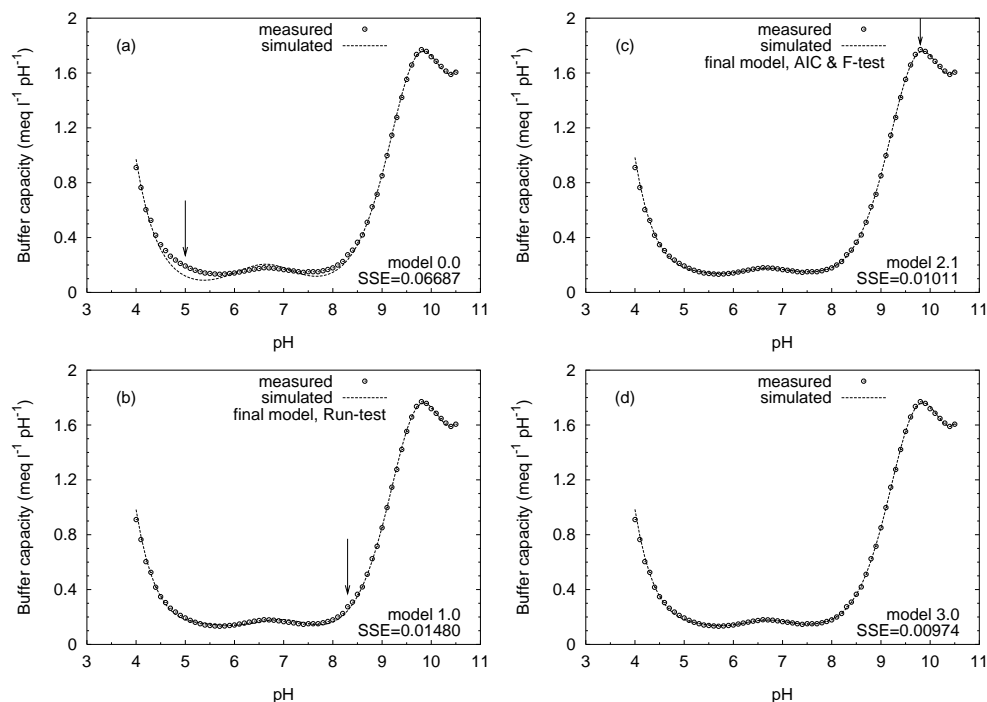


Figure 9.10: Experimental and simulated buffer capacity curves of one selected manure sample. The stepwise model building process starts with plot (a) (the zero model) and ends with plot (d). The final model for each model selection criterion is indicated on the graph. The arrows indicate the automatically proposed pK_a positions for model extension

entered in the final model (mostly the case with AIC), their pK_a values are around 4, 5, 8 and 10.

The selected sample that illustrated the buffer capacity model development in section 8.4.7 on page 210 is reconsidered for the illustration of the automatic model building process. The stepwise model building results are illustrated in Figure 9.10 and the corresponding estimated concentrations of ammonium and ortho-phosphate are presented in Table 9.13. First, it can be remarked that the zero model gives the best estimates, especially of ortho-phosphate. This is in correspondence with the results previously obtained in chapter 8. Second, the two known interfering buffers around pH 5 and 8 are correctly introduced in the buffer capacity model in order of importance (model 1.0 and model 2.1). Third, the fit of the model with 1 blind buffer is already acceptable, such that the Run-test criterion is fulfilled ($u = -2.96$ or $p = 0.003$) at the model 1.0 stage. The AIC and F-test criterion both select the model with 2 blind buffers, which is the most realistic choice, because the buffer at pH 8 is to be expected from a theoretical point of view, and this buffer has an estimated concentration which is still significantly different from zero ($\alpha = 0.05$). For this type of destructed manure samples, a better choice for the critical significance level in the Run-test and the F-test would be $\alpha = 0.001$ instead

Table 9.13: Ammonium and ortho-phosphate model building results for the selected manure sample. The concentrations are expressed as $mg\ N\ l^{-1}$ or $mg\ P\ l^{-1}$ and the table entries are estimate \pm standard deviation

Buffer	Model 0.0	Model 1.0	Model 2.1	Model 3.0	laboratory
NH_4^+	38.3 ± 0.41	38.4 ± 1.52	38.4 ± 0.89	$30.9 \pm ?^a$	36.5
$o-PO_4$	9.62 ± 0.52	8.11 ± 1.47	6.83 ± 1.33	7.44 ± 1.34	9.82

^a Standard deviation cannot be calculated (NaN detected in variance-covariance matrix).

of the previously used $\alpha = 0.0001$. This modification would allow that both the Run-test and the F-test select model 2.1. Fourth, the model 3.0 is considered as an ‘overfitted’ model. The estimated ammonium concentration is much lower and worse than with the previous models, because of the blind3 buffer introduced at pH 9.8. Fifth, the standard deviations on the parameter estimates of ammonium and ortho-phosphate with model 2.1 (the most realistic model) are twice the respective standard deviations with model 0.0 (the most adequate model for accurate estimation of N and P). However, it is considered ‘safer’ and more realistically to use the standard deviations on the estimates with model 2.1 instead of the standard deviations with model 0.0. The latter statement is justified by the fact that the most adequate fixed model neglects the influence of the two interfering buffers around pH 5 and pH 8 because these buffers are a priori excluded from the model (the only reason for this was to obtain better estimates of N and P), whereas in chapter 8 it was found that these two interfering buffers are indeed present in reality. The automatically built models incorporate these two ‘real’ buffers and are thus considered to represent the real number of buffers more closely compared to the fixed model.

Another aspect that was investigated is the possibility of the automatic model development to detect unexpected buffer capacity changes caused by e.g. the experimental titration conditions. A randomly selected example for this purpose is a manure sample for which a number of replicate titration curves were recorded under various conditions.⁶ Three replicates of 1 sample, illustrated in Figure 9.11(a), were prepared and titrated under various conditions:

Replicate 1 : Correct experimental conditions

Replicate 2 : The NaOH 0.1 N titrant solution was contaminated with IC and silicates

Replicate 3 : A stirring problem prior to titration introduced extra IC in the buffer capacity profile, originating from the NaOH 1.5 N stock solution

Each of these replicate buffer capacity profiles was used for automatic model building with a slightly modified zero model, because the IC buffer was no longer incorporated. This allowed to investigate whether the automatic model building algorithm is able to separate the IC buffer from the ortho-phosphate buffer as two individual buffers. The results of the final model (with the AIC criterion) for each of the replicates are illustrated in respectively Figure 9.11(b)–(d). Replicate 1 is modelled with 2 extra blind buffers around pH 5 and pH 8, which was earlier

⁶Titrant related problems (see section 8.5 on page 216) caused a bad reproducibility of the experimental buffer capacity profiles. Consequently, a number of titration curves were omitted from the validation experiment described in chapter 8.

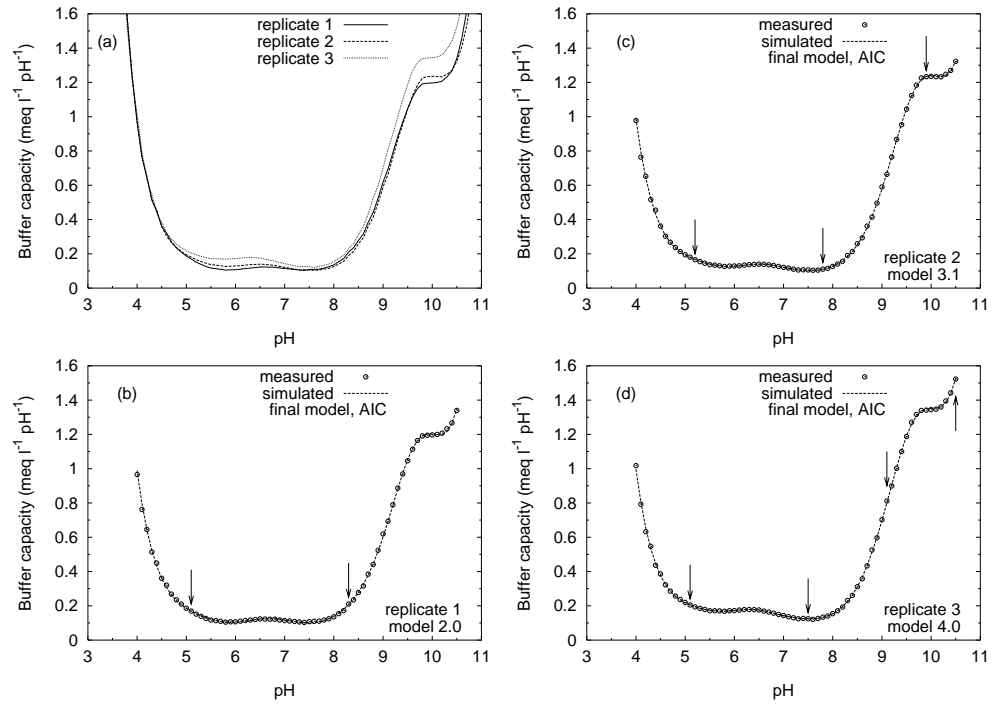


Figure 9.11: Plot (a): Experimental buffer capacity profiles of three replicates of one destructed and diluted manure sample, under various conditions. Plots (b)–(d): The experimental and final model simulated buffer capacity curves of each replicate of Plot (a) respectively. The arrows indicate the positions of the incorporated blind buffers

described as the most appropriate model for this type of samples. However, the same model building algorithm applied to replicate 2 and 3 results in final models of a higher degree (respectively 3 and 4 blind buffers were added). The extra modelled buffers have an estimated concentration significantly different from 0, except the buffer at pH 9.1 added in replicate 3. This example illustrates that extra information about the sample can potentially be obtained by applying the automatic buffer capacity model building algorithm to the experimental data. If the selected final model contains extra blind buffers between pH 9 and pH 10.5, this is a first indication that additional interfering buffers could be present. The extra IC buffer capacity around pH 6 in replicate 2 and 3 (first dissociation step of H_2CO_3^*) is not recognized as an extra buffer at that pH, but spread out over the ortho-phosphate buffer and the other neighbouring blind buffer. The latter finding points to an important aspect related to the interfering IC around pH 6, i.e. the impossibility of automatic separation of the interfering IC buffer from the neighbouring ortho-phosphate buffer (the pK_a separation between both buffers is only between 0.1 and 1).

9.5.3 Conclusions

Due to the ample a priori knowledge that is available about the destructed manure samples, and the earlier finding (chapter 8) that the best fitting model does not yield the best N and P estimates, the automatic model building benefits have to originate from the extra information that can be generated.

The automatic model building algorithm easily detects and quantifies the two most important interferences originating from complexation reactions around pH 5 and pH 8. Despite the fact that the zero model often results in the most accurate estimates of ammonium and ortho-phosphate (see results in chapter 8), it is suggested that for confidence calculations on these estimates, it is safer to use the standard deviations from the automatically built final model. In most cases such final model includes one or more blind buffers compared to the zero model.

It has also been demonstrated with a randomly selected example that a potential benefit of the automatic modelling approach is the detection of problems related to the experimental titration conditions. If there is e.g. a titrant contamination with IC or silicates, this is reflected in the number of blind buffers incorporated in the final model. This is an interesting property for robustness and verification of the produced results in later field-use.

It was experienced that no simple model selection criterion can be considered as the 'best' criterion. The AIC criterion was experienced most useful. However, a well-chosen modification of the critical significance level α for the Run-test and F-test would make the performance of these tests more realistic. The α was earlier equal to 0.0001, but for this particular manure application it is proposed that 0.001 is a better choice.

9.6 Summarizing conclusions

The automatic model building algorithm that is implemented in the software *bomb* has been applied to many titration curves of diverse samples, with the objective to develop tailor-made buffer capacity models. A number of shortcomings that were detected and described in the first

development stage of this algorithm [299] are now completely solved. At present, the model building algorithm has been evaluated as robust and fail-safe.

Six different model selection criteria were evaluated for the purpose of selecting the most appropriate model from the pool of automatically built models for each individual sample. The AIC, AIC_C, FPE and SIC criteria were found to perform very similar. The Run-test and F-test criteria often have a different behaviour compared to each other and compared to the AIC and related criteria. There is no 'best' criterion for general purposes, because all criteria have their advantages and disadvantages. On the one hand, the AIC and related criteria sometimes select overparametrized models, but on the other hand, they have the advantage of generally satisfying performance, and being independent of a user-defined critical significance level α . The Run-test sometimes suffers from the problem that its solution criterion is not fulfilled for any of all models built, whereas the F-test sometimes selects a model with a too low model degree. The necessity of a user-defined α for the Run-test and the F-test has advantages and disadvantages. The advantage is that the user has an extra tuning facility, by choosing a critical significance level that best suits the practical purposes. The disadvantage is that the best choice for α is case dependent and should be tuned in function of the application. An interesting perspective for further research could be to use a combination of the final model results with the different model selection criteria. The final model selected by each of the criteria could be introduced in an 'expert system' that can make a choice based on the pro's and contra's known for each criterion.

The benefits of automatic model building compared to a fixed model approach are different for various applications. In situations where the a priori knowledge about the sample is already high (e.g. the algal and manure samples), the main benefit of the automatic model building is that extra information about the sample can be obtained. This includes the detection of unexpected or interfering buffers (e.g. silicates) and the detection of experimental problems in the titration system. The estimates of ammonium and ortho-phosphate with a fixed modelling approach are often better compared to the automatic modelling results. However, the calculated standard deviations on the concentration estimates with the automatically built models are suggested to be superior compared to the standard deviations obtained with a fixed model. In the other situations, where the a priori knowledge is not high (e.g. many river and effluent samples), some spectacular increases in the accuracy of the estimated ammonium and ortho-phosphate concentrations occurred with the automatically built models compared to a fixed model. For some applications (e.g. the industrial effluent), a fixed model approach is not useful because the buffer composition of the effluent stream can continuously change. The automatic modelling approach is also advantageous for alarm generating purposes on e.g. river waters, because unexpected buffers are easily detected and can be added in the buffer capacity model. The list of blind buffers with their respective concentrations and standard deviations can then be used to report extra buffer systems on top of the a priori expected buffers defined in the zero model. Again, a small 'expert system' could be implemented to interpret these automatic model building results, with the purpose of alarm triggering.

For fixed model implementations, mostly a narrow simulation pH interval is chosen, in function of the buffers to be quantified and to avoid the influences of neighbouring interfering buffers (e.g. for the manure samples fixed model, a simulation interval between pH 5.6 and pH 10.5 was chosen for this purpose). The automatic model building environment can be applied by an expert user as a supporting tool for a quick characterisation of unknown buffer capacity

profiles. In practical situations where a fixed buffer capacity model has to be developed, applying the automatic modelling approach on a number of preliminary samples can help the expert user to define the most appropriate fixed model. The automatic modelling approach allows the user to choose a wider pH simulation interval (e.g. from pH 3 to pH 11) in order to detect and quantify more buffer systems.

A final, concluding remark can be made about the results obtained in this chapter. The automatic model building approach was investigated and evaluated at the end of this Ph.D. study. More particularly, the data collected for various applications described in the previous chapters were reconsidered here for possible new applications such as alarm generation, titrator problem detection, expert user support, etc. The obtained results point to certain benefits resulting from the automatic model building approach, however, further research should be performed in order to validate and confirm the preliminary results obtained in this chapter. As an example, it would be very useful to incorporate a buffer capacity based sensor in a river monitoring network, while measuring other water quality variables at the same site and time. Under such conditions, the interpretation of continuously collected buffer capacity profiles would allow a more thorough evaluation of the new ideas presented in this chapter.

Chapter 10

General discussion and conclusions

In this work, a multipurpose titrimetric sensor was developed. Initially, the aim was to develop an automated on-line sensor for use in water quality monitoring of rivers and effluents (AQMON project, see chapter 6). Since 1991, the quality of surface waters and effluents in Flanders is expressed in 'polluting units'. The mathematical expression for the calculation of the 'polluting units' considers oxygen binding substances (COD and BOD), suspended solids, nitrogen, phosphorus and heavy metals. Within this framework, the primary goal was to develop a sensor that is capable to quantify several components of the 'polluting units' with one measurement principle. The application of such a sensor was seen in the context of an automatic measurement network (e.g. to monitor a river network). Continuous monitoring of surface waters and potentially polluting river inputs (e.g. effluents) is a promising support tool for a better supervision and control of surface water quality. The initial research performed in the AQMON project was exploratory, and rather ambitious. With appropriate sample pre-treatments, research was performed to measure BOD_{st} , NO_3^- , NH_4^+ and $o-PO_4$ from buffer capacity profiles. In further stages of the project, the ambition was tuned down and the attention was focussed towards those topics that had the best potential value for field application. The ammonium and ortho-phosphate assessment from the buffer capacity profile showed the best potentials for field-use, and it was expected that the buffer capacity curve itself could serve as a kind of 'fingerprint' of the water quality. The AQMON sensor was thus proposed as an automatic buffer capacity based multipurpose hard- and software sensor.

In a later phase, the same methodology was implemented for the monitoring of an algal tertiary wastewater treatment plant (see chapter 7). Besides the ortho-phosphate and ammonium measurements, a new and interesting aspect was that the monitoring of the inorganic carbon buffer with the same buffer capacity based sensor offered extra information that is useful for control purposes.

With the obtained experiences on rivers, effluents and the algal treatment plant, a new application area was explored and investigated, being the automatic and in the field monitoring of ortho-phosphate and ammonium in animal manure (FASTNAP project, chapter 8). The developed methodology is innovative because in this application area, automatic nutrient sensors are not available yet. The developed automatic buffer capacity based sensor was evaluated for its potential as an alternative to the traditional laboratory analyses, of which the results are only

available after five to ten working days.

In this concluding chapter, a general discussion of the obtained results in relation to the literature is given. Also, the most important conclusions with their perspectives will be presented. First, the various buffer capacity simulation approaches will be discussed. Second, the developed multipurpose hard- and software sensor will be discussed. The third section deals with the realized application results, whereas the fourth section describes the applications in the framework of alarm generation. The fifth section discusses the possibilities of automatic buffer capacity model building. At last, a list of important conclusions is summarized.

10.1 Various buffer capacity simulation approaches

In literature, various approaches are considered to model pH buffer capacity [198, 251, 263, 273]. Depending on the aim of the modelling, different approaches should be selected. However, the majority of approaches focuses on assessing the composition or species distribution (including pH) of a sample under a certain set of conditions. This work, on the contrary, is focussed on buffer capacity modelling. Therefore, some models and methods described in the literature needed to be modified or extended for the purpose of this work. An example is the 'tableau method' [273] used for speciation calculations which was adopted and extended for buffer capacity modelling. Also, the literature contains many different ways of handling buffer capacities. Some authors [138, 273] present buffer capacities in terms of protolysis degree (α_i), being the ratio of the concentration of the species to the total concentration. In another approach [235–237], the buffer capacity is defined as a dimensionless value. As a consequence, parts of chapter 3 are redevelopments of a number of existing models, however, presented in a consistent framework.

In chapter 3, three different approaches of buffer capacity modelling are presented in a single framework. The mathematical models and related methods were presented for the simulation of titrations of aquatic samples with a strong acid or base. The three approaches are described in a consistent framework in which simple as well as more complicated chemical equilibria are handled. If only simple acid-base equilibria have to be modelled, the linear buffer capacity model is by far to be preferred. If complexation and/or precipitation reactions have to be considered, the tableau-based method is a good choice, because of its flexibility and widest range of possibilities. However, if only acid-base and complexation equilibria have to be considered, and speed and numerical robustness are important (e.g. in on-line field applications), the non-linear symbolic model is the preferred model.

The constructive approach followed in chapter 3, illustrated with didactic examples, and supported with the chemical background of chapter 2, should allow the reader to obtain a solid introduction and a consistent overview of pH buffer capacity modelling. This overview was partially based on literature research, however, major parts were adapted or further developed to fit the requirements of this work. Furthermore, a number of pitfalls and serious confusions related to this subject were encountered in the literature. An important source of errors that was experienced is related to the many different ways equilibrium constants are presented in the literature (K , β , *K , K' , cK , ...). Caution is needed when using values from tables in which it is not straightforward to assess what the tabulated values exactly mean. Some examples in chapter 2 illustrate that popular aquatic chemistry textbooks like [263] or widely used

software packages like MINTEQA2 [257] are sensitive to such type of errors. Consequently, when wrongly used K -values are implemented for simulation purposes, they can have a very significant influence on the simulation result.

Based on a literature research of existing chemical equilibrium software, it was found that the freely available and well documented program MINTEQA2 [10] is very popular among environmental professionals. The package is suitable for equilibrium problems in natural waters (acid-base, precipitation-dissolution, complexation, surface complexation and redox reactions). However, this package is meant as a speciation program and is not well-suited for the simulation of buffer capacity curves resulting from titration experiments. In view of the later field applications, some other packages [20, 210, 295] were evaluated too, but these packages were not found suitable for our purposes. Therefore, specific software was developed for each of the described modelling approaches, discussed in the next paragraph.

The linear buffer capacity modelling approach was implemented in the software *bomb* (see chapter 5). This software was further extended as a complete data processing tool for experimental titration curves, and can be considered the brain of the developed buffer capacity based hard- and software sensor of this work. Therefore, it is further discussed in section 10.2. The non-linear symbolic model approach was evaluated with some prototype software programs, and found not appropriate for research purposes, however, having good potentials for robust field applications. The non-linear tableau-based method was implemented in the software *bctab*, and was found very convenient for research purposes. In *bctab*, the chemical equilibrium problem has to be structured in a stoichiometric matrix and supplied to the simulation program by means of an input file. This might require extra work to write down in advance all the equilibrium equations in function of the chosen components, however, this structural approach is less sensitive to conceptual errors, compared to e.g. the non-linear symbolic model approach. An important advantage compared to e.g. the program MAGIK [20] found in literature, is that the simulation program *bctab* doesn't need to be compiled again for each particular problem. The application of the developed software program *bctab* can be situated as a supporting tool for students and researchers who need more insight in the buffer capacity behaviour as function of pH for simple and complicated chemical equilibrium problems. A further perspective is to integrate the simulation software *bctab* into the complete data processing software *bomb*. This would allow to fit complex chemical equilibrium buffer capacity models to experimental data and stepwise build adequate buffer capacity models including complexation and precipitation reactions.

Despite the fact that complexation and precipitation reactions can be integrated successfully into buffer capacity models and simulated with *bctab*, their practical influence on the experimental buffer capacity is not always as the models predict. More particularly, precipitation reactions may be determined much more by kinetic and other factors, which are not taken into account in the equilibrium based approach that is followed in this work [198]. Indeed, it was practically experienced in the destructed manure samples, that precipitation reactions are sluggish and non-reproducible, making it impractical to model their effect on the experimental buffer capacity.

10.2 Buffer capacity based hard- and software sensor

In the titrimetric sensor developed in this work, a sample is titrated with a strong base and/or acid (hardware part of the sensor), followed by the calculation of experimental buffer capacities, and subsequently the fitting of mathematical models to the data (software part of the sensor). An important difference compared to most existing titrimetric sensors is that no endpoint detection methods are applied, and that the whole and detailed titration curve is used for mathematical modelling purposes. Similar sensors found in literature mostly work with only a few titration points and a simplified data interpretation e.g. in [46, 65, 197]. The interpretation of the complete titration or buffer capacity profile is performed in a wide variety of systems, especially environmental systems, e.g. in [38, 66, 115, 124, 169, 248, 305]. However, most of these applications are limited to a qualitative approach, to find or to illustrate the most important buffer systems in the titrated sample. The approach developed in this work is undoubtedly more advanced than the applications mentioned above, because of the incorporation of an extra and automatic mathematical modelling step of the complete buffer capacity profile.

The developed methodology can be realistically implemented in an on-line automatic measurement system. Literature research showed that sampling systems and more particularly filtration systems are among the weakest parts of on-line environmental sensors, especially nutrient sensors. Most NH_4^+ , NO_3^- and PO_4^{3-} -analyzers require a sample stream free of suspended solids, which necessitates the use of a membrane filter sampling system [87, 250, 288, 289, 317]. Up to 46 % of the investment costs for the installation of an on-line analyzer can be due to the installation of a sampling and filtration system [250]. In the past, other filter systems, like dialysis [220], a gauze filter equipped with a compressor for cleaning purposes [261], or smaller filter systems [289] have been tested but they often suffer from limited lifetime or clogging problems. The sensor developed in this work does not need any sample filtration, a major advantage for field-use. Also, maintenance and surveillance are key factors in on-line measurements. On the one hand, on-line analyzer companies often suggest maintenance intervals of 1 week, or even 1 month, but practical field studies, on the other hand, show that for complicated on-line sensors (e.g. N and P analyzers), a daily inspection should be carried out with all on-line analyzers [250]. This inspection can vary from a visual inspection to a full cleaning and calibration. In general, 20 minutes per instrument and per day, including sample pre-treatment, are to be expected [250]. For the applications resulting from this research, the maintenance requirements of the titration vessel and the electrode are comparable to the maintenance of an on-line pH sensor. The chemicals used (NaOH and HCl) are environmentally friendly and inexpensive.

Because of the necessity of accurately recording a complete titration profile, the maximum measurement frequency is only around 2 measurements per hour. However, one measurement cycle results in the estimation of several variables (e.g. ammonium and ortho-phosphate), which is an important advantage compared to existing sensors. Another aspect of the developed sensor is its multipurpose functionality. On the one hand, if the sample matrix is exactly known (e.g. the destructed manure samples), the sensor has an analyzer function, capable of making accurate estimations of e.g. ammonium and ortho-phosphate. On the other hand, if the sample matrix is not exactly known (e.g. river waters), the sensor has to be seen in the context of alarm generation. The latter functionality can be compared with other non-specific sensors like UV absorbance based sensors [58, 201, 287]. Useful correlations have been established

between the COD or BOD in various types of waters and the UV absorbance at 254 nm [201] or the absorbance at 650 nm [58]. The results obtained in chapter 6 show that the correlations between the ‘soap’ buffer capacity and the BOD and/or COD in effluents and river waters are comparable to the correlations found in similar samples between UV absorbances at various wavelengths and the BOD and/or COD. The advantage of the absorbance measurements is that they are very rapid, however, the spectrophotometric developments are waiting for the design of a simple field portable device [287].

Commercial automatic titrators have expensive built-in dynamic algorithms for the control of a titration experiment. The details of titration algorithms are kept secret by the titrator developers, because of their commercial value. In the framework of this research, only a limited number of functionalities that commercial titration algorithms offer, are needed. The DET algorithm of Metrohm [168] was used for the collection of titration curves throughout this work. However, a disadvantage that was encountered is that the DET algorithm results in unnecessarily high measurement point density in the less interesting pH regions ($\text{pH} < 5$ and $\text{pH} > 9$), and a too low measurement point density in parts of the titration curve that contain the most useful information for data processing (e.g. the pH region around pH 7). An equidistant measurement point density is advantageous for the further data processing, more particularly for the calculation of the buffer capacities from the titration profile. In the literature, it was found that pH control by conventional means (e.g. PI control) is very difficult because of the highly non-linear response of the pH value to the addition of acid or base [188]. An innovative and combined data- and model-driven titration algorithm was developed, capable of performing the titration task as needed for the purpose of this work. The algorithm has a user-defined set-point for ΔpH and was developed to obtain an equidistant measurement point density. The algorithm was implemented and validated, and was found sufficiently robust for field-use.

The complete data processing part of the titrimetric sensor is implemented in the software *bomb*. During the development phase of this software, strong emphasis was put on the robustness for field-use. For example, the parabolic regression algorithm for the calculation of the experimental buffer capacity switches automatically to a linear algorithm in case numerical problems are detected. Further, the public domain parameter estimation routine PRAXIS was preferred over the commercial mathematical function library M++ for robustness reasons, despite the attractive features of the M++ package. Further, the variance-covariance calculation of the parameter estimates is performed with a well-proven robust method developed by Nelder and Mead (1964). And last, the automatic buffer capacity model building algorithm was modified several times throughout this work in function of its later use in the field. The software *bomb* was tested intensively, and was used for all buffer capacity calculations, simulations and optimization exercises in this work. In the literature, only one similar stepwise approach for building buffer capacity models for unknown solutions was found, named the Gordon algorithm [101, 102]. Unfortunately, this method was developed 15 years ago, and no recent literature based on this approach was found. In this work, important progress was realized compared to the above mentioned older method. The old method should be considered as an off-line laboratory research tool rather than a functional part of an on-line sensor. Also, the Gordon algorithm uses a priori information about the buffers to be expected in the sample only to a minor extent and does not use advanced model selection criteria as in the new method. For the Gordon algorithm, the limit of resolution for a minimal $\text{p}K_a$ separation of two buffers is

reported to be between 0.1 and 0.5 [101, 102]. In this study (chapter 9), it was experienced that two buffers with a pK_a separation less than 0.5 are pooled together in the model as one buffer.

The developed buffer capacity based sensor also offers new perspectives for use in the laboratory as an alternative to traditional end-point titrators. As mentioned above, these commercial titrators are expensive if they are equipped with a dynamic equivalence-point titration algorithm. However, with the methodology developed in this work, it is possible to replace such advanced titrator with a simple and less expensive dosing unit, coupled to a computer and using the constant ΔpH titration algorithm. As a consequence, the concentration of the titrated species would no longer be calculated from the titrant volume required to reach an equivalence-point, but would be the result of buffer capacity modelling, in which the complete titration curve is used rather than only a few points around the equivalence-point. Further research should investigate what the consequences are for the accuracy and precision for such applications.

10.3 Nutrient measurements from buffer capacities

Standard addition experiments of ammonium and ortho-phosphate in various types of samples showed that the minimum amount of ammonium and ortho-phosphate that can be successfully recovered with the buffer capacity based sensor is around 0.5 mg N l^{-1} and 0.5 mg P l^{-1} respectively. These values are only indicative, because they are case dependent. In a literature review on a wide variety of nutrient sensors (chapter 4), it was found that the detection limit of on-line ammonium sensors is mostly lower than reported with the buffer capacity based sensor (e.g. an NH_3 sensitive electrode has a detection limit of 0.05 mg N l^{-1}). Similarly, the detection limit of on-line ortho-phosphate analyzers was found to be lower than reported with the buffer capacity based sensor (e.g. ortho-phosphate sensors based on the colorimetric principle typically have a detection limit between 0.05 and 0.2 mg P l^{-1}). Based on these findings, it is concluded that buffer capacity based measurements of N and P are not well-suited for analytical purposes in low concentrated samples. The reproducibility or precision of the buffer capacity based measurements of N and P can be expressed as a relative standard deviation (r.s.d.), and is around 2 and 5 % for ammonium and ortho-phosphate respectively (chapter 6). Ortho-phosphate estimations are generally found to be less accurate and less reproducible compared to ammonium estimations. This is possibly due to a higher number of interferences present in the buffer capacity region where ortho-phosphate is buffering. Also, ortho-phosphate is more sensitive to complexation reactions with other components, potentially masking its buffer capacity effect. The reported reproducibility values (expressed as r.s.d.) in the literature of on-line ammonium and ortho-phosphate analyzers (chapter 4) show very high variability, depending on the study and the measurement technique. For example, r.s.d. values ranging from 0.7–120 and 1–32 % are reported for ammonium and ortho-phosphate respectively. Generally spoken, the reproducibility obtained with the buffer capacity based sensor is very acceptable compared to the reported literature values. If a number of interferences related to the NaOH titrant (silicates and inorganic carbon) would have been better controlled in most of the experiments ¹, the accuracy, reproducibility and detection limits would possibly be better than reported. A detailed com-

¹Indeed, the finding of the interferences occurred only at the end of the Ph.D. study.

parison between self prepared NaOH titrant stock solutions and commercially prepared NaOH stock solutions was made. It was concluded that commercially prepared NaOH stock solutions (e.g. Titripack[®], Merck) are a strong and reliable alternative to avoid interferences, both from inorganic carbon and silicates. These solutions are stored in completely closed, headspace free plastic bags of 10 l, and are not necessarily more expensive than self prepared stock solutions.

Generally, for the discussion of nutrient measurements (N and P) in environmental samples, an important distinction has to be made between raw titrated samples (e.g. river water and effluent samples) and destructed samples (e.g. destructed manure samples). For the first category, a useful correlation was obtained between laboratory analyses and titration based estimations of ammonium and ortho-phosphate. The results obtained show that the buffer capacity based sensor is a useful measurement system for on-line monitoring of ammonium and ortho-phosphate in effluents, river waters and algal treatment systems. For a better interpretation, the obtained results were compared with the between-laboratory variability and the experiences with on-line sensors found in the literature. First, based on the river water and effluent results in chapter 6, it was concluded that the variability between the two laboratories for the same sample is comparable to the variability between the titrimetric sensor and each of the laboratories. This conclusion is also in correspondence with recent Aquacheck tests [62, 301], where it was found that the relative standard deviation (r.s.d.) of measurements of 1 sample in several laboratories is 6 % and 5 % for ammonium and ortho-phosphate respectively. Although the reported accuracy of commercial sensors is mostly acceptable, one should realize that these specifications are not always reached in the field. A detailed field test with 9 commercial ammonium sensors on the same location reported differences of more than 200 % between measurements performed by the different sensors under test [326]. An important offset difference between different sensors was noticed. The main concern was that some monitors often failed and needed extra intervention and cleaning, multiple trials of calibration, changing of plastic pipes or other parts, . . . This field test has shown that every detail is important when installing and running a monitor. Particularly the filtration unit and piping are among the high maintenance parts. As presented earlier in this discussion, the buffer capacity based sensor is not very sensitive to this type of particular problems.

For applications, like anaerobic wastewater treatment [12, 46, 71] and algal wastewater treatment [199, 259, 277, 279], the inorganic carbon (IC) buffer is an interesting process control parameter. In waters which are low or even limiting in IC buffer capacity (like in algal treatment plants), standard alkalinity measurements can give an overestimation of the IC buffer system, because the alkalinity is a general composite measurement, including all pH buffering components in the considered pH interval. In the case study with the algal pilot plant, the alkalinity measurement (T-2C) could overestimate the $[\text{HCO}_3^-]$ buffer with up to 22 % compared to the IC from the buffer capacity based approach. For this particular case study, an automated alkalinity measurement possibly would reveal similar process information as the IC determination with the buffer capacity sensor. However, because the hardware and the hardware related practical difficulties (maintenance, calibration, . . .) of an automated alkalinity measurement are very similar to this buffer capacity sensor, the main advantage of the developed sensor is that ammonium, ortho-phosphate and inorganic carbon are obtained with one single measurement device.

For the destructed manure samples, the interpretations of the results are different because organic interferences in the samples are absent due to the destruction step prior to titration.

The effect of ionic strength on the buffer capacity had to be taken into account, however, and a dilution factor between 3 and 6 was experimentally found to give the best results. Complexation reactions with Ca^{2+} and Fe^{3+} were investigated in more detail, and it was found that iron and calcium complexes could be responsible for buffer capacities around pH 5, pH 8 and pH 10. It was also found that the buffer capacities of $o\text{-PO}_4$ and NH_4^+ (the buffers of main interest) are only influenced to a limited extent by the complex formation reactions. The ammonium concentrations found with the titrimetric analyses are all between -7 and $+8$ % relative error compared to the laboratory measurements. The relative errors for the titrimetric ortho-phosphate concentrations are between -15 and $+25$ % compared to the laboratory results, after eliminating some important interferences that were found to originate from the NaOH stock solutions. On-line manure nutrient sensors were not found in the literature or on the market, thus making comparisons with other systems impossible. However, a recent small scale study [2] showed differences between the minimum and maximum reported laboratory analysis results of 24 % and 87 % for respectively N and P measurements in 1 pig manure sample. A similar comparative test in Flanders (called ‘ringtest’) [64] in which 30 laboratories were involved, found differences between the minimum and maximum reported analysis results of 54 % and 39 % for respectively N and P. This official test was also used in an accreditation procedure to select the laboratories that are officially allowed to perform these measurements. From these two recent studies, one can conclude that nutrient measurements in manure are sensitive to many sources of error which are not completely under control yet in some of the tested laboratories. Finally, the obtained statistical results with the buffer capacity based method were compared with the requirements for an official accreditation in the Netherlands [1] for nitrogen and phosphorus measurement in animal manure. These requirements include the minimum measurable concentration (expressed as three times the residual standard deviation s_X) and the reproducibility (including the subsampling or duplo effect and the analysis effect). The obtained minimum measurable concentrations N and P, calculated from the residual standard deviations of the titrimetric measurements are still higher than the required values. Especially for P, the results are not fully acceptable yet. However, it should be taken into account that the titrimetric data used in this validation study (see chapter 8) were obtained without appropriate control and minimizations of the interferences discovered afterwards (silicates and IC). Therefore, it is expected that by taking care of the described interferences, the minimum measurable concentrations for N and P will be within the requirements for accreditation. The obtained reproducibility (including the effects of subsampling and analysis) is already within the requirements.

From detailed analysis of the experimental and corresponding simulated buffer capacity profiles and their relationship with laboratory analyses, a number of conclusions could be drawn. For the undestructed samples (river waters and effluents) it is concluded that no strict relationship exists between the goodness of fit and the agreement between the titrimetric results and the ammonium, respectively ortho-phosphate laboratory analyses. Examples with a perfect model fit often show good estimates for ammonium and ortho-phosphate, but sometimes suffer from interferences present at the same pK_a value of the modelled buffer systems. Among different evaluated mathematical models (i.e. fixed or variable pK_a values, fixed or variable amount of IC buffer, wide or small simulation interval), a best ‘general purpose’ model useful for domestic effluents and river waters was formulated. Similarly, for the destructed manure samples an adequate model useful for all manure samples was developed. Remarkable is that

the best N and P estimations are obtained with a rather simple model, that did not take into account known interferences around pH 5 and pH 8. The use of a fixed model is an important aspect for field implementations, because it is not always possible or realistic to set up preliminary experiments to define the best site-specific buffer capacity model. For the tested industrial effluent, the ‘general purpose’ buffer capacity model of domestic effluents was not successful for N and P estimations, because of too many interferences present in the time-varying effluent. In this framework, it was also investigated whether it is advantageous for ammonium and ortho-phosphate assessment, to use the automatic buffer capacity model builder algorithm (available in the software *bomb*). In situations where the a priori knowledge about the sample is already high (e.g. the algal and manure samples), the estimates of ammonium and ortho-phosphate obtained with a fixed modelling approach are often better compared to the automatic modelling results. In the other situations, where the a priori knowledge is not high (e.g. many river and effluent samples), some spectacular increases in the accuracy of the estimated ammonium and ortho-phosphate concentrations were achieved with the automatically built models compared to the fixed model. For some applications (e.g. the industrial effluent), a fixed model approach is certainly not useful because the buffer composition of the effluent stream can continuously change.

The results obtained show that the buffer capacity sensor is a useful measurement system for on-line monitoring of ammonium and ortho-phosphate in effluents and river waters. Because the titrimetric measurement methodology is undoubtedly sensitive to interferences, the sensor application should in the first place be seen in the context of alarm generation. This aspect is further discussed in section 10.4. Interesting perspectives for the buffer capacity based sensor for the quantification of the IC buffer are noticed in recent literature, because this particular measurement becomes increasingly important for assessing stoichiometric carbon balances in e.g. river water modelling [234] or trickling filter modelling and control [314]. The perspectives for nutrient measurements in manure are twofold. First, increasing demands for nutrient measurements in animal manure (e.g. in the framework of MINAS in the Netherlands) are to be expected in the coming years. Due to the benefit for the receiving farmer to have the measurements available prior to application of the manure on soil, a market potential for on-line manure sensors is expected. Second, taking into account some further optimizations discussed in this work, the analysis results with this titrimetric sensor are expected to be as reliable as the laboratory results. A first comparison between the results obtained and the requirements for accreditation was performed, and it could be concluded that the developed methodology is promising for official acceptance. Moreover, the developed titrimetric measurement technique can be implemented in the laboratory, with a laboratory titrator coupled to a computer, and act as a reliable alternative for the classical laboratory methods. The strongest points of the titrimetric method are: simultaneous N and P measurement with 1 method, minor sample manipulations, N and P results within 30 minutes, low and inexpensive chemical consumption, consumption of only one and non-hazardous reagent (NaOH) and the possibility to measure continuously in the lab with a sample carousel coupled to the titrating unit.

10.4 Buffer capacity based alarm generation

A first possible alarm indicator found in effluents and river waters is the ‘soap’ buffer around pH 5. The concentration of this buffer showed an useful correlation with the COD of the sample. In the industrial effluent, two unexpected COD peak loadings were perfectly recognized by the increasing ‘soap’ buffer concentration. This illustrates that the buffer capacity based sensor is suited for alarm generating purposes in case of unexpected COD discharge peaks. However, on theoretical basis a strict relationship may not exist between buffer capacities and COD (e.g. sugars have no buffer capacity, but a high COD). The approach followed for COD estimation can therefore be compared with other non-specific measurement techniques for similar purposes, like UV absorbance based sensors [201, 287] (see also discussion in section 10.2).

A new idea developed in this work is ‘quality proportional sampling’ in effluents and river waters. This is proposed as an alternative to time or flow proportional sampling. It is suggested that the buffer capacity profile is used as a fingerprint for the water composition. When the fingerprint is changing, an alarm is triggered and a sample is automatically taken for further laboratory analysis. The quality dependent sampling is superior to the time- or flow proportional sampling if such sampling strategy would lead to a significantly lower number of laboratory analyses to be performed. The alarm triggering function was developed by means of the automatic buffer capacity model building approach in chapter 9. The model building algorithm will add ‘blind’ buffers in order of importance. The corresponding standard deviations on the estimated concentrations can be used to test statistically if the reported concentrations are significantly different from previous concentrations or significantly different from 0. The developed ‘alarm triggering’ methodology was only developed and validated with titration curves obtained off-line. The practical implementation should be further investigated and validated with field experiments.

10.5 Automatic pH buffer capacity model building

Besides the application of alarm generation, the automatic buffer capacity model building approach also offers a number of interesting perspectives compared to the use of fixed buffer capacity models. The approach can be applied by an expert user as a support tool for characterisation of unknown buffer capacity profiles or to develop an appropriate fixed model for a specific application. For a number of selected samples (e.g. the industrial effluent samples in the last weeks of the measurement period), the estimations with automatically built models were highly superior to the fixed model approach, because the buffer composition was drastically changing during the measurement period. In retrospect a lot of time could have been gained if the automatic modeller would have been available for the development of adequate models for the various applications investigated in this work. Another benefit of the automatic modelling approach is the detection of problems related to experimental titration conditions. For example, in the destructured manure titration curves, it was found that a titrant contamination with IC or silicates is directly reflected in the number of blind buffers incorporated in the final model. This is an interesting property for robustness and verification of the produced results in later field-use. A new application for automatic model building is the evaluation of the correctness of end-point titrations used in many analytical laboratory methods. Automatic titrators

search for an equivalence-point, and the corresponding equivalence titrant volume is attributed to the expected buffer. However, such algorithms are not able to detect small interferences like IC, silicates, Therefore, automatic buffer capacity modelling can be used to find out if there is indeed only one buffer system present, or if other (interfering) buffers are present as well. However, further research is necessary for a practical validation of this new application.

A number of suggestions for further research suggestions on the automatic buffer capacity model building approach were also formulated in this work. The investigated model selection criteria (AIC, AIC_C, SIC, FPE, Run-test, F-test) all have advantages and disadvantages. There appeared no 'best' criterion for general purposes. In another field, the same model selection criteria were compared for the selection of oxygen uptake rate (OUR) models fitted to respirometric data [315]. It was found that traditional information criteria (AIC, AIC_C, FPE and SIC) result in overfitting of the model compared to the 'human expert advice'. An interesting perspective for further research could be to use a combination of the different model selection criteria. The final model selected with each of the criteria could be introduced in an 'expert system' that can make a choice based on the pro's and contra's known for each criterion. It was also experienced that automatically added buffers in the model sometimes lead to estimated concentrations which are not significantly different from 0. A stepwise modelling approach as used in multiple linear regression would allow to remove a buffer from the model if the concentration of this buffer is not significantly different from 0. Finally, although the parameter estimation routine PRAXIS is very robust, it was noticed in the automatic modelling approach that it sometimes returns local minima solutions. Further research could add supplementary optimization techniques to further increase the automatic model building robustness.

10.6 Summarized conclusions

Based on the discussion presented in this chapter, the following main realisations of this study can be summarized:

- Three different approaches of buffer capacity modelling are developed and evaluated in a single and consistent framework. This framework allows the simulation of the effects of simple (acid-base) as well as more complicated (complexation, precipitation) chemical equilibria on the pH buffer capacity. Appropriate software was developed, to support the implementation of an automatic, field-usable buffer capacity based sensor.
- A multipurpose titrimetric sensor has been developed, which can realistically be implemented in a robust and on-line automatic measurement system, which does not need complicated sample pretreatments such as filtration. An important difference compared to most existing titrimetric sensors is that no end-point detection methods are applied, and that the whole and detailed titration curve is interpreted using mathematical models.
- Most titration curves in this work were successfully collected with a commercial titrator with a built-in dynamic titration algorithm. However, for the purpose of the implementation of the developed methodology in an automatic sensor, an innovative combined data- and model-driven titration algorithm was developed, implemented and validated. The added value of this new titration algorithm is that it generates an equidistant pH measurement density, which is expected to be advantageous for the data processing.

- An automatic and robust model building algorithm was developed and implemented, of which the purpose is to efficiently find an useful and adequate buffer capacity model, tailor-made for each individual sample. The two most important benefits of the automatic model approach compared to the fixed model approach were: First, new and useful buffer information about the titrated sample became available, and second, for a number of samples, the concentration estimations with automatically built models were highly superior to the fixed model approach.
- The first developed application is the effluent and surface water monitoring of pH buffering substances. The sensor is capable to give an indication of the ammonium and ortho-phosphate level in the tested effluents and surface waters. Experiences with different types of samples have shown that the accuracy and precision are affected by the composition of the sample. Due to possible interferences of buffering components and the presence of unmodelled buffering components in the effluent, this titration sensor cannot be proposed for use as an analytical instrument. Rather it should be used as an effluent or surface water quality indicator and detector of possible changes in the sample composition. The sensor can be used for alarm triggering when the buffer capacity profile changes. However, this should be further investigated with field experiments.
- The second developed application is the monitoring of tertiary wastewater treatment with algae. This application has to be seen in the context of process monitoring and alarm generation. An innovative aspect of the presented buffer capacity sensor, is that it gives a multivariate response (IC, NH_4^+ , $o\text{-PO}_4$) supplemented with extra information, e.g. the appearance or disappearance of extra buffer systems, that are useful for process monitoring.
- The third developed application concerns the N and P measurements in destructed animal manure. The most important difference compared to the previous applications is that the titrated sample is now free of extra buffer capacities because of the destruction step prior to titration. Inorganic complexation reactions only influenced the buffer capacities of ammonium and ortho-phosphate to a limited extent. Taking into account some further optimizations discussed in this work, the analysis results with this titrimetric sensor are expected to be comparable with the laboratory results.

On the whole, this work has introduced a number of new concepts, for instance, the on-line measurement of animal manure nutrients and quality proportional sampling of e.g. effluents and river waters. However, the major benefits of this work are undoubtedly the result of the interdisciplinary approach of existing methods, technologies and necessities. More particularly, the traditional and well-proven titration technique was revisited and upgraded for use in advanced mathematical modelling. This has created a number of interesting perspectives, of which some new applications were developed in the field of on-line environmental measurements.

Bibliography

- [1] Accreditatieprogramma dierlijke mest; samenstelling. Bijlage bij de regeling hoeveelhedsbepaling dierlijke en overige organische meststoffen. Ministerie van Landbouw, Natuurbeheer en Visserij, 's Gravenhage, 1998. pp. 38.
- [2] Twijfel aan mestanalyse. *Boerderij*, 83(51):18, 1998.
- [3] A.J. Acher and B.J. Juven. Destruction of coliforms in water and sewage water by dye-sensitized photooxidation. *Appl. Environ. Microbiol.*, 33(5):1019–1022, 1977.
- [4] A.J. Acher and I. Rosenthal. Dye-sensitized photo-oxidation – a new approach to the treatment of organic matter in sewage effluents. *Wat. Res.*, 11:557–562, 1977.
- [5] A.J. Acher and S. Saltzman. Dye-sensitized photooxidation of bromacil in water. *J. Environ. Qual.*, 9(2):190–194, 1980.
- [6] Mettler-Toledo AG. Practice and theory of pH measurement. Urdorf, Switzerland, 1996.
- [7] S.R. Ahmad and D.M. Reynolds. Monitoring of water quality using fluorescence technique: Prospect of on-line process control. *Wat. Res.*, 33(9):2069–2074, 1999.
- [8] H. Akaike. A Bayesian analysis of the minimum AIC procedure. *Ann. Inst. Statist. Math.*, 30:9–14, 1978.
- [9] A. Al-Wehaid and A. Townshend. Spectrophotometric flow-injection determination of nitrate based on reduction with titanium(iii) chloride. *Anal. Chim. Acta*, 186:289–294, 1986.
- [10] J.D. Allison, D.S. Brown, and K.J. Novo-Gradac. *MINTEQA2/PRODEFA2 – A Geochemical Assessment Model for Environmental Systems*. U.S. Environmental Protection Agency, Environmental Research Laboratory, Athens, 1991.
- [11] K.L. Andersen and P. Wagner. Testing on-line monitors for ammonia, nitrate, orthophosphate and suspended solids in activated sludge sewage treatment plants. In R. Briggs, editor, *Instrumentation, control and automation of water and wastewater treatment and transport systems*, pages 667–675. IAWPRC Workshop held in Yokohama and Kyoto, Japan, July 26 - August 3 1990, Pergamon Press, 1990.

- [12] G.K. Anderson and G. Yang. Determination of bicarbonate and total volatile acid concentration in anaerobic digesters using a simple titration. *Water Environ. Res.*, 64(1):53–59, 1992.
- [13] G.M. Anderson and D.A. Crerar. *Thermodynamics in geochemistry - The equilibrium model*. Oxford University Press, New York, 1993.
- [14] K.N. Andrew, P.J. Worsfold, and M. Comber. On-line flow injection monitoring of ammonia in industrial liquid effluents. *Anal. Chim. Acta*, 314:33–43, 1995.
- [15] T. Aoki, S. Uemura, and M. Munemori. Continuous flow method for simultaneous determination of nitrate and ammonia in water. *Environ. Sci. Technol.*, 20(5):515–517, 1986.
- [16] F.A.J. Armstrong and S. Tibbitts. Photochemical combustion of organic matter in sea water, for nitrogen, phosphorus and carbon determination. *J. mar. biol. Ass. U.K.*, 48:143–152, 1968.
- [17] F.A.J. Armstrong, P.M. Williams, and J.D.H. Strickland. Photo-oxidation of organic matter in sea water by ultra-violet radiation, analytical and other applications. *Nature*, 211(5048):481–484, 1966.
- [18] H. Aspegren, B. Andersson, U. Nyberg, and J. la C. Jansen. Model and sensor based optimization of nitrogen removal at Klagshamn wastewater treatment plant. *Wat. Sci. Tech.*, 26(5–6):1315–1323, 1992.
- [19] H. Aspegren, B. Andersson, G. Olsson, and U. Jeppsson. Practical full scale experiences of the dynamics of biological nitrogen removal. In R. Briggs, editor, *Instrumentation, control and automation of water and wastewater treatment and transport systems*, pages 283–290. IAWPRC Workshop held in Yokohama and Kyoto, Japan, July 26 - August 3 1990, Pergamon Press, 1990.
- [20] M. Bader. Exact computer solutions to complex problems in chemical equilibria using matrix mechanics methods. *International Laboratory*, 11:10–12, 1997.
- [21] D.S. Baldwin. Reactive “organic” phosphorus revisited. *Wat. Res.*, 32(8):2265–2270, 1998.
- [22] P. Balslev, A. Lynggaard-Jensen, and C. Nickelsen. Nutrient sensor based real time on-line process control of a wastewater treatment plant using recirculation. *Wat. Sci. Tech.*, 33(1):183–192, 1996.
- [23] T.E. Barnard and J.J. Bisogni Jr. Errors in Gran function analysis of titration data for dilute acidified water. *Wat. Res.*, 19(3):393–399, 1985.
- [24] R.L. Bassett and D.C. Melchior. Chemical modeling of aqueous systems - an overview. In D.C. Melchior and R.L. Bassett, editors, *Chemical Modeling of Aqueous Systems 2*, number 416 in ACS Symposium Series, pages 1–14, Washington, DC, 1990. American Chemical Society.

- [25] G. Bastin and D. Dochain. *On-line estimation and adaptive control of bioreactors*. Elsevier, Amsterdam, 1990. 379 pp.
- [26] M. Beccari and R. Ramadori. Nutrient removal from wastewaters. *Chimicaoggi*, 9(3), 1991.
- [27] M. Bekbölet and G. Özkösemen. A preliminary investigation on the photocatalytic degradation of a model humic acid. *Wat. Sci. Tech.*, 33(6):189–194, 1996.
- [28] L.D. Benefield, J.F. Judkins Jr., and B.L. Weand. *Process chemistry for water and wastewater treatment*. Prentice-Hall, Englewood Cliffs, New Jersey, 1982.
- [29] F.J. Benitez, J. Beltran-Heredia, J.L. Acero, and M.L. Pinilla. Simultaneous photodegradation and ozonation plus UV radiation of phenolic acids - major pollutants in agro-industrial wastewaters. *J. Chem. Technol. Biotechnol.*, 70(3):253–260, 1997.
- [30] R.L. Benson, I.D. McKelvie, B.T. Hart, and I.C. Hamilton. Determination of total phosphorus in waters and wastewaters by on-line microwave-induced digestion and flow-injection analysis. *Anal. Chim. Acta*, 291:233–242, 1994.
- [31] R.L. Benson, I.D. McKelvie, B.T. Hart, Y.B. Truong, and I.C. Hamilton. Determination of total phosphorus in waters and wastewaters by on-line UV/thermal induced digestion and flow injection analysis. *Anal. Chim. Acta*, 326:29–39, 1996.
- [32] R.L. Benson, Y.B. Truong, I.D. McKelvie, and B.T. Hart. Monitoring of dissolved reactive phosphorus in wastewaters by flow injection analysis: Part 1. Method development and validation. *Wat. Res.*, 30(9):1959–1964, 1996.
- [33] R.L. Benson, Y.B. Truong, I.D. McKelvie, B.T. Hart, G.W. Bryant, and W.P. Hilkmann. Monitoring of dissolved reactive phosphorus in wastewaters by flow injection analysis: Part 2. On-line monitoring system. *Wat. Res.*, 30(9):1965–1971, 1996.
- [34] H.-U. Bergmeyer. *Methods of Enzymatic Analysis*. Academic Press, New York and London, 1965.
- [35] D. Bilanovic, R.E. Loewenthal, Y. Avnimelech, and M. Green. Potentiometric measurement of chemical oxygen demand. *Water SA*, 23(4):301–309, 1997.
- [36] J.J. Bisogni Jr. Measurement of volatile acid concentration in anaerobic processes by least squares regression of overdetermined titration data. *Water Environ. Res.*, 66(1):16–20, 1994.
- [37] J.J. Bisogni Jr and S.L. Arroyo. The effect of carbon dioxide equilibrium on pH in dilute lakes. *Wat. Res.*, 25(2):185–190, 1991.
- [38] J.J. Bisogni Jr., S.W. Witzmann, and J.R. Stedinger. A simple method for determination of volatile acid concentration with corrections for ionic strength. *Water Environ. Res.*, 70(7):1303–1306, 1998.

- [39] M. Blonda, A. Brunetti, S. Morrone, R. Ramadori, and J.W. May. Determination of orthophosphate in activated sludges from wastewater-treatment systems showing enhanced biological phosphate removal. *Wat. Res.*, 28(1):155–159, 1994.
- [40] H. Bogaert, A. Vanderhasselt, K. Gernaey, Z. Yuan, C. Thoeye, and W. Verstraete. New sensor based on pH effect of denitrification process. *J. Environ. Eng.*, 123(9):884–891, 1997.
- [41] J. Bols, P.L.M. Goethals, J. Meirlaen, A. van Griensven, V. Vandenberghe, L. Van Vooren, N. De Pauw, P.A. Vanrolleghem, and W. Bauwens. Automated measurement stations for river water quality monitoring. *Proceedings 13th Forum Applied Biotechnology. Med. Fac. Landbouww. Univ. Gent*, (64/5a):107–110, 1999.
- [42] W. Boschmann, S. Pohl, and B. Klüßendorf. TOC-bestimmung in der prozeß-analytik. In B. Böhnke, editor, *Industrieabwasser vermeiden, vermindern, behandeln*, pages 596–604, Aachen, May 1991. Gesellschaft zur förderung der siedlungswasserwirtschaft an der RWTH Aachen.
- [43] P.V. Brady and J.V. Walther. Controls on silicate dissolution rates in neutral and basic pH solutions at 25 °C. *Geochim. Cosmochim. Acta*, 53:2823–2830, 1989.
- [44] R.P. Brent, editor. *Algorithms for minimization without derivatives*. Prentice-Hall, Englewood Cliffs, New Jersey, 1973. 195 pp.
- [45] R. Briggs, J.W. Schofield, and P.A. Gorton. Instrumental methods of monitoring organic polluton. *Journal of The Institute of Water Pollution Control*, (1):47–57, 1976.
- [46] K. Buchauer. A comparison of two simple titration procedures to determine volatile fatty acids in influents to waste-water and sludge treatment processes. *Water SA*, 24(1):49–56, 1998.
- [47] P. Burman and D. Nolan. A general Akaike-type criterion for model selection in robust regression. *Biometrika*, 82(4):877–886, 1995.
- [48] J.N. Butler. *Ionic equilibrium - A mathematical approach*. Addison-Wesley Publishing Company, Reading, Massachusetts, 1964.
- [49] W.-J. Cai, Y. Wang, and R.E. Hodson. Acid-base properties of dissolved organic matter in the estuarine waters of Georgia, USA. *Geochim. Cosmochim. Acta*, 62(3):473–483, 1998.
- [50] J. Carstensen, P. Harremoës, and H. Madsen. Statistical identification of Monod-kinetic parameters from on-line measurements. *Wat. Sci. Tech.*, 31(2):125–133, 1995.
- [51] S.C. Chapra. *Surface Water-Quality Modeling*. The McGraw-Hill Companies, New York, 1997.
- [52] J. Chen, W.H. Rulkens, and H. Bruning. Photochemical elimination of phenols and COD in industrial wastewaters. *Wat. Sci. Tech.*, 35(4):231–238, 1997.

- [53] X. Chucai and L. Helin. Heterogeneous sensitized photooxidation of phenol in water. *Water Treatment*, 3:171–184, 1988.
- [54] A. Clement, L. Somlyódy, and L. Koncsos. Modeling the phosphorus retention of the Kis-Balaton upper reservoir. *Wat. Sci. Tech.*, 37(3):113–120, 1998.
- [55] F. Coen, B. Vanderhaegen, I. Boonen, P.A. Vanrolleghem, and P. Van Meenen. Nitrogen removal upgrade of a WWTP within existing reactor volumes: A simulation supported scenario analysis. *Wat. Sci. Tech.*, 34(3–4):339–346, 1996.
- [56] F. Coen, B. Vanderhaegen, I. Boonen, P.A. Vanrolleghem, and P. Van Meenen. Improved design and control of industrial and municipal nutrient removal plants using dynamic models. *Wat. Sci. Tech.*, 35(10):53–61, 1997.
- [57] F. Coen, B. Vanderhaegen, L. Van Eyck, and P. Van Meenen. Simulation for improved design and performance of activated sludge systems. case study of an industrial and a municipal WWTP. *Proceedings Workshop Modelling, Monitoring and Control of Wastewater Treatment Plants. Med. Fac. Landbouww. Univ. Gent*, 60:2385–2394, 1995.
- [58] S.D.W. Comber, M.J. Gardner, and A.M. Gunn. Measurement of absorbance and fluorescence as potential alternatives to BOD. *Environ. Technol.*, 17(7):771–776, 1996.
- [59] D.L. Correll. The role of phosphorus in the eutrophication of receiving waters: A review. *J. Environ. Qual.*, 27:261–266, 1998.
- [60] P.A. Corrigan, V.E. Lyons, G.D. Barnes, and F.G. Hall. Conductivity measurements monitor waste streams. *Environ. Sci. Technol.*, 4(2):116–121, 1970.
- [61] M. Cumps. Ontwikkeling van een net-effekt-biosensor voor organische belasting en nitraat in oppervlaktewaters. Master's thesis, Universiteit Gent, Coupure links 653, B-9000 Gent, 1994.
- [62] R. Dams, K. Tirez, and R. Cautaerts. Verslag analytische kwaliteitscontrole op de heffingsparameters. Technical report, Vlaamse Milieumaatschappij – Afdeling Meetnetten en Onderzoek, 1998.
- [63] W. Davison, M. Hill, C. Woof, M. Rouen, and D. Aspinall. Continuous measurement of stream pH. Evaluation of procedures and comparison of resulting hydrogen ion budgets with those from flow-weighted integrating samplers. *Wat. Res.*, 28(1):161–170, 1994.
- [64] N. De Brucker and P. Van Bree. Interlaboratoriumvergelijking voor analyse van dierlijke mest, kunstmest, water, bodem en veevoeder. Technical report, Vlaamse Instelling voor Technologisch Onderzoek (VITO), Mol, July 1999.
- [65] D.W. de Haas and N. Adam. Use of a simple titration procedure to determine H_2CO_3 alkalinity and volatile fatty acids for process control in waste-water treatment. *Water SA*, 21(4):307–318, 1995.
- [66] B. De Heyder. Acid diffusion in canned vegetables. Final report, Universidade Catolica Portuguesa, Escola Superior de Biotecnologia, Porto, 1990.

- [67] J. de la Noüe and N. De Pauw. The potential of microalgal biotechnology: a review of production and uses of microalgae. *Biotech. Adv.*, 6:725–770, 1988.
- [68] J. de la Noüe, R. van Coillie, L. Brunel, and Y. Pouliot. Traitement des eaux usées par culture de micro-algues: Influence de la composition du milieu sur la croissance de *Scenedesmus sp.* *Annls Limnol.*, 25(3):197–203, 1989.
- [69] H. De Schepper, P. Bauwens, and J. Van Dijck. Ringonderzoek: BOD en COD. *Water*, 8(45):51–54, 1989.
- [70] T. Deksissa Chuco. Determination of nitrate in low loaded waters. Master's thesis, Universiteit Gent, Coupure links 653, B-9000 Gent, 1998.
- [71] A.C. Di Pinto, N. Limoni, R. Passino, A. Rozzi, and M.C. Tomei. Anaerobic process control by automated bicarbonate monitoring. In R. Briggs, editor, *Instrumentation, control and automation of water and wastewater treatment and transport systems*, pages 51–59. IAWPRC Workshop held in Yokohama and Kyoto, Japan, July 26 - August 3 1990, Pergamon Press, 1990.
- [72] E. Diamadopoulos and A. Benedek. The precipitation of phosphorus from wastewater through pH variation in the presence and absence of coagulants. *Wat. Res.*, 18(9):1175–1179, 1984.
- [73] D. Diamond and N. Liao. Total nitrogen and total phosphorus in water and waste waters by flow injection analysis using in-line UV digestion. *International Environmental Technology*, 7:12–14, 1996.
- [74] H.B.F. Dixon, G.A. Clarke, S.D. Smith, and T.K. Carne. The origin of multiply sigmoid curves of pH-dependence. The partitioning of groups among titration pK values. *Biochem. J.*, 278:279–284, 1991.
- [75] N.M. Dixon and D.B. Kell. The control and measurement of CO_2 during fermentations. *J. Microbiol. Methods*, 10:155–176, 1989.
- [76] Dyad Software, Washington, U.S.A. *M++ class library; OPTIM Optimization module*, 1991.
- [77] W. Eckert, T. Frevert, and H.G. Trüper. A new liquid-junction free probe for the in situ determination of pH, pH_2S and redox values. *Wat. Res.*, 24(11):1341–1346, 1990.
- [78] Eijkelkamp Agrisearch Equipment. Fastnap (ref 161404) werkwijze voor het bepalen van het gehalte aan stikstof en/of fosfor in drijfmest, monsternemer voor het uitvoeren van een dergelijke werkwijze. Patent submitted at Octrooibureau Vriezendorp & Gaade, Den Haag, march 2000.
- [79] A.B. Estrada. Determination of biodegradable organic matter in low loaded waters. Master's thesis, Universiteit Gent, Coupure links 653, B-9000 Gent, 1993.
- [80] G.R. Findenegg. Inorganic carbon transport in microalgae. 2: Uptake of HCO_3^- ions during photosynthesis of five microalgal species. *Plant Sci. Lett.*, 18:289–297, 1980.

- [81] J.P. Frizado. Ion exchange on humic materials - a regular solution approach. In E.A. Jenne, editor, *Chemical Modeling in Aqueous Systems - Speciation, Sorption, Solubility, and Kinetics*, number 93 in ACS Symposium Series, pages 133–145, Washington, DC, 1979. American Chemical Society.
- [82] M. Fukushima, S. Tanaka, K. Hasebe, M. Taga, and H. Nakamura. Interpretation of the acid-base equilibrium of humic acid by a continuous pK distribution and electrostatic model. *Anal. Chim. Acta*, 302:365–373, 1995.
- [83] K. Fytianos, E. Voudrias, and N. Raikos. Modelling of phosphorus removal from aqueous and wastewater samples using ferric iron. *Environ. Pollut.*, 101(1):123–130, 1998.
- [84] H. Galster. *pH Measurement - Fundamentals, Methods, Applications, Instrumentation*. VCH Verlagsgesellschaft mbH, Weinheim, Germany, 1991.
- [85] R.M. Garrels and C.L. Christ. *Solutions, Minerals, and Equilibria*. Harper & Row, New York, 1965.
- [86] K.R. Gegenfurtner. PRAXIS: Brent's algorithm for function minimization. *Behaviour Research Methods, Instruments, & Computers*, 24(4):560–564, 1992.
- [87] K. Gernaey. *Development of sensors for on-line monitoring of nitrification in activated sludge*. PhD thesis, Universiteit Gent, Coupure links 653, B-9000 Gent, 1997.
- [88] K. Gernaey, H. Bogaert, A. Massone, P. Vanrolleghem, and W. Verstraete. On-line nitrification monitoring in activated sludge with a titrimetric sensor. *Environ. Sci. Technol.*, 31(8):2350–2355, 1997.
- [89] K. Gernaey, H. Bogaert, P. Vanrolleghem, L. Van Vooren, and W. Verstraete. Sensors for nitrogen removal monitoring in wastewater treatment. In J.M. Lynch and A. Wiseman, editors, *Environmental Biomonitoring - The Biotechnology Ecotoxicology Interface*, volume 7 of *Biotechnology Research series*, pages 180–207. Cambridge University Press, 1998.
- [90] K. Gernaey, D. Maffei, P. Vanrolleghem, and W. Verstraete. Model-based interpretation of titration experiments to quantify inhibitory effects on NH_4^+ oxidizing bacteria in activated sludge. *J. Chem. Technol. Biotechnol.*, 1999.
- [91] K. Gernaey, A. Vanderhasselt, H. Bogaert, P. Vanrolleghem, and W. Verstraete. Sensors to monitor biological nitrogen removal and activated sludge settling. *J. of Microbiol. Methods*, 32:193–204, 1998.
- [92] K. Gernaey, P. Vanrolleghem, and W. Verstraete. On-line estimation of *Nitrosomas* kinetic parameters in activated sludge samples using titration in-sensor-experiments. *Wat. Res.*, 32(1):71–80, 1998.
- [93] P. Geuzens, P. Van Bree, N. De Brucker, and H. Van den Broeck. Bemonsterings- en analyseprocedures voor mest, bodem en veevoeder in het kader van het Mestdecreet. Technical report, Vlaamse Instelling voor Technologisch Onderzoek (VITO), Mol, March 1999.

- [94] J. Gibs, R.J. Schoenberger, and I.H. Suffet. A simplified buffer capacity model for sanitary landfill leachate. *Wat. Res.*, 16:699–705, 1982.
- [95] E.T. Gjessing and T. Källqvist. Algicidal and chemical effect of UV-radiation of water containing humic substances. *Wat. Res.*, 25(4):491–494, 1991.
- [96] P. Goethals, A. van Griensven, J. Bols, N. De Pauw, P.A. Vanrolleghem, L. Van Vooren, and W. Bauwens. Automated measurement stations and water quality modelling. In *Proceedings 9th European Congress on Biotechnology*, Brussels, Belgium, July 11–15 1999.
- [97] J.C. Goldman, M.R. Dennett, and C.B. Riley. Inorganic carbon sources and biomass regulation in intensive microalgal cultures. *Biotechnol. Bioeng.*, 23:995–1014, 1981.
- [98] R. González-Herrera. Temperature dependence of Eh probe equilibration times in potable waters. In R. Briggs, editor, *Instrumentation, control and automation of water and wastewater treatment and transport systems*, pages 631–637. IAWPRC Workshop held in Yokohama and Kyoto, Japan, July 26 - August 3 1990, Pergamon Press, 1990.
- [99] G.C. Goodwin, M. Gevers, and B. Ninness. Quantifying the error in estimated transfer functions with application to model order selection. *IEEE Trans. Autom. Control*, 37(7):913–928, 1992.
- [100] J.T.H. Goossen and J.G. Kloosterboer. Determination of phosphate in natural and waste waters after photochemical decomposition and acid hydrolysis of organic phosphorus compounds. *Analytical Chemistry*, 50(6):707–711, 1978.
- [101] W.E. Gordon. Component discrimination in acid-base titration. *J. Phys. Chem.*, 83(11):1365–1377, 1979.
- [102] W.E. Gordon. Data analysis for acid-base titration of an unknown solution. *Anal. Chem.*, 54(9):1595–1601, 1982.
- [103] K.T.V. Grattan. Water quality monitoring – technological advantages and potential developments in the use of fiber optic technology. *Wat. Sci. Tech.*, 37(12):247–253, 1998.
- [104] A.E. Greenberg, L.S. Clesceri, A.D. Eaton, and M.A.H. Franson. *Standard methods for the examination of water and wastewater*. American Public Health Association, Washington, 18th edition, 1992.
- [105] D. Guang, D.E. Wiley, M. Hlavacek, and A.G. Fane. On-line automatic sampling for real time monitoring of wastewaters. *Wat. Res.*, 30(11):2651–2654, 1996.
- [106] H. Gupta and S. Tanaka. Photocatalytic mineralisation of perchloroethylene using titanium dioxide. *Wat. Sci. Tech.*, 31(9):47–54, 1995.
- [107] F. Gustafsson and H. Hjalmarsson. Twenty-one ML estimators for model structure selection. *Automatica*, 31(10):1377–1392, 1995.

- [108] A.J. Guwy, D.L. Hawkes, F.R. Hawkes, and A.G. Rozzi. Characterization of a prototype industrial on-line analyzer for bicarbonate/carbonate monitoring. *Biotechnol. Bioeng.*, 44(11):1325–1330, 1994.
- [109] M.C. Hascoet and M. Florentz. Influence of nitrates on biological phosphorus removal from wastewater. *Water SA*, 11(1):1–8, 1985.
- [110] F.R. Hawkes, A.J. Guwy, D.L. Hawkes, and A.G. Rozzi. On-line monitoring of anaerobic digestion: Application of a device for continuous measurement of bicarbonate alkalinity. *Wat. Sci. Tech.*, 30(12):1–10, 1994.
- [111] F.R. Hawkes, A.J. Guwy, A.G. Rozzi, and D.L. Hawkes. A new instrument for on-line measurement of bicarbonate alkalinity. *Wat. Res.*, 27(1):167–170, 1993.
- [112] A.C. Hearn. *REDUCE user's manual version 3.6*. RAND, Santa Monica, 1995. <http://www.uni-koeln.de/REDUCE/3.6/doc/reduce/>.
- [113] A. Henriksen. Determination of total nitrogen, phosphorus and iron in fresh water by photo-oxidation with ultraviolet radiation. *Analyst*, 95:601–608, 1970.
- [114] M. Hikuma, H. Matsuoka, M. Takeda, and Y. Tonooka. Microbial electrode for nitrate based on *Pseudomonas aeruginosa*. *Biotechnology Techniques*, 7(3):231–236, 1993.
- [115] A.R. Hill, D.M. Irvine, and D.H. Bullock. Buffer capacity of cheese wheys. *Journal of Food science*, 50:733–738, 1985.
- [116] M. Hirsch and O. Hutzinger. Naturally occurring proteins from pond water sensitize hexachlorobenzene photolysis. *Environ. Sci. Technol.*, 23(10):1306–1307, 1989.
- [117] T.-F.L. Ho and J.R. Bolton. Toxicity changes during the UV treatment of pentachlorophenol in dilute aqueous solution. *Wat. Res.*, 32(2):489–497, 1998.
- [118] P. Hoeksma. De samenstelling van drijfmest die naar akkerbouwbedrijven wordt afgezet. 141 pp., Instituut voor Mechanisatie, Arbeid en Gebouwen (IMAG), Wageningen, Nederland, 1988.
- [119] P. Hoeksma, P.J.L. Derikx, N.W.M. Ogink, and G.W.M. Willems. Toetsing van het prototype monsternamen-apparaat voor drijfmest in transportwagens. 20 pp. P96-52, DLO instituut voor milieu- en agritechniek (IMAG-DLO), Wageningen, Nederland, 1996.
- [120] C.-P. Huang, H.-W. Wang, and P.-C. Chiu. Nitrate reduction by metallic iron. *Wat. Res.*, 32(8):2257–2264, 1998.
- [121] C.M. Hurvich, R. Shumway, and C.-L. Tsai. Improved estimators of Kullback-Leibler information for autoregressive model selection in small samples. *Biometrika*, 77(4):709–719, 1990.
- [122] C.M. Hurvich and C.-L. Tsai. Regression and time series model selection in small samples. *Biometrika*, 76(2):297–307, 1989.

- [123] C.M. Hurvich and C.-L. Tsai. Bias of the corrected AIC criterion for underfitted regression and time series models. *Biometrika*, 78(3):499–509, 1991.
- [124] S. Husted, L.S. Jensen, and S.S. Jørgensen. Reducing ammonia loss from cattle slurry by the use of acidifying additives: the role of the buffer system. *Journal Sci. Food Agric.*, 57:335–349, 1991.
- [125] S. Isaacs and M. Henze. Fluorescence monitoring of an alternating activated sludge process. *Wat. Sci. Tech.*, 30(4):229–238, 1994.
- [126] S. Isaacs and H. Sjøberg. Flow injection analysis for on-line monitoring of a wastewater treatment plant. In J. Van Impe, P. Vanrolleghem, and D. Iserentant, editors, *Advanced instrumentation, Data Interpretation and Control of Biotechnical processes*. Kluwer Academic, 1994.
- [127] S. Isaacs and H. Temmink. Experiences with automatic N and P measurements of an activated sludge process in a research environment. *Wat. Sci. Tech.*, 33(1):165–173, 1996.
- [128] S.H. Isaacs, H. Sjøberg, and M. Kümmel. Monitoring and control of a biological nutrient removal process: rate data as a source of information. Poster Presentation: IFAC/BIO5, Keystone, Colorado, 1992.
- [129] J.J.L. Iversen, J.K. Thomsen, and R.P. Cox. On-line growth measurements in bioreactors by titrating metabolic proton exchange. *Appl. Microbiol. Biotechnol.*, 42(2-3):256–262, 1994.
- [130] W.F. Jardim and J.J.R. Rohwedder. Chemical oxygen demand (COD) using microwave digestion. *Wat. Res.*, 23(8):1069–1071, 1989.
- [131] P.J. Johnes and A.L. Heathwaite. A procedure for the simultaneous determination of total nitrogen and total phosphorus in freshwater samples using persulphate microwave digestion. *Wat. Res.*, 26(10):1281–1287, 1992.
- [132] D. Jolley, W. Maher, and P. Cullen. Rapid method for separating and quantifying orthophosphate and polyphosphates: Application to sewage samples. *Wat. Res.*, 32(3):711–716, 1998.
- [133] C. Jordan. The mean pH of mixed fresh waters. *Wat. Res.*, 23(10):1331–1334, 1989.
- [134] L.-C. Juang, D.-H. Tseng, and Yang S.-C. Treatment of petrochemical wastewater by UV/H₂O₂ photodecomposed system. *Wat. Sci. Tech.*, 36(12):357–365, 1997.
- [135] W.L.M.N. Karim, A.J. Morris, and E.B. Martin. Control relevant identification of a pH waste water neutralisation process using adaptive radial basis function networks. *Computers chem. Engng*, 20:S1017–S1022, 1996.
- [136] C.-H. Kiang, S.S. Kuan, and G.G. Guilbault. Enzymatic determination of nitrate: Electrochemical detection after reduction with nitrate reductase and nitrite reductase. *Anal. Chem.*, 50(9):1319–1322, 1978.

- [137] C.-H. Kiang, S.S. Kuan, and G.G. Guilbault. Enzymatic determination of nitrate: Fluorometric detection after reduction with nitrate reductase. *Anal. Chem.*, 50(9):1323–1325, 1978.
- [138] D.W. King and D.R. Kester. A general approach for calculating polyprotic acid speciation and buffer capacity. *J. Chem. Educ.*, 67(11):932–933, 1990.
- [139] W.S. Kisaalita, P.J. Slininger, R.J. Bothast, J.F. McCarthy, and R.L. Magin. Application of fiber-optic fluorescence measurements to on-line pH monitoring of a pseudomonad fermentation process. *Biotechnol. Prog.*, 7:564–569, 1991.
- [140] R.K. Kobos, D.J. Rice, and D.S. Flournoy. Bacterial membrane electrode for the determination of nitrate. *Anal. Chem.*, 51(8):1122–1125, 1979.
- [141] T. Korenaga, T. Takahashi, T. Moriwake, and S. Sanuki. Water quality monitoring system using a flow-through sensing device. In R. Briggs, editor, *Instrumentation, control and automation of water and wastewater treatment and transport systems*, pages 625–631. IAWPRC Workshop held in Yokohama and Kyoto, Japan, July 26 - August 3 1990, Pergamon Press, 1990.
- [142] C. Kormann, D.W. Bahnemann, and M.R. Hoffmann. Photolysis of chloroform and other organic molecules in aqueous TiO₂ suspensions. *Environ. Sci. Technol.*, 25(3):494–500, 1991.
- [143] H.A. Kramer, J.R. Moed, and H. de Haan. Nitrogen analysis in eutrophic, alkaline and peaty waters: a comparison of different methods to analyse ammonia-nitrogen. *Wat. Res.*, 24(2):221–224, 1990.
- [144] J.R. Kramer, P. Brassard, and P.V. Collins. Automatic electrode correction in binding site analysis. *Environ. Sci. Technol.*, 26(9):1844–1846, 1992.
- [145] H. Kroon. Determination of nitrogen in water: comparison of a continuous-flow method with on-line UV digestion with the original Kjeldahl method. *Anal. Chim. Acta*, 276:287–293, 1993.
- [146] G. Laliberté, P. Lessard, J. de la Noüe, and S. Sylvestre. Effect of phosphorus addition on nutrient removal from wastewater with the cyanobacterium *Phormidium bohneri*. *Biores. Technol.*, 59:227–233, 1997.
- [147] G. Laliberté, D. Proulx, N. De Pauw, and J. de la Noüe. Algal technology in wastewater treatment. In H. Kausch and W. Lampert, editors, *Advances in Limnology - Algae and water pollution*, volume 42, pages 283–302. E. Schweizerbart'sche Verlagsbuchhandlung, Stuttgart, 1994.
- [148] A. LeDuy and J.E. Zajic. A geometrical approach for differentiation of an experimental function at a point: Applied to growth and product formation. *Biotechnol. Bioeng.*, 15:805–810, 1973.
- [149] Y.-W. Lee, S.-K. Ong, and C. Sato. Effects of heavy metals on nitrifying bacteria. *Wat. Sci. Tech.*, 36(12):69–74, 1997.

- [150] P.J. Leslie. Removing phosphorus without chemicals. Kelowna's new Bardenpho wastewater treatment plant. *Water and Pollution Control*, pages 20–22, October 1985.
- [151] P. Lessard, D. Proulx, and J. de la Noüe. Nutrient removal using cyanobacteria (*Phormidium bohneri*): Experimental results with a batch reactor. *Wat. Sci. Tech.*, 30(6):365–368, 1994.
- [152] N. Lewis, K. Topudurti, G. Welshans, and R. Foster. A field demonstration of the UV/oxidation technology to treat ground water contaminated with VOCs. *J. Air Waste Manage. Assoc.*, 40(4):540–547, 1990.
- [153] X.Z. Li and M. Zhang. Decolorization and biodegradability of dyeing wastewater treated by a TiO₂-sensitized photo-oxidation process. *Wat. Sci. Tech.*, 34(9):49–55, 1996.
- [154] X.Z. Li, M. Zhang, and H. Chua. Disinfection of municipal wastewater by sensitized photooxidation. *Wat. Sci. Tech.*, 33(3):111–118, 1996.
- [155] C.-F. Lin and M.M. Benjamin. The effects of strongly complexing ligands on the adsorptive partitioning of metal ions. *Wat. Res.*, 26(4):397–407, 1992.
- [156] P. Linares, M.D.L. de Castro, and M. Valcárcel. Sequential automatic on-line determination of aquiculture nutrients: phosphate and nitrate. *Journal of Automatic Chemistry*, 14(5):173–175, 1992.
- [157] L. Ljung. *System Identification: Theory for the User*. Prentice Hall, Englewood Cliffs, New Jersey, 1987.
- [158] J.R. Lobry, L. Rosso, and J.P. Flandrois. A FORTRAN subroutine for the determination of parameter confidence limits in non-linear models. *Binary*, 3:86–93, 1991.
- [159] G. Locher, B. Sonnleitner, and A. Fiechter. Automatic bioprocess control. 2. Implementations and practical experiences. *J. Biotechnol.*, 19:127–144, 1991.
- [160] G. Locher, B. Sonnleitner, and A. Fiechter. Automatic bioprocess control. 3. Impacts on process perception. *J. Biotechnol.*, 19:173–192, 1991.
- [161] G. Locher, B. Sonnleitner, and A. Fiechter. On-line measurement in biotechnology : Exploitation, objectives and benefits. *J. Biotechnol.*, 25:55–73, 1992.
- [162] R.E. Loewenthal, D. Bilanovic, T.M. Thebe, and M. Green. Determination of low chemical oxygen demand using potentiometry and a modified Gran function. *Water SA*, 23(4):293–299, 1997.
- [163] J. Lohmann. Development of wastewater standards in the federal republic of Germany and the impact on automation engineering. In R. Briggs, editor, *Instrumentation, control and automation of water and wastewater treatment and transport systems*, pages 401–410. IAWPRC Workshop held in Yokohama and Kyoto, Japan, July 26 - August 3 1990, Pergamon Press, 1990.

- [164] J. Londong. Strategies for optimized nitrate reduction with primary denitrification. *Wat. Sci. Tech.*, 26(5–6):1087–1096, 1992.
- [165] J. Londong and P. Wachtl. Six years of practical experience with the operation of on-line analysers. *Wat. Sci. Tech.*, 33(1):159–164, 1996.
- [166] L.H. Lotter and A.R. Pitman. The usefulness of on-line monitoring in effecting savings in combined biological and chemical removal of phosphorus in activated sludge plants. *Wat. Sci. Tech.*, 28(11-12):539–548, 1993.
- [167] R.H. Lowe and M.C. Gillespie. An *Escherichia coli* strain for use in nitrate analysis. *Journal of Agricultural Food Chemistry*, 23(4):783–785, 1975.
- [168] Metrohm Ltd. *716 DMS Titrino, Instructions for use*. Metrohm AG, Herisau, Switzerland, August 1992.
- [169] J.A. Lucey, C. Gorry, and P.F. Fox. Changes in the acid-base buffering curves during the ripening of Emmental cheese. *Milchwissenschaft*, 48(4):183–186, 1993.
- [170] F. Lücking, H. Köser, M. Jank, and A. Ritter. Iron powder, graphite and activated carbon as catalysts for the oxidation of 4-chlorophenol with hydrogen peroxide in aqueous solution. *Wat. Res.*, 32(9):2607–2614, 1998.
- [171] A. Lynggaard-Jensen, N.H. Eismum, I. Rasmussen, H.S. Jacobsen, and T. Stenstrøm. Description and test of a new generation of nutrient sensors. *Wat. Sci. Tech.*, 33(1):25–35, 1996.
- [172] H. Maeckelberghe, R. Depamelaere, H. Sluyts, and F. Van Hoof. Het automatisch meetstation op het Albertkanaal te Grobbendonk. *Water*, (66):168–174, 1992.
- [173] S. Mahimairaja, N.S. Bolan, M.J. Hedley, and A.N. Macgregor. Evaluation of methods of measurement of nitrogen in poultry and animal manures. *Fertilizer Research*, 24:141–148, 1990.
- [174] K.B. Male and J.H.T. Luong. An FIA biosensor system for the determination of phosphate. *Biosensors & Bioelectronics*, 6:581–587, 1991.
- [175] D. Manca, J. de la Noüe, J.E. Côté, and J. Turcotte. Evaluation of a gas-phase selective electrode for the quantitation of ammonia in liquid piggery wastes. *Intern. J. Environ. Anal. Chem.*, 36:55–68, 1989.
- [176] D. Marani, G. Macchi, and M. Pagano. Lead precipitation in the presence of sulphate and carbonate: Testing of thermodynamic predictions. *Wat. Res.*, 29(4):1085–1092, 1995.
- [177] D. Marani, J.W. Patterson, and P.R. Anderson. Alkaline precipitation and aging of the Cu(II) in the presence of sulfate. *Wat. Res.*, 29(5):1317–1326, 1995.
- [178] J. March. *Advanced organic chemistry: Reactions, Mechanisms, and Structure*. McGRAW-HILL International Book Company, 2nd edition, 1984.

- [179] J. Maschlanka. Phosphate elimination: process and control fundamentals. *Wastewater International*, pages 37–42, February 1992.
- [180] A. Massone, K. Gernaey, A. Rozzi, and W. Verstraete. Measurement of ammonium concentration and nitrification rate by a new titrimetric biosensor. *Water Environ. Res.*, 70(3):343–350, 1998.
- [181] A.G. Massone, K. Gernaey, H. Bogaert, A. Vanderhasselt, A. Rozzi, and W. Verstraete. Biosensors for nitrogen control in wastewaters. *Wat. Sci. Tech.*, 34(1–2):213–220, 1996.
- [182] N. Matsché and Stumwöhrer. UV absorption as control-parameter for biological treatment plants. *Wat. Sci. Tech.*, 33(12):211–218, 1996.
- [183] R.W. Matthews. Photo-oxidation of organic material in aqueous suspensions of titanium dioxide. *Wat. Res.*, 20(5):569–578, 1986.
- [184] R.W. Matthews. Purification of water near-UV illuminated suspensions of titanium dioxide. *Wat. Res.*, 24(5):653–660, 1990.
- [185] M.M. Mazet, J. Ayele, and I. Rigaudie. Elimination des acides humiques contenus dans l'eau par les celluloses greffées. *Wat. Res.*, 26(4):409–417, 1992.
- [186] R.F. McCurdy, R. Boss, and J. Dale. Determination of ammonia in water by centrifugal analysis. *Wat. Res.*, 23(6):779–784, 1989.
- [187] J.A. Meima and R.N.J. Comans. Application of surface complexation/precipitation modeling to contaminant leaching from weathered municipal solid waste incinerator bottom ash. *Environ. Sci. Technol.*, 32(5):688–693, 1998.
- [188] S. Menzl, M. Stühler, and R. Benz. A self adaptive computer-based pH measurement and fuzzy-control system. *Wat. Res.*, 30(4):981–991, 1996.
- [189] W. Mertens. Aktiviteit / evenwichtsconstanten: Bepaal zelf de pK_a en maak de aktiviteit zichtbaar. *KVCV-Tijdingen*, 16(1):24–35, 1989.
- [190] W. Mertens. Vergelijkende studie over de verschillende methodes om de zuurgraad (pH) te berekenen en titratiecurven theoretisch te volgen. *KVCV-Tijdingen*, 16(3):49–65, 1989.
- [191] Vlaamse Milieumaatschappij. Jaarverslag meetnet oppervlaktewater. Technical report, Bestuur Meetnetten en Onderzoek, Dienst Water, 1993.
- [192] Vlaamse Milieumaatschappij. VMM Aktiviteitenverslag. Technical report, 1998.
- [193] Vlaamse Milieumaatschappij. Waterkwaliteit – Lozingen in het water. Technical report, 1998.
- [194] M. Miller, G.M. Singer, J.D. Rosen, and R. Bartha. Sequential degradation of chlorophenols by photolytic and microbial treatment. *Environ. Sci. Technol.*, 22(10):1215–1219, 1988.

- [195] C. Minero, V. Maurino, L. Campanella, C. Morgia, and E. Pelizzetti. Photodegradation of 2-ethoxy- and 2-butoxyethanol in the presence of semiconductor particles or organic conducting polymer. *Environ. Technol. Lett.*, 10:301–310, 1989.
- [196] W. Moerman. *Improvement of the effluent quality of activated sludge treated carbonization wastewater*. PhD thesis, Universiteit Gent, Coupure links 653, B-9000 Gent, 1994.
- [197] R.E. Moosbrugger, M.C. Wentzel, G.A. Ekama, and G.v.R. Marais. A 5 pH point titration method for determining the carbonate and SCFA weak acid/bases in anaerobic systems. *Wat. Sci. Tech.*, 28(2):237–245, 1993.
- [198] F.M.M. Morel and J.G. Hering. *Principles and Applications of Aquatic Chemistry*. John Wiley & Sons, New York, 1993.
- [199] J.-L. Mouget, A. Dakhama, M.C. Lavoie, and J. de la Noüe. Algal growth enhancement by bacteria: Is consumption of photosynthetic oxygen involved? *FEMS Microbiol. Ecol.*, 18:35–44, 1995.
- [200] T. Moutin, J.Y. Gal, H. El Halouani, B. Picot, and J. Bontoux. Decrease of phosphate concentration in a high rate pond by precipitation of calcium phosphate: Theoretical and experimental results. *Wat. Res.*, 26(11):1445–1450, 1992.
- [201] M. Mrkva. Evaluation of correlations between absorbance at 254 nm and COD of river waters. *Wat. Res.*, 17:231–235, 1983.
- [202] C. Mussche. Validatie en uitbreiding van een pH gebaseerde sensor voor laagbelaste waters. Master's thesis, Universiteit Gent, Coupure links 653, B-9000 Gent, 1997.
- [203] E.V. Musvoto, M.C. Wentzel, R.E. Loewenthal, and G.A. Ekama. Kinetic-based model for mixed weak acid/base systems. *Water SA*, 23(4):311–322, 1997.
- [204] G.H. Nancollas, Z. Amjad, and P. Koutsoukos. Calcium phosphates - speciation, solubility and kinetic considerations. In E.A. Jenne, editor, *Chemical Modeling in Aqueous Systems - Speciation, Sorption, Solubility, and Kinetics*, number 93 in ACS Symposium Series, pages 475–497, Washington, DC, 1979. American Chemical Society.
- [205] J.A. Nelder and R. Mead. A simplex method for function minimization. *The Computer Journal*, 7:308–313, 1964.
- [206] J.A. Nelder and R. Mead. A simplex method for function minimization: Errata. *The Computer Journal*, 8:27, 1965.
- [207] J. Neter, M.H. Kutner, C.J. Nachtsheim, and W. Wasserman. *Applied linear statistical models*. Irwin, London, 4th edition, 1990.
- [208] H.J. Noorman, G.C.A. Luijkx, K.Ch.A.M. Luyben, and J.J. Heijnen. Modeling and experimental validation of carbon dioxide evolution in alkalophilic cultures. *Biotechnol. Bioeng.*, 39:1069–1079, 1992.

- [209] G. Ogner. Digestion of plants and organic soils using nitric acid, hydrogen peroxide and UV irradiation. *Commun. in Soil Sci. Plant Anal.*, 14(10):937–943, 1983.
- [210] H. Okamoto, K. Mori, K. Ohtsuka, H. Ohuchi, and H. Ishii. Theory and computer programs for calculating solution pH, buffer formula, and buffer capacity for multiple component system at a given ionic strength and temperature. *Pharmaceutical Research*, 14(3):299–302, 1997.
- [211] W. Olthuis, M.A.M. Robben, P. Bergveld, M. Bos, and W.E. Van Der Linden. pH sensor properties of electrochemically grown iridium oxide. *Sensors and Actuators B*, 2:247–256, 1990.
- [212] D. Osbild, M. Babut, and P. Vasseur. Review - state of the art: Biosensors for environmental monitoring and water control. *Revue des Sciences de l'Eau*, 8(4):505–538, 1995.
- [213] R. Otterpohl, T. Rolfs, and J. Londong. Optimizing operation of wastewater treatment plants by offline and online computer simulation. *Wat. Sci. Tech.*, 30(2):165–174, 1994.
- [214] J.P. Ottoy and G.C. Vansteenkiste. A computer program for non-linear curve fitting. *Adv. Eng. Software*, 3(2):55–61, 1981.
- [215] J.D. Owens, D.S. Thomas, P.S. Thompson, and J.W. Timmerman. Indirect conductimetry: a novel approach to the conductimetric enumeration of microbial populations. *Letters in Applied Microbiology*, 9:245–249, 1989.
- [216] J.F. Pankow. *Aquatic Chemistry Concepts*. Lewis Publishers, Chelsea, Michigan, 1991.
- [217] J.R. Parker. *Model based multi-agent object classification*. PhD thesis, Faculty of Sciences, University Gent, Belgium, 1998.
- [218] J.J. Pauer, H.R. van Vliet, and J.F. Staden. The automated determination of nitrate in water. *Water SA*, 16(2):105–108, 1990.
- [219] A. Pauss, A. Rozzi, M.J. Ledrut, H. Naveau, and E.J. Nyns. Bicarbonate determination in complex acid-base solutions by a back-titration method. *Environ. Technol.*, 11:469–476, 1990.
- [220] K.M. Pedersen, M. Kümmel, and H. Sørensen. Monitoring and control of biological removal of phosphorus and nitrogen by flow-injection analysers in a municipal pilot-scale waste-water treatment plant. *Anal. Chim. Acta*, 238:191–199, 1990.
- [221] K.M. Pedersen, M. Kümmel, and H. Sørensen. A real time measurement system for an activated sludge wastewater treatment plant. In R. Briggs, editor, *Instrumentation, control and automation of water and wastewater treatment and transport systems*, pages 171–178. IAWPRC Workshop held in Yokohama and Kyoto, Japan, July 26 - August 3 1990, Pergamon Press, 1990.

- [222] L. Pehrsson, F. Ingman, and A. Johansson. Acid-base titrations by stepwise additions of equal volumes of titrant with special reference to automatic titrations – 1 Theory, discussion of the Gran functions, the Hofstee method and two proposed methods for calculating equivalence volumes. *Talanta*, 23:769–780, 1976.
- [223] L. Pehrsson, F. Ingman, and A. Johansson. Acid-base titrations by stepwise additions of equal volumes of titrant with special reference to automatic titrations – 2 Theory of titration of mixtures of acids, polyprotic acids, acids in mixture with weak bases, and ampholytes. *Talanta*, 23:781–788, 1976.
- [224] E. Pelizzetti, V. Maurino, C. Minero, V. Carlin, E. Pramauro, O. Zerbinati, and M. Tosato. Photocatalytic degradation of atrazine and other *s*-triazine herbicides. *Environ. Sci. Technol.*, 24:1559–1565, 1990.
- [225] E. Pelizzetti, C. Minero, V. Maurino, A. Sclafani, H. Hidaka, and N. Serpone. Photocatalytic degradation of nonylphenol ethoxylated surfactants. *Environ. Sci. Technol.*, 23(11):1380–1385, 1989.
- [226] E.M. Perdue. Solution thermochemistry of humic substances - acid-base equilibria of river water humic substances. In E.A. Jenne, editor, *Chemical Modeling in Aqueous Systems - Speciation, Sorption, Solubility, and Kinetics*, number 93 in ACS Symposium Series, pages 99–114, Washington, DC, 1979. American Chemical Society.
- [227] D. Peterson, D. Watson, and W. Winterlin. Destruction of pesticides and their formulations in water using short wavelength UV light. *Bull. Environ. Contam. Toxicol.*, 44(5):744–750, 1990.
- [228] G.E. Powell and D.B. Archer. On-line titration method for monitoring buffer capacity and total volatile fatty acid levels in anaerobic digesters. *Biotechnol. Bioeng.*, 33:570–577, 1989.
- [229] W.H. Press, S.A. Teukolsky, W.T. Vetterling, and B.P. Flannery, editors. *Numerical Recipes in C. The art of scientific computing*. Cambridge University Press, Cambridge, United Kingdom, 2th edition, 1995.
- [230] D. Proulx, P. Lessard, and J. de la Noüe. Traitement tertiaire d'un effluent domestique secondaire par culture intensive de la cyanobactérie *Phormidium bohneri*. *Environ. Technol.*, 15:449–458, 1994.
- [231] R. Ramadori, A. Rozzi, and V. Tandoi. An automated system for monitoring the kinetics of biological oxidation of ammonia. *Wat. Res.*, 14:1555–1557, 1980.
- [232] C. Ranger. Determination of low level nutrients in environmental water samples using flow injection analysis. *Int. Environ. Technol.*, pages 21–23, 1993.
- [233] P. Reichert. *Concepts underlying a computer program for the identification and simulation of aquatic systems*. Number 7 in Schriftenreihe der EAWAG. Swiss Federal Institute for Environmental Science and Technology (EAWAG), Dübendorf, Switzerland, 1994.

- [234] P. Reichert. River water quality model no. 1: case study ii. oxygen and nitrogen conversion processes in the river Glatt. Submitted to the IWA World congress in Paris, 2000.
- [235] H. Rilbe. On the use of dimension-less parameters in acid-base theory: 1. The buffer capacity of simple ampholyte solutions. *Electrophoresis*, 13(11):811–816, 1992.
- [236] H. Rilbe. On the use of dimensionless parameters in acid-base theory: 2. The molar buffer capacities of bivalent weak acids and bases. *Electrophoresis*, 14(3):202–204, 1993.
- [237] H. Rilbe. On the use of dimensionless parameters in acid-base theory: 3. The molar buffer capacity of trivalent protolytes. *Electrophoresis*, 14(7):591–596, 1993.
- [238] W.S. Rovira, G. Kalis, and A. Fowler. Water and wastewater monitoring and analysis: state of the art in on-line accurate pH measurement. *Journal A*, 33(3):50–62, 1992.
- [239] A. Rozzi. Physico-chemical equilibria in anaerobic digesters. In R. Buvet, M.F. Fox, and D.J. Picken, editors, *Biomethane, Production and Uses*, pages 79–94. Turret-Wheatland, Rickmansworth, 1984.
- [240] A. Rozzi. Alkalinity considerations with respect to anaerobic digesters. *Proceedings 5th Forum Applied Biotechnology. Med. Fac. Landbouww. Rijksuniv. Gent*, 56:1499–1514, 1991.
- [241] A. Rozzi, A.C. Di Pinto, and A. Brunetti. Anaerobic process control by bicarbonate monitoring. *Environ. Technol. Lett.*, 6(594–601), 1985.
- [242] A. Rozzi, A. Massone, and M. Antonelli. A VFA measuring biosensor based on nitrate reduction. *Wat. Sci. Tech.*, 36(6-7):183–189, 1997.
- [243] R.L. Runkel, K.E. Bencala, R.E. Broshears, and S.C. Chapra. Reactive solute transport in streams 1. Development of an equilibrium-based model. *Water Resour. Res.*, 32(2):409–418, 1996.
- [244] R.L. Runkel, D.M. McKnight, and K.E. Bencala. Reactive solute transport in streams 2. Simulation of a pH modification experiment. *Water Resour. Res.*, 32(2):419–430, 1996.
- [245] A. Safarzadeh-Amiri, J.R. Bolton, and S.R. Cater. Ferrioxalate-mediated photodegradation of organic pollutants in contaminated water. *Wat. Res.*, 31(4):787–798, 1997.
- [246] F.F. Sanders. Watch out for instrument errors. *Chemical Engineering Progress*, pages 62–66, July 1995.
- [247] E.B.H. Santos and A.C. Duarte. The influence of pulp and paper mill effluents on the composition of the humic fraction of aquatic organic matter. *Wat. Res.*, 32(3):597–608, 1998.
- [248] D.E. Sawyers and S.K. Dentel. Anoxic, zero-headspace titrations of landfill leachate. *Wat. Sci. Tech.*, 26(9–11):2265–2268, 1992.

- [249] S.N. Scarce, R.W. Benninger, A.S. Weber, and J.H. Sherrard. Prediction of alkalinity changes in the activated sludge process. *J. Water Pollut. Control Fed.*, 52(2):399–405, 1980.
- [250] S. Schlegel and P. Baumann. Requirements with respect to on-line analyzers for N and P. *Wat. Sci. Tech.*, 33(1):139–146, 1996.
- [251] J.L. Schnoor. *Environmental modeling - Fate and transport of pollutants in water, air, and soil*. John Wiley & Sons, New York, 1996.
- [252] H.Fr. Schröder. Non-biodegradable wastewater compounds treated by ozone or ozone/UV-conversion monitoring by substance-specific analysis and biotoxicity testing. *Wat. Sci. Tech.*, 33(6):331–338, 1996.
- [253] G. Schwarz. Estimating the dimension of a model. *Ann. Statist.*, 6(2):461–464, 1978.
- [254] I. Sekerka and J.F. Lechner. Determination of alkalinity and acidity of water by conductometric acid-base titration. *J. Assoc. off. Anal. chem.*, 67(5):893–895, 1984.
- [255] W. Sellien, R. Czolk, J. Reichert, and H.J. Ache. Development of an optical-chemical sensor for the detection of ammonium ions. *Anal. Chim. Acta*, 269:83–88, 1992.
- [256] D. Sen, C.W. Randall, and T.J. Grizzard. Alkalinity and turbidity measurements as feedback controls to improve performance of a biological nitrogen and phosphorus removal system. In R. Briggs, editor, *Instrumentation, control and automation of water and wastewater treatment and transport systems*, pages 291–298. IAWPRC Workshop held in Yokohama and Kyoto, Japan, July 26 - August 3 1990, Pergamon Press, 1990.
- [257] S.M. Serkiz, J.D. Allison, E.M. Perdue, H.E. Allen, and D.S. Brown. Correcting errors in the thermodynamic database for the equilibrium speciation model MINTEQA2. *Wat. Res.*, 30(8):1930–1933, 1996.
- [258] J.B. Sérodes, E. Walsh, O. Goulet, J. de la Noüe, and C. Lescelleur. Tertiary treatment of municipal wastewater using bioflocculating micro-algae. *Can. J. Civ. Eng.*, 18:940–944, 1991.
- [259] J. Sevrin-Reyssac, S. Sylvestre, and J. de la Noüe. Stimulation de la production de microalgues et de la dépollution pendant l’hiver par des apports de gaz carbonique et une élévation de la température. *Comptes rendus de l’académie d’agriculture de France*, 79(7):77–92, 1993.
- [260] L. Sigg, W. Stumm, and P. Behra. *Chimie des milieux aquatiques - chimie des eaux naturelles et des interfaces dans l’environnement*. Masson, Paris, 1992.
- [261] M. Sikow and J. Pursiainen. Use and maintenance of on-line measurements at Suomenoja wastewater plant. In *Proceedings IAWQ Specialized Conference on Sensors in Waste Water Technology*, Copenhagen, Denmark, October 1995. IAWQ.
- [262] W.R. Smith and R.W. Missen. *Chemical Reaction Equilibrium Analysis: Theory and Algorithms*. John Wiley & Sons, New York, 1982.

- [263] V.L. Snoeyink and D. Jenkins. *Water Chemistry*. John Wiley & Sons, New York, 1980.
- [264] T. Söderström and P. Stoica. Model validation and model structure determination. In *System Identification*, chapter 11, pages 422–467. Prentice Hall, Englewood Cliffs, New Jersey, 1989.
- [265] B. Sonnleitner, G. Locher, and A. Fiechter. Automatic bioprocess control. 1. A general concept. *J. Biotechnol.*, 19:1–18, 1991.
- [266] J. Sørensen, J. Andersen, K. Andreasen, and K. Hald. Experience with the upgrading of 14 treatment plants to N & P removal in the municipality of Aarhus. *Wat. Sci. Tech.*, 37(9):201–208, 1998.
- [267] M. Sörensen and F.H. Frimmel. Photochemical degradation of hydrophilic xenobiotics in the UV/H₂O₂ process: Influence of nitrate on the degradation rate of EDTA, 2-amino-1-naphthalenesulfonate, diphenyl-4-sulfonate and 4,4'-diaminostilbene-2,2'-disulfonate. *Wat. Res.*, 31(11):2885–2891, 1997.
- [268] W. Spendley, G.R. Hext, and F.R. Himsforth. Sequential application of simplex designs in optimisation and evolutionary operation. *Technometrics*, 4(4):441–461, 1962.
- [269] M.A. Stanley, J. Maxwell, M. Forrestal, A.P. Doherty, B.D. MacCraith, D. Diamond, and J.G. Vos. Comparison of the analytical capabilities of an amperometric and an optical sensor for the determination of nitrate in river and well water. *Anal. Chim. Acta*, 299:81–90, 1994.
- [270] S.K. Stephens, I.E. Tohill, P.J. Warner, and A.P.F. Turner. Detection of silage effluent pollution in river water using biosensors. *Wat. Res.*, 31(1):41–48, 1997.
- [271] J.P. Stephenson, E.G. Luxon, B.A. Monaghan, and R.G. Gillespie. Evaluation of instruments for continuous activated sludge monitoring. *Wat. Sci. Tech.*, 13:721–728, 1981.
- [272] A.V. Stoyanov and P.G. Righetti. Can amphoteric substances with very small (or negative) ΔpK differences exist and what properties would their water solutions exhibit? *Electrophoresis*, 19(2):187–191, 1998.
- [273] W. Stumm and J.J. Morgan. *Aquatic chemistry - Chemical equilibria and rates in natural waters*. John Wiley & Sons, New York, 1996.
- [274] C.J. Swinnerton, D.J. Palmer, and P.N. Williams. “Sherlock”: An integrated approach to pollution monitoring. In J. Bau, J.P.L. Ferreira, J.D. Henriques, and J. de Oliveira Raposo, editors, *Integrated approaches to water pollution problems*, pages 115–121. Elsevier Applied Science, 1992.
- [275] S. Sylvestre, P. Lessard, and J. de la Noüe. Performance d’un photobioréacteur utilisant la cyanobactérie *Phormidium bohneri* pour l’enlèvement de l’azote et du phosphore. *Environ. Technol.*, 17:697–706, 1996.

- [276] K. Takeda and K. Fujiwara. Characteristics on the determination of dissolved organic nitrogen compounds in natural waters using titanium dioxide and platinized titanium dioxide mediated photocatalytic degradation. *Wat. Res.*, 30(2):323–330, 1996.
- [277] P. Talbot and J. de la Noüe. Tertiary treatment of wastewater with *Phormidium bohneri* (schmidle) under various light and temperature conditions. *Wat. Res.*, 27(1):153–159, 1993.
- [278] P. Talbot, M.P. Gortares, R.W. Lencki, and J. de la Noüe. Absorption of CO₂ in algal mass culture systems: A different characterization approach. *Biotechnol. Bioeng.*, 37:834–842, 1991.
- [279] P. Talbot, R.W. Lencki, and J. de la Noüe. Carbon dioxide absorption characterization of a bioreactor for biomass production of *Phormidium bohneri*: Comparative study of three types of diffuser. *J. Appl. Phycol.*, 2:341–350, 1990.
- [280] P. Talbot, J.-M. Thébault, A. Dauta, and J. de la Noüe. A comparative study and mathematical modeling of temperature, light and growth of three microalgae potentially useful for wastewater treatment. *Wat. Res.*, 25(4):465–472, 1991.
- [281] M. Tardat-Henry and J.-P. Beaudry. *Chimie des eaux*. Les éditions le Griffon d'argile, Sainte-Foy (Québec), Canada, 1992.
- [282] B. Tartakovsky, L.A. Lishman, and R.L. Legge. Application of multi-wavelength fluorometry for monitoring wastewater treatment process dynamics. *Wat. Res.*, 30(12):2941–2948, 1996.
- [283] B. Teichgräber. Alkalinity and pH-control in activated sludge plants with nitrification. In R. Briggs, editor, *Instrumentation, control and automation of water and wastewater treatment and transport systems*, pages 179–185. IAWPRC Workshop held in Yokohama and Kyoto, Japan, July 26 - August 3 1990, Pergamon Press, 1990.
- [284] The MuPAD Group, Benno Fuchssteiner et al. *MuPAD User's Manual - MuPAD Version 1.2.2*. John Wiley and sons, Chichester, New York, first edition, March 1996.
- [285] J.-M. Thébault. Representation of phosphorus in lake ecosystem models. *Annl's Limnol.*, 31(2):143–149, 1995.
- [286] J. Thielmann, N.E. Tolbert, A. Goyal, and H. Senger. Two systems for concentrating CO₂ and bicarbonate during photosynthesis by *Scenedesmus*. *Plant Physiol.*, 92:622–629, 1990.
- [287] O. Thomas, F. Theraulaz, C. Agnel, and S. Suryani. Advanced UV examination of wastewater. *Environ. Technol.*, 17:251–261, 1996.
- [288] H.A. Thomsen and K. Kisbye. N and P on-line meters: Requirements, maintenance and stability. *Wat. Sci. Tech.*, 33(1):147–157, 1996.

- [289] H.A. Thomsen and M.K. Nielsen. Practical experience with on-line measurements of NH_4 , NO_3 , PO_4 , redox, MLSS and SS in advanced activated sludge plants. In *Colloquium "The City and the Water"*, pages 1–11. Hydrotop 92, 8-10 April 1992.
- [290] D.E. Thornberg, M. Nielsen, and J. Eriksson. Upgrading of Borås wastewater treatment plant based on intelligent process and operation control. *Wat. Sci. Tech.*, 37(9):57–63, 1998.
- [291] D.E. Thornberg, M.K. Nielsen, and K.L. Andersen. Nutrient removal: On-line measurements and control strategies. *Wat. Sci. Tech.*, 28(11-12):549–560, 1993.
- [292] D.E. Thornberg and H.A. Thomsen. Interaction between computer simulations and control using on-line nitrogen measurements. *Wat. Sci. Tech.*, 30(4):199–206, 1994.
- [293] U. Tinner. Electrodes in potentiometry. Metrohm AG, Herisau, Switzerland, 1989.
- [294] L. Tranvik and S. Kokalj. Decreased biodegradability of algal DOC due to interactive effects of UV radiation and humic matter. *Aquat. Microb. Ecol.*, 14(3):301–307, 1998.
- [295] R.R. Trussell. Spreadsheet water conditioning. Spreadsheets are a powerful tool for solving water chemistry problems. *Journal AWWA*, 90(6):70–81, 1998.
- [296] K. Tsukada, Y. Miyahara, Y. Shibata, and H. Miyagi. An integrated chemical sensor with multiple ion and gas sensors. *Sensors and Actuators B*, 2:291–295, 1990.
- [297] H. Twist, A.C. Edwards, and G.A. Codd. Algal growth responses to waters of contrasting tributaries of the river Dee, North-East Scotland. *Wat. Res.*, 32(8):2471–2479, 1998.
- [298] E. v. Münch and P.F. Greenfield. Estimating VFA concentrations in fermenters by measuring pH. *Wat. Res.*, 32(8):2431–2441, 1998.
- [299] M. Van De Steene. Modelgebaseerde on-line alarmgenerator voor laagbelaste waters. Master's thesis, Universiteit Gent, Coupure links 653, B-9000 Gent, 1998.
- [300] M. Van De Steene, L. Van Vooren, and P. Vanrolleghem. Eindverslag FASTNAP projekt. Technical report, BIOMATH, Universiteit Gent, December 1999.
- [301] H. Van den Broeck. Meetonzekerheid: Een slag in het water? KVCV sectie milieu & veiligheid, November 1999.
- [302] P. Van der Meeren, J. Vanderdeelen, and L. Baert. Vergelijkingen voor de berekening van aktiviteitskoefficienten: een vrije keuze? *KVCV-Tijdingen*, 13(3), 1986.
- [303] A.J. Van Der Veer and C.E. Zagt. Het ontwerp van een UV-reactor. *H₂O*, 30(26):806–810, 1997.
- [304] K. Van Hecke, O. Van Cleemput, and L. Baert. Chemo-denitrification of nitrate-polluted water. *Environ. Pollut.*, 63:261–274, 1990.

- [305] A. Van Molle. Implementatie van een digitale pH-regelaar als net-effect sensor van biotechnologische processen. Master's thesis, Universiteit Gent, Coupure links 653, B-9000 Gent, 1985.
- [306] J.F. van Staden. Simultaneous flow-injection analysis for two components with on-line dialysis and gas diffusion in series: Determination of chloride and ammonia nitrogen in industrial effluent water. *Anal. Chim. Acta*, 261:453–459, 1992.
- [307] J. van Tuijnen and J. van Konijnenburg. On-line meetapparatuur voor emissiegegevens. *MilieuMarkt*, pages 47–55, January/February 1993.
- [308] L. Van Vooren, P. Lessard, J.-P. Ottoy, and P.A. Vanrolleghem. pH buffer capacity based monitoring of algal wastewater treatment. *Environ. Technol.*, 20:547–561, 1999.
- [309] L. Van Vooren, M. Van De Steene, J.-P. Ottoy, and P.A. Vanrolleghem. Automatic buffer capacity model building for the purpose of water quality monitoring. *Submitted for WATERMATEX 2000 conference*, 2000.
- [310] L. Van Vooren and P. Willems. Chemische en microbiologische monitoring van de waterkwaliteit. deel 2. Net-effekt sensor voor oppervlaktewater monitoring. In *Verhandelingen van de Fac. L & TBW*, pages 6/1–4, Gent, Belgium, December 1992. Post-Universitaire Onderwijsdag, Universiteit Gent.
- [311] L. Van Vooren, P. Willems, J.P. Ottoy, G.C. Vansteenkiste, and W. Verstraete. Automated buffer capacity based sensor for effluent quality monitoring. *Wat. Sci. Tech.*, 33(1):81–87, 1996.
- [312] A. Vanderhasselt. Decados: een nieuwe sensor voor nitraatverwijdering. *Het Ingenieursblad*, (8–9):26–30, 1996.
- [313] G. Vanhooren. Gebruik van een globale biologische index ter bepaling van de biotoop en de waterkwaliteit van de oppervlaktewateren. *Water*, (45):45–50, 1989.
- [314] H. Vanhooren, D. Demey, I. Vannijvel, and P.A. Vanrolleghem. Monitoring and modelling an industrial trickling filter using on-line off-gas analysis and respirometry. Submitted to ISEB 4, Noordwijkerhout, April 10–12, 2000.
- [315] P. Vanrolleghem. *On-line modelling of activated sludge processes: Development of an adaptive sensor*. PhD thesis, Universiteit Gent, Coupure links 653, B-9000 Gent, 1994.
- [316] P. Vanrolleghem and F. Coen. Optimal design of in-sensor-experiments for on-line modelling of nitrogen removal processes. *Wat. Sci. Tech.*, 31(2):149–160, 1995.
- [317] P. Vanrolleghem and W. Verstraete. On-line monitoring equipment for wastewater treatment processes: state of the art. In *Studiedag Optimalisatie van waterzuiveringsinstallaties door procescontrole en -sturing*, pages 1–22, Gent, Belgium, 1993. TI-KVIV.
- [318] P.A. Vanrolleghem, B. De Clercq, M. Devisscher, J. Meirlaen, and H. Vanhooren. *Kursus Bioprocessregeling*. Universiteit Gent, Coupure links 653, B-9000 Gent, 1998.

- [319] P.A. Vanrolleghem and D. Dochain. Bioprocess model identification. In J.F. Van Impe, P.A. Vanrolleghem, and D. Iserentant, editors, *Advanced instrumentation, Data interpretation, and Control of biotechnological processes*, chapter 10, pages 251–318. Kluwer Academic Publishers, Dordrecht, The Netherlands, 1998.
- [320] P.A. Vanrolleghem, Z. Kong, and F. Coen. Full-scale on-line assessment of toxic wastewaters causing change in biodegradation model structure and parameters. *Wat. Sci. Tech.*, 33(2):163–175, 1996.
- [321] P.A. Vanrolleghem, W. Schilling, W. Rauch, P. Krebs, and H. Aalderink. Setting up measuring campaigns for integrated wastewater modelling. *Wat. Sci. Tech.*, 39(4):257–268, 1999.
- [322] P.A. Vanrolleghem, M. Van Daele, and D. Dochain. Practical identifiability of a biokinetic model of activated sludge respiration. *Wat. Res.*, 29(11):2561–2570, 1995.
- [323] G.C. Vansteenkiste, J. Spriet, and J. Bens. Structure characterization for system modeling in uncertain environments. In B.P. Zeigler, M.S. Elzas, G.J. Klir, and T.I. Ören, editors, *Methodology in systems modelling and simulation*, pages 789–303. North-Holland Publishing Company, 1979.
- [324] M.D.R. Vaz, A.C. Edwards, and C.A. Shand. Determination of dissolved organic phosphorus in soil solutions by an improved automated photo-oxidation procedure. *Talanta*, 39(11):1479–1487, 1992.
- [325] L. Vermeersch, B. Kroes, and P. Vanrolleghem. Feature-based model identification of nonlinear biotechnological processes. *Ecol. modelling*, 75/76:629–640, 1994.
- [326] H. Wacheux, J.-L. Million, C. Guillo, and E. Alves. NH₄ automatic analysers for WWTP: Evaluation test at laboratory and field level. *Wat. Sci. Tech.*, 33(1):193–201, 1996.
- [327] N. Walraven. Verslag van het bezoek aan ANALYTICA te München. 10 pp. P98-57, DLO instituut voor milieu- en agritechniek (IMAG-DLO), Wageningen, Nederland, 1998.
- [328] N. Walraven and P.J.L. Derikx. Sub-bemonstering van drijfmest: een inventarisatie van mogelijke technieken. 13 pp. P98-79, DLO instituut voor milieu- en agritechniek (IMAG-DLO), Wageningen, Nederland, 1998.
- [329] N. Walraven, P.J.L. Derikx, N.W.M. Ogink, and J.H. Slangen. Magnetrondestructie van dierlijke mest voor de bepaling van stikstof en fosfor. 13 pp. P98-71, DLO instituut voor milieu- en agritechniek (IMAG-DLO), Wageningen, Nederland, 1998.
- [330] N. Walraven, H.C. Willers, P.J.L. Derikx, J.H. Slangen, and N.W.M. Ogink. Perspectives for on-line measurement of manure composition. In *Dutch-Japanese Workshop on Precision Dairy Farming*, pages 109–119, Wageningen, The Netherlands, September 1998.

- [331] J. Wang, C.P. Huang, H.E. Allen, L.R. Takiyama, I. Poesponegoro, H. Poesponegoro, and D. Pirestani. Acid characteristics of dissolved organic matter in wastewater. *Water Environ. Res.*, 70(5):1041–1048, 1998.
- [332] J.B. Watts, K. Evans, and A. Molloy. A wastewater/water process monitoring system allowing operational control – developed by an operational manager. In R. Briggs, editor, *Instrumentation, control and automation of water and wastewater treatment and transport systems*, pages 143–154. IAWPRC Workshop held in Yokohama and Kyoto, Japan, July 26 - August 3 1990, Pergamon Press, 1990.
- [333] R.J. Watts, V.D. Adams, and E.J. Middlebrooks. Dissolved oxygen requirements for the indirect photolysis treatment of two refractory herbicides. *J. Environ. Qual.*, 17(4):723–729, 1988.
- [334] W.F. Watts, J.B. and Garber. Instrument and system maintenance: A design and operational necessity. In B. Jank and IAWQ Program committee, editors, *Instrumentation, control and automation of water & wastewater treatment and transportation systems*, pages 328–337. IAWQ, June 1993.
- [335] R.C. Weast and M.J. Astle, editors. *CRC Handbook of chemistry and physics*. CRC Press inc., Florida, U.S.A., 60th edition, 1981.
- [336] R.B. Webber. *The book of pH*. George Newnes Limited, London, 1957.
- [337] W.J. Weber Jr. and F.A. DiGiano. *Process Dynamics in Environmental Systems*. John Wiley & Sons, New York, 1996.
- [338] S.R. Weijers, J.J. Kok, H.A. Preisig, A. Buunen, and T.W.M. Wouda. Parameter identifiability in the IAWQ model no. 1 for modelling activated sludge plants for enhanced nitrogen removal. *Computers chem. Engng*, 20:S1455–S1460, 1996.
- [339] T. Wik. Modelling dynamics of nitrifying trickling filters and ammonium meters. *Proceedings 11th Forum Applied Biotechnology. Med. Fac. Landbouww. Univ. Gent*, 62:1641–1648, 1997.
- [340] W. Willems. Neurale technieken bij parameterschatting van biologische processen. Master's thesis, Universiteit Gent, Coupure links 653, B-9000 Gent, 1993.
- [341] H.C. Willers, N. Walraven, P.J.L. Derikx, and J.H. Slangen. On-line meten van P en N in mest: een inventarisatie van vier analysetechnieken. 11 pp. P98-19, DLO instituut voor milieu- en agritechniek (IMAG-DLO), Wageningen, Nederland, 1998.
- [342] I. Willner, E. Katz, and N. Lapidot. Bioelectrocatalysed reduction of nitrate utilizing polythiophene bipyridinium enzyme electrodes. *Bioelectrochemistry and Bioenergetics*, 29:29–45, 1992.
- [343] J.F. Wright, P.D. Armitage, M.T. Furse, and D. Moss. Prediction of invertebrate communities using stream measurements. *Regulated Rivers: Research and Management*, 4:147–155, 1989.

- [344] J.F. Wright, M.T. Furse, and P.D. Armitage. RIVPACS - a technique for evaluating the biological quality of rivers in the U.K. *European Water Pollution Control*, 3(4):15–25, 1993.
- [345] M. Yang, J. Hu, and K. Ito. Characteristics of $\text{Fe}^{2+}/\text{H}_2\text{O}_2/\text{UV}$ oxidization process. *Environ. Technol.*, 19(2):183–191, 1998.
- [346] S. Yeoman, T. Stephenson, J.N. Lester, and R. Perry. Biotechnology for phosphorus removal during wastewater treatment. *Biotech. Adv.*, 4:13–26, 1986.
- [347] Z. Yuan, Bogaert H., P.A. Vanrolleghem, C. Thoeye, G.C. Vansteenkiste, and W. Verstraete. Control of external carbon addition to predenitrifying systems. *J. Environ. Eng.*, 123:1080–1086, 1997.
- [348] L. Zaiyou and W. Limin. Determination of total phosphorus in water by photochemical decomposition with ultraviolet irradiation. *Talanta*, 33(1):98–100, 1986.

Summary

In this work, a multipurpose titrimetric sensor was developed. The hardware part of the sensor developed in this work consists of a titrator unit, capable to perform acid-base titrations of aquatic samples. A titration curve has a typical S-shape, and can be transformed into a buffer capacity profile with an appropriate mathematical algorithm. The software sensor part of this work can be seen as the complete data interpretation of the recorded titration curves. The developed hard- and software sensor differentiates itself from most existing sensors by the fact that the whole and detailed titration profile is used for model-based interpretation. It is a multipurpose sensor because, on the one hand, it is useful for the quantification of buffering components (e.g. ammonium and ortho-phosphate in effluents or in destructed animal manure samples), and, on the other hand, it can be used as an alarm generator or early warning system (e.g. the detection of accidental pollutant discharges in rivers). An important part of the research described in this thesis was performed in the framework of research projects in which industrial partners were involved. Therefore, the research described in this thesis is interdisciplinary and practically oriented.

The first part of the thesis describes the fundamentals and the background of the research work. The constructive approach, illustrated with didactic examples should allow the reader to obtain a solid introduction and a consistent overview of pH buffer capacity modelling. This overview was partially based on literature research, however, major parts were adapted or further developed to fit the requirements of this work. Furthermore, in the literature a number of pitfalls and serious confusions related to this subject were pointed out. An interesting aspect is that not only buffer capacity models were developed for the simplest type of chemical reactions (acid-base equilibria), but that also more complicated buffer systems (i.e. where complexation and/or precipitation reactions occur) could be considered in the same framework. Appropriate simulation software was developed for each of the presented approaches. Further, a literature review on field technologies for on-line measurement in wastewater treatment systems, rivers and other aquatic streams is presented.

The second part of the thesis summarizes the main software developments. A commercial automatic titrator with a built-in dynamic titration algorithm was used to collect the experimental titration curves. Using this algorithm, some disadvantages were encountered, and therefore a combined data- and model-driven titration algorithm was developed, capable of performing the titration task as needed for the purpose of this work. A dosing system, coupled to a computer and using the developed algorithm also offers perspectives for use in the laboratory as an alternative for traditional end-point titrators. The complete data processing part of the titrimetric sensor is implemented in the software *bomb* (buffer capacity optimal model builder), with

strong emphasis on the robustness for field-use. From a particular titration curve, this software extracts information about individual buffer systems and estimates their concentrations. Further, the same software is capable to automatically build buffer capacity models.

The third part of this work is application oriented. Three on-line (field) application areas for the developed sensor were investigated in detail: effluent and river water monitoring, algal wastewater treatment monitoring and animal manure nutrient measurements. The minimum amount of ammonium and ortho-phosphate that can be successfully recovered with the buffer capacity based sensor is around 0.5 mg N l^{-1} and 0.5 mg P l^{-1} respectively. These values are only indicative, because they are case dependent. The results obtained show that the buffer capacity based sensor is a useful measurement system for on-line monitoring of ammonium and ortho-phosphate in effluents, river waters and algal wastewater treatment systems. Because the titrimetric measurement methodology is undoubtedly sensitive to interferences, the sensor application should in the first place be seen in the context of alarm generation. In an algal wastewater treatment plant, the inorganic carbon buffer could accurately be assessed with the developed sensor, and this measurement was interpreted as a useful control input. The simultaneous measurement of ammonium, ortho-phosphate and inorganic carbon with one single device was experienced as an important advantage of the developed methodology.

The on-line measurement of nitrogen and phosphorus in animal manure is a new application area, for which the developed sensor was evaluated. In Flanders, a taxation system on the production and surplus of nitrogen and phosphorus has been approved (Mestdecreet, May 11th, 1999). In this framework, increasing demands for analyses of N and P in animal manure and other organic streams are to be expected in the coming years. The most important difference compared to the other applications is that the titrated sample is now free of organic interferences because of a destruction step with H_2SO_4 and H_2O_2 prior to titration. Complexation reactions with Ca^{2+} and Fe^{3+} were modelled and pointed to be responsible for extra buffer capacities around pH 5, pH 8 and pH 10. It was also found that the buffer capacities of $o\text{-PO}_4$ and NH_4^+ (the buffers of main interest) are only influenced to a limited extent by the complex formation reactions. Taking into account some further optimizations discussed in this work, the analysis results with this titrimetric sensor are expected to be comparable with the laboratory results. The strongest points of the titrimetric method are: Simultaneous N and P measurement with one method, minor sample manipulations, N and P results within 30 minutes, low and inexpensive chemical consumption, consumption of only one and non-hazardous reagent (NaOH).

The fourth part of this work describes the automation of buffer capacity model building, of which the purpose is to efficiently find an useful and adequate buffer capacity model, tailor-made for each individual sample. This methodology supports a new idea developed in this work, being 'quality proportional sampling' in effluents and river waters. This is proposed as an alternative to time or flow proportional sampling. It is suggested that the buffer capacity profile is used as a fingerprint for the water composition. When the fingerprint is changing, an alarm is triggered and a sample is automatically taken for further laboratory analysis. For a number of selected samples (e.g. industrial effluent samples), the estimations with automatically built models were highly superior to the fixed model approach, because the buffer composition was drastically changing during the measurement period. Other benefits of the automatic modelling approach are its usefulness for titrator problem detection and its application as a support tool for the characterization of unknown buffer capacity profiles.

Samenvatting

In dit werk werd een multifunctionele titrimetrische sensor ontwikkeld. De hardware van deze sensor bestaat uit een titratie-eenheid, die zuur-base titraties van aquatische stalen kan verrichten. Een titratiecurve heeft een typische S-vorm, en kan mits een gepast mathematisch algoritme omgezet worden in een buffercapaciteitsprofiel. Het softwaregedeelte van dit werk omhelst de volledige data-interpretatie van de opgenomen titratiecurves. De ontwikkelde hard- en softwaresensor differentieert zich van bestaande sensoren doordat het volledige en gedetailleerde titratieprofiel geïnterpreteerd wordt met een modelgebaseerde aanpak. Het is een multifunctionele sensor omdat hij ten eerste nuttig is voor het quantificeren van bufferende componenten (bv. ammonium en ortho-fosfaat in effluenten of gedestrueerde dierlijke mest), en ten tweede, omdat hij gebruikt kan worden als een alarmgenerator (bv. het detecteren van accidentele lozingen in rivieren). Een aanzienlijk deel van het onderzoek is uitgevoerd in functie van onderzoeksprojecten waarin industriële partners betrokken waren. Als gevolg hiervan is het in dit werk beschreven onderzoek interdisciplinair en praktisch georiënteerd.

Het eerste deel van dit proefschrift beschrijft de fundamenteën en de achtergrond van het onderzoekswerk. De opbouwende aanpak, geïllustreerd met didactische voorbeelden, stelt de lezer in staat een degelijke introductie en een consistent overzicht van het modelleren van pH-buffercapaciteit te verwerven. Dit overzicht is gedeeltelijk opgebouwd rond literatuuronderzoek, doch er moesten belangrijke gedeeltes gemodificeerd of verder ontwikkeld worden teneinde te voldoen aan de vereisten van dit werk. Tevens werden er in de literatuur hieromtrent een aantal verwarringen ontrafeld. Een interessant aspect is dat niet alleen buffercapaciteitsmodellen voor eenvoudige systemen (zuur-base evenwichten) ontwikkeld werden, maar dat ook meer gecompliceerde systemen (complexaties en/of neerslagreacties) in dit raamwerk behandeld konden worden. Voor elk van de beschreven methodes werd aangepaste simulatiesoftware ontwikkeld. Er wordt ook een literatuuroverzicht van on-line meettechnieken gegeven voor afvalwaterbehandelingssystemen, rivieren en andere aquatische stromen.

Het tweede deel van dit proefschrift vat de belangrijkste software-ontwikkelingen samen. Er werd een commerciële titrator met een ingebouwd dynamisch titratie-algoritme gebruikt om de experimentele titratiecurves op te nemen. Met deze opstelling werden een aantal nadelen vastgesteld, en daarom werd een gecombineerd data- en modelgebaseerd algoritme ontwikkeld, dat beter geschikt was in functie van dit werk. Een doseereenheid, gekoppeld aan een computer, en gebruik makend van het ontwikkelde titratie-algoritme biedt ook interessante mogelijkheden tot gebruik in het laboratorium als alternatief voor de traditionele eindpunttitratoren. Het volledige dataverwerkingsgedeelte van de titrimetrische sensor is geïmplementeerd in de software *bomb* (optimaal buffercapaciteitsmodel bouwer), met een sterke nadruk op de robuustheid voor gebruik in het veld. Deze software kan uit een titratiecurve informatie extraheren over de individuele buffersystemen, en hun respectievelijke concentraties schatten. Met

dezelfde software kunnen ook automatisch buffercapaciteitsmodellen gebouwd worden.

Het derde deel van dit proefschrift is toepassingsgericht. Er werden drie on-line (ten velde) toepassingen voor de ontwikkelde sensor in detail bestudeerd: het bewaken van effluenten en rivierwaters, het meten van nutriënten in tertiaire waterzuiveringssystemen gebaseerd op algen, en het meten van nutriënten in gedestruerde dierlijke mest. De kleinste concentraties aan ammonium en ortho-fosfaat die succesvol konden bepaald worden, liggen respectievelijk rond 0.5 mg N l^{-1} en 0.5 mg P l^{-1} . Deze waarden zijn slechts indicatief, omdat ze sterk situatieafhankelijk zijn. De resultaten toonden aan dat de op buffercapaciteit gebaseerde sensor een nuttig meetsysteem is voor het on-line bewaken van ammonium en ortho-fosfaat in effluenten, rivieren en op algen gebaseerde waterzuiveringssystemen. Omdat de gebruikte meetmethodologie ongetwijfeld gevoelig is aan interferenties, kadert het toepassingsdomein van deze sensor in de eerste plaats binnen de context van alarmgeneratie. In een pilootreactor met algen kon de concentratie aan inorganische koolstof accuraat geschat worden met de ontwikkelde sensor, en deze meting werd nuttig beschouwd voor controledoelinden. De simultane meting van ammonium, ortho-fosfaat en inorganische koolstof met één en hetzelfde apparaat werd als een belangrijk voordeel voor de ontwikkelde methodologie bevonden.

De on-line meting van stikstof en fosfor in dierlijke mest is een nieuw toepassingsdomein waarvoor de ontwikkelde sensor geëvalueerd werd. In Vlaanderen werd een taxatiesysteem op de productie en overschotten van stikstof en fosfor ingevoerd (Mestdecreet, 11 mei 1999). In dit raamwerk worden toenemende behoeften voor analyses van N en P in dierlijke mest en andere organische stromen verwacht. Het belangrijkste verschil vergeleken met de vorige toepassingen is dat het getitreerde staal vrij is van organische interferenties wegens de destructiestap met H_2SO_4 en H_2O_2 vóór de titratie. Complexatiereacties met Ca^{2+} en Fe^{3+} werden gemodelleerd en verantwoordelijk geacht voor extra buffercapaciteiten rond pH 5, pH 8 en pH 10. Er werd ook gevonden dat de buffercapaciteiten van o-PO_4 en NH_4^+ (de buffers van belang) slechts miniem beïnvloed werden door deze complexatiereacties. Rekening houdend met een aantal verdere optimalisaties besproken in dit werk, wordt verwacht dat de titrimetrische metingen de vergelijking met de laboratoriumresultaten kunnen doorstaan. De sterkste punten van de titrimetrische methode zijn: simultane N- en P-meting met één methode, weinig manipulaties van de stalen, N- en P-metingen binnen de 30 minuten, een laag en goedkoop chemicaliënverbruik, en het gebruik van slechts één en vrij ongevaarlijk reagens (NaOH).

Het vierde deel van dit proefschrift tenslotte beschrijft de automatisering van het bouwen van buffercapaciteitsmodellen. De doelstelling hierbij is om op efficiënte wijze een bruikbaar en adequaat buffercapaciteitsmodel te bouwen, dat aangepast is aan een individueel staal. Deze methodologie onderbouwt een nieuw idee dat ontwikkeld werd in de werk, nl. 'kwaliteitsafhankelijke staalname' in rivieren en effluenten. Dit wordt voorgesteld als een alternatief voor tijds- of debietsproportionele monsternamen. Er wordt hierbij aangenomen dat een buffercapaciteitsprofiel gebruikt kan worden als een soort van vingerafdruk van de waterkwaliteit. Als de vingerafdruk wijzigt, wordt een alarm geactiveerd, en wordt automatisch een staal genomen voor verdere analyse in het laboratorium. Voor een aantal geselecteerde stalen (bv. industrieel effluent) waren de schattingen met de automatisch gebouwde buffercapaciteitsmodellen duidelijk superieur vergeleken met de schattingen via een vast model, omdat de buffersamenstelling drastisch wijzigde tijdens de uitgevoerde meetcampagne. Andere voordelen van de automatische modelaanpak zijn de mogelijkheid om titratorproblemen te detecteren en de ondersteuning bij het karakteriseren van onbekende buffercapaciteitsprofielen.

Curriculum Vitae

Lieven Van Vooren

Geboren te Assenede op 9 augustus 1967

Gehuwd met Ria Perneel op 18 juli 1992

Vader van Sander (geboren op 23 juli 1994) en Daan (geboren op 10 januari 1997)

Persoonlijk adres:

Rijschootstraat 23

9940 Ertvelde

Tel: (09) 344 75 09

Werkadres:

Universiteit Gent (U.G.)

Faculteit Landbouwkundige en Toegepaste Biologische Wetenschappen

Vakgroep Toegepaste Wiskunde, Biometrie en Procesregeling

Coupure links 653, 9000 Gent

Tel: (09) 264 59 33

Fax: (09) 223 49 41

E-mail: Lieven.VanVooren@rug.ac.be

Studies

- Secundair onderwijs (1979-1985)
St.-Laurensinstituut, Zelzate
Wetenschappelijke A
- Hoger onderwijs (1985-1990)
Universiteit Gent
Faculteit Landbouwkundige en Toegepaste Biologische Wetenschappen
Coupure links 653, 9000 Gent
 - Kandidaat landbouwkundig ir. (1987)
Grote onderscheiding
 - Landbouwkundig ir. – biotechnologie (1990)

Keuzevakken: systeemsimulatie en radio-agrologie

Afstudeerwerk: Computersimulatie van het actief slib waterzuiveringsproces met de RODTOX als biosensor

Promotoren:

Prof. W. Verstraete – Laboratorium voor Microbiële Ecologie

Prof. G. Vansteenkiste – Seminarie voor Toegepaste Wiskunde en Biometrie

Grote onderscheiding

Militaire dienst

Van 1 augustus 1990 tot 31 juli 1991

Assistent leerstoel Toegepaste Scheikunde

Koninklijke Militaire School – Brussel

Werk:

Retrospectieve identifikatie van zenuwgassen en pesticiden in menselijk serum

Gaschromatografie

Beroepsactiviteiten

- Van 1 november 1990 tot 31 juni 1991
Repetitor organische scheikunde, fysica en dieetleer
STUDIDAC, St. Pietersplein 44, 9000 Gent, tel: (09) 220 15 62
- Van 15 september 1991 tot 31 maart 1994
Onderzoeksassistent op een VLIM-project
(Vlaams Impulsprogramma voor Milieutechnologie)
Ontwikkeling van een sensor voor de bepaling van de oppervlaktewaterkwaliteit
Universiteit Gent (U.G.)
Faculteit Landbouwkundige en Toegepaste Biologische Wetenschappen
Laboratorium voor Microbiële Ekologie, tel: (09) 264 59 76
Seminarie voor Toegepaste Wiskunde en Biometrie, tel: (09) 264 59 32
Coupure links 653, 9000 Gent
HEMMIS NV, Leopold III-laan 2, 8500 Kortrijk, tel: (056) 37 26 37
- Vanaf 1 april 1994
Assistent aan de Vakgroep Toegepaste Wiskunde, Biometrie en Procesregeling
Universiteit Gent
Begeleidende en sturende rol bij extern gefinancierde onderzoeksprojecten:
 - Van 1 april 1994 tot 1 oktober 1994: Ontwikkeling van een sensor voor de bepaling van de oppervlaktewaterkwaliteit
 - Van 15 november 1995 tot 15 november 1996: Gebruik van statistische methoden voor doorgedreven interpretatie van data uit de meetdatabank van de VMM (Vlaamse Milieumaatschappij)
 - Van 1 januari 1998 tot 1 januari 2000: FASTNAP: Snelle bepaling van stikstof en fosfor in mengmest

Buitenlandse werkzaamheden in dienstverband:

- Van 9 mei 1994 tot 11 mei 1994: Nancy (Frankrijk), EG-COST682 working group meeting “Fullscale activated sludge database”
- Van 30 mei 1995 tot 4 juni 1995: Lyngby (Denemarken) en Lund (Zweden), werkbezoek “Ontwikkeling van een databank voor volschalige actief slib installaties”
- Van 5 juni 1995 tot 11 juni 1995: Cracow (Polen), TEMPUS lesgever statistiek in M.Sc. “European Food and Beverage Quality Management”
- Van 2 mei 1997 tot 4 mei 1997: Wiesbaden (Duitsland), volgen van cursus “Generalised linear models and multivariate responses”
- Van 20 juli 1997 tot 24 augustus 1997 en van 1 augustus 1998 tot 1 december 1998: Quebec (Canada), onderzoeker in het kader van “Internationale wetenschappelijke en technologische samenwerking Quebec–Vlaanderen”, gefinancierd door de Vlaamse gemeenschap

Extra verworvenheden:

- Verantwoordelijke in een onderzoekslaboratorium
- Ontwikkeling van milieu-sensoren in een commercieel kader
- Begeleiden van thesisstudenten en project-onderzoekers
- Lesgeven in post-academische opleidingsprogramma’s (praktijkstatistiek)
- Geven van presentaties op symposia, congressen enz.
- Statistische consultancy voor bedrijven en onderzoekers
- Aanvragen en opvolgen van nationale en internationale projecten

Talenkennis

Nederlands, Engels en Frans: vlot

Duits: elementair

Diverse

- Laureaat K.VIV-studentenprijs 1990
- Laureaat Studieprij Water 1990 - W.E.L. vzw
- Lesgever ‘Praktijkgerichte statistiek’, Instituut Permanente Vorming, Faculteit Toegepaste Wetenschappen, Gent, 1998–2000
- Mede-indiener van het patent FASTNAP (ref 161404) “Werkwijze voor het bepalen van het gehalte aan stikstof en/of fosfor in drijfmest, monsternemer voor het uitvoeren van een dergelijke werkwijze” (Octrooibureau Vriezendorp & Gaade, Den Haag)

Publikaties

J. Bols, P.L.M. Goethals, J. Meirlaen, A. van Griensven, V. Vandenberghe, L. Van Vooren, N. De Pauw, P.A. Vanrolleghem, and W. Bauwens. Automated measurement stations for river water quality monitoring. *Proceedings 13th Forum Applied Biotechnology. Med. Fac. Landbouww. Univ. Gent*, 64/5a:107–110, 1999.

W.N. Camargo, L. Van Vooren, and P. Sorgeloos. Effects of lunar cycles on artemia density sampling in hypersaline environments. *In preparation*, 2000.

L.A. Danneels, H.J. De Cuyper, G.G. Vanderstraeten, D.C. Cambier, C.K. Goemaere, and L. Van Vooren. Electronically processed EMG and lumbar paravertebral muscle function. *Accepted in Clinical Biomechanics*, 1999.

L.A. Danneels, H.J. De Cuyper, G.G. Vanderstraeten, D.C. Cambier, C.K. Goemaere, and L. Van Vooren. Natural lifting movements evaluated electronically: a subdivision between the multifundus and the iliocostalis lumborum. *Submitted to Manual Therapy*, 1999.

K. Gernaey, H. Bogaert, P. Vanrolleghem, L. Van Vooren, and W. Verstraete. Sensors for nitrogen removal monitoring in wastewater treatment. In J.M. Lynch and A. Wiseman, editors, *Environmental Biomonitoring - The Biotechnology Ecotoxicology Interface*, volume 7 of *Biotechnology Research series*, pages 180–207. Cambridge University Press, 1998.

P. Goethals, A. van Griensven, J. Bols, N. De Pauw, P.A. Vanrolleghem, L. Van Vooren, and W. Bauwens. Automated measurement stations and water quality modelling. In *Proceedings 9th European Congress on Biotechnology*, Brussels, Belgium, July 11–15 1999.

C. Hellinga, P. Vanrolleghem, and L. Van Vooren. Meten en regelen in de praktijk gebracht - verslag congres 'sensors in waste water technology'. *H₂O*, 30(4):122–125, 1997.

I. Kersters, L. Van Vooren, G. Huys, P. Janssen, K. Kersters, and W. Verstraete. Influence of temperature and process technology on the occurrence of *Aeromonas* species and hygienic indicator organisms in drinking water production plants. *Microbial Ecology*, 30:203–218, 1995.

I. Kersters, L. Van Vooren, L. Verschuere, L. Vauterin, A. Wouters, J. Mergaert, J. Swings, and W. Verstraete. Utility of the Biolog system for the characterization of heterotrophic microbial communities. *System. Appl. Microbiol.*, 20:439–447, 1997.

I. Kersters, L. Van Vooren, L. Verschuere, L. Vauterin, J. Wouters, J. Mergaert, W. Verstraete, and J. Swings. Characterisation of heterotrophic microbial communities by means of the Biolog system. In *Substrate use tests for characterisation of microbial communities in terrestrial ecosystems*, poster, Innsbruck, Austria, October 16-18 1996. University of Innsbruck, Institute of Microbiology.

- J.-P. Ottoy, Van Vooren L., Willems P., Van Welden D., Vanrolleghem P.A., and Thierens K. Opzet, verwerking en interpretatie van dierproeven. Statistische basistechnieken. In *Proceedings TI-KVIV Studiedag Opzet, Verwerking en Interpretatie van Dierproeven*, pages 1–37, Gontrode, Belgium, May 1995. KVIV.
- O. Thas, L. Van Vooren, and J.-P. Ottoy. Graphical models: Applicability and software. In *Proceeding of the 6th HARMA workshop*, pages 33–48, Berlin, Germany, September, 20 1996. HARMA Workshop.
- O. Thas, L. Van Vooren, and J.-P. Ottoy. Modellen voor categorische data. In *Verhandelingen van de Fac. L & TBW*, pages 5/1–38, Gent, Belgium, December 1996. Post-Universitaire Onderwijsdag, Universiteit Gent.
- O. Thas, L. Van Vooren, and J.-P. Ottoy. Selection of nonparametric methods for monotonic trend detection in water quality. In *Proceeding of the 5th HARMA workshop*, Bari, Italy, February 23 1996. HARMA Workshop.
- O. Thas, L. Van Vooren, and J.P. Ottoy. Nonparametric test performance for trends in water quality with sampling design applications. *JAWRA*, 34(2):347–357, 1998.
- O. Thas, P. Vanrolleghem, B. Kops, L. Van Vooren, and J.P. Ottoy. Extreme value statistics: Potential benefits in water quality management. *Wat. Sci. Tech.*, 36(5):133–140, 1997.
- M. Van De Steene, L. Van Vooren, O. Thas, and J.P. Ottoy. *GLM procedure in SPSS voor Windows*. Faculteit Landbouwkundige en Toegepaste Biologische Wetenschappen, Universiteit Gent, 1998. 72 pp.
- H. Van de Werf, G. Genouw, L. Van Vooren, and W. Verstraete. The determination of active microbial biomass by the respiration simulation method. In Kassem Alef and Paolo Nannipieri, editors, *Methods in Applied Soil Microbiology and Biochemistry*, chapter 8, pages 405–408. Academic Press Ltd., London, U.K., 1995.
- L. Van Vooren, N. Huyghe, O. Thas, and J.-P. Ottoy. *Inleiding tot SPSS voor Windows*. Faculteit Landbouwkundige en Toegepaste Biologische Wetenschappen, Universiteit Gent, 1998. 193 pp.
- L. Van Vooren, P. Lessard, J.-P. Ottoy, and P.A. Vanrolleghem. pH buffer capacity based monitoring of algal wastewater treatment. *Environ. Technol.*, 20:547–561, 1999.
- L. Van Vooren, M. Van De Steene, J.-P. Ottoy, and P.A. Vanrolleghem. Automatic buffer capacity model building for the purpose of water quality monitoring. *Submitted for WATERMATEX 2000 conference, Gent, 2000*.
- L. Van Vooren, W. Verstraete, and G.C. Vansteenkiste. Dynamisch computermodel van het actief slib waterzuiveringsproces. *Water*, 64:72–80, 1992.

L. Van Vooren and P. Willems. Chemische en microbiologische monitoring van de waterkwaliteit. deel 2. Net-effekt sensor voor oppervlaktewater monitoring. In *Verhandelingen van de Fac. L & TBW*, pages 6/1–4, Gent, Belgium, December 1992. Post-Universitaire Onderwijsdag, Universiteit Gent.

L. Van Vooren and P. Willems. Analyse van organische stoffen: groepsparameters. In *Milieumetingen: uitvoering en interpretatie*, Antwerpen, Belgium, March 1993. Vlomitech cursus, KVIV.

L. Van Vooren, P. Willems, J.P. Ottoy, G.C. Vansteenkiste, and W. Verstraete. Automated buffer capacity based sensor for effluent quality monitoring. *Wat. Sci. Tech.*, 33(1):81–87, 1996.

L. Verschuere, V. Fievez, L. Van Vooren, I. Kersters, and W. Verstraete. Biolog profiles of model microbial communities: single point analysis vs. kinetic profiles. In *Substrate use tests for characterisation of microbial communities in terrestrial ecosystems*, page poster, Innsbruck, Austria, October 16-18 1996. University of Innsbruck, Institute of Microbiology.

L. Verschuere, V. Fievez, L. Van Vooren, G. Rombaut, and W. Verstraete. Modeling the color development in Biolog microtiter plates by the gompertz function. *Syst. Appl. Microbiol.*, 21:609–617, 1998.

L. Verschuere, V. Fievez, L. Van Vooren, and W. Verstraete. The contribution of individual populations to the Biolog pattern of microbial communities. *FEMS Microbiol. Ecol.*, 24:353–362, 1997.

P. Willems and L. Van Vooren. Chemische en microbiologische monitoring van de waterkwaliteit. deel 1. Algemene methodes. In *Verhandelingen van de Fac. L & TBW*, pages 5/1–12, Gent, Belgium, December 1992. Post-Universitaire Onderwijsdag, Universiteit Gent.

P. Willems, L. Van Vooren, and J.-P. Ottoy. *Inleiding tot het Internet*. Faculteit Landbouwkundige en Toegepaste Biologische Wetenschappen, Universiteit Gent, 1995. 75 pp.